UNIVERSITY OF
BIRMINGHAM

STRUCTURAL BEHAVIOUR OF STRUCTURAL INSULATED PANELS (SIPS)

by

PRATHAN RUNGTHONKIT

A Thesis submitted to
The University of Birmingham
For the degree of
DOCTOR OF PHILOSOPHY

School of Civil Engineering
College of Engineering and Physical Sciences
The University of Birmingham
April 2012

ABSTRACT

The Structural Insulated Panel System (SIP system) has recently attracted continuingly growing interest since it is strong, energy efficient, easy to use in construction and hence has a potential to become a new alternative building material. It is anticipated that Structural Insulated Panels (SIPs) are required to withstand loads in various directions either individually or in combinations, e.g., the axial, racking and transverse loadings. Very few publications report the performance of SIPs when subjected to loads in multiple directions. Moreover, when applying SIPs as a load bearing material, there is another major concern related to their long-term performance, mainly caused by creep.

This research presents studies on structural behaviours of the SIPs under both short-term and long-term loadings under single and multi-axial loadings together with two typical joint designs i.e. mini-SIP and dimensional timber spline joints with and without openings by experimental, analytical and numerical investigations. It has been demonstrated that the developed numerical models can well predict the initiation of failure load and the failure mode of SIPs. Interactive failure load curves between axial and transverse loadings have been developed by carrying out a parametric analysis for SIPs with/without openings by using two types of joint construction.

ACKNOWLEDGEMENTS

First and foremost, I would like to thank Dr. Jian Yang, my supervisor, for his generous help, encouragement, and advice throughout the research. I will always remember his kind patience and assistant not only on technical matters, but also with life issues. With his encouragement and support, I won the research category 2010 and 2011 awards organised by the Midland Counties Branch of the Institution of Structural Engineers. In addition, I was also awarded the Guest, Keen and Nettlefolds Academic Excellence Scholarship 2010.

I would also like to thank my co-supervisor, Professor Leslie Clark, for his technical support during the course of this research.

This study was financially supported by the EPSRC, ErgoHome Ltd and the University of Birmingham and this support is gratefully acknowledged.

Thanks to the School of Civil Engineering, University of Birmingham for the use of school facilities and the support of the technical staff including David Cope, Michael Vanderstam, James Guest and John Edgerton.

Last but not least, sincere thanks to my family and especially my wife and my lovely son, Pornsawan and Thames. Without their unending support and constant encouragement, this work would never have been completed.

TABLE OF CONTENTS

ABSTRACT i
ACKNOWLEDGEMENTS ii
TABLE OF CONTENTS iii
LIST OF FIGURES ix
LIST OF TABLES xvii
LIST OF NOTATIONS xxii
LIST OF ABBREVIATIONS xxiv

CHAPTER ONE **1**
INTRODUCTION 1
1.1 Structural Insulated Panel System 1
1.2 History of SIPs 1
1.3 Strengths and weaknesses of the SIP system 4
1.4 Gaps in knowledge 6
1.4.1 SIP performance subjected to multiple load combinations 7
1.4.2 Effects of opening areas 7
1.4.3 Effects of long-term loading 8
1.4.4 SIP connections 8
1.5 Aim and Objectives of this research 8
1.6 Thesis outline 9
1.7 Publication of research 10

CHAPTER TWO **12**
LITERATURE REVIEW 12
2.1 SIP system 12
2.1.1 Structural Insulated Panels (SIPs) 12
2.1.1.1 Outer face 14
2.1.1.2 Inner Core 16
2.1.1.3 Adhesive 18
2.1.2 SIP connections 19
2.1.3 Header, footer and sole plate 22
2.1.4 Fixing 24
2.1.5 Internal lining 24
2.1.6 External cladding 24

2.2 SIP standards and guidance 26
2.2.1 ISO 22452 (ISO, 2011) *26*
2.2.2 PRS-610 (APA, 2008) *26*
2.2.3 TR 019 (EOTA, 2005) *26*
2.2.4 APA supplement No.4 (APA, 1993) *27*
2.2.5 Prescriptive Method for Structural Insulated Panels (SIPs) Used in Wall Systems in Residential Construction (HUD, 2006) *27*
2.3 Structural analysis techniques 27
2.3.1 Classical sandwich panel theory *28*
2.3.2 Finite Element Method *31*
2.4 Failure mode in SIPs 33
2.4.1 Transverse load *33*
2.4.1.1 Face failure *34*
2.4.1.2 Inner core shear failure *35*
2.4.1.3 Debonding *35*
2.4.1.4 Indentation *36*
2.4.2 Axial compression load *36*
2.4.2.1 Buckling *38*
2.4.2.2 End bearing *39*
2.4.2.3 Debonding *39*
2.4.3 Racking *39*
2.5 Structural performance 40
2.5.1 Axial compression test *40*
2.5.2 Transverse load test *42*
2.5.3 Racking test *44*
2.5.4 Combined bending and compression test *45*
2.5.5 SIPs with openings *46*
2.5.6 Fire performance *48*
2.5.7 Creep test *48*
2.5.7.1 Creep tests on SIPs *50*
2.5.7.2 Creep tests on sandwich beams *51*
2.5.7.3 Creep testing standards for sandwich beams *55*
2.5.7.4 Creep analysis method summary *56*
2.6 Summary 57

CHAPTER THREE **58**

RESEARCH METHODOLOGY 58

AND 58

MECHANICAL PROPERTIES OF SIP CONSTITUENT MATERIALS 58

3.1 Introduction 58

3.2 Research methodology 58

3.3 Mechanical properties of OSBs 60
3.3.1 Compressive test on OSBs 61
3.3.2 Tensile test on OSBs 65
3.4 Mechanical properties of PUR 70
3.4.1 Compressive test on PURs 70
3.4.2 Shear test on PURs 76
3.5 Mechanical properties of SIPs 81
3.5.1 Compressive test on SIPs 81
3.5.2 Tensile test of SIPs 84
3.5.3 Shear test on SIPs 87
3.5.4 Shear/Skewed test on SIPs 89
3.6 Three-point bending test on SIP beams 91
3.6.1 Experimental investigations on SIP beams 92
3.6.2 Analytical analysis of the shear modulus 94
3.6.3 Numerical investigation of SIP beams 96
3.7 Summary 108

CHAPTER FOUR 109

SIPS UNDER SINGLE LOADINGS 109

4.1 Introduction 109

4.2 Experimental investigations on SIPs with different joint constructions 109

4.2.1 SIP specimens 110
4.2.2 Experimental apparatus 113
4.2.3 Experimental investigation 115
4.2.4 Analytical investigation 125
4.2.5 Numerical investigation 131
4.2.6 Investigation summary of the four-point bending on SIPs 147
4.3 Combined loading test investigation 149
4.3.1 SIP testing samples 149
4.3.1.1 SIP typical panel (STP) 150
4.3.1.2 SIP with mini-SIP connection (SMC) 150
4.3.1.3 SIP with dimensional timber spline connection (SDC) 151
4.3.1.4 SIP typical panel with opening (STPO) 151
4.3.1.5 SIP with mini-SIP connection and opening (SMCO) 151
4.3.2 Test load cases 157
4.4 Load case No. 1 - Transverse loading 158
4.4.1 Experimental investigations for panels without opening 164
4.4.2 Analytical investigation 173
4.4.3 Numerical investigation 176
4.4.4 Investigation summary for panels with different joints 189
4.4.5 Experimental investigations to SIPs with openings 191

4.4.6 Numerical investigation..... 198
4.4.7 Investigation summary for panels with different joints and openings208
4.5 Load case No. 2 – Uniform axial compression 210
4.5.1 Experimental investigations for SIPs without openings..... 211
4.5.2 Axial compression analytical method..... 214
4.5.2.1 Outer face crushing failure 214
4.5.2.2 Buckling failure 215
4.5.3 Numerical investigation..... 216
4.5.4 SMCO experimental investigation..... 221
4.5.5 SMCO axial compression analytical method 222
4.5.6 Numerical investigation..... 224
4.5.7 Investigation summary for panels with different joints and openings228
4.6 Load case No.3 – Racking loading 229
4.6.1 Experimental investigation 231
4.6.2 Racking analytical investigation 236
4.7 Summary 237

CHAPTER FIVE **239**

SIPS UNDER COMBINED LOADINGS 239

5.1 Introduction 239

5.2 Load case No. 4 - Combined axial and transverse loadings 239

5.2.1 Experimental investigation 240
5.2.2 Numerical investigation..... 246
5.2.3 Discussion of results for panels with different joints and openings.. 249
5.3 Load case No. 5 - Combined racking and transverse loadings 251

5.3.1 Experimental investigation 254
5.4 Load case No. 6 - Combined axial and racking loadings 258

5.4.1 Experimental investigation 259
5.4.2 Racking analytical investigation 264
5.5 Load cases No. 7 & 8 - Combined axial, racking and transverse loadings 265

5.5.1 Experimental investigation 267
5.5.2 Numerical investigation on SIPs with combined axial and transverse loadings..... 274
5.7 Summary 276

CHAPTER SIX **278**

SIPS UNDER LONG-TERM LOADINGS 278

6.1 Introduction 278

6.2 Experimental study of OSB subjected to long-term loading 278

6.2.1 Experimental investigation of long-term performance of OSB 279
6.2.2 Numerical investigation of long-term performance of OSBs 281

6.3 Long-term double shear experimental study of SIPs 285

6.3.1 Experimental investigation of long-term double shear of SIPs 285
6.3.2 Numerical investigation of long-term SIPs 287

6.4 Long-term experimental investigation on SIP beams 290

6.4.1 Experimental investigation of SIP beams under long-term loading . 291
6.4.2 Numerical investigation of long-term SIP beams 294
6.4.3 Creep prediction methods for SIP beams 296
6.4.3.1 Taylor's models 297
6.4.3.2 BS EN 1606 (BSI, 1996) 302
6.4.3.3 BS EN 14509 (BSI, 2006) 305
6.4.3.4 Just's model 308
6.4.3.5 Huang and Gibson's model 308
6.4.4 Unloaded experimental investigation of SIP beams 309
6.4.5 Unloaded prediction methods for SIP beams 311
6.4.5.1 Modified Taylor's models 311
6.4.5.2 Modified BS EN 1606 (BSI, 1996) 315
6.4.5.3 Huang and Gibson's model 317
6.4.6 Discussion of SIP beam creep and recovery 318

6.5 Long-term investigation on SIPs with different joint designs 318

6.5.1 Experimental investigation of SIPs with different joint designs 319
6.5.2 Numerical investigation of long-term SIPs with different joint designs 323
6.5.3 Creep prediction methods for SIPs with different joint designs 325
6.5.3.1 Taylor's models 326
6.5.3.2 BS EN 1606 (BSI, 1996) 328
6.5.4 Ultimate load after the creep experiment 329
6.5.5 60 year SIP performances with different joint designs 331
6.5.6 Discussion of SIPs with different joint designs 334

6.6 Summary 336

CHAPTER SEVEN **337**

CONCLUSIONS AND RECOMMENDATIONS 337

7.1 Contribution to knowledge 337

7.2 Implications for design practice 339

7.3 Recommendations for future work..... 340
REFERENCES..... 343
APPENDICES..... A
Appendix A - Analytical method calculations..... A1
Appendix B - Published Paper..... B1

LIST OF FIGURES

Figure 1.1: Structural Insulated Panels (Kingspan TEK Ltd, 2007) 2
Figure 1.2: ErgoHome (ErgoHome Ltd, 2010) 2
Figure 1.3: Alden B. Dow with SIPs (Morley, 2000) 3
Figure 2.1: Cross-section of a typical SIP (Bregulla and Enjily, 2004) 13
Figure 2.2: Comparison of SIP with an I beam (Morley, 2000) 13
Figure 2.3: OSB fibre alignment (Sunley and Bedding, 1995) 15
Figure 2.4: OSB thin spline (Morley, 2000) 20
Figure 2.5: Foam block spline or Mini-SIP (Morley, 2000) 20
Figure 2.6: Dimensional timber spline (Morley, 2000) 20
Figure 2.7: Other sections of SIP connections (Hemsec SIPs Ltd, 2007) 22
Figure 2.8: Footer and Sole Plate Details (SIP Build Ltd, 2008) 23
Figure 2.9: External claddings (Kingspan TEK Ltd, 2007) 25
Figure 2.10: The geometry and coordinate system used in this research 28
Figure 2.11: Three-point bending load on SIP 30
Figure 2.12: A complex shape that can be represented by finite elements (Case et al., 1999) 32
Figure 2.13: Commonly used finite element forms (ABAQUS, 2010) 32
Figure 2.14: Typical failure modes when subjected to transverse load 34
Figure 2.15: Typical failure modes when subjected to axial compression load 37
Figure 2.16: Combined bending and axial compression load resistance (BBA, 2004) 46
Figure 2.17: Three stages of creep (Findley, 1976) 49
Figure 2.18: Long-term creep tests on sandwich beams (Just, 1983) 52
Figure 3.1: OSB compressive test specimen 61
Figure 3.2: Experimental apparatus for OSB compressive test 62
Figure 3.3: Stress vs strain of OSB specimens in the major axis 63
Figure 3.4: Crushing failure 63
Figure 3.5: Stress vs Strain of the minor axis OSB specimens 64
Figure 3.6: OSB tensile specimen details 66
Figure 3.7: Apollo structural adhesive A5086 part A and B 66
Figure 3.8: Experimental apparatus for OSB tensile test 67

Figure 3.9: Stress vs Strain of the major axis OSB specimens 68
Figure 3.10: Tensile failure mode 69
Figure 3.11: Stress vs Strain of the minor axis OSB specimens 69
Figure 3.12: PUR compressive test 72
Figure 3.13: 50% displacement of specimen thickness 72
Figure 3.14: Force-Displacement of the longitudinal direction PUR specimens 73
Figure 3.15: Force-Displacement of the through thickness direction PUR specimens 74
Figure 3.16: Force-Displacement of the transverse direction PUR specimens 75
Figure 3.17: Single shear on PUR test specimens 77
Figure 3.18: Force-displacement curve of PUR specimens 78
Figure 3.19: Delaminated failure mode 79
Figure 3.20: Double shear on PUR test specimens 79
Figure 3.21: Force-displacement curve of PUR specimens 80
Figure 3.22: Delaminated and slippage failure mode 81
Figure 3.23: Compressive test on SIP specimen 82
Figure 3.24: 50% displacement of specimen thickness 83
Figure 3.25: Force-displacement curve of SIP specimens 83
Figure 3.26: Tensile test on SIP specimen 85
Figure 3.27: Tearing of PUR 85
Figure 3.28: Force-displacement curve of SIP specimens 86
Figure 3.29: Double shear test on SIP specimens 87
Figure 3.30: Force-displacement curve of SIP specimens 88
Figure 3.31: Debonding and slip failure mode 88
Figure 3.32: Shear/Skewed test on SIP specimens 89
Figure 3.33: Force-Displacement of shear/skew SIP test results 90
Figure 3.34: Delaminated failure mode 91
Figure 3.35: Three-point bending experimental apparatus 92
Figure 3.36: Applied load vs mid-span deflection curves 93
Figure 3.37: Bending failure mode 94
Figure 3.38: SIP beam finite element model 98
Figure 3.39: Deflections comparison between FEM and mean test results 100
Figure 3.40: Deflections comparison between FEM and mean test results 101

Figure 3.41: Deflections comparison between FEM and mean test results 102
Figure 3.42: Distribution of the longitudinal stress (S_{11}) of the outer faces 106
Figure 3.43: Distribution of the shear stress (S_{22}) of the PUR inner core..... 106
Figure 3.44: Distribution of the shear stress (S_{12}) of the PUR inner core..... 107
Figure 3.45: Deflection comparison between the FEM and the mean test results 107
Figure 4.1: Four-point bending test (BS EN 14509, 2006) 111
Figure 4.2: STP specimen details 112
Figure 4.3: SMC specimen details 112
Figure 4.4: SDC specimen details 113
Figure 4.5: Experimental apparatus and sign convention of displacement 114
Figure 4.6: Dial gauge arrangement for the tests..... 115
Figure 4.7: Central vertical displacement at the mid-span (Dial Gauge No.1)..... 118
Figure 4.8: Vertical displacement at the mid-span (Dial Gauge No.2) 119
Figure 4.9: Typical mean vertical displacements at Dial Gauges No.1 and 2 120
Figure 4.10: Vertical displacement at the edge (Dial Gauge No.3) 121
Figure 4.11: Horizontal displacement at the edge (Dial Gauge No. 4) 123
Figure 4.12: Failure modes of panels subjected to four-point bending loads 125
Figure 4.13: Comparison between the mean STP test result with different methods..... 128
Figure 4.14: Comparison between the mean STP test result with different methods..... 131
Figure 4.15: STP finite element model..... 132
Figure 4.16: Finite element mesh for all specimens 134
Figure 4.17: Distribution of the outer face stresses 139
Figure 4.18: Distribution of the stresses of the PUR inner core 141
Figure 4.19: Central displacement comparison between the FEM and the mean test results 143
Figure 4.20: Vertical displacement comparison between the FEM and the mean test results 144
Figure 4.21: Vertical displacements comparison between the FEM and the mean test results 146
Figure 4.22: Horizontal displacements comparison 147
Figure 4.23: SIP typical panel (STP) details 152
Figure 4.24: SIP with mini-sip connection (SMC) details 153

Figure 4.25: SIP with dimensional timber spline connection (SDC) details 154
Figure 4.26: SIP typical panel with opening (STPO) details 155
Figure 4.27: SIP with mini-sip connection and opening (SMCO) details 156
Figure 4.28: Experimental apparatus for transverse loading test 159
Figure 4.29: Test panel was bolted at 150 mm and 750 mm to the test rig 160
Figure 4.30: Roller support at another end 160
Figure 4.31: LVDT arrangement and sign convention of displacement 163
Figure 4.32: LVDT arrangement for panels with openings 164
Figure 4.33: Load versus central vertical displacement (LVDT No.1) 166
Figure 4.34: Debonding failure modes 168
Figure 4.35: Load versus vertical displacement (LVDT No.2) 169
Figure 4.36: Typical load versus vertical displacement at the central span and at the panel edge 170
Figure 4.37: Load versus horizontal displacement (LVDT No. 3) 172
Figure 4.38: Comparison between the STP mean test result with the three analytical methods 174
Figure 4.39: Comparison between the mean SDC test result with different methods 175
Figure 4.40: Comparison between the mean SDC test result with different methods 176
Figure 4.41: STP finite element model 178
Figure 4.42: Distribution of the outer face stresses 180
Figure 4.43: Distribution of the stresses of the PUR inner core 181
Figure 4.44: Central deflection comparison between the FEM and the mean test results . 186
Figure 4.45: Edge deflection comparison between the FEM and the mean test results 187
Figure 4.46: Deflection comparison between the FEM and the mean test results 189
Figure 4.47: Test result comparison of SIPs with different connections 191
Figure 4.48: Load versus vertical displacement (LVDT No.1) 193
Figure 4.49: Flexure-shear failure 194
Figure 4.50: Load versus vertical displacement (LVDT No.2) 195
Figure 4.51: Load versus horizontal displacement (LVDT No. 3) 196
Figure 4.52: Load versus vertical displacement at the opening edge (LVDT No.1) 197
Figure 4.53: Test result comparison of STPO and SMCO 198
Figure 4.54: STPO finite element model 199

Figure 4.55: Distribution of the outer face stresses 203
Figure 4.56: Distribution of the stresses of the PUR inner core 204
Figure 4.57: Central deflection comparison between the FEM and the mean test results . 205
Figure 4.58: Edge deflection comparison between the FEM and the mean test results 206
Figure 4.59: Horizontal displacement comparison between the FEM and the mean test results 207
Figure 4.60: FEM result comparison of STPO, SMCO and SDCO 210
Figure 4.61: Experimental apparatus for uniform axial loading test..... 211
Figure 4.62: Load versus axial displacement 212
Figure 4.63: End bearing failure 213
Figure 4.64: SMC finite element model 217
Figure 4.65: Distribution of the longitudinal stress (S33) of the outer faces 218
Figure 4.66: Distribution of the stresses of the PUR inner core 219
Figure 4.67: Displacement comparison between the FEM and the mean test results 220
Figure 4.68: Load versus axial displacement 221
Figure 4.69: Face crushing failure..... 222
Figure 4.70: SMCO finite element model 224
Figure 4.71: Distribution of the longitudinal stress (S33) of the outer faces 225
Figure 4.72: Distribution of the stresses of the PUR inner core 226
Figure 4.73: Displacement comparison between the FEM and the mean test results 227
Figure 4.74: 120 x 120 mm square bearing pads..... 230
Figure 4.75: Racking test arrangement 230
Figure 4.76: LVDT arrangement and sign convention of displacement 231
Figure 4.77: Load versus racking displacement (LVDT No.1) 232
Figure 4.78: Racking failure modes 233
Figure 4.79: Load versus horizontal displacement (LVDT No.2) 234
Figure 4.80: Load versus vertical displacement (LVDT No. 3) 235
Figure 5.1: Experimental apparatus layout 240
Figure 5.2: LVDT arrangement 241
Figure 5.3: Load versus central vertical displacement (LVDT No.1)..... 242
Figure 5.4: Failure mode 243
Figure 5.5: Load versus vertical displacement (LVDT No.2) 244

Figure 5.6: Load versus axial displacement (LVDT No. 3) 245
Figure 5.7: Central displacement comparison between the FEM and the test results 248
Figure 5.8: Numerical result comparison of SIPs with different connections 250
Figure 5.9: Numerical result of SIPs with different connections and openings 250
Figure 5.10: Experimental apparatus layout for 253
Figure 5.11: LVDT arrangement 253
Figure 5.12: Load versus vertical displacement (LVDT No.1) 254
Figure 5.13: Failure modes 255
Figure 5.14: Load versus vertical displacement (LVDT No.2) 256
Figure 5.15: Load versus racking displacement (LVDT No. 3) 257
Figure 5.16: Experimental apparatus layout for 259
Figure 5.17: Load versus racking displacement 260
Figure 5.18: Disjointed failure 261
Figure 5.19: Load versus horizontal displacement (LVDT No.2) 262
Figure 5.20: Load versus vertical displacement (LVDT No. 3) 263
Figure 5.21: Experimental apparatus layout for 266
Figure 5.22: LVDT arrangement 267
Figure 5.23: Load versus central vertical displacement (LVDT No.1) 268
Figure 5.24: Load versus vertical displacement (LVDT No.2) 269
Figure 5.25: Load versus racking displacement (LVDT No.3) 270
Figure 5.26: Load versus axial axis displacement (LVDT No.4) 271
Figure 5.27: Failure modes 272
Figure 5.28: Combined axial-transverse capacity of SIPs with different joints 275
Figure 5.29: Combined axial-transverse capacity of SIPs with openings 276
Figure 6.1: Long-term OSB experimental apparatus 280
Figure 6.2: Three month creep test results 280
Figure 6.3: OSB finite element model 282
Figure 6.4: 1,000 hour experimental and FEM predicted creep deflections of OSBs 283
Figure 6.5: Three month experimental and FEM predicted creep deflections of OSBs 284
Figure 6.6: Long-term double shear SIP experimental apparatus 286
Figure 6.7: Three month creep test results 287
Figure 6.8: SIP double shear finite element model 288

Figure 6.9: 1,000 hour experimental and FEM predicted creep deflections of SIPs..... 289
Figure 6.10: Three month experimental and FEM predicted displacements of SIPs 290
Figure 6.11: Long-term experimental apparatus 292
Figure 6.12: Three month creep test results 293
Figure 6.13: Mean creep deflections of two duplicated test specimens 293
Figure 6.14: Three month comparison of SIP beams 295
Figure 6.15: Five month comparison of SIP beams 296
Figure 6.16: 1,000 hour mean experimental and predicted creep deflections of SIP-BLT-1&2 298
Figure 6.17: 1,000 hour mean experimental and predicted creep deflections of SIP-BLT-3&4 298
Figure 6.18: 1,000 hour mean experimental and predicted creep deflections of SIP-BLT-5&6 299
Figure 6.19: Three month experimental and predicted deflections of SIP-BLT-1&2..... 299
Figure 6.20: Three month experimental and predicted deflections of SIP-BLT-3&4..... 300
Figure 6.21: Three month experimental and predicted deflections of SIP-BLT-5&6..... 300
Figure 6.22: Five month experimental and predicted creep deflections of SIP beams 301
Figure 6.23: Mean 1,000 hour experimental and predicted deflections of SIP beams..... 303
Figure 6.24: Three month mean experimental and predicted deflections of SIP beams ... 303
Figure 6.25: Five month experimental and predicted creep deflections of SIP beams 304
Figure 6.26: OSB face FEM model..... 306
Figure 6.27: Three month experimental and predicted creep deflections of SIP beams ... 307
Figure 6.28: Three month experimental and predicted deflections of SIP beams 308
Figure 6.29: Three month mean experimental and predicted creep deflections of SIP beams 309
Figure 6.30: Unloaded experiment..... 310
Figure 6.31: Unloaded test results for all SIP beams..... 310
Figure 6.32: Unloaded one month test and predicted deflections of SIP-BLT-2..... 312
Figure 6.33: Unloaded one month test and predicted deflections of SIP-BLT-4..... 313
Figure 6.34: Unloaded one month test and predicted deflections of SIP-BLT-6..... 313
Figure 6.35: Unloaded two month test and predicted deflections of SIP-BLT-2..... 314
Figure 6.36: Unloaded two month test and predicted deflections of SIP-BLT-4..... 315

Figure 6.37: Unloaded two month test and predicted deflections of SIP-BLT-6..... 315
Figure 6.38: Unloaded one month test and predicted deflections of SIP beams..... 316
Figure 6.39: Unloaded two month test and predicted deflections of SIP beams 317
Figure 6.40: Unloaded two month test and predicted deflections of SIP beams 317
Figure 6.41: Experimental apparatus..... 320
Figure 6.42: Three month creep displacements at the mid-span (Dial Gauge No.1) 321
Figure 6.43: Three month vertical creep displacements at the edge (Dial Gauge No.2) ... 322
Figure 6.44: Three month vertical creep displacements (Dial Gauge No.3) 322
Figure 6.45: Three month horizontal creep displacements (Dial Gauge No.4) 323
Figure 6.46: Three month comparison of STP..... 324
Figure 6.47: Three month comparison of SMC 324
Figure 6.48: Three month comparison of SDC..... 325
Figure 6.49: Three month experimental and predicted creep deflections of STP..... 326
Figure 6.50: Three month experimental and predicted creep deflections of SMC 327
Figure 6.51: Three month experimental and predicted creep deflections of SDC..... 327
Figure 6.52: Three month experimental and predicted creep deflections 329
Figure 6.53: Debonding failure..... 331
Figure 6.54: Predicted deflections for 2400 mm SIPs with different joint designs..... 333
Figure 6.55: Predicted deflections for 3600 mm SIPs with different joint designs..... 333
Figure 6.56: Predicted deflections for 4800 mm SIPs with different joint designs..... 334

LIST OF TABLES

Table 2.1: SIP weight with various thicknesses (Hemsec SIPs Ltd, 2007) 14
Table 2.2: Some mechanical properties of 11 mm thick OSB 17
Table 2.3: Some mechanical properties of inner core materials (Thomas et al., 2005)..... 17
Table 2.4: Strengths and weaknesses of the wall-to-wall panel connections 21
Table 2.5: Compression test details and results (Kermani, 2006) 41
Table 2.6: Permissible axial loads for SIPs with different heights (BBA, 2004)..... 42
Table 2.7: Permissible transverse load for different span lengths (BBA, 2006)..... 43
Table 2.8: Racking design load of tested SIPs (Kermani and Hairstans, 2006) 44
Table 2.9: Basic racking resistances with different panel heights (BBA, 2006b)..... 45
Table 2.10: Combined bending and axial compression test results (Kermani, 2006) 46
Table 2.11: Effects of opening size on basic racking resistance of walls (Kermani and Hairstans, 2006) 47
Table 2.12: Creep deflection models proposed by Taylor et al. (1997) 50
Table 2.13: Creep analysis method summary 57
Table 3.1: OSB specimen test results in the major axis 63
Table 3.2: Minor axis OSB specimen test results..... 64
Table 3.3: Comparison between the test results and BS EN 12369 values 65
Table 3.4: Major axis OSB specimen test results..... 68
Table 3.5: Minor axis OSB specimen test results..... 70
Table 3.6: Comparison between the test results and BS EN 12369-1 characteristic values 70
Table 3.7: PUR longitudinal axis specimen test results 73
Table 3.8: PUR through thickness direction specimen test results 74
Table 3.9: PUR transverse direction specimen test results..... 75
Table 3.10: Comparison of PUR in three principal directions 75
Table 3.11: PUR single shear test results..... 78
Table 3.12: PUR single shear test results..... 80
Table 3.13: Comparison between the single and double shear test results..... 81
Table 3.14: Compressive SIP specimen test results 84
Table 3.15: Comparison of compressive SIP and PUR test results 84
Table 3.16: Tensile SIP specimen test results 86

Table 3.17: Comparison between SIP tensile test result and other published values 86
Table 3.18: SIP double shear test results 88
Table 3.19: Comparison between the PUR and SIP shear test results 89
Table 3.20: SIP shear/skewed test results 90
Table 3.21: Comparison between SIP shear/skewed test result and Kermani's finding 91
Table 3.22: Summary of experimental results for SIP beam test 94
Table 3.23: Shear modulus analytical analysis of SIP beam specimens 97
Table 3.24: Elastic material properties 99
Table 3.25: Material failure stresses 105
Table 3.26: Numerical analysis on OSB outer faces 105
Table 3.27: Numerical analysis on PUR 105
Table 4.1: Experimental result summary 125
Table 4.2: Analytical equations to determine the central displacement 127
Table 4.3: STP details and material properties 128
Table 4.4: SDC details and material properties 130
Table 4.5: Elastic material properties 134
Table 4.6: Stresses results in the OSB outer faces 137
Table 4.7: Stress results in the PUR core 138
Table 4.8: Experimental and numerical finding summary 148
Table 4.9: Details of loading combination and panel specimen 157
Table 4.10: Experimental result summary 173
Table 4.11: STP details and material properties 174
Table 4.12: SDC details and material properties 175
Table 4.13: Stresses results in the OSB outer faces 183
Table 4.14: Stress results in the PUR core 184
Table 4.15: Experimental and numerical finding summary 191
Table 4.16: Experimental result summary 198
Table 4.17: Stress results in the OSB outer faces 201
Table 4.18: Stress results in the PUR core 202
Table 4.19: Numerical analysis on the OSB outer faces for SDCO panels 208
Table 4.20: Numerical analysis on the PUR for SDCO panels 208
Table 4.21: Experimental and numerical finding summary 209

Table 4.22: Experimental result summary 214
Table 4.23: SMC details, material properties and axial loading capacity 215
Table 4.24: Specimen details, material properties and buckling load capacity 216
Table 4.25: Numerical analysis on SIPs when subjected to axial load 220
Table 4.26: Numerical analysis on SIPs when subjected to axial load 221
Table 4.27: SMCO experimental finding summary 222
Table 4.28: SMCO details, material properties and axial loading capacity..... 223
Table 4.29: SMCO details, material properties and buckling load capacity..... 223
Table 4.30: Numerical analysis on SMCO when subjected to axial load 227
Table 4.31: Summary of FEM investigations for all panels with openings 228
Table 4.32: Uniform axial compression test result summary 228
Table 4.33: Summary of FEM investigations for all panels..... 229
Table 4.34: Racking result summary..... 236
Table 4.35: Comparison between the test result and EC5 method 237
Table 5.1: Experimental result summary..... 246
Table 5.2: SMC - numerical analysis on the OSB outer faces 246
Table 5.3: SMC - numerical analysis on the PUR..... 247
Table 5.4: SMCO - numerical analysis on the OSB outer faces..... 247
Table 5.5: SMCO - numerical analysis on the PUR 247
Table 5.6: Summary of numerical results for STP and SDC panels 249
Table 5.7: Summary of numerical results for STPO and SDCO panels 249
Table 5.8: STP, SMC and SDC experimental and numerical finding summary..... 251
Table 5.9: STPO, SMCO and SDCO experimental and numerical finding summary 251
Table 5.10: Experimental finding summary 258
Table 5.11: SMC result summary 264
Table 5.12: SMCO result summary..... 264
Table 5.13: Comparison between the test result and EC5 method 265
Table 5.14: SMC result summary 272
Table 5.15: SMCO result summary..... 273
Table 5.16: SMC result summary 274
Table 5.17: SMCO result summary..... 274
Table 6.1: The applied loads and the instantaneous deflection of each OSB specimen 281

Table 6.2: 1,000 hour ABAQUS power-law creep parameters 283
Table 6.3: Comparison between the three month creep test results and FEM predictions 284
Table 6.4: The applied loads and the initial deflection of each SIP specimens 287
Table 6.5: 1,000 hour ABAQUS power-law creep parameters 289
Table 6.6: Comparison between the three month creep test results and FEM predictions 290
Table 6.7: The applied loads and the instantaneous deflection of each SIP specimen 294
Table 6.8: 1,000 hour ABAQUS power-law creep parameters 294
Table 6.9: Comparison between the three month creep test results and FEM predictions 295
Table 6.10: Comparison between the five month creep test results and FEM predictions 296
Table 6.11: Creep deflection models proposed by Taylor et al. (1997) 297
Table 6.12: 1,000 hour creep parameters from regression analysis 297
Table 6.13: the creep deflection at mid-span test results with various creep models 301
Table 6.14: Five month creep test results and predictions from the power model 302
Table 6.15: 1,000 hour material constants from BS EN 1606 method 302
Table 6.16: Comparison between the three month test results and BS EN 1606 predictions 304
Table 6.17: Comparison between the five month test results and BS EN 1606 predictions304
Table 6.18: Comparison between BS EN 1606 and power model 305
Table 6.19: Creep coefficient from BS EN 14509 method 306
Table 6.20: Comparison between the conservative and experimental φ_t values 307
Table 6.21: Recovery of each SIP specimen 310
Table 6.22: Modified Taylor's models for recovery deflection 311
Table 6.23: One month recovery parameters 312
Table 6.24: Remaining deflection at mid-span test results with various models 314
Table 6.25: One month material constants 316
Table 6.26: The applied loads and the initial deflection of each SIP specimen 319
Table 6.27: Creep test results of all SIP specimens 321
Table 6.28: Comparison between the three month test results and FEM predictions 325
Table 6.29: 1,000 hour creep parameters from regression analysis 326
Table 6.30: Creep deflection at the mid-span test results with the two creep models 328
Table 6.31: 1,000 hour material constants from BS EN 1606 method 328
Table 6.32: Creep deflection at the mid-span test results with the two creep models 329

Table 6.33: Ultimate loads at 3 months 330
Table 6.34: Panel specimen details 332
Table 6.35: Creep deflections of different numerical models 335

LIST OF NOTATIONS

Latin Alphabet

A_C	Effective area of the foam core
A_i	Creep parameters associated with creep deflection equations
A_{F1}	Measured area of cross-section of the top face
A_{F2}	Measured area of cross-section of the bottom face
B	Measured width of the specimen
B_{F1}	Bending stiffness of the top face
B_{F2}	Bending stiffness of the bottom face
B_s	Flexural rigidity
D	Sum of flexural rigidity
d_c	Depth of the core material
E_c	Compressive modulus of elasticity
E_F	Modulus of elastic of the faces
E_{F1}	Modulus of elastic of the top face
E_{F2}	Modulus of elastic of the bottom face
E_t	Tensile modulus of elasticity
e	Measured depth between the centroids of the faces
F	Applied load
f	Face thickness
f_c	Compressive strength
f_t	Tensile strength
f_{xx}	Failure stress in the x-x axis direction
G	Shear modulus of the core
G_t	Reduced shear modulus
G_{eff}	Effective shear modulus of the core
I_{F1}	Moment of inertia of the top face
I_{F2}	Moment of inertia of the bottom face
$J_c(t)$	Shear creep compliance of core at time t
L	Span length
P_C	Shear critical load

P_E	Euler critical load
S_{xx}	Applied stress in the x-x axis direction
t	Time
w_0	Instantaneous deflection measured at time t = 0
w_b	Deflection caused by the elastic extension of the faces
w_t	Deflection measured at time t
X_t	Creep deflection at time t
X_0	Initial deflection
z	Vertical distance

Greek Alphabet

ε_c	Compressive strain
ε_t	Tensile strain
Δ_0	Initial deflection
$\Delta_i(t)$	Total time dependent deflection
Δw	Total displacement
Δw_B	Bending displacement
Δw_s	Shear displacement
$\gamma(t)$	Shear strain of foam at time t
ϕ_t	Creep coefficient at time t
φ_t	Creep coefficient at time t
τ_{xx}	Applied shear stress in the x-x axis direction
ν	Possion's ratio

LIST OF ABBREVIATIONS

CBPB	Cement Bonded Particle Board
EPS	Expanded Polystyrene
LVDTs	Linear Variable Differential Transformers
MDF	Medium Density Fibreboard
OSB	Oriented Strand Board
PF	Phenolic Foam
PIR	Polyisocyanurate
PUR	Polyurethane
PW	Plywood
SDC	SIP with dimensional timber spline connection
SIP	Structural Insulated Panel
SIPs	Structural Insulated Panels
SMC	SIP with mini-SIP connection
SMCO	SIP with mini-SIP connection and opening
SMW	Structural Mineral Wool
STP	SIP typical panel
STPO	SIP typical panel with opening
XPS	Extruded Polystyrene

CHAPTER ONE

INTRODUCTION

1.1 Structural Insulated Panel System

The Structural Insulated Panel System (SIP system) comprises of high performance load-bearing panels, which are considered to be a low impact construction material. The main component of the SIP system is Structural Insulated Panels (SIPs) of which a typical make-up comprises insulation core materials adhesively bonded to outer faces such as oriented strand board (OSB) or plywood. As a novel structural load bearing system which offers distinguished advantages including adequate structural strength, superior thermal performance, high strength-to-weight ratio and great environmental friendliness.

SIPs are mainly used as internal and external walls, roofs and floors in residential and light commercial buildings such as houses, restaurants, schools, hospitals, churches and office buildings. ErgoHome Ltd (the industrial sponsor) uses the SIP system for its offsite SIP home that is ready for delivery at an affordable price (ErgoHome Ltd, 2010). Figure 1.1 and 1.2 show typical buildings constructed with this material.

1.2 History of SIPs

The first concept of SIPs as panels emerged in 1935 by engineers at the Forest Products Laboratory (FPL) in the USA (SIPA, 2010). These panels were made in a way of bonding structural sheathing, insulation core and framing members together. The first SIP houses (namely Usonian houses) were built by Frank Lloyd Wright, a famous architect during the 1930s (Morley, 2000). Some of the wall panels of the Usonian houses were made of three layers

of plywood together with two layers of tar paper. There was no insulation for this type of wall panels.

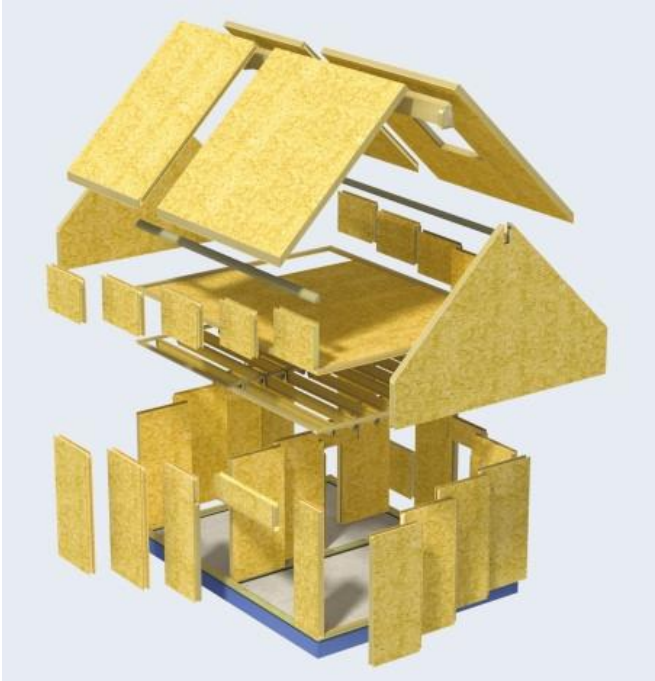

Figure 1.1: Structural Insulated Panels (Kingspan TEK Ltd, 2007)

Figure 1.2: ErgoHome (ErgoHome Ltd, 2010)

The first foam core SIP, in the similar form to nowadays, was developed by Alden B. Dow (one of Wright's students) in 1952 as shown in Figure 1.3.

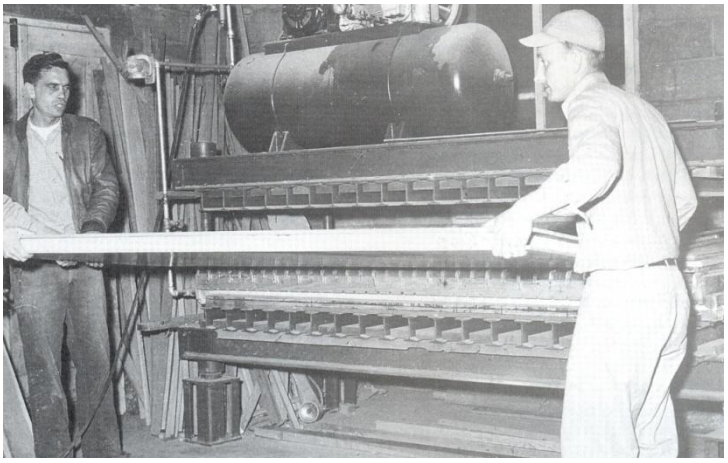

Figure 1.3: Alden B. Dow with SIPs (Morley, 2000)

To meet the rising demand for affordable and energy-efficient housings in the UK during the 1980s, the SIP system was introduced by importing from the USA (Bregulla and Enjily, 2004). The use of the system has been increased since then, and several SIP manufacturers have therefore been established in the UK and Europe. Nowadays, this system used in the UK is manufactured either within the country or imported from Europe rather than the USA.

A large volume of applications of the SIP system have been reported worldwidely as in the USA, Canada, Europe and it is becoming increasingly popular as an alternative construction system in the UK (Bregulla and Enjily, 2004). The numbers of new built homes with the SIP system is forecast to be increased significantly throughout the next decade (Communities and Local Government, 2008). This is due to the fact that this system is light, strong, excellent in thermal performance, environmentally friendly and faster to erect. Hairstans and Kermani (2008) state that the SIP system passes all building regulation requirements and hence becomes a favourable option of material for domestic buildings. In addition, several SIP manufacturers, third party approval bodies and researchers have carried out various structural tests on their system and demonstrated that they are structurally adequate. Moreover, they were proven to have excellent thermal properties by Kawasaki and Kawai (2006).

To raise awareness and increase the use of the SIP system, and also providing technical and information assistance, the Structural Insulated Panels Association (SIPA) was established by SIP manufacturers in 1990 in the USA (SIPA, 2010). Similarly, the UK Structural Insulated Panel Association (UKSIPS) has been recently established in the UK in 2009 (UKSIPS, 2010).

1.3 Strengths and weaknesses of the SIP system

The SIP system has been established and used in the USA since the 1940s. Bregulla and Enjily (2004) indicate that 3,000 SIP homes have been built in the UK since 1980. However, the popularity of the SIP system is increasing because of its favourable characteristics:

- Light and strong structure – SIPs have excellent in-plane, flexure and shear resistance and behave as thin sandwich structures. They have been extensively tested and certified by third-party approval bodies such as BBA and IAB certifications. Not only does SIP system perform well in tests, but in real-life natural disasters, such as the earthquakes in Kobe Japan and North Ridge, hurricane Andrew, a Colorado tornado, a Portland gas explosion and an Omaha fire in the USA, the SIP system has also proven its strong structural system without any structural damage as described by Kingspan Ltd (2007) and Tracy (2000).

- Excellent thermal performance – the inner foam core of SIPs offers extremely efficient U-values. According to SIP Build Ltd (2007), SIP homes can reduce up to 70% of energy use in comparison to other traditional homes. Moreover, SIPA (2008) reports on the tests undertaken by Oak Ridge National Laboratories (ORNL) that the SIP system is almost 15 times more airtight than wood-frame construction.

- Save construction time and cost – SIPs can be manufactured in large sizes and are faster and easier to install than other traditional systems. Since they are faster and easier to erect, SIP building is constructed with by requiring a few workers, which can significantly save labour and equipment costs and as well as construction time. In addition, the study on labour time saving for wall and roof installation in the SIP system was undertaken by Mullens and Arif (2006). Their study revealed approximate two-thirds of the time on site could be saved in comparison to timber frame construction.

- Environmentally friendly – minimal site wastage as SIPs are factory made. OSB, which is commonly used in a SIP system, is manufactured with sustainable forest resources (Forestry, 2010). In addition, the inner core is manufactured free of Chlorofluoro-Carbon (CFC) or Hydrochloro-fluorocarbon (HCFC), and so does not deplete the ozone layer. SIPs are also 100% end of life recyclable according to Hemsec Ltd (2010) and Innovaré Systems Ltd (2010).

- The SIP system is favourable to post-disaster due to Hurricane Katrina according to McIntosh (2008). Her study discovers that the use of the SIP system can achieve sustainable building features and reduce the construction time.

- Said (2006) pointed out that the amount of structural framing is lower in the SIP system. As a result, less wood will be required and this also results into a reduction in heat loss due to the thermal bridging effect. Furthermore, he also reported that, in the post inspection of the SIP system after one year construction, SIPs lead to smaller structural movements and no indication of nails popping out nor drywall cracks.

Despite the various strengths of the SIP system, there are several weaknesses when compared to traditional building systems as follows:

- Neither British nor European standards are currently available for designing the SIP system. However, it has been extensively tested and certified by third-party approval bodies that their performances are above the building requirements.

- Bregulla and Enjily (2004) believe that there might be some difficulties to get SIP buildings approved by building control authorities as they may not be familiar with the SIP system. However, with the continuity use of this system as an alternative construction system and many third-party approval certificates in place, these difficulties will be one day solved.

- Bregulla and Enjily (2004) also claim that the long-term durability of the SIP system is still unknown. However, when it is installed and maintained as detailed in third-party approval body certificates, it will be fit for its intended use for 60 years. Moreover, there is evidence that some SIP buildings have been in service for 50 years in the USA.

- As a non-standard material, SIP structures are 2-10% more expensive than traditional wood-frame structures as stated by Hairstans and Kermani (2008). However, labour and energy savings can help offset these initial building costs.

- Customising the SIP system in the future is more difficult than other traditional systems and will require consultation with the manufacturer's structural engineers (PATH, 2010).

1.4 Gaps in knowledge

The volume of SIP system usage is increasing as previously described. However, the knowledge of the SIP system is still very limited and this considerably hinders its application. This section describes the identified knowledge gaps with regard to the SIP system in

construction, which have not been addressed before and are considered as part of the research project.

1.4.1 SIP performance subjected to multiple load combinations

In reality, it is envisaged that SIPs are required to sustain various load combinations, including part or all of the following loads:

- Axial loading – dead load and/or imposed load
- Racking loading – wind load in the plane of panels or due to the imperfection
- Transverse loading – dead, imposed and wind loads perpendicular to panels

To date, no publications have been reported on the performance of SIPs when subjected to load combinations including all the above loads.

1.4.2 Effects of opening areas

The number, size, shape and location of openings such as windows or doors can affect the structural performance of a panel. Increasing the number or size of openings will result in a decreased strength and stiffness.

In most recent studies, the effect of opening areas of SIPs has been reported in the racking tests by Kermani and Hairstans (2006) and Structural Insulated Panels Scotland (BBA, 2004). No information is available for the performance of SIPs with the opening areas when subjected to combined loads in multiple axes.

1.4.3 Effects of long-term loading

Due to the fact that SIPs comprises an inner foam core, which is a viscoelastic material and experiences creep at ambient and elevated temperature. SIPs subjected to sustained loads will generate continuingly increased deflection. There is currently limited information on the long-term SIP performance.

1.4.4 SIP connections

The connections between SIP to SIP vary from manufacturer to manufacturer. Although they have been used and approved by several third-party approval bodies, knowledge of their structural performance is still limited. Moreover, there has been little discussion on designing and detailing SIP connections.

1.5 Aim and Objectives of this research

The aim of this research is to investigate structural performance of SIPs when subjected to short-term and long-term, and multi-axial loadings. This research will specifically focus on SIPs with oriented strand board (OSB) and polyurethane (PUR) only. However, the research findings will be applicable to other SIP configurations in terms of their structural behaviour and numerical model. To achieve the aim of the research, the specific research objectives are as follows:

- Characterise the mechanical properties of OSB and PUR, which can be used as input in the numerical investigation.
- Experimental investigation of the structural performance of SIPs under multi-axial loadings with typical joint designs.

- Investigate the effect of opening on the structural performance of SIPs.
- Investigate the long-term behaviours of SIPs and identify appropriate creep models for predicting the creep behaviour.
- Develop an appropriate finite element modelling methodology which predicts the initiation of damage and deformation behaviour of SIPs during the loading process.
- Propose an interactive failure load curve for SIPs with combined axial and transverse loadings.

1.6 Thesis outline

This thesis has been divided into six chapters. Following this introduction, the thesis is composed as follows:

Chapter 2 begins by presenting a comprehensive literature review of the SIP system. The literature review is divided into four main sections: starting with a brief account of each component of the SIP system, followed by standards and guidance for SIPs. The review then moves on to present the existing analytical and numerical techniques, failure modes and structural performance of SIPs.

Chapter 3 describes the research methodology in order to achieve the aim of the research, including the objectives of each investigation, methods and specimen details. The first investigation starts with the experimental investigations to determine the mechanical properties of OSB and PUR are then presented. These tests include tensile and compressive tests on OSB and PUR and shear tests on PUR and SIPs. These mechanical properties obtained through

experimental investigations were then used in numerical modelling and numerical results were compared with the SIP beam experimental results for verification.

Chapter 4 is concerned with the experimental, analytical and numerical investigations on SIPs with different joint designs and the effect of opening when subjected to individual loadings.

Chapter 5 presents SIPs subjected to combined loadings. The interactive failure load curves for SIPs with combined axial and transverse loadings are also provided.

Chapter 6 examines the long-term performance of SIPs. The investigation to determine appropriate creep models for predicting the creep behaviours is also presented.

Chapter 7 presents the summaries of the research findings which have contributed to knowledge. The implications for design practice and recommendations for future work are outlined.

1.7 Publication of research

Some of the work presented in this thesis has been published in the conference proceedings and can be found in the Appendix B, which is:

Rungthonkit, P. and Yang, J. (2009) **Behaviour of Structural Insulated Panels (SIPs) under both short-term and long-term loadings.** 11th International Conference on Non-conventional Materials and Technologies Materials for Sustainable and Affordable Construction, University of Bath, Bath, UK, 6th - 9th Sep 2009.

Other four unpublished papers are currently being prepared for submission as listed below:

- Rungthonkit, P., Yang, J. and Clark, L. A. (2012) **Past, Current Status and Future of Structural Insulated Panel Construction System.**

- Rungthonkit, P., Kenyangi, O., Yang, J. and Clark, L. A. (2012) **A study of the use of Structural Insulated Panels (SIPs) in the UK construction industry**.

- Rungthonkit, P., Yang, J. and Clark, L. A. (2012) **Behaviour of Structural Insulated Panels (SIPs) under combined axial and transverse loadings.**

- Rungthonkit, P., Yang, J. and Clark, L. A. (2012) **Behaviour of Structural Insulated Panel (SIP) beams under both Short-term and Long-term Loadings.**

CHAPTER TWO

LITERATURE REVIEW

This chapter presents a comprehensive literature review of the SIP system. It has been divided into four main sections as follows:

- A brief account of each component of the SIP system.
- A summary of standards and guidance of SIPs.
- Description on the existing research on analytical and numerical techniques for studying SIPs and the failure modes
- Structural performance of SIPs.

2.1 SIP system

In review literature, there are six main components in the SIP system. This section presents a brief account of each component.

2.1.1 Structural Insulated Panels (SIPs)

The first and also the main component of the SIP system is the SIP. SIP consists of three layers: two outer faces of high-density face layers and one inner core of a low-density insulating material as shown in Figure 2.1. Two main fabrication techniques to bond the outer faces with the inner core are described by Kermani (2006). In the first technique, a pre-cut inner core is sprayed with a proprietary adhesive and then the cold press technique is used to bond to the two outer faces and then left until the adhesive is cured. In the second technique, the inner core foam

is poured or injected into the spacing between the two outer faces and the foam then cures to bond to the outer faces. Either method produces a monolithic unit, which is much stronger than the simple addition of their individual structural performance as stated by Pugh (2006).

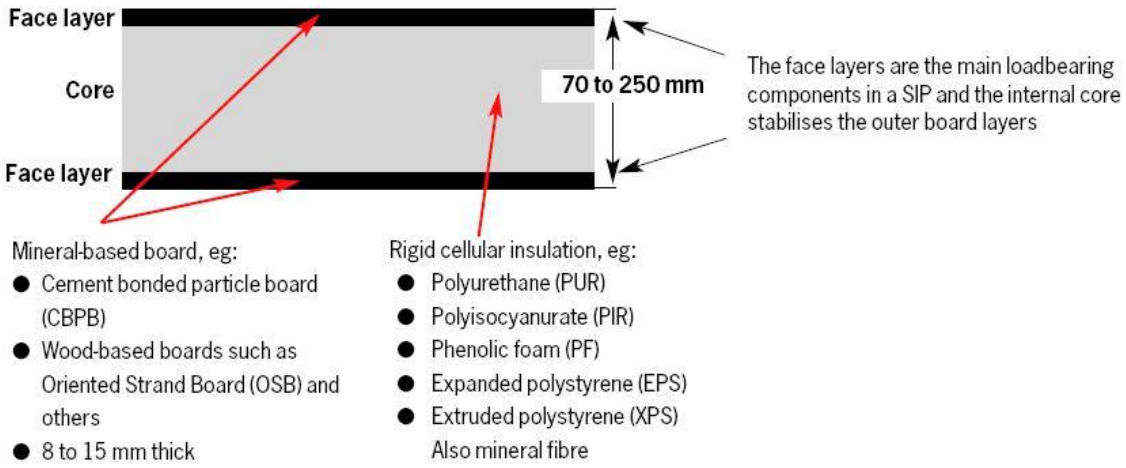

Figure 2.1: Cross-section of a typical SIP (Bregulla and Enjily, 2004)

SIPs work in a similar manner to an I-beam (Morley, 2000) in that the outer faces act as the flanges which primarily withstand tension and compression stresses caused by bending, while the inner core acts as the web to resist shear and support the outer faces against buckling as illustrated in Figure 2.2.

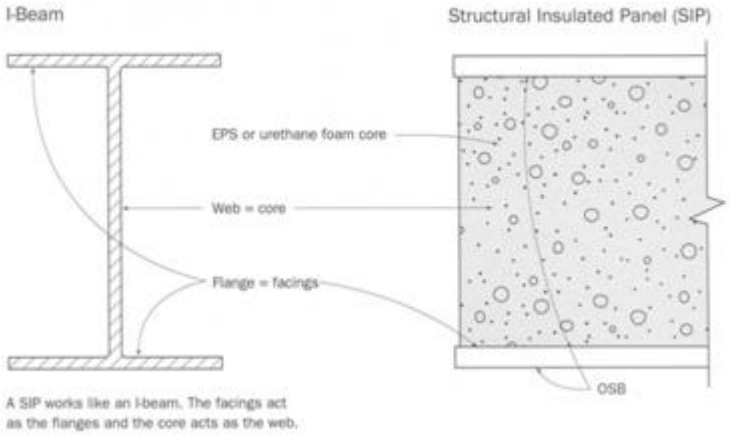

Figure 2.2: Comparison of SIP with an I beam (Morley, 2000)

Typical size of SIPs is 1220 mm x 2440 mm (4' x 8'). A larger size up to 2440 mm x 7315 mm (8' x 24') can be manufactured as stated by APA and SIPA (2007). Unidek Ltd (2010) can manufacture a free span roof up to 8000 mm, which claims to be the largest span in Europe.

Typical SIP thickness is between 70 to 250 mm as previously shown in Figure 2.1. Currently, the thickness of SIPs depends upon the insulation requirement rather than the strength of the panel. In order to provide an acceptable bending stiffness, the inner core should be reasonably thick to space the outer faces. The American Plywood Association supplement No. 4 (APA, 1993) recommends a minimum of 89 mm (3.5 in.) inner core thickness for SIP walls subjected to wind loads.

SIPs are light-weight and better thermal insulation can be obtained by increasing the inner core thickness, but the panel weight is slightly increased as presented in Table 2.1 (Hemsec SIPs Ltd, 2007). According to BS EN 1991 (BSI, 2002), reinforced concrete walls or floors with a 150 mm depth are 360 kg/m^2, which is somewhat 14.9 times heavier than SIPs.

SIP thickness (mm)	100	125	150	180
Weight (kg/m^2) for 15/15 mm OSB	22.1	23.1	24.2	25.5

Table 2.1: SIP weight with various thicknesses (Hemsec SIPs Ltd, 2007)

The following sections describe the individual component of SIPs in detail. These are the outer face, the inner core and adhesive.

2.1.1.1 Outer face

As previously shown in Figure 2.1, the outer faces can be made from a number of materials, including Oriented Strand Board (OSB), Plywood (PW), Cement Bonded Particle Board (CBPB) and Medium Density Fibreboard (MDF). Kenyangi (2009) conducted a survey of the

leading SIP manufacturers in the UK and found 93% of respondents have encountered OSB as the more commonly used structural facings.

This research focuses on the OSB as the outer faces for SIPs since ErgoHome Ltd (the industrial sponsor) utilises OSB as the structural facings. OSB is an engineered wood panel manufactured from sustainable forest resources (Forestry, 2010). In addition, OSB does not suffer from any wood defects that are typically found on the timber blocks. The typical wood defects are, for example, knots, wane and twist as summarised by Lyons (2010).

OSB normally comprises three layers of strands that have been bonded together by using synthetic resin and later pressed and cut to make a requirement size. In Europe, strands are typically from Spruces, whereas Aspens are used in the USA and Canada (Dinwoodie and Enjily, 2003). Strands in the outer layers are oriented in the direction of the panel and the strands in the inner layers can be random or roughly oriented at right angles of the panel as shown in Figure 2.3.

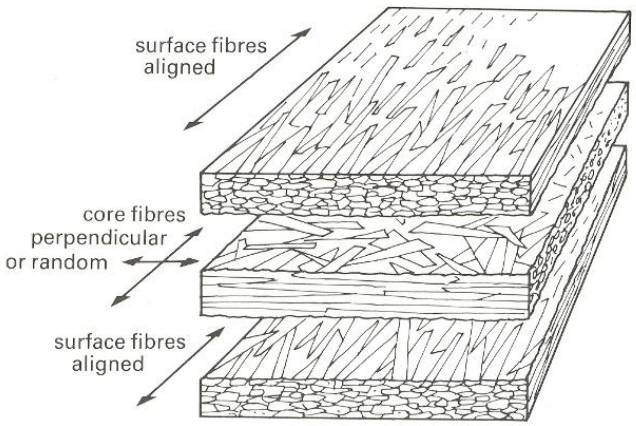

Figure 2.3: OSB fibre alignment (Sunley and Bedding, 1995)

Typical OSB sizes are 2440 x 1200 mm, 2440 x 1220 mm and 3660 x 1220 mm with available thickness of 6, 8, 9, 11, 15, 18, 22, 25 and 38 mm (Dinwoodie and Enjily, 2003). BS EN 300

(BSI, 2006) classifies four types of OSB as listed below and OSB/3 has been typically used in SIPs.

- OSB/1 general purpose non load-bearing boards, and boards for interior fitments for use in dry conditions.
- OSB/2 load-bearing boards for use in dry conditions.
- OSB/3 load-bearing boards for use in humid conditions.
- OSB/4 heavy duty load-bearing boards for use in humid conditions.

This research will only examine OSB/3 with 11 mm thick as the outer faces. However, the research investigations and findings can be applied to other outer faces.

BS EN 12369-1 (BSI, 2001) and TR 019 (EOTA, 2005) provides comprehensive mechanical properties for OSB panels used in the structure design, which are summarised in Table 2.2. It has been suggested by Zhu et al. (2005) that the mechanical properties of OSB depend upon various factors e.g. its constituents (wood species and resin type) and test conditions (temperature, moisture content and etc.). Accordingly, selected mechanical properties i.e. compressive and tensile modulus of elasticity and strengths were determined through experiments. These properties are required in the numerical investigation and will be presented in more detail in Chapter 3.

2.1.1.2 Inner Core

Likewise, the inner core can also be made from a number of materials like Expanded Polystyrene (EPS), Extruded Polystyrene (XPS), Polyurethane (PUR), Polyisocyanurate (PIR) and Phenolic Foam (PF). The material properties of the inner cores depend upon many factors,

for instance, density, recipe, temperature and humidity. Table 2.3 presents the material properties of some inner core materials.

Material properties	Along grain of face veneer	Perpendicular to grain of face veneer
In plane - bending modulus, E	3,800 N/mm^2	3,000 N/mm^2
In plane - shear modulus, G	1,080 N/mm^2	1,080 N/mm^2
In plane - bending strength	16.4 N/mm^2	8.2 N/mm^2
In plane - tensile strength	9.4 N/mm^2	7.0 N/mm^2
In plane - compressive strength	15.4 N/mm^2	12.7 N/mm^2
Possion's ratio, υ	0.24	0.24

Table 2.2: Some mechanical properties of 11 mm thick OSB

extracted from TR 019 (EOTA, 2005)

Inner core material	Density (kg/m^3)	Shear Modulus (N/mm^2)	Modulus of Elasticity (N/mm^2)	Shear Strength (N/mm^2)
EPS	14	2.1	1.4	0.14
	18	2.7	2.1	0.17
	22	3.3	2.3	0.20
	29	4.3	3.3	0.24
XPS	26	2.9	9.3	0.10
	29	3.1	12	0.14
	35	5.1	18	0.24
	48	6.2	26	0.28
PUR	48	2.8	2.9	0.29
	64	4.5	5.8	0.43
	80	6.4	10	0.60

Table 2.3: Some mechanical properties of inner core materials (Thomas et al., 2005)

Since ErgoHome Ltd utilises PUR in its product, this research will therefore focus only on the PUR. According to Davies (2001), the rigid PUR foam includes polyol, isocyanate, a blowing agent and activator as its main components. After mixing, the liquid foam will expand rapidly and can be autohesively bonded to the outer faces. This does not require any other adhesives or other processes to bond to the outer faces.

PUR contained in SIPs is a closed-cell foam filled with a blowing agent that has an excellent thermal property which is better than EPS and XPS. Although the thermal property is better, it has been reported that PUR does degrade its thermal performance over time as the blowing agent escapes and the air is substituted in the cell (Morley, 2000).

Typical PUR density in the sandwich construction is in the range of 35 - 50 kg/m^3 according to Davies (2001). It has been found that the inner PUR core of SIP Build Ltd is 45 kg/m^3.

Some mechanical properties, which are required in the numerical investigation i.e. compressive and shear modulus of elasticity and strengths, were determined through experiment and will be presented in Chapter 3.

2.1.1.3 Adhesive

The adhesive is another important element of SIP components. Morley (2000) states that the adhesive has to provide a strong bond between the outer faces and the inner core in order to sustain buckling and racking forces. Moreover, it should also be able to resist moisture penetration and does not delaminate over SIPs' service life.

For the inner core, which has the autohesively bonded characteristic like PUR and PIR, the adhesive to bond the outer faces with the inner core is not required. Nevertheless, for the inner core without the bonding characteristic such as EPS and XPS, the adhesive is required. Noakes (2008) outlines some suitable adhesives that are used in the modern composites including Polyurethane, Polyvinyl Acetate (PVA), Acrylic, Phenolic and epoxy adhesives. I-S Manufacturing Ltd produces I-S and I-SIP building system by using two-part polyurethane adhesive for bonding the OSBs to the EPS inner core (BBA, 2009). SIP Industries Ltd (2010) utilises PVA glue to manufacture their SIPs.

NAHB Research Centre Inc. and Building Works Inc. (2007) states the adhesive to bond the outer faces and inner core of SIPs must conform to ASTM D2559 (ASTM, 2010) or type II class 2 in accordance with ICC ES Acceptance Criteria AC05 (ICC-ES, 2008). AC05 presents the minimum performance requirements for adhesive with respect to moisture, temperature, accelerated ageing, creep, oxidation or ozone, mold, chemical reagents and compatibility. In addition, AC05 also details various tests that an adhesive requires to satisfy.

2.1.2 SIP connections

Morley (2000) emphasises that connecting each SIP element is a very important part of the SIP system. Apart from assuring structural integrity and long-term durability, the air leakage must be avoided at each joint in order to maintain energy efficiency.

There are many different connection types which vary from manufacturer to manufacturer. None of the standards are currently available for designing and detailing SIP connections. In reviewing the literature, there are three typical panel-to-panel joints, including OSB thin spline, foam block spline (or referred to as mini-SIP spline) and dimensional timber spline. Morley (2000) states that the OSB thin spline is the most commonly used joint in the industry as it is inexpensive and does not produce any thermal breaks. Nevertheless, the OSB thin spline will not be included in this research. This is due to the fabrication difficulty in engineering practice, in comparison with other two connection types because the inner core is required to be pre-routed to accommodate the OSB thin spline. Moreover, it is expected that SIPs with the OSB thin spline joint should have similar structural performance to SIPs with the mini-SIP spline joint. Figures 2.4 - 2.6 illustrates the typical panel connections and Table 2.4 describes the strengths and weaknesses of the typical connections.

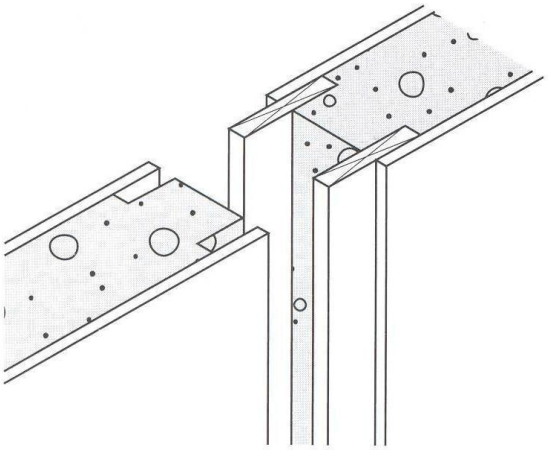

Figure 2.4: OSB thin spline (Morley, 2000)

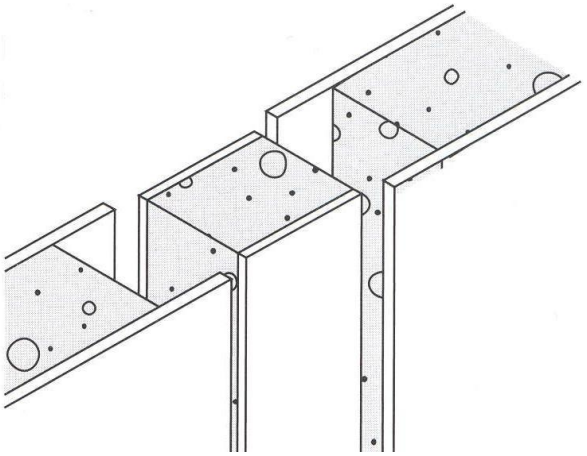

Figure 2.5: Foam block spline or Mini-SIP (Morley, 2000)

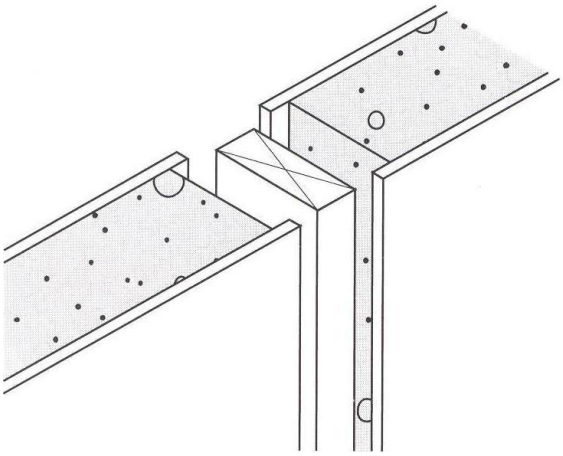

Figure 2.6: Dimensional timber spline (Morley, 2000)

Panel connections	Strengths	Weaknesses
OSB thin spline	• Light-weight panel connection. • No thermal break at the connection.	• Difficult to form this connection as the inner core required to be pre-routed to accommodate the OSB thin spline. • Less stiffness in comparison with dimensional timber spline connection.
Foam block spline or Mini-SIP spline	• Light-weight panel connection. • Easier to form than the OSB thin spline. • No thermal break at the connection. • Slightly increase the panel strength at the connection in comparison to the typical panel as found in the four-point bending experimental test and will be presented in Chapter 4.	• Less stiffness in comparison with dimensional timber spline connection. Experimental and numerical studies are presented in Chapter 4.
Dimensional timber spline	• High stiffness along joint as found in the four-point bending experimental test. • Less panel deflection. • Easier to form than the OSB thin spline.	• Heavier panel connection than the others. • Thermal break at the connection. • More expensive than the other two joints.

Table 2.4: Strengths and weaknesses of the wall-to-wall panel connections

It should be noted that there are various connection types in the SIP system, for example corner junction, eaves and ridge details as depicted in Figure 2.7. Nevertheless, these connections will not be investigated in this research.

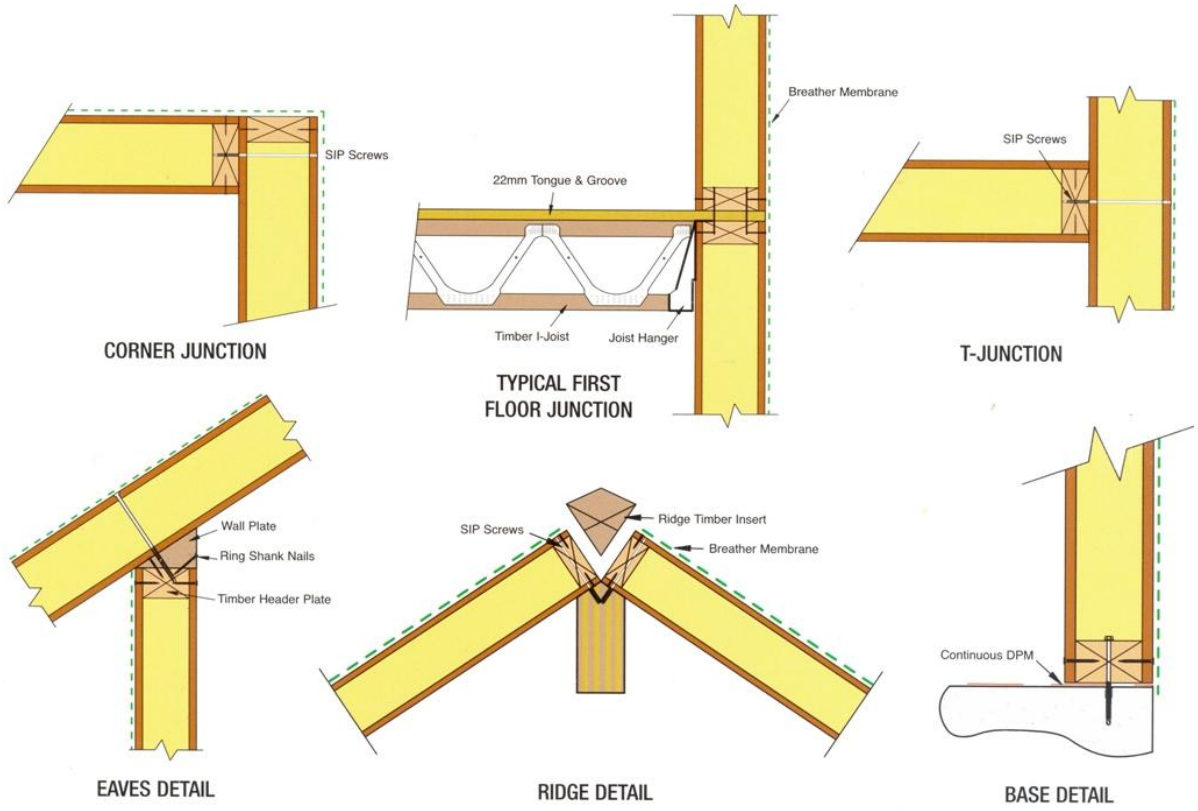

Figure 2.7: Other sections of SIP connections (Hemsec SIPs Ltd, 2007)

2.1.3 Header, footer and sole plate

Two elements, typically timber blocks, at the top and bottom of the panel are called header and footer. The header and footer depths are as same as the recesses at both ends of the panel and are fastened to the panel by using proprietary adhesive and fixings at regular intervals. They are continuous throughout the wall length and typically 4.8 m long each.

Kermani (2006) investigated the impact of header and footer on structural performance by carrying out the axial loading on SIPs. As expected, his investigations revealed that installation of the header and footer along the edge of the SIP could result in increasing the panel strength.

Sole plate is used to support the panel by bolting through the base and attaching to the footer. TRADA (2007) provides a good practice guideline for the sole plates in timber construction,

which can be adopted to be used in the SIP system. The sole plate joint details are also vary from manufacture to manufacture and Figure 2.8 shows the SIP Build Ltd joint detail of the sole plate and the footer (SIP Build Ltd, 2008). This joint detail is used in the experimental programme and C16 timbers are used for the header, footer and sole plate in this research.

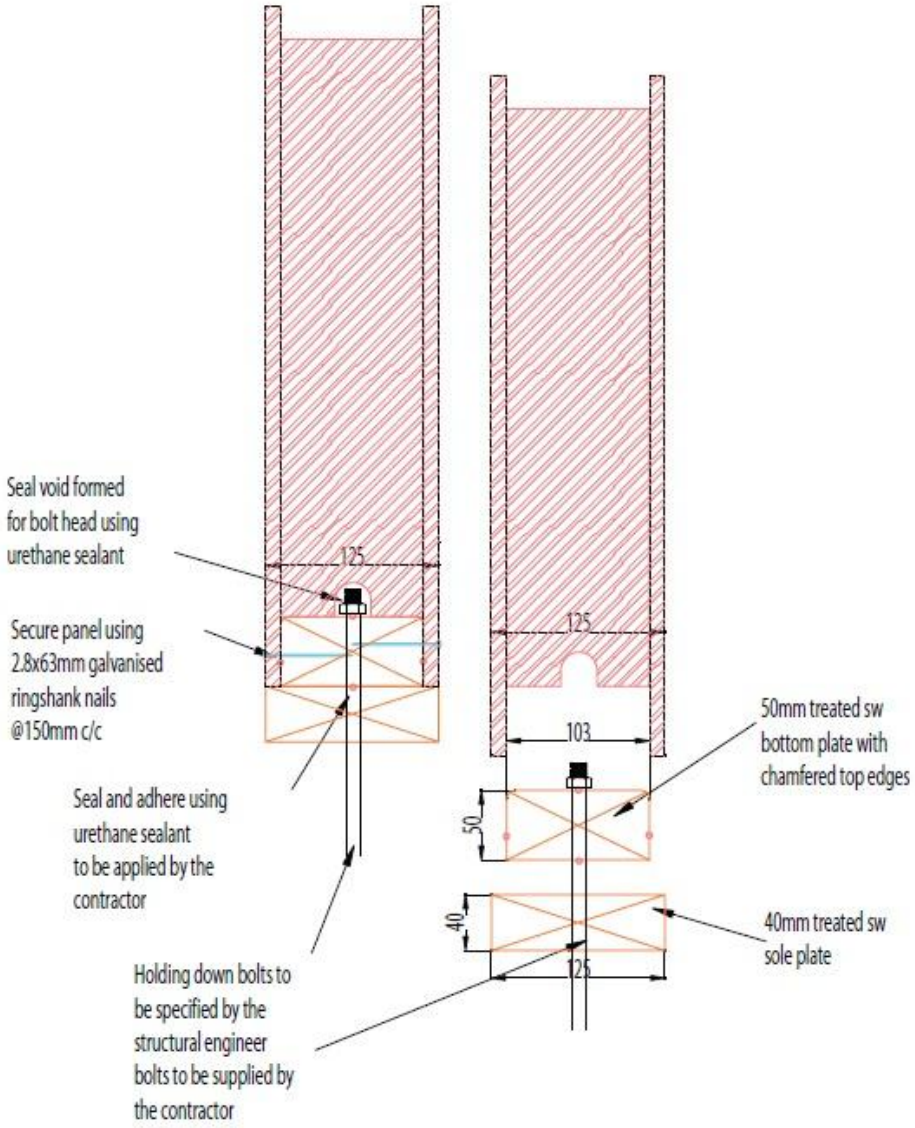

Figure 2.8: Footer and Sole Plate Details (SIP Build Ltd, 2008)

2.1.4 Fixing

Fixing in the SIP system is varying from manufacturer to manufacturer. NAHB Research Centre Inc. and Building Works Inc. (2007) details the fixing in the SIP system that shall have corrosion resistance and the thread should penetrate at least 25.4 mm (1 in.) into the elements that are adhered to. Galvanised ring shank nails or screws are typically used in the SIP system. In this research, 2.8 mm diameter and 63 mm long Galvanised ring shank nails at a 150 mm spacing are used as specified by SIP Build Ltd.

2.1.5 Internal lining

Internal lining is another part of the SIP system. Although it is classified to be another part of the system, it is not required to sustain a heavy load as it is only used for the interior finishing. It should have a fire resistance characteristic as SIPs are combustion materials. Gypsum plasterboards are normally used as the internal lining as their characteristic can resist fire for 60 minutes when two layers of 15 mm plasterboards are used.

2.1.6 External cladding

Kingspan TEK Ltd (2007) presents some exterior claddings which are brickwork, proprietary brick slip system, timber boarding and tile/slate hanging claddings as shown in Figure 2.9. Bregulla and Enjily (2004) states that brick skin or wooden claddings are typically used for external cladding in the SIP system.

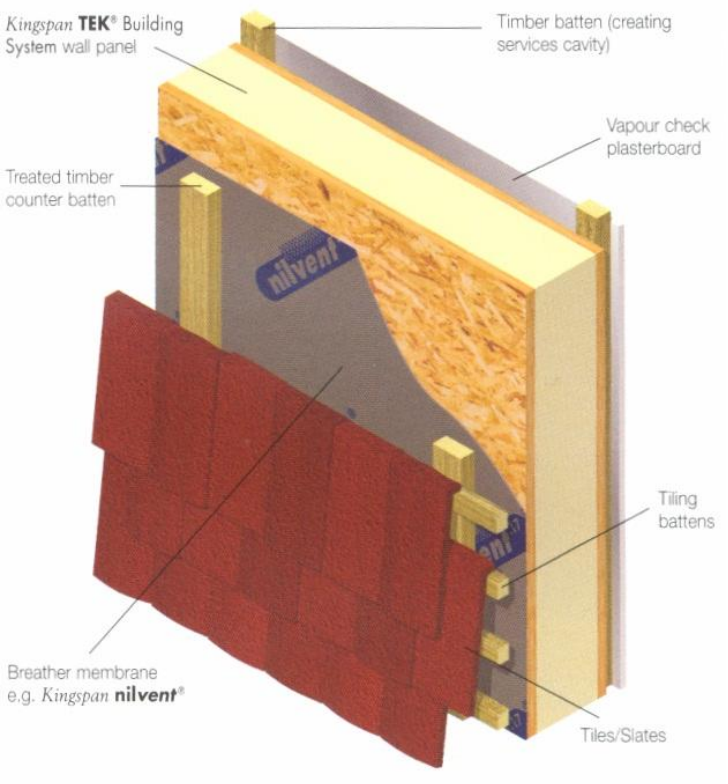

(a) Tile hanging cladding

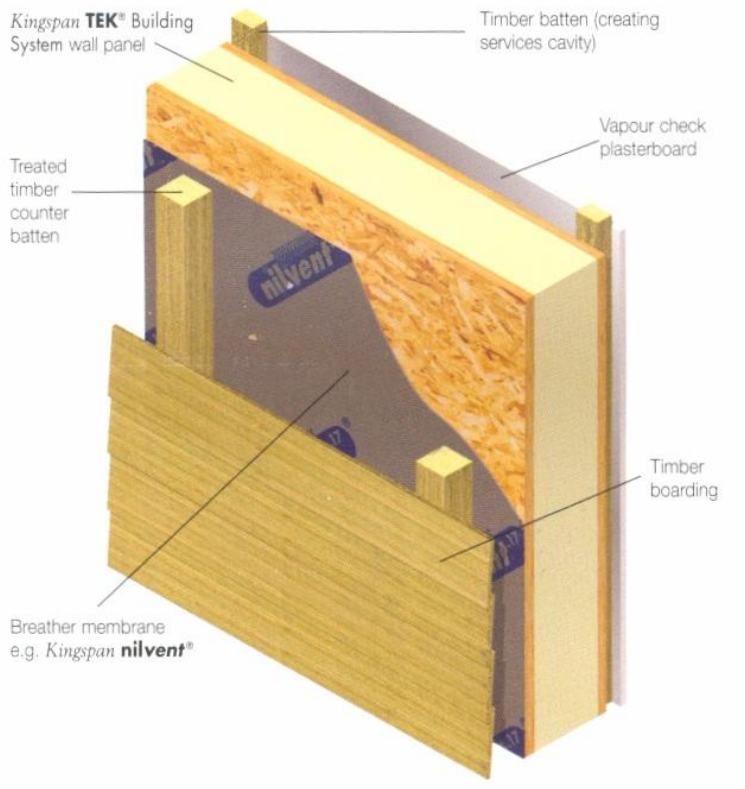

(b) Timber boarding cladding

Figure 2.9: External claddings (Kingspan TEK Ltd, 2007)

2.2 SIP standards and guidance

Lack of relevant standards and guidance limit the usage of the SIP system. Various organisations have been working on the development of SIP standards. A brief detail of each standard and guidance is as follows.

2.2.1 ISO 22452 (ISO, 2011)

ISO 22452 were published in June 2011. This ISO standard presents the test methods for SIP walls to determine their structural properties, including tensile bonding strength of the panels, ageing, shear, vertical load, racking and bending performance. This standard will contribute great deal to standardise the SIP tests.

2.2.2 PRS-610 (APA, 2008)

A series of consensus-based standards for Performance-Rated Structural Insulated Panels (PRS-610) are currently being developed by the American National Standards Institute (ANSI), APA and SIPA. There will be three series, beginning with the first standard for wall applications (PRS-610.1). This will be followed by PRS-610.2 and PRS-610.3 for roof and floor applications, respectively.

2.2.3 TR 019 (EOTA, 2005)

European Organisation for Technical Approvals (EOTA) is currently developing the Technical Report No.19 (TR 019) which details the calculation models for prefabricated wood-based load-bearing stressed skin panels for use in roofs. These models can also be adequately used for walls and floors. The analytical method will be investigated and compared with the experimental results in Chapter 4.

2.2.4 APA supplement No.4 (APA, 1993)

This publication is divided into two major parts. The first part presents the method for design of plywood sandwich panels when subjected to horizontal, vertical and combined loadings. The second part details the requirements for each plywood sandwich panel component, its fabrication process and methods of taking test samples from various parts of the panels.

2.2.5 Prescriptive Method for Structural Insulated Panels (SIPs) Used in Wall Systems in Residential Construction (HUD, 2006)

The Engineered Wood Association (APA) carried out transverse, axial, racking and lintel tests on SIPs with three inner core types i.e. EPS, PUR and XPS (APA 2006, 2007 and 2008b). At present, only the test results of SIPs with EPS core is used to establish the design capacities in the prescriptive method for Structural Insulated Panels (SIPs) used in wall systems in residential construction. This prescriptive method provides "wall thickness selection tables, and construction details to design and construct residential wall systems using SIPs" (HUD, 2006).

2.3 Structural analysis techniques

Comprehensive overview of methods to determine sandwich panel behaviour have been presented by several authors, for instance, Davies (1987), Burton and Noor (1994), Forstig (2003) and Sun (2007). In review literature, there are six methods: namely classical sandwich panel theory, first shear order, higher order sandwich panel theory, elasticity theory, superposition approach, and finite element method. The current SIP and sandwich panel standards employ the classical sandwich panel theory to design panels. This is mainly due to its simplification that can be used for general panel design. Furthermore, this theory can be analysed by simple statics approach. Other methods comprise cumbersome mathematical

operations that include numbers of simultaneous differential equations and require the use of the computer programme such as MATLAB or Maple or programming language (e.g. FORTRAN) to obtain the numerical results.

This research will focus on the classical sandwich panel theory and finite element method. This is due to the fact that this approximation approach is available in the current SIP and sandwich panel standards, whereas the finite element method shows a good agreement by various authors such as Pokharel (2003) and Del Coz Diaz et al. (2008). Other techniques are not used in this research, but can be found in Burton and Noor (1994), Kim and Swanson (2001), Forstig (2003) and Apetre et al. (2008). The brief details of the classical sandwich panel theory and finite element method are presented in the following sections. Figure 2.10 presents the geometry and coordinate system used in this research.

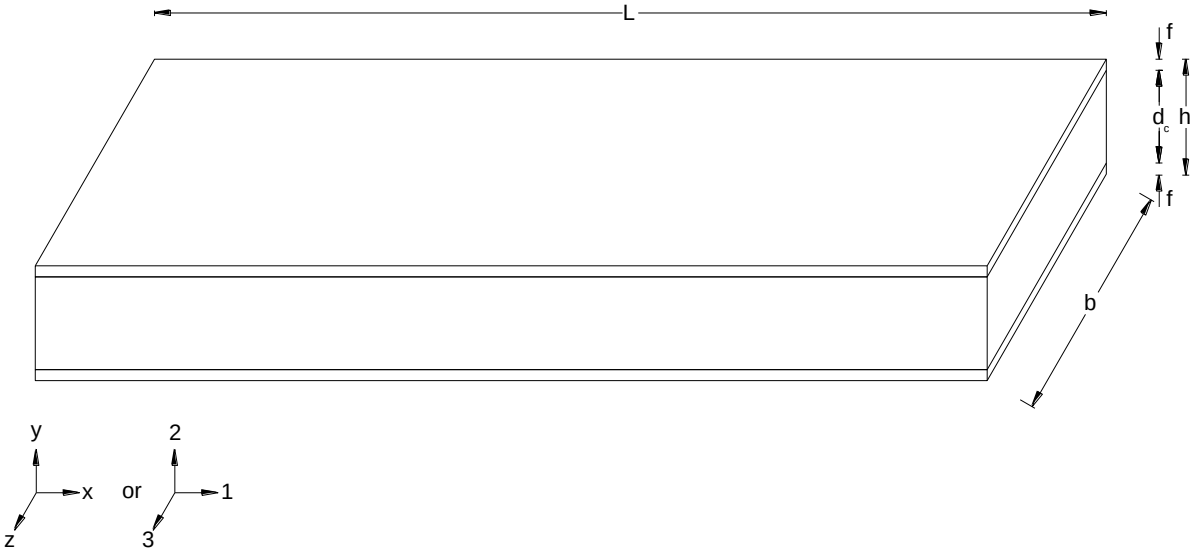

Figure 2.10: The geometry and coordinate system used in this research

2.3.1 Classical sandwich panel theory

Classical sandwich panel theory has been presented in various well-known sandwich panel books by Plantema (1966), Allen (1969), Zenkert (1995 and 1997), Vinson (1999) and Davies

(2001). In addition, the current SIP and sandwich panel standards and guidance are referred to this theory in panel design. These include TR019 (EOTA, 2005), APA supplement No. 4 (APA, 1993), BS EN 14509 (BSI, 2006), Sandwich concept (Diab, 2008) and Design Guide (SIP Building Systems Ltd, 2009). The assumptions of the classical sandwich panel theory are given by Davies (1993) and are listed below.

- The faces and the inner core are linearly elastic.
- The deflections are small (i.e. curvature can be represented by the second derivative of the deflection as in conventional bending theory).
- The shear stress in the inner core is constant across its thickness.
- There is no slip at the interface between the core and the faces.
- There is no deformation of the inner core in a direction perpendicular to the faces (i.e. the inner core does not squash).

The total displacement (Δw) of a panel consists of two components i.e. bending displacement (Δw_B) and shear displacement (Δw_s) as shown in equation 2.1.

$$\Delta w = \Delta w_B + \Delta w_s \tag{2.1}$$

For a SIP beam or panel when subjected to a three-point bending load as shown in Figure 2.11, the total displacement at the mid-span can be determined by:

- Allen's method (equation 2.2).
- BS EN 14509 method (equation 2.3).

- TR 019 method (equation 2.4).

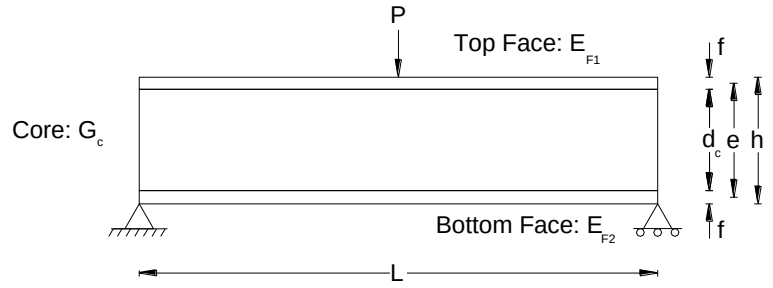

Figure 2.11: Three-point bending load on SIP

Allen's method: $$\Delta w = \frac{FL^3}{48D} + \frac{FL}{4BeG} \quad (2.2)$$

where F is the applied load.

L is the span length.

D is the sum of flexural rigidity, $E_F \frac{Bf^3}{6} + E_F \frac{Bfe^2}{2} + E_c \frac{Bd_c^3}{12}$

E_F is the E-modulus of the faces.

E_c is the E-modulus of the core.

B is the measured width of the specimen.

f is the face thickness.

d_c is the depth of the core material.

e is the measured depth between the centroids of the faces.

G is the shear modulus of the core material.

BS EN 14509 method: $$\Delta w = \frac{FL^3}{48B_s} + \frac{FL}{4Bd_cG} \quad (2.3)$$

where F, L, B, d_c and G are previously defined in equation (2.2).

B_s is the flexural rigidity, equals to $\frac{E_{F1} \cdot A_{F1} \cdot E_{F2} \cdot A_{F2}}{E_{F1} \cdot A_{F1} + E_{F2} \cdot A_{F2}} e^2$

E_{F1} is the E-modulus of the top face.

A_{F1} is the measured area of cross-section of the top face.

E_{F2} is the *E*-modulus of the bottom face.

A_{F2} is the measured area of cross-section of the bottom face.

TR 019 method:
$$\Delta w = \frac{FL^3}{48B_s} + \frac{FL}{4Bd_cG} \tag{2.4}$$

where F, L, B, d_c and G are previously defined in equation (2.2).

B_s is the flexural rigidity, equals to $B_{F1} + B_{F2} + \frac{E_{F1} \cdot A_{F1} \cdot E_{F2} \cdot A_{F2}}{E_{F1} \cdot A_{F1} + E_{F2} \cdot A_{F2}} e^2$

B_{F1} is the bending stiffness of the top face, equals to $E_{F1} \frac{Bf^3}{12}$

B_{F2} is the bending stiffness of the bottom face, equals to $E_{F2} \frac{Bf^3}{12}$

The different between Allen's method and both TR 019 and BS EN 14509 is due to the lower shear deflection. The shear deflection is determined using the depth between the centroids of the outer faces (e) in Allen's method. In contrast, TR 019 and BS EN 14509 methods use the depth of the core material (d_c). These equations will be compared to the experimental results in Chapter 4 to verify which methods are appropriate to predict SIP behaviour.

2.3.2 Finite Element Method

Finite element method has been found favourable to design a sandwich panel. It can be used to deal with irregular loading shapes with any types of support conditions (Davies, 1993). Other methods are limited when these non-standard circumstances arisen.

In finite element method, a complex shape is represented by a series of simpler shapes as shown in Figure 2.12. This method can be used to analyse any simpler and more complex structures ranging from an integrated circuit to legs of an offshore drilling. Moreover, it is currently employed in various applications such as structural dynamics, fluid flow, heat transfer and magneto statics (Case et al., 1999 and Kim and Sankar, 2009).

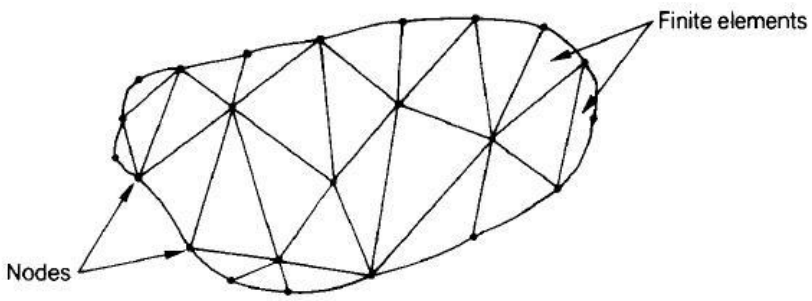

Figure 2.12: A complex shape that can be represented by finite elements (Case et al., 1999)

Finite element method can be employed in many forms in stress analysis, the commonly used element forms are shown in Figure 2.13. In this research, the shell and continuum elements will be employed in the numerical investigations since they have been observed and provided a good agreement with the experimental findings by various researchers, for example, Kim and Swanson (2001), Alwin (2002), Pokharel (2003) and Rizov et al. (2005).

Numerical investigation will be presented and compared to the experimental findings, which will be presented in the subsequent chapters.

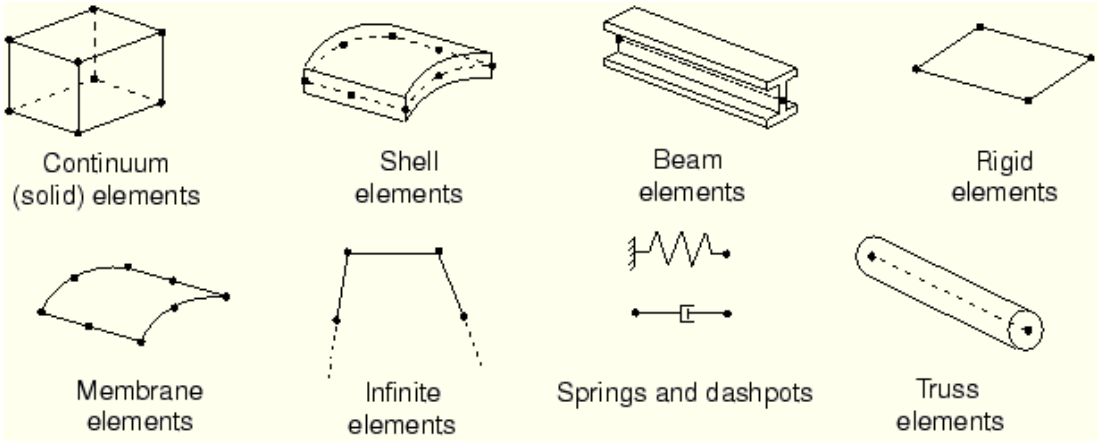

Figure 2.13: Commonly used finite element forms (ABAQUS, 2010)

2.4 Failure mode in SIPs

2.4.1 Transverse load

Extensive studies of failure mode of sandwich beams were carried out by various researchers, e.g., Triantafillou and Gibson (1987), McCormack et al. (2001) and Lim et al. (2004). Triantafillou and Gibson (1987) investigated failure modes of sandwich beams with aluminium faces and rigid polyurethane foam cores and provided a failure mode map that can be used to design the minimum-weight sandwich beam for a given strength. Their failure mode studies are applicable with SIP failure modes.

When a panel subjected to an applied transverse load, the failure mode can occur by one or in combination of several modes, including face failure, inner core shear failure, debonding and indentation at the loading point as shown in Figure 2.14.

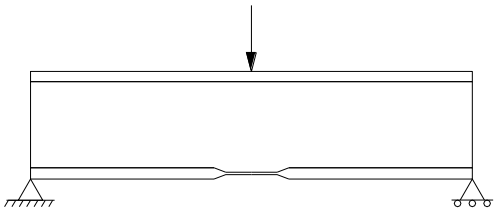

(a) Face failure

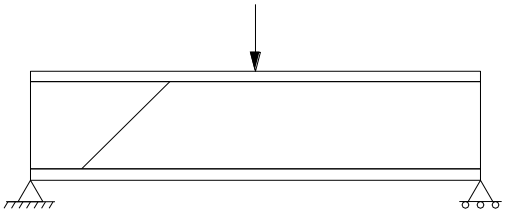

(b) Inner core shear failure

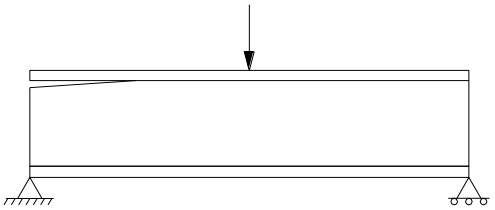

(c) Debonding

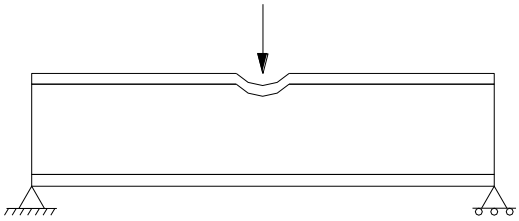

(d) Indentation

Figure 2.14: Typical failure modes when subjected to transverse load

2.4.1.1 Face failure

According to Allen (1969), the outer faces of SIP panel fail in bending or tension or compression when the applied stress in the faces higher than the failure strength as given in equation 2.5.

$$S_{n,xx} > f_{n,xx} \tag{2.5}$$

where $S_{n,xx}$ is the applied bending or tensile or compressive stress in the x-x axis direction.

$f_{n,xx}$ is the bending or tensile or compressive strength in the x-x axis direction.

For a three-point bending load using the classical sandwich panel theory, the applied stress can be determined by using the equation 2.6.

$$S_{n,xx} = \frac{FLz}{D} E_F \tag{2.6}$$

where z is the distance; and

F,L,D and E_F are previously defined in equation 2.2.

2.4.1.2 Inner core shear failure

The inner core will fail due to shear when the applied shear stress is higher than the shear strength as given in equation 2.7.

$$\tau_{xx} > f_{xx} \tag{2.7}$$

where τ_{xx} is the applied shear stress in the x-x axis direction.

f_{xx} is the shear strength in the x-x axis direction.

Similarly for the three-point bending load, the τ_{12} can be obtained by using equation 2.8.

$$\tau_{12} = \frac{F}{2Be} \tag{2.8}$$

where *F,B and e* are previously defined in equation 2.2.

2.4.1.3 Debonding

Debonding failure can be predicted by using Hashin-Rotem's criterion, which has been studied and presented by various researchers, for example, Sun and Tao (1998) and Zhou (2008). This failure mode occurs by the following quadratic stress based criterion as shown in equation 2.9. It should be noted that it is not practical to determine the applied stresses by using the classical sandwich panel theory, the finite element method has been found appropriate to be employed.

$$\text{PUR debonding failure} = \frac{(S_{22})^2}{(f_{t,22})^2} + \frac{(S_{12})^2}{(f_{v,12})^2} + \frac{(S_{23})^2}{(f_{v,23})^2} > 1.0 \tag{2.9}$$

where S_{22} is the tensile stress in the through thickness direction.

$f_{t,22}$ is the tensile strength in the through thickness direction.

S_{12} is the shear stress in the 1-2 axis direction.

$f_{v,12}$ is the shear strength in the 1-2 axis direction.

S_{23} is the shear stress in the 2-3 axis direction.

$f_{v,23}$ is the shear strength in the 2-3 axis direction.

Studies conducted by Dai and Hahn (2003) and Dean (2008) found that the debonding failure agrees well with the linear stress criterion as shown in equation (2.10).

$$\text{PUR debonding failure} = \frac{S_{22}}{f_{t,22}} + \frac{S_{12}}{f_{v,12}} + \frac{S_{23}}{f_{v,23}} > 1.0 \qquad (2.10)$$

This research will further study both linear and quadratic criteria to investigate the most appropriate criterion for SIP debonding, and will be presented in Chapter 4.

2.4.1.4 Indentation

SIPs can fail by indentation at the loading point when the applied compressive stress is higher than the compressive strength as shown in equation 2.11.

$$S_{n,xx} > f_{n,xx} \qquad (2.11)$$

where $S_{n,xx}$ is the applied compressive stress in the x-x axis direction.

$f_{n,xx}$ is the compressive strength in the x-x axis direction.

2.4.2 Axial compression load

When SIP is subjected to an axial compression load, it can fail in buckling, end bearing and debonding. Figure 2.15 illustrates the typical failure of SIP when subjected to an axial compression load.

(a) Buckling

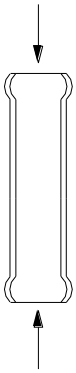

(b) End bearing

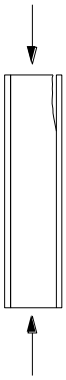

(c) Debonding

Figure 2.15: Typical failure modes when subjected to axial compression load

2.4.2.1 Buckling

Analytical methods to determine the buckling critical load (P_{cr}) of the sandwich panel when subjected to axial compression load are given by Allen (1969), the APA supplement No. 4 (APA, 1993) and Davies (2001). Equations 2.12 and 2.13 present Davies' method and Allen's method to determine the buckling critical load calculation.

Allen's method:

$$P_{cr} = \frac{P_E}{1 + \frac{P_E}{AG}} \tag{2.12}$$

where P_E is Euler critical = $\pi^2 D/L^2$.

D is the sum of flexural rigidity = $E_F \frac{Bf^3}{6} + E_F \frac{Bfe^2}{2} + E_c \frac{Bd_c^3}{12}$

E_F is the E-modulus of the faces.

E_c is the E-modulus of the core.

B is the measured width of the specimen.

f is the face thickness.

d_c is the depth of the core material.

e is the measured depth between the centroids of the faces.

G is the shear modulus of the core material.

L is effective height.

A is the effective area of the foam core = Be.

Davies' method:

$$P_{cr} = \frac{P_E P_{EF} - P_{EF}^2 + P_E P_C}{P_E - P_{EF} + P_C} \tag{2.13}$$

where P_E is Euler critical load of the complete panel = $\pi^2 B/L^2$

P_{EF} is Euler critical load of the flanges only = $\pi^2 B_D/L^2$

P_C is the shear critical load = $A_C G_{eff}$

B is $B_D + B_S$

B_D is $B_{F1} + B_{F2}$

B_S is bending stiffness of the sandwich part of the cross-section
= $E_{F1}A_{F1}E_{F2}A_{F2}e^2/(E_{F1}A_{F1}+E_{F2}A_{F2})$

B_{F1} is bending stiffness of the upper face = $E_{F1}I_{F1}$

B_{F2} is bending stiffness of the lower face = $E_{F2}I_{F2}$

E_{F1}, E_{F2} is Young's moduli of the faces.

A_{F1}, A_{F2} is areas of the faces.

I_{F1} ,I_{F2} is moment of inertias of the faces.
A_C is the effective area of the foam core = be
b is width of the panel.
G_{eff} is effective shear modulus of the core = Ge/d_c
G, e, d_c and L are previously defined in equation 2.12.

Both equations will be used to determine the buckling critical load and later compared to the experimental results, which will be presented in Chapter 4.

2.4.2.2 End bearing

As observed by Kermani (2006) and will be presented in more detail in Chapter 4, SIPs can fail due to end bearing. This failure mode occurs when the applied compressive stress is higher than the face compressive strength as given in equation 2.14.

$$S_{n,xx} > f_{n,xx} \tag{2.14}$$

where $S_{n,xx}$ is the applied compressive stress in the x-x axis direction.
$f_{n,xx}$ is the face compressive strength in the x-x axis direction.

2.4.2.3 Debonding

SIPs can fail due to debonding with insufficient bonding strength, this failure mode can be determined by using previously presented equations 2.9 and 2.10.

2.4.3 Racking

Since the SIP system employs footer and sole plates in similar way with timber construction, the current Eurocode 5 (EC5) (BSI, 2004) can be adequately used to design SIPs when subjected to the racking load. There are two methods available (Method A and B) in the racking design to EC5. Method B is adopted in the UK as stated by Kermani and Hairstans (2006).

Studies by Kermani and Haristans (2006) and Bregulla (2003) revealed SIPs were better performance than the EC5 prediction. This research has also been found that SIPs perform better than the EC5 prediction. More detail is presented in Chapter 4.

2.5 Structural performance

SIP structural performance has been reported better than timber frame construction by various researchers, for example Kermani and Hairstans (2006) and Carradine et al. (2004). This section summarises and reports the performance and behaviour of SIPs that have been extensively tested by several researchers and SIP manufacturers. The literature review purely on SIPs does not show sufficient existing research records and therefore the scope of review has been extended to other sandwich structural and non-structural panels. It has been recognised that some of the knowledge may be useful for SIPs.

2.5.1 Axial compression test

The structural performances of SIPs subjected to axial compression load have been carried out by various SIP manufacturers to attain their panel strengths. A study on SIPs was carried out on SIPs with different panel sizes with and without headers, footers and studs by Kermani (2006). All SIPs were comprised of 11 mm OSB/3 facings and a 95 mm expanded polystyrene core (117 mm overall thickness). The header, footer and stud were grade C16 timber sections of 47 x 95 mm. These were fastened by 2.65 mm diameter screws, that were 35 mm long at a 250 mm spacing. Table 2.5 provides a summary of the test results.

The test results are consistent with the expectation that installation of a stiffener along the edge of the SIP can result in an increase of panel strength. Conversely, the strength decreases as the panel height increases as the panel fails due to buckling at lower load. The typical failure modes

of SIPs when subjected to the uniform axial compression were end bearing and buckling, where buckling failure mode is more likely when the height of panel is increased.

A strength based on discontinuity of the joint was also investigated by ungluing the joint between the insulated core blocks at the mid-height of the panel. This resulted in up to 20% strength reduction as reported by Kermani (2006). This suggests providing the continuity of the insulated core blocks is important in maintaining panel strength.

Not only SIPs can fail due to end bearing and buckling as observed by Kermani (2006). Vaidya et al. (2010) found SIPs were more likely to fail by delamination between the inner core and outer face when axial load was applied at an eccentricity. This can induce more compressive strain in the facesheet, which generates more strain at the interface.

Width (mm)	**Height (mm)**	**Configuration**	**Mean ultimate load (kN/m)**	**Typical failure modes**
600	600	Without any stiffeners	227.3	End bearing
	1200		189.3	Buckling
	1800		177.9	Buckling
	600	With header and footer	230.4	End bearing
	1200		211.8	
	1800		202.3	
400	2400		128.6	Buckling with some end bearing
	3000		68.7	Buckling
600	600	With header, footer and studs	244.5	End bearing
	1200		231.7	
	1800		204.9	

Table 2.5: Compression test details and results (Kermani, 2006)

Prior to ISO 22452 (ISO, 2011), various SIP manufacturers carried out the axial compression tests by using methods described in BS 5268 Part 2 (BSI, 2002) or ASTM E72 (ASTM, 2005) to determine their permissible axial loads. These were then certified by various third party approval bodies such as British Board of Agrément (BBA) and Irish Agrément Board (IAB).

BBA is one of the UK's major approval bodies, which carries out tests and certifies new construction products and installers (BBA, 2007). Table 2.6 lists the permissible axial loads for SIPs with different heights from Structural Insulated Panels Ltd (BBA, 2004).

Width (mm)	Height (mm)	Permissible axial load (kN/m)
2400	1200	75
	1600	70
	2000	63
	2400	45
	2800	30
	3000	25

Table 2.6: Permissible axial loads for SIPs with different heights (BBA, 2004)

As shown in Table 2.6, an increase in panel height results in a decrease in panel strength. This research will investigate SIPs with different joint designs and openings when subjected to axial compression load, more detail is presented in Chapter 4.

2.5.2 Transverse load test

SIPs as floor and roof panels are required to sustain transverse loads such as self-weight, wind and snow loads. Esvelt (1997) conducted 115 full-size panel tests under uniformed distributed transverse loading and compared findings with the APA supplement No. 4 (APA, 1993) prediction in order to determine their adequacy. She found the majority of panels failed in either shear at a wire chase or bearing at a support. This revealed failures that could not be predicted by using APA supplement No. 4. In addition, APA supplement No. 4 generally predicts over conservative deflected values in comparison to the test results.

Del Coz Diaz et al. (2008) compared the displacements obtained from the experiment and TR019 (EOTA, 2005) prediction under transverse loadings. They found that TR019 provides a higher displacement (i.e. more conservative) to their experimental results.

Prior to ISO 22452, permissible transverse loads on SIPs were based on test results in accordance with BS 5268 part 2 (BSI, 2002) or ASTM E72 (ASTM, 2005) from various manufacturers. Table 2.7 summaries the permissible transverse loads obtained from Structural Insulated Panels Ltd (BBA, 2004).

SIP Details			**Permissible Transverse Load**
Outer – Core – Outer	**Width**	**Span**	
(mm – mm – mm)	**(mm)**	**(mm)**	**(kN/m^2)**
11 – 95 – 11 (117 mm SIP) OSB/3-EPS-OSB/3	2400	2400	3.02
		3000	1.54
		3600	0.89
		4200	0.57
11 – 165 – 11 (187 mm SIP) OSB/3-EPS-OSB/3		2400	6.00
		3000	4.00
		3600	2.46
		4200	1.55
		4800	1.04

Table 2.7: Permissible transverse load for different span lengths (BBA, 2006)

As illustrated in Table 2.7, an increase in the panel height causes a reduction in the permissible transverse load. This finding can be explained by the fact that the panel will be required to sustain higher stresses when the panel is increased. As a result, the panel will fail at a lower applied load.

This research will investigate SIPs when subjected to transverse loading with different joint designs and openings. It has been found that different type of joint can make a different impact on panel behaviour. More detail of the transverse loading investigations is presented in Chapter 4.

2.5.3 Racking test

Extensive racking behaviour of SIPs have been studied by Bregulla (2003), and Kermani and Hairstair (2006). Bregulla found that type of outer face, connection joint, header and footer joint and fixing were the major influence factors of the racking behaviour.

Kermani and Hairstans (2006) carried out the racking load tests on SIP walls in accordance with BS 5268 (BSI, 1996) and BS EN 594 (BSI, 1996). All tested SIP walls comprised of two panels of 1200 x 2400 mm with 117 mm overall thickness, and were joined in the centre by an OSB spline connection. The header and footer were grade C16 timber sections of 47 x 95 mm fastened by 2.65 mm diameter screws, 35 mm long that were located at 250 mm centres. Racking resistances of SIP walls were evaluated under a series of applied vertical loading (0, 12.5 and 25 kN) together with racking loads. The results of the tests are detailed in Table 2.8.

As shown in Table 2.8, an increase in the applied vertical load results in a higher racking resistance. This is due to the vertical load is restraining the panel causing the reduction of the uplift in front of the panel.

Width (mm)	**Height (mm)**	**Vertical load (kN)**	**Test racking design load (R_d) (kN/m)**	**Failure mode**
2x1200 (2400)	2400	0	2.8	OSB panels were disjointed from the soleplate.
		12.5	3.8	
		25	6.3	

Table 2.8: Racking design load of tested SIPs (Kermani and Hairstans, 2006)

Similarly, racking tests have been carried out by various SIP manufacturers. Hemsec SIPs Ltd (BBA, 2006a) provides basic racking resistances with different panel heights as listed in Table

2.9. It should be noted that an increase in the panel height attracts more applied load due to higher lever arm and results in a decrease in racking resistance.

Width (mm)	Height (mm)	Basic racking resistance (kN/m)
2400	2000	4.08
	2200	3.71
	2400	3.40
	2600	3.14
	2800	2.91
	3000	2.72

Table 2.9: Basic racking resistances with different panel heights (BBA, 2006b)

There is limited knowledge of SIPs with different joint designs when subjected to racking loads. This research will investigate the behaviour of SIPs with different joint designs and also with openings. More detail is presented in Chapter 4.

2.5.4 Combined bending and compression test

Combined bending and compression tests were carried out by various SIP manufacturers and Kermani (2006). A series of constant axial loads of 0, 8, 16 and 24 kN together with an increasing four-point lateral bending load were applied to 400 x 2400 mm and 117 mm thick panels by Kermani (2006). As expected, the results indicated that increasing the axial compression load causes the reduction in the lateral bending moment resistance. The failure mode for all panels was governed by the bending moment as shown in Table 2.10.

The combined bending and axial compression load resistance of a wall panel with a height of 2400 mm and 117 mm thickness (11 mm OSB/3 – 95 mm EPS – 11 mm OSB/3) provided by Structural Insulated Panels Scotland were approved by the BBA (BBA, 2004). Figure 2.16 shows characteristic and basic design capacity for the SIP wall when subjected to the combined

bending and axial compression loads. It should be noted that a linear interaction model appears to be a good representation of combined bending and axial compression load.

Axial compression load (constant and uniform) (kN/m)	Ultimate lateral bending moment (kNm/m)	Failure mode
0	4.80	Bending
8	3.50	
16	3.10	
24	2.45	

Table 2.10: Combined bending and axial compression test results (Kermani, 2006)

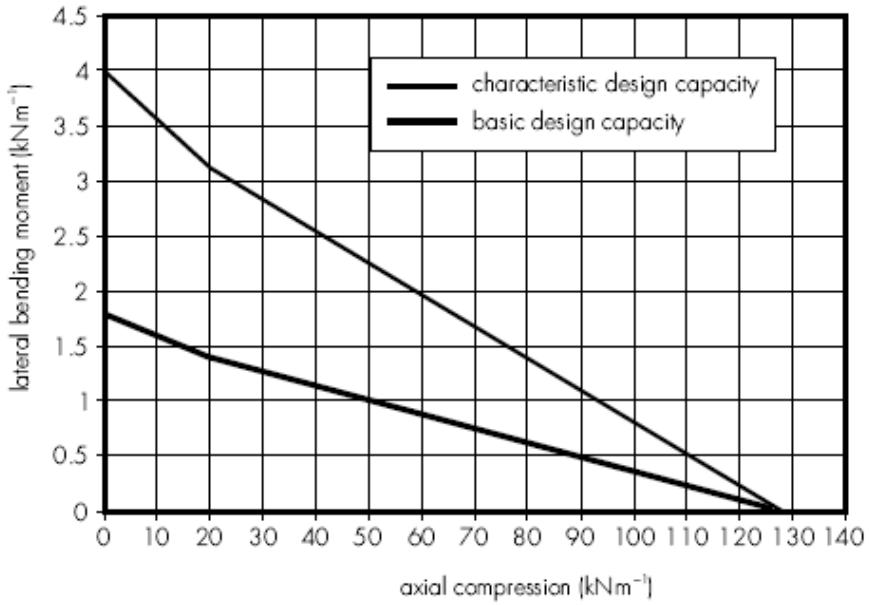

Figure 2.16: Combined bending and axial compression load resistance (BBA, 2004)

2.5.5 SIPs with openings

So far, however, there has been little discussion about SIPs with openings. The effects of openings for windows and doors were examined by Kermani and Hairstans (2006). It was determined that an increase in the percentage of the opening area causes a reduction in racking resistance as shown in Table 2.11.

Opening (%)	Vertical load (kN)	Basic test racking resistance (kN)	Failure mode
6	0	3.12	Panel tore at the top corners of the opening.
9		2.82	OSB panels were disjointed from the soleplate.
19		2.48	Panel tore at the top corners of the opening.
33		1.34	Panel tore at the top corners of the opening and also disjointing from the soleplate.
56		0.67	Panel tore at the top corners of the opening
65		0.28	
6	25	1.67	
9		3.75	
19		2.05	OSB panels were disjointed from the soleplate.
33		1.36	Panel tore at the top corners of the opening
56		0.50	
65		0.30	

Table 2.11: Effects of opening size on basic racking resistance of walls (Kermani and Hairstans, 2006)

In their tests, two failure modes were identified as the panels tore at the top corners of the openings and the OSB panels disjointed from the soleplate. The test result of 6% opening area together with 25 kN vertical load (1.67 kN) shows an anomaly as the result of 9% opening suggests it should be less than 3.75 kN. No explanation is available for this finding.

Sun (2007) investigated a sandwich panel with an opening by experimental and numerical investigations. He concluded that experimental work or finite element analysis should be carried out prior to use sandwich panels with openings due to the lack of analytical analysis available.

Further studies on SIPs with openings when subjected to individual and combined loadings were carried out to investigate their structural performance and will be presented in Chapter 4.

2.5.6 Fire performance

It is expected that the fire resistance period of 30 to 60 minutes of SIP system is required as identified by Bregulla and Enjily (2004). Three typical methods to enhance fire resistance of SIP interior faces are presented as follows (International Barrier Technology, 2008).

- Attach a plasterboard or gypsum board to the entire interior face.
- Paint or coat with an approved fire-retardant.
- Attach a proprietary sheathing, for example, Blazeguard Fire-Rated Sheathing.

Milner (2003) states that installation of the plasterboard or gypsum board is the most commonly used in the SIP system. Most manufacturers have carried out testing on their SIP systems in accordance with BS 476-21 (BSI, 1987) and guarantee a fire resistance of 60 minutes (BBA 2004, 2006a and 2006b).

Large-scale fire tests for the SIP system was undertaken and found that the lining was the most important element in providing the required fire resistance. Two layers of 15 mm fire resistant plasterboard were also reported to be adequate for 60 minute fire resistance (DCLG, 2010).

2.5.7 *Creep test*

SIP manufacturers claim that SIPs will be fitted for their intended use for 60 years when they are installed and maintained to the standard as detailed in third-party approval body certificates (BBA 2004, 2006a and 2006b). However, the current knowledge of SIPs under long-term loading is limited as there are few publications, which report the creep behaviour of SIPs. This is due to the fact that SIPs comprise an inner foam core, which is a viscoelastic material and experiences creep at ambient and elevated temperatures. SIPs subjected to sustained loading will generally result in a gradual increase in deflection.

Creep behaviour of SIPs is influenced by many factors such as the magnitude of applied load, type of the inner core, the inner core density, temperature and humidity as stated by Taylor et al. (1997). This research will only focus on loading magnitudes, which are 10%, 20% and 30% of the mean ultimate load found in the short-term loading test and SIPs with different connection types. More detail is presented in Chapter 6.

There are typically three different stages of creep behaviour as illustrated in Figure 2.17. The "primary creep" is where deflection/strain rises rapidly initially and then gradually slows down. The "secondary creep" stage occurs when the creep deflection/strain is at a constant rate. Finally, the "tertiary creep" stage occurs when an increasing rate of deflection/strain occurs and then terminates at one of the failure modes (Findley, 1976). This research will consider the primary and secondary creep stages of SIPs. The tertiary creep stage will not be considered as this occurs with high applied load/stress or in high temperature environments, which are not relevant to this research.

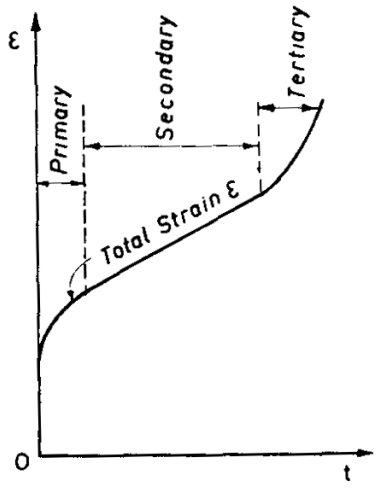

Figure 2.17: Three stages of creep (Findley, 1976)

There are few publications currently available that report the creep behaviour of SIPs. Several publications and standards have been produced for sandwich panels and these can assist in understanding the creep of SIPs.

2.5.7.1 Creep tests on SIPs

Although extensive investigation of the viscoelastic behaviour has been undertaken and reported for materials such as wood and plastic, few publications currently describe this behaviour for SIPs as stated by Taylor et al. (1997). Taylor investigated SIP beam behaviours with four creep compliance models in order to predict the total creep deflection as summarised in Table 2.12.

Taylor found that a three element creep compliance model was unsuitable to predict the creep behaviour of both EPS and PUR SIPs. However, the four element creep compliance model was found marginally acceptable to predict the three month creep behaviour, but not suitable for six month prediction. The five element and power creep compliance models were reported to adequately predict the creep behaviour for three months. It has been suggested that the three month creep parameters from both models (five element and power) could be used to predict the six month creep behaviour.

Model	**Equation**
Power	$\Delta_p(t) = \Delta_0 + A_1 t^{A_2}$
Three element	$\Delta_3(t) = \Delta_0 + A_1[1 - \exp(-A_2 t)]$
Four element	$\Delta_4(t) = \Delta_0 + A_1[1 - \exp(-A_2 t)] + A_3 t$
Five element	$\Delta_5(t) = \Delta_0 + A_1[1 - \exp(-A_2 t)] + A_3 t^{A_4}$
where $\Delta_i(t)$ is total time dependent deflection (minutes); Δ_0 is initial deflection (mm); and A_i is creep parameters associated with creep deflection equations.	

Table 2.12: Creep deflection models proposed by Taylor et al. (1997)

The long-term transverse creep tests on SIPs without joint and with mini-SIP and dimensional timber spline joints were carried out by Rungthonkit and Yang (2009) and will be presented in more detail in Chapter 6. It was found that the panel with dimensional timber spline connection had the lowest creep deflections within the same duration. Furthermore, the five element creep compliance model was found to be able to adequately describe creep test results and could be used to predict the creep behaviour in longer durations. This further support Taylor et al. (1997) findings.

Kermani (2006) conducted a creep test on SIPs under axial compression loads. He concluded the creep effect was negligible under axial compression loads. Furthermore, the panels showed recovery after removing the applied load. Neither debonding nor bulging of the outer faces was found under his creep test.

Zarghooni and Sennah (2010) investigated SIP performances over nine months. They found the maximum nine month deflection increased by 70.10% of the initial deflection. They recommended using a creep constant of 0.74, which is 74% increment of the initial deflection, in a design of long-term creep since it is expected that the snow load does not last longer than nine months in Canada. Nevertheless, this recommended creep constant depends up on the SIP constituent materials and adhesive type.

2.5.7.2 Creep tests on sandwich beams

Just (1983) investigated on the long-term creep tests of sandwich beams. The beams comprised plain metal faces with a variety of polyurethane inner foam cores, and were sustained for 10 years. The findings of the tests are summarised as follows:

- The creep of the inner foam core was still ongoing after 10 years.

- When plotting the creep test results on the double logarithmic scale, the creep function was approximately linear as shown in Figure 2.18. The upper bound equation representing this linear plot on the double logarithmic scale is given by the equation 2.15.

$$\phi_t = 0.12t^{0.36} \tag{2.15}$$

where ϕ_t is creep coefficient.

t is time (hours).

- When unloading, at least 50% could be recovered but the speed of recovery is somewhat slower than the speed of creeping.

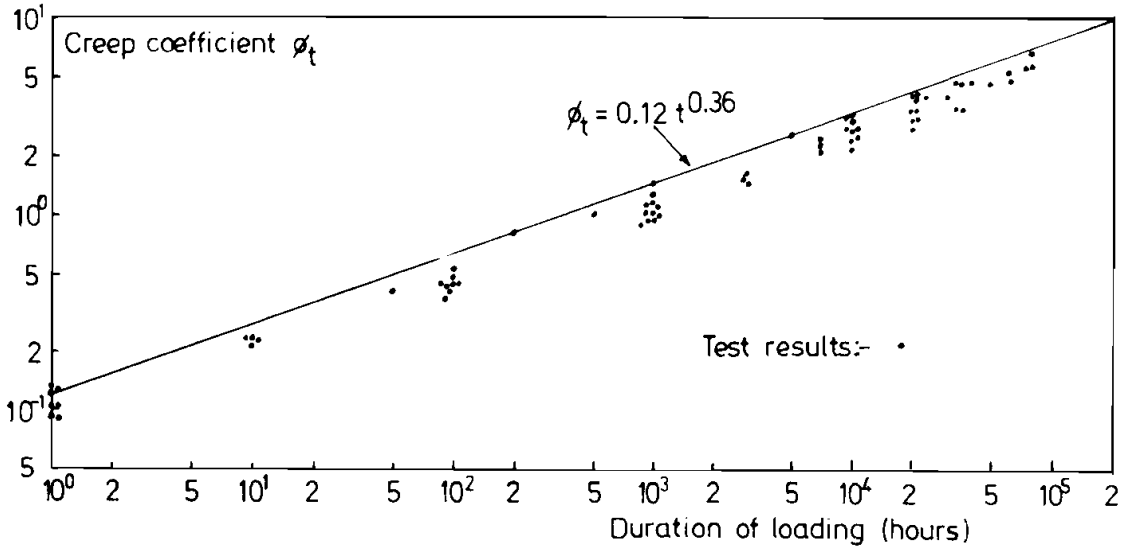

Figure 2.18: Long-term creep tests on sandwich beams (Just, 1983)

Davies (1987) investigated creep tests on sandwich beams and suggested conservative ϕ_t values in the design of sandwich panels for polyurethane and polystyrene cores subjected to permanent loads such as self-weight of materials (at t = 2,000 hours) or quasi-permanent loads such as snow loads (at t = 100,000 hours). These ϕ_t values can be used to calculate the reduced shear modulus (G_t) at the corresponding time t by equation 2.16.

$$G_t = \frac{G}{1+\phi_t} \tag{2.16}$$

where G_t is reduced shear modulus.

G is instantaneous shear modulus of the core.

ϕ_t is creep coefficient as follows:

For polyurethane foam core:

permanent loads - t = 100,000 hours, ϕ_t = 7.0

quasi-permanent loads - t = 2,000 hours, ϕ_t = 2.4

For polystyrene foam core:

permanent loads - t = 100,000 hours, ϕ_t = 3.0

quasi-permanent loads - t = 2,000 hours, ϕ_t = 1.2

For other core materials, Davies suggests to carry out a creep test for up to 1,000 hours (6 weeks) and plot the test results on a double logarithmic scale in order to obtain ϕ_t at time t = 2,000 and 100,000 hours ($\phi_{2,000}$ and $\phi_{100,000}$) by linear extrapolation for each core material.

Huang and Gibson (1990) undertook a creep test on 16 sandwich beams: four for each inner core density of 32, 48, 64 and 96 kg/m^3. The sandwich beams comprised rigid urethane foam cores and aluminium faces bonding by using polyester resin. The beams were subjected to three-point bending by weight loads at 10, 20, 30 and 40% of their shear strengths for 1,200 hours. The temperature and relative humidity were controlled at 23°C ± 1°C and 20 ± 2%, respectively. The deflections of the beams were then recorded at regular intervals for 1,200 hours.

For a three-point bending test, the time-dependent deflection, $\delta(t)$ of the sandwich beam at time t is given in equation 2.17.

$$\delta(t) = \frac{PL^3}{48(EI)_{eq}} + \frac{PLJ_c(t)}{4bc} \tag{2.17}$$

where $\delta(t)$ is total deflection at time t

P is applied load

L is beam span

$(EI)_{eq}$ is equivalent flexural rigidity

$J_c(t)$ is shear creep compliance of core at time t

b is beam width

c is inner core thickness

The first term in the equation 2.17 is the deflection due to bending, which is assumed to be a time independent parameter, whereas the second term is a time dependent parameter due to shear. The shear creep compliance $J_c(t)$ of the inner core is given in equation 2.18:

$$J_c(t) = \frac{\gamma(t)}{\tau} = \frac{(\gamma'_0 + m' t^n)}{G} \tag{2.18}$$

where $J_c(t)$ is shear creep compliance of core at time t

$\gamma(t)$ is shear strain of foam at time t

τ is shear stress of foam

γ'_0, m' and n are creep parameters of form wall material solid

G is instantaneous shear modulus of the core

t is time

They also carried out another shear test, which reported in Huang and Gibson (1991), on sandwich beams with different polyurethane densities in order to determine γ'_0, m' and n values. They were found to be 0.761, 0.384 hour$^{1/n}$ and 0.155, respectively. Huang and Gibson (1991) state all the above coefficients are independent values of both stress and inner core density. However, it is worth noting that G is a foam density dependent quantity.

2.5.7.3 Creep testing standards for sandwich beams

BS EN 1606 (BSI, 1997) presents the recommended method for the compressive creep test to determine the deformation of a test specimen under a constant compressive stress by dead weight with 23°C ± 2°C temperature and 50 ± 5% relative humidity. This standard also details the recommending specimen size, applied stresses and recording times. The creep displacement at time *t* can then be determined using equation (2.19).

$$X_t = X_0 + mt^b \tag{2.19}$$

where X_t is creep deflection at time t (mm).

X_0 is initial deflection (mm).

m and *b* are material constants.

The equation (2.19) is the same as the power creep compliance model provided by Taylor as described in section 2.5.7.1. However, the determination of the parameters is different. The material constant (*m* and *b*) values are determined using the double logarithmic scale from the 1,000 hour creep test results, whereas Taylor's parameters are determined by regression analysis.

BS EN 14509 (BSI, 2006) provides a procedure to test a simply-supported sandwich panel with a uniformly distributed dead load in order to determine the creep coefficient (φ_t). The dead load should be in the range of 30% to 40% of the average shear failure, in which can be found from Cl. A.3. The test should be carried out at a minimum of 1,000 hours and the creep deflection should be recorded regularly.

BS EN 14509 and its predecessor ECCS (2001) suggests to use the measured creep deflection at t = 200 and 1,000 hours to determine the creep coefficients $\varphi_{2,000}$ and $\varphi_{100,000}$ by following equation (2.20).

$$\varphi_t = \frac{1.2[\varphi_{\exp 2}(\log(t) - \log(t_1)) - \varphi_{\exp 1}(\log(t) - \log(t_2))]}{\log(t_2) - \log(t_1)} \quad (2.20)$$

where: φ_t is the creep coefficient at time t.

φ_{exp1} and φ_{exp2} is the experimental creep coefficient at time t_1 and t_2 respectively and they can be calculated by following equation (2.21).

1.2 is a factor which increases the experimentally defined creep coefficient by 20%.

$$\varphi_t = \frac{w_t - w_0}{w_0 - w_b} \quad (2.21)$$

where: w_t is the deflection measured at time t (mm).

w_0 is the initial deflection at the time t = 0 (mm).

w_b is the deflection caused by the elastic extension of the faces – without shear deformation (mm).

BS EN 14509 also provides φ_t values with different core materials and load durations as follows: For polyurethane, expanded and extruded polystyrene foam cores, $\varphi_{100,000}$ = 7.0 and $\varphi_{2,000}$ = 2.4; and for mineral wool, $\varphi_{100,000}$ = 3.0 and $\varphi_{2,000}$ = 1.2.

2.5.7.4 Creep analysis method summary

Table 2.13 below summarises the analysis methods in order to determine the required creep parameters. It should be noted that all model methods are purely empirical expression without taking into account any sound theoretical basis i.e. mechanism of creep behaviour (Illston and Domone, 2010).

Regression analysis		Double logarithmic scale	
Models	**Creep parameters**	**Models**	**Creep parameters**
Taylor	A_i	Huang and Gibson	γ'_0, m' and n
		Just	ϕ_t
		Davies	φ_t
		BS EN 1606	m and b
		BS EN 14509	φ_t

Table 2.13: Creep analysis method summary

2.6 Summary

This Chapter presented the comprehensive literature review of the SIP system. Several studies have investigated SIP performances and revealed their structural adequate. However, there is still insufficient data for SIPs with different joints, and with and without openings when subjected to individual and combined loads. In addition, there has been little discussion on their long-term behaviour. It would be interesting to study the effects of different joint designs to the SIP performance under short-term and long-term loadings.

These identified knowledge gaps will be investigated by experimental, analytical and numerical methods in this research. The research findings will enhance the understanding of SIP performance and behaviour to which will help in an increase the usage of SIP system.

CHAPTER THREE

RESEARCH METHODOLOGY
AND
MECHANICAL PROPERTIES OF SIP CONSTITUENT MATERIALS

3.1 Introduction

This Chapter describes the methodology in order to achieve the aim of the research, including the objectives of each investigation, methods and specimen details. The first investigation starts with the experimental investigation to determine the mechanical properties of OSB, PUR and small SIP specimens. These mechanical properties obtained through experimental investigations were then used in numerical modelling and numerical results were compared with the SIP beam experimental results for verification.

3.2 Research methodology

The aim of this research was to investigate structural performance of the SIPs when subjected to loadings applied for both short-term and long-term durations, or in multi-axial directions. This research specifically focuses on the SIPs with 11 mm thick OSB type 3 and 103 mm thick PUR (overall 125 mm thickness), manufactured by SIP Build Ltd.

The experimental investigations began with various tests on SIP constituent materials to determine their own mechanical properties. As previously stated, their mechanical properties depend upon various factors e.g. type of constituents, density and test conditions. Accordingly, selected mechanical properties, which were required in both analytical and numerical investigations, were determined including tensile and compressive tests on OSB and PUR, and

shear tests on PUR and small SIP specimens. The obtained mechanical properties were later used in the analytical investigations by using the classical sandwich panel theory, as well as in the numerical investigations. Both analytical and numerical results were then compared to the SIP beam experimental results for verification purpose. More detail on this will be presented in this Chapter.

There has been little discussion on SIP performances with different joint designs. The research then moved on to the experimental investigations on SIPs with two typical joint designs subjected to four-point bending loads as floor and roof condition and will be presented in Chapter 4. Six panels of approximately 600 mm wide by 1200 mm long (half-size scaled of standard size samples) were tested. The selection of sample size has been deemed to be economic and still be able to supply adequate results to fulfil the designated purpose i.e. the effect of joint construction and critical governing design factors for SIPs. Test samples comprise typical panels without joints (STP), SIPs with 100 mm mini-SIP joints (SMC), and SIPs with 47 mm C16 dimensional timber spline joints (SDC), each of two duplicated specimens. These samples were chosen in order to study the effect of joint designs on the behaviour of SIPs in term of strength and stiffness. The failure modes and governing design factors were also identified. Analytical and numerical investigations were then undertaken and later compared to the experimental results.

To address the knowledge gaps of SIP performances when subjected to multi-axial loadings, SIPs were then investigated as wall panel condition. Thirty-four SIP specimens of standard size panel, i.e. 1200 x 2440 mm were subjected to eight experimental load cases, including single and combined transverse, axial and racking load tests with the following objectives:

- To investigate the structural behaviours of SIPs with and without connections.

- To investigate the effect of opening on the structural performance of SIPs.

- To establish failure load curves for SIPs under individual and combined loads.

There has been also little discussion on long-term SIP behaviour, experimental investigations on the creep behaviour of SIP constituents (OSB and PUR) and SIPs as beams and panels were therefore undertaken. Numerical investigations were also carried out to determine the power-law creep parameters of OSB and PUR and later employed in the prediction of SIP creep behaviour. The investigations to determine appropriate creep models for predicting the creep behaviours without employing numerical investigation were also undertaken. More information regarding these investigations will be presented in Chapter 6.

3.3 Mechanical properties of OSBs

BS EN 12369-1 (BSI, 2001) provides comprehensive mechanical properties for OSB panels used in the structure design. Zhu et al. (2005) stated that the mechanical properties of OSB depend upon various factors e.g. its constituents (wood species and resin type) and test conditions (temperature, moisture content and etc.). Accordingly, it is important to determine some mechanical properties of OSB which provided by SIP Build Ltd and used in this research. Selected mechanical properties included the compressive and tensile modulus of elasticity and strength, were determined through corresponding experiments.

It should be noted that this research does not focus on the product quality control that requires testing a sufficient number of specimens. The purpose of performing material tests is to determine the mechanical properties of the tested specimen which can be later used in the subsequent numerical analysis. Accordingly, only two specimens from each test were investigated.

3.3.1 Compressive test on OSBs

OSBs were tested in compression in order to determine their compressive modulus of elasticity (E_c) and strength (f_c). The test coupon size was chosen at approximately 50 mm wide, 66 mm long and 11 mm thick cut from a standard sized panel. The length was chosen to be six times of the thickness as recommended in BS EN 408 (BSI, 2003) to avoid the buckling failure mode. It is also believed that this specimen size should adequately provide the compressive modulus and strength for the numerical investigation. The test results will be compared and expected to be higher than the characteristic values provided by BS EN 12369-1 (BSI, 2001).

Four specimens were prepared and tested, two of them (OSB-L1 and 2) were cut from the major axis (parallel to the length of the OSB panel), and the other two (OSB-P1 and 2) were from the minor axis (perpendicular to the length of the OSB panel). A 120 ohm strain gauge was mounted to each specimen at the centre point to record the vertical strains by using SG401 adhesive as illustrated in Figure 3.1. Both strain gauge and adhesive are supplied by Omega Engineering Limited.

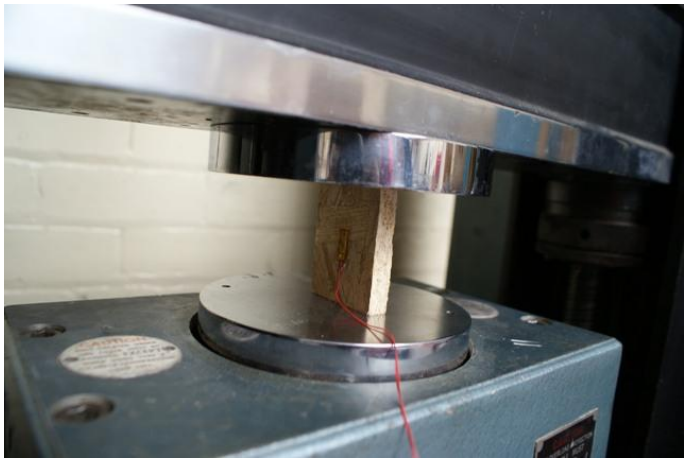

Figure 3.1: OSB compressive test specimen

Each specimen was then subjected to the uniform compressive load by using the Instron testing machine (model number: AC8301-D) with the capacity up to 60 kN. The loads were applied at a constant rate of 0.5 mm/min in cross-head movement. By utilising this loading rate, the maximum load was reached in approximately 240 seconds. This is within 300±120 seconds in accordance with BS EN 789 (BSI, 1997). The applied load readings were taken from the integral data logging system of the Instron machine and the corresponding vertical strain data were recorded through the Grant data logging system. Figure 3.2 shows the experimental apparatus of the OSB compressive test.

Figure 3.2: Experimental apparatus for OSB compressive test

Figure 3.3 shows the plot between stress and strain of the two major axis OSBs. It can be seen that the behaviour of OSB is almost linear up to failure. Table 3.1 illustrates the summary of the major axis OSB specimen test results. The mean values of the modulus of elasticity in compression, compressive strength and the corresponding strain are 3,872 N/mm^2, 15.75 N/mm^2 and 0.000392, respectively. The failure mode in this compressive test is crushing as presented in Figure 3.4.

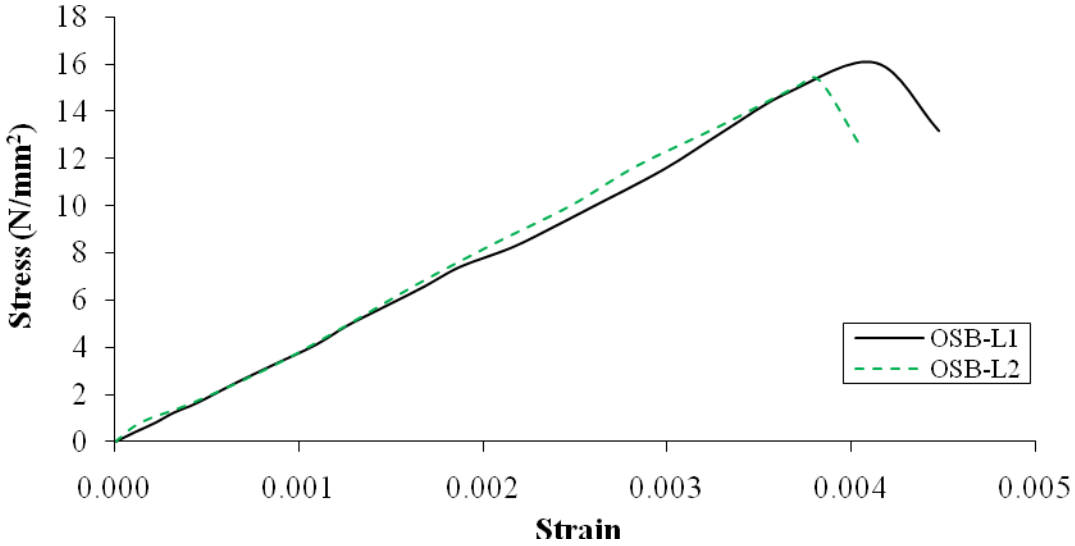

Figure 3.3: Stress vs strain of OSB specimens in the major axis

Specimen	OSB-L1	OSB-L2	Mean
Width (mm)	52.60	52.34	**52.48**
Length (mm)	65.27	64.95	**65.11**
Thickness (mm)	11.54	11.45	**11.50**
Weight (g)	26.30	26.30	**26.30**
Density (kg/m^3)	663.82	675.67	**669.75**
E_c (N/mm^2)	3,814	3,929	**3,872**
f_c (N/mm^2)	16.47	15.02	**15.75**
ε_c	0.00414	0.00370	**0.00392**

Table 3.1: OSB specimen test results in the major axis

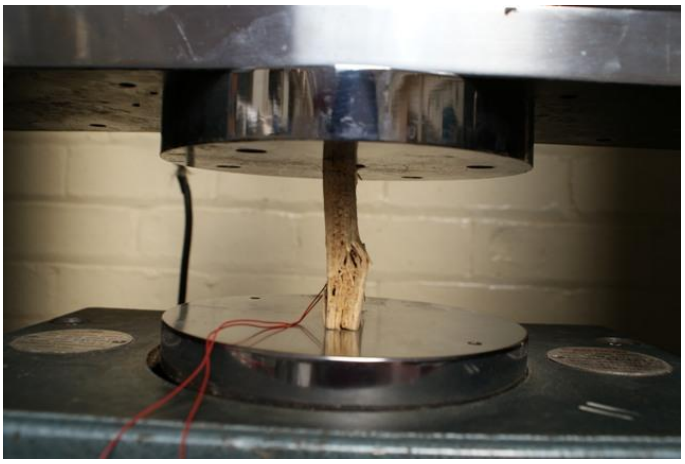

Figure 3.4: Crushing failure

Figure 3.5 shows the figure between stress and strain of the two minor axis OSBs. Similar to the major axis specimens, the behaviour of OSB in the minor axis is also almost linear up to failure. The minor axis OSB specimen test results are listed in Table 3.2. The mean of the modulus of elasticity in compression, compressive strength and strain are 3,824 N/mm^2, 13.00 N/mm^2 and 0.00352, respectively.

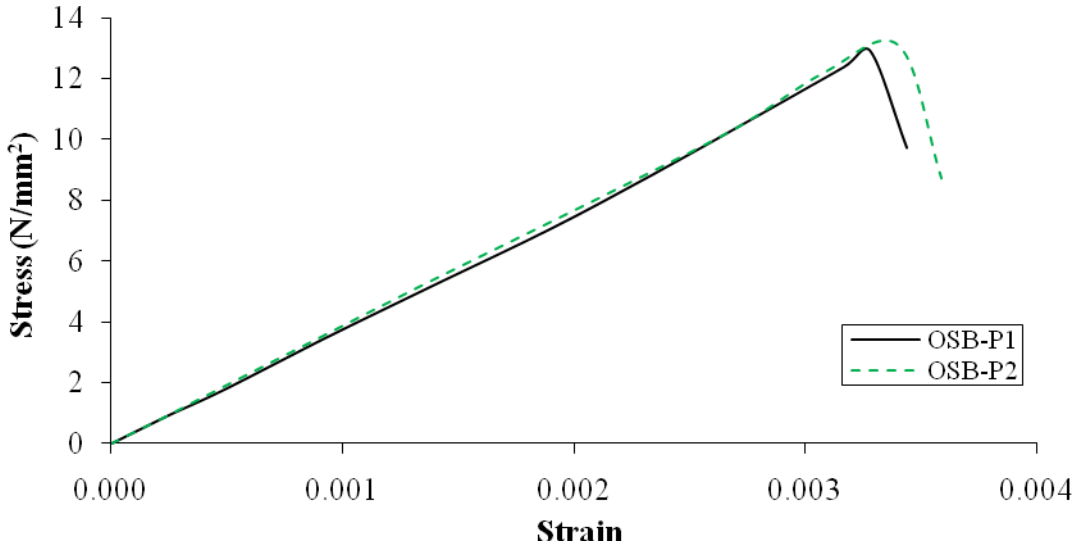

Figure 3.5: Stress vs Strain of the minor axis OSB specimens

Specimen	OSB-P1	OSB-P2	Mean
Width (mm)	50.80	50.75	**50.78**
Length (mm)	66.00	65.75	**65.88**
Thickness (mm)	11.12	11.30	**11.21**
Weight (g)	21.20	25.50	**23.35**
Density (kg/m^3)	568.62	676.29	**622.45**
E_c (N/mm^2)	3,759	3,888	**3,824**
f_c (N/mm^2)	12.92	13.08	**13.00**
ε_c	0.00344	0.00359	**0.00352**

Table 3.2: Minor axis OSB specimen test results

In line with expectation, the OSB test results are higher than the characteristic values, which are given in BS EN 12369-1 (BSI, 2001) and presented in Table 3.3.

From	Major axis specimen		Minor axis specimen	
	E_c (N/mm^2)	f_c (N/mm^2)	E_c (N/mm^2)	f_c (N/mm^2)
Test results	3,872	15.75	3,824	13.00
BS EN 12369-1	3,800	15.40	3,000	12.70
Difference (%)	1.90	2.27	27.47	2.36

Table 3.3: Comparison between the test results and BS EN 12369 values

3.3.2 Tensile test on OSBs

A tensile test on OSBs was carried out in order to determine the tensile modulus of elasticity (E_t) and tensile strength (f_t). The Instron test machine, which was detailed in the previous section, was used to carry out this tensile test with a small specimen. Since the grips of the Instron testing machine can only accommodate up to a 50 mm width specimen, hence an 80% reduction in width from the standard specimen size in accordance with BS EN 789 (BSI, 1997) was adopted and tested. Figure 3.6 shows the details of the OSB tension test coupon. Four OSB test specimens, of which two of them are from the major axis and the other two from the minor axis, were tested. The 120 ohm strain gauge was mounted to each specimen at the centre point to record the vertical strains by using SG401 adhesive.

The 80% reduction size of the OSB specimen was weak and might be fractured near the grip jaws. In order to prevent this fracture, both sides of the OSB specimen were bonded to the 50x100x10 mm steel plates by using the Apollo structural adhesive A5086 part A and B. This adhesive is generally known as two-part epoxy resin as shown in Figure 3.7. The two steel plates were then connected to other steel plates by screws and were inserted to the grips of the Instron testing machine as shown in Figure 3.8.

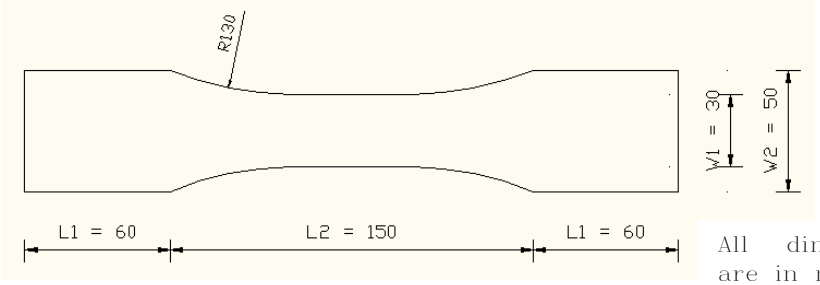

(a)

(b)

Figure 3.6: OSB tensile specimen details

Figure 3.7: Apollo structural adhesive A5086 part A and B

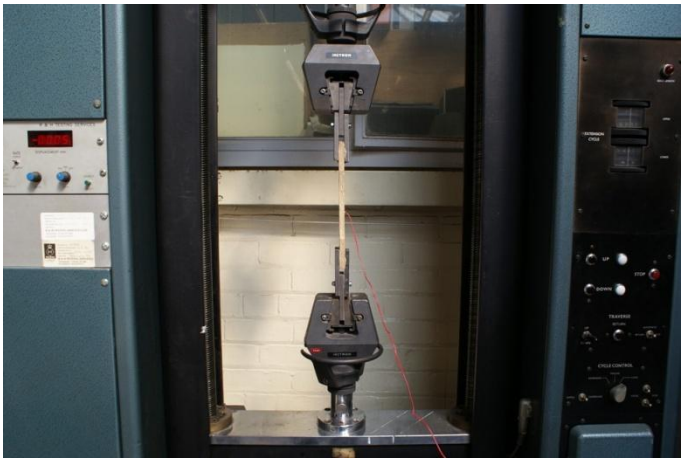

(a)

(b)

Figure 3.8: Experimental apparatus for OSB tensile test

The loads were applied at a constant rate of cross-head movement of 0.5 mm/min and the maximum load was reached in approximately 200 seconds. This is also within 300±120 seconds in accordance with BS EN 789 (BSI, 1997). The applied load readings were again taken from the integral data logging system of the Instron machine and the corresponding vertical strain data were recorded through the Grant data logging system.

Figure 3.9 shows the curve between the tensile stress and strain of the OSB specimens cut in the major axis. It can be seen that the behaviour of OSB is almost linear up to failure. Table 3.4 illustrates the summary of the major axis OSB specimen test results. The mean of the modulus

of elasticity in tension, tensile strength and strain are 3,844 N/mm^2, 10.85 N/mm^2 and 0.00313, respectively. The tensile failure mode is observed as presented in Figure 3.10.

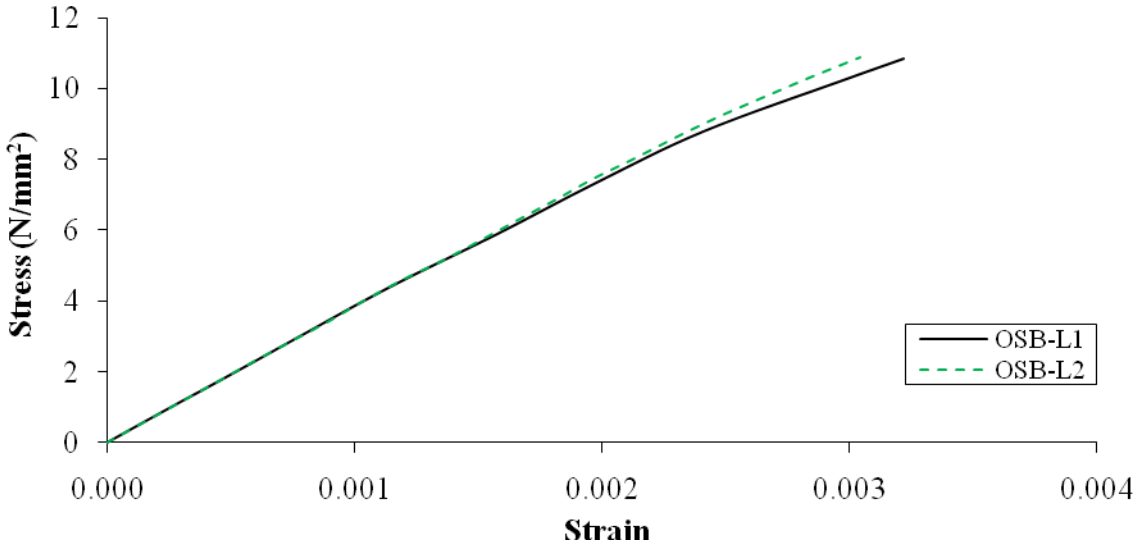

Figure 3.9: Stress vs Strain of the major axis OSB specimens

Specimen	OSB-L1	OSB-L2	Mean
W1-Width (mm)	30.58	30.60	**30.59**
W2-Width (mm)	50.00	50.00	**50.00**
L1-Length (mm)	60.00	60.00	**60.00**
L2-Length (mm)	150.00	150.00	**150.00**
Thickness (mm)	11.17	11.42	**11.30**
R (mm)	130.00	130.00	**130.00**
Weight (g)	76.10	79.30	**77.70**
E_t (N/mm^2)	3834	3854	**3844**
f_t (N/mm^2)	10.83	10.87	**10.85**
ε_t	0.00322	0.00304	**0.00313**

Table 3.4: Major axis OSB specimen test results

Figure 3.11 shows the curves between the tensile stress and strain of the two minor axis OSBs. Similar to the finding in the major axis specimen, the behaviour of OSB also reveals brittle failure nature. Table 3.5 illustrates the summary of the minor axis OSB specimen test results.

The mean value of the tensile modulus of elasticity, strength and strain are 3,615 N/mm^2, 8.97 N/mm^2 and 0.00271, respectively.

Figure 3.10: Tensile failure mode

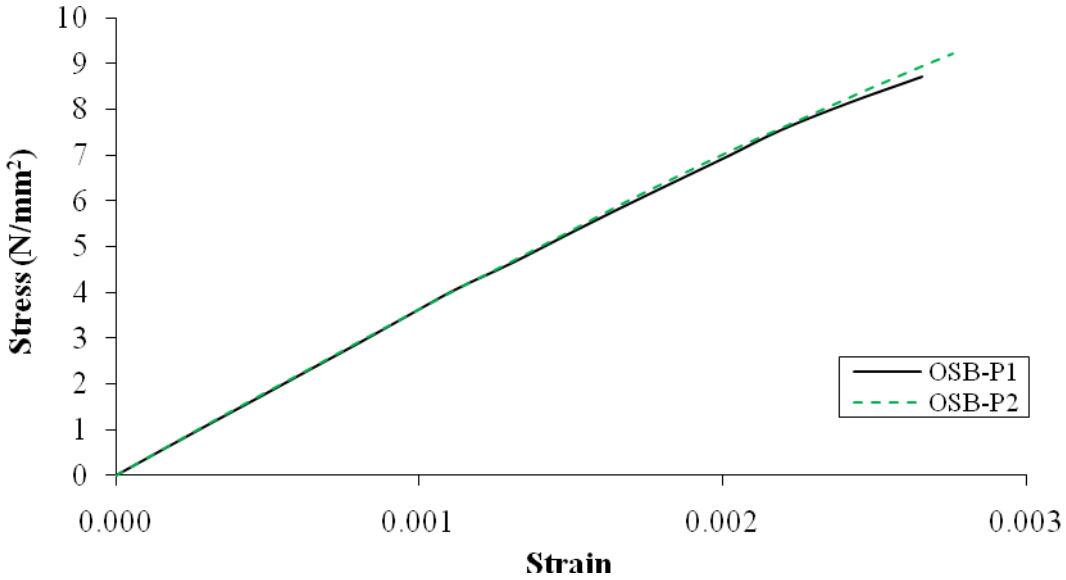

Figure 3.11: Stress vs Strain of the minor axis OSB specimens

The comparison between the OSB test results and the characteristic values given in BS EN 12369-1 is presented in Table 3.6. The test results are higher than the BS EN 12369-1 characteristic values.

Specimen	OSB-L1	OSB-L2	Mean
W1-Width (mm)	30.12	30.17	**30.15**
W2-Width (mm)	50.00	50.00	**50.00**
L1-Length (mm)	60.00	60.00	**60.00**
L2-Length (mm)	150.00	150.00	**150.00**
Thickness (mm)	11.42	11.14	**11.28**
R (mm)	130.00	130.00	**130.00**
Weight (g)	74.40	73.80	**74.10**
E_t **(N/mm^2)**	3624	3606	**3615**
f_t **(N/mm^2)**	8.72	9.22	**8.97**
ε_t	0.00266	0.00276	**0.00271**

Table 3.5: Minor axis OSB specimen test results

From	Major axis specimen		Minor axis specimen	
	E_t (N/mm^2)	f_t (N/mm^2)	E_t (N/mm^2)	f_t (N/mm^2)
Test results	3,844	10.85	3,615	8.97
BS EN 12369-1	3,800	9.40	3,000	7.00
Differece (%)	1.16	15.43	20.50	28.14

Table 3.6: Comparison between the test results and BS EN 12369-1 characteristic values

3.4 Mechanical properties of PUR

The mechanical properties of PUR are influenced by various factors, for instance, the type, density, and manufacturing method as previously described in section 2.1.1.2. Some mechanical properties, which are required in the numerical investigation, i.e. compressive and shear modulus of elasticity and strengths, were determined through experiment in accordance with BS EN 12090 (BSI, 1997) and BS EN 14509 (BSI, 2006).

3.4.1 Compressive test on PURs

SIPs are required to sustain an applied load and should not be indented at the loading point. Sufficient compressive strength of PUR is required to ensure that they will not subjected to the indentation failure. Compressive tests on PURs in three principal directions were carried out in

order to determine the modulus of elasticity in compression and compressive strength in accordance with BS EN 14509 (BSI, 2006).

Two PUR specimens were taken from each three principal direction, i.e. longitudinal (x-axis), through thickness (y-axis) and transverse (z-axis) directions. Each specimen is approximately 100 mm wide, 100 mm long and 100 mm deep. A total of six PUR specimens were subjected to compressive tests in order to determine the modulus of elasticity in compression and compressive strength in each direction by using the Instron testing machine as presented in Figure 3.12. The loads were applied at a constant rate of cross-head movement of 10 mm/min. This movement is within 10% of thickness ± 25 % per minute (7.5 mm – 12.5 mm per minute) in accordance with BS EN 14509. The forces and displacements were then recorded at regular intervals. Since the specimens were not subjected to any failures, the loads and displacements were recorded until a displacement equivalent to 50% of the specimen thickness i.e. 50 mm as presented in Figure 3.13. SIPs will not be intended to deflect for 50% of their thickness in a SIP design.

The compressive strength (f_{Cc}) is calculated using Equation (A.3) in BS EN 14509 with the ultimate load determined at 10% relative deformation, whilst the compressive modulus (E_{Cc}) is calculated using Equation (A.4) in accordance with BS EN 14509.

The force-displacement data obtained from the experiment is presented in Figure 3.14. The behaviour of the PUR reveals three phases according to Gibson and Ashby (1999). The first phase is called “linear elasticity” which involves the cell wall bending (in open cell) and the cell face stretching (in closed cell). The second phase namely “plateau” is concerned with the elastic buckling of the cells. The final phase “densification” reveals the rapidly increasing compressive stress that happens when the cell walls buckle and touch together.

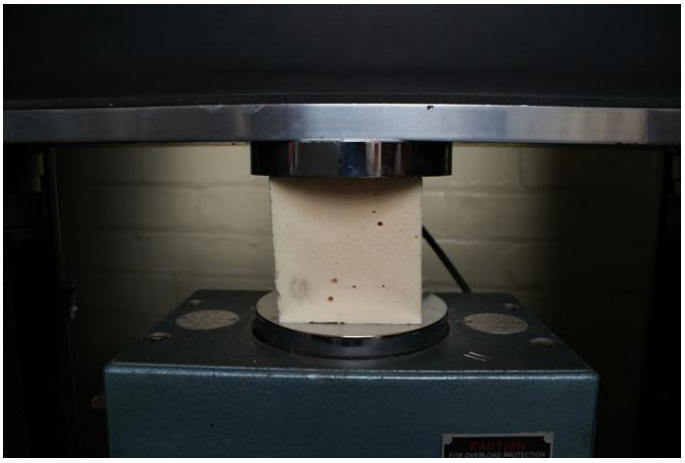

Figure 3.12: PUR compressive test

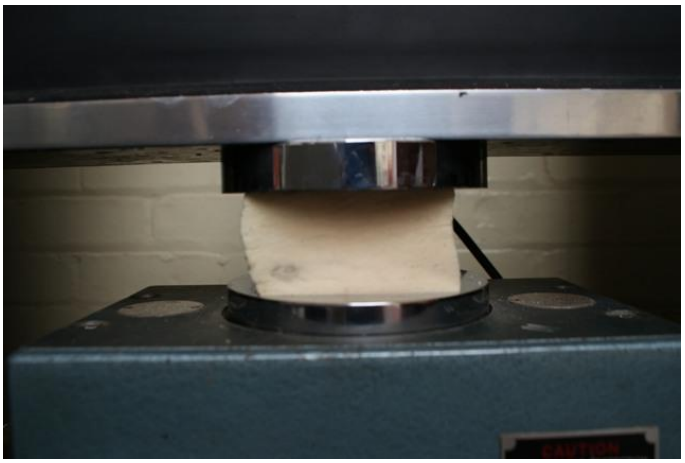

Figure 3.13: 50% displacement of specimen thickness

Table 3.7 illustrates the summary of the PUR specimen test results in the longitudinal axis. The mean value of the compressive modulus of elasticity and strength are 5.447 N/mm^2 and 0.196 N/mm^2, respectively.

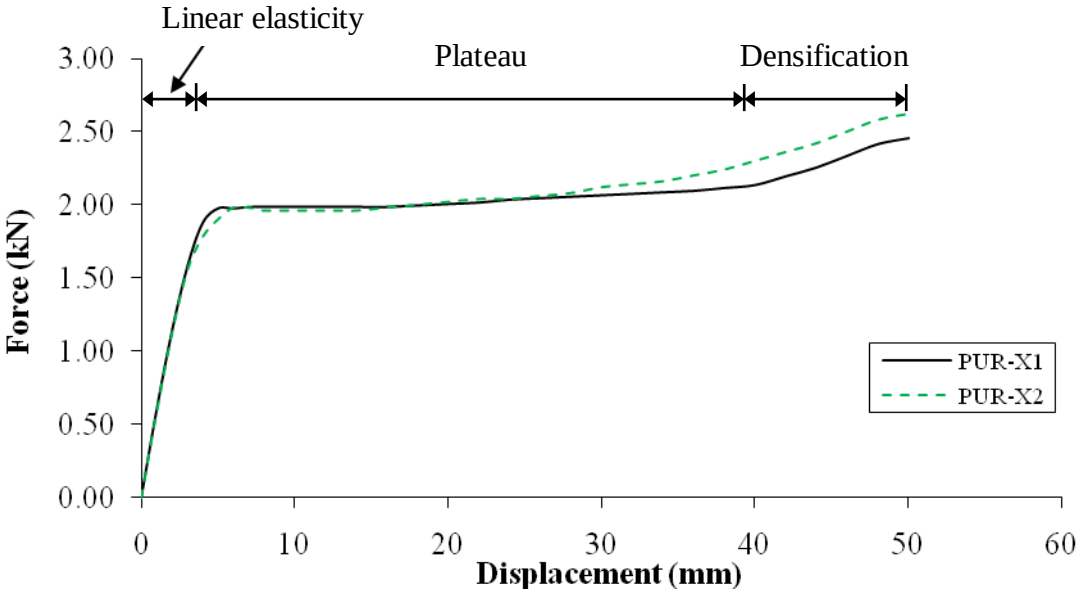

Figure 3.14: Force-Displacement of the longitudinal direction PUR specimens

Specimen	PUR-X1	PUR-X2	Mean
Width (mm)	100.28	97.90	**99.09**
Length (mm)	103.89	99.60	**101.75**
Depth (mm)	101.09	99.47	**100.28**
Weight (g)	41.10	40.50	**40.80**
Density (kg/m^3)	39.03	41.76	**40.39**
E_{Cc} (N/mm^2)	5.517	5.376	**5.447**
f_{Cc} (N/mm^2)	0.191	0.201	**0.196**

Table 3.7: PUR longitudinal axis specimen test results

Similarly, the force-displacement of the through thickness direction obtained from the experiment is presented in Figure 3.15. Table 3.8 illustrates the summary of the PUR specimen test results. The mean of the compressive modulus of elasticity and strength are 6.442 N/mm^2 and 0.202 N/mm^2, respectively.

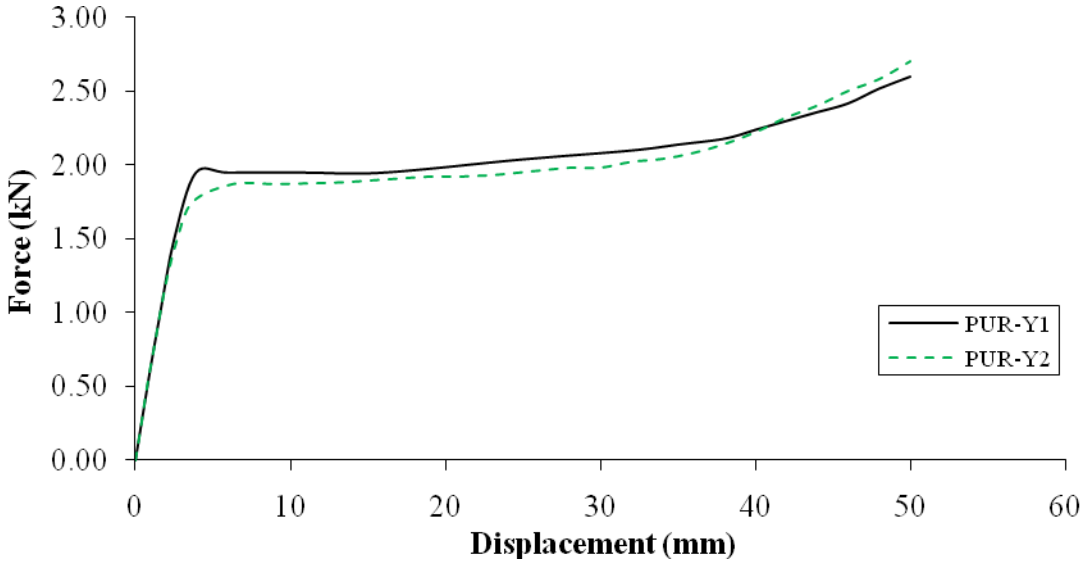

Figure 3.15: Force-Displacement of the through thickness direction PUR specimens

Specimen	PUR-Y1	PUR-Y2	Mean
Width (mm)	96.40	95.73	**96.07**
Length (mm)	98.53	98.10	**98.32**
Depth (mm)	100.44	100.13	**100.29**
Weight (g)	42.40	42.80	**42.60**
Density (kg/m^3)	44.44	45.52	**44.98**
E_{Cc} (N/mm^2)	6.444	6.440	**6.442**
f_{Cc} (N/mm^2)	0.205	0.199	**0.202**

Table 3.8: PUR through thickness direction specimen test results

Finally, the force-displacement of the transverse direction is showed in Figure 3.16 and the summary is listed in Table 3.9. The mean of the compressive modulus of elasticity and strength are 5.703 N/mm^2 and 0.192 N/mm^2, respectively.

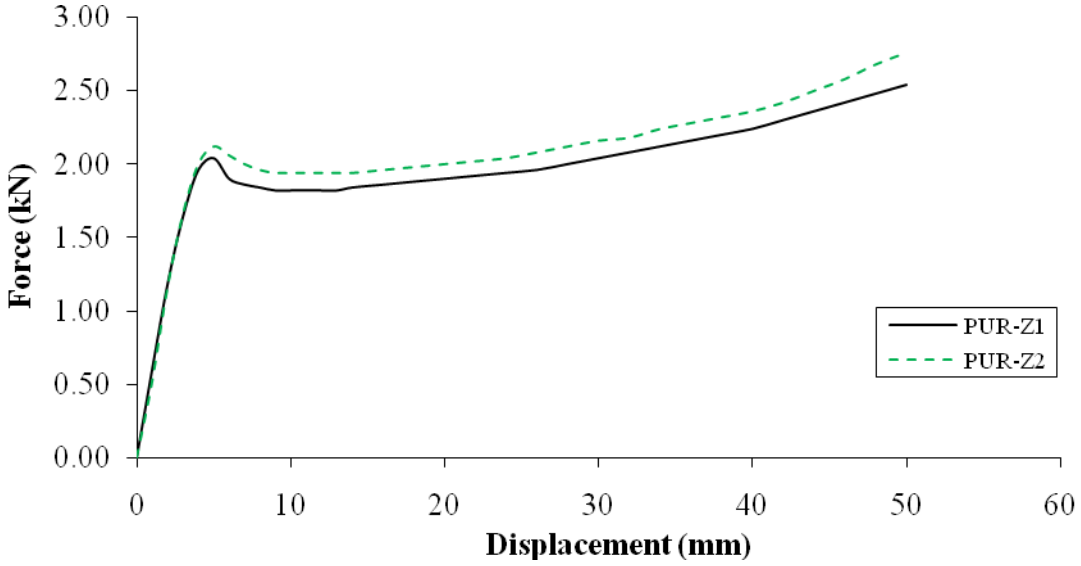

Figure 3.16: Force-Displacement of the transverse direction PUR specimens

Specimen	PUR-Z1	PUR-Z2	Mean
Width (mm)	98.13	97.60	**97.87**
Length (mm)	100.14	100.13	**100.14**
Depth (mm)	101.58	98.02	**99.80**
Weight (g)	41.50	39.50	**40.50**
Density (kg/m^3)	41.57	41.24	**41.41**
E_{Cc} (N/mm^2)	5.847	5.559	**5.703**
f_{Cc} (N/mm^2)	0.185	0.199	**0.192**

Table 3.9: PUR transverse direction specimen test results

The comparison between the PUR test results in each direction is presented in Table 3.10. As can be seen in the Table 3.10, the E_{Cc} of the through thickness direction (Y-axis) is 11% higher than other two directions. All directions f_{Cc}, which are determined at 10% relative deformation, are almost equal.

Specimen	PUR-X	PUR-Y	PUR-Z
E_{Cc} (N/mm^2)	5.447	6.442	5.703
f_{Cc} (N/mm^2)	0.196	0.202	0.192

Table 3.10: Comparison of PUR in three principal directions

3.4.2 Shear test on PURs

The characteristic of the inner core in SIPs is to resist shear and support the outer faces against buckling. Literature review shows that the material properties of the inner core, i.e., shear modulus (G) and shear strength (τ) vary depending upon, for example, inner core type, density and manufacturer's technique. In addition, Esvelt (1999) states the deflection of SIP is very shear sensitive.

The shear modulus and shear strength was required in the design of SIPs and numerical investigation. Accordingly, shear tests on PUR were undertaken in accordance with BS EN 12090 (BSI, 1997). This standard requires a single shear test arrangement for the inner core specimen with a 50 mm thickness. For the thickness greater than 50 mm, a double shear test arrangement is employed in order to avoid the additional moment applied to the specimen from the eccentricity.

Two PUR specimens (PUR-SS1 and 2) of approximately 50 mm wide, 200 mm long and 50 mm thick were subjected to the single shear test. It should be noted that the length of PUR in the single shear test was reduced to be 200 mm (instead of 250 mm) so that the same specimen length for both single and double shear tests was investigated. All specimens were obtained from small SIP specimens provided by SIP Build Ltd.

The PUR inner core specimens were bonded on two steel plates by using the Apollo structural adhesive A5086 part A and B. The steel plates are 50 mm wide, 300 mm long and 10 mm thick. Although the steel plate thickness of 16 mm is recommended in BS EN 12090, this thickness is thicker than the grips of the Instron testing machine. Consequently, the 10 mm thickness was used instead and the test results would not be affected from the steel plate thickness. The two

steel support plates were then connected to other steel plates of 50x100x10 mm by bolts and were jaw clamped in the grips of the Instron testing machine as shown in Figure 3.17.

Figure 3.17: Single shear on PUR test specimens

BS EN 12090 states a force (F) shall be applied at a 3±0.5 mm/min constant rate of movement of the movable head. Nevertheless, the Instron machine can accommodate the constant rate of movement of 2 mm/min or 5 mm/min. The 2 mm/min constant rate of movement of the movable head was therefore chosen. The applied loads together with the displacements were then taken from the Instron machine reading at regular intervals until shear failure occurred. The shear modulus (G) and shear strength (τ) are determined as given in BS EN 12090.

The forces and shear displacements of two PUR specimens are shown in Figure 3.18. The test results indicate a linear and non-linear behaviour of PUR specimens when subjected to shear forces. The mean values of shear modulus and shear strength are 1.70 N/mm^2 and 0.126 N/mm^2 respectively, as summarised in Table 3.11. The slip and debonding leading to shear failure mode is observed as presented in Figure 3.19.

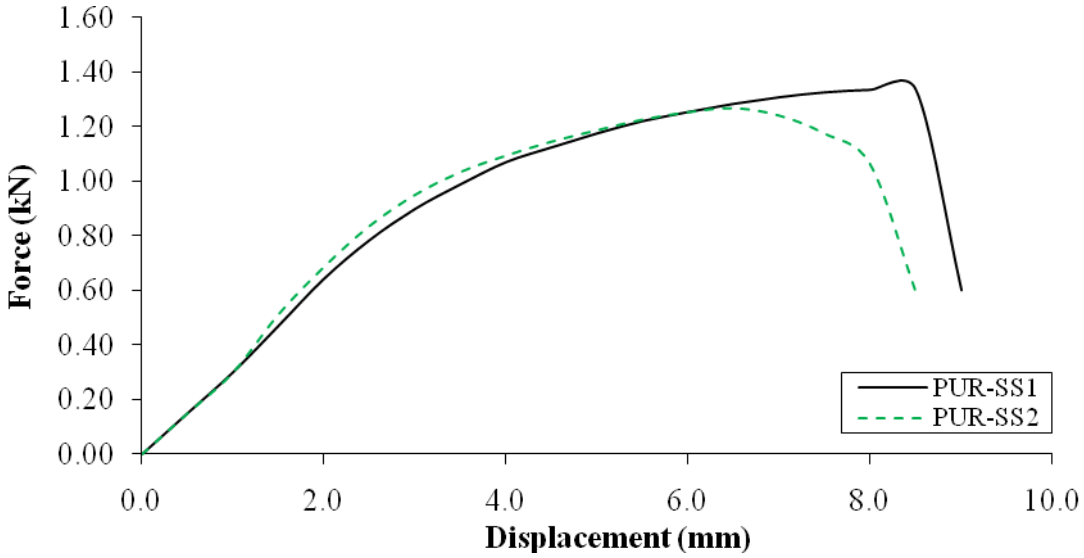

Figure 3.18: Force-displacement curve of PUR specimens

Specimen	PUR-SS1	PUR-SS2	Mean
Width (mm)	49.95	53.39	**51.67**
Length (mm)	199.65	199.15	**199.40**
Depth (mm)	49.69	48.91	**49.30**
Weight (g)	22.50	23.50	**23.00**
Density (kg/m^3)	45.41	45.19	**45.30**
***G* (N/mm^2)**	1.71	1.69	**1.70**
τ (N/mm^2)	0.134	0.119	**0.126**

Table 3.11: PUR single shear test results

Two sets of PUR specimens (PUR-DS1 and 2) of approximately 100 mm wide, 200 mm long and 100 mm thick were subjected to the double shear test. PUR inner core specimens were bonded on two steel supported plates and one steel loading plate by again using the Apollo structural adhesive A5086 part A and B. The steel supported plates are 250 mm wide, 300 mm long and 10 mm thick. Four 17 mm diameter holes were drilled through the support plates, four 16 mm all thread steel bars with washers and nuts were used to hold the support plates. The steel loading plate, initially 100 mm wide, 300 mm long and 10 mm thick, were cut to the width of a 50 mm at the top section in order to attach firmly to the grip of the Instron testing machine.

Additional four steel equal size angles were assembled to the testing rig and then attached to the moving part of the Instron testing machine by four all thread steel bars as illustrated in Figure 3.20.

Figure 3.19: Delaminated failure mode

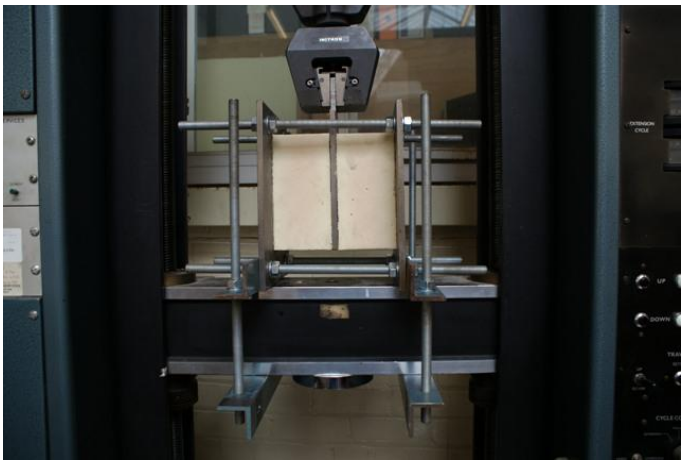

Figure 3.20: Double shear on PUR test specimens

Prior to performing the test, all of the nuts at the steel supported plates were loosen to avoid any additional compressive load to the specimens which could yield an inaccurate result. Figure 3.21 shows the forces and shear displacements of two PUR specimens subjected to the double shear test. Similar to the single shear test, the test results demonstrate a linear and non-linear behaviour. The mean values of shear modulus and shear strength are 1.71 N/mm^2 and 0.108

N/mm^2 respectively, as listed in Table 3.12. The debonding and slip failure mode was found in this investigation as presented in Figure 3.22.

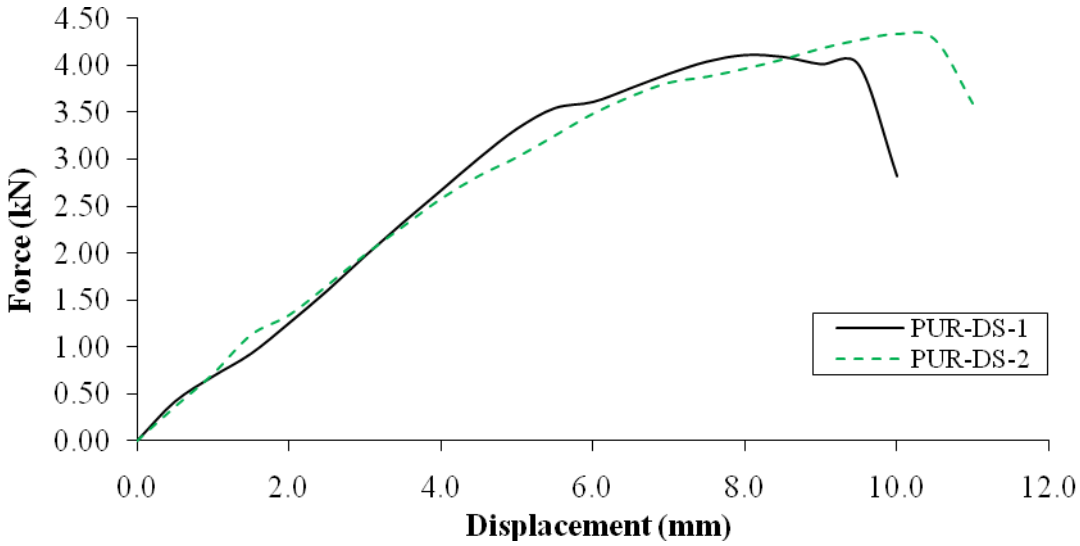

Figure 3.21: Force-displacement curve of PUR specimens

Specimen	PUR-DS1		PUR-DS2		Mean
Width (mm)	99.15	98.88	98.85	99.11	**99.00**
Length (mm)	198.91	198.80	197.83	197.58	**198.28**
Depth (mm)	99.40	99.97	98.91	97.94	**99.06**
Weight (g)	89.40	89.20	88.00	87.90	**88.63**
Density (kg/m^3)	45.60	45.39	45.50	45.83	**45.58**
***G* (N/mm^2)**	1.72		1.70		**1.71**
τ (N/mm^2)	0.104		0.111		**0.108**

Table 3.12: PUR single shear test results

The comparison between the PUR test results is presented in Table 3.13. As can be seen in the Table 3.13, the *G* values from both single and double shear tests are approximately equal, whereas τ is less conformable. The τ value from double shear test is 14.29% less than the single shear. This may be due to the additional eccentric bending moment applied to the specimens, causing failure at slightly lower loads.

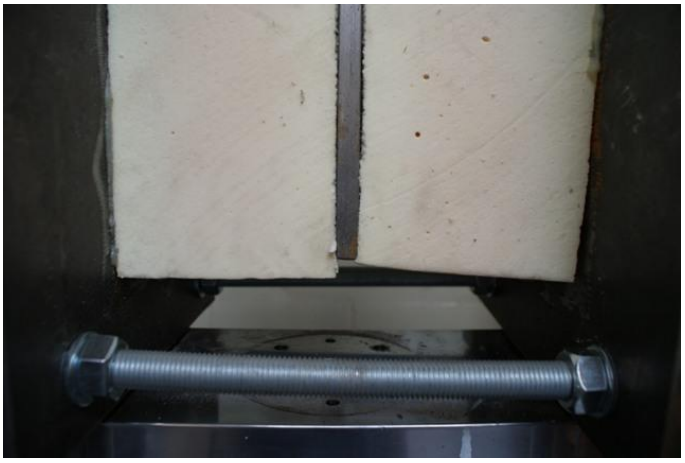

Figure 3.22: Delaminated and slippage failure mode

From	G (N/mm^2)	τ (N/mm^2)
PUR-SS	1.70	0.126
PUR-DS	1.71	0.108
Difference (%)	0.59	-14.29%

Table 3.13: Comparison between the single and double shear test results

3.5 Mechanical properties of SIPs

In this section, selected mechanical properties (compressive, tensile and shear) of SIPs were carried out. These mechanical properties will be compared with the PUR test results and the published values, and later used in the numerical investigations.

3.5.1 Compressive test on SIPs

Compressive test on SIP specimens was carried out in the through thickness direction only in order to determine the modulus of elasticity in compression and compressive strength in accordance with BS EN 14509 and to compare with the PUR test results. Two SIP specimens, approximately 200 mm wide, 200 mm long and 125 mm thick (11 mm OSB thick and 103 mm PUR thick), were subjected to compressive loads as shown in Figure 3.23. The loads were applied at a constant cross-head movement rate of 10 mm/min using the Instron testing

machine. This movement is within 10% of thickness ± 25 % per minute (7.5 mm - 12.5 mm per minute) in accordance with BS EN 14509. The forces and displacements were then recorded at regular intervals. Initially mounted strain gauges were used to record the strains at the centre of the specimens. Nevertheless, the recordings from the strain gauge were disregarded as they were out of range at the higher load applied. Hence, the displacements of the cross-head movements were employed. Since the specimens were not subjected to any failures, the loads and displacements were recorded until a displacement equivalent to 50% of the specimen thickness i.e. 60 mm as shown in Figure 3.24.

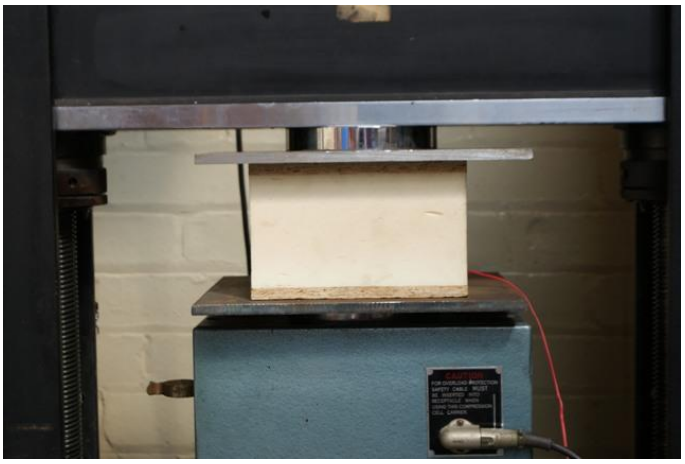

Figure 3.23: Compressive test on SIP specimen

Figure 3.25 shows the force and displacement curves of SIP specimens. The behaviour of SIP specimen comprises three phases, which is as same as to the compressive test of PUR as previously described in the section 3.4.1.

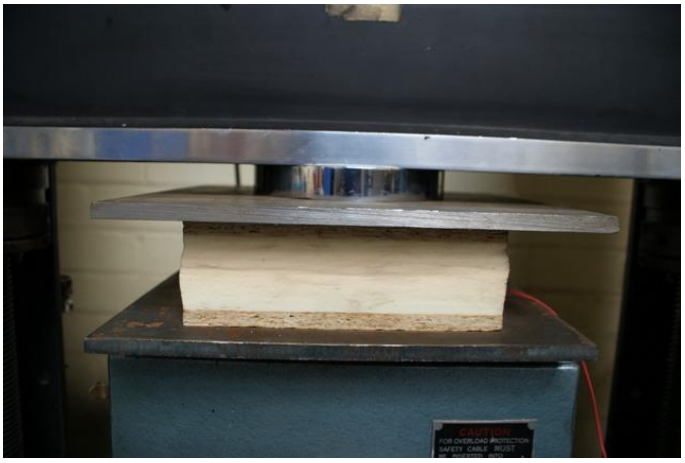

Figure 3.24: 50% displacement of specimen thickness

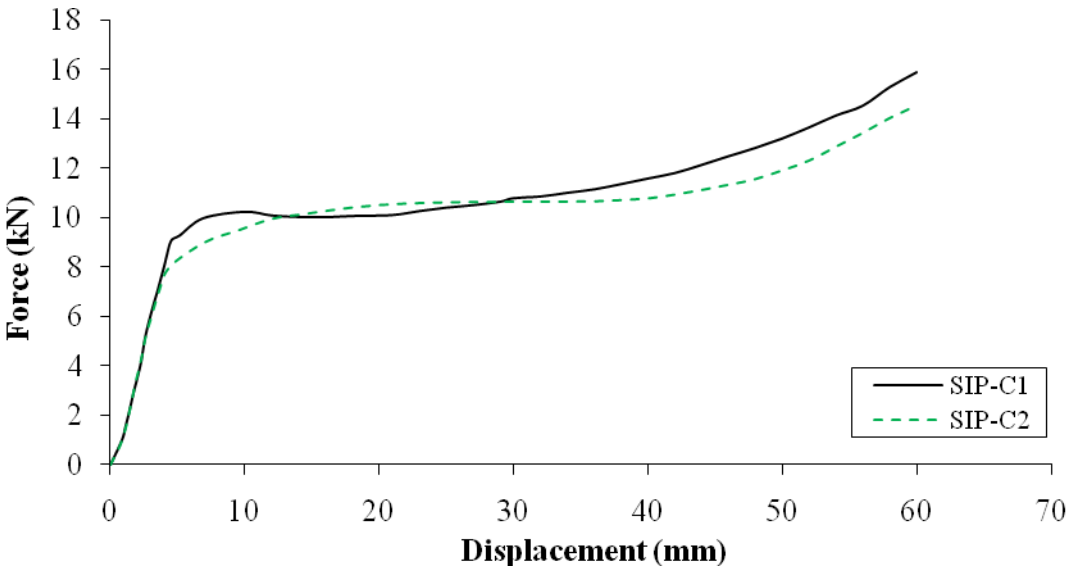

Figure 3.25: Force-displacement curve of SIP specimens

Table 3.14 shows the summary of the SIP specimen test results. The mean of the modulus of elasticity in compression and compressive strength are 6.665 N/mm^2 and 0.254 N/mm^2, respectively. The compressive modulus values are in similar range as previously found on the PUR test, whereas the compressive strength is approximately 25.7% higher. This indicates that SIPs (as composite materials) can provide a higher strength than the PUR only as illustrated in Table 3.15.

Specimen	SIP-C1	SIP-C2	Mean
Width (mm)	198.51	197.27	**197.89**
Length (mm)	198.83	198.44	**198.64**
Depth (mm)	124.92	124.72	**124.82**
Weight (g)	746.50	730.00	**738.25**
E_{Cc} **(N/mm^2)**	6.779	6.550	**6.665**
f_{Cc} **(N/mm^2)**	0.261	0.247	**0.254**

Table 3.14: Compressive SIP specimen test results

Specimen	SIP	PUR-Y
E_{Cc} **(N/mm^2)**	6.665	6.442
f_{Cc} **(N/mm^2)**	0.254	0.202

Table 3.15: Comparison of compressive SIP and PUR test results

3.5.2 Tensile test of SIPs

Tensile test of SIP specimens in the through thickness direction was carried out in order to determine the tensile modulus of elasticity in tension and strength in accordance with BS EN 14509 (BSI, 2006). Each specimen is approximately 200 mm wide, 200 mm long and 125 mm thick. SIP specimens were bonded two T-shape steel plates by using the Apollo structural adhesive and were inserted to the grips of the Instron testing machine as illustrated in Figure 3.26.

The loads were applied at a constant cross-head movement rate of 10 mm/min (according to BS EN 14509). The forces and displacements were then recorded at regular intervals. The corresponding strains that recorded by the strain gauges at the central of the specimens were found to be small and underestimate the strain movement. Accordingly, the strain records were disregarded and the displacements were used instead. The failure mode was found to be due to tearing of the PUR as presented in Figure 3.27.

Figure 3.26: Tensile test on SIP specimen

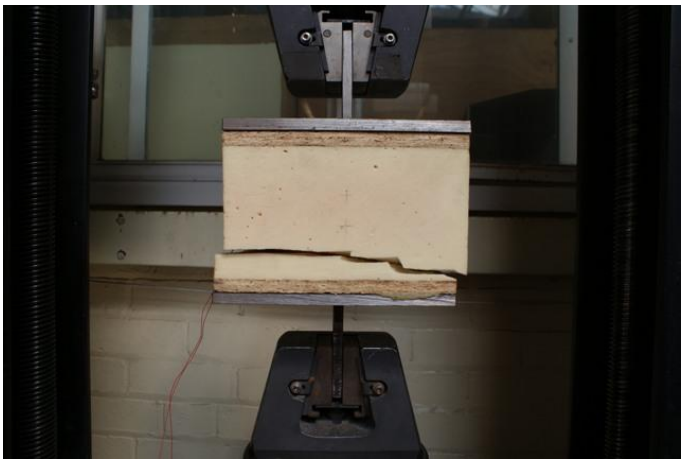

Figure 3.27: Tearing of PUR

Figure 3.28 shows the force and displacement curves of SIP specimens. Table 3.16 shows the summary of the SIP specimen test results. The means of the tensile modulus of elasticity and strength are 7.156 N/mm^2 and 0.254 N/mm^2, respectively. The tensile modulus is higher than the compressive modulus. This agrees well with Koschade (2002)'s finding that the tensile modulus is higher than the compressive modulus.

The SIP tensile test results are compared to Kermani (2006) and Esvelt (1999)'s findings as presented in Table 3.17. The tensile strength is almost double as Kermani's value. This finding

may be explained by the fact that the different types of the inner core materials and densities can vary the strength and stiffness.

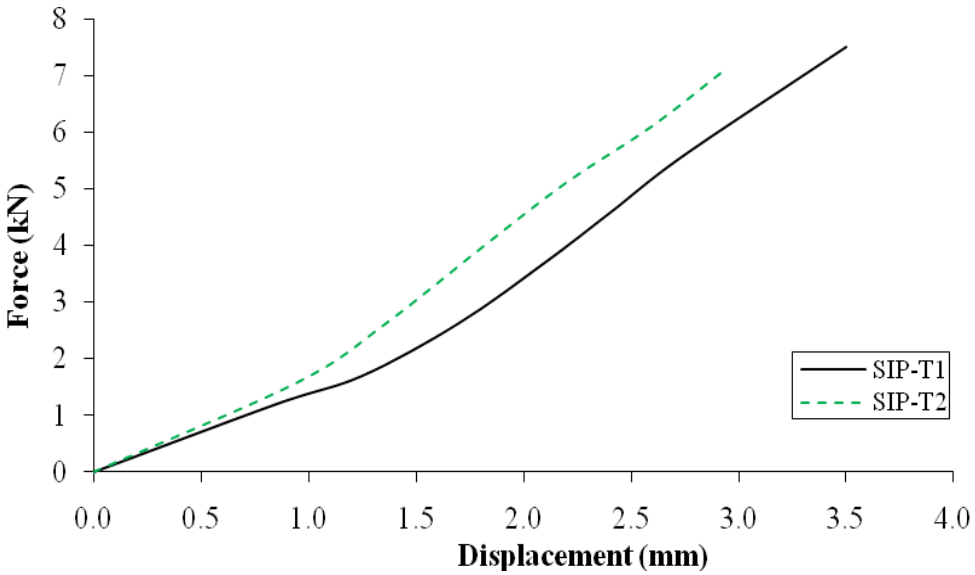

Figure 3.28: Force-displacement curve of SIP specimens

Specimen	SIP-T1	SIP-T2	Mean
Width (mm)	196.45	198.25	**197.35**
Length (mm)	196.56	198.44	**197.50**
Depth (mm)	124.45	124.5	**124.475**
Weight (g)	766.20	786.40	**776.30**
E_{Ct} (N/mm^2)	7.061	7.251	**7.156**
f_{Ct} (N/mm^2)	0.194	0.182	**0.188**

Table 3.16: Tensile SIP specimen test results

By	Test result (PUR)	Kermani (2006) (EPS)	Esvelt (1999) (EPS)
Width (mm)	197.35	200	89
Length (mm)	197.50	200	89
Thickness (mm)	OSB – PUR – OSB 11 – 103 – 11	OSB – EPS – OSB 11 – 95 – 11	OSB – EPS – OSB 11 – 92 – 11
Tensile strength (N/mm^2)	0.188	0.097	0.196
Displacement at failure (mm)	3.23	20.00	6.00
Failure mode	Tearing of the inner core.		

Table 3.17: Comparison between SIP tensile test result and other published values

3.5.3 Shear test on SIPs

As the SIP thickness in this research is a 125 mm thick, the double shear test was therefore carried out. Two sets of SIP specimens, approximately 100 mm wide, 200 mm long and 125 mm thick, were subjected to the double shear test. These specimen sizes are in accordance with BS EN 12090 requirement. The experimental apparatus and procedure in this SIP test are as same as the double shear test on PUR as previously detailed in section 3.4.2. Figure 3.29 illustrates the experimental apparatus and SIP specimens subjected to the double shear test.

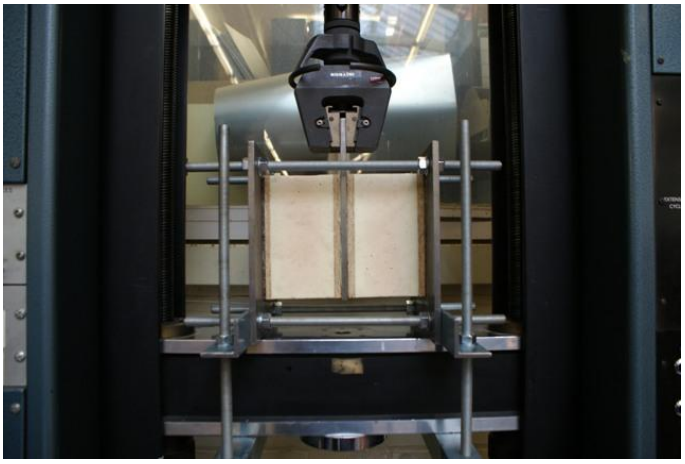

Figure 3.29: Double shear test on SIP specimens

Figure 3.30 shows the forces and shear displacements of two SIP specimens subjected to the double shear test. The specimens failed due to debonding and excessive slip as presented in Figure 3.31.

The mean of shear modulus and shear strength are 1.77 N/mm^2 and 0.116 N/mm^2, respectively as listed in Table 3.18. These values are in the similar range of the PUR only tests as shown in Table 3.19.

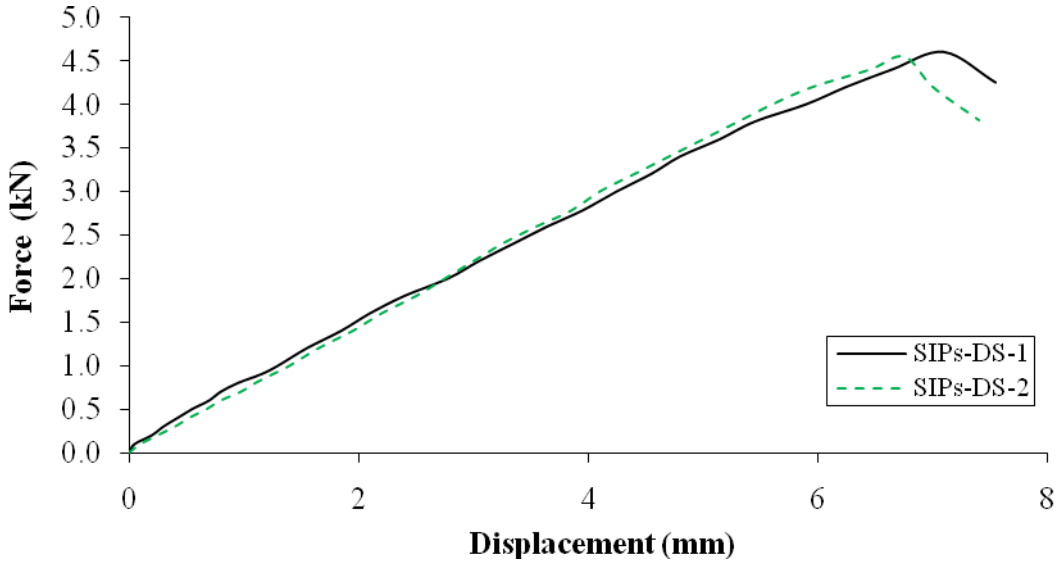

Figure 3.30: Force-displacement curve of SIP specimens

Specimen	SIP-DS1		SIP-DS2		Mean
Width (mm)	100.02	100.01	98.46	100.23	**99.68**
Length (mm)	198.35	199.23	197.74	198.58	**198.48**
Depth (mm)	125.09	125.29	124.91	125.35	**125.16**
Weight (g)	381.40	392.80	349.10	374.10	**374.35**
***G* (N/mm^2)**	1.71		1.82		**1.77**
τ (N/mm^2)	0.116		0.116		**0.116**

Table 3.18: SIP double shear test results

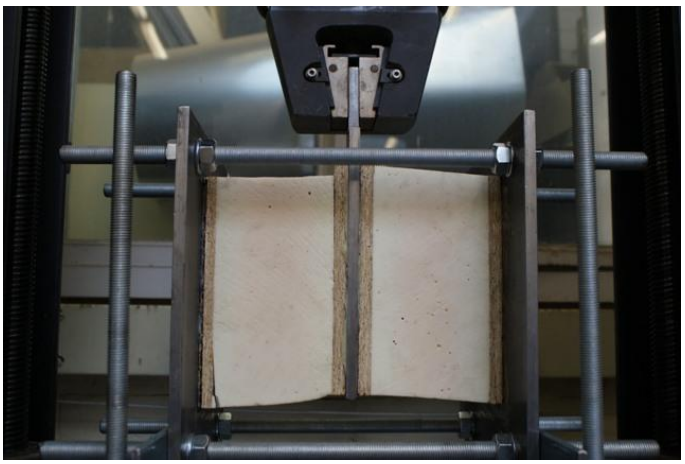

Figure 3.31: Debonding and slip failure mode

From	G (N/mm^2)	τ (N/mm^2)
PUR-SS	1.70	0.126
PUR-DS	1.71	0.108
SIP-DS	1.77	0.116

Table 3.19: Comparison between the PUR and SIP shear test results

3.5.4 Shear/Skewed test on SIPs

The shear/skewed test was undertaken to two SIP specimens in order to determine the shear strength at the interface. Each specimen is approximately 200 mm wide, 200 mm long and 125 mm thick. The loads were applied at a constant cross-head movement rate of 10 mm/min by using the Instron testing machine as shown in Figure 3.32. The forces and displacements were then recorded at regular intervals.

Figure 3.32: Shear/Skewed test on SIP specimens

Figure 3.33 shows the forces and displacements of two SIP specimens subjected to the shear/skewed test. The test results demonstrate linear and non-linear behaviour. The mean of shear strength is 0.109 N/mm^2 as listed in Table 3.20. This value is in the similar range of the shear tests on PUR and SIPs only as previously described in the preceding sections.

The failure mode was found due to the debonding as shown in Figure 3.34. This finding differs from Kermani (2006)'s study, who found the failure was due to the tearing of the foam and the glue lines remained intact. This can be explained that his SIP specimens consist of a higher bond strength than the EPS foam strength. Nevertheless, the shear strength test result is 46.8% higher than Kermani's results for EPS as listed in Table 3.21. This finding may be again explained by the fact that the different types of the inner core materials and also densities can vary the strength and behaviour.

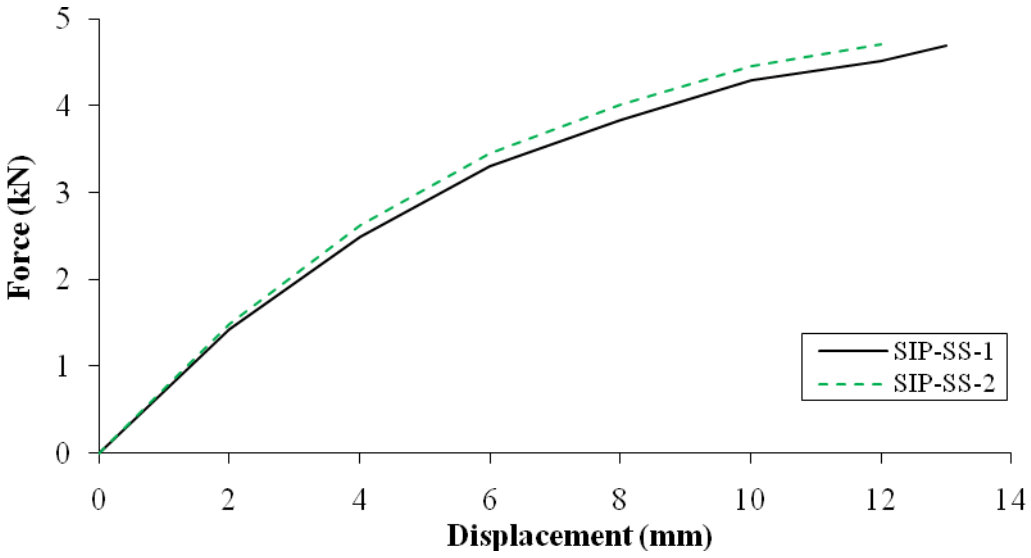

Figure 3.33: Force-Displacement of shear/skew SIP test results

Specimen	SIP-SS1	SIP-SS2	Mean
Width (mm)	196.95	197.08	**197.02**
Length (mm)	197.61	198.80	**198.21**
Depth (mm)	123.99	124.40	**124.20**
Weight (g)	743.10	750.20	**746.65**
τ (N/mm^2)	0.109	0.109	**0.109**

Table 3.20: SIP shear/skewed test results

Figure 3.34: Delaminated failure mode

By	Test result (PUR)	Kermani (2006) (EPS)
Width (mm)	197.02	200
Length (mm)	198.21	200
Thickness (mm)	OSB – PUR – OSB 11 – 103 – 11	OSB – EPS – OSB 11 – 95 – 11
Shear strength (N/mm^2)	0.109	0.058
Displacement (mm)	12.50	25.54
Failure mode	Debonding	Tearing of foam, glue lines remained intact

Table 3.21: Comparison between SIP shear/skewed test result and Kermani's finding

3.6 Three-point bending test on SIP beams

The experimental investigations moved on to SIPs as a beam. Three-point bending tests on SIP beams were undertaken in order to determine the failure loads and to investigate the structural behaviour when subjected to transverse loads. Moreover, the failure load obtained from short-terming loading test would then be used to determine the applied loads in the long-term experimental investigation, which is presented in Chapter 5.

3.6.1 Experimental investigations on SIP beams

Two SIP beams (SIP-BST-1 and 2) were subjected to the three-point bending tests. Each beam is 200 mm wide, 800 mm long with 11 mm thick OSB facings and a 103 mm thick polyurethane inner core (overall thickness of 125 mm). The beams were supported on two movable steel rollers which were placed on two steel boxes. Two 100 mm wide steel plates were placed between the support rollers and the SIP beams in order to distribute the reaction. The loads were then applied using Mand Testing Machine through a steel I-beam with a 100 mm load spreader at the mid-span point. The applied loads and the mid-span displacements were recorded by Linear Variable Differential Transformers (LVDTs) which were connected to the Grant data logging system until failure occurred. Figure 3.35 illustrates the three-point bending test apparatus and instrumentations used. Although LVDTs were used to record the displacements at various locations i.e. horizontal displacements and vertical displacement at the support, these displacements were found negligible in comparison to the mid-span displacement and were less concerned in engineering practice. Accordingly, only the mid-span displacements have been studied and presented.

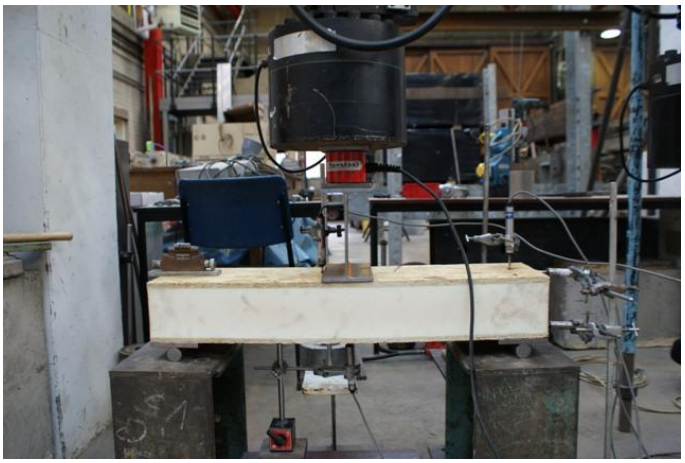

Figure 3.35: Three-point bending experimental apparatus

Figure 3.36 shows the applied load against mid-span deflection curves for specimens SIP-BST-1 and 2. The test results reveal a proportional limit at 6 kN. Both beams failed due to the fracture of the lower surface at the point of load application as shown in Figure 3.37. The mean ultimate load at failure is 8.78 kN as summarised in Table 3.22.

Prior to the publication of ISO 22452 (ISO, 2011), neither British nor European standard were available for designing and testing SIPs. EC5 (BSI, 2004), which is the standard for timber design, was therefore used to determine the serviceability deflection limit. EC5 provides the limiting instantaneous deflection value in the range of ℓ/300 to ℓ/500 for a simply supported beam. However, in accordance with BS 5268-2 (BSI, 2002) cl. 2.10.7, the deflection limit of a simply supported span is the lesser of ℓ/333 or 14 mm. This indicates clearly that the deflection limit provided by BS 5268-2 is in the range of ℓ/300 to ℓ/500 in accordance with EC5. Accordingly, the limiting deflection value has been chosen to be ℓ/333 (2.10 mm) for this experimental study.

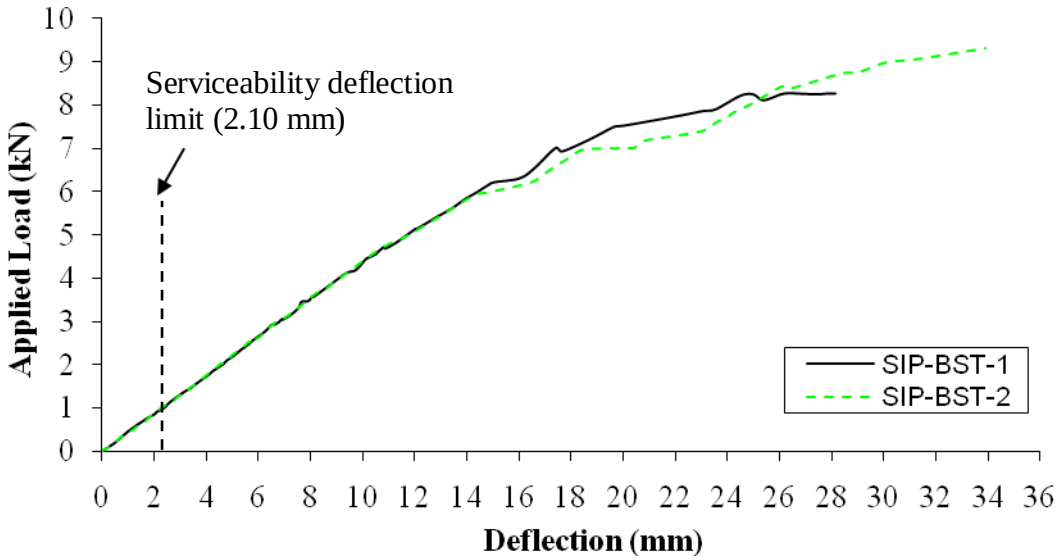

Figure 3.36: Applied load vs mid-span deflection curves

Figure 3.37: Bending failure mode

It should be noted that the mean serviceability load at the deflection limit (0.91 kN) is approximately 10% of the mean ultimate load (8.78 kN). This indicates that SIPs have a high degree of capacity reserve, i.e. up to 9.65 times the imposed load effects. However, it should be noted that the reserve capacity is influenced by many factors such as the span length, load type and support conditions.

Specimen	***Load at failure***	***Deflection at failure***	***Load at deflection limit (ℓ/333 = 2.10 mm)***	***Failure mode***
	(kN)	***(mm)***	***(kN)***	
SIP-BST-1	8.26	26.42	0.91	Bending
SIP-BST-2	9.30	33.90	0.91	
Mean	**8.78**	**30.16**	**0.91**	

Table 3.22: Summary of experimental results for SIP beam test

3.6.2 Analytical analysis of the shear modulus

In this section, the shear modulus (G) of the PUR inner core material is determined and presented by adapting the method in BS EN 14509. Since the SIP beam specimens do not failed due to shear, the shear capacity cannot be determined.

The shear modulus can be determined by the gradient of the applied load vs deflection at mid-span curve by using the following procedures.

The first step is to calculate the flexural rigidity (B_s) which can be determined by the following equation 3.1:

Flexural rigidity: $$B_s = \frac{E_{F1} \cdot A_{F1} \cdot E_{F2} \cdot A_{F2}}{E_{F1} \cdot A_{F1} + E_{F2} \cdot A_{F2}} e^2 \quad (3.1)$$

where E_{F1} is the E-modulus of the top face.

A_{F1} is the measured area of cross-section of the top face.

E_{F2} is the E-modulus of the bottom face.

A_{F2} is the measured area of cross-section of the bottom face.

e is the measured depth between the centroids of the faces.

Now by substituting the B_s value together with ΔF and L into the equation 3.2, the bending deflection (Δw_B) can be obtained. This equation has been modified for the three-point bending load.

Bending deflection: $$\Delta w_B = \frac{\Delta F L^3}{48 B_s} \quad (3.2)$$

where Δw_B is the deflection at mid-span for a load increment ΔF taken from the slope of the linear part of load-deflection curve.

L is the clear span of test specimen.

After that, the shear deflection (Δw_s) can be obtained by subtracting Δw with Δw_B as shown in the equation 3.3.

Shear deflection: $$\Delta w_s = \Delta w - \Delta w_B \quad (3.3)$$

Finally, the shear modulus (G) can then be determined by using the following equation 3.4.

Shear modulus: $$G = \frac{\Delta F L}{4 B d_c \Delta w_s} \quad (3.4)$$

where d_c is the depth of the core material; and

B is the measured width of the specimen.

Table 3.23 tabulates the shear modulus (G) for the SIP-BST-1 and 2. The shear modulus (G = 3.96 N/mm^2) obtained by the adaptation of BS EN 14509 method is 133% higher than the single or double shear test (G = 1.70 N/mm^2) as described in the section 3.2. According to Davies (2001), the above stated formulae for the shear modulus calculation is not valid when using wide patch loading zone, in which the deflection is lower than that for the point load. Consequently, the shear modulus will be over estimated. There is currently no such formulae to determine the mid-span deflection with the wide loading zone in sandwich or SIP beams. Finite element analysis is therefore used to determine the shear modulus in such cases. This will be presented in the following section.

3.6.3 Numerical investigation of SIP beams

Numerical investigation was analysed using the ABAQUS v.6.9-1 finite element programme. The material properties required in the modelling were obtained from the experiment as previously described in the sections 3.3 and 3.4. The SIP beam specimen was analysed using a two-dimensional model. The assumption of perfect bond at the OSB-PUR interface was adopted. The steel load plate was not modelled since the load could be applied directly to the SIP model. Steel support plates were modelled and connected to the lower OSB face by the

contact interaction with a coefficient of friction equal to 0.2 (wood-steel coefficient) obtained from Cobb (2009).

Specimen	SIP-BST-1	SIP-BST-2	Mean
F_u (kN)	8.26	9.30	**8.78**
ΔF (kN)	0.91	0.91	**0.91**
Δw (mm)	2.10	2.10	**2.10**
B (mm)	197.70	198.28	**197.99**
L (mm)	699	699	**699**
f (mm)	11	11	**11**
d_c (mm)	101.97	102.94	**102.46**
e (mm)	112.97	113.94	**113.46**
$E_{F1} = E_{F2}$ (N/mm^2)	3844	3844	**3844**
$A_{F1} = A_{F2}$ (mm^2)	2174.70	2181.08	**2177.89**
B_s (Nmm^2)	5.33E+10	5.44E+10	**5.39E+10**
Δw_B (mm)	0.121	0.119	**0.120**
Δw_s (mm)	1.979	1.981	**1.980**
G (N/mm^2)	3.99	3.93	**3.96**

Table 3.23: Shear modulus analytical analysis of SIP beam specimens

As the geometry of the specimen and loading are symmetric about the mid-span section, only half of the specimen was modelled. Thus the XSYMM boundary condition was applied in the vertical section at the mid-span. This technique can save the computational efforts considerably. Finally, a restraint in the vertical direction ($U_y = 0$) was applied at the centre of the bottom face of the steel support plate. Figure 3.38 depicts the finite element mesh for SIP beam model.

The structured mesh technique was employed in this model by utilising an eight-node biquadratic plane strain element with reduced integration (CPE8R). This meshing technique can render the most favourable results with minimal computational efforts. OSB faces were divided into two divisions in depth with a 10 mm element size in the longitudinal directions. Other materials, i.e. PUR and steel plate, were discretised into 10 x 10 mm elements. A sensitivity

analysis on the density of mesh element was carried out and found that these elements were fine enough to provide satisfactory results in both stresses and displacements output.

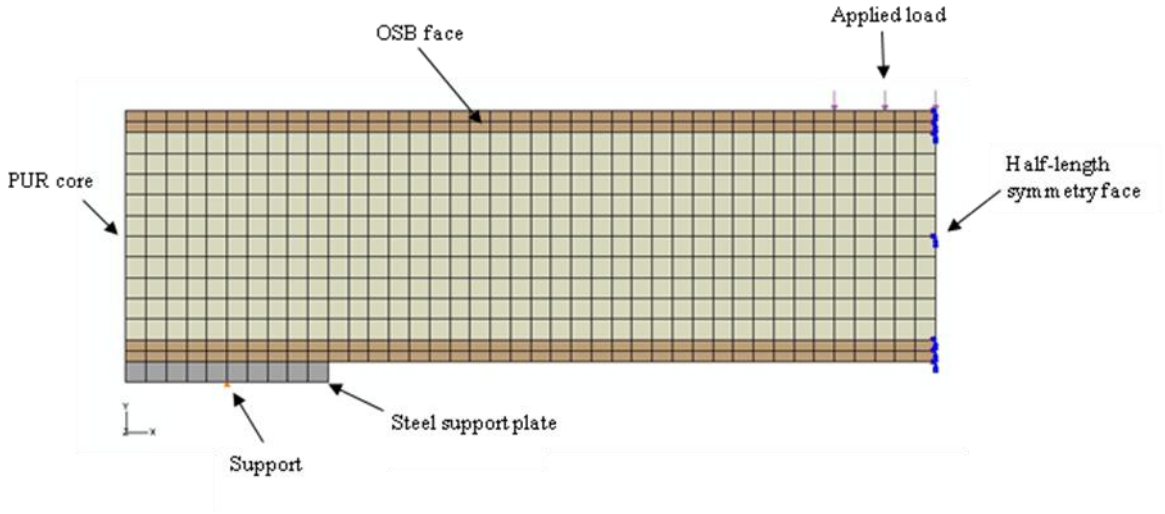

Figure 3.38: SIP beam finite element model

OSB is effectively an orthotropic material, the material properties of OSB were hence specified as an elastic-orthotropic material. It should be noted that normal materials properties were from the mechanical properties tests as presented in section 3.2 and the shear material properties were obtained from BS EN 12369-1 as such data were not measured by tests. The modulus of elasticity in the through thickness direction (E_{22}) was not determined by the experiment, it was therefore assumed equal to the minor axis modulus of elastic. The experiment was not carried out to determine the Poisson's ratio (υ) in each direction. The Poisson's ratio was obtained from TR 019 (EOTA, 2005), where υ equals to 0.24 along and perpendicular to the grain directions. Accordingly, the υ was assumed to be 0.24 for all directions in this research.

As observed in the mechanical property tests, the OSB material failed in a brittle manner. As a result, an elastic material model was assumed in this modelling exercise.

PUR inner core, provided by SIP Build Ltd, is also an orthotropic material that has been identified by the mechanical properties in section 3.3. Similar, the υ of PUR was not investigated. Gibson and Ashby (1999) present a large variation of the Poisson's ratio of foams with different foam types and densities. They suggest the Poisson's ratio equals to 0.33 (in all directions) which is the average value of their presented data. Accordingly, the same value for Poisson's ratio for the PUR core was employed.

The nonlinear (plastic) part of the PUR core behaviour was implemented using the *PLASTIC option with perfectly plastic bi-linear stress-strain model. From the compressive test on the PUR through thickness direction, the initial yield stress at zero plastic strain was found equal to 0.2 N/mm^2 following by the stress of 0.33 N/mm^2 at the plastic strain of 0.29.

Steel support plate was specified as an isotopic material and its material property was obtained from BS EN 1993-1-1 (BSI, 2005). Table 3.24 lists the elastic material properties of each component in this numerical investigation.

Material	E_{11}	E_{22}	G_{12}	υ
	(N/mm^2)	**(N/mm^2)**	**(N/mm^2)**	
OSB	3,844	3,615	1,080	0.24
PUR	5.447	6.442	1.7	0.33
Steel	210,000	210,000	81,000	0.30

Table 3.24: Elastic material properties

The nonlinear geometry, i.e. *NLGEOM option in the ABAQUS, was also included because it was expected that the model would undergo large deformations. The applied load and the mid-span deflection curves from the FEM numerical investigation and the mean experiment of SIP beam specimens are presented in Figure 3.40. It has been found that the deflection is very sensitive to the shear modulus (G) of the inner core, rather than the material properties of the

OSB outer faces and the modulus of elastic (E) of the inner core. This finding agrees with the statement of Esvelt (1999), who found that the deflection of SIP was very shear sensitive.

As illustrated in Figure 3.39, the FEM result with the PUR material properties obtained from the shear tests does not agree with the SIP beam test results. The result over-predicts the deflection, but it has been found conservative in the design with the shear modulus determined by the single/double shear in accordance with BS 12090. This finding supports Caprino and Langella (2000)'s study that the single shear test provides less agreement to the sandwich beam behaviour in comparison to three-point bending test.

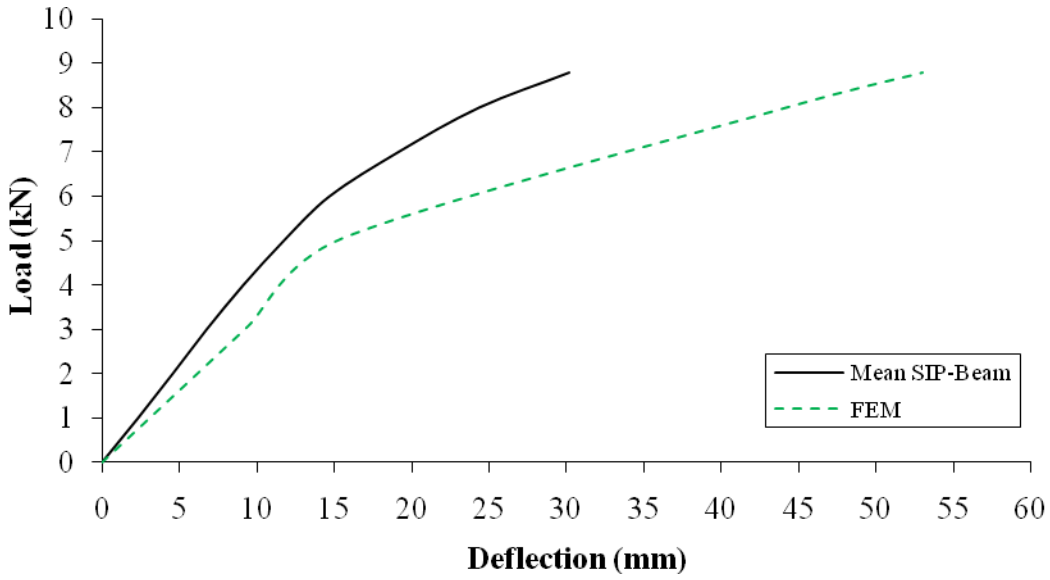

Figure 3.39: Deflections comparison between FEM and mean test results

In the next investigation, the *HYPERFOAM elastic material option in the ABAQUS was used. ABAQUS provides the hyper-elastic behaviour of the foams, which is based on the strain energy function (ABAQUS, 2010). The purpose of this investigation was to examine whether the *HYPERFOAM option can predict the behaviour of SIPs well.

The stress-strain test data of the PUR inner core in the uniaxial compression and tension in the through thickness direction and shear were entered in the *HYPERFOAM material option. The parametric study of the strain energy potential order (N), up to six terms, was also entered and investigated. It was found that the FEM results were converged when N equaled to 2, 3 and 4. Furthermore, the N values were found to have negligible impact on the deflection behaviour. Figure 3.40 presents the comparison between the FEM results and the mean experiment of SIP beam specimens. Similarly, both results do not agree and reveal the use of *HYPERFOAM option is more unfavourable. This finding supports the idea of Alwin (2002) that the *HYPERFOAM option obtained from the uniaxial compression and shear test data is inappropriate to use in prediction of SIP beam behaviour.

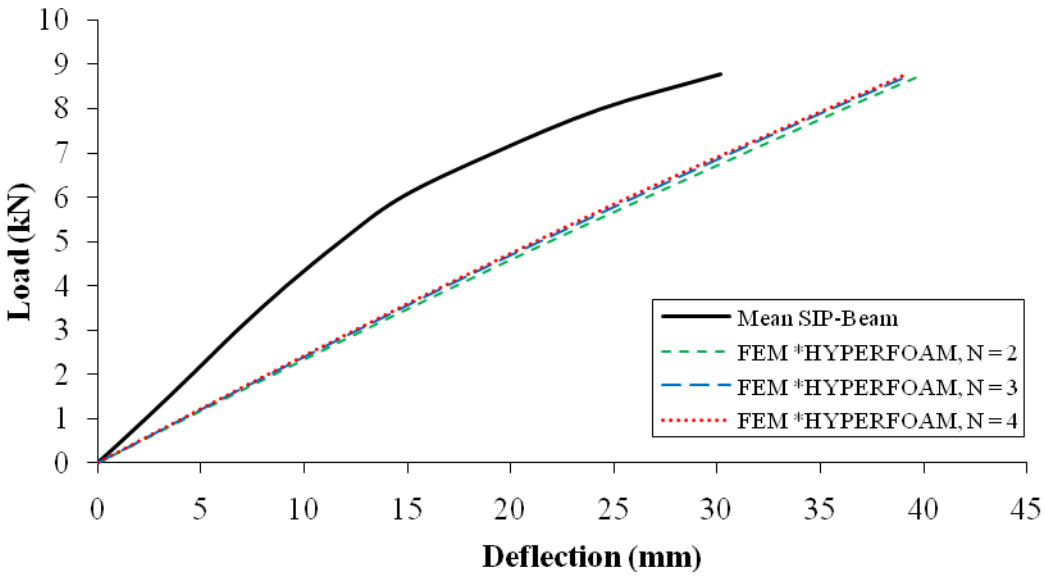

Figure 3.40: Deflections comparison between FEM and mean test results

Since the test shear modulus and *HYPERFOAM provides less conformity in comparison with the SIP beam test results, parametric study on the PUR material properties in both elastic and plastic parts was then investigated further. As previously described that the SIP deflection is very sensitive to the shear modulus (G), rather than the modulus of elastic (E). Hence, the

modulus of elasticity remains the same as previously listed in the Table 3.24. The FEM result agrees with the mean experiment of SIP specimens (see Figure 3.41) when the shear modulus is selected to be 2.3 N/mm^2 together with perfectly plastic bi-linear stress-strain model. The initial yield stress is equal to 0.2 N/mm^2 followed by the stress of 0.3 N/mm^2 at the plastic strain of 0.033. This shear modulus also agrees well with SIPs as panels which will be presented in the next chapter.

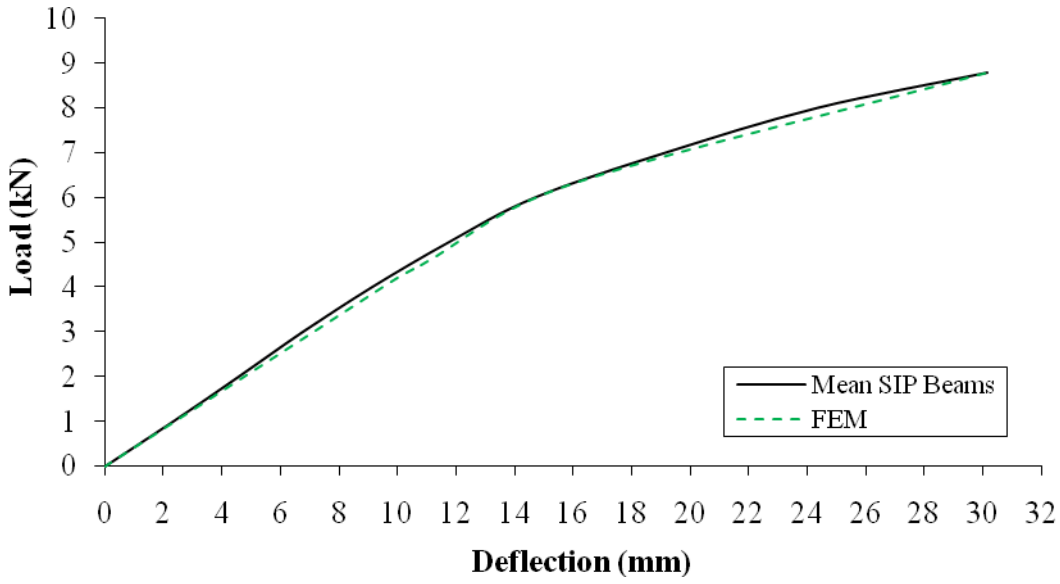

Figure 3.41: Deflections comparison between FEM and mean test results

The following FEM investigation deals with the determination of the initial failure. It should be noted that the FEM investigation in this research mainly focuses on the structural response of SIPs up to the onset of the initial failure. The modelling of the damage evolution has not been included. Nevertheless, the initial failure mode, which is obtained from the numerical investigation, can be used to predict the ultimate failure mode of SIP as a beam or a panel. The initial failure modes to be examined in this research were focused on bending, tensile and compressive failures of the OSB, and debonding and shear failures of the PUR. The procedure to determine the initial failure load is listed below.

(i) The experimental failure load was first applied in the FEM model.

(ii) Due to the nonlinear nature of the model, the analysis was conducted in a number of sub-steps before reaching the experimental failure loading level. The obtained stresses were evaluated at the final sub-step first by using the followings:

- The maximum axial stress criteria for OSB (equation 3.5).
- The linear interaction failure criteria for debonding of the PUR (equation 3.6).
- The Hashin Rotem's failure criteria for debonding of the PUR (equation 3.7).
- The shear failure criteria for the PUR (equation 3.8).

(iii) If there was no failure occurred, the applied load would then be increased until one of the failure criteria (as detected by using equations 3.5 to 3.8) was greater than or equal to 1.0. If one of the failure criteria has been breached, the penultimate sub-step would be checked to determine whether the initial damage has started in this sub-step. The similar process would be repeated until no failure occurred in this sub-step and the initial damage would be determined by the interpolation of the current sub-step and the next sub-step. The corresponding load was then recorded as the load at the initial failure load.

$$\text{OSB failure} = \max\left(\frac{S_{b,11}}{f_{b,11}}, \frac{S_{c,11}}{f_{c,11}}, \frac{S_{t,11}}{f_{t,11}}\right) \geq 1.0 \qquad (3.5)$$

where $S_{b,11}$ is the bending stress in parallel to the grain direction.

$f_{b,11}$ is the bending strength in parallel to the grain direction.

$S_{c,11}$ is the compressive stress in parallel to the grain direction.

$f_{c,11}$ is the compressive strength in parallel to the grain direction.

$S_{t,11}$ is the tensile stress in the parallel to the grain direction.

$f_{t,11}$ is the tensile strength in parallel to the grain direction.

$$\text{PUR debonding failure} = \frac{S_{22}}{f_{t,22}} + \frac{S_{12}}{f_{v,12}} \geq 1.0 \tag{3.6}$$

where S_{22} is the tensile stress in the through thickness direction.

$f_{t,22}$ is the tensile strength in the through thickness direction.

S_{12} is the shear stress in the 1-2 axis direction.

$f_{v,12}$ is the shear strength in the 1-2 axis direction.

$$\text{PUR debonding failure} = \left(\frac{S_{22}}{f_{t,22}}\right)^2 + \left(\frac{S_{12}}{f_{v,12}}\right)^2 \geq 1.0 \tag{3.7}$$

where S_{22}, S_{12}, $f_{t,22}$ and $f_{v,12}$ are previously defined in equation 3.6.

$$\text{PUR shear failure} = \frac{S_{12}}{f_{v,12}} \geq 1.0 \tag{3.8}$$

where S_{12} and $f_{v,12}$ are previously defined in equation 3.6.

Most OSB and PUR strengths have been determined from the material property tests as previously presented in the sections 3.3 and 3.4. Since the bending strengths of the OSB had not been determined through tests, they were obtained from BS EN 12369-1. Table 3.25 lists the material strengths of the OSB and PUR.

The mean failure loads, i.e. 8.78 kN found from the experimental investigation, were first applied to the SIP beam FEM model. Tables 3.26 and 3.27 present the maximum stresses obtained from the finite element analysis for OSB and PUR, respectively. At the mean experimental failure load, the upper faces were subjected to bending failure as shown in Figure 3.42. The inner core also failed in debonding and shear as depicted in Figures 3.43 and 3.44.

Material	Strength	Direction	Failure stress (N/mm^2)
OSB	Tension	Parallel to the grain ($f_{t,OSB,11}$)	10.85
	Compression	Parallel to the grain ($f_{c,OSB,11}$)	15.75
	Bending	Parallel to the grain ($f_{b,OSB,11}$)	16.40
PUR	Shear	Transverse ($f_{v,PUR,12}$)	0.116
	Tension	Through thickness ($f_{t,PUR,22}$)	0.188

Table 3.25: Material failure stresses

Further nonlinear analysis was performed in order to determine the loading level that the specimen began to fail. The initial failure load has been found to be 4.48 kN, which is approximately 51% of the experimental ultimate load. The initial damage reveals the bending damage of the OSB was first detected in the specimen and apparently it could further endure further loads until the panel system collapse. This bending failure occurs prior to the debonding and shear failures of the inner core.

Load (kN)	Failure	S_{11} (N/mm^2)	S_{11} / f_{11}	Remark
8.78	Bending	37.35	2.28	Fail
4.48		16.14	0.98	Pass

where f_{11} is bending failure stress, equal to 16.40 N/mm^2.

Table 3.26: Numerical analysis on OSB outer faces

Load (kN)	Failure	S_{22} (N/mm^2)	S_{12} (N/mm^2)	$S_{22} / f_{22} + S_{12} / f_{12}$	$(S_{22} / f_{22})^2 + (S_{12} / f_{12})^2$	Remark
8.78	Debonding	0.347	0.102	2.72	4.18	Fail
	Shear	-	0.188	-	-	Fail
4.50	Debonding	0.130	0.039	0.99	0.59	Pass
5.42	Shear	-	0.116	-	-	Pass

where f_{22}, and f_{12} are failure stresses, equal to 0.188 N/mm^2 and 0.116 N/mm^2, respectively.

Table 3.27: Numerical analysis on PUR

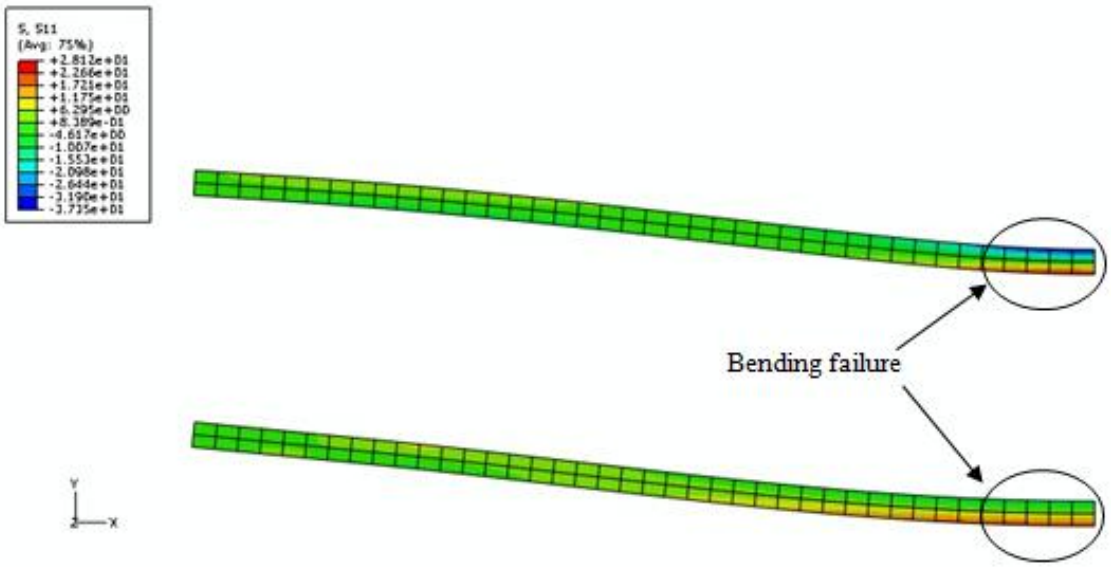

Figure 3.42: Distribution of the longitudinal stress (S_{11}) of the outer faces

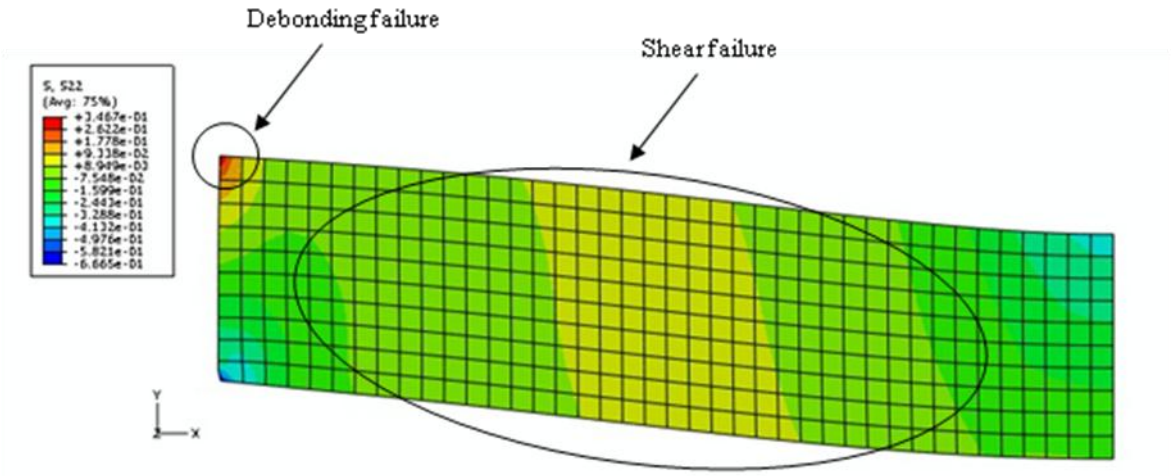

Figure 3.43: Distribution of the shear stress (S_{22}) of the PUR inner core

Figure 3.45 shows the applied load and deflection curves comparison between the FEM and the mean test results. It should be noted that the current FEM study is unable to precisely predict the post-initial damage behaviour i.e. the structural behaviour beyond the initial damage. Consequently, the deflection after the initial damage (as shown in Figure 3.45) may be unrealistic and is presented as a dash-line.

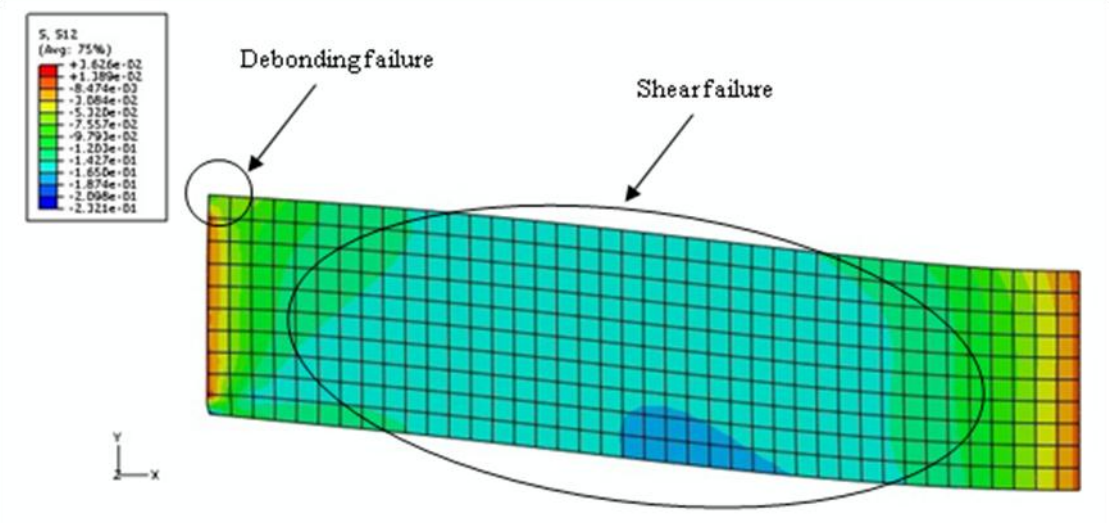

Figure 3.44: Distribution of the shear stress (S_{12}) of the PUR inner core

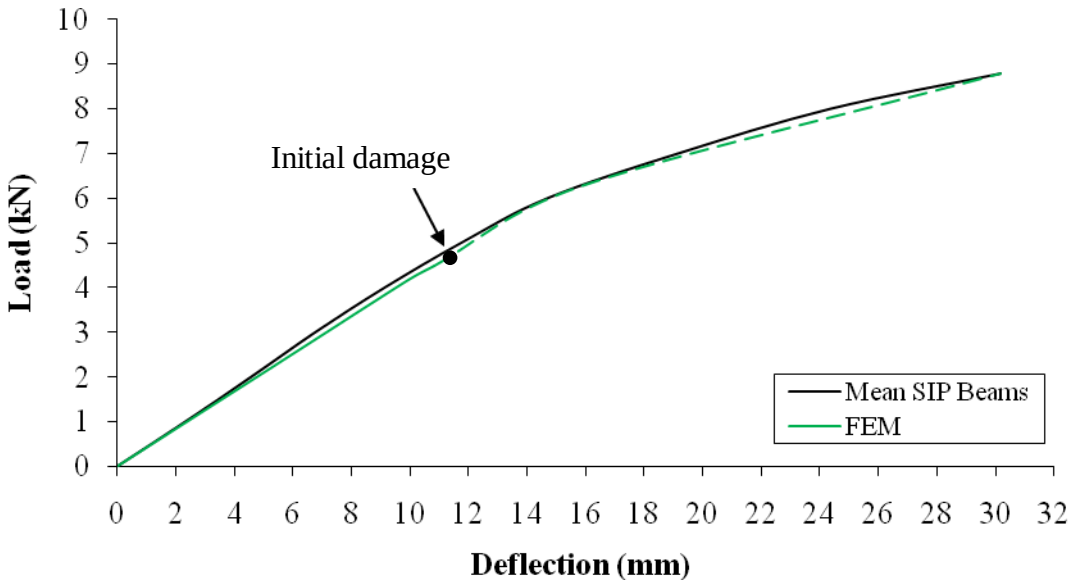

Figure 3.45: Deflection comparison between the FEM and the mean test results

In order to obtain the realistic structural behaviour after the initial damage, further work can be undertaken by considering the post-damage behaviour to track the damage evolution process that eventually leads to ultimate failure.

3.7 Summary

This Chapter presented the research methodology and various experimental investigations to determine the mechanical properties of SIP constituents. It has been found that the deflection of SIP beam is very shear sensitive and the numerical investigation with the PUR material properties obtained from the single or double shear test does not agree well with the SIP beam test results.

Further numerical investigation was undertaken and found in a good agreement with the SIP beam test results when the shear modulus equals to 2.3 N/mm^2 together with perfectly plastic bi-linear stress-strain model of the initial yield stress equals to 0.2 N/mm^2 followed by the stress of 0.3 N/mm^2 at the plastic strain of 0.033. These parameters will be later used and found in a good agreement with SIPs as panels which will be presented in the next Chapter.

The initial failure mode, which is obtained from the numerical investigation, can be used to predict the ultimate failure mode of SIP as a beam. Furthermore, it can be also used to predict as a panel that will be presented in more details in the next Chapter.

CHAPTER FOUR

SIPS UNDER SINGLE LOADINGS

4.1 Introduction

In review literature, there is still insufficient data for structural performance of SIPs with different joint designs. A series of experimental, analytical and numerical investigations on the structural behaviour of SIPs with different joint designs and openings are presented in this Chapter. The investigation begins with different joint constructions and subjected to a four-point bending test as in the floor or roof condition. It has been found that those panel samples jointed by the dimensional timber spline connections (SDC) are the stiffest and can offer highest load capacity, whereas these jointed by the mini-SIP connections (SMC) exhibit almost identical stiffness and failure loads to the typical panels without joints. The structural behaviour of SIPs under single (transverse, axial and racking) as wall condition was later investigated and presented.

4.2 Experimental investigations on SIPs with different joint constructions

Like-for-like comparison of structural performance of SIPs with different joint constructions is lacking in the published literature. The first experiment in this study investigates SIPs with different joint constructions subjected to four-point bending loading. As previously described in Chapter 2, there are three typical panel-to-panel joints, including OSB thin spline, foam block spline (or referred to as mini-SIP spline) and dimensional timber spline. Nevertheless, in this research, the OSB thin spline was not included due to the fabrication difficulty in engineering practice in comparison with other two connection types. Moreover, it is envisaged that SIPs

with the OSB thin spline joint should exhibit similar structural performance to SIPs with the mini-SIP spline joint. The aims of this study are as follows:

- To study the impact of joint construction on the behaviour of SIPs in term of strength and stiffness.

- To determine failure modes and governing factors in the design of SIPs with different joint designs.

- To compare the experimental results with the analytical and numerical ones to establish methods which are appropriate and agree well with the experimental results.

Prior to ISO 22452 (ISO, 2011), British and European standards were not available for testing SIPs. Four-point bending test recommended by BS EN 14509 (BSI, 2006), which is a product specification standard for sandwich panels, was found suitable and hence employed. Figure 4.1 illustrates the four-point bending test details. The loads were applied at suitable increments and the displacements were recorded until failure.

4.2.1 SIP specimens

Six SIP specimens of three groups, i.e. two typical panels without connections (STP-1 and 2), two panels with mini-SIP connections (SMC-1 and 2) and two panels with dimensional timber spline connections (SDC-1 and 2), were subjected to four-point bending test until failure. All test panel specimens are 600 mm x 1200 mm and supplied by SIP Build Ltd. The selection of sample size has been deemed to be economic and still be able to supply adequate results to fulfil the designated purpose. For instance, conclusions on the impact of joints can be equally drawn through these half-size scaled samples, and the results may adequately serve as the benchmark of the numerical modelling.

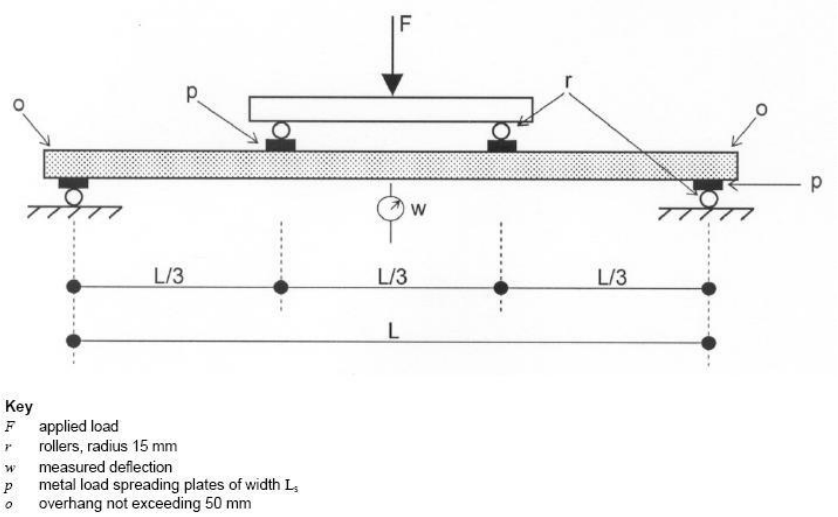

Figure 4.1: Four-point bending test (BS EN 14509, 2006)

The first group of panel specimens, as shown in Figure 4.2, comprises two duplicated single standard panels i.e. STP-1 and STP-2. They were approximately 600 mm wide by 1200 mm long with 11 mm OSB/3 facings and a 103 mm polyurethane inner core (overall thickness of 125 mm). Both short edges of the panels were inserted with C16 timber sections of 47 x 103 mm fastened by 2.8 mm diameter and 63 mm long nails at an interval of 150 mm, and also glued to the OSB faces and the PUR core. Both long edges of the specimens were not inserted with any timber sections and are left with 50 x 103 mm edge recesses, which represent a typical standard panel without any joints. In addition to the edge recesses, the inner core failure mode would be clearly visible rather than was blocked by the installation of the long edge timber blocks.

The second group of panel specimens comprises two panels (SMC-1 and SMC-2). All configurations were as same as the first group except there were 100 mm mini-SIP joints in the middle of the panels as shown in Figure 4.3.

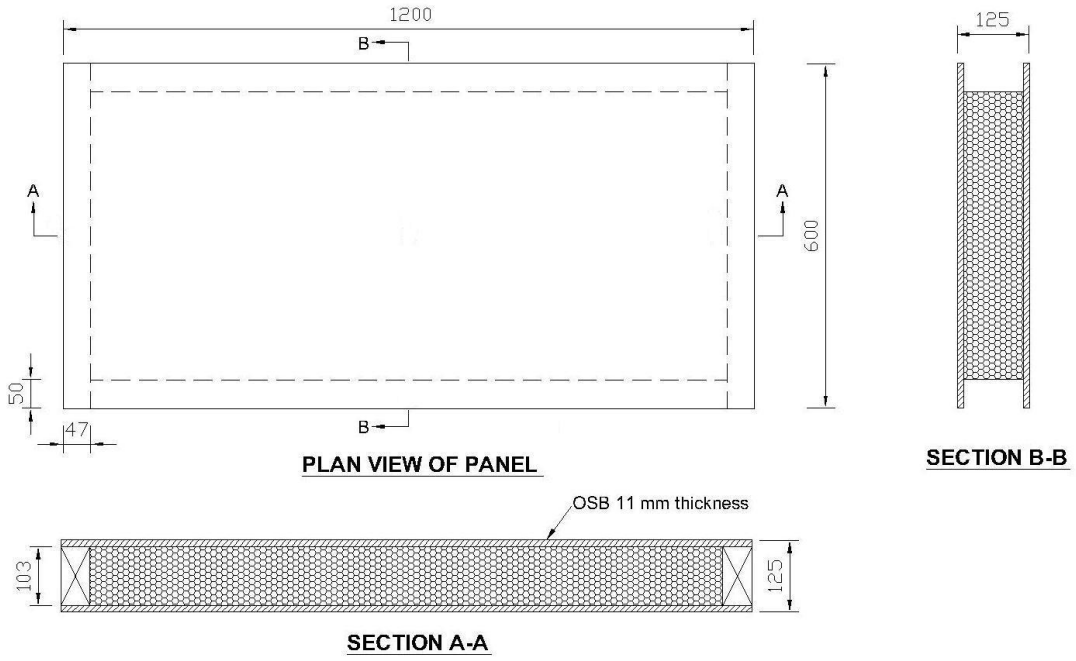

Figure 4.2: STP specimen details

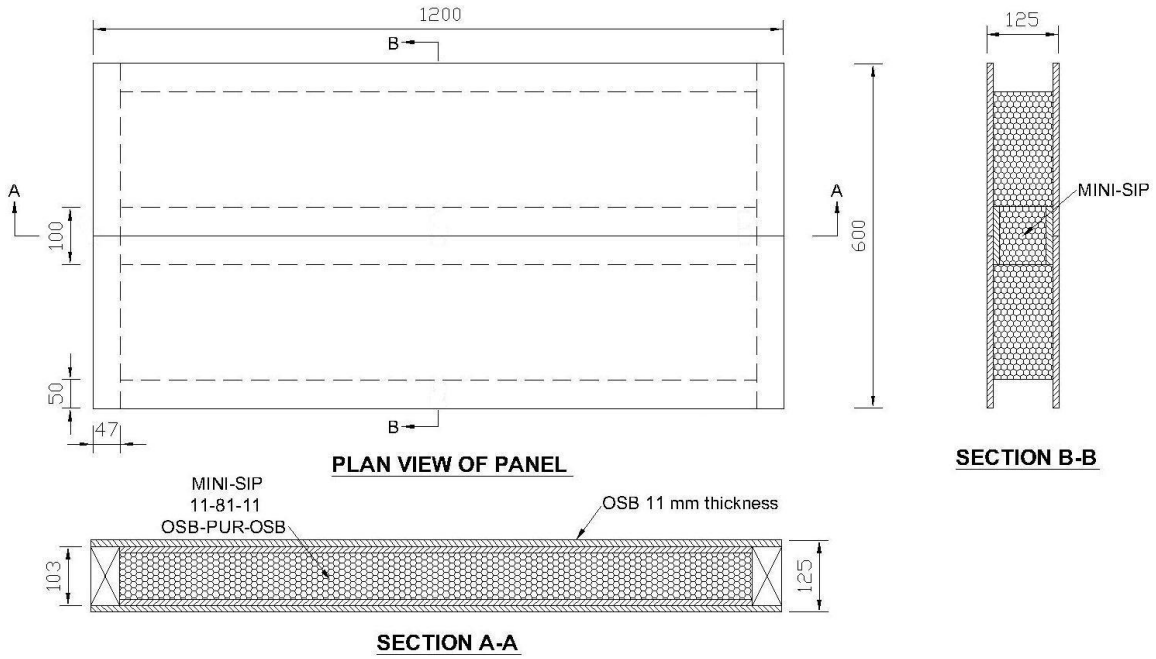

Figure 4.3: SMC specimen details

The third group of panel specimens also comprises two panels (SDC-1 and SDC-2). All configurations were as same as both former groups except there were 47 mm C16 dimensional timber joints in the middle of the panels as shown in Figure 4.4.

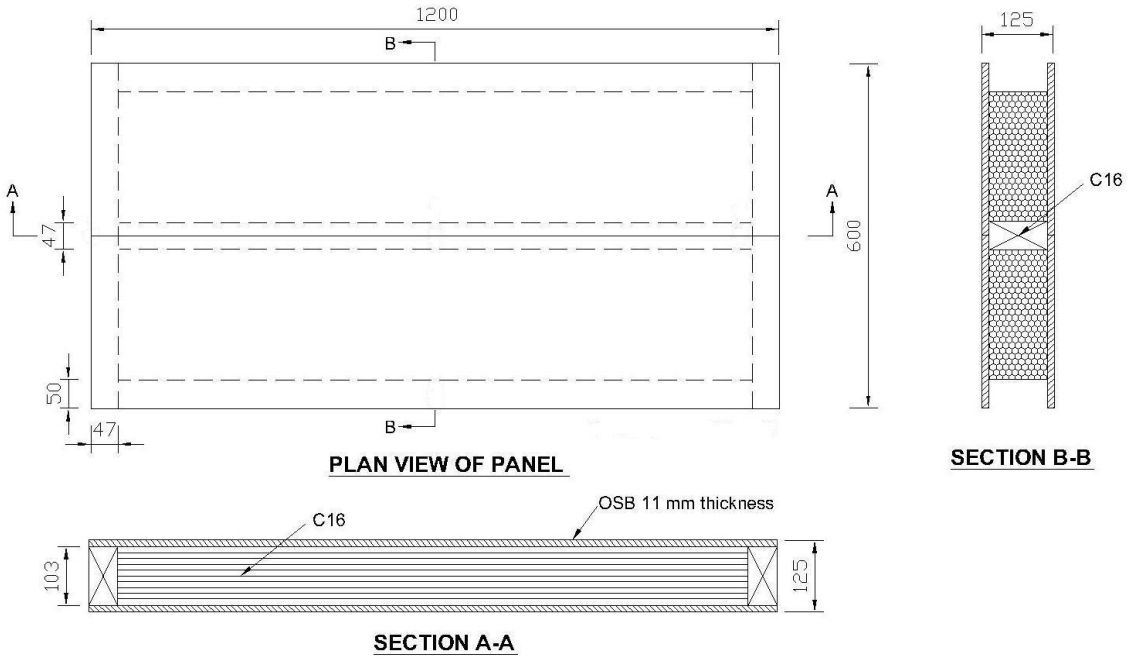

Figure 4.4: SDC specimen details

4.2.2 Experimental apparatus

The four steel load spreading plates used in this experimental test were 100 mm wide by 600 mm long and 10 mm thick, together with four steel rollers of 30 mm diameter. Two steel rollers (free to move horizontally) were supported on two equal height I-beam steels. Afterwards, the panel was positioned on both steel plates with flush outer edges. Then, two other steel plates together with two steel rollers were positioned on the test panel as two loading lines. They were set to divide the span into three equal parts of approximately 367 mm each.

As the Mand Testing Machine could not reach the top of two steel rollers, three I-beam steel sections together with a half roller were then placed on top of the rollers. Consequently, the initial applied load from the weight of these three I-beams and the half roller was 0.32 kN. Figure 4.5 shows the layout of experimental apparatus for this test and the sign convention of displacement.

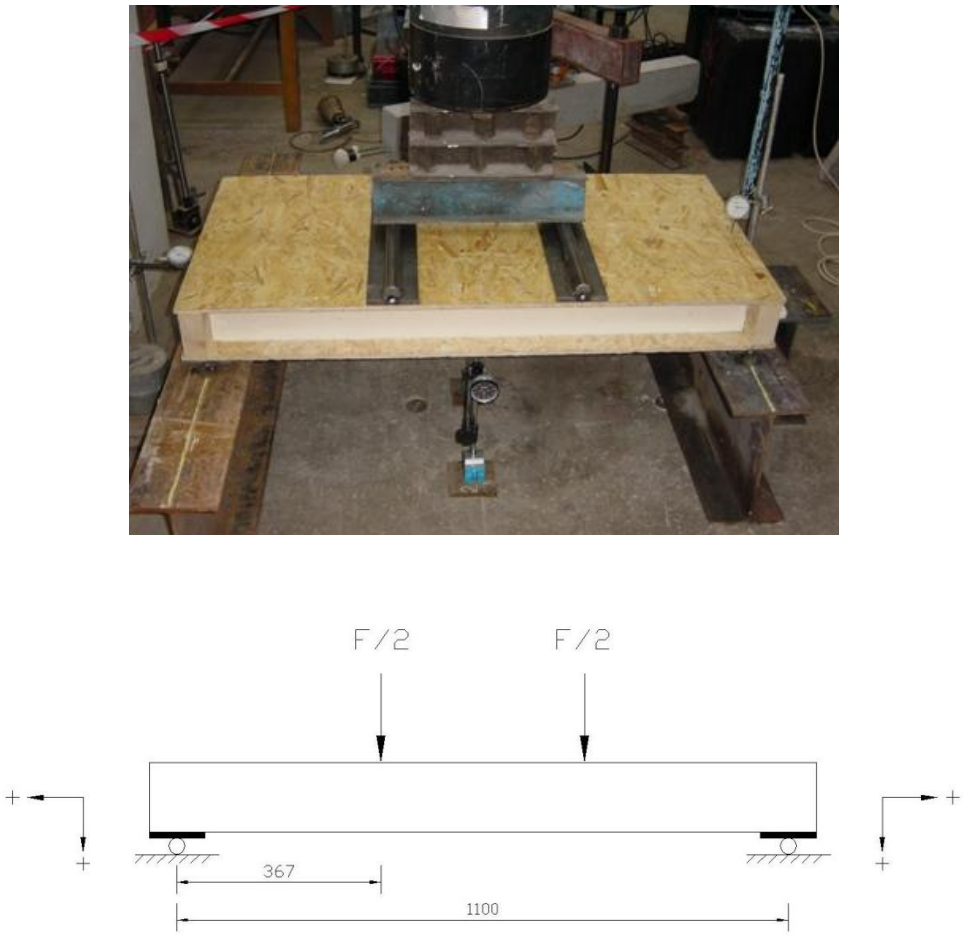

Figure 4.5: Experimental apparatus and sign convention of displacement

Four dial gauges were positioned at the following locations in order to measure the vertical and horizontal displacements as shown in Figure 4.6:

- Dial Gauge No.1 was positioned at mid-length and mid-width (central) of the panel for measuring the vertical displacement at the central span.

- Dial Gauge No.2 was positioned at mid-length and approximately at 10 mm from the edge of the panel for measuring the vertical displacement at the mid-span.

- Dial Gauge No.3 was positioned at approximately 60 mm from the edge of the panel for measuring the vertical displacement near the support.

- Dial Gauge No.4 was positioned at the edge of the panel for measuring the horizontal displacement at the panel edge.

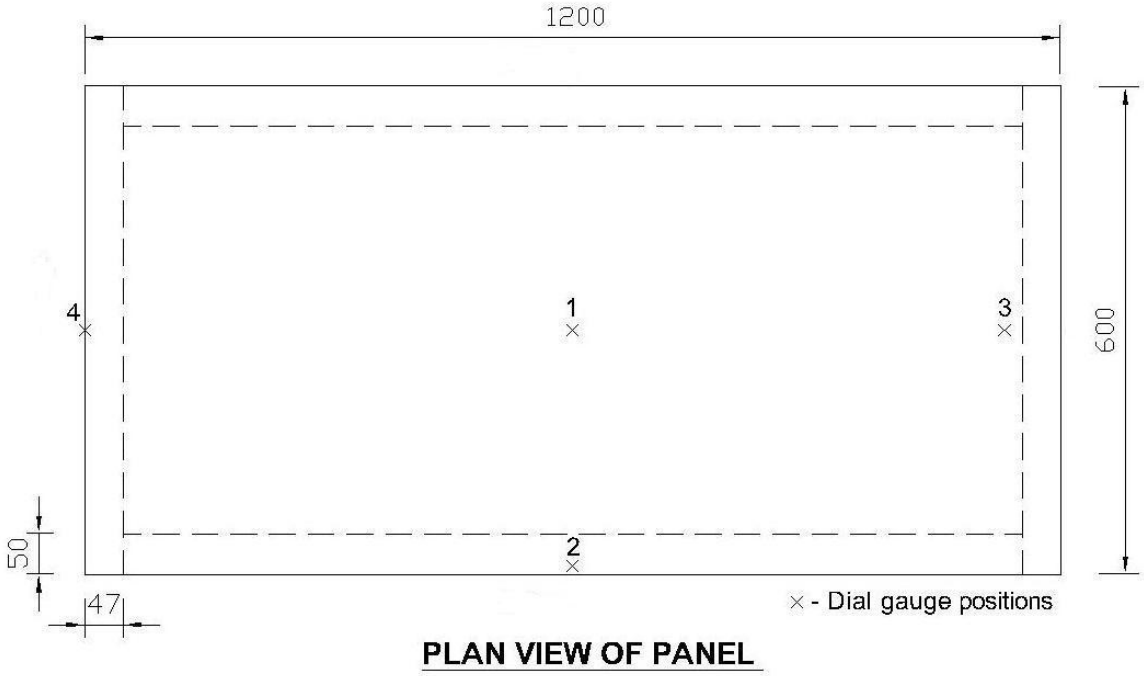

Figure 4.6: Dial gauge arrangement for the tests

The loads were applied at suitable increments and the displacements were recorded until one of the failure modes was occurred. The expected failure modes were face bending, core shear and debonding.

4.2.3 Experimental investigation

The applied loads and the displacements recorded at each dial gauge of all specimens subjected to four bending tests are presented in Figures 4.7 - 4.11.

As previously detailed in Chapter 3.6, the limiting deflection value has also been chosen to be $\ell/333$ (3.30 mm) for this experimental study. Further investigation in Figure 4.7 indicates that the serviceability limit loads (SLL) at the deflection limit (3.30 mm deflection) are found to be

approximately at 2.87 kN (for STP), 3.06 kN (for SMC) and 7.98 kN (for SDC), whereas the mean ultimate limit loads (ULL) at failure are 19.32 kN, 19.82 kN and 40.32 kN, respectively. It should be noted that the deflection of the panel becomes the limiting factor of the loading capacity. The SLLs are approximately 15% (for both STP and SMC) and 20% (for SDC) of the ULLs.

Figure 4.7(d) shows the applied loads and the mean central displacements of all three groups of the panels (Dial Gauge No. 1). As expected, SDC panels (jointed by the dimensional timber spline connections) are the stiffest which offer the highest load capacity, whereas the SMC panels (jointed by the mini-SIP connections) exhibit almost identical stiffness and failure loads to the STP panels.

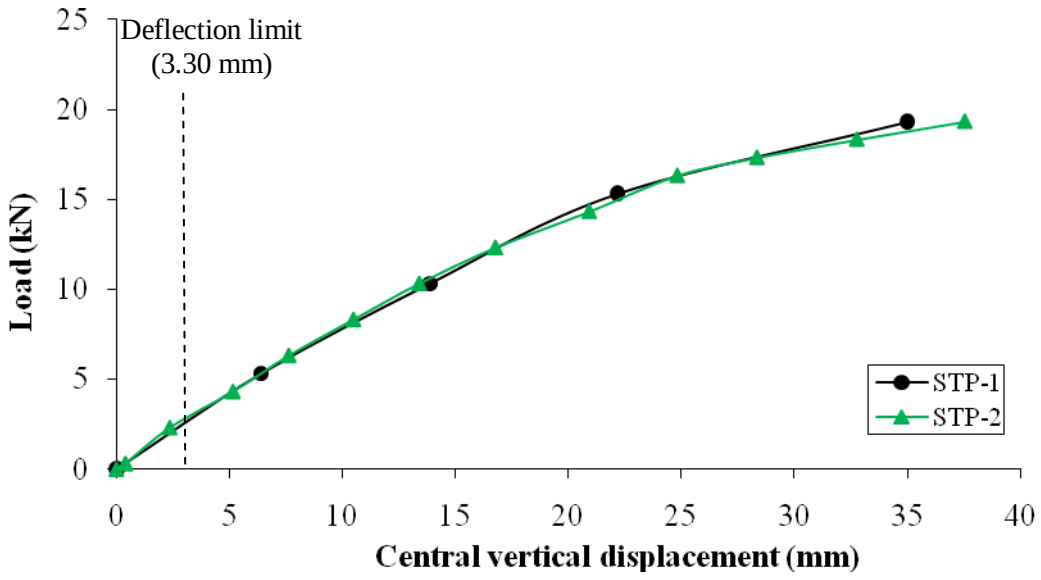

(a) STP

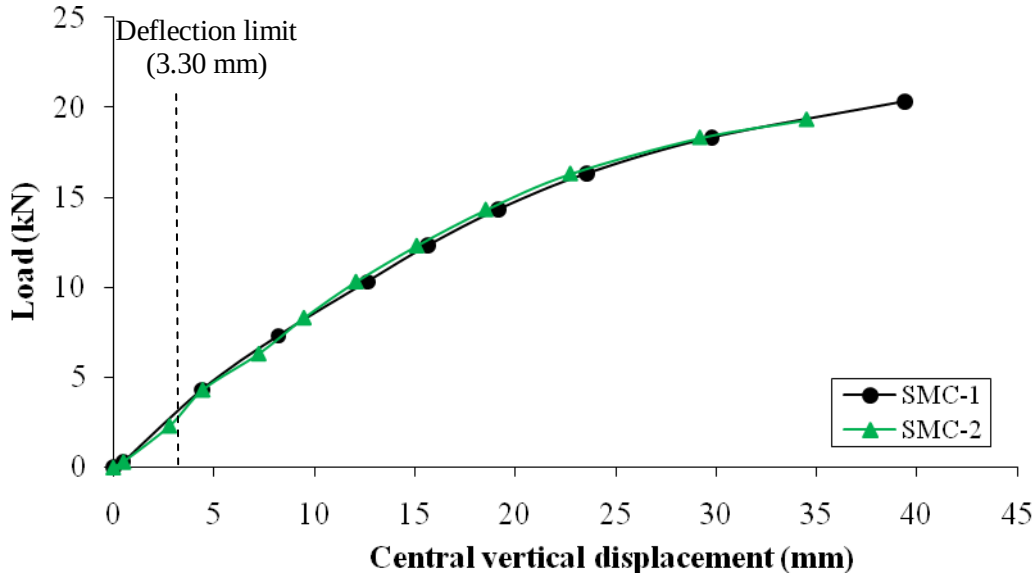
Deflection limit
(3.30 mm)
Load (kN)
Central vertical displacement (mm)
SMC-1
SMC-2

(b) SMC

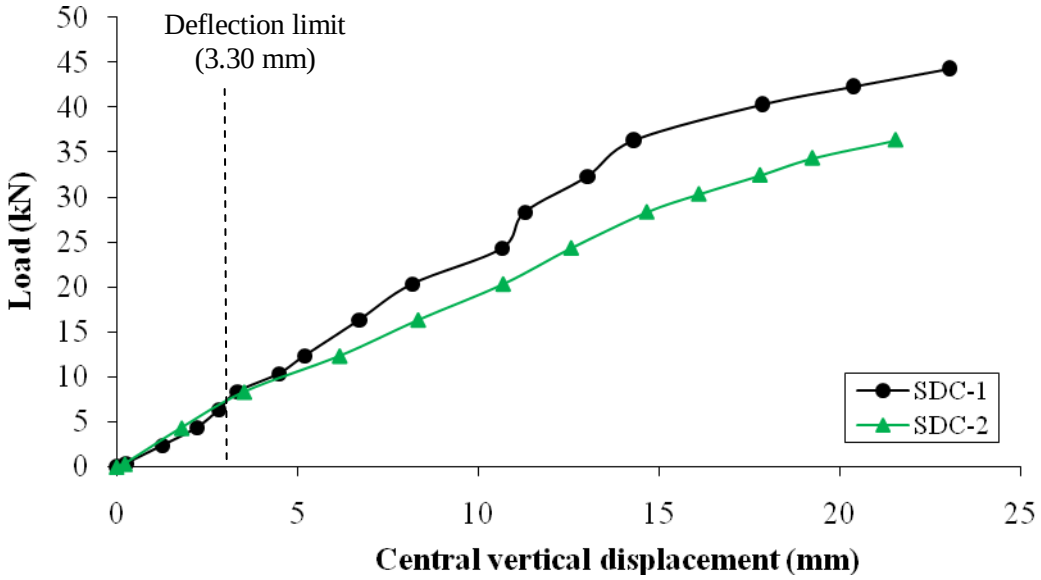
Deflection limit
(3.30 mm)
Load (kN)
Central vertical displacement (mm)
SDC-1
SDC-2

(c) SDC

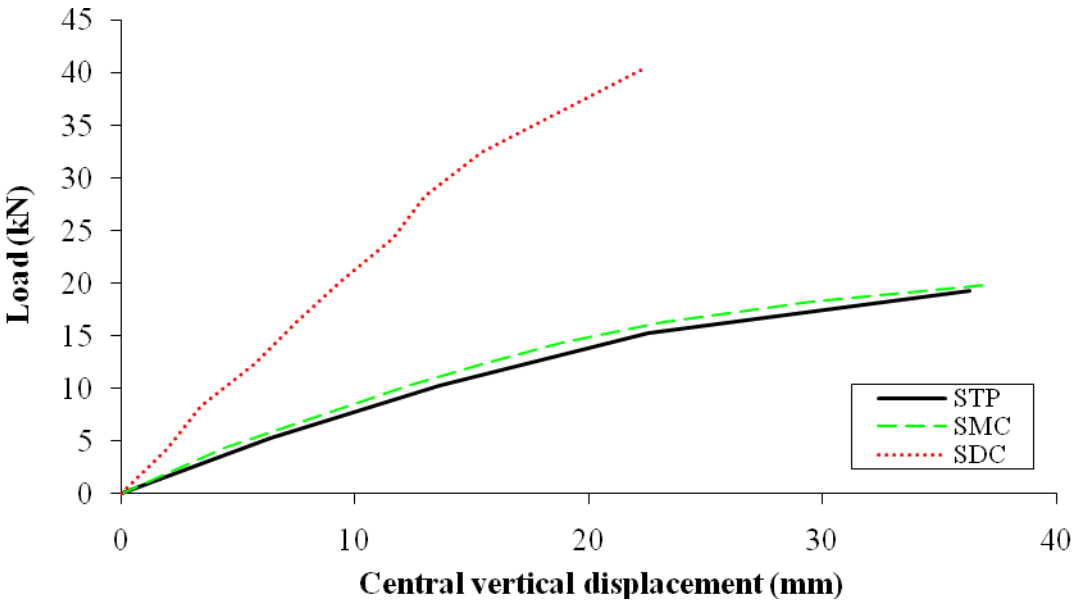

(d) Mean central displacements of all group panels

Figure 4.7: Central vertical displacement at the mid-span (Dial Gauge No.1)

Figure 4.8 shows the applied loads and the vertical edge displacements at the mid-span of panels recorded at the Dial Gauge No.2. These test results are typically found in the same trend with those obtained from the Dial Gauge No.1 as illustrated in Figure 4.9.

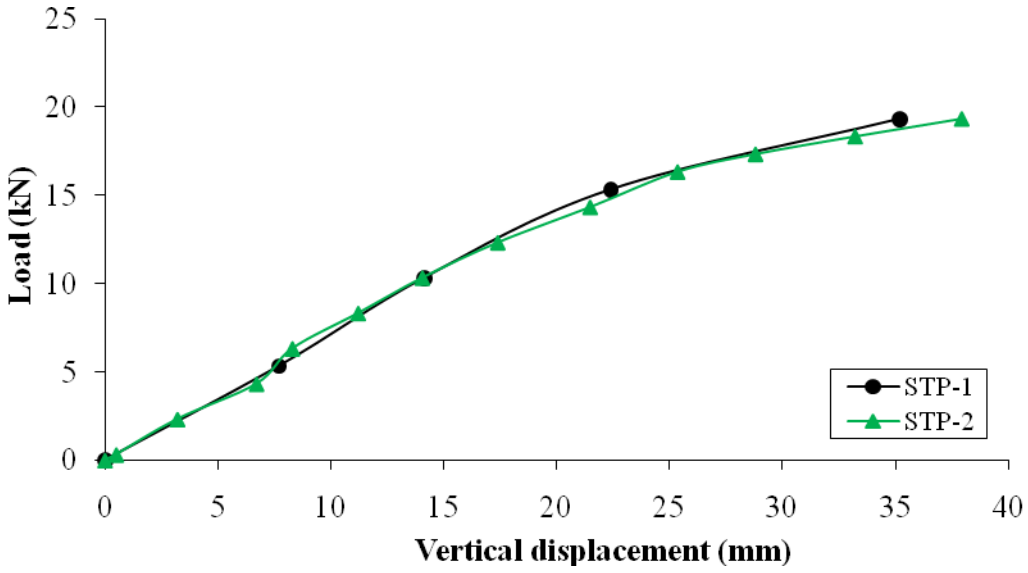

(a) STP

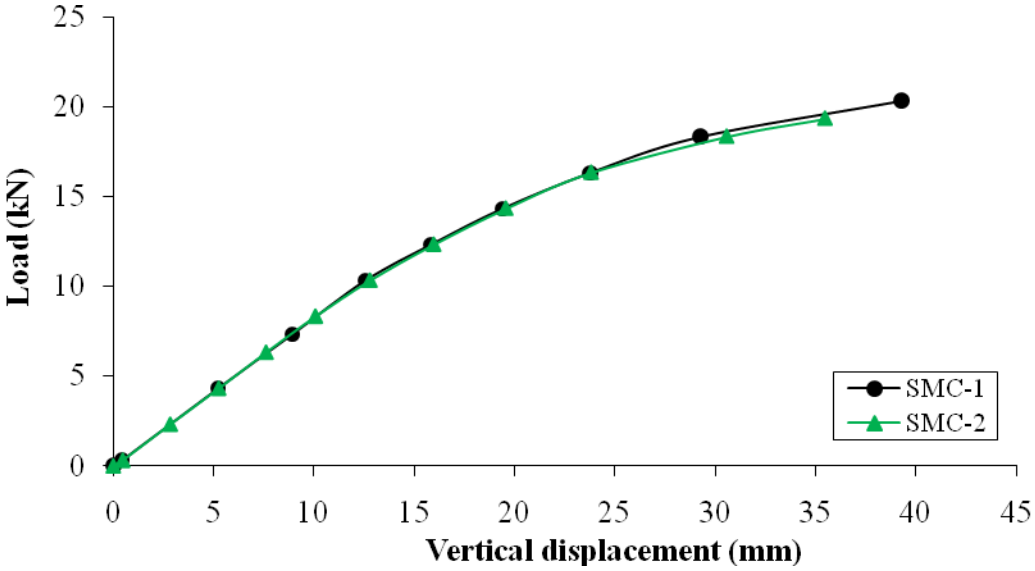

(b) SMC

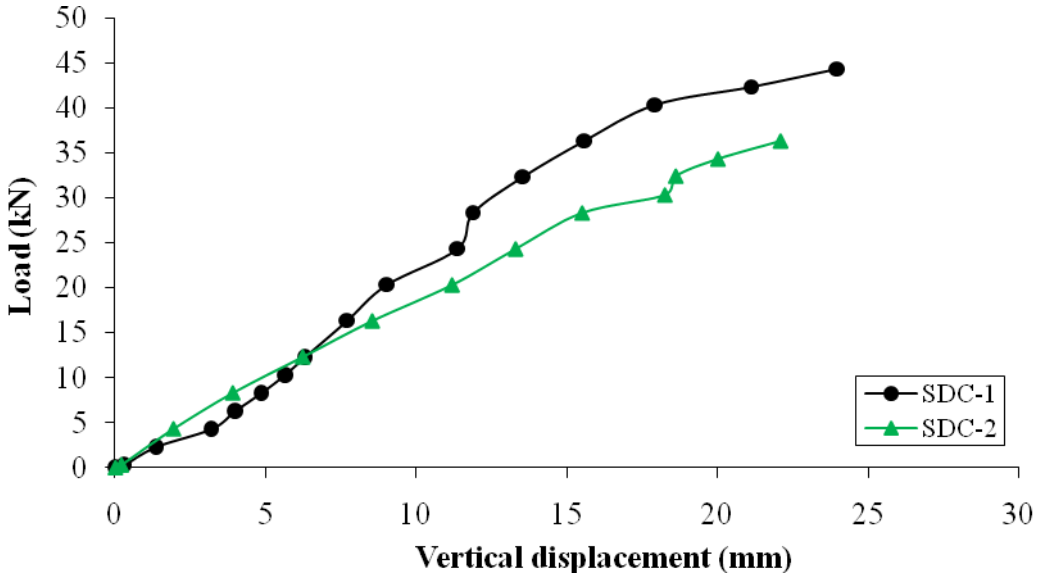

(c) SDC

Figure 4.8: Vertical displacement at the mid-span (Dial Gauge No.2)

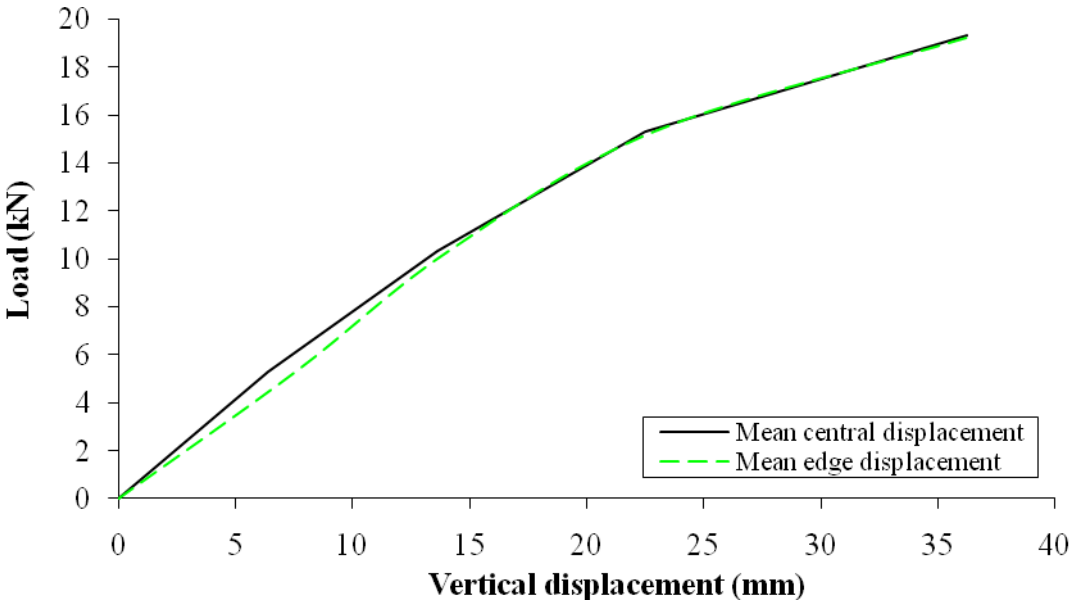

Figure 4.9: Typical mean vertical displacements at Dial Gauges No.1 and 2

Figure 4.10 shows the applied loads and the vertical displacements of tested panels recorded at the Dial Gauge No.3. The maximum vertical displacement is 2.01 mm (from SDC-1), this is approximately 11% of the central displacement (23.05 mm from SDC-1). This is as expected that the timber blocks at both header and footer supports retained the height of the core space and did not cause any significant bearing deformation at the support.

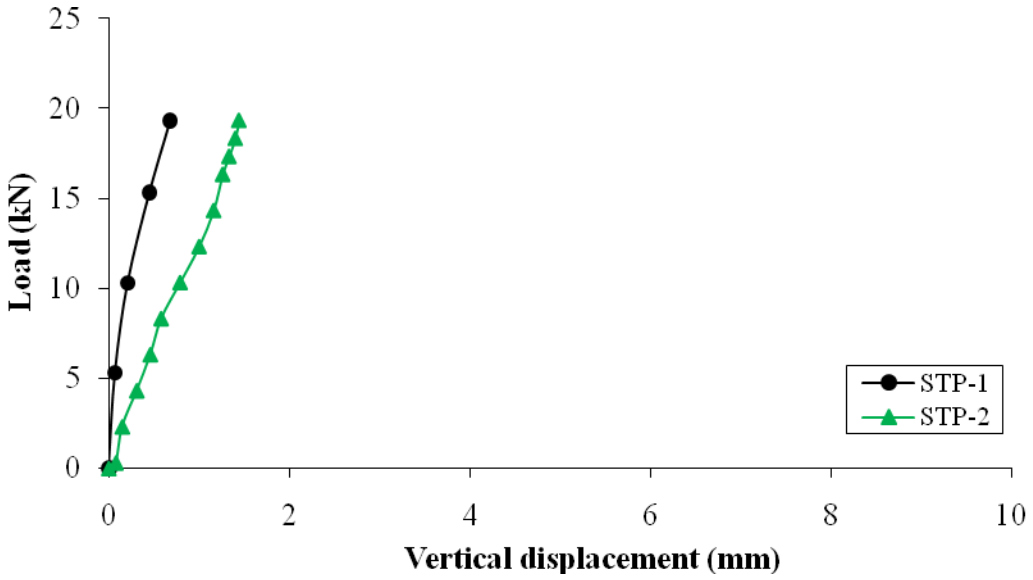

(a) STP

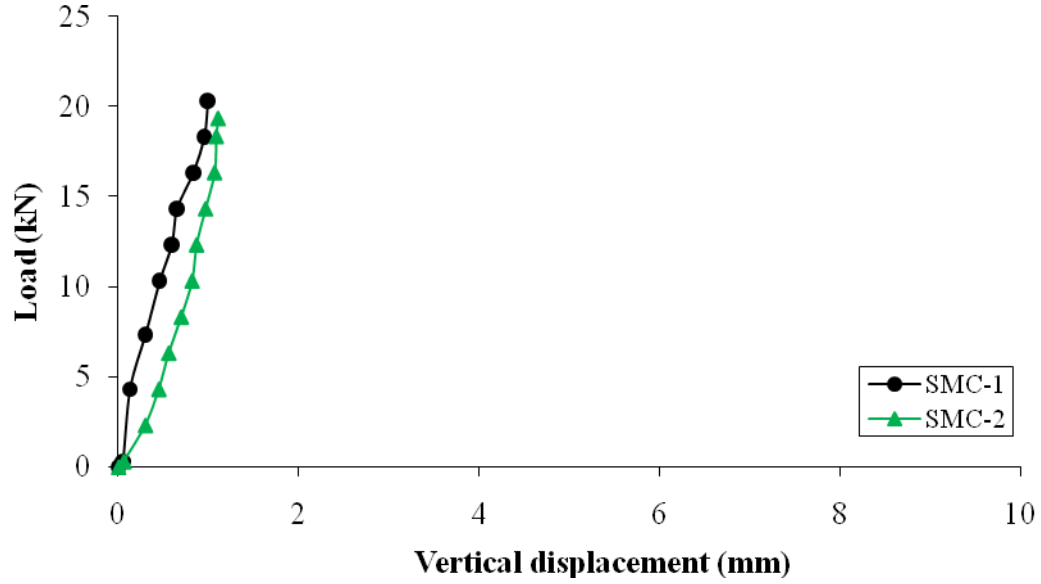

(b) SMC

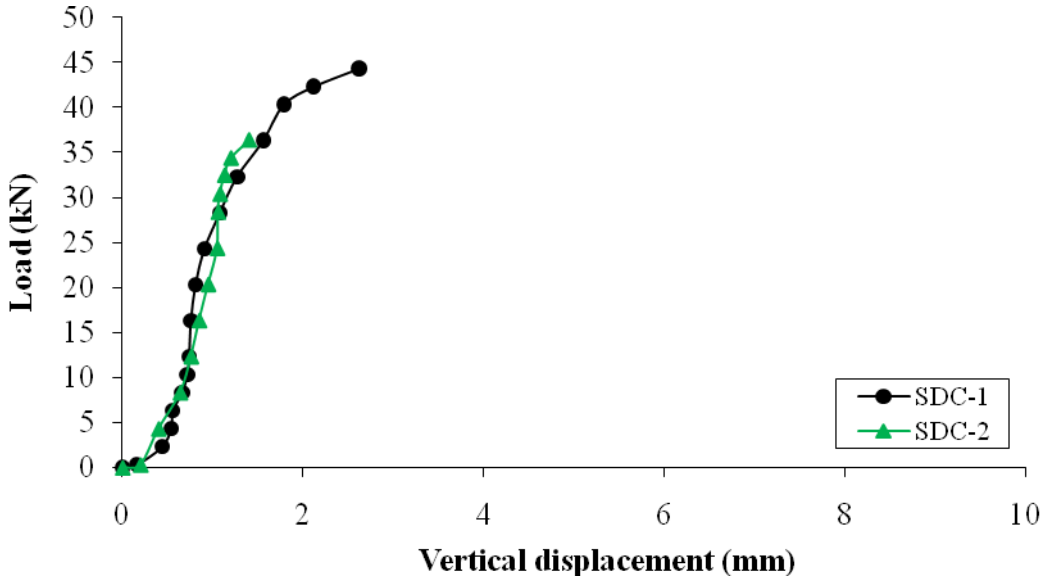

(c) SDC

Figure 4.10: Vertical displacement at the edge (Dial Gauge No.3)

The loads and the horizontal displacements of panel specimens recorded at the Dial Gauge No.4 are presented in Figure 4.11. In comparison to the displacement at the central span, the horizontal displacement is small. This is because the high shear deformation rendering the top of the header/footer to move outwards.

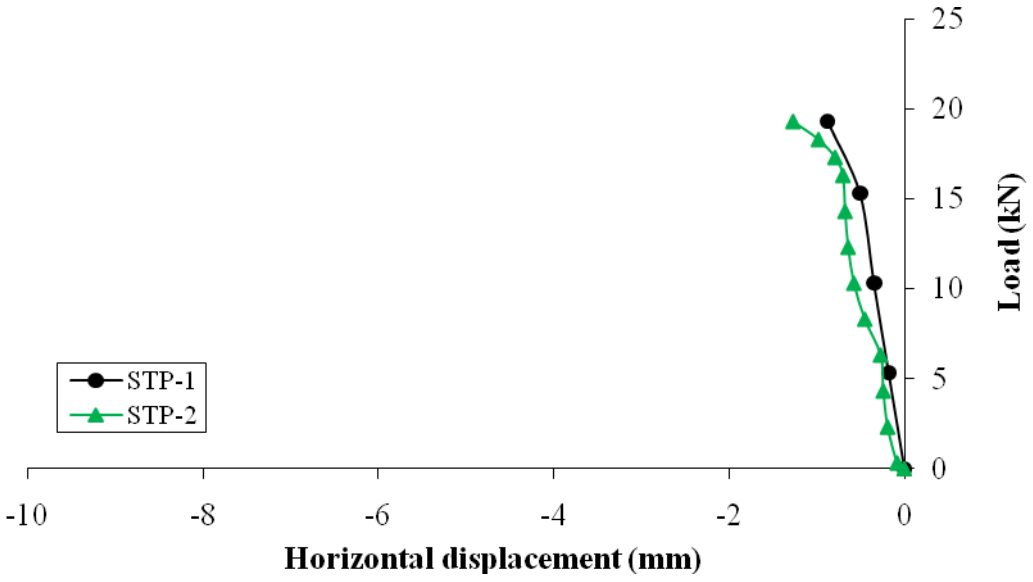
25
20
15
10
5
0
Load (kN)
STP-1
STP-2
-10
-8
-6
-4
-2
0
Horizontal displacement (mm)

(a) STP

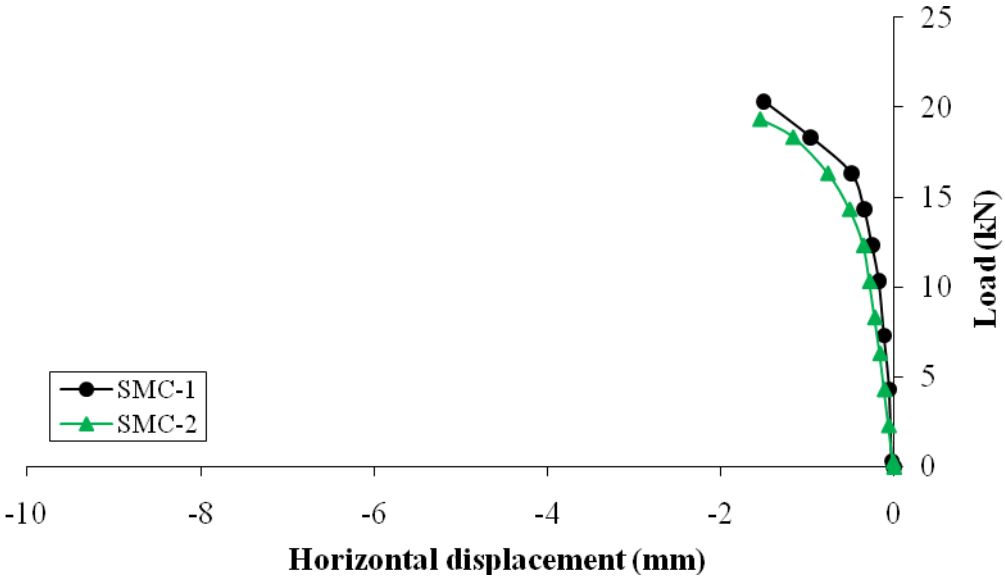
25
20
15
10
5
0
Load (kN)
SMC-1
SMC-2
-10
-8
-6
-4
-2
0
Horizontal displacement (mm)

(b) SMC

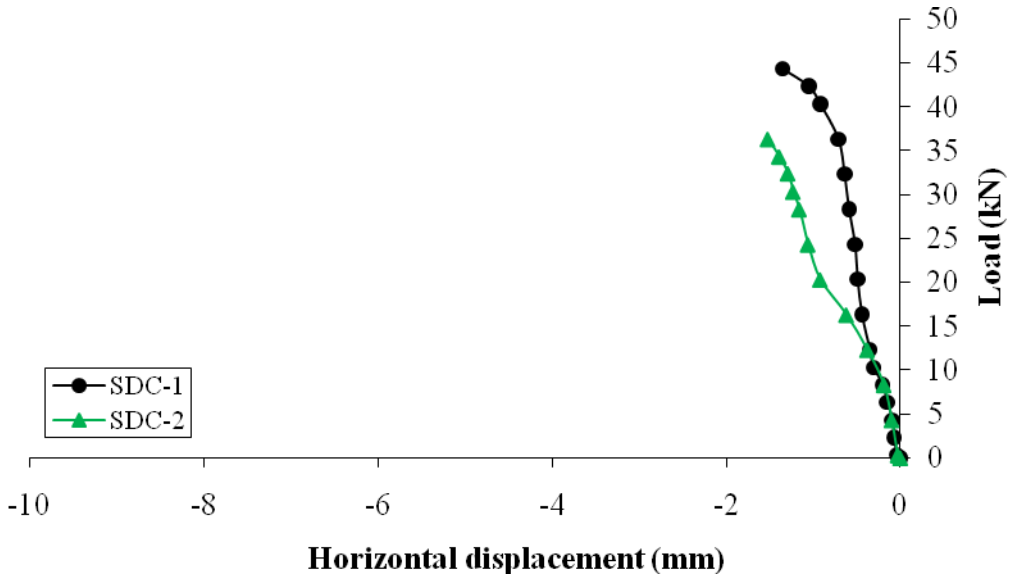

(c) SDC

Figure 4.11: Horizontal displacement at the edge (Dial Gauge No. 4)

Figure 4.12 presents the failure modes of all specimens. Although the applied loads at failure are found identical, the failure modes of STP panels are different. The failure mode of STP-1 is a typical shear failure in the core material as shown in Figure 4.12(a), whereas the failure mode of STP-2 is due to the debonding of the edge header/footer from the core as illustrated in Figure 4.12(b). The first failure mode is attributed to the high shear force in the core material near the edge and is therefore classified as shear failure, and whereas the second one is due to the outward of the header/footer. Both failure modes are associated with high shear deformation that the tested panels have experienced.

The failure modes of both SMC-1 and SMC-2 are found to be both inner cores debonded from the top outer faces and the timber sections as illustrated in Figures 4.12(c) and (d).

Both SDC-1 and SDC-2 failure modes are due to the cracking of the bottom outer face and inner core shear as shown in Figures 4.12(e) and (f). The cracking direction and location indict that this failure is due to the combined action of flexure and shear.

Table 4.1 summarises the experimental results of the three types of panel specimens. It should be noted that the deflection of the panel becomes the governing factor of the loading capacity as previously demonstrated. As can be seen from Table 4.1, SDC panels (jointed by the dimensional timber spline connections) are the stiffest which offers highest load capacity, whereas the SMC panels (jointed by the mini-SIP connections) exhibit almost identical stiffness and failure loads. The ULL of SDC has been found 109% higher than STP. This observation reveals that the mini-SIP joint has negligible impact on the structural performance of SIPs whereas the dimensional timber spline joint has significant impact. To increase the structural efficiency, the dimensional timber spline joint is preferred. However, it has been reported that more thermal break can occur at this joint and also more expensive than the mini-SIP joint.

(a) STP-1 shear failure

(b) STP-2 debonding failure

(c) SMC-1 debonding failure

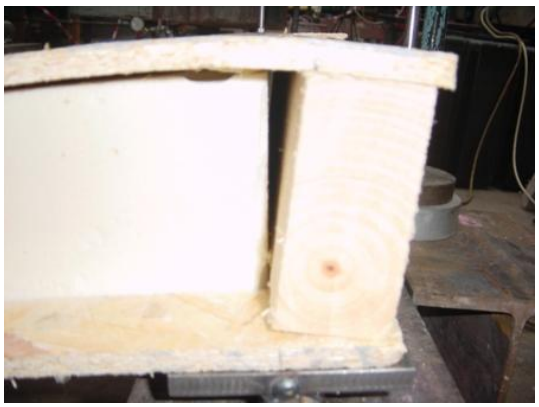

(d) SMC-2 debonding failure

(e) SDC-1 flexural-shear failure

(f) SDC-2 flexural-shear failure

Figure 4.12: Failure modes of panels subjected to four-point bending loads

Specimen	STP	SMC	SDC
Ultimate Limit Load, ULL (kN)	19.32	19.82	40.32
Increase of ULL (%)	0	2.59	108.70
Load at deflection limit ℓ/333 (kN)	2.87	3.06	7.98
Serviceability load / Ultimate load (%)	14.9	15.4	19.8
Maximum central displacement (mm)	36.25	36.96	22.30
Maximum edge displacement (mm)	36.56	37.39	23.03
Maximum vertical displacement at edge (mm)	1.06	1.05	2.01
Maximum horizontal displacement (mm)	1.08	1.52	1.44
Experimental failure mode	Debonding	Debonding	Flexure-Shear

Table 4.1: Experimental result summary

4.2.4 Analytical investigation

As one of the tests was carried out on the typical panels without any connections, the central span deflection can be predicted by using the classical sandwich panel theory by various authors as previously presented in Chapter 2. This section will focus on the analytical methods provided by Allen (1969), TR 019 (EOTA, 2005) and BS EN 14509 (BSI, 2006). Table 4.2 presents the analytical equations to determine the central displacement.

The panel details and material properties (presented in Chapter 3) are reproduced and listed in Table 4.3. Figure 4.13 illustrates the comparison between the mean test result with the three analytical methods. Although the analytical results from TR 019 and BS EN 14509 yield similar results, they are overestimate and less agreement in comparison with the Allen's method. The difference between Allen's method and both TR 019 and BS EN 14509 is due to the lower shear deflection. The shear deflection is determined using the depth between the centroids of the outer faces (e) in Allen's method. In contrast, TR 019 and BS EN 14509 methods use the depth of the core material (d_c). Since the outer face thickness in this case is 11 mm, the e value is therefore 1.11 times higher than d_c value. As a result, the shear deflection is thus reduced by 22.5% in this analysis. The detailed calculation using Allen's method is shown in Appendix A.

Allen's method	TR 019	BS EN 14509
$\Delta w = \frac{23FL^3}{648D} + \frac{FL}{3BeG}$	$\Delta w = \frac{23FL^3}{648B_s} + \frac{FL}{3Bd_cG}$	

where F is the applied load;

L is the span length;

D is the sum of flexural rigidity, $E_F \frac{Bf^3}{6} + E_F \frac{Bfe^2}{2} + E_c \frac{Bd_c^3}{12}$;

E_F is the E-modulus of the faces;

E_c is the E-modulus of the core;

f is the face thickness;

B is the measured width of the specimen;

G is the shear modulus;

e is the measured depth between the centroids of the faces;

B_s is the flexural rigidity (BS EN 14509), equals to $\frac{E_{F1} \cdot A_{F1} \cdot E_{F2} \cdot A_{F2}}{E_{F1} \cdot A_{F1} + E_{F2} \cdot A_{F2}} e^2$;

E_{F1} is the E-modulus of the top face;

A_{F1} is the measured area of cross-section of the top face;

E_{F2} is the E-modulus of the bottom face;

A_{F2} is the measured area of cross-section of the bottom face.

B_s is the flexural rigidity (TR 019), equals to $B_{F1} + B_{F2} + \frac{E_{F1} \cdot A_{F1} \cdot E_{F2} \cdot A_{F2}}{E_{F1} \cdot A_{F1} + E_{F2} \cdot A_{F2}} e^2$;

B_{F1} is the bending stiffness of the top face, equals to $E_{F1} \frac{Bf^3}{12}$;

B_{F2} is the bending stiffness of the bottom face, equals to $E_{F2} \frac{Bf^3}{12}$;

d_c is the depth of the core material.

Table 4.2: Analytical equations to determine the central displacement

F (kN)	19.32
B (mm)	500
L (mm)	1,100
f (mm)	11
d_c (mm)	103
e (mm)	114
$E_{F1} = E_{F2}$ (N/mm^2)	3,844
E_c (N/mm^2)	6.442
G (N/mm^2)	2.30

Table 4.3: STP details and material properties

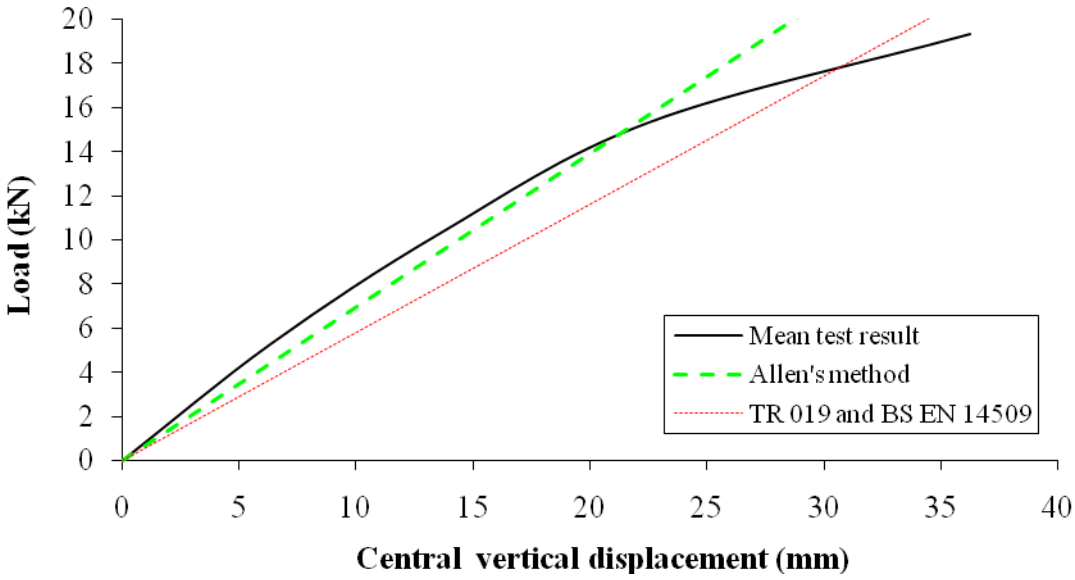

Figure 4.13: Comparison between the mean STP test result with different methods

For a four-point bending load using the classical sandwich panel theory, the applied tensile and compressive stresses in the outer faces can be determined by using the modified equation 2.6 as given in equation 4.1.

$$S = \frac{FLe}{12D} E_F \tag{4.1}$$

With the applied load of 19.32 kN, the applied tensile and compressive stresses in the outer faces are 5.62 N/mm^2, which are less than 10.85 N/mm^2 (tensile strength) and 15.75 N/mm^2 (compressive strength). No tensile and compressive failures of the outer faces occur.

Similarly for the four-point bending load, the shear stress (τ) in the inner core can be obtained by using equation 4.2.

$$\tau = \frac{F}{2Be} \tag{4.2}$$

With the applied load of 19.32 kN, the applied shear stress is 0.188 N/mm^2, which is higher than 0.116 N/mm^2 shear strength. These panels would fail due to shear by this theory. The allowable applied load of 12 kN is adequate for the inner core that will not fail due to shear. This is approximately 22% less than the allowable applied load of 15.3 kN determined by the numerical investigation, which will be presented in the next section.

For SDC panels, TR 019 and EC5 (BS EN 1995-1-1, BSI 2004) present the methods to calculate the central span deflection with C16 joints. Both methods deal with the determination of the effective flange width of the top and bottom outer faces. EC5 provides the maximum values to determine the effective flange width due to the effects of shear lag and plate buckling without taking into account neither the material properties of the outer face material nor the loadbearing insulation inner core. Nevertheless, TR 019 states the plate bucking may not be considered as the outer faces are supported by the loadbearing insulation core. The effective flange width is then determined due to the effect of shear lag only with taking into account the material properties of the outer faces and the shear property of the wooden joint. The panel details and material properties are again reproduced and listed in Table 4.4. The effective flange width of both compression and tension obtained from EC5 (212 mm) is less than TR 019 (406

mm). Accordingly, the central deflection determined by EC5 is hence higher than TR 019. The detailed calculation using TR 019 is presented in the Appendix A.

Figure 4.14 illustrates the comparison between the mean test result with the TR 019 and EC5 analytical methods. As shown in Figure 4.14, the mean test result is significantly higher than both TR 019 and EC5 calculations. This may be due to the edge recesses and also the small width of the panel. The maximum vertical displacement at the edge mid-span (23.03 mm) is almost 2.4 times of the TR 019 central displacement (9.58 mm). However, the experimental investigation shows the vertical displacements at both central (22.30 mm) and edge (23.03 mm) are similar. The central deflection may be influenced by the edge displacement i.e. edge recesses and the small width of the panel, causing the central to displace more. In addition, the loads were applied through rigid spread steel plates, which forced the central and edge deflection to be almost identical.

F **(kN)**	40.32
B **(mm)**	500
L **(mm)**	1,100
f **(mm)**	11
d_c **(mm)**	103
e **(mm)**	114
E_{11} **(N/mm^2)**	3,844
E_{33} **(N/mm^2)**	3,615
G_{c16} **(N/mm^2)**	500
v	0.24

Table 4.4: SDC details and material properties

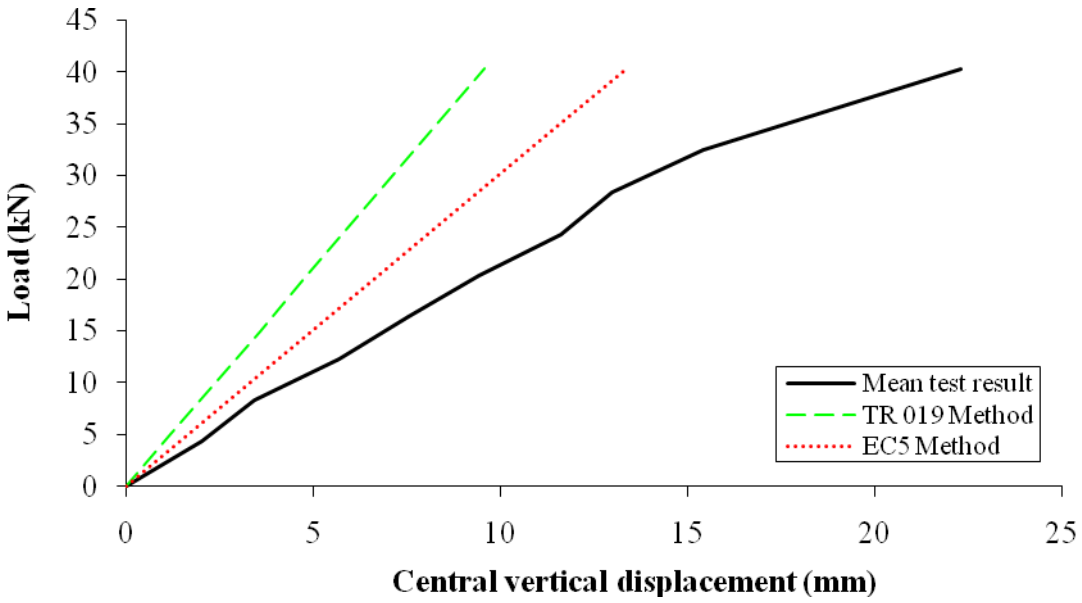

Figure 4.14: Comparison between the mean STP test result with different methods

4.2.5 Numerical investigation

All panels could not be modelled as two-dimensional models due to the edge recesses along the length of the specimens. Accordingly, three-dimensional models with a deformable body were employed as depicted in Figure 4.15 for STP panel.

The assumption of the perfect bond at the OSB-PUR interface was adopted as previously described in section 3.6. Despite the fact that structural adhesive bonding (zigzag pattern) and nail connections were both used to connect the C16 header/footer and the OSB faces, they were not fully perfect bond as the OSB-PUR interface. As a result, the surface tie-constraint was used at the C16-OSB interface since they could be classified as a strong bond, whereas the default ABAQUS contact was employed at the C16-PUR interface. This would only ensure that there would be no penetration at the C16-PUR interface. Finally, a steel support plate was modelled and connected to the bottom OSB face by the contact interaction with a coefficient of friction equal to 0.2.

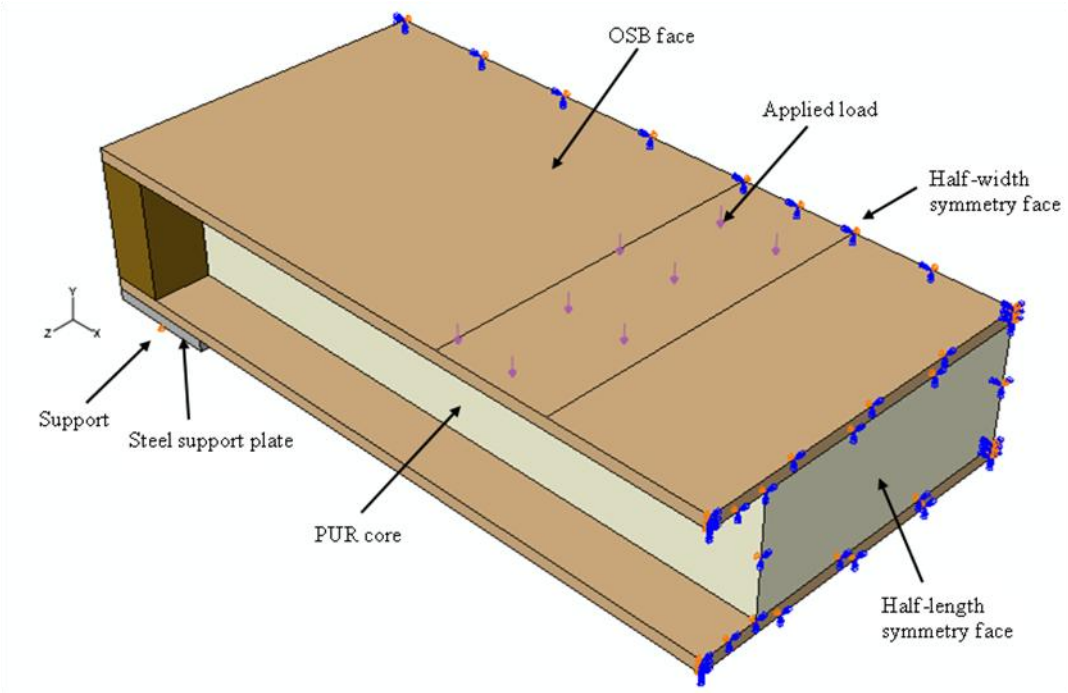

Figure 4.15: STP finite element model

As the geometry of the specimen and the loading were symmetric in both longitudinal and transverse directions, a quarter of the whole specimen was modelled. Thus the XSYMM boundary condition was applied to the vertical surface at the mid-span section, whereas the ZSYMM boundary condition was applied to the mid-width section. This technique can save the computation efforts significantly. Finally, a restraint in the vertical direction ($U_y = 0$) was applied along the central line of the bottom surface of the steel support plate.

The structured mesh technique for these models was 20-node hexahedral elements with reduced integration (C3D20R). This technique is recommended for general analysis work (ABAQUS, 2010) and found to be in a good agreement with the experimental results. The OSB faces were again divided into two elements in the thickness direction and were 10 mm wide in the panel length directions. The panel in the width direction was then discretised into 20 mm uniform elements. Other components (PUR, C16 header and footer, and steel plate) were discretised into 10 x 10 x 20 mm elements. A sensitivity analysis on the density of the mesh element was also

carried out and found that these elements were fine enough to provide satisfactory results in terms of both stress and displacement. Figure 4.16 illustrates the finite element mesh for the specimen models.

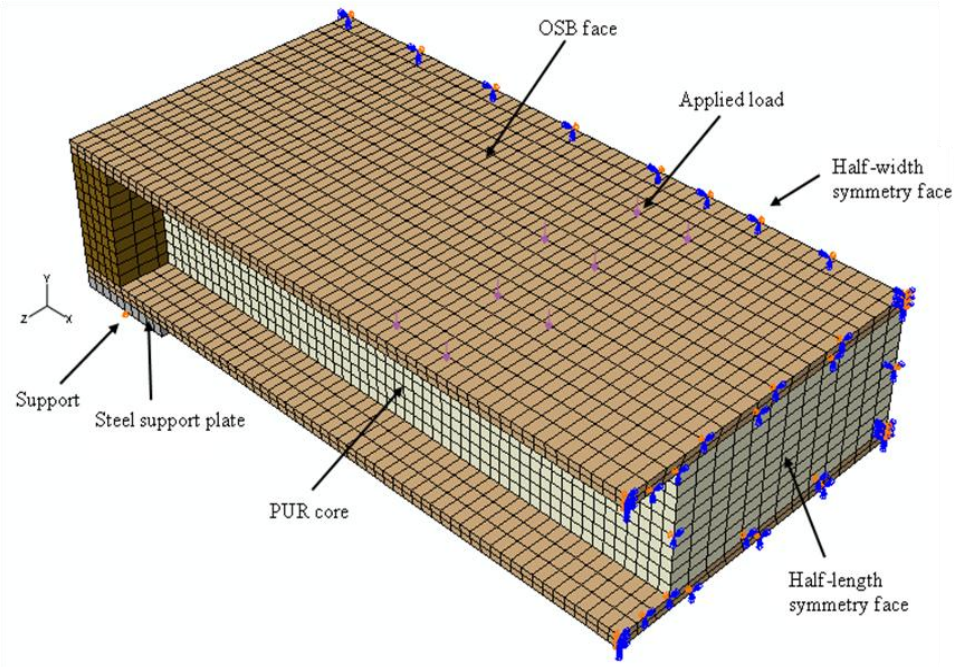

(a) STP

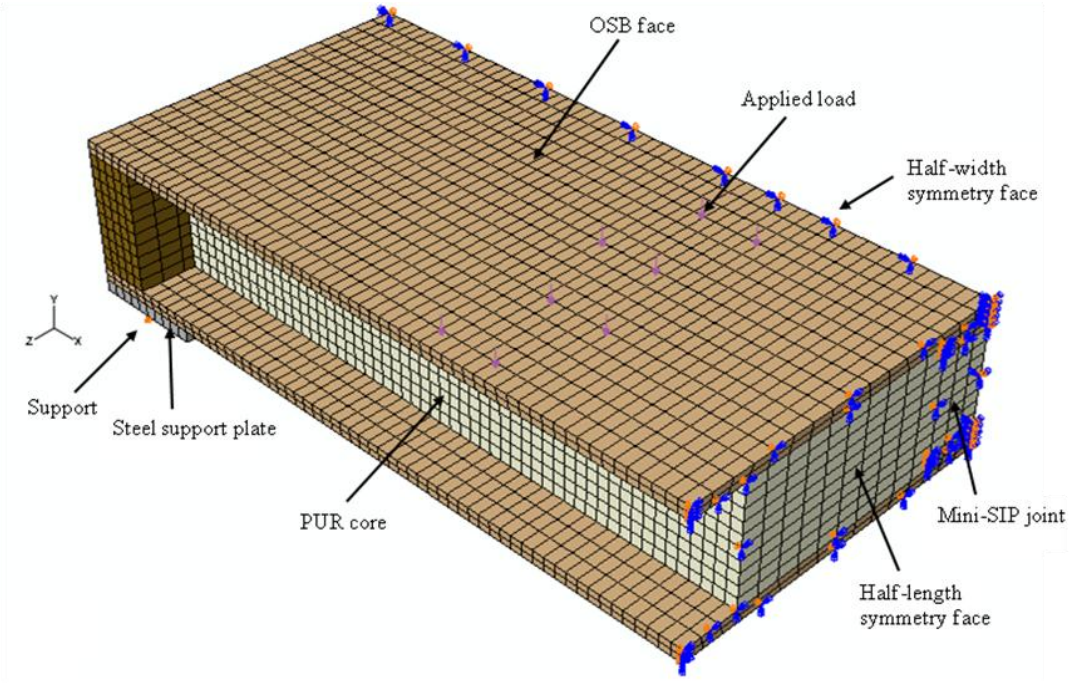

(b) SMC

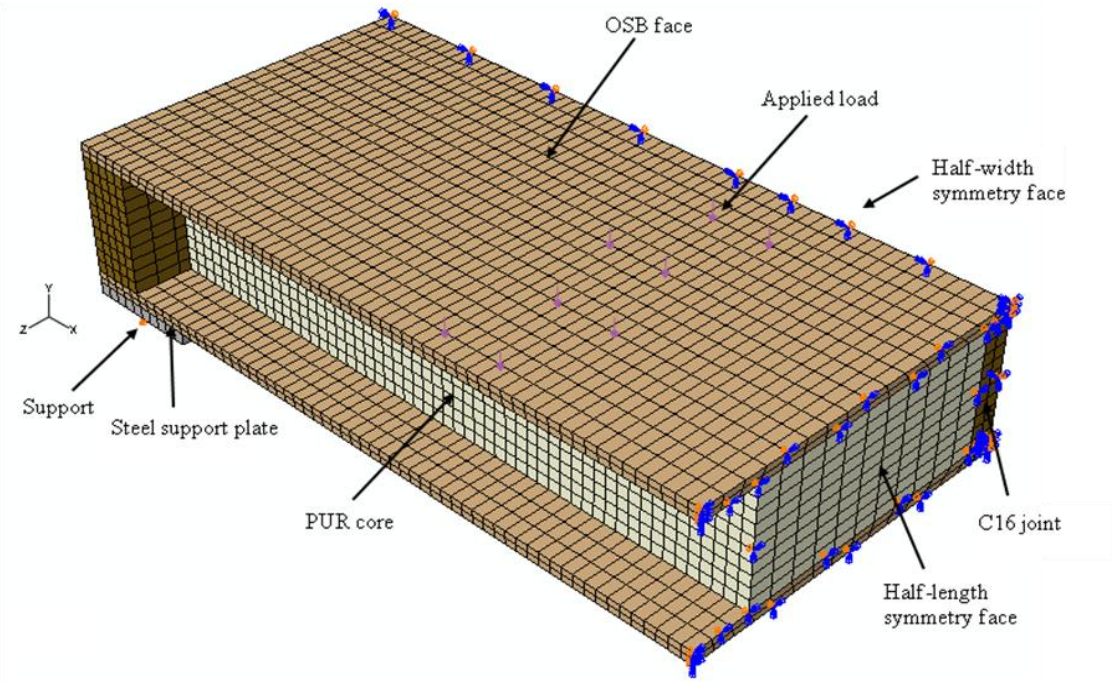

(c) SDC

Figure 4.16: Finite element mesh for all specimens

The material properties of SIP components are tabulated in Table 4.5. The nonlinear geometry, i.e. *NLGEOM option in the ABAQUS, was also included in this investigation.

Material	E_{11} (N/mm^2)	E_{22} (N/mm^2)	E_{33} (N/mm^2)	G_{12} (N/mm^2)	G_{13} (N/mm^2)	G_{23} (N/mm^2)	ν_{12}	ν_{13}	ν_{23}
OSB	3,844	3,615	3,615	1,080	50	1,080	0.24	0.24	0.24
PUR	5.447	6.442	5.703	2.3	2.3	2.3	0.33	0.33	0.33
C16	8,000	270	270	500	500	500	0.24	0.24	0.24
Steel	210,000	210,000	210,000	81,000	81,000	81,000	0.30	0.30	0.30

Table 4.5: Elastic material properties

The applied loads equal to 25 kN were applied to the STP and SMC models, whereas 50 kN was applied to the SDC model in order to ensure that the failure would occur in the FEM investigations. Figures 4.17 and 4.18 present the distributions of the stresses of the SIP constituents for the STP model i.e. OSB and PUR. The stress distributions and the maximum

stresses of SMC and SDC models have been found at the same locations as in the case of the STP model. As a result, the contour plots of SMC and SDC are therefore not presented.

Tables 4.6 present the numerical results of maximum stresses developed in the OSB faces, in which S_{11} and S_{33} are the normal stresses in the OSB faces along the x and z directions; and f_{11} and f_{33} are the respective failure stress under each stress component acted alone. As can be seen from Table 4.6, these stresses were examined at two load levels. At the applied loads of 25 kN (for STP and SMC) and 50 kN (for SDC), the longitudinal stresses S_{11} have exceeded the failure stresses, which indicates that OSB have failed at these lower load levels. The stress contour plots for both S_{11} and S_{33} in the OSB faces are presented in Figures 4.17(a) and 4.17(b). Backward examinations of the stress results along the incremental loading path suggest that at the load levels of 19.3 kN (for STP), 20.3 kN (for SMC) and 21.0 kN (for SDC), their S_{11} have just reached the failure stresses; these values have therefore been captured as the loads at the initial failure of OSB bending failure.

Tables 4.7 present the numerical results of maximum stresses developed in the inner core PUR. S_{22} is the normal stress in the PUR normal to its thickness direction, whereas S_{12} and S_{23} are the shear stresses in the x-y and y-z planes. The coordinate system is presented in Figure 4.18. f_{22}, f_{12} and f_{23} are also the respective failure stress under each stress component acted alone. These results were examined again at 25 kN applied load (for both STP and SMC) and 50 kN (for SDC), the inner cores of all specimens fail due to shear and debonding (at the interface of longitudinal end of PUR to OSB/C16) in both linear stress and Hashin Rotem's criteria as shown in Figures 4.18(b) to 4.18(c) and Table 4.7.

Further backward examinations of the stress results along the incremental loading path suggest that at the load levels of 15.3 kN (for STP), 15.5 kN (for SMC) and 29.0 kN (for

SDC), their S_{12} of the inner core elements have just reach the failure stresses (as shown in Figure 4.18(b)); therefore, these values have been captured as the loads at the initial failure of shear failures. For debonding failure, the failure occurs at the top corner elements (adhered to the outer face and header/footer elements) where the stress values have been taken. Generally, the linear stress criterion provides a lower initial failure load. Although the initial failure loads due to debonding from Hashin Rotem's criterion provide better agreement to the experimental failure loads (in this investigation), the initial failure loads from linear stress criterion will be used instead. The subsequent numerical investigations (presented in Chapter 4.3) will show the linear stress criterion provides better agreement than the Hashin Rotem's criterion.

Specimen	Load (kN)	Failure	S_{11} (N/mm^2)	S_{33} (N/mm^2)	S_{11} / f_{11}	S_{33} / f_{33}	Remark
STP	25.0	Bending	23.37	5.15	1.43	0.63	Fail due to S_{11}
	19.3		16.35	-	0.99	-	Pass
SMC	25.0		22.12	4.78	1.35	0.58	Fail due to S_{11}
	20.3		16.25	-	0.99	-	Pass
SDC	50.0		44.47	9.07	2.71	1.11	Fail both S_{11} and S_{33}
	21.0		16.38	3.91	0.99	0.48	Pass

where f_{11} and f_{33} are bending failure stresses, equal to 16.40 N/mm^2 and 8.20 N/mm^2, respectively.

Table 4.6: Stresses results in the OSB outer faces

Specimen	Load (kN)	Failure	S_{12} (N/mm^2)	S_{12} / f_{12}	Remark
STP	25.0	Shear	0.160	1.38	Fail
	15.3		0.115	0.99	Pass
SMC	25.0		0.158	1.36	Fail
	15.5		0.115	0.99	Pass
SDC	50.0		0.152	1.31	Fail
	29.0		0.115	0.99	Pass

where f_{12} is shear failure stress, equals to 0.116 N/mm^2.

(a) Shear

Specimen	Load (kN)	Failure	S_{22} (N/mm^2)	S_{12} (N/mm^2)	S_{23} (N/mm^2)	Linear stress criterion $S_{22}/f_{22}+S_{12}/f_{12}+S_{23}/f_{23}$	Remark
STP	25.0	Debonding	0.237	0.033	0.051	1.98	Fail
	11.9		0.111	0.021	0.029	0.99	Pass
SMC	25.0		0.235	0.032	0.050	1.96	Fail
	12.0		0.115	0.019	0.027	0.99	Pass
SDC	50.0		0.195	0.043	0.025	1.62	Fail
	30.0		0.121	0.026	0.015	0.99	Pass

where f_{22}, f_{12} and f_{23} are failure stresses, equal to 0.188 N/mm^2, 0.116 N/mm^2 and 0.116 N/mm^2, respectively.

(b) Debonding – Linear stress criterion

Specimen	Load (kN)	Failure	S_{22} (N/mm^2)	S_{12} (N/mm^2)	S_{23} (N/mm^2)	Hashin Rotem's criterion $(S_{22}/f_{22})^2+(S_{12}/f_{12})^2+(S_{23}/f_{23})^2$	Remark
STP	25.0	Debonding	0.237	0.033	0.051	1.86	Fail
	18.3		0.172	0.027	0.037	0.99	Pass
SMC	25.0		0.235	0.032	0.050	1.82	Fail
	18.4		0.172	0.025	0.037	0.99	Pass
SDC	45.0		0.195	0.043	0.025	1.26	Fail
	44.0		0.173	0.038	0.022	0.99	Pass

where f_{22}, f_{12} and f_{23} are failure stresses, equal to 0.188 N/mm^2, 0.116 N/mm^2 and 0.116 N/mm^2, respectively.

(c) Debonding – Hashin Rotem's criterion

Table 4.7: Stress results in the PUR core

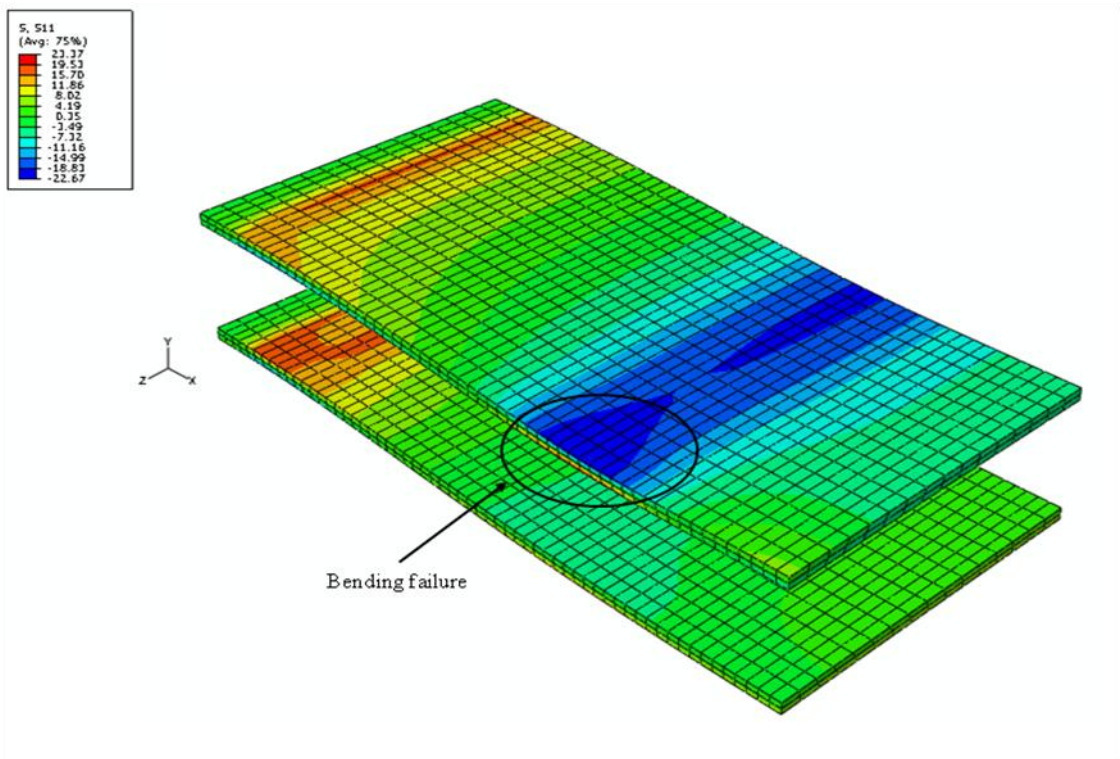

(a) Distribution of the longitudinal stress (S_{11}) of the outer faces

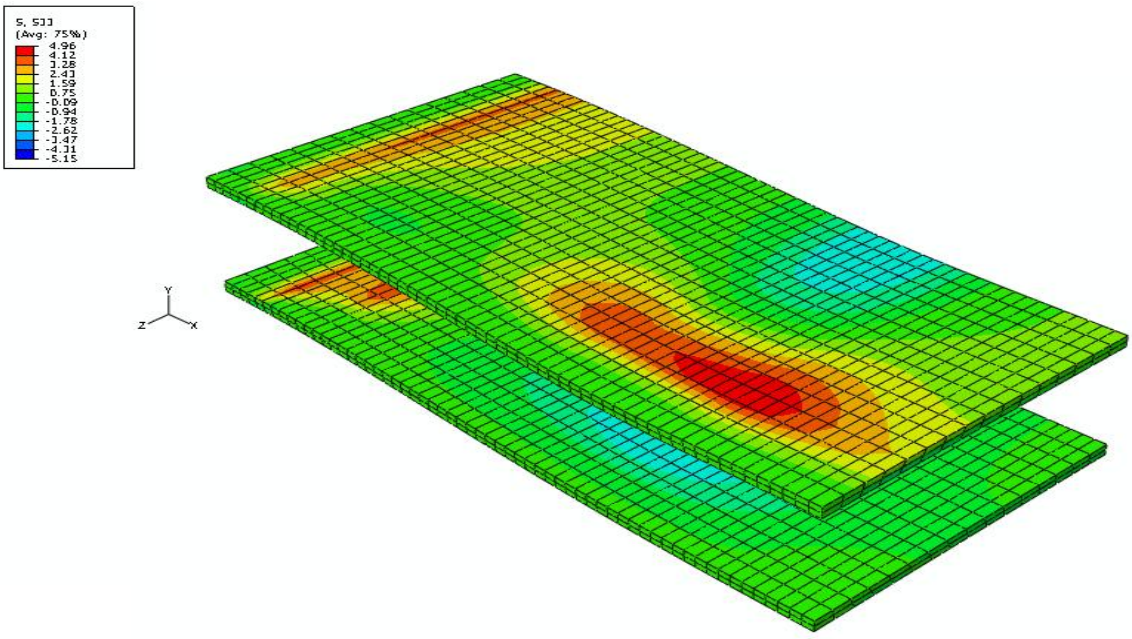

(b) Distribution of the transverse stress (S_{33}) of the outer faces

Figure 4.17: Distribution of the outer face stresses

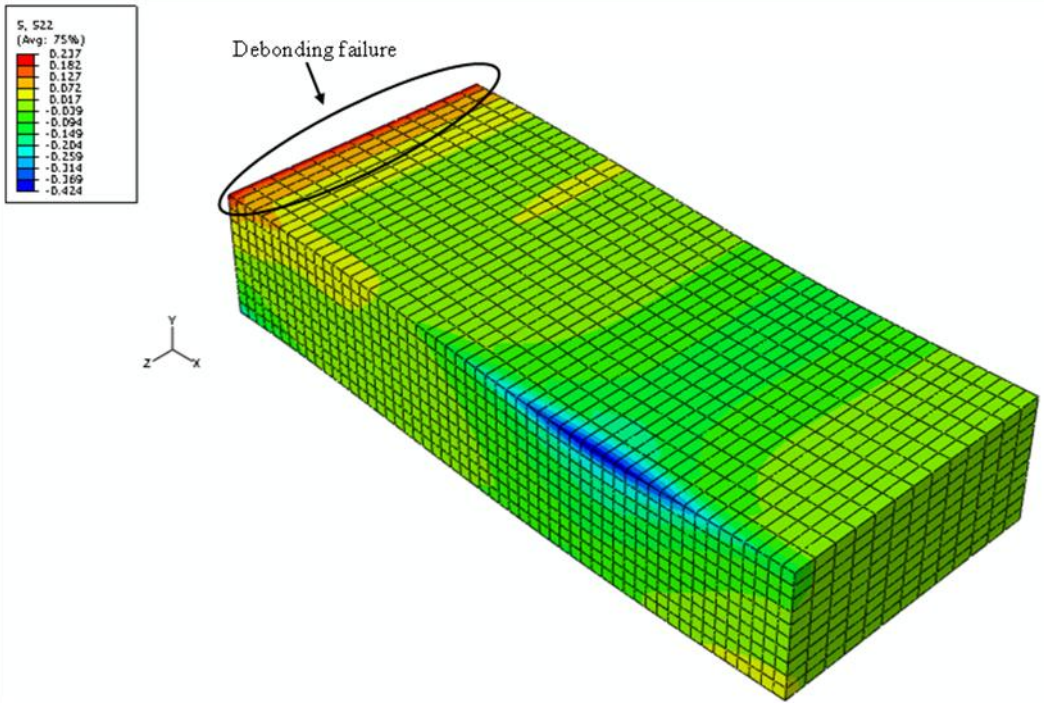

(a) Distribution of the normal stress (S_{22}) of the PUR inner core

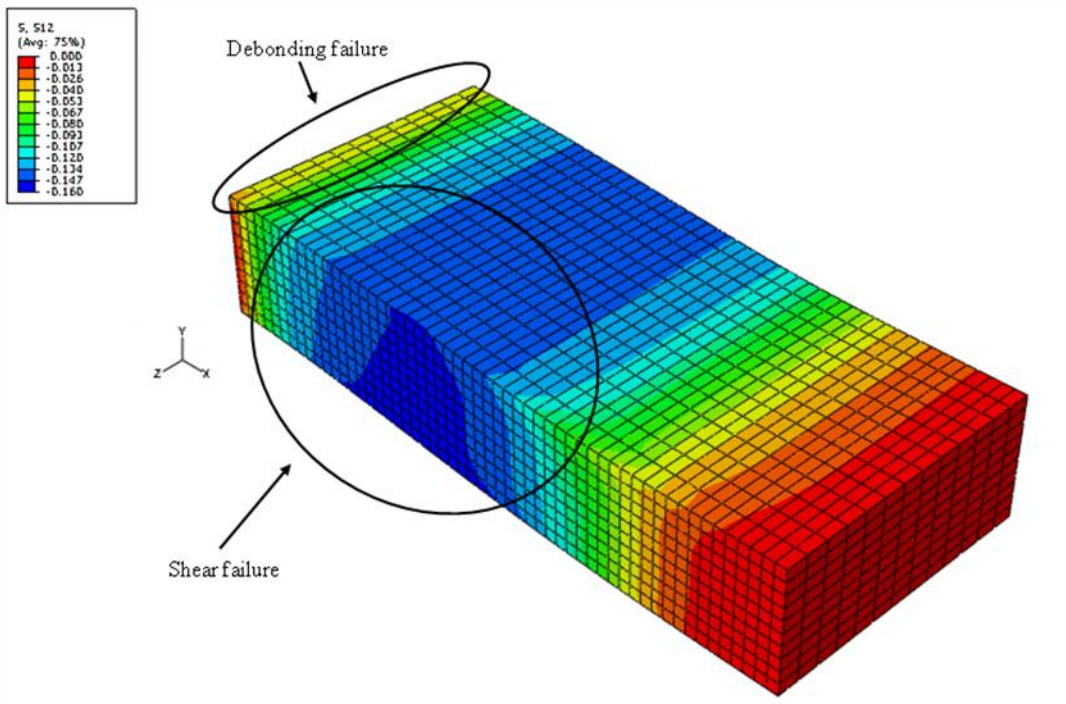

(b) Distribution of the shear stress (S_{12}) of the PUR inner core

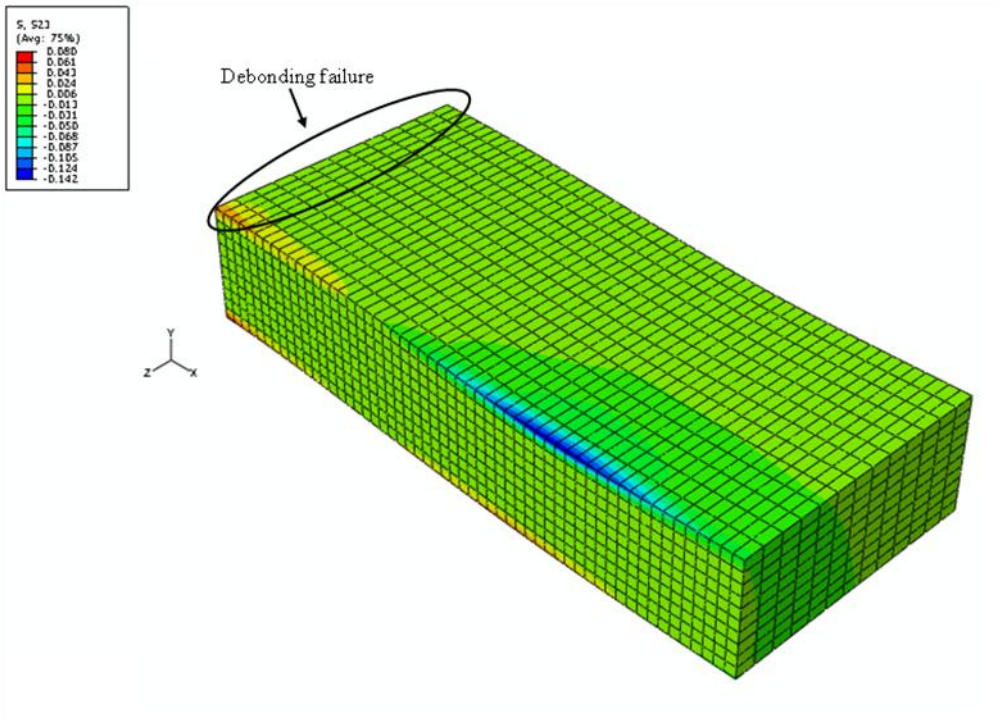

(c) Distribution of the shear stress (S_{23}) of the PUR inner core

Figure 4.18: Distribution of the stresses of the PUR inner core

As previously described in section 3.6 the current FEM study is unable to precisely predict the behaviour following the onset of the first failure unless the post-damage laws for the SIP constituents are utilised in the model. Consequently, the load and the deflection curves (presented in this investigation) are only up to the initial failure load. Figures 4.19 to 4.22 show the comparison between the FEM and the mean test result.

The agreement of the central displacements at the mid-span (Dial Gauge Nos. 1) for STP and SMC is encouraging as shown in Figures 4.19(a) and (b). Nevertheless, the FEM central displacement for SDC is significantly different to the mean test result. It seems possible that the higher central displacement is due to the influence of the edge displacement, causing the central to displace more since the loads were applied through the rigid spread steel plates, which forced

the central and edge deflection to be almost identical. The mean central displacement agree wells with the edge displacement (Dial Gauge No.2) as shown in Figure 4.19(c).

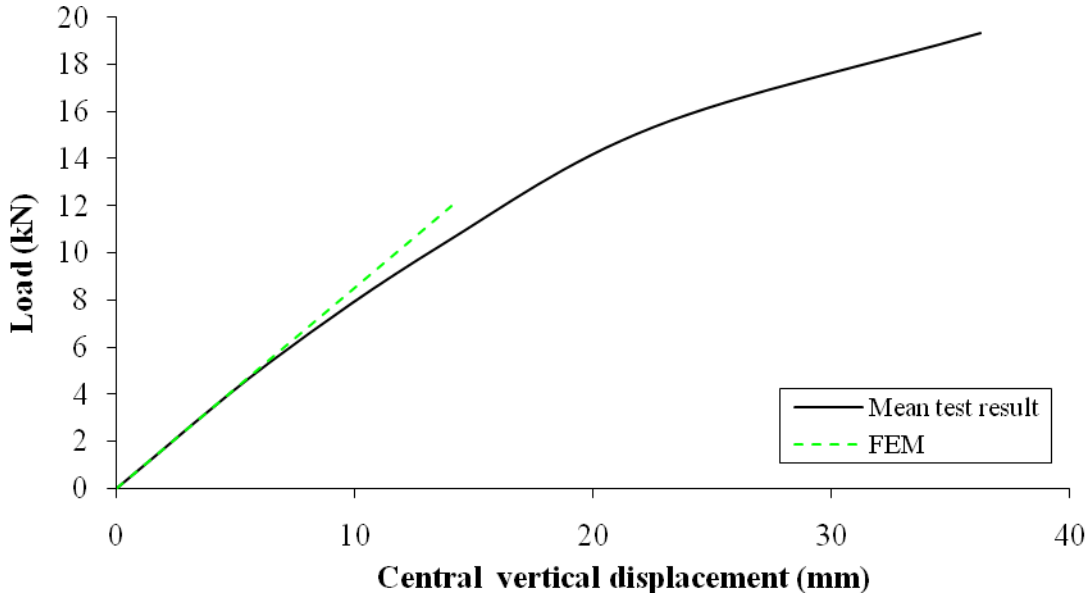

(a) STP

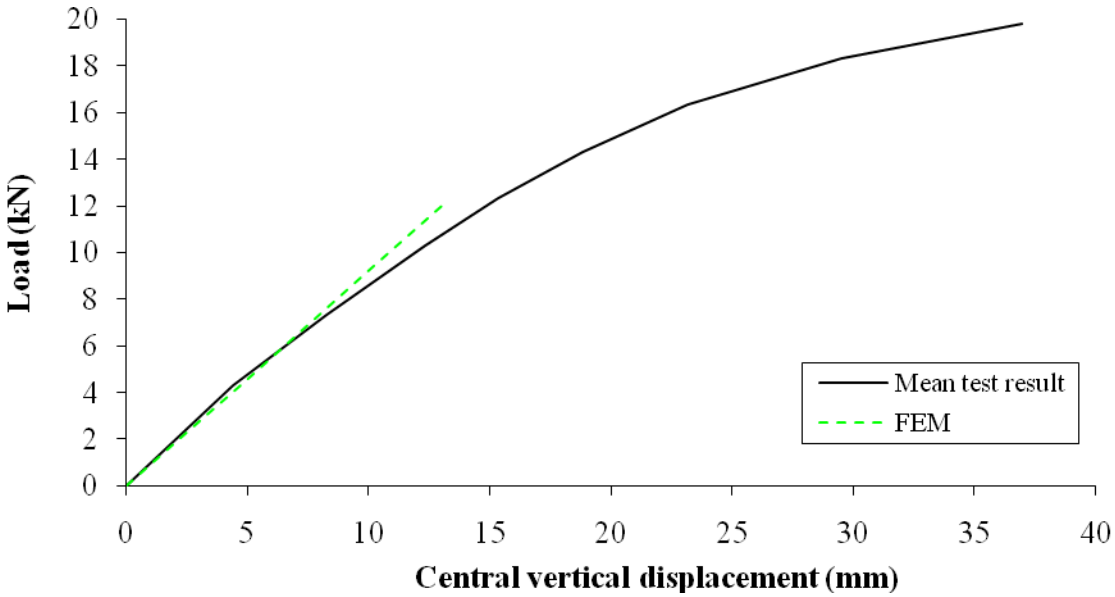

(b) SMC

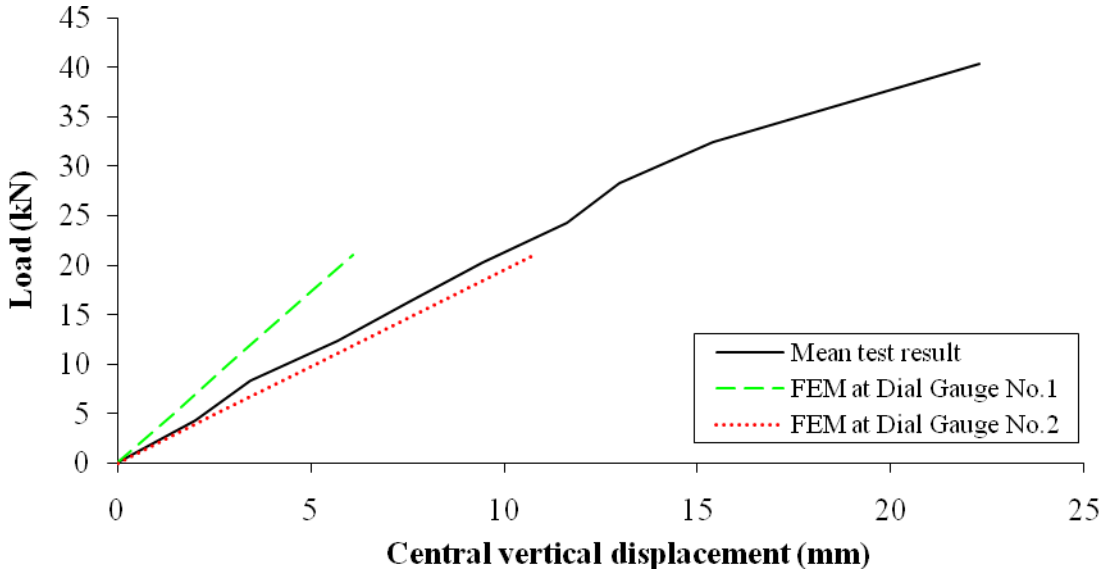

(c) SDC

Figure 4.19: Central displacement comparison between the FEM and the mean test results

The FEM edge displacements up to the initial failure loads are in good agreement with the mean test result as shown in Figure 4.20.

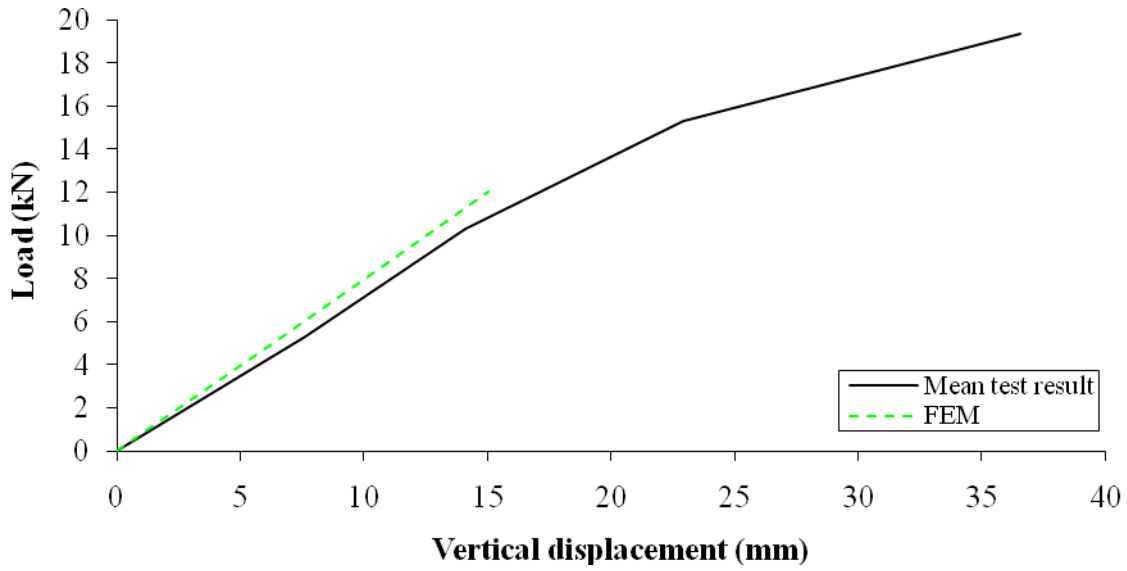

(a) STP

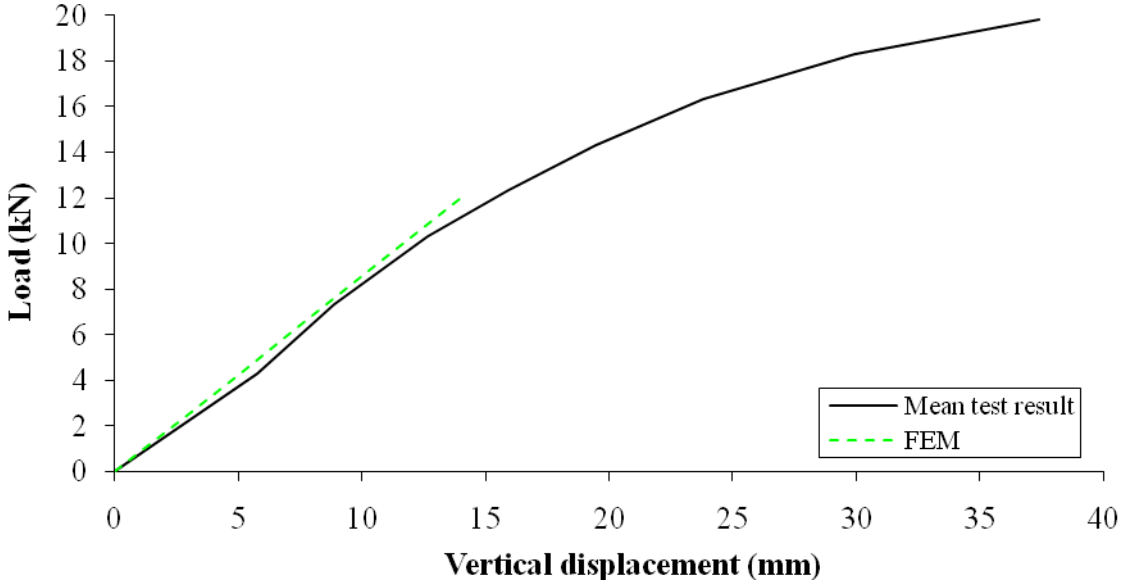

(b) SMC

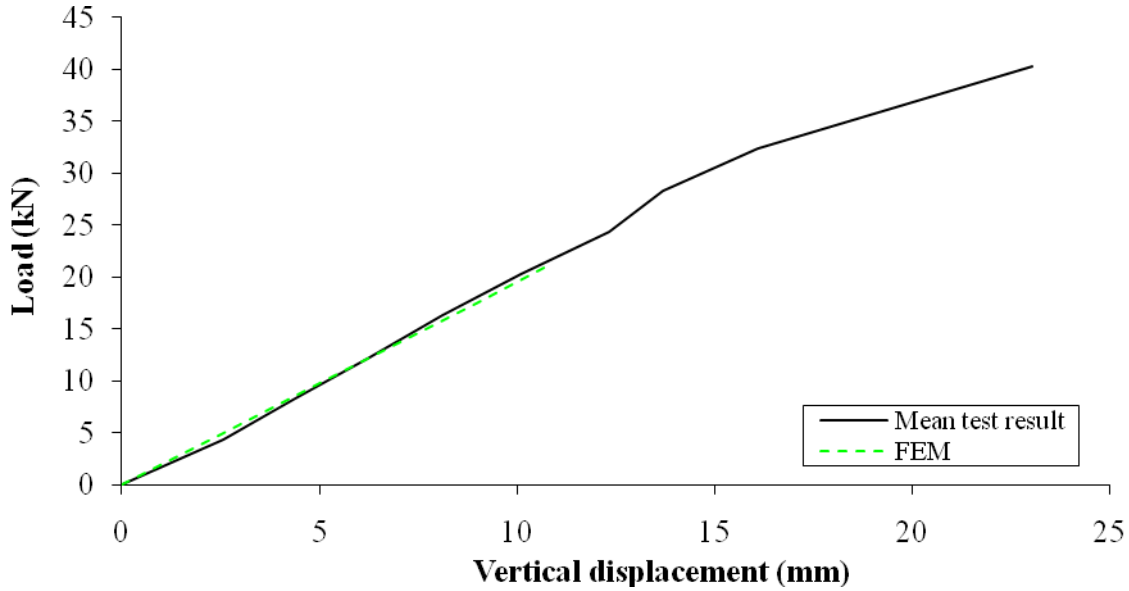

(c) SDC

Figure 4.20: Vertical displacement comparison between the FEM and the mean test results

The vertical and horizontal displacements at the edge of the panels from the FEM investigation are significantly less than the mean test results as illustrated in Figures 4.21 and 4.22. The discrepancies were due to two reasons: (1) any movements near the edge are sensitive to the

edge construction details associated with nails and adhesive, and these details are not readily predictable; (2) both movements were of small amount and any small difference would yield a large relative error. However, it is believed that these two movements have less concern in engineering practice in comparison to the central deflection.

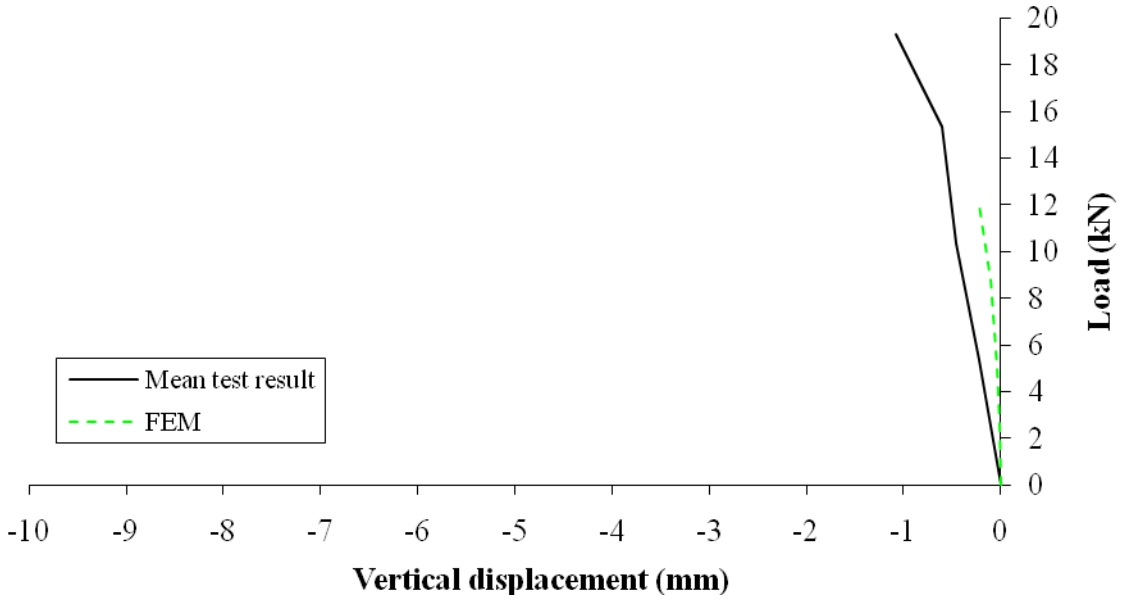

(a) STP

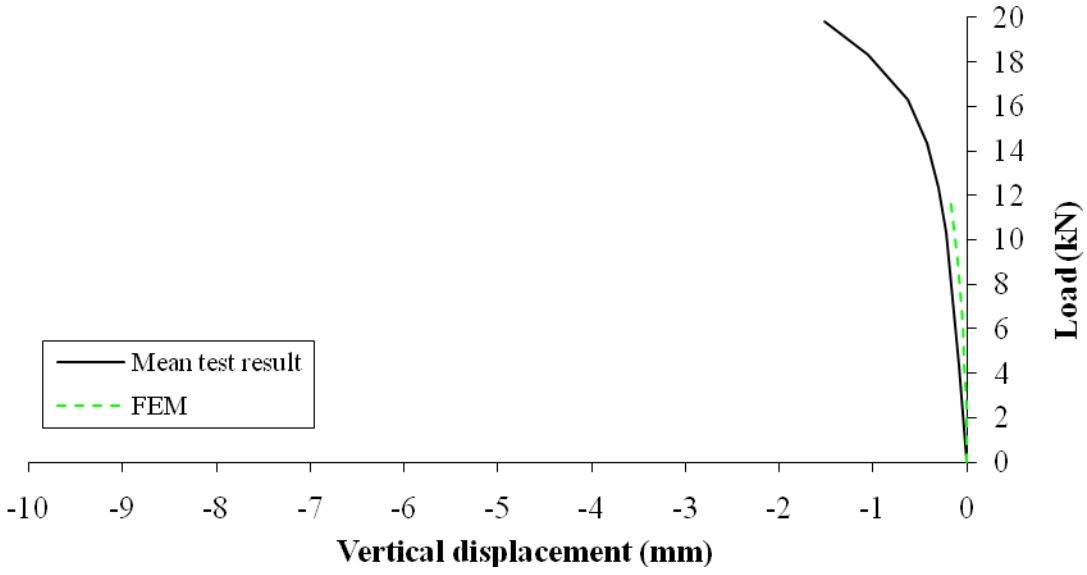

(b) SMC

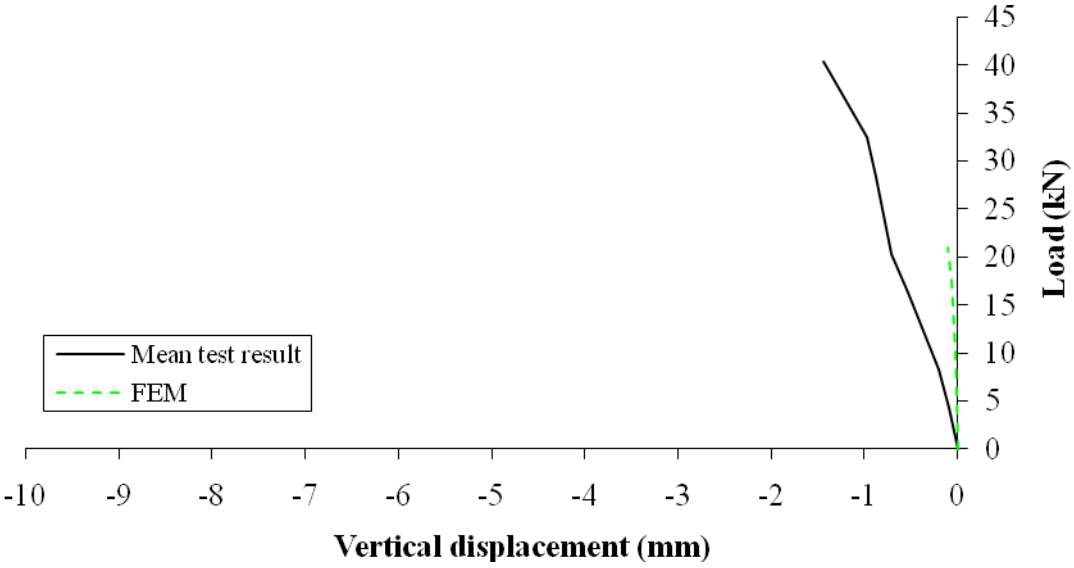

(c) SDC

Figure 4.21: Vertical displacements comparison between the FEM and the mean test results

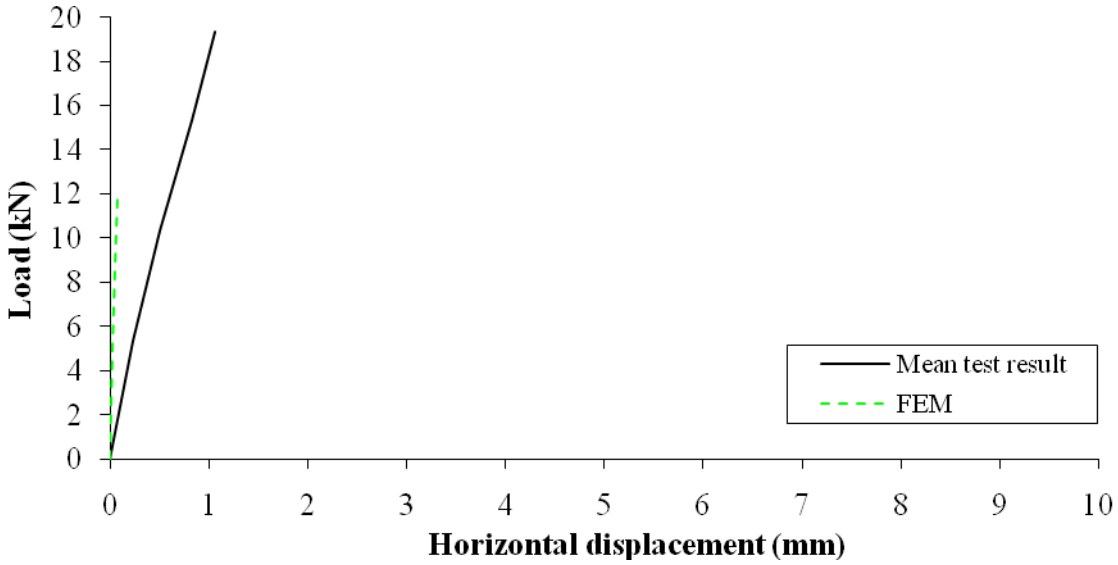

(a) STP

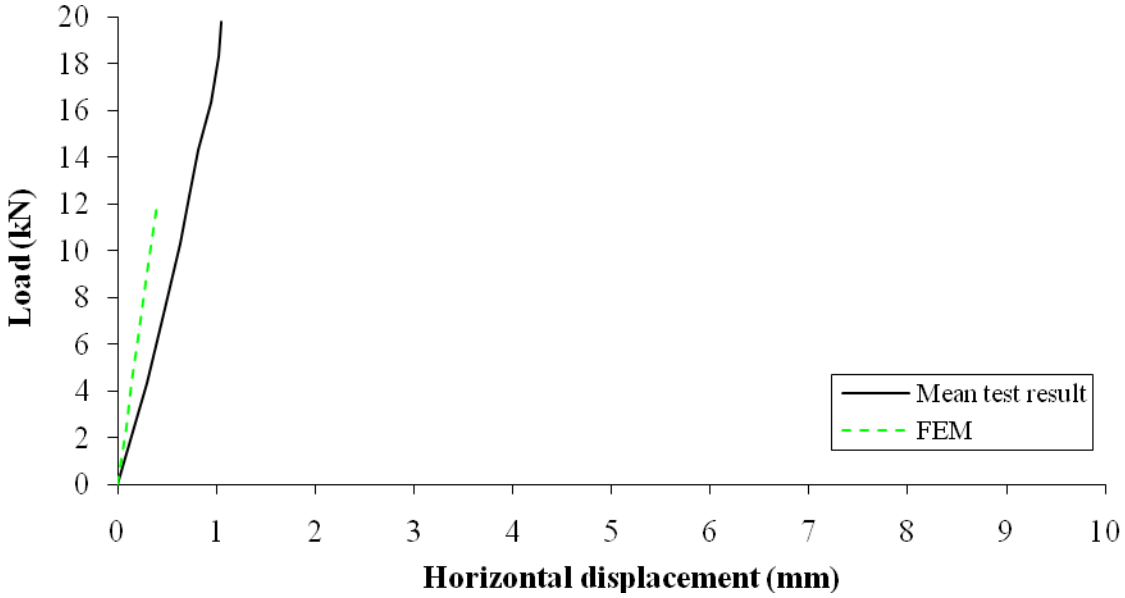

(b) SMC

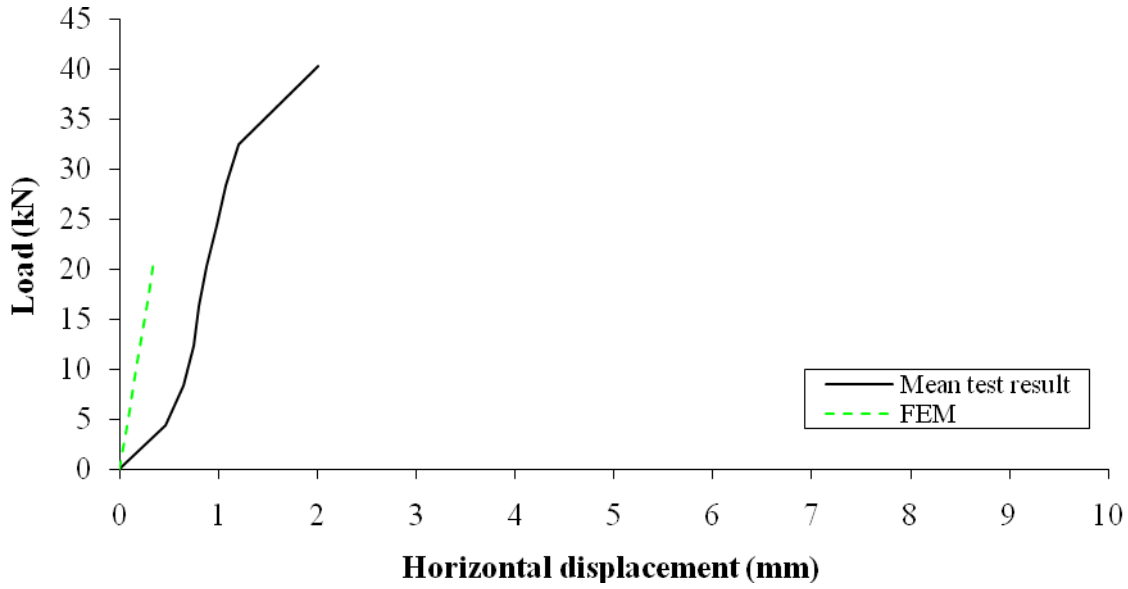

(c) SDC

Figure 4.22: Horizontal displacements comparison

between the FEM and the mean test results

4.2.6 Investigation summary of the four-point bending on SIPs

Table 4.8 summarises the experimental and numerical findings of the three specimen types. It

should be noted that the deflection of the panel becomes the governing factor of the loading capacity as previously demonstrated.

Specimen	STP	SMC	SDC
Ultimate Limit Load, ULL (kN)	19.32	19.82	40.32
Increase of ULL (%)	0	2.59	108.70
Load at deflection limit ℓ/333 (kN)	2.87	3.06	7.98
Serviceability load / Ultimate load (%)	14.9	15.4	19.8
FEM initial failure (kN)	11.9	12.0	21.0
Initial failure/ULL (%)	62	61	52
Mean central displacement (mm)	36.25	36.96	22.30
Mean edge displacement (mm)	36.56	37.39	23.03
Mean vertical displacement at edge (mm)	1.06	1.05	2.01
Mean horizontal displacement (mm)	1.08	1.52	1.44
Experimental failure mode	Debonding	Debonding	Flexure-Shear
FEM initial failure mode	Debonding	Debonding	Bending

Table 4.8: Experimental and numerical finding summary

As can be seen from Table 4.8, SDC panels (jointed by the dimensional timber spline connections) are the stiffest which offers highest load capacity, whereas the SMC panels (jointed by the mini-SIP connections) exhibit almost identical stiffness and failure loads. The ULL of SDC has been found 109% higher than STP. This observation reveals that the mini-SIP joint has negligible impact on the structural performance of SIPs whereas the dimensional timber spline joint has significant impact. To increase the structural efficiency, the dimensional timber spline joint is preferred.

Numerical investigation can only predict the load for the initiation of the failure; whereas the experimental can record the ultimate failure load as the initiation of failure usually occurred inside the panel. Nevertheless, the numerical results can indicate the ultimate failure mode, which are presented in Table 4.8 and it can be seen that both match very well.

The vertical displacements at the mid-span determined by the numerical analysis (up to the initial failure loads) agree well with the experimental results. Although, the vertical and horizontal displacements at the header/footer have been found less conformity to the experimental results, these displacements are small (within 2.63 mm) in comparison with the central displacements and less concern in engineering practice.

4.3 Combined loading test investigation

Very little was found in the literature on the structural behaviours of SIPs with different joint designs when subjected to combined loadings. The structural behaviours of SIPs under individual (transverse, axial and racking) and combined loading tests were investigated with the following objectives.

- To investigate the structural behaviours of SIPs with and without connections.
- To investigate the effect of opening on the structural performance of SIPs.
- To provide interactive failure load curves between axial and transverse loadings for SIPs with different joint designs and without and with openings.

4.3.1 SIP testing samples

Thirty-four SIP specimens of standard size panel, i.e. 1200 x 2440 mm were subjected to eight experimental load cases, including single and combined transverse, axial and racking load tests. All specimens comprise 11 mm thick OSB type 3 facings and a 103 mm thick polyurethane inner core (overall thickness of 125 mm) and were manufactured by SIP Build Ltd. SIP specimens can be classified into five groups as detailed in the following sections.

4.3.1.1 SIP typical panel (STP)

The first group is a typical type of SIP panel (STP), consisting of two testing panels for individual transverse loading test only. A C16 timber section of 47 x 103 mm header was inserted into the rebate at the top section of the panel by SIP Build adhesive to the OSB faces and the PUR core, and also fastened by 2.8 mm diameter and 63 mm long ring shank nails at 150 mm spacing. The footer was connected to the sole plate by SIP Build adhesive and also bolted through both sections by two M8 bolts grade 8.8 together with 25 mm diameter and 3 mm thick washers at 150 mm and 750 mm away from the panel edge. The position of the bolts is in accordance with the racking test requirement in BS 594 (BSI, 1996), i.e., 150 mm away from one end of the panel and a 600 mm spacing for the next bolt. The size and thickness of washer are also in accordance with EC5 (BSI, 2004), which are slightly greater than 3 and 0.3 times the bolt diameter (25 mm and 3 mm), respectively. The footer and the sole plate are C16 timber sections of 47 x 103 mm and 47 x 125 mm, respectively. By using the same assembly as the header, the footer was inserted into the rebate at the bottom section of the panel. Figure 4.23 illustrates the specimen details of STP.

4.3.1.2 SIP with mini-SIP connection (SMC)

The second group is known as SIP with mini-SIP connection (SMC) which consists of 12 testing panels. Each SMC comprises two small panels of 600 mm wide by 2440 mm long which are joined along the centre-line by a 100 mm width mini-SIP fastened by 2.8 mm diameter and 63 mm long nails at 150 mm spacing. The configurations for the header, footer and sole plate are as same as the first group. Figure 4.24 shows the specimen details of the second group (SMC).

4.3.1.3 SIP with dimensional timber spline connection (SDC)

The third group, i.e. SIP with dimensional timber spline connection (SDC), consists of four testing panels. Each SDC comprises two small panels of 600 mm wide by 2440 mm long that are joined along the centre-line by a C16 timber section of 47 x 103 mm fastened by the same nail type at 150 mm spacing. The configurations for the header, footer and sole plate are as same as the first group. Figure 4.25 shows the specimen details of the third group (SDC).

4.3.1.4 SIP typical panel with opening (STPO)

The fourth group is SIP typical panel with opening (STPO), consists of two testing panels for individual transverse loading test only. The configurations of this panel group are as same as previously described in the first group, however the panel is cut in the middle for a 600 x 1200 mm^2 opening area (25% of the panel area). All four sides of the opening area are reinforced with C16 timber sections of 47 x 103 mm and are bonded to the OSB faces and PUR core by SIP Build adhesive and also fastened by the same ring shank nails at 150 mm spacing. Figure 4.26 shows the specimen details of the fourth group (STPO).

4.3.1.5 SIP with mini-SIP connection and opening (SMCO)

The last group is SIP with mini-SIP connection and opening (SMCO), consists of 14 testing panels. The configurations of this panel group are as same as previously detailed in the second group, however the panel is cut in the middle for a 600 x 1200 mm^2 opening area (25% of the panel area). All four sides of the opening area are reinforced with C16 timber sections of 47 x 103 mm and are bonded to the OSB faces and PUR core by SIP Build adhesive and also fastened by 2.8 mm diameter and 63 mm long ring shank nails at 150 mm spacing. Figure 4.27 shows the specimen details of the fifth group (SMCO).

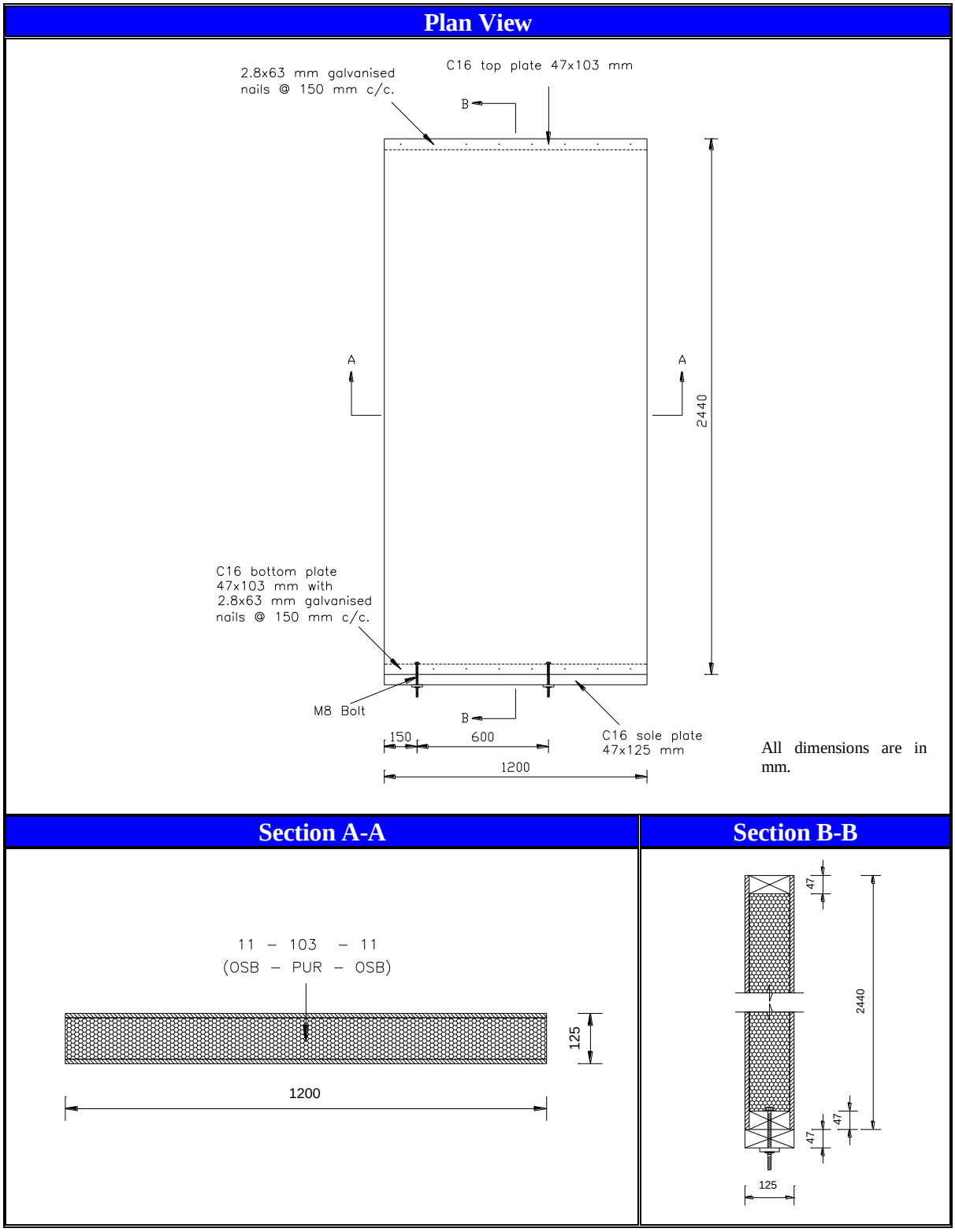

Figure 4.23: SIP typical panel (STP) details

Plan View

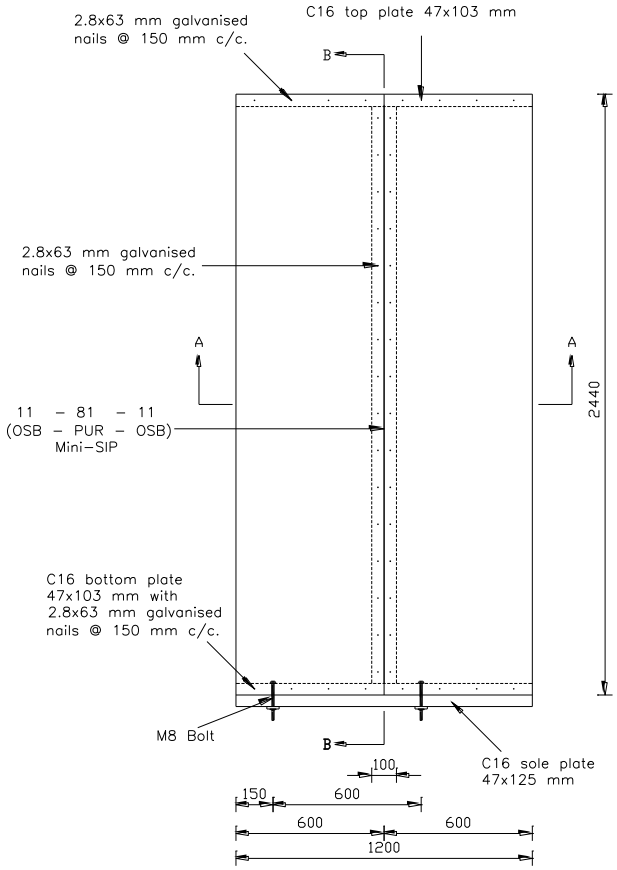

All dimensions are in mm.

Section A-A

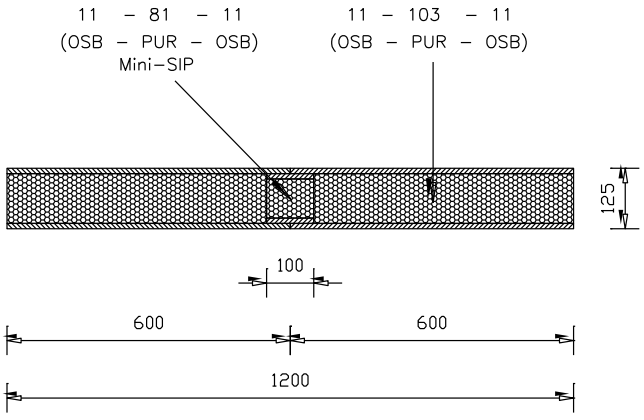

Section B-B

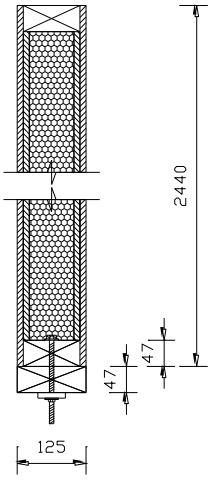

Figure 4.24: SIP with mini-sip connection (SMC) details

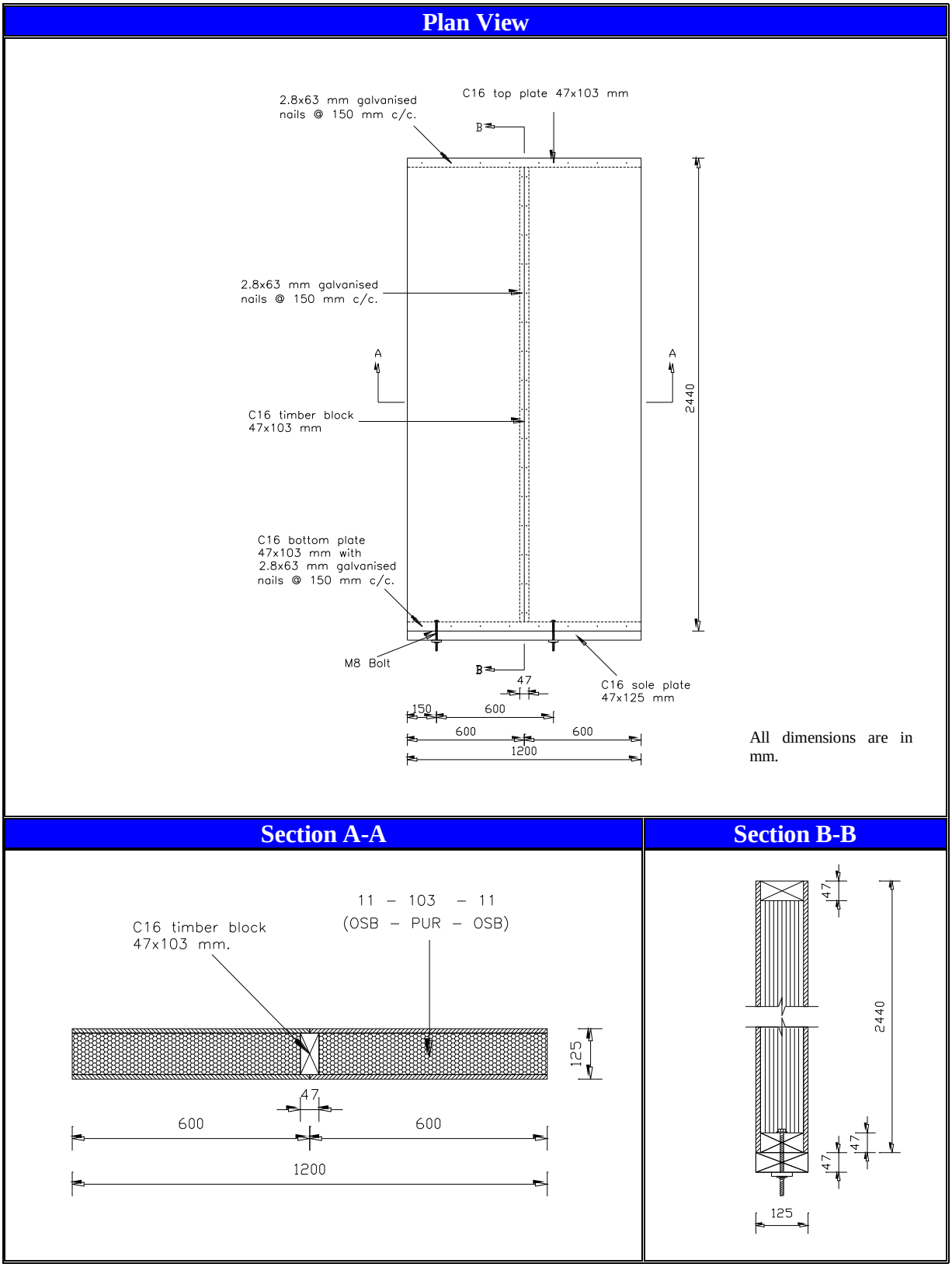

Figure 4.25: SIP with dimensional timber spline connection (SDC) details

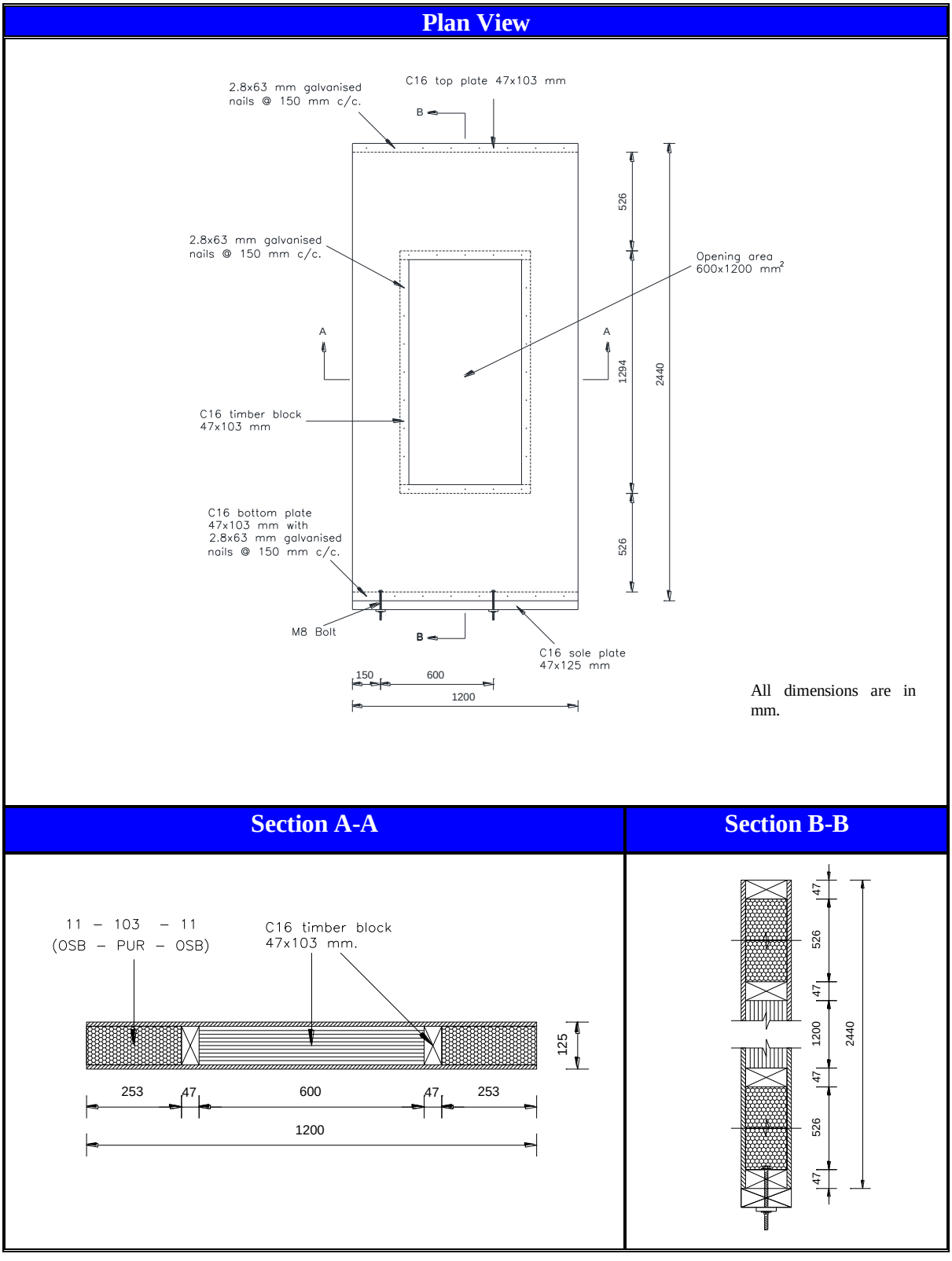

Figure 4.26: SIP typical panel with opening (STPO) details

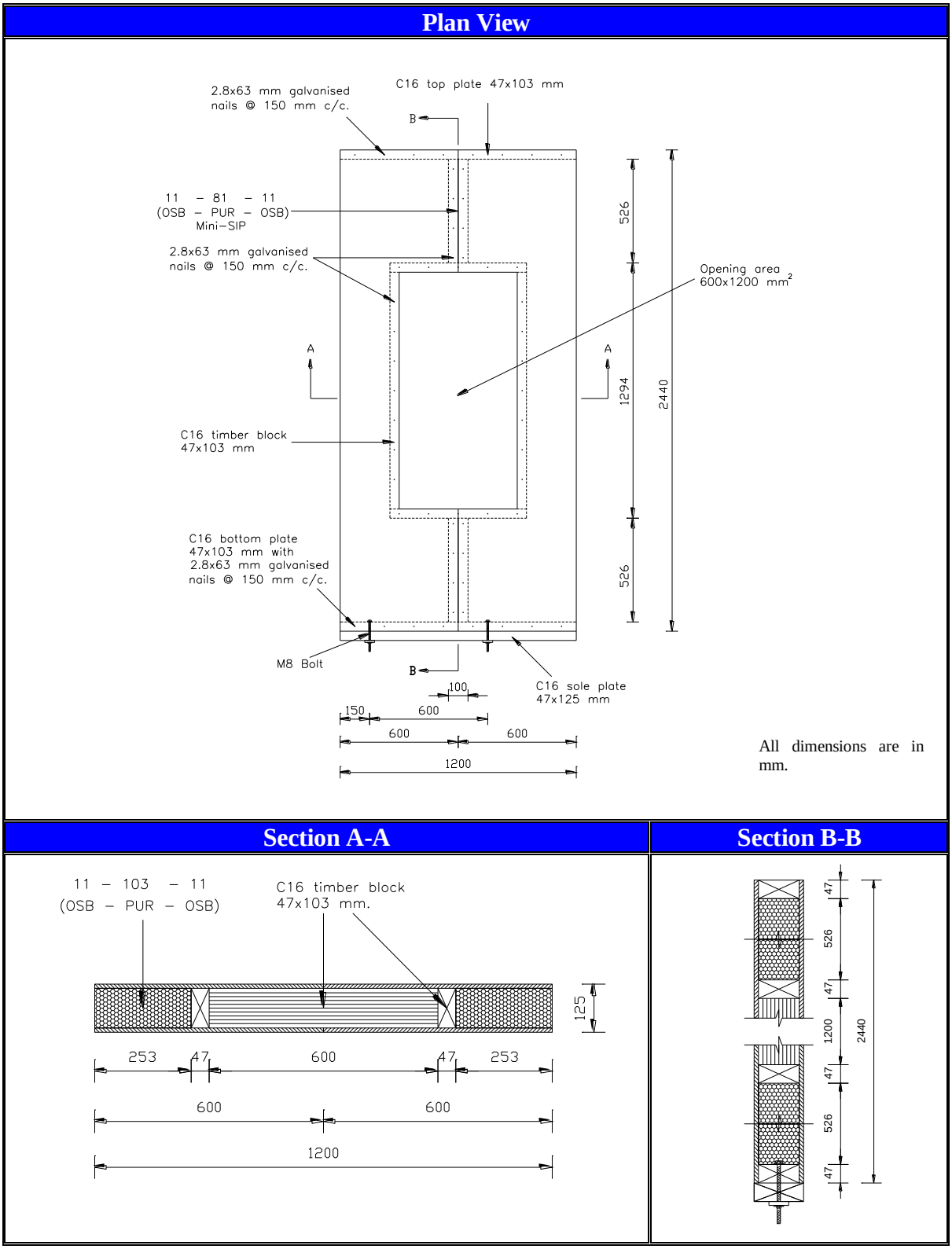

Figure 4.27: SIP with mini-sip connection and opening (SMCO) details

4.3.2 Test load cases

In this test programme, 34 panel specimens were investigated with eight different load cases. Table 4.9 presents the details of load combinations and number of panel specimens in each load case scenario.

Load case	**Panel specimen type and number of panel tested**				
	STP	**SMC**	**SDC**	**STPO**	**SMCO**
No.1: Transverse loading	2	2	2	2	2
No.2: Axial loading		2	2		2
No.3: Racking loading		2			2
No.4: Combined axial (8 kN/m) and transverse loadings		2			2
No.5: Combined racking and transverse loadings		1			2
No.6: Combined axial (8kN/m) and racking loadings		1			2
No.7: Combined axial (8kN/m), racking (1 kN) and transverse loadings		1			1
No.8: Combined axial (16 kN/m), racking (2 kN) and transverse loadings		1			1

Table 4.9: Details of loading combination and panel specimen

The first testing programme began with the individual transverse loading test of 10 SIP specimens i.e. two from each group panel as described in section 4.3.1. The test results obtained from the individual transverse only are served as a baseline for the study of SIP strength and stiffness when subjected to other individual and combined loading tests. Therefore, only this individual transverse test was carried out to all groups and other load cases would focus on the panels with mini-SIP connections (SMC) and with openings (SMCO). Other groups i.e. typical SIPs (STP), SIPs with dimensional timber spline connections (SDC), SIPs with openings (STPO), and additional SIPs with dimensional timber spline connections with openings (SDCO) were investigated by using the numerical investigation only.

The investigations on SIPs with two typical connections (SMC and SDC) and SMCO were then undertaken under the individual uniform axial compression test. After that, the individual racking loading test was undertaken. This racking test was initially planned to apply the racking loads on to the specimens (i.e. SMC, SDC and SMCO) as those subjected to uniform axial compression (load case No. 2). However, after testing the panels with SMC and SMCO, the failure mode was found mainly to be the OSB faces were disjointed from the footers and no structural damage was found. This indicates that the racking load capacity does not depend upon the panel configurations i.e. connections and openings of this experimental programme. Accordingly, the SDC panels were not tested as it was expected that the failure mode and the load capacity would be similar.

After undertaking the individual applied loading tests (load case Nos. 1-3), the combined loadings with different combinations were carried out. Each load case (Nos. 4-8) was initially planned to test two repeated panels of SMC and SMCO. Nevertheless, the test results have been found with little differences. This was due to the arrangement that the pre-applied loads of uniform axial compression and racking are applied at a level that panels are normally required to sustain in their service life, which were small. As a result, some of the load cases were tested to only one SIP specimen as it was expected that the test result on another panel would provide similar results as found in the load case No. 4.

The test results and discussions of this experimental programme are presented in the following sections.

4.4 Load case No. 1 - Transverse loading

The first load case is the single transverse loading test. In this test, panels with different

connections and openings were tested and the test results are presented in this section.

Ten SIP specimens, i.e. two from each group panel specimen as previously detailed in section 4.3.1, were subjected to transverse loadings until failure. The test results obtained from the individual transverse only are served as a baseline for the study of SIP strength and stiffness when subjected to other individual and combined loading tests.

Figure 4.28 shows the test rig which was purposely built for this experimental study. The test rig consisted of steel C-Sections which were assembled by using M16 bolts. The test rig was then bolted to the strong floor.

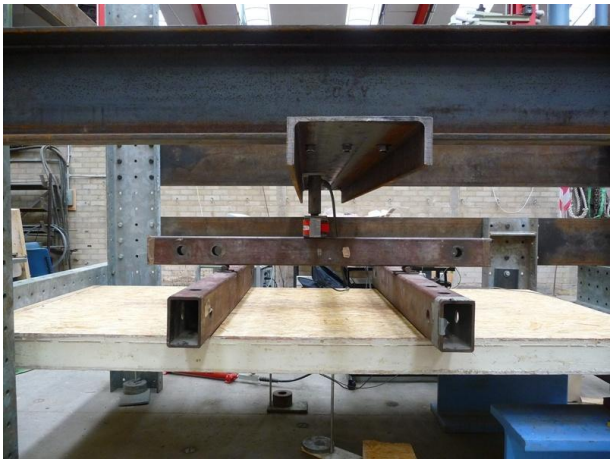

Figure 4.28: Experimental apparatus for transverse loading test

The test panels were then attached to the test rig by using two M8 bolts at the bottom of the panel specimens as illustrated in Figure 4.29. Although these bolt positions were in accordance with the racking test requirement, in order to keep an consistent support condition, it was decided to use the same arrangement in this transverse test as well. It is worth nothing that these bolt positions yield similar structural performance to the symmetric bolt arrangement, i.e. at 300 mm and 900 mm. Another end of the panel was supported by a 30 mm diameter steel roller

providing freedom to move horizontally (see Figure 4.30). Two line loads, which are 806 mm apart, were symmetrically applied through load spreader on two 100 mm width steel box beams. On the top of these steel box beams, a third steel box beam was placed in the orthogonal direction, supported by steel plates with one side welded to the 15 mm diameter steel roller and another free to move horizontally to create a simply supported condition. The loads were then applied by using a hydraulic hand pump through the load-cell that connected to the Grant data logging system in order to record the applied load.

Figure 4.29: Test panel was bolted at 150 mm and 750 mm to the test rig

Figure 4.30: Roller support at another end

Three LVDTs were used to measure the displacements. They were positioned on top of the test panels at the following locations for those test panels without openings. It should be noted that the positions of the LVDT were on top of the panels because the panels at failure could fall in a brittle manner and would damage the equipment otherwise. Figure 4.31 shows the LVDT positions and the sign convention of the displacement.

- LVDT No.1 was positioned at the central of the panel for measuring the vertical displacement.

- LVDT No.2 was positioned at mid-length and approximately at 10 mm from the edge of the panel for measuring the vertical displacement.

- LVDT No.3 was positioned at the mid-plane and the edge of the panel for measuring the horizontal displacement.

For the test panels with openings, LVDT No.1 was repositioned to be at the mid-length and approximately at 10 mm from the edge of the opening as illustrated in Figure 4.32.

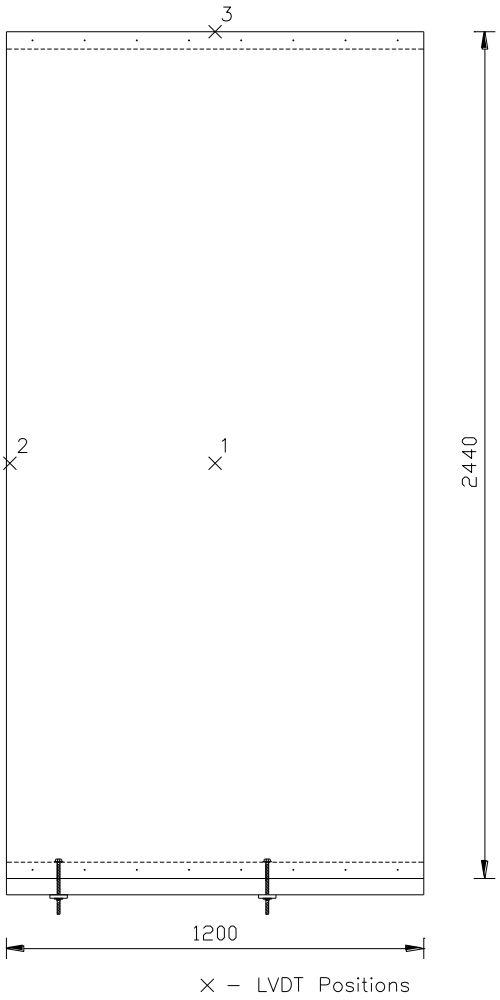

(a) Three LVDT locations

(b) LVDT No.1 and 2 locations

(c) LVDT No.3 location

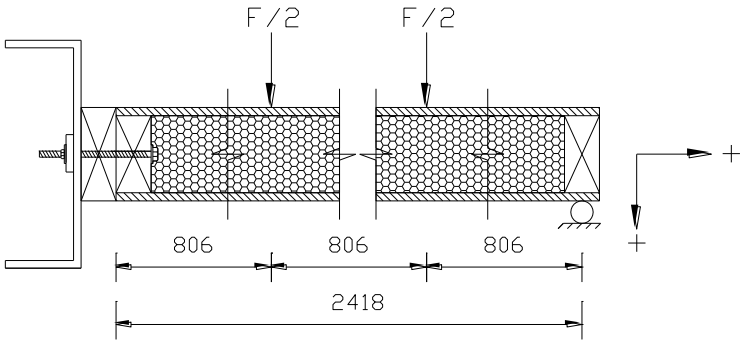

(d) Sign convention of displacement

Figure 4.31: LVDT arrangement and sign convention of displacement

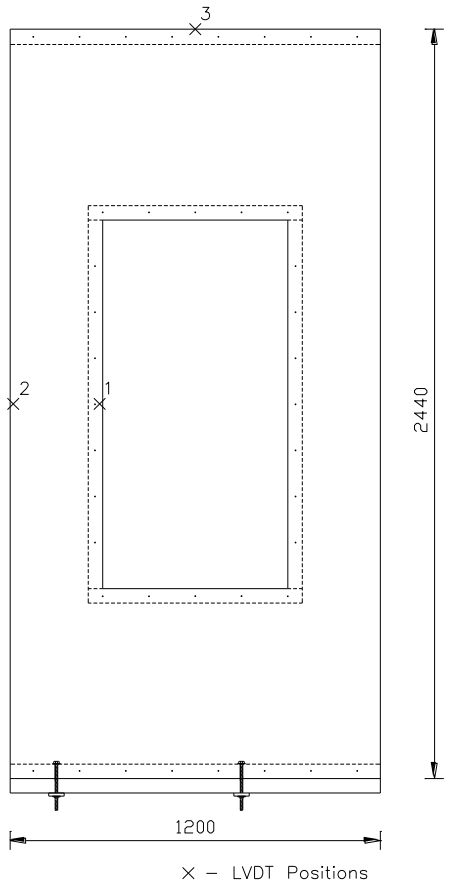

Figure 4.32: LVDT arrangement for panels with openings

4.4.1 Experimental investigations for panels without opening

Figure 4.33 shows the applied loads against the central vertical displacements of the two typical panels (STP), two panels with mini-SIP connections (SMC) and two panels with dimensional timber spline connections (SDC).

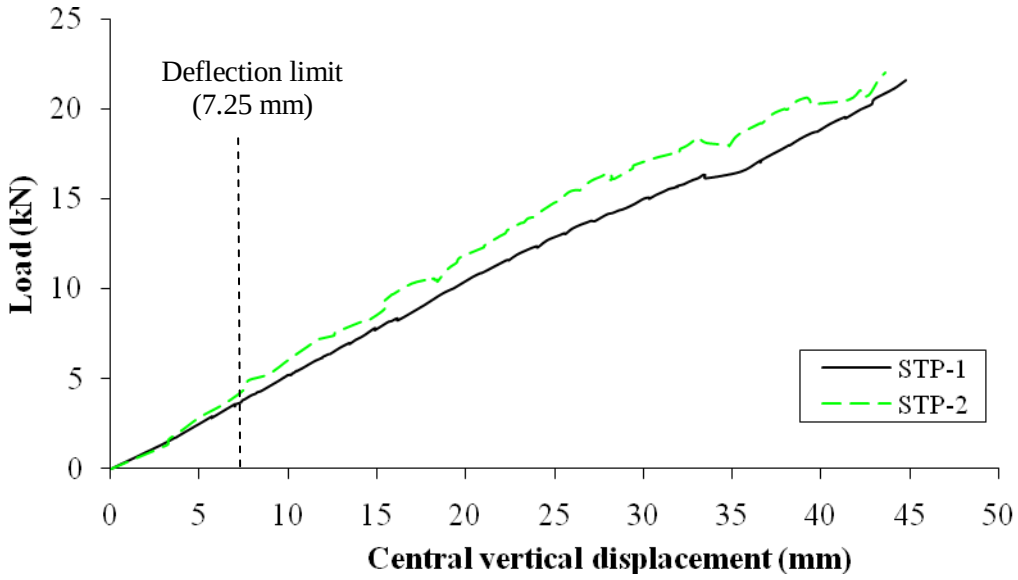
Deflection limit
(7.25 mm)
Load (kN)
Central vertical displacement (mm)
STP-1
STP-2
0
5
10
15
20
25
30
35
40
45
50

(a) STP

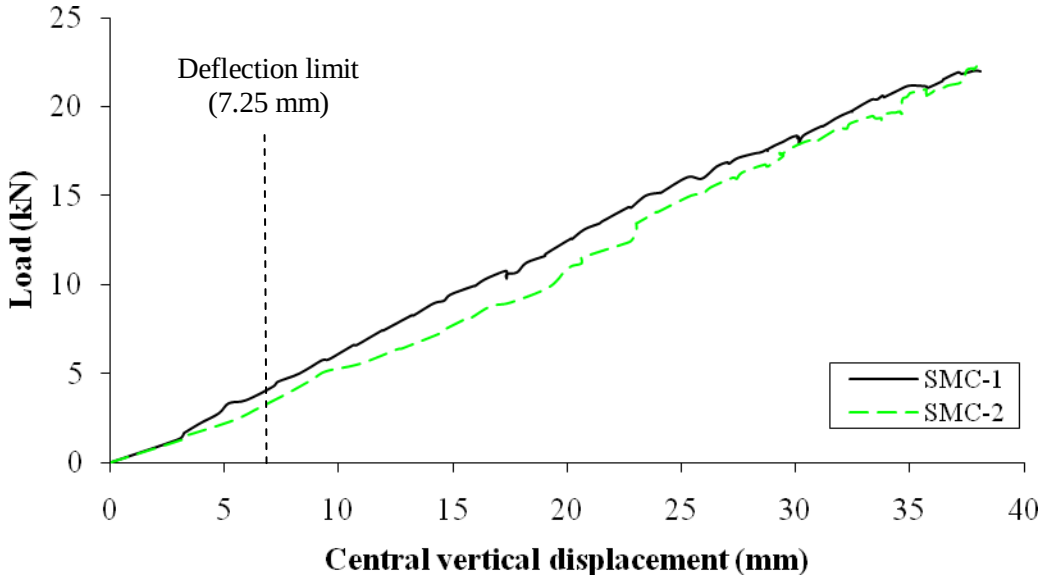
Deflection limit
(7.25 mm)
Load (kN)
Central vertical displacement (mm)
SMC-1
SMC-2
0
5
10
15
20
25
30
35
40

(b) SMC

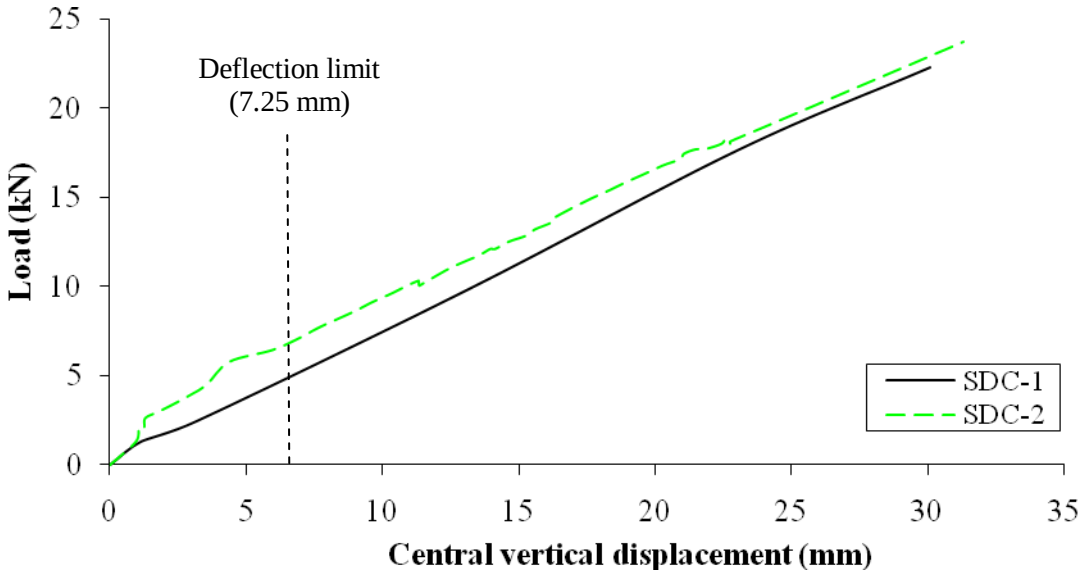

(C) SDC

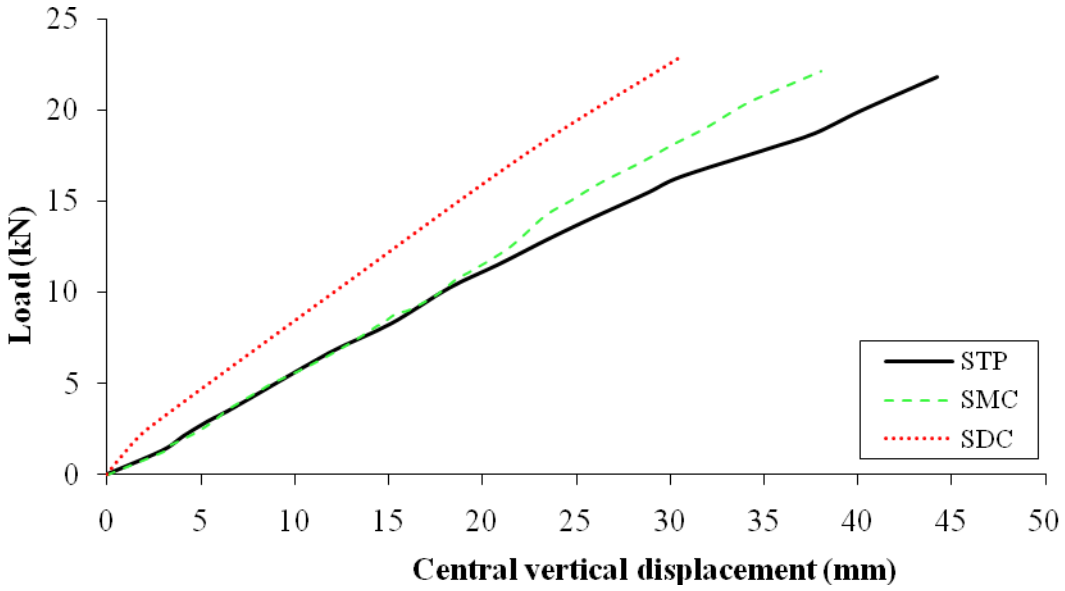

(d) Mean test result comparison of SIPs with different connections

Figure 4.33: Load versus central vertical displacement (LVDT No.1)

As previously mentioned with regards to the deflection limit in section 3.6, the limiting deflection value has been also chosen to be $\ell/333$ (7.25 mm) for this experimental study. From the test results, it should be noted that the deflection of the panel becomes the governing factor of the loading capacity. The failure modes were found to be the inner core debonded from the

top outer faces adjacent to the footer as shown in Figure 4.34. A close examination of failure point revealed that the footer was firmly connected to the sole plate and then supporting frame through bolts. While both facial panels were nailed to the rather fixed footer, it creates a discontinued course of line between the core and timber footer. This could lead to a higher interfacial shear together with a high peeling stress between the top outer face and the inner core, which would trigger the debonding failure. This failure mode indicates a brittle nature of SIP specimen when subjected to transverse loading as can be seen in the load-deflection curve (Figure 4.33) where the deflection is almost linear up to failure.

(a) STP-1

(b) STP-2

(c) SMC-1

(d) SMC-2

(e) SDC-1 (f) SDC-2

Figure 4.34: Debonding failure modes

Figure 4.35 plots the applied loads against the vertical displacements at 10 mm from the edge of the panels (LVDT No.2).

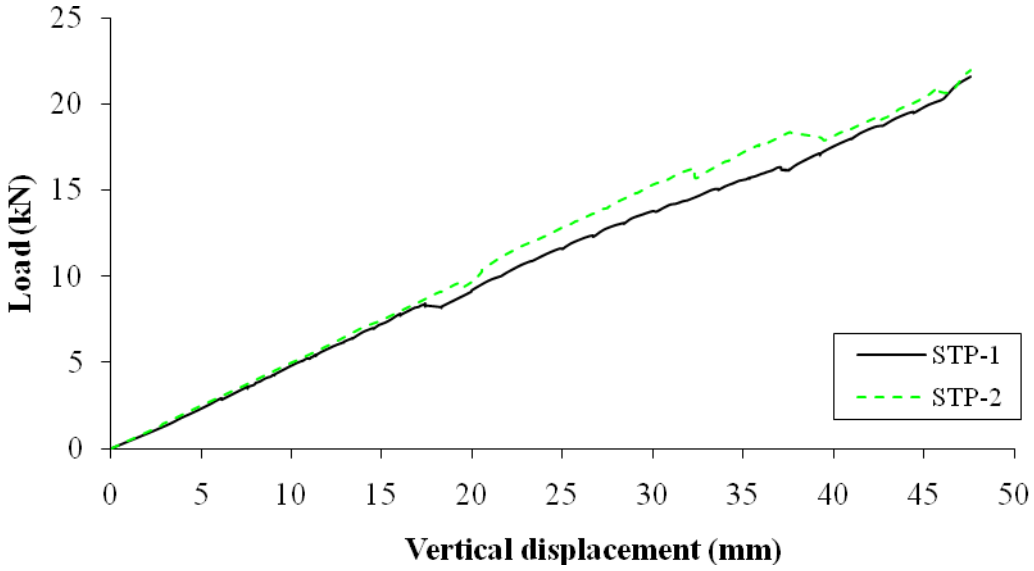

(a) STP

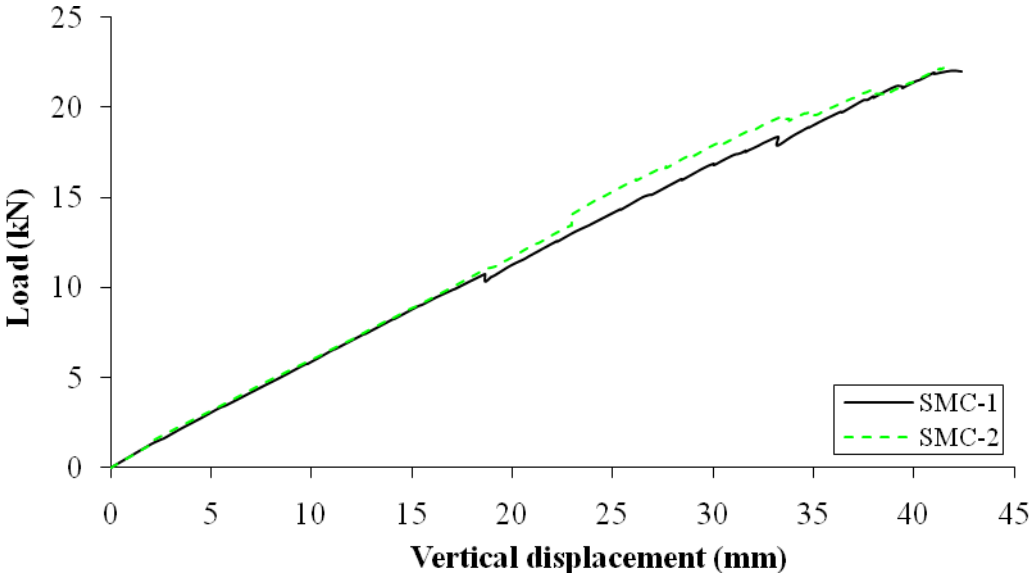

(b) SMC

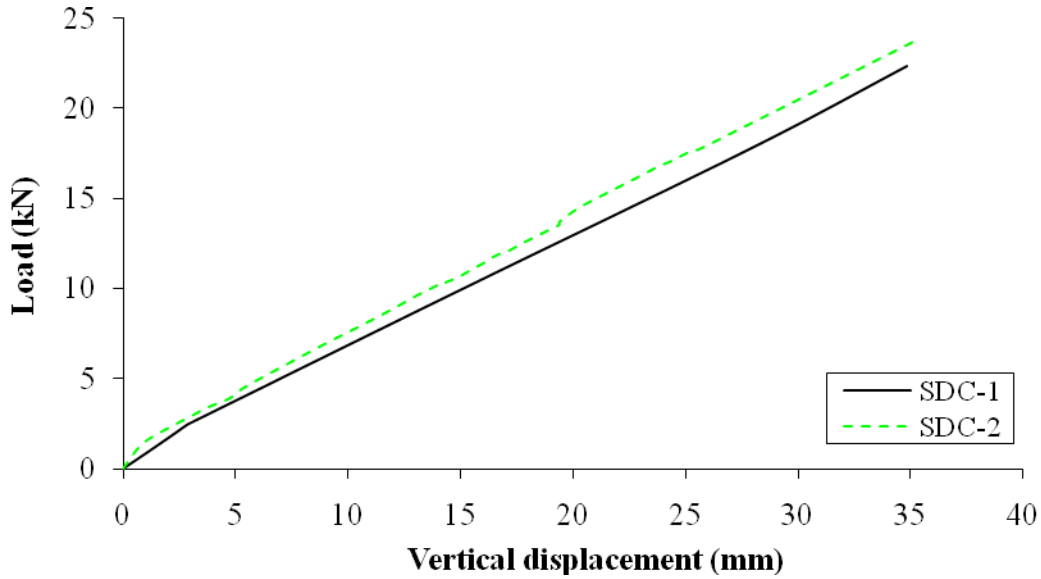

(C) SDC

Figure 4.35: Load versus vertical displacement (LVDT No.2)

The mean displacement at 10 mm from the panel edge (LVDT No.2) is slightly higher than the mean displacement at the central span (LVDT No.1) as shown in Figure 4.36. This is due to the well-acknowledged Poisson effect (Swanson, 2001) that the deflections near both edges, having no anticlastic curvature prevention, are higher than that at the mid-width. Although the load

applied at the top of steel box beams was as two point loads, the test panels were loaded as two uniformly distributed line loads. This is due to the fact that the steel box beams are much stiffer than the panel and the applied load is relatively low. Therefore, there is barely any variation in loading distribution in the panel width direction. This has also been proven by the observation from the test that the deflections measured at the centre and the edge of the panel are very close as presented in Figure 4.36.

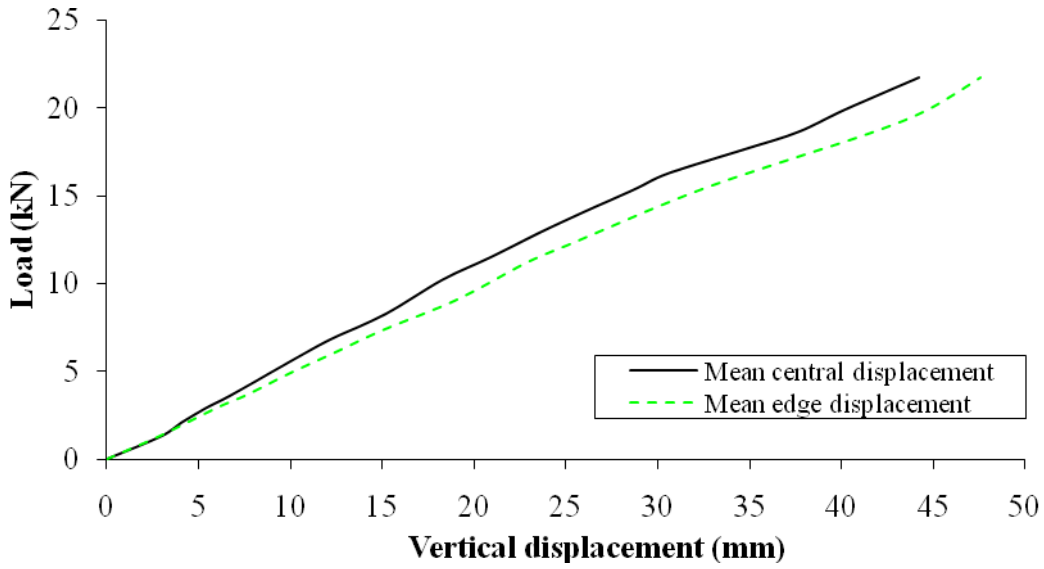

Figure 4.36: Typical load versus vertical displacement

at the central span (LVDT No.1) and at the panel edge (LVDT No.2)

The horizontal movements at the edge of the panels (LVDT No.3) are small (within 2.3 mm) as illustrated in Figure 4.37. The SMC panels did not initially move horizontally, moreover their movements are small (within 0.35 mm) as shown in Figure 4.37(b). It should be noted the horizontal displacement of the panel under the transverse load is negligible in comparison to the central displacement.

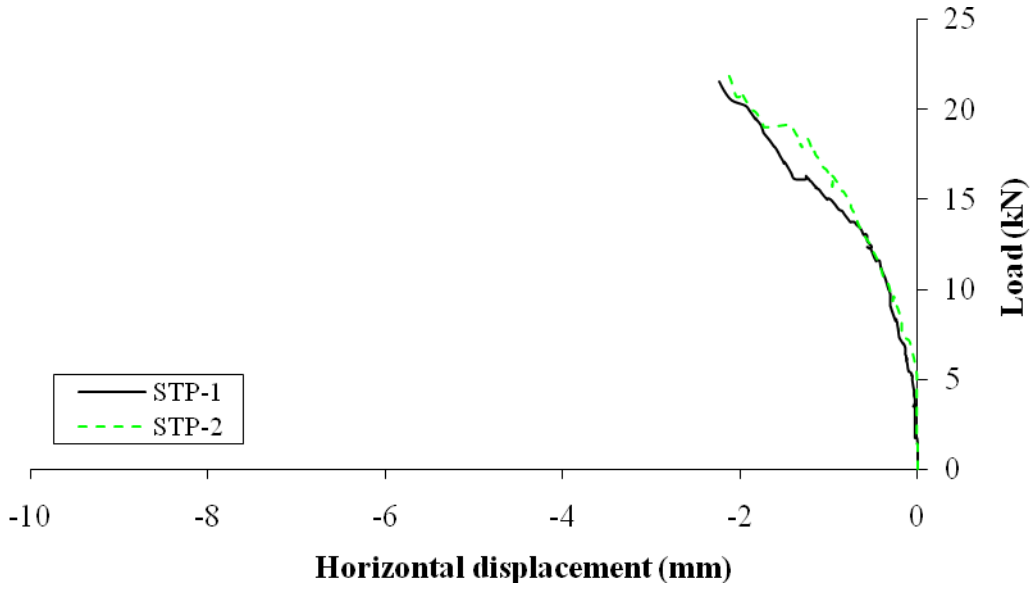
25
20
15
10
5
0
Load (kN)
STP-1
STP-2
-10
-8
-6
-4
-2
0
Horizontal displacement (mm)

(a) STP

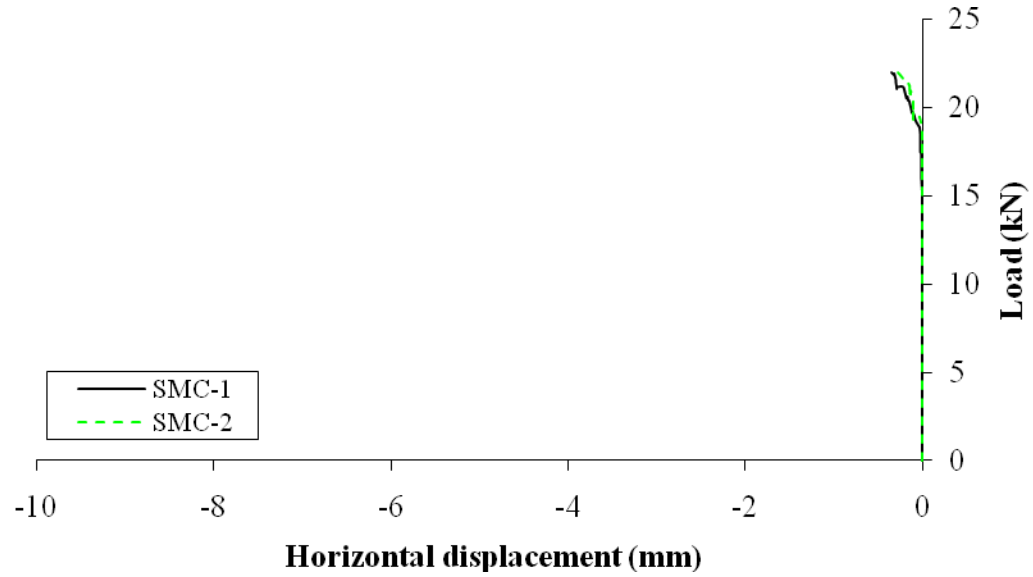
25
20
15
10
5
0
Load (kN)
SMC-1
SMC-2
-10
-8
-6
-4
-2
0
Horizontal displacement (mm)

(b) SMC

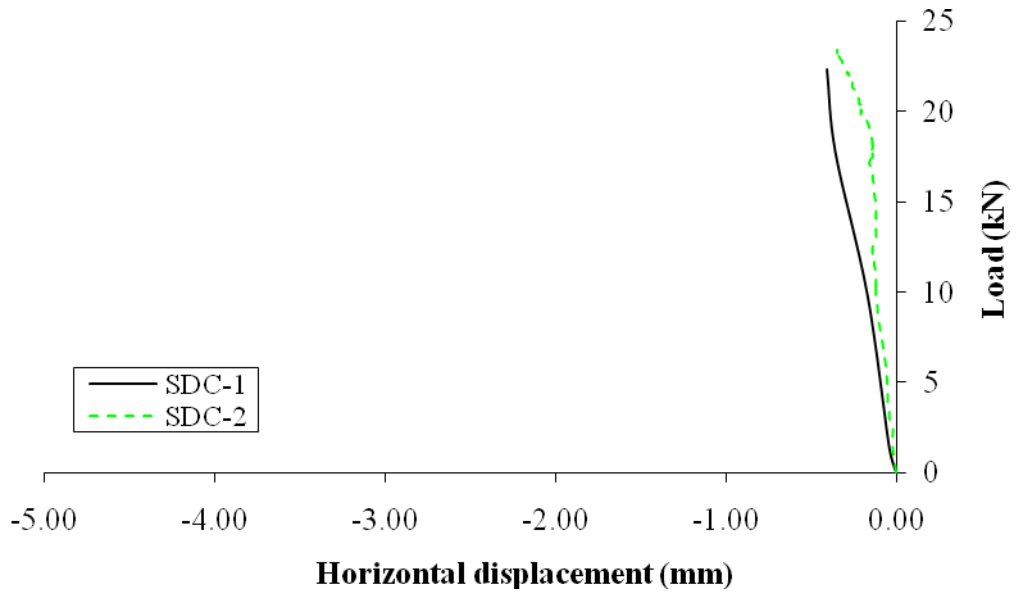

(c) SDC

Figure 4.37: Load versus horizontal displacement (LVDT No. 3)

Table 4.10 summarises the test results of the STP, SMC and SDC panels when subjected to transverse loading. Despite the mean loads at failure of typical panels, panels with mini-SIP connections and panels with dimensional timber spline connections are different by 5.65% (21.78 kN and 23.01 kN). It should be noted that in this experimental study, the ultimate load and the failure mode are not influenced by the type of joint designs and were physically tested as wall conditions. In contrast to the earlier findings in the four-point bending test on SIPs with different joints as floor or roof conditions (section 4.2), the test results illustrated that the mean ultimate load of the SDC (40.32 kN) that are 2.09 times of the similar mean ultimate loads of the STP and SMC (19.32 kN).

Specimen	STP	SMC	SDC
Ultimate Limit Load, ULL (kN)	21.78	22.16	23.01
Increase of ULL (%)	0	1.74	5.65
Load at deflection limit ℓ/333 (kN)	3.97	4.03	6.36
Serviceability load / Ultimate load (%)	18.3	18.2	27.6
Maximum central displacement (mm)	44.19	38.05	30.70
Maximum edge displacement (mm)	47.57	42.04	34.97
Maximum horizontal displacement (mm)	2.19	0.33	0.38
Experimental failure mode	Debonding		

Table 4.10: Experimental result summary

4.4.2 Analytical investigation

The central span deflection of the typical panel (STP) can be determined by using the classical theory. Three analytical methods were again employed, i.e. Allen (1969), TR 019 (EOTA, 2005) and BS EN 14509 (BSI, 2006). Although one end of the test panel is attached to the test rig by using two M8 bolts at the bottom of the panel specimen, it has been conservatively assumed to be a simply supported condition.

The panel details and material properties are listed in Table 4.11. Figure 4.38 illustrates the comparison between the STP mean test result with the three analytical methods. The present comparison further supports the previous finding in section 4.2 that Allen's method yields a good agreement than other methods as shown in Figure 4.38.

The applied tensile and compressive stresses in the outer faces can be determined by using equation 4.1. With the applied load of 21.78 kN, the applied tensile and compressive stresses in the outer faces are 5.80 N/mm^2, which are less than 10.85 N/mm^2 (tensile strength) and 15.75 N/mm^2 (compressive strength). As a result, no tensile and compressive failures of the outer faces occur.

***F* (kN)**	21.78
***B* (mm)**	1,200
***L* (mm)**	2,416.5
***f* (mm)**	11
d_c (mm)	103
***e* (mm)**	114
$E_{F1} = E_{F2}$ (N/mm^2)	3,844
E_c (N/mm^2)	6.442
***G* (N/mm^2)**	2.30

Table 4.11: STP details and material properties

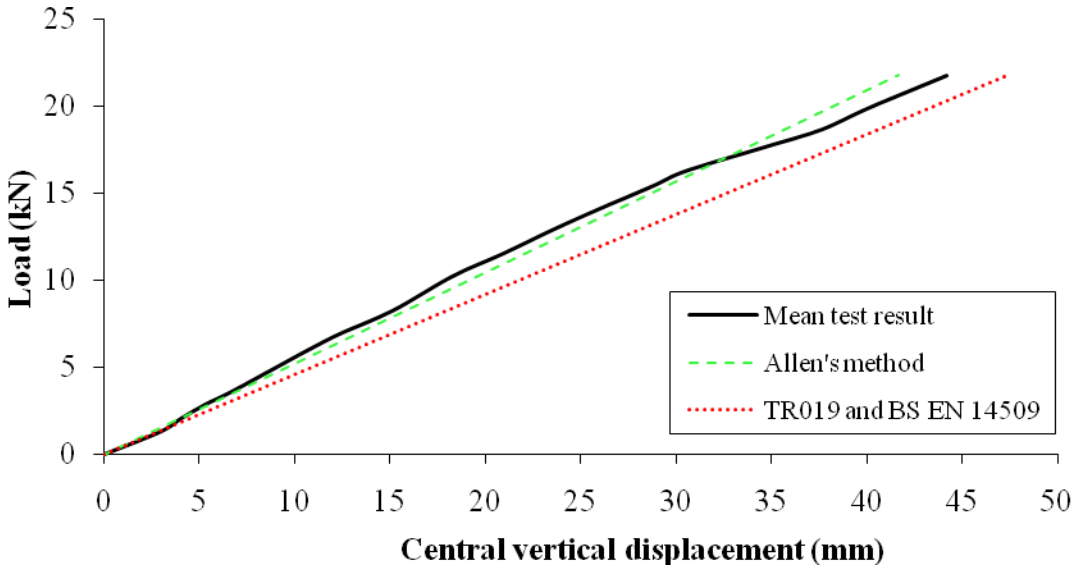

Figure 4.38: Comparison between the STP mean test result with the three analytical methods

The shear stress (τ) in the inner core can be obtained by using equation 4.2. With the applied load of 21.78 kN, the applied shear stress is 0.088 N/mm^2, which is less than 0.116 N/mm^2 shear strength. These panels would therefore not fail due to shear by the classical sandwich panel theory.

The central span deflection of SDC can be determined using TR 019 and EC5 analytical methods. Both TR 019 and EC5 methods were previously described in section 4.2. The panel details and material properties are again reproduced and listed in Table 4.12. The effective

flange width of both compression and tension obtained from EC5 (322 mm) is less than TR 019 (816 mm). Accordingly, the central deflection determined by EC5 is higher than TR 019.

***F* (kN)**	23.01
***B* (mm)**	1,200
***L* (mm)**	2,416.5
***f* (mm)**	11
d_c **(mm)**	103
***e* (mm)**	114
E_{11} **(N/mm^2)**	3,844
E_{33} **(N/mm^2)**	3,615
G_{C16} **(N/mm^2)**	500
υ	0.24

Table 4.12: SDC details and material properties

Figure 4.39 illustrates the comparison between the mean test result with the TR 019 and EC5 analytical methods. As shown in Figure 4.39, the mean test result agrees well with the TR 019 method, but less consistent at the higher applied load.

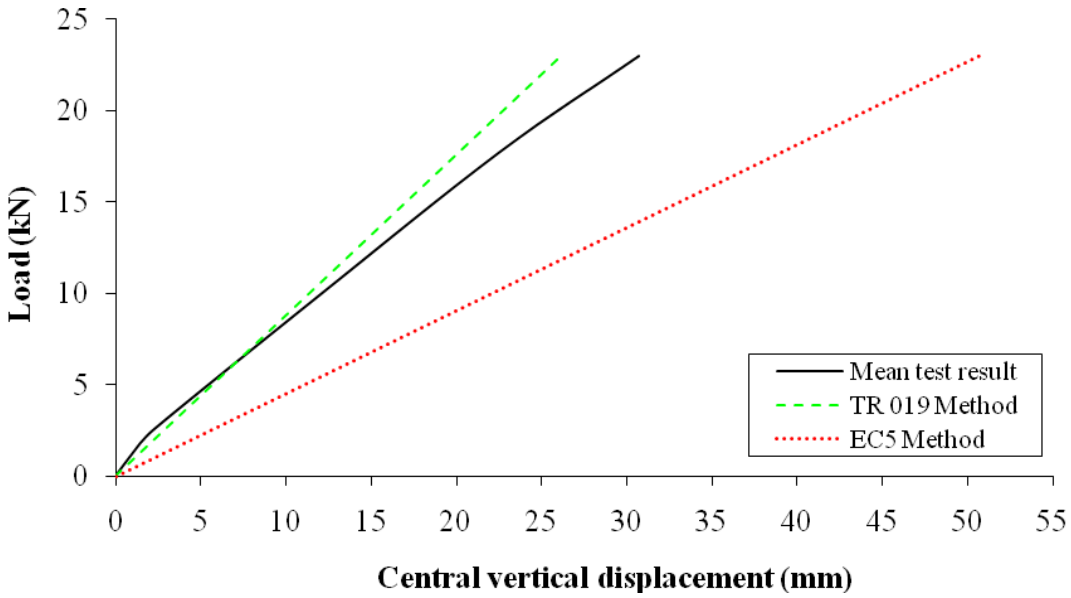

Figure 4.39: Comparison between the mean SDC test result with different methods

Due to the fact that these SDC panels are manufactured without recesses, the analytical and FEM methods can obviously be compared. The FEM result, which will be presented in the next section, is consistent with the TR 019 rather than EC5 method as illustrated in Figure 4.40. This finding indicates the TR 019 is preferable to be used in determination of the central span deflection.

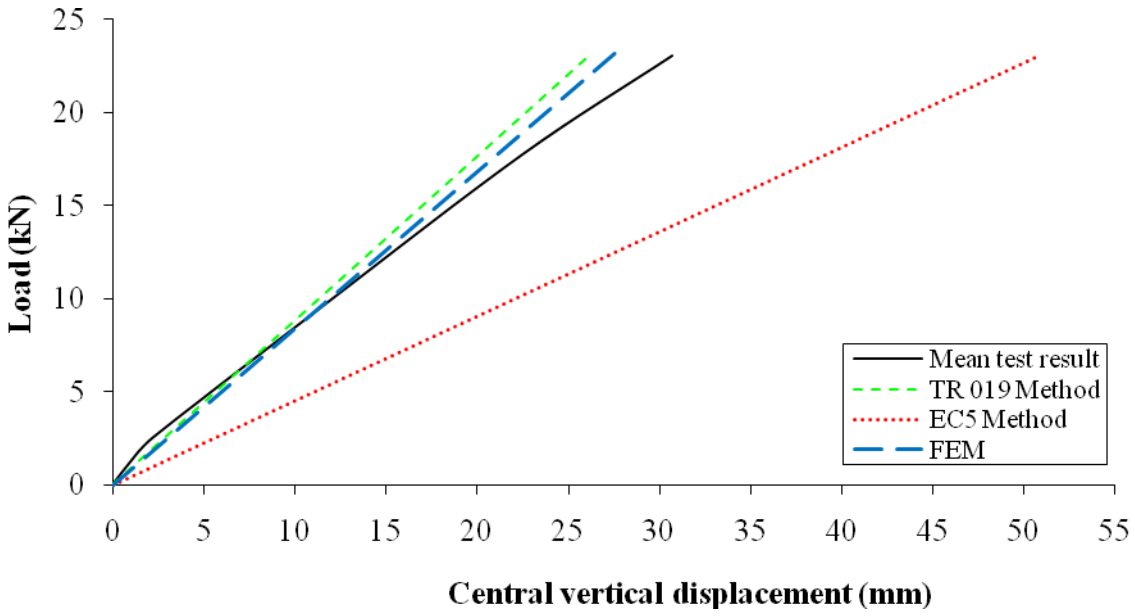

Figure 4.40: Comparison between the mean SDC test result with different methods

4.4.3 Numerical investigation

All panels were modelled as three-dimensional models. The concept to model the panels is as same as the panels in the four-point bending test in which has been presented in section 4.2.

The sole plates were not modelled since they were used to support the panels and did not contribute to the strengths of the panels. This could reduce the computational effort.

All panels cannot be modelled as a quarter of the whole specimen since the two end supports are different. The bolt positions in this numerical investigation were assumed to be at 300 mm

and 900 mm instead of 150 mm and 750 mm. By using this assumption, a half of the whole specimen was modelled and it was expected that the structural performance should be similar. A full model was carried out and found that the structural performance is similar to the half model. Thus, the XSYMM boundary condition was applied to the vertical surface at the mid-width. This technique can save the computational efforts significantly.

A line of pin support through the footer was applied to the centre of the footer. At the other end, the roller support ($U_y = 0$) was applied at the OSB bottom face at the 23.5 mm off the panel edge. In order to save more computational efforts, the four-point bending loads were applied directly to the OSB top surface. Thus, the steel loading plates were not modelled. Figure 4.41 presents the finite element model for STP model. SMC and SDC models are similar to the STP model.

The structured mesh technique for these models was also 20-node hexahedral elements with reduced integration (C3D20R). OSB faces were again divided into two elements in the thickness direction. In addition, 10 mm wide fine element sizes were used in the region of high stress gradients which are at approximately 150 mm from both panel ends and at the applied load positions. Meanwhile, 20 mm wide coarse element sizes were used elsewhere. The cross panel direction was subsequently discretised with 20 mm elements.

PUR inner core was discretised into 10 x 20 x 20 mm elements in the region of high stress gradients as described in the OSB faces. Likewise, 20 x 20 x 20 mm elements were used elsewhere. Finally, the C16 header and footer, located in the high stress regions, were discretised with 10 x 10 x 20 fine element sizes. A sensitivity analysis on the density of mesh element was also carried out and found that these elements were fine enough to provide satisfactory results.

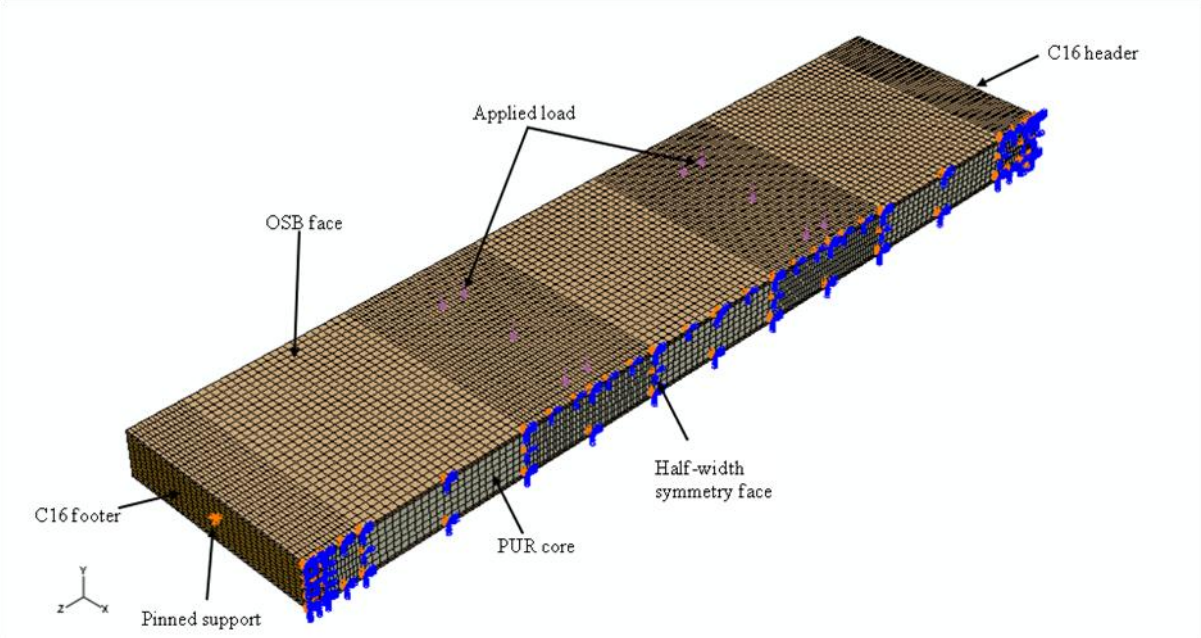

(a)

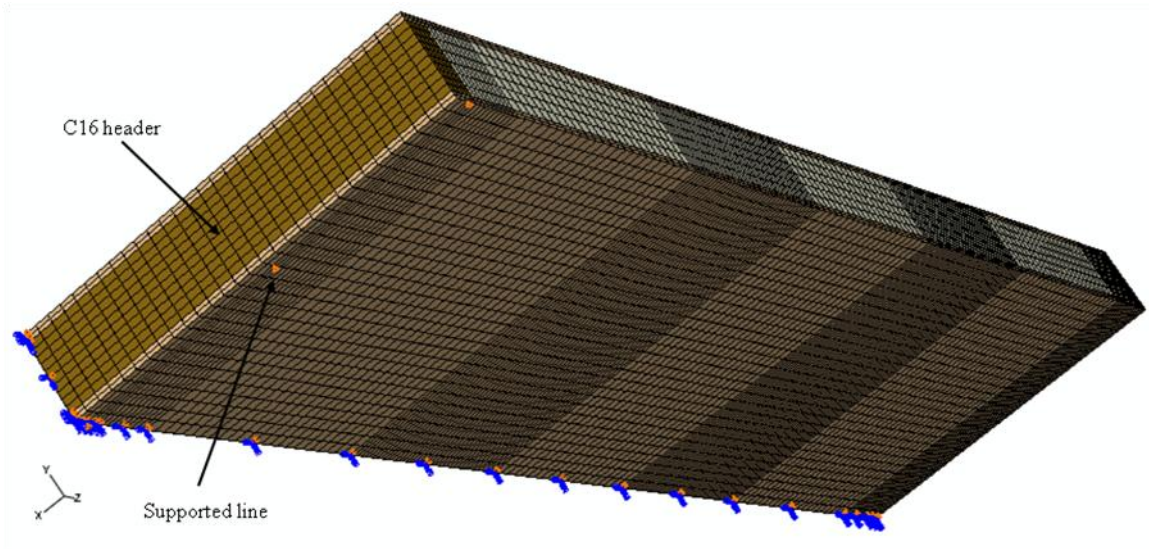

(b)

Figure 4.41: STP finite element model

The material properties of the SIP components are as same as previously used in the preceding sections. The nonlinear geometry, i.e. *NLGEOM option in the ABAQUS, was also included in this investigation.

In order to ensure that the failure would occur in the FEM investigations, the applied loads equal to 25 kN was applied to the STP and SMC models, whereas 30 kN was applied to the SDC model. These loads are higher than the mean failure loads found from the experimental investigations. Figures 4.42 and 4.43 present typical distributions of the stresses of the SIP constituents for the STP model. The stress distributions and the maximum stresses of SMC and SDC models have been found at the same locations as in the case of the STP model. As a result, the contour plots of SMC and SDC are therefore not presented.

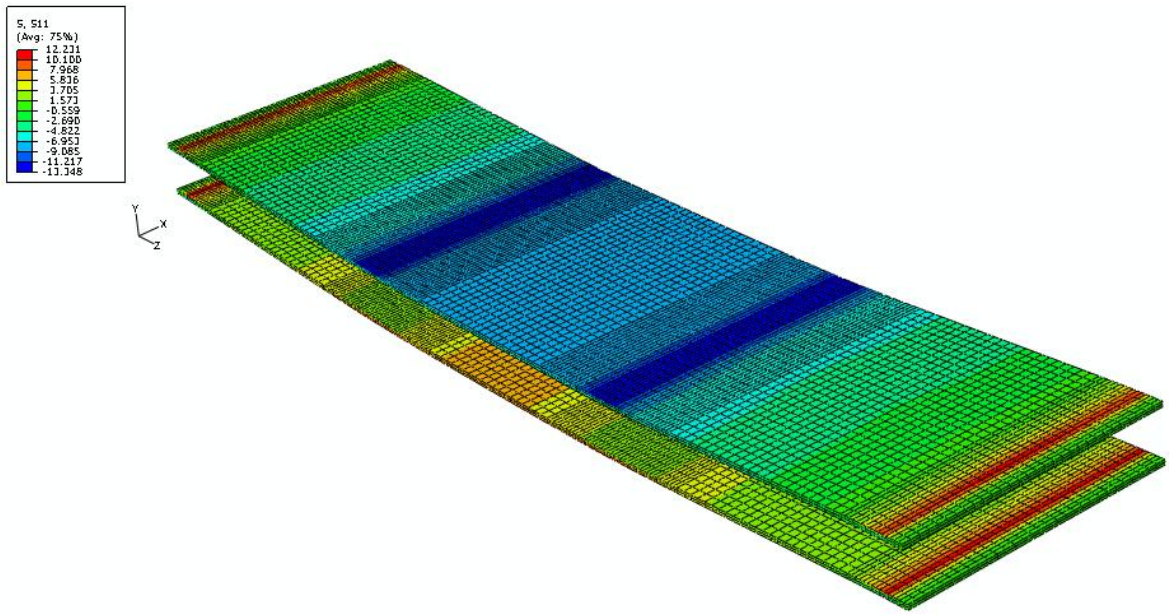

(a) Distribution of the longitudinal stress (S_{11}) of the outer faces

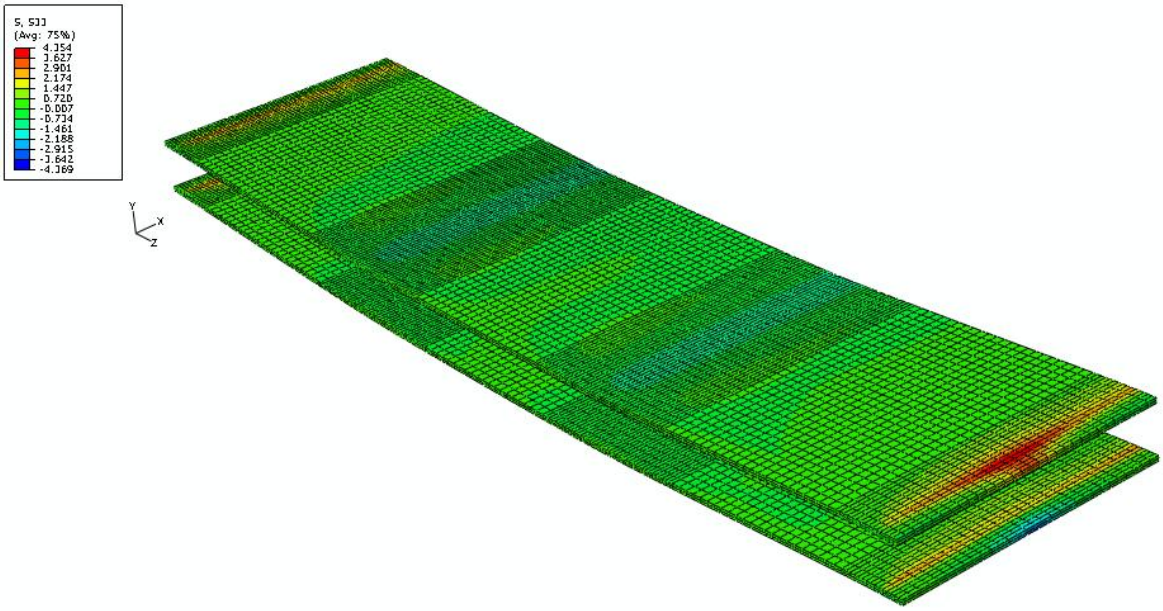

(b) Distribution of the transverse stress (S_{33}) of the outer faces

Figure 4.42: Distribution of the outer face stresses

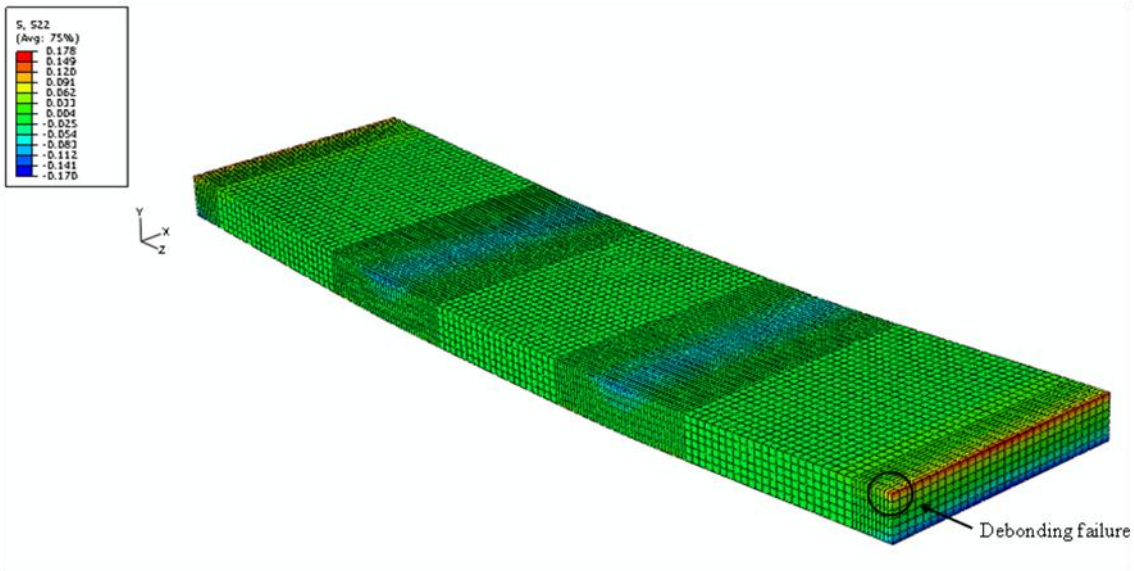

(a) Distribution of the normal stress (S_{22}) of the PUR inner core

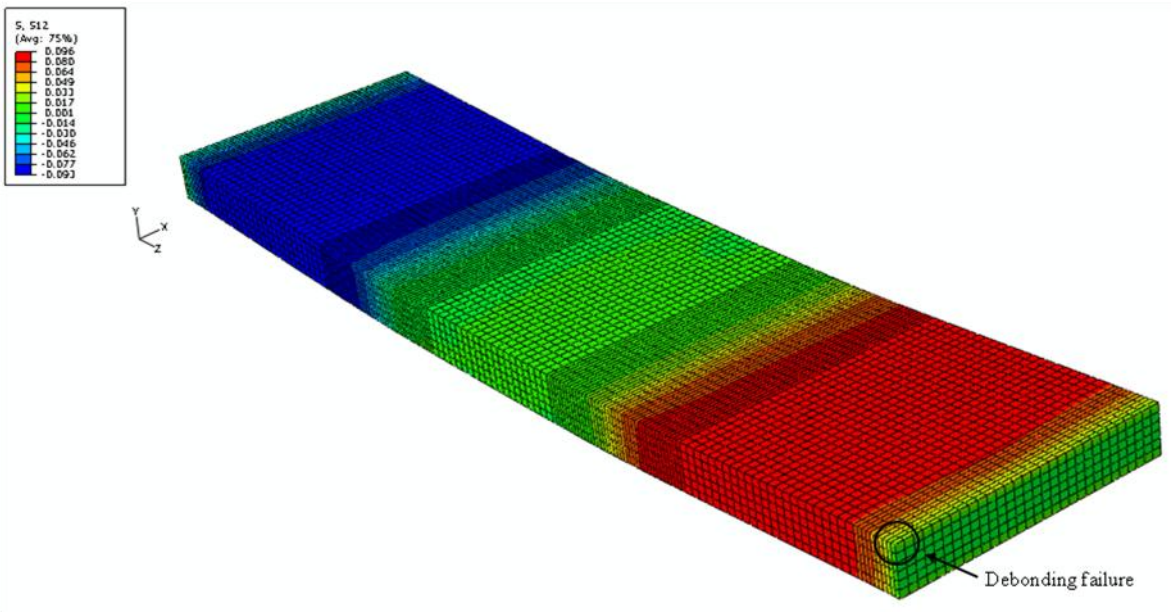

(b) Distribution of the shear stress (S_{12}) of the PUR inner core

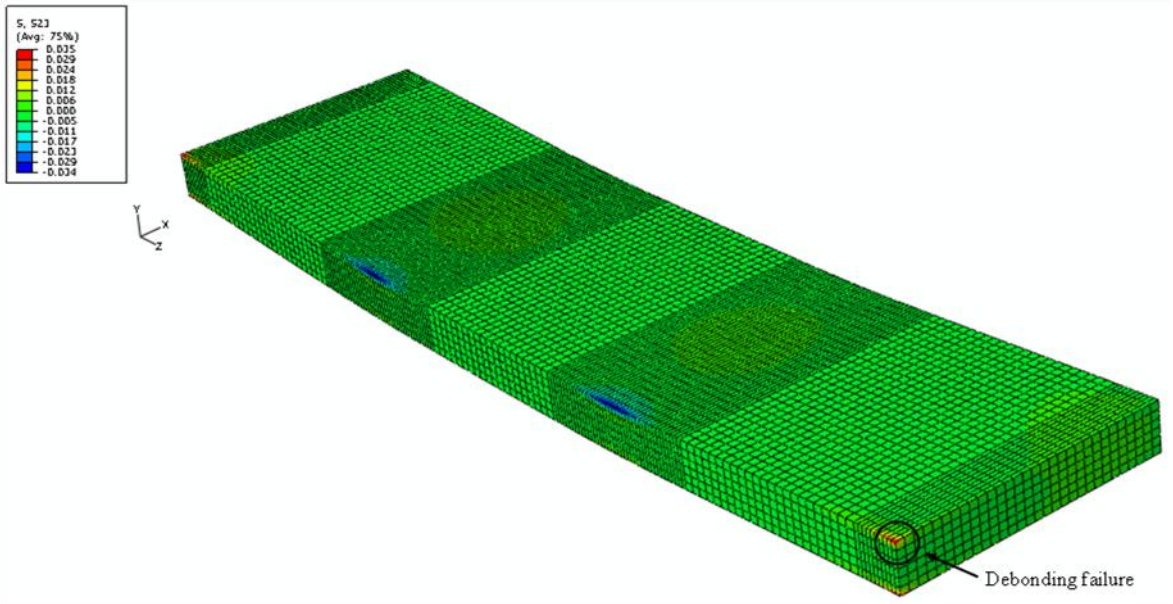

(c) Distribution of the shear stress (S_{23}) of the PUR inner core

Figure 4.43: Distribution of the stresses of the PUR inner core

Tables 4.13 and 4.14 present the maximum stresses obtained from the finite element analysis of the OSB and the PUR, respectively. At 25 kN (for STP and SMC) and 30 kN (for SDC) applied loads, the outer faces are able to sustain without any failures in both longitudinal and transverse directions Figures 4.43(a) and 4.43 (b). Meanwhile, the inner cores fail due to the debonding in both linear stress and Hashin Rotem's criteria as tabulated in Table 4.14 and indicated in Figures 4.44(a) to 4.44(c).

Further back track analysis was performed in order to determine the loading levels that the FEM specimens began to fail. The initial failure reveals the debonding failure at the OSB-PUR interface that has been found to agree with the experimental finding. It is interesting to note that the initial failure loads due to the debonding from Hashin Rotem's criterion are higher than the experimental failure loads as tabulated in Table 4.14(c). As a result, Hashin Rotem's criterion provides less agreement to the experimental results. The initial failure loads due to the debonding from the linear stress criterion are in favourable and subsequently used in this investigation as tabulated in Table 4.14(b).

Specimen	Load (kN)	Failure	S_{11} (N/mm^2)	S_{33} (N/mm^2)	S_{11} / f_{11}	S_{33} / f_{33}	Remark
STP	25.0	Bending	13.35	4.37	0.81	0.53	Pass
SMC	25.0		13.65	4.31	0.83	0.53	
SDC	30.0		14.03	4.09	0.86	0.50	

where f_{11} and f_{33} are bending failure stresses, equal to 16.40 N/mm^2 and 8.20 N/mm^2, respectively.

Table 4.13: Stresses results in the OSB outer faces

Specimen	Load (kN)	Failure	S_{12} (N/mm^2)	S_{12} / f_{12}	Remark
STP	25.0	Shear	0.096	1.38	Pass
SMC	25.0		0.096	1.36	
SDC	30.0		0.093	1.31	

where f_{12} is shear failure stress, equals to 0.116 N/mm^2.

(a) Shear

Specimen	Load (kN)	Failure	S_{22} (N/mm^2)	S_{12} (N/mm^2)	S_{23} (N/mm^2)	Linear stress criterion $S_{22}/f_{22}+S_{12}/f_{12}+S_{23}/f_{23}$	Remark
STP	25.0	Debonding	0.158	0.022	0.035	1.33	Fail
	18.7		0.118	0.016	0.026	0.99	Pass
SMC	25.0		0.146	0.023	0.030	1.23	Fail
	20.2		0.118	0.019	0.024	0.99	Pass
SDC	30.0		0.146	0.027	0.031	1.28	Fail
	23.4		0.114	0.021	0.024	0.99	Pass

where f_{22}, f_{12} and f_{23} are failure stresses, equal to 0.188 N/mm^2, 0.116 N/mm^2 and 0.116 N/mm^2, respectively.

(b) Debonding – Linear stress criterion

Specimen	Load (kN)	Failure	S_{22} (N/mm^2)	S_{12} (N/mm^2)	S_{23} (N/mm^2)	Hashin Rotem's criterion $(S_{22}/f_{22})^2+(S_{12}/f_{12})^2+(S_{23}/f_{23})^2$	Remark
STP	25.0	Debonding	0.158	0.022	0.035	0.83	Pass
	27.3		0.172	0.024	0.038	0.99	
SMC	25.0		0.146	0.023	0.030	0.71	
	29.5		0.172	0.027	0.035	0.99	
SDC	30.0		0.146	0.027	0.031	0.73	
	35.0		0.170	0.031	0.036	0.99	

where f_{22}, f_{12} and f_{23} are failure stresses, equal to 0.188 N/mm^2, 0.116 N/mm^2 and 0.116 N/mm^2, respectively.

(c) Debonding stress results

Table 4.14: Stress results in the PUR core

Figures 4.44 to 4.46 show the load and the deflection curves comparison between the FEM and the mean test results up to the initial failure load. The agreement of the vertical displacements is pretty encouraging as shown in Figures 4.44 and 4.45.

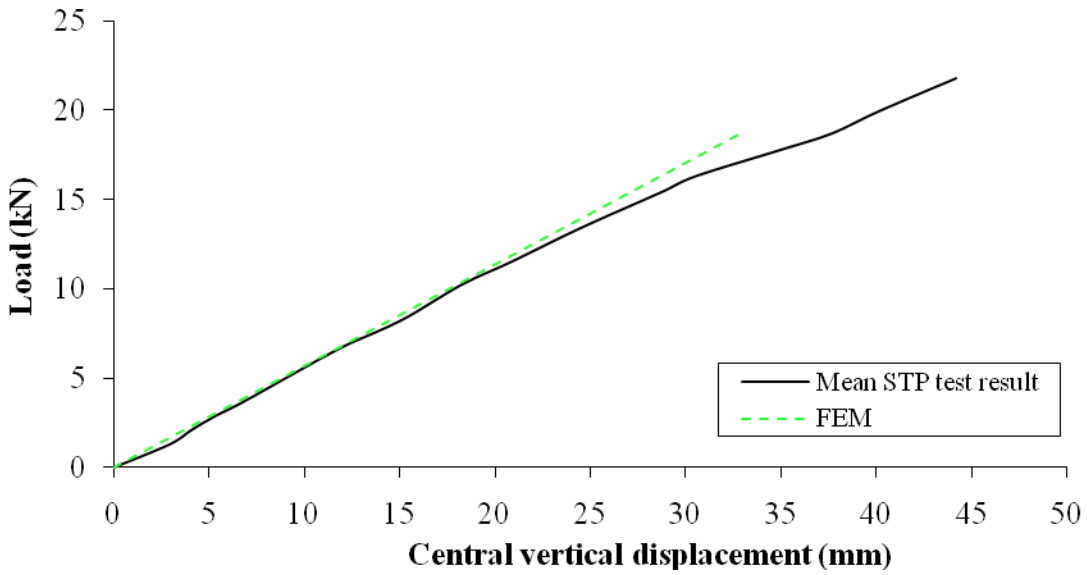

(a) STP

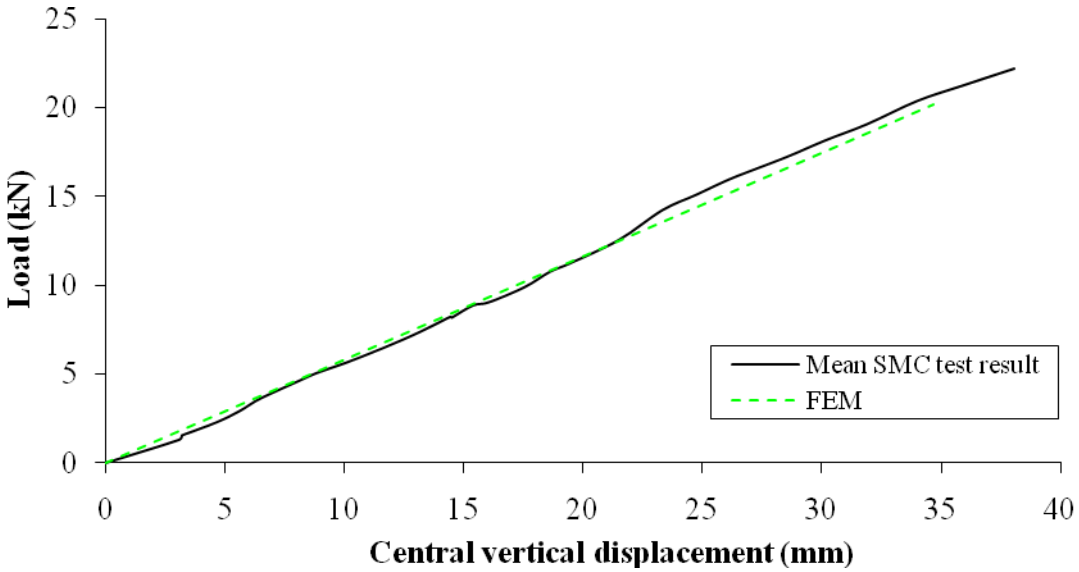

(b) SMC

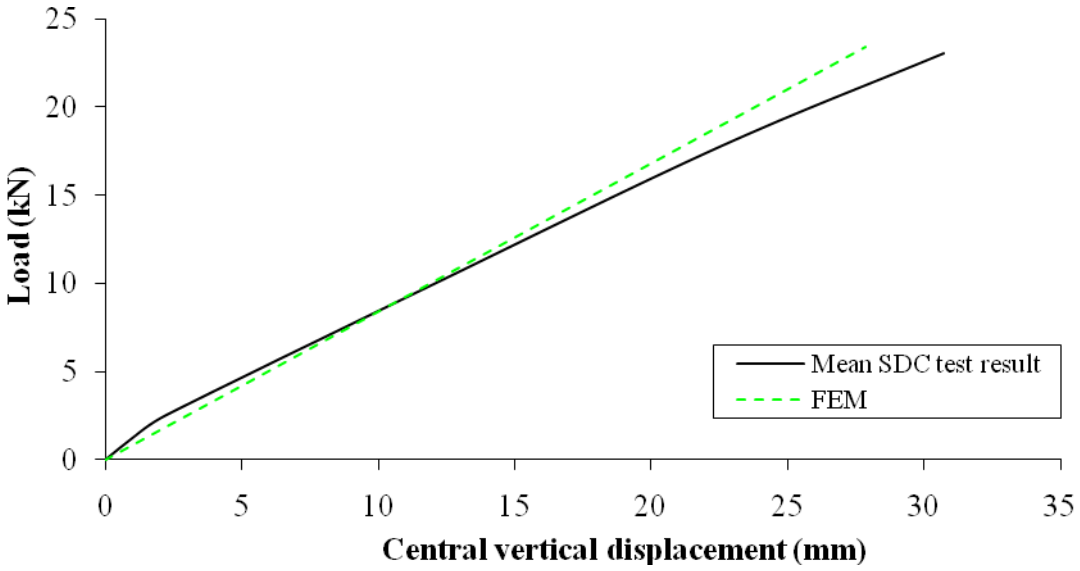

(c) SDC

Figure 4.44: Central deflection comparison between the FEM and the mean test results

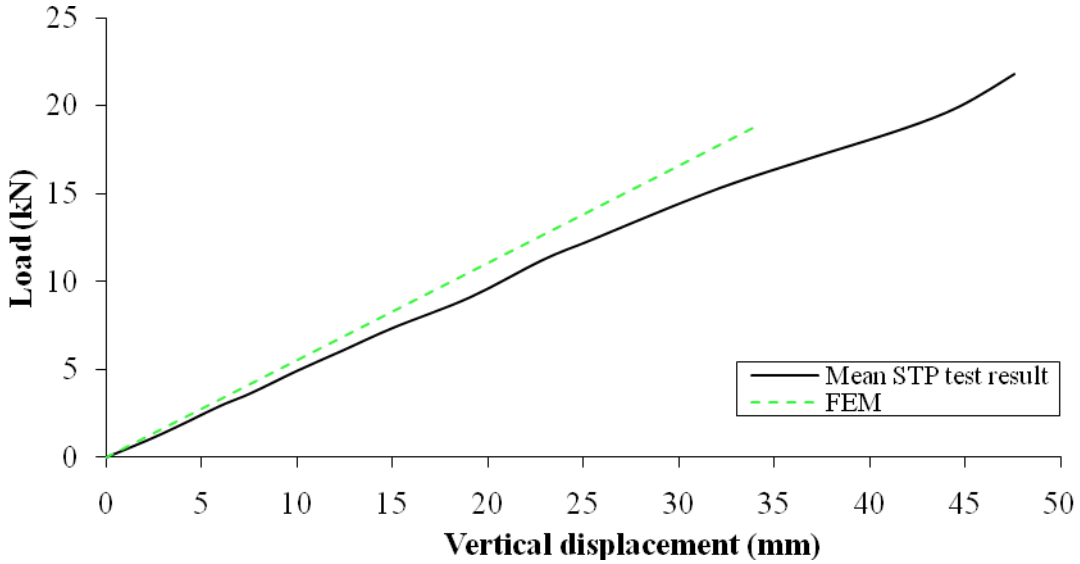

(a) STP

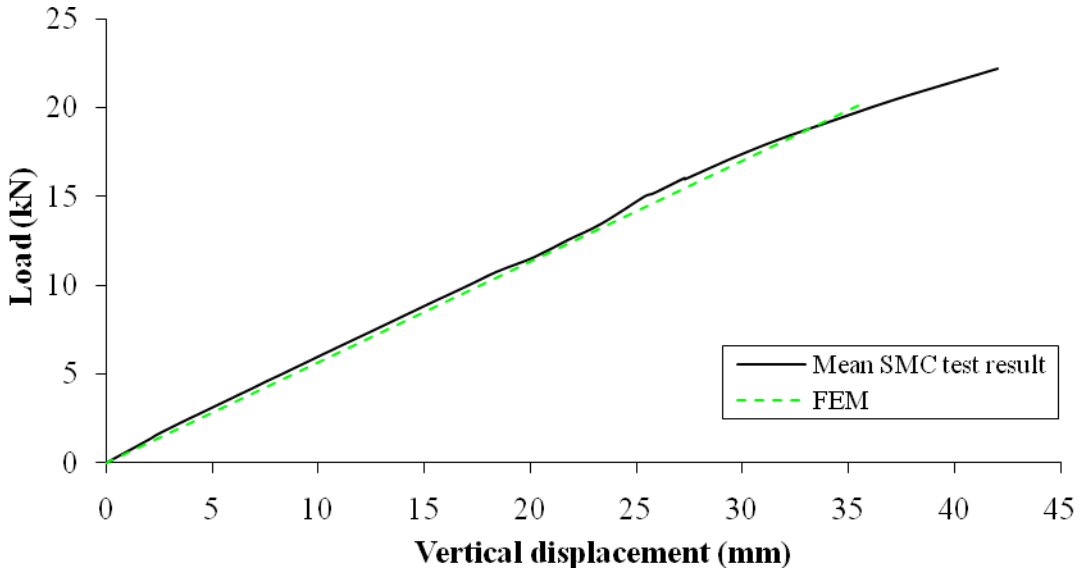

(b) SMC

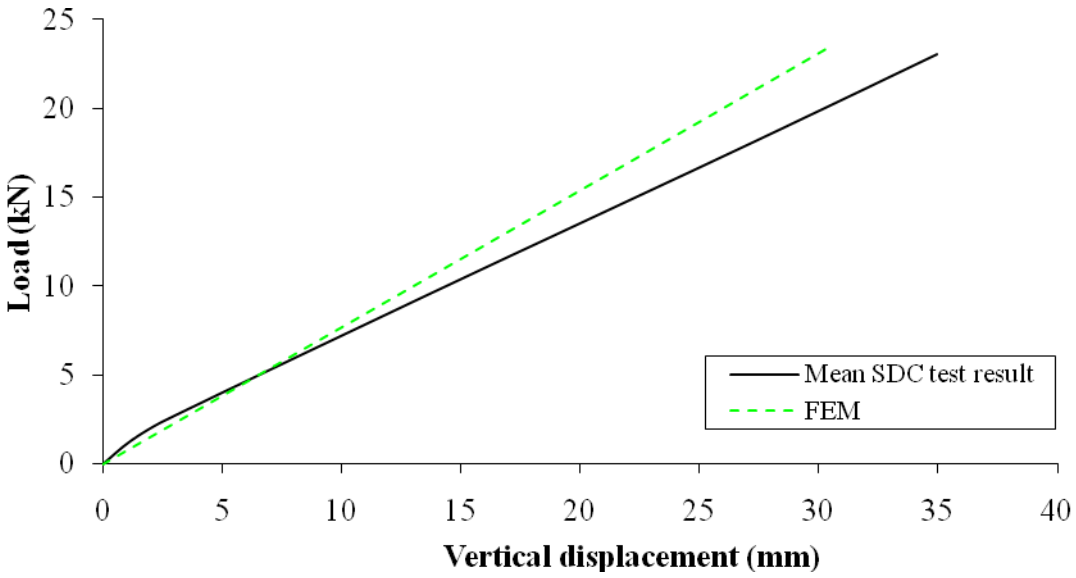

(c) SDC

Figure 4.45: Edge deflection comparison between the FEM and the mean test results

The horizontal displacements at the edge from the FEM investigation are also small as illustrated in Figure 4.46. These horizontal movements have again revealed their less concern in engineering practice in comparison to the central deflections.

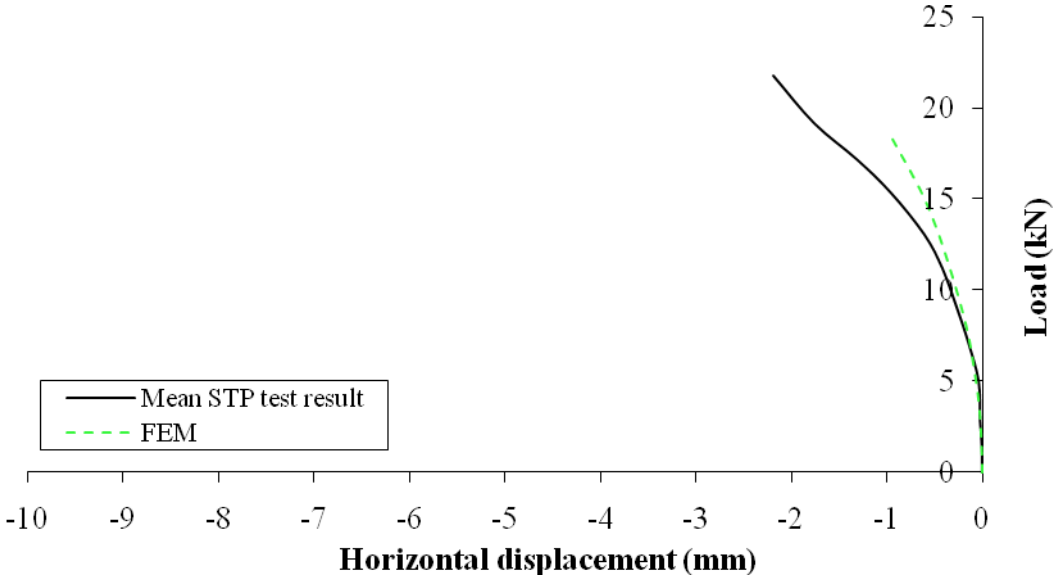
25
20
15
10
5
0
Load (kN)
Mean STP test result
FEM
-10
-9
-8
-7
-6
-5
-4
-3
-2
-1
0
Horizontal displacement (mm)

(a) STP

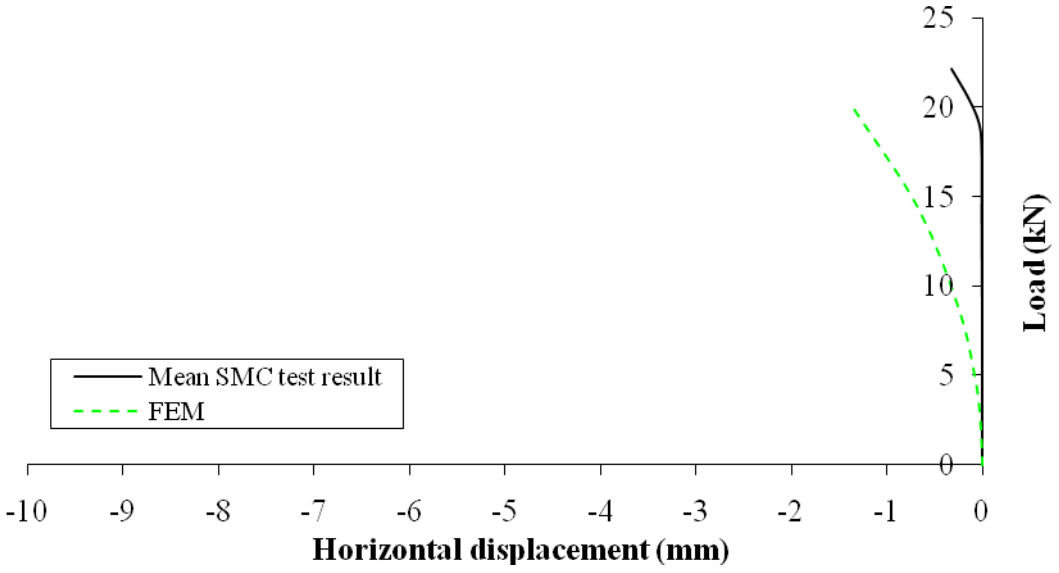
25
20
15
10
5
0
Load (kN)
Mean SMC test result
FEM
-10
-9
-8
-7
-6
-5
-4
-3
-2
-1
0
Horizontal displacement (mm)

(b) SMC

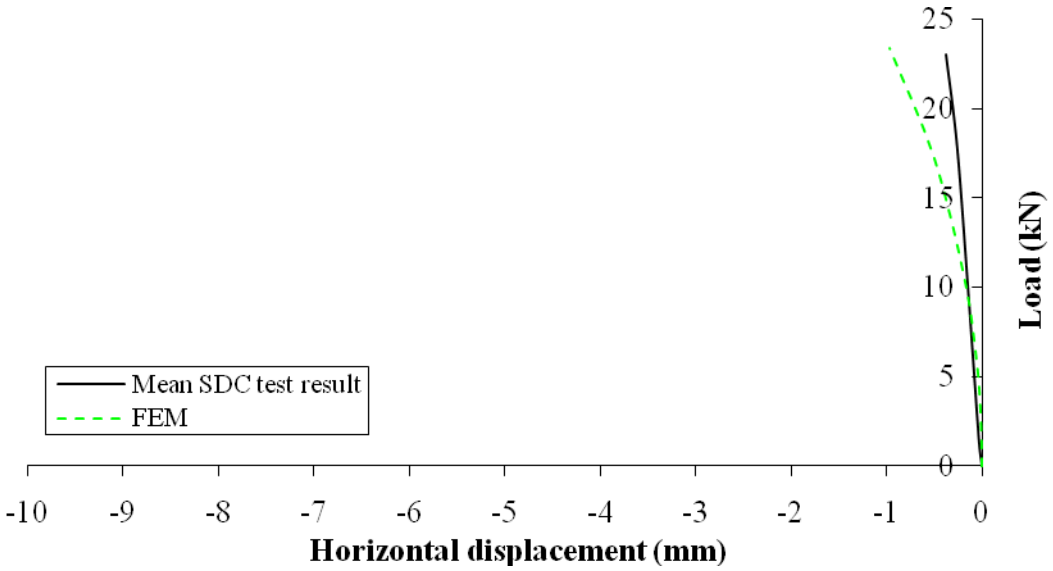

(c) SDC

Figure 4.46: Deflection comparison between the FEM and the mean test results

4.4.4 Investigation summary for panels with different joints

Figure 4.47 presents the mean central displacement results of STP, SMC and SDC. These results are consistent with the expectations in which the SDC shows the best stiffness than the other two.

Table 4.15 summarises the test results of the STP, SMC and SDC panels when subjected to transverse loading. The key notes from this transverse loading test are as follows:

- Despite the mean loads at failure of typical panels, panels with mini-SIP connections and panels with dimensional timber spline connections are different by 5.65% (21.78 kN and 23.01 kN). It should be noted that in this experimental study, the ultimate load and the failure mode are not influenced by the type of joint designs and were physically tested as wall conditions. In contrast to the earlier findings in the four-point bending test on SIPs with different joints as floor or roof conditions (section

4.2), the test results illustrated that the mean ultimate load of the SDC (40.32 kN) that are 2.09 times of the similar mean ultimate loads of the STP and SMC (19.32 kN).

- In line with expectation that the ranking (high to low) of the panel stiffness found from this experiment is SDC, SMC and STP, respectively.

- The failure mode found in this study is the debonding of SIP walls when subjected to transverse loading. This debonding failure is due to the discontinue line of course between the core and footer and hence a high interfacial shear stress together with high peeling stress between the top outer face and the inner core since the top outer face is held with the footer and the inner core is bent. The brittle nature of SIP walls with these panel configurations as detailed in the section 4.3.1 has been found in this experiment since the test panels all suddenly collapse without excessive pre-failure deformations.

- The serviceability load becomes the governing factor of the loading capacity as summarised in the Table 4.15.

- The central displacement is slightly lower than at the edge of the panel. This finding is in agreement with the well-acknowledged Poisson effect.

- The horizontal displacement is negligible in comparison with the vertical displacement and less concerned in engineering practice.

- Allen's and TR 019 analytical methods have been found in favourable to analyse the central displacements for STP and SDC, respectively.

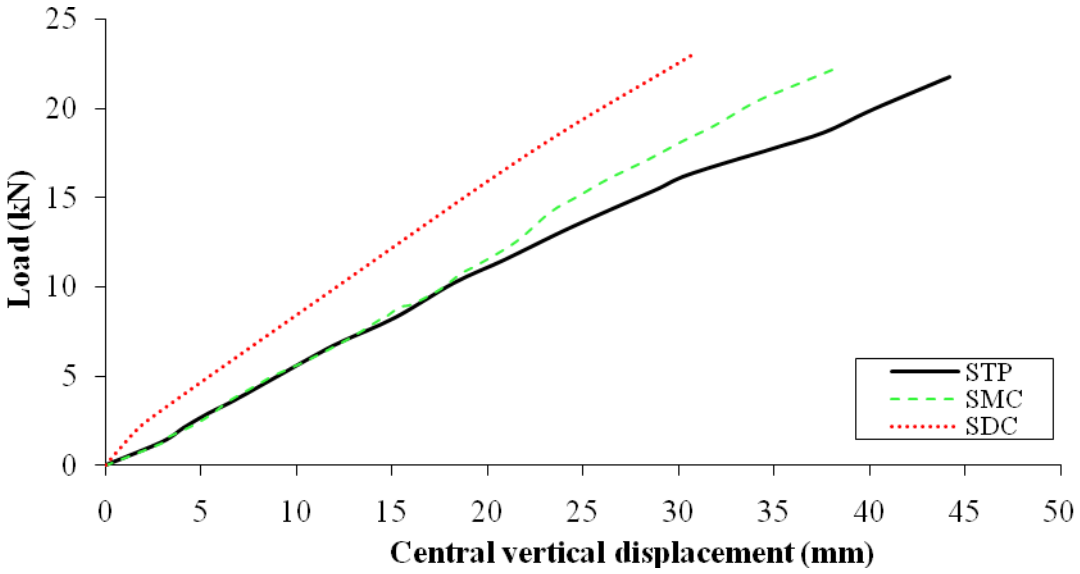

Figure 4.47: Test result comparison of SIPs with different connections

Specimen	STP	SMC	SDC
Ultimate Limit Load, ULL (kN)	21.78	22.16	23.01
Increase of ULL (%)	0	1.74	5.65
Load at deflection limit ℓ/333 (kN)	3.97	4.03	6.36
Serviceability load / Ultimate load (%)	18.3	18.2	27.6
FEM initial failure load (kN)	18.70	20.20	23.40
Initial failure load/ULL (%)	86	91	102
Maximum central displacement (mm)	44.19	38.05	30.70
Maximum edge displacement (mm)	47.57	42.04	34.97
Maximum horizontal displacement (mm)	2.19	0.33	0.38
Experimental failure mode	Debonding		
FEM initial failure mode	Debonding		

Table 4.15: Experimental and numerical finding summary

4.4.5 Experimental investigations to SIPs with openings

The effect of opening on the panels when subjected to transverse loading was examined by testing two panels with openings (STPO-1 and 2) and two panels with mini-SIP connections and openings (SMCO-1 and 2). Figure 4.48 shows the loads against the vertical displacements at 10 mm from the edge of the openings (LVDT No.1).

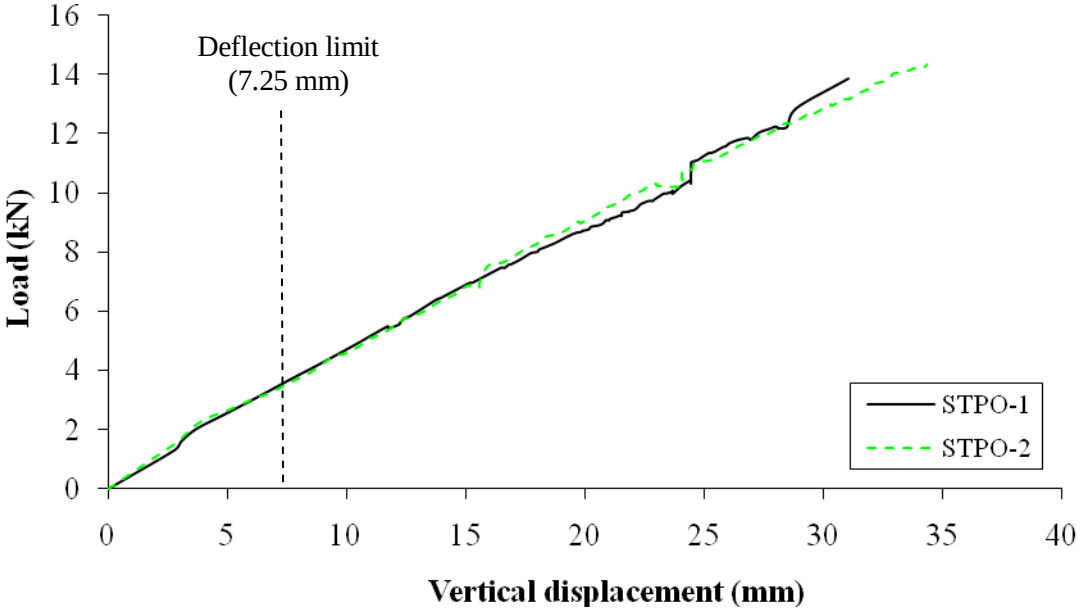
Deflection limit
(7.25 mm)
Load (kN)
Vertical displacement (mm)
STPO-1
STPO-2

(a) STPO

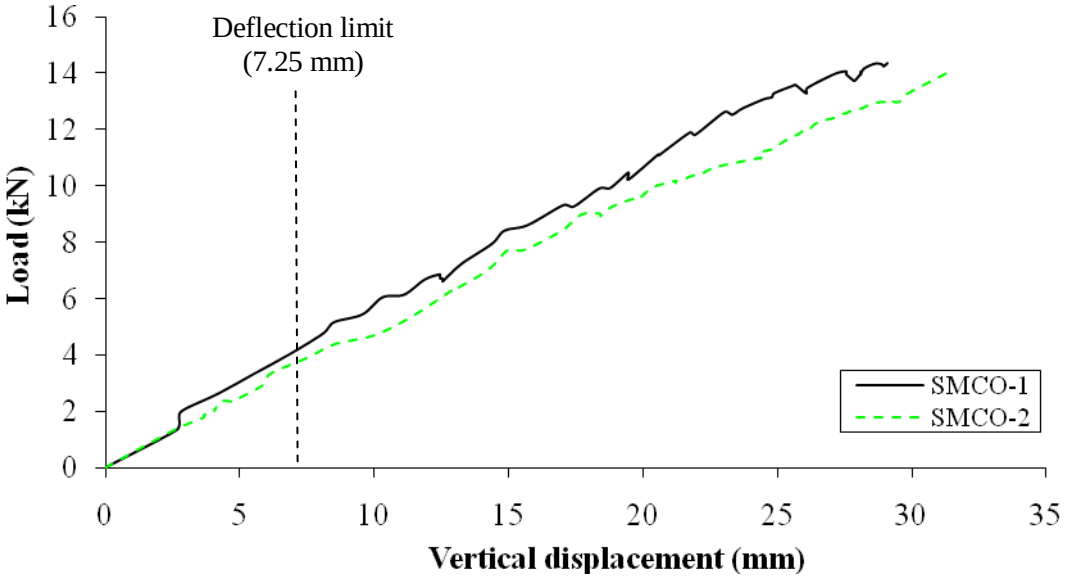
Deflection limit
(7.25 mm)
Load (kN)
Vertical displacement (mm)
SMCO-1
SMCO-2

(b) SMCO

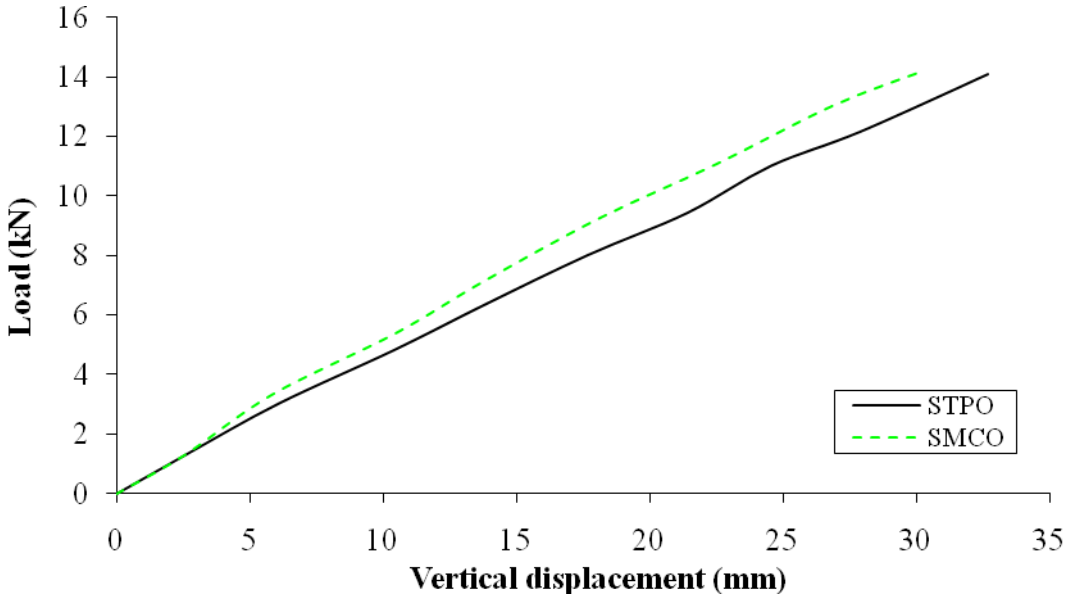

(c) Mean test result comparison of STPO and SMCO

Figure 4.48: Load versus vertical displacement (LVDT No.1)

The mean ultimate loads of STPO and SMCO are 14.11 kN and 14.18kN, this is approximately 64% of the panel without opening. The serviceability load also becomes the limiting factor of the loading capacity. The failure mode is the flexure-shear as shown in Figure 4.49. The outer face facture and the inner core shear occur at one of the corner of the openings where the maximum shear force and bending moment are presented concurrently. This failure mode is as expected due to an obvious reduced section. This failure mode shows again a brittle nature behaviour.

(a) STPO-1

(b) STPO-2

(a) SMCO-1

(b) SMCO-2

Figure 4.49: Flexure-shear failure

Figure 4.50 plots the applied loads against vertical displacements at 10 mm from the edge of the panels.

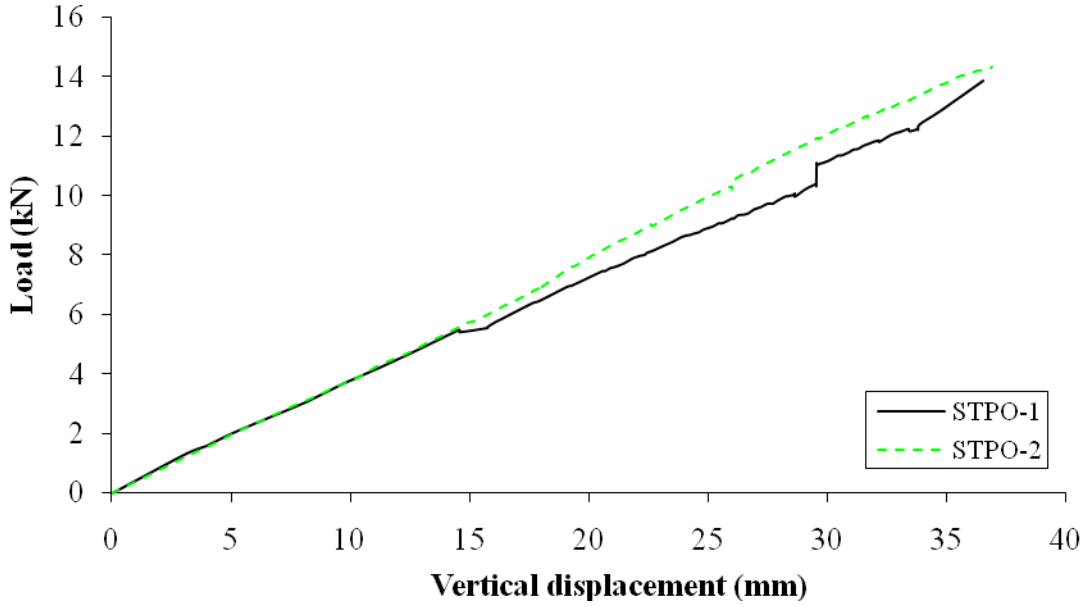

(a) STPO

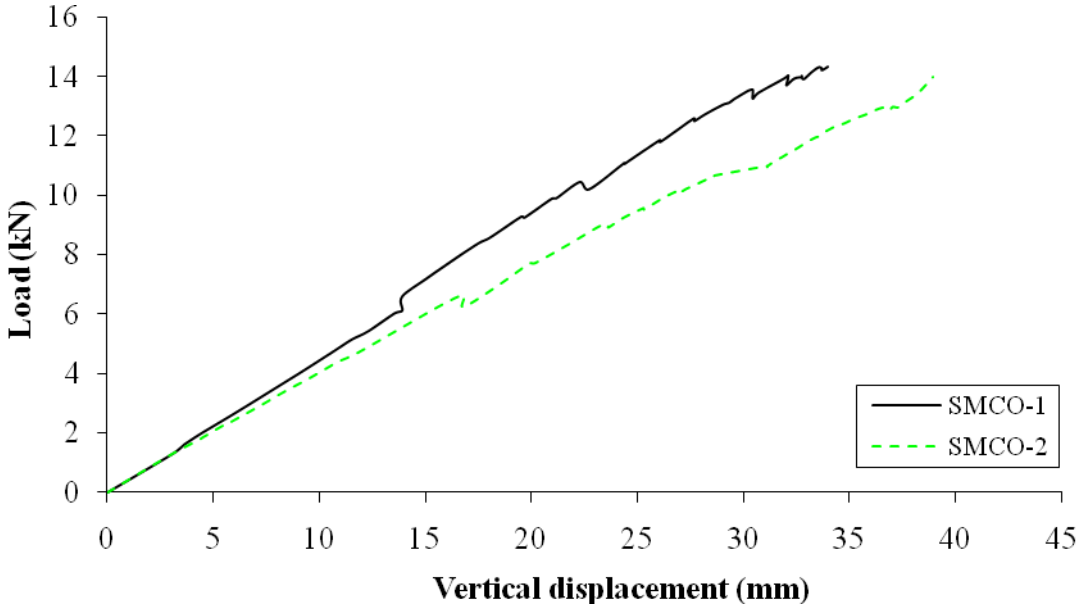

(b) SMCO

Figure 4.50: Load versus vertical displacement (LVDT No.2)

The horizontal movements at the edge of the panels (LVDT No.3) are small (within 1.45 mm) as illustrated in Figure 4.51.

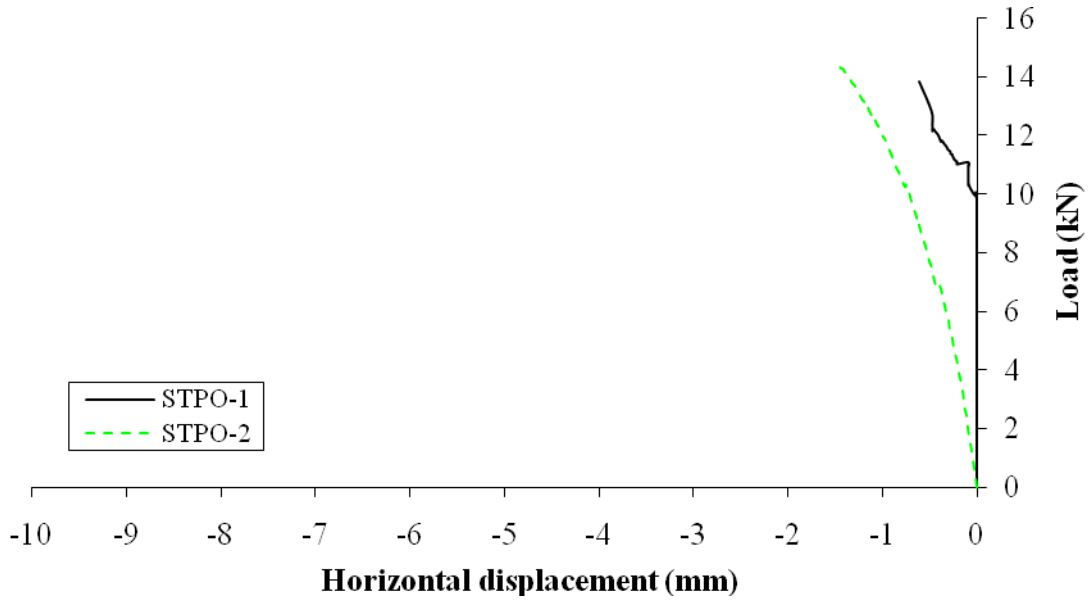

(a) STPO

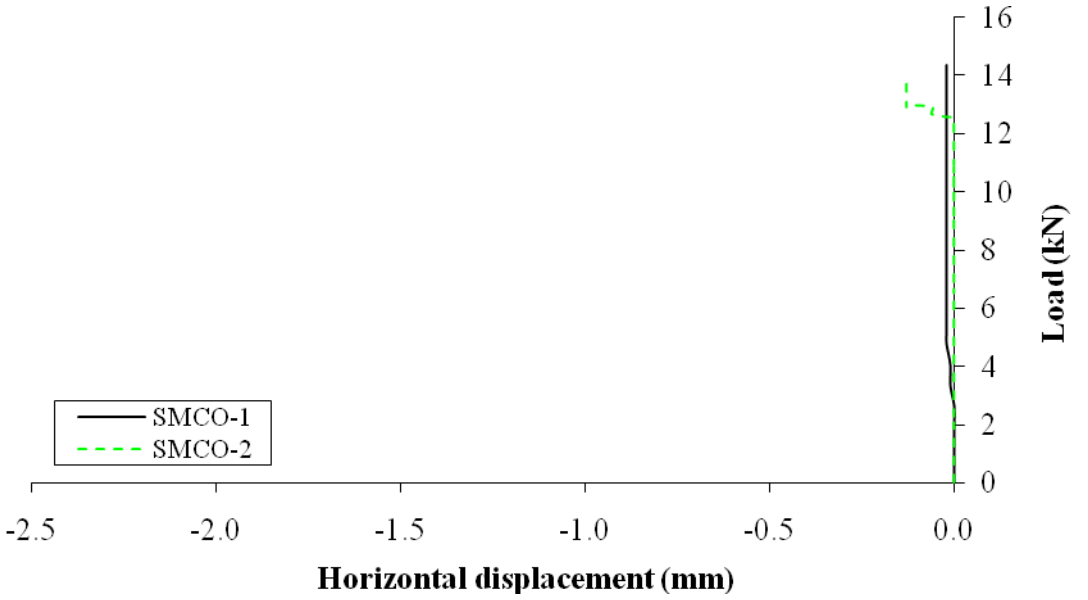

(b) SMCO

Figure 4.51: Load versus horizontal displacement (LVDT No. 3)

The mean vertical displacement at the mid-span near the opening edge (LVDT No.1) is lower than the mean displacement at the mid-span near the panel edge (LVDT No.2). Figure

4.52 shows typical displacements at LVDT No.1 and LVDT No.2. This indicates that the stiffeners at the opening can reduce the vertical displacement.

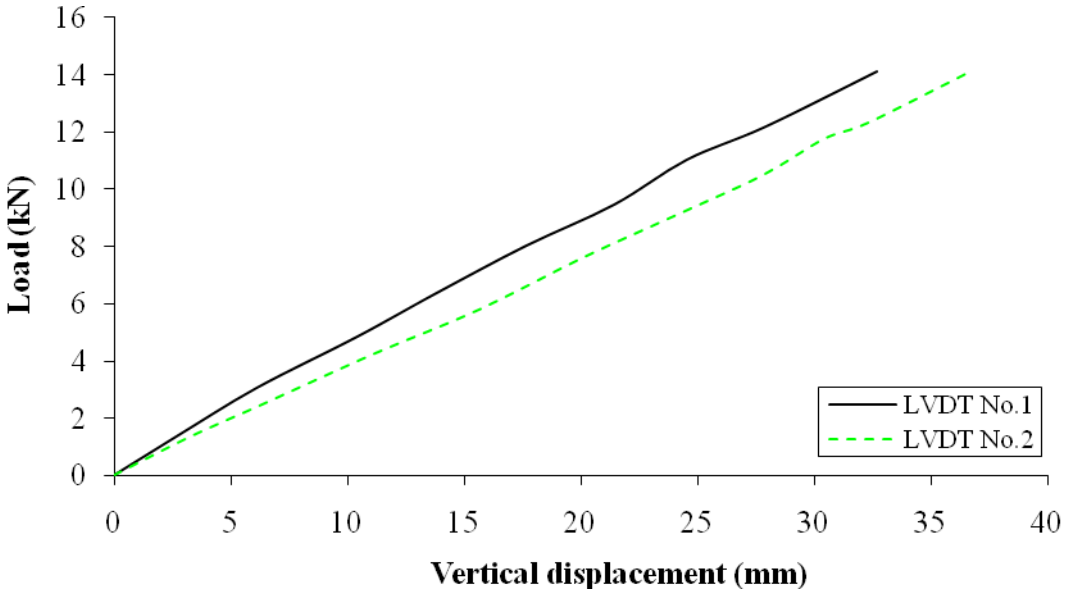

Figure 4.52: Load versus vertical displacement at the opening edge (LVDT No.1) and at the panel edge (LVDT No.2)

Figure 4.53 compares the mean test results of STPO and SMCO, and the experimental results are summarised in Table 4.16.

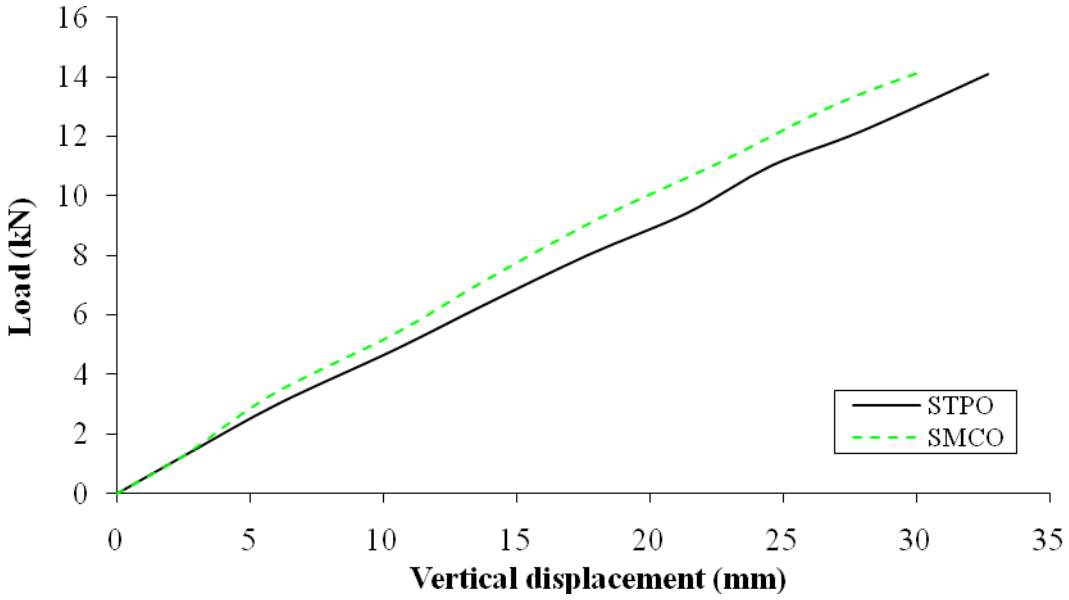

Figure 4.53: Test result comparison of STPO and SMCO

Specimen	STPO	SMCO
Ultimate Limit Load, ULL (kN)	14.11	14.18
Increase of ULL (%)	0	0.50
Load at deflection limit ℓ/333 (kN)	3.49	4.03
Serviceability load / Ultimate load (%)	24.7	28.4
Mean displacement at the opening (mm)	32.68	30.19
Mean displacement at the edge (mm)	36.72	36.48
Mean horizontal displacement (mm)	1.03	0.08
Experimental failure mode	Flexure-Shear	

Table 4.16: Experimental result summary

4.4.6 Numerical investigation

Berner and Pfaff (2005) points out there is a lack of simple analytical calculation to determine the stress peaks at the corners of a sandwich panel with an opening. They recommend to determine the stress peaks by employing finite element or rod model methods. Consequently, the structural behaviour of SIPs with openings was investigated by using the finite element method.

The concept to model the STPO and SMCO panels is as similar as the STP panel in the previous section. Figure 4.54 depicts finite element for STPO model. The material properties of SIP components are as same as previously used in the preceding sections.

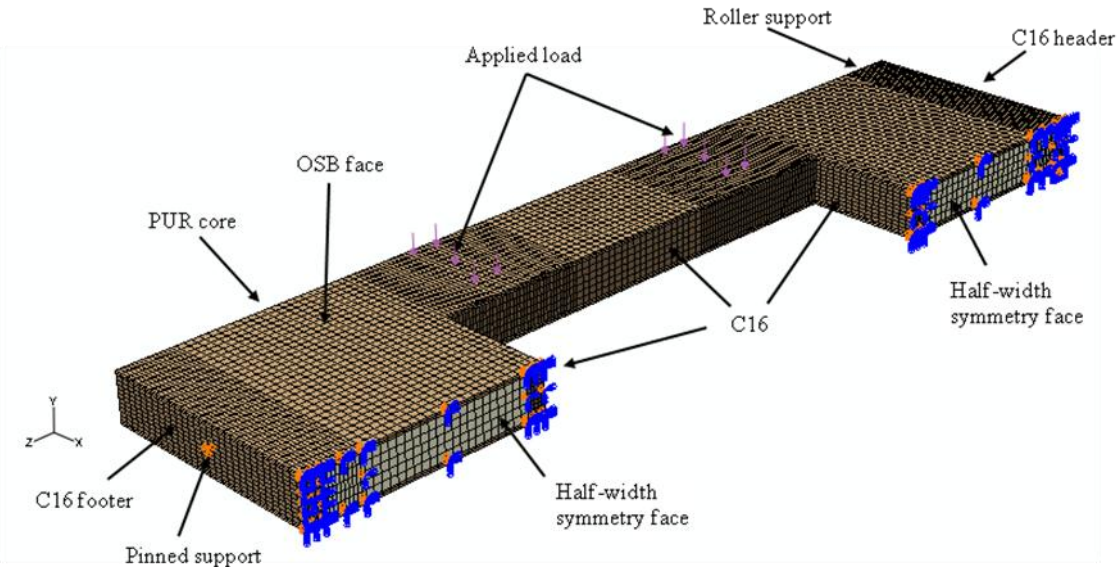

Figure 4.54: STPO finite element model

In order to ensure that the failure mode would occur in the FEM investigation, the applied load equals to 15 kN was applied to the FEM model. This load is higher than the mean failure loads found from the experimental investigations. Figures 4.55 and 4.56 present typical distributions of the stresses of the SIP constituents.

The stress peaks at the corners of the openings have been found as shown in Figures 4.55(a) and 4.55(b). Nevertheless, these stress peaks are ignored and not investigated further since this will lower the initial failure load (to an inappropriate value) in this numerical investigation. The maximum stresses are obtained in the vicinity of the opening area (not at the corners) and listed in Tables 4.17 and 4.18 for the OSB and PUR, respectively. Since Hashin Rotem's criterion provides less agreement to the experimental results as presented in

the previous section, the linear stress criterion for debonding is only presented here as tabulated in Table 4.18(b).

At the 15 kN applied load, the outer faces fail in both longitudinal and transverse bending stresses as shown in Figures 4.55(a) and 4.55(b). Moreover, the inner core fails due to debonding as depicted in Figure 4.56.

Further back track analysis was again performed, the initial failure loads have been found to be 9.4 kN (for STPO) and 9.6 kN (for SMCO), which are approximately 67% of the experimental ultimate loads. The lowest initial failure load reveals the debonding failure at the OSB-PUR interface. It is also possible to see the outer faces fail due to bending since the initial failure is in similar range of the debonding initial failure (10.5 kN for STPO and 10.6 kN for SMCO).

Specimen	Load (kN)	Failure	S_{11} (N/mm^2)	S_{33} (N/mm^2)	S_{11} / f_{11}	S_{33} / f_{33}	Remark
STPO	15.0	Bending	23.42	9.85	1.43	1.20	Fail – both S_{11} and S_{33}
	10.5		16.38	6.87	0.99	0.84	Pass
SMCO	15.0		23.19	7.98	1.41	0.97	Fail only S_{11}
	10.6		16.33	-	0.99	-	Pass

where f_{11} and f_{33} are bending failure stresses, equal to 16.40 N/mm^2 and 8.20 N/mm^2, respectively.

Table 4.17: Stress results in the OSB outer faces

Specimen	Load (kN)	Failure	S_{12} (N/mm^2)	S_{12} / f_{12}	Remark
STPO	15.0	Shear	0.077	0.66	Pass
SMCO	15.0		0.074	0.64	

where f_{12} is shear failure stress, equals to 0.116 N/mm^2.

(a) Shear stress results

Specimen	Load (kN)	Failure	S_{22} (N/mm^2)	S_{12} (N/mm^2)	S_{23} (N/mm^2)	Linear stress criterion $S_{22}/f_{22}+S_{12}/f_{12}+S_{23}/f_{23}$	Remark
STPO	15.0	Debonding	0.191	0.048	0.018	1.59	Fail
	9.4		0.121	0.030	0.011	0.99	Pass
SMCO	15.0		0.177	0.046	0.022	1.53	Fail
	9.6		0.116	0.030	0.014	0.99	Pass

where f_{22}, f_{12} and f_{23} are failure stresses, equal to 0.188 N/mm^2, 0.116 N/mm^2 and 0.116 N/mm^2, respectively.

(b) Debonding – Linear stress criterion

Table 4.18: Stress results in the PUR core

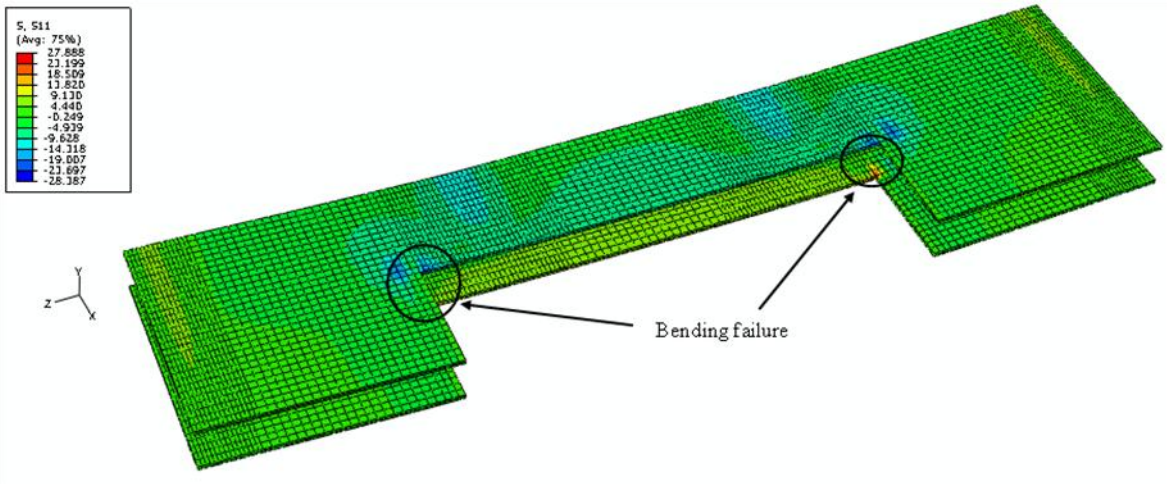

(a) Distribution of the longitudinal stress (S11) of the outer faces

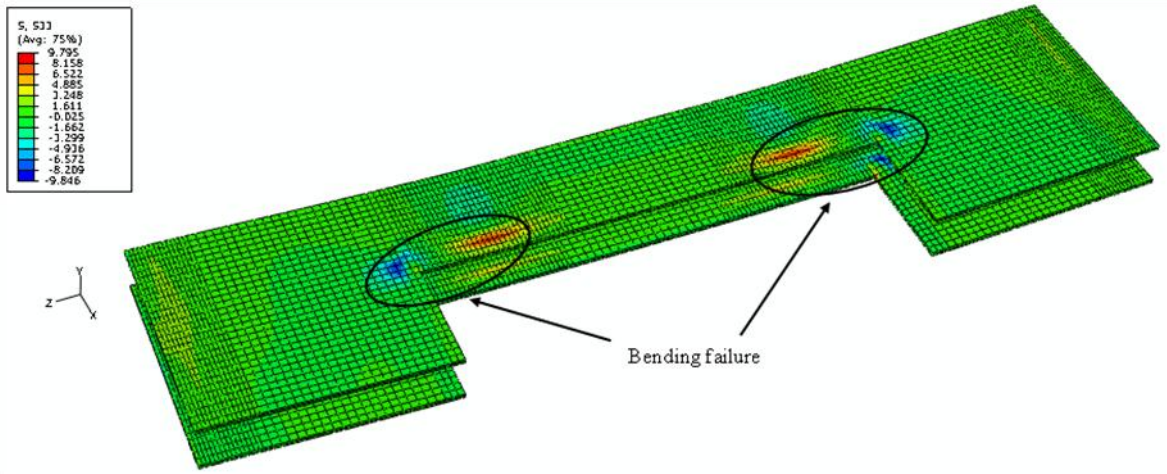

(b) Distribution of the transverse stress (S33) of the outer faces

Figure 4.55: Distribution of the outer face stresses

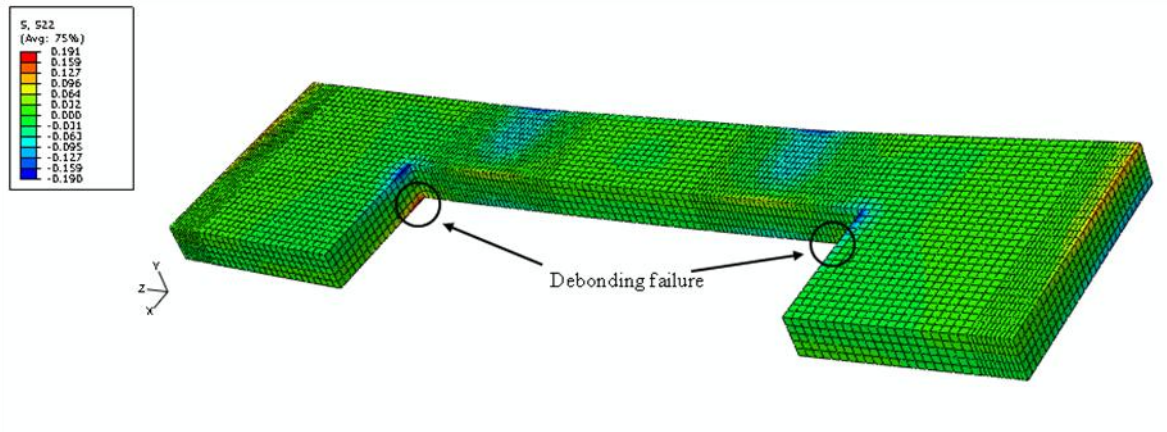

(a) Distribution of the normal stress (S22) of the PUR inner core

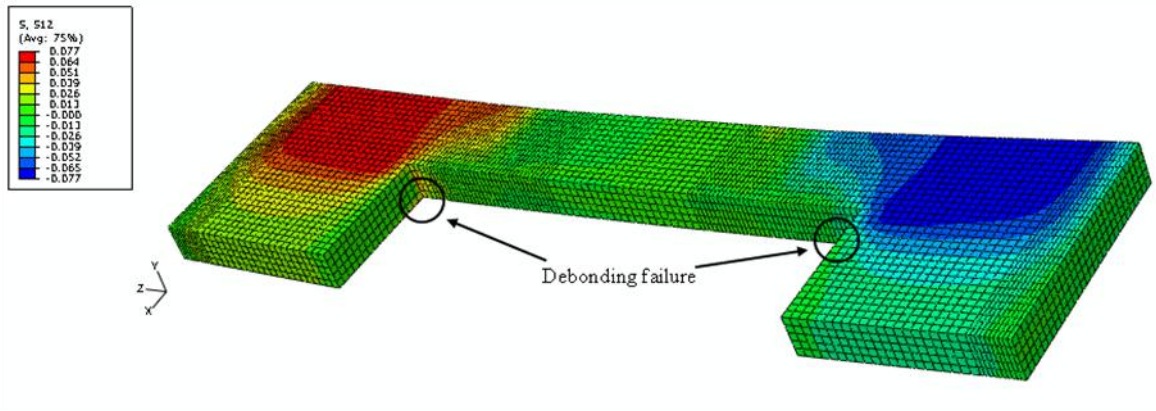

(b) Distribution of the shear stress (S12) of the PUR inner core

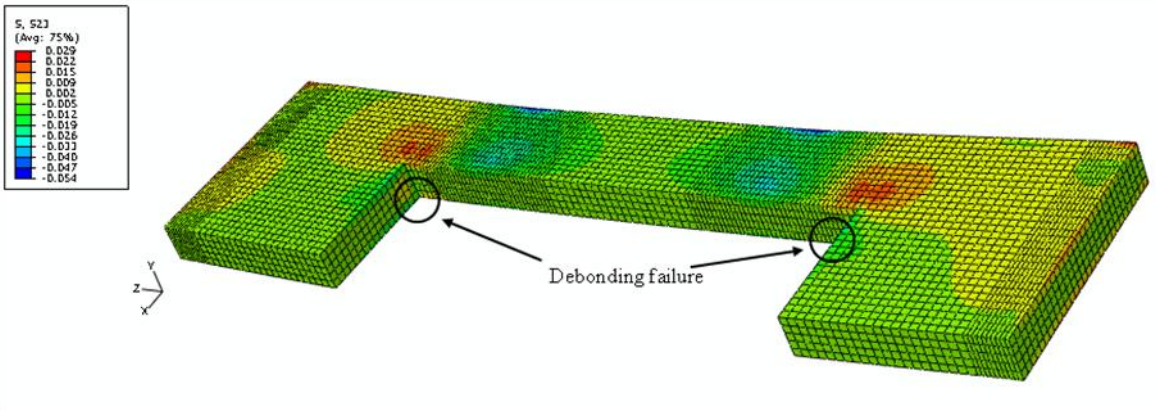

(c) Distribution of the shear stress (S23) of the PUR inner core

Figure 4.56: Distribution of the stresses of the PUR inner core

Figures 4.57 to 4.59 show the load and the deflection curves comparison between the FEM and the mean test results up to the initial failure. The agreement of the displacements at three locations is encouraging.

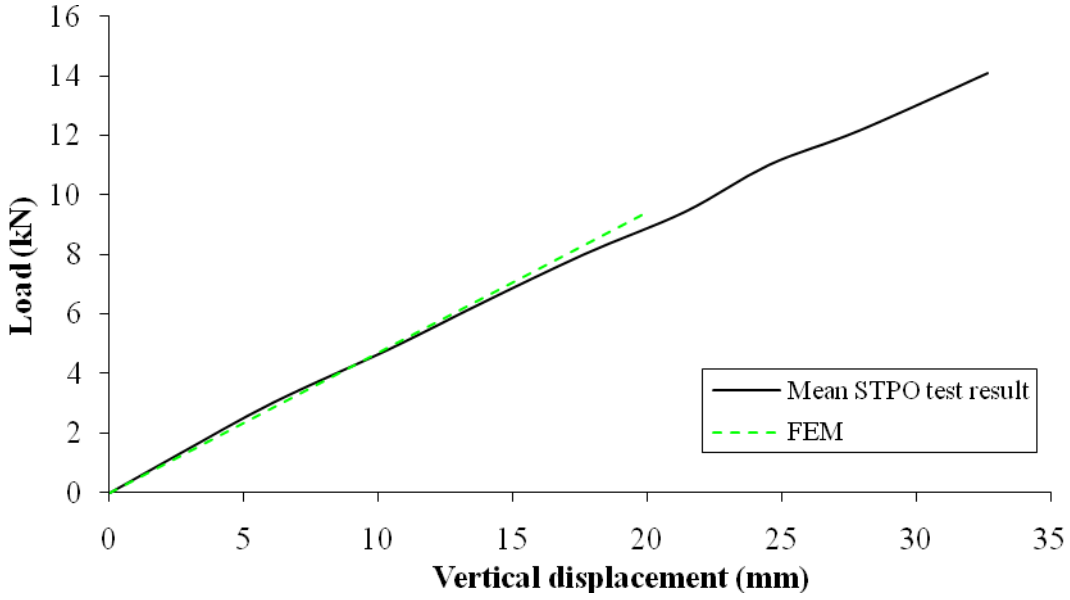

(a) STPO

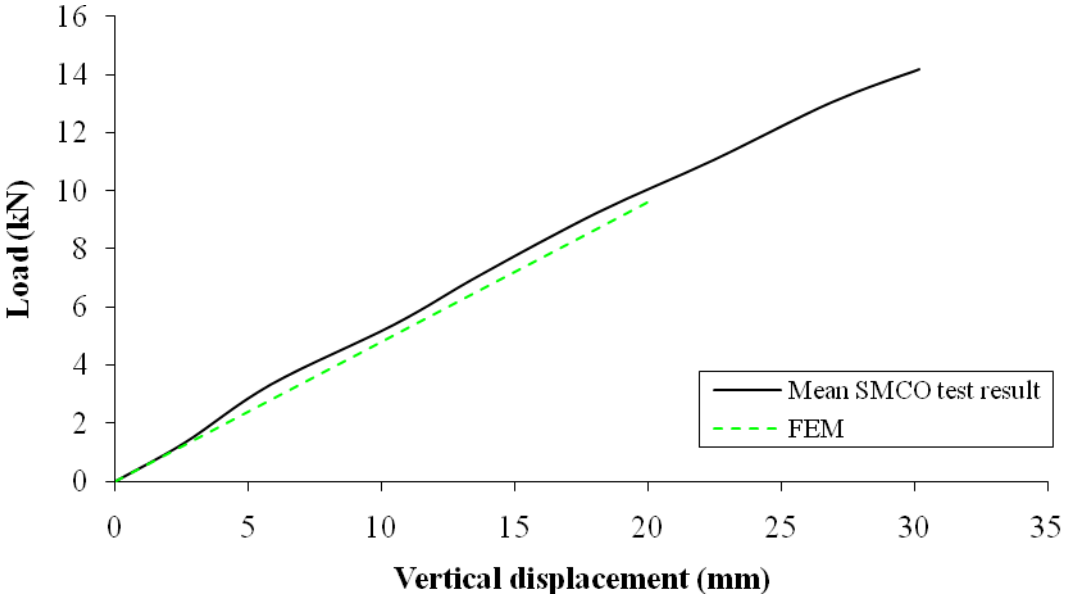

(b) SMCO

Figure 4.57: Central deflection comparison between the FEM and the mean test results

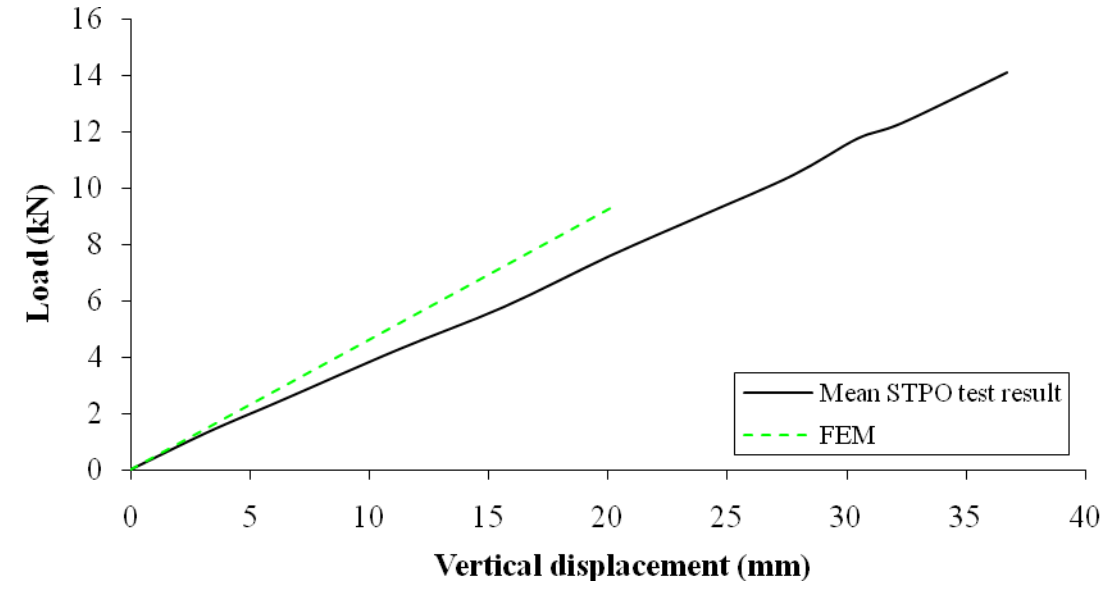

(a) STPO

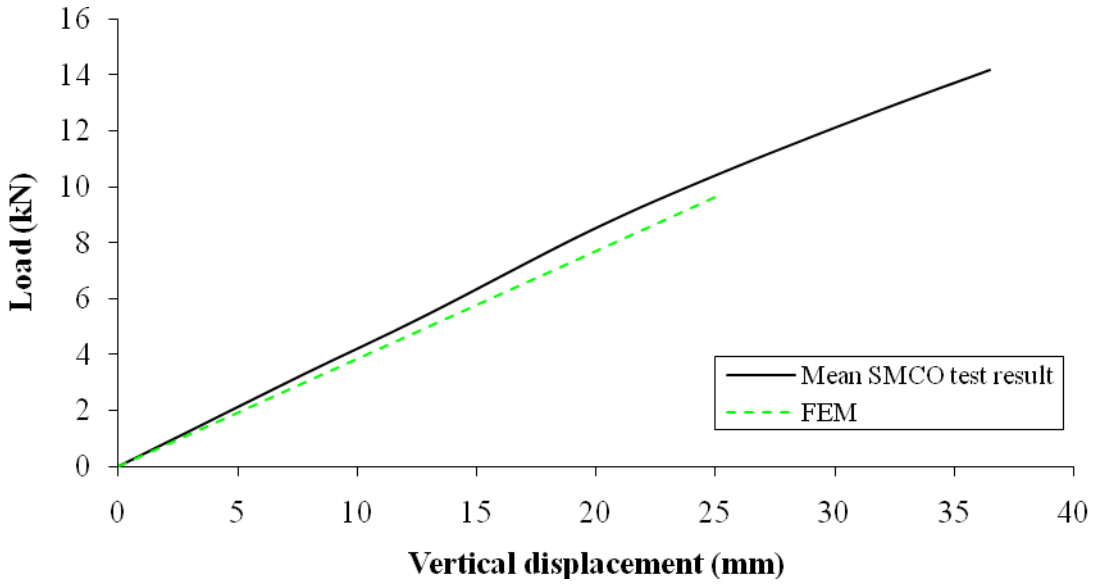

(b) SMCO

Figure 4.58: Edge deflection comparison between the FEM and the mean test results

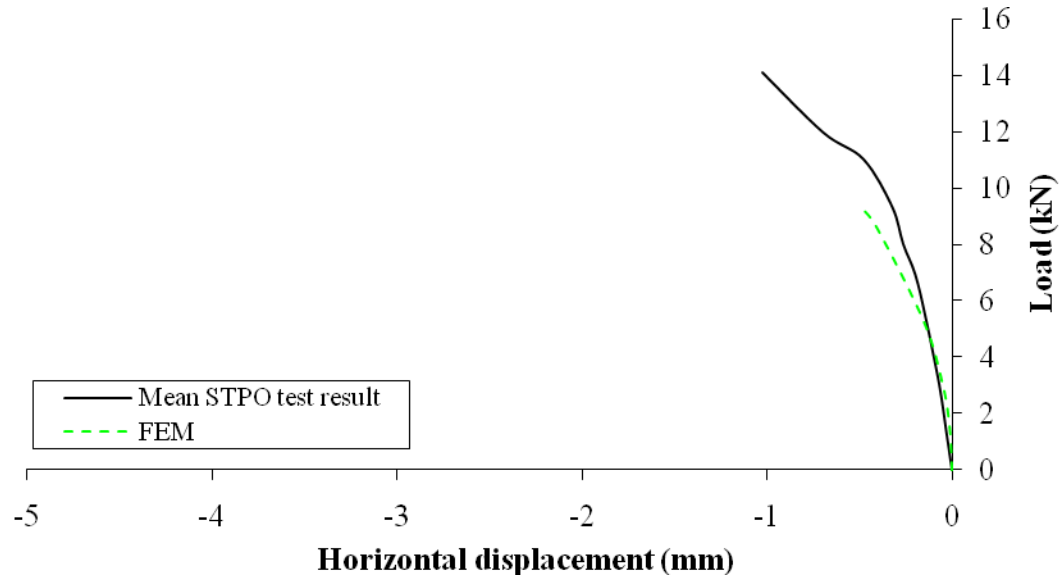

(a) STPO

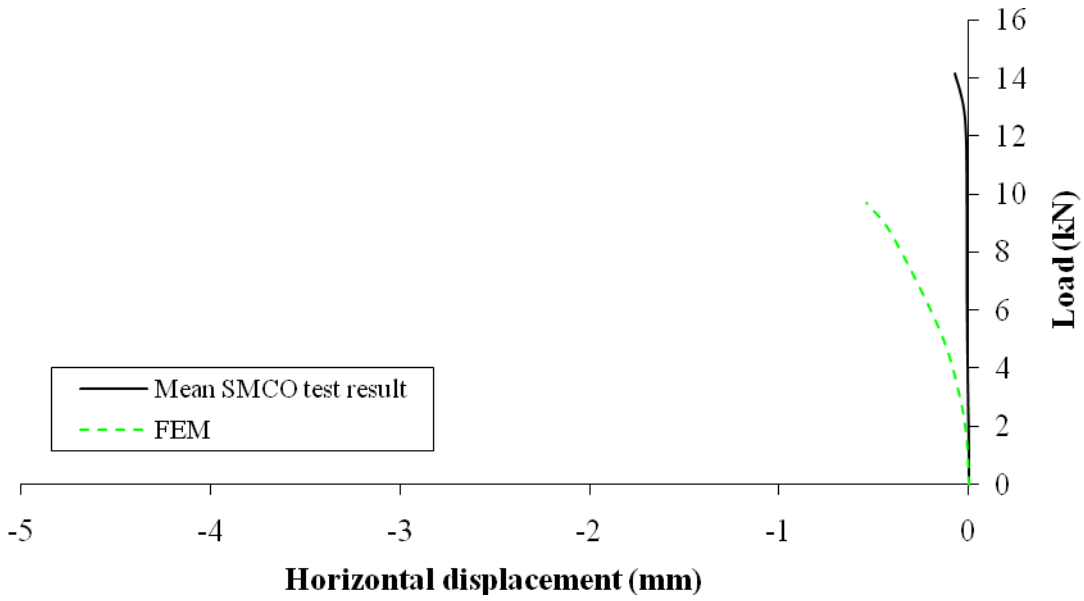

(b) SMCO

Figure 4.59: Horizontal displacement comparison between the FEM and the mean test results

SIPs with dimensional timber spline connections and openings (SDCO) have not been tested as previously described. This section presents the numerical investigation on SDCO. The concept to model the SDCO panel is similar to both STPO and SMCO panels. As these panels were connected by C16 joint at the middle, only half width of the C16 joint was modelled.

Tables 4.19 and 4.20 present the maximum stresses obtained from the finite element analysis with 20 kN applied load for the OSB and the PUR, respectively. The stress distributions and the maximum stresses have been found at the same locations of STPO and SMCO, therefore the contour plots are not presented. Like the STPO and SMCO findings, the outer faces fail in both longitudinal and transverse bending stresses, and also the inner core fails due to debonding. The initial failure load has been found to be 9.7 kN.

Load (kN)	**Failure**	S_{11} **(N/mm^2)**	S_{33} **(N/mm^2)**	S_{11} / f_{11}	S_{33} / f_{33}	**Remark**
20.0	Bending	31.56	12.95	1.92	1.58	Fail - both
10.4		16.37	6.67	0.99	0.81	Pass

Table 4.19: Numerical analysis on the OSB outer faces for SDCO panels

Load (kN)	**Failure**	S_{22} **(N/mm^2)**	S_{12} **(N/mm^2)**	S_{23} **(N/mm^2)**	$S_{22} / f_{11} + S_{12} / f_{12} + S_{23} / f_{23}$	**Remark**
20.0	Debonding	0.225	0.057	0.023	1.886	Fail
9.7		0.120	0.030	0.012	0.99	Pass

Table 4.20: Numerical analysis on the PUR for SDCO panels

4.4.7 Investigation summary for panels with different joints and openings

Table 4.21 summarises the test results of the panels with openings when subjected to transverse loadings. The findings from this transverse loading test are summarised as follows:

- With a 600 x 1200 mm^2 opening area, the ultimate load is approximately 64% of the panel without opening.

- The failure mode is due to the flexure-shear. The outer face facture and the inner core shear occur at one of the corner of the openings where the maximum shear force and bending moment are presented concurrently.

- The serviceability load also becomes the limiting factor of the loading capacity.

- Since the opening is stiffened by C16 timber blocks around the entire edge, the displacement near the edge of the opening has been found smaller than at the edge.

- The horizontal displacement is negligible in comparison with the vertical displacement.

- Under these SIP connection configurations, it can be concluded that the structural behaviour of SIPs with different joint designs is not influenced as shown in Figure 4.60 from both experimental and FEM investigation. This is because the critical section is away from the panel joint line.

Specimen	**STPO**	**SMCO**	**SDCO**
Ultimate Limit Load, ULL (kN)	14.11	14.18	-
Increase of ULL (%)	0	0.50	-
Load at deflection limit ℓ/333 (kN)	3.49	4.03	-
Serviceability load / Ultimate load (%)	24.7	28.4	-
FEM initial failure (kN)	9.4	9.6	9.7
Initial failure/ULL (%)	67	68	-
Mean displacement at the opening (mm)	32.68	30.19	-
Mean displacement at the edge (mm)	36.72	36.48	-
Mean horizontal displacement (mm)	1.03	0.08	-
Experimental failure mode	Flexure-Shear		-
FEM initial failure mode	Debonding		

Table 4.21: Experimental and numerical finding summary

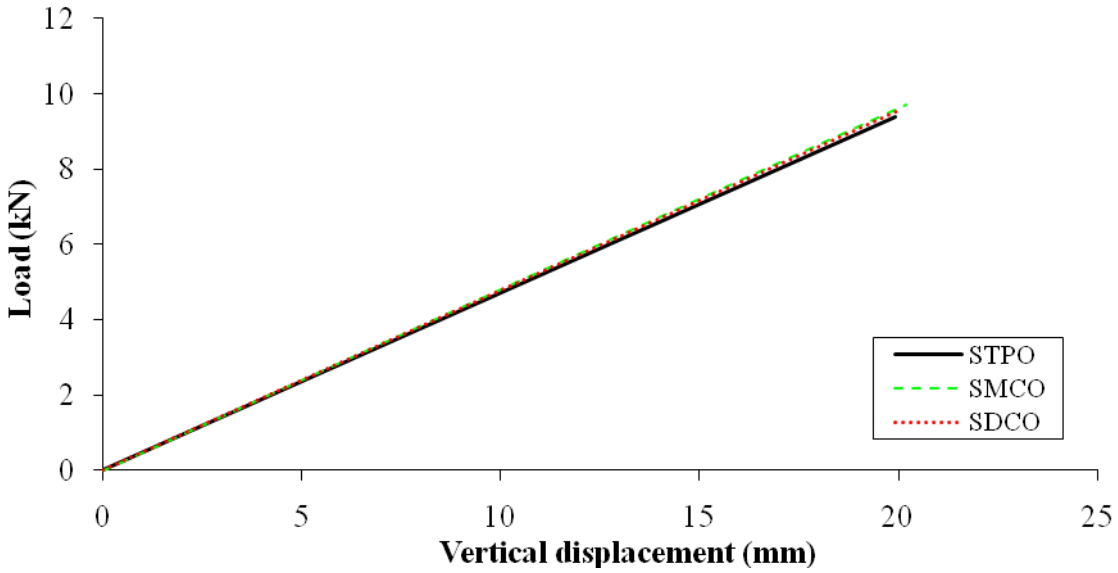

Figure 4.60: FEM result comparison of STPO, SMCO and SDCO

4.5 Load case No. 2 – Uniform axial compression

As SIPs are load bearing elements, the structural performances of SIPs with mini-SIP connections (SMC), dimensional timber spline connections (SDC) and mini-SIP connections with openings (SMCO) were examined under uniform axial compression.

Six SIP specimens which are two SMCs, two SDCs and two SMCOs without sole plates and M8 holding down bolts were subjected to uniform axial compression until failure.

It was estimated that the ultimate loads of the panel specimens when subjected to uniform axial compression would be beyond 150 kN. The custom-built test rig would therefore not be able to support the loads that cause the panel failure. An Avery-Denison testing machine that has a 500 kN capacity was used for the axial compression test. Since the panel is wider than the cross heads of the testing machine, two steel box beams (bolted to the cross heads) were used to spread and support the panel. Each SIP specimen was then inserted and held in place by the two

steel box beams as shown in Figure 4.61. The load was then applied by the bottom pad movement and the axial displacement was recorded by a dial gauge with a 0.01 mm accuracy.

Figure 4.61: Experimental apparatus for uniform axial loading test

4.5.1 Experimental investigations for SIPs without openings

Figure 4.62 shows the applied loads against the axial displacements of two panels with mini-SIP connections (SMC-1 and 2) and two panels with dimensional timber spline connections (SDC-1 and 2). The axial displacements were found to be small and could yield more variations in the test results as shown in Figure 4.62. However, these different from two specimens are approximately 2 mm at the higher load.

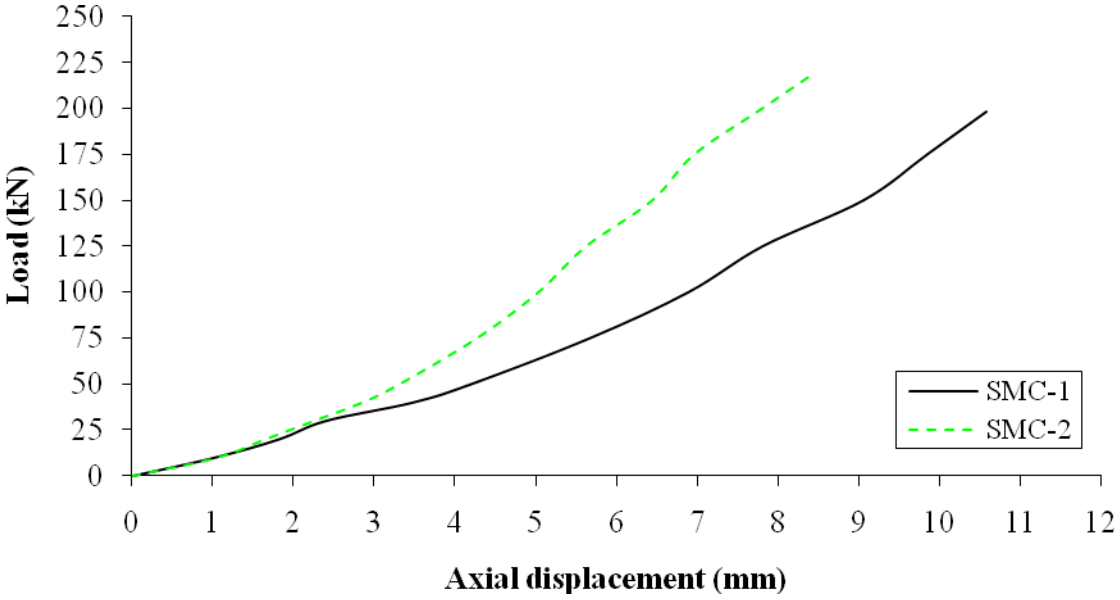

(a) SMC

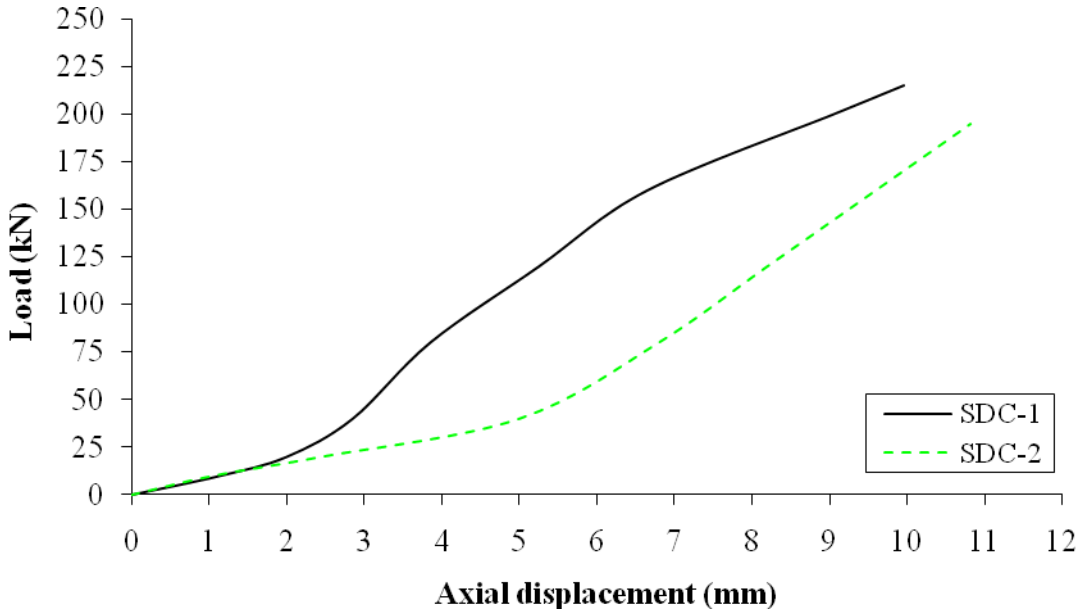

(b) SDC

Figure 4.62: Load versus axial displacement

The mean ultimate loads are 209 kN (for SMC) and 205 kN (for SDC). The failure modes (Figure 4.63) for these specimens are end bearing since the axial force is carried by the compression in the outer faces, while the inner core supports the outer faces against buckling as

stated by APA (1993). It should be noted that only one face was failed due to face crushing as shown in Figure 4.63. A possible explanation for this is the due to the dimensional tolerance of facial panels, bearing ends do not provide a flush bearing surface and therefore it may be likely that only part of facial panels have endured the bearing load. This causes the panel specimen to fail due to the end bearing. The experimental results are tabulated in Table 4.22.

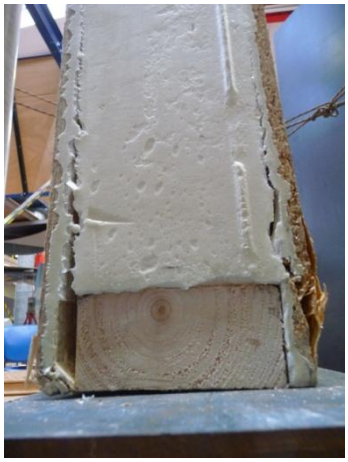

(a) SMC-1

(b) SMC-2

(a) SDC-1

(b) SDC-2

Figure 4.63: End bearing failure

Specimen	Dimension (mm)			Ultimate load		Axial displacement at failure (mm)	Failure mode
	W	L	D	(kN)	(kN/m)		
SMC-1	1,193	2,440	125	198.0	165.0	10.58	End bearing
SMC-2	1,194	2,442	125	220.0	183.3	8.47	
Mean	**1,193**	**2,441**	**125**	209.0	**174.2**	**9.53**	

(a) SMC

Specimen	Dimension (mm)			Ultimate load		Axial displacement at failure (mm)	Failure mode
	W	L	D	(kN)	(kN/m)		
SDC-1	1,193	2,440	125	215.0	179.2	9.95	End bearing
SDC-2	1,193	2,440	125	195.0	162.5	10.83	
Mean	**1,193**	**2,440**	**125**	205.0	**170.9**	**10.39**	

(b) SDC

Table 4.22: Experimental result summary

4.5.2 Axial compression analytical method

4.5.2.1 Outer face crushing failure

The axial loading capacity ($F_{u,ax}$) due to the outer face crushing failure can be determined by using the equation 4.3. It should be noted that this load capacity is independent of the SIP longitudinal joint designs and configurations. The panel details, material properties and the axial loading capacity are listed in Table 4.23.

$$F_{u,ax} = f_{c,33} 2A = f_{c,33} 2Bf \tag{4.3}$$

where $f_{c,33}$ is the compressive strength of OSB in parallel to the grain direction, equals to 15.75 N/mm^2 which has been determined in section 3.3.1;

A is the area of the outer face;

B is the measured width of the specimen; and

f is thickness of the outer face.

$f_{c,33}$ (N/mm^2)	15.75
B (mm)	1,193
f (mm)	11
$F_{u,ax}$ (kN)	413.4

Table 4.23: SMC details, material properties and axial loading capacity

It can be seen in Table 4.23 that the axial loading capacity (413.4 kN) is almost double of the mean SMC ultimate load (209 kN). This axial loading capacity, determined by using equation 4.3, does not show a good agreement on the ultimate load between the analytical and the experimental results. As previously mentioned, a possible explanation for this is the due to the dimensional tolerance of facial panels, bearing ends do not provide a flush bearing surface and therefore it may be likely that only part of facial panels have endured the bearing load. This causes the panel specimen to fail due to the end bearing. Numerical investigation has been found that the axial loading capacity is consistent with the analytical method which is also double of the mean SMC ultimate load.

4.5.2.2 Buckling failure

Although the buckling failure of the panel does not present in the experimental investigation, the buckling failure load (P_{cr}) is determined in order to verify whether the buckling failure can take place.

Analytical methods to determine P_{cr} of the sandwich panel when subjected to axial compression load are given by Allen (1969) and Davies (2001) as previously detailed in section 2.4. The panel details, material properties and the buckling failure load are listed in Table 4.24.

The buckling load capacities determined by Allen and Davies' methods are similar (198.47 kN and 198.69 kN) as illustrated in Table 4.24. These load capacities are also in the similar range

(within 5%) to the end bearing failure load (209 kN), but the buckling failure mode was not envisaged in the experiment. This result can be explained by the fact that only part of facial panels have endured the bearing load, causing the panels to fail at the lower loads.

B (mm)	1,193
L (mm)	2,441
f (mm)	11
d_c (mm)	103
e (mm)	114
E_f (N/mm^2)	3,844
E_c (N/mm^2)	6.442
G (N/mm^2)	2.30
ν_f	0.24
ν_c	0.33
Allen's method, P_{cr} (kN)	198.47
Davies' method, P_{cr} (kN)	198.69

Table 4.24: Specimen details, material properties and buckling load capacity

4.5.3 Numerical investigation

The concept to model the SMC and SDC panels is generally as similar as the previous FEM numerical sections. Since the panel is symmetric in both longitudinal and transverse directions, a quarter of the whole specimen was modelled. The XSYMM boundary condition was applied to the vertical surface at the mid-width, whereas the ZSYMM boundary condition was applied to the vertical surface at the mid-length.

The structured mesh technique for this model was again 20-node hexahedral elements with reduced integration (C3D20R). OSB faces were also divided into two elements in the thickness direction. In addition, 10 mm wide fine element sizes were used in the region of high stress gradients which are at approximately 150 mm from the panel end (at the applied load position).

Meanwhile, 20 mm wide coarse element sizes were used elsewhere. The through width panel direction was afterward discretised with 20 mm elements.

PUR inner core was discretised with 10 x 20 x 20 mm elements in the region of high stress gradients as described in the OSB faces. Likewise, 20 x 20 x 20 mm elements were used elsewhere. Finally, the C16 header located in the high stress region, was discretised with 10 x 10 x 20 fine element sizes. Figure 4.64 depicts finite element for SMC model. The material properties of SIP components are the same as those used previously.

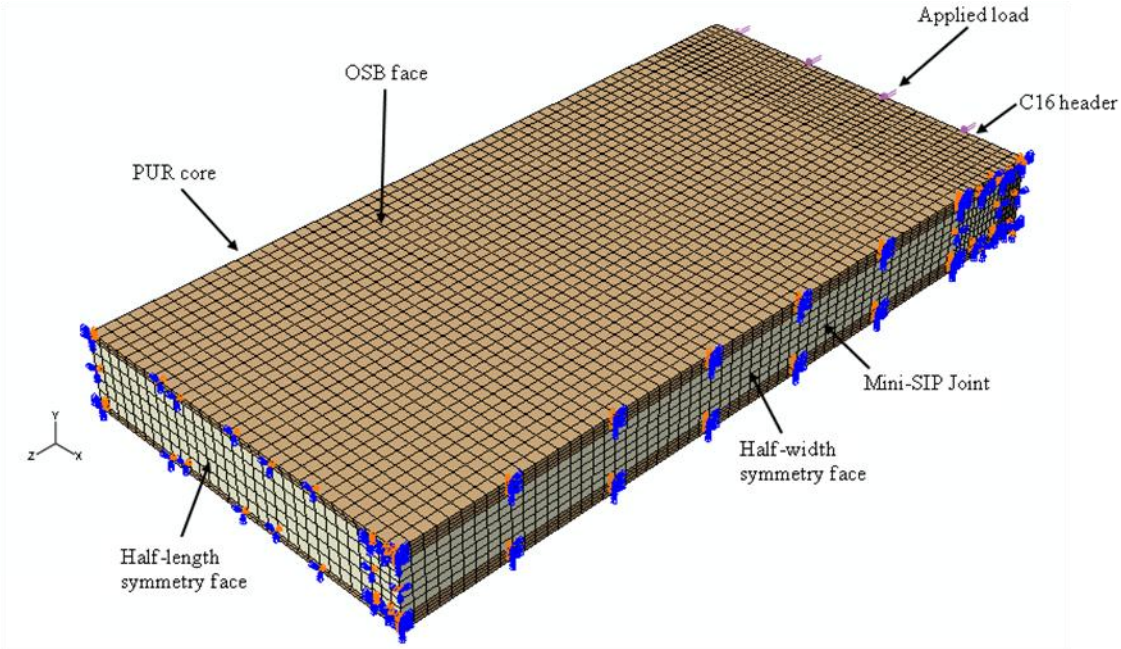

Figure 4.64: SMC finite element model

It has been found that the initial failure loads for the end bearing failure of the outer faces are 421.5 kN and 436.5 kN for SMC and SDC, respectively. These findings are consistent with the analytical findings. Figure 4.65 shows the distribution of the longitudinal stress (S33) of the outer faces for SMC model only at the initial failure load of 421.5 kN. The inner cores are not subjected to any failures as shown in Figure 4.66.

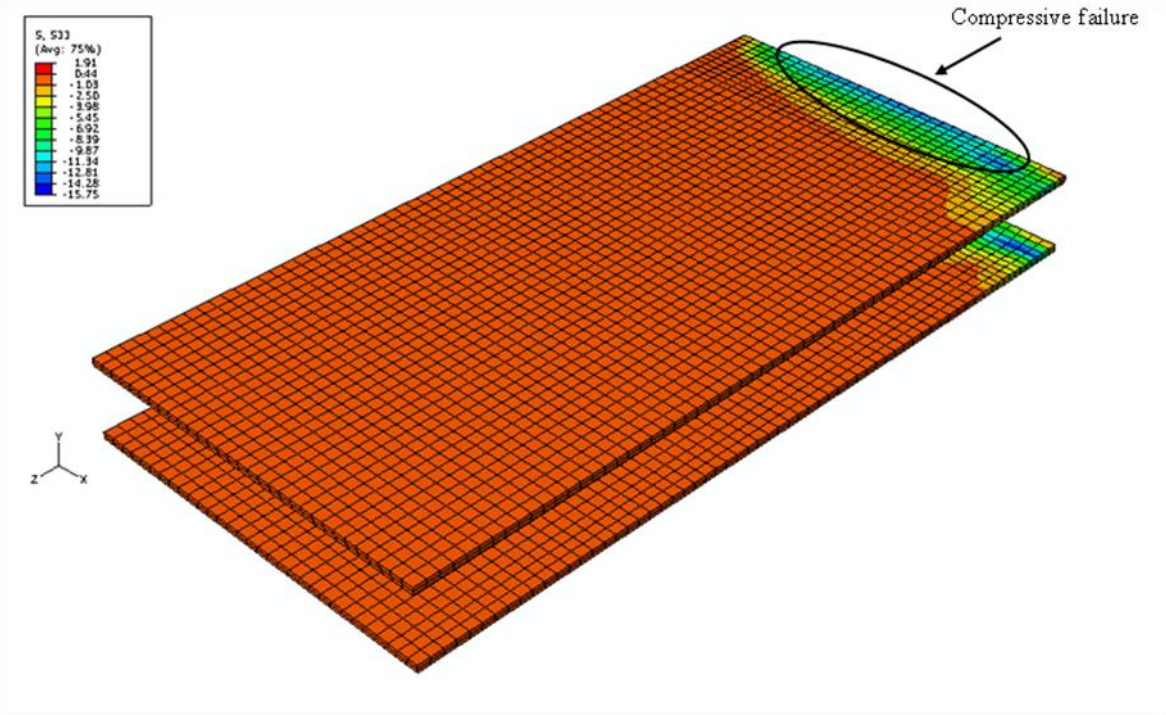

Figure 4.65: Distribution of the longitudinal stress (S33) of the outer faces

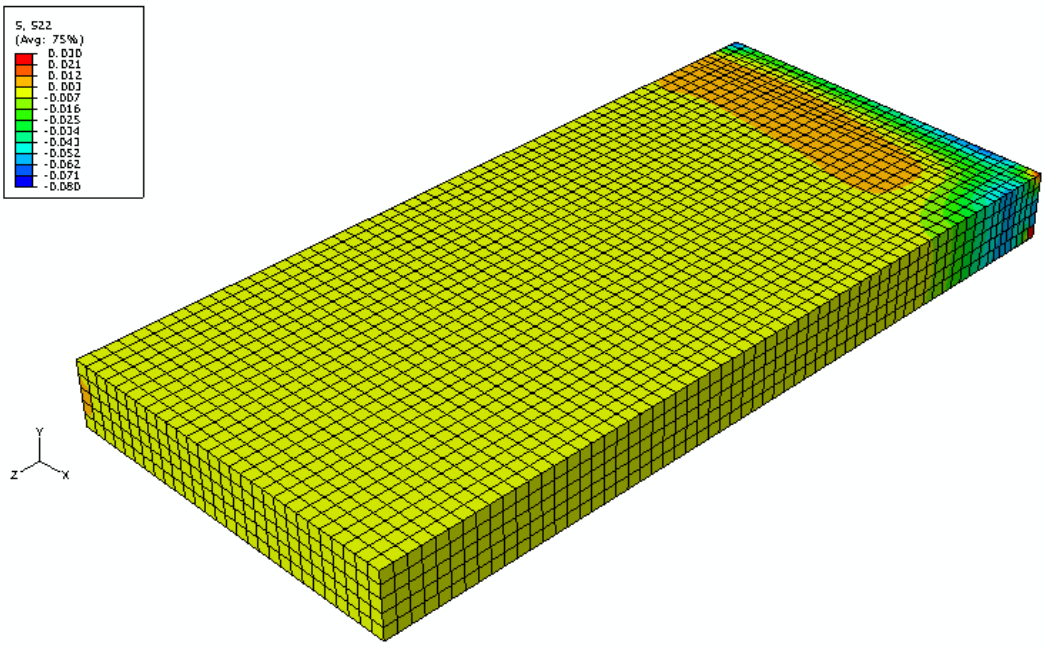

(a) Distribution of the normal stress (S22) of the PUR inner core

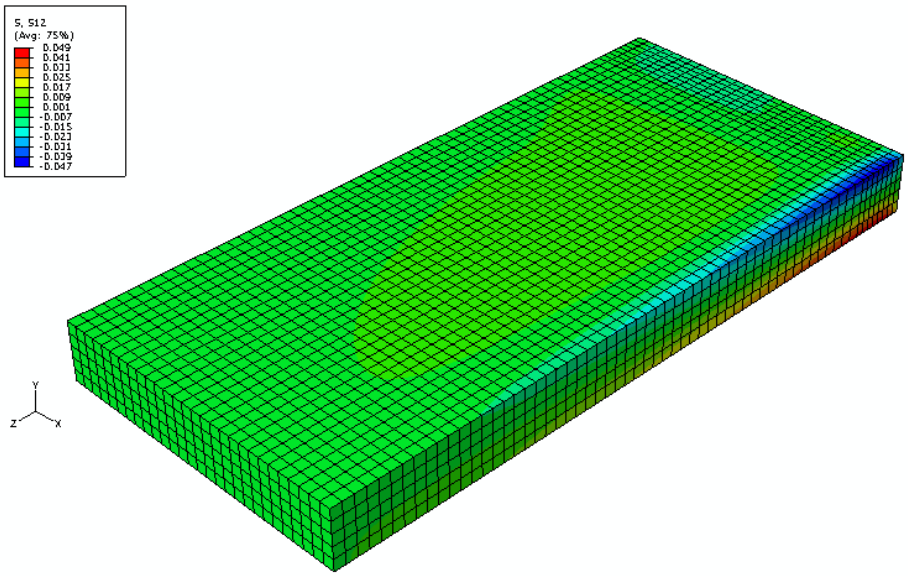

(b) Distribution of the shear stress (S12) of the PUR inner core

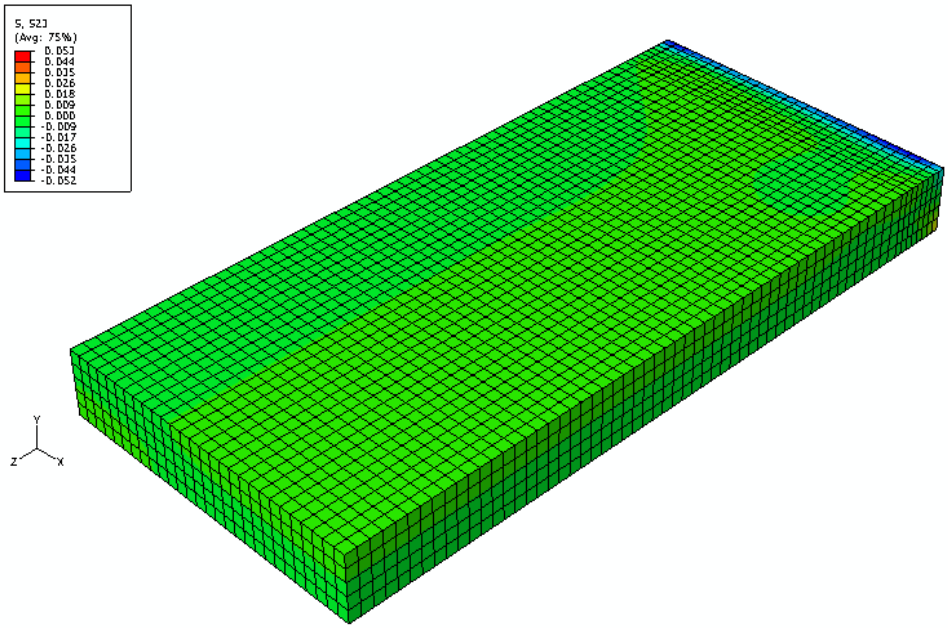

(c) Distribution of the shear stress (S23) of the PUR inner core

Figure 4.66: Distribution of the stresses of the PUR inner core

Further investigations to determine the buckling failure by using *BUCKLE step, the buckling failure loads are 237.1 kN (for SMC) and 307.3 kN (for SDC). It should be noted that the type

of longitudinal joint can make an impact on the buckling failure load. Table 4.25 tabulated the initial failure loads found from the numerical investigations.

Specimen	Load (kN)	Failure
SMC	237.1	Buckling
	421.5	End bearing
SDC	307.3	Buckling
	436.5	End bearing

Table 4.25: Numerical analysis on SIPs when subjected to axial load

Figure 4.67 shows the load and the displacement curves comparison between the FEM and the mean test results up to the initial failure loads i.e. buckling failure loads. Although less agreement on the displacement has been found, the displacements are small only 0.45% of the panel height. This reveals that the axial displacement less concerned in engineering practice.

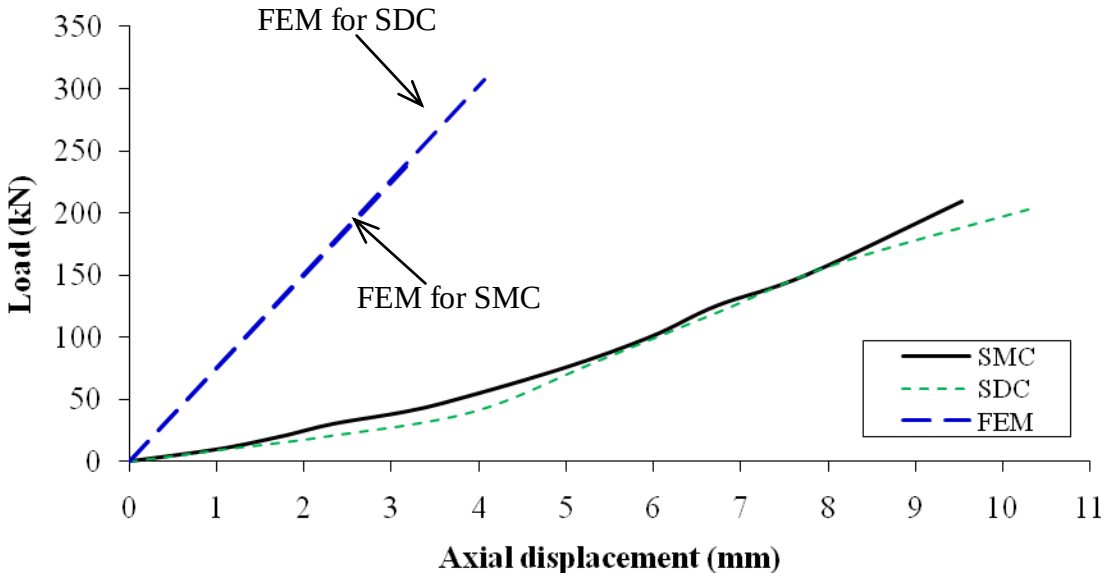

Figure 4.67: Displacement comparison between the FEM and the mean test results

Typical SIPs (STP) have not been subjected to physical test as previously described. This section presents the numerical investigation on STP. The concept to model the STP panel is

similar to the SMC and SDC panels. Table 4.26 tabulated the initial failure loads found from the STP numerical investigations, it should be noted that the initial failure loads are similar to the SMC panels.

Specimen	Load (kN)	Failure
STP	210.5	Buckling
	415.6	End bearing

Table 4.26: Numerical analysis on SIPs when subjected to axial load

4.5.4 SMCO experimental investigation

The effects of opening when subjected to uniform axial compression were evaluated by testing two panels i.e. SMCO-1 and 2. Figure 4.68 shows the applied loads against the axial displacements.

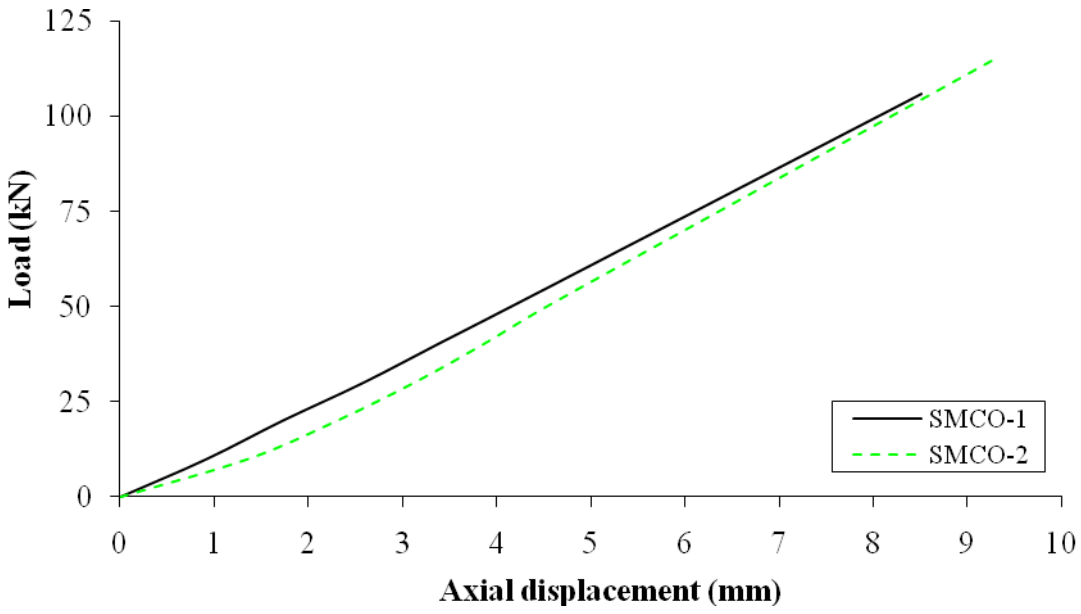

Figure 4.68: Load versus axial displacement

The mean ultimate load at failure and mean axial displacement are 110.5 kN (92.1 kN/m) and 8.90 mm, respectively. The failure mode for both specimens is due to face crushing at the small

section of the opening on one side only as shown in Figure 4.69. The SMCO experimental results are summarised in Table 4.27.

(a) SMCO-1

(b) SMCO-2

Figure 4.69: Face crushing failure

Specimen	**Dimension (mm)**			**Ultimate load**		**Axial axis displacement at failure (mm)**	**Failure mode**
	W	**L**	**D**	**(kN)**	**(kN/m)**		
SMCO-1	1,194	2,445	125	106.0	88.3	8.51	Face crushing
SMCO-2	1,193	2,440	125	115.0	95.8	9.29	
Mean	**1,193**	**2,443**	**125**	110.5	**92.1**	**8.90**	

Table 4.27: SMCO experimental finding summary

4.5.5 SMCO axial compression analytical method

An analytical method to determine the axial loading capacity is currently not available. However, the axial loading capacity with the remaining cross section is investigated and determined by using the equation 4.3. Table 4.28 presents the panel details, material properties and the axial loading capacity of SMCO.

$f_{c,33}$ (N/mm^2)	15.75
B (mm)	600
f (mm)	11
$F_{u,ax}$ (kN)	207.90

Table 4.28: SMCO details, material properties and axial loading capacity

As can be seen in Table 4.29 that the axial loading capacity (207.90 kN) is almost 1.88 times the mean SMCO ultimate load (110.50 kN). This axial loading capacity, determined by using the equation 4.3, does not again provide a good agreement between the analytical load capacity and the experimental ultimate load. This is due to bearing ends again do not provide a flush bearing surface and thus it may be likely only part of facial panels have endured the compressive load.

An analytical method to determine the buckling load capacity is not available either. However, the buckling capacity with the remaining cross section is investigated and determined by using Allen's and Davies' method, respectively. Table 4.29 presents the panel details, material properties and the buckling failure load of SMCO. The buckling load capacities determined by Allen and Davies' methods are again similar (99.75 kN and 99.87 kN).

B (mm)	600
L (mm)	2,443
f (mm)	11
d_c (mm)	103
e (mm)	114
E_f (N/mm^2)	3,844
E_c (N/mm^2)	6.442
G (N/mm^2)	2.30
ν_f	0.24
ν_c	0.33
Allen's method, P_{cr} (kN)	99.75
Davies' method, P_{cr} (kN)	99.87

Table 4.29: SMCO details, material properties and buckling load capacity

4.5.6 Numerical investigation

The concept to model the SMCO panel is generally as similar as the previous numerical model without opening. Figure 4.70 depicts finite element for SMCO model. The material properties of SIP components are same as those used in the preceding sections.

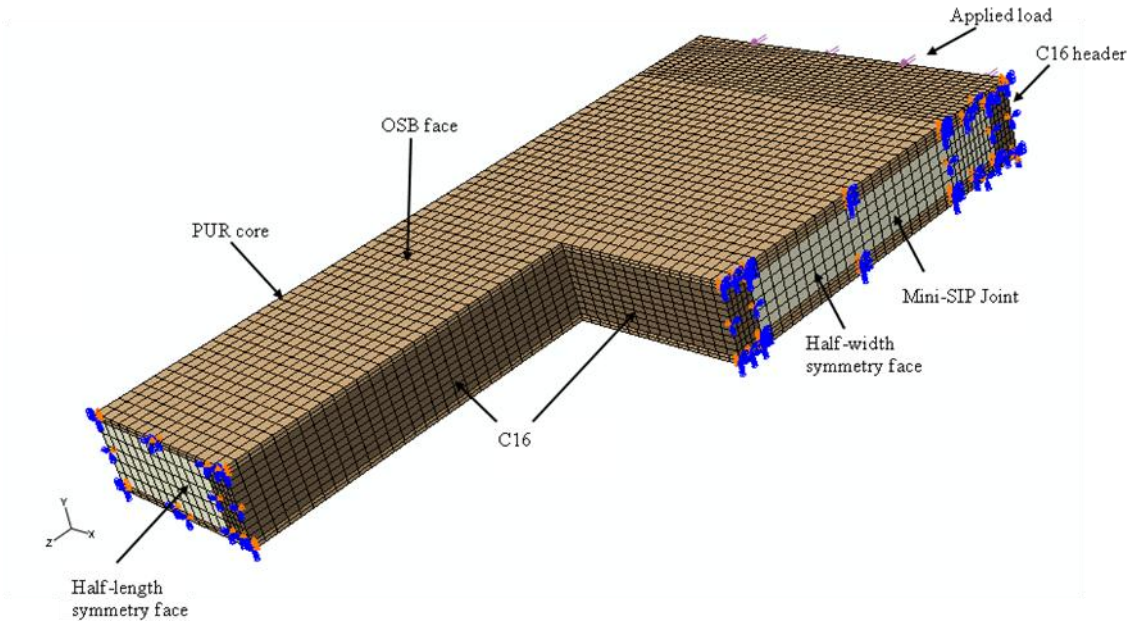

Figure 4.70: SMCO finite element model

It has been found that the initial failure load for the crushing failure of the outer faces is 220.1 kN. This load is consistent with the analytical findings. Figure 4.71 shows the distribution of the longitudinal stress (S33) of the outer faces for SMCO model only. The inner core is also subjected to debonding failure at 220.1 kN applied load as shown in Figure 4.72. Further back track analysis was performed, the initial failure load due to debonding has been found to be 147.1 kN.

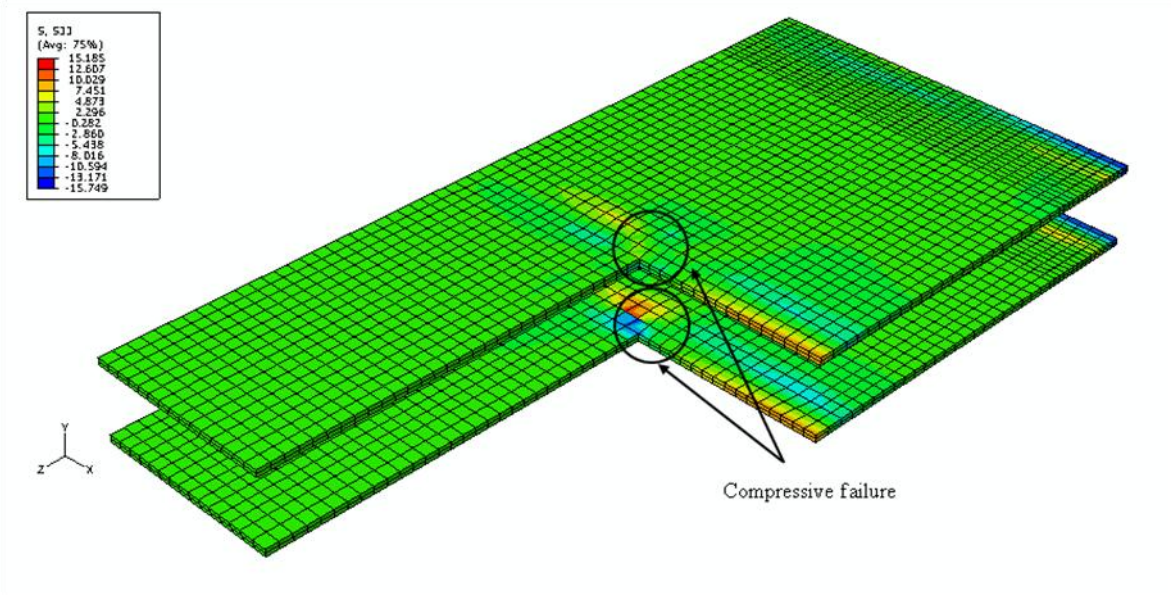

Figure 4.71: Distribution of the longitudinal stress (S33) of the outer faces

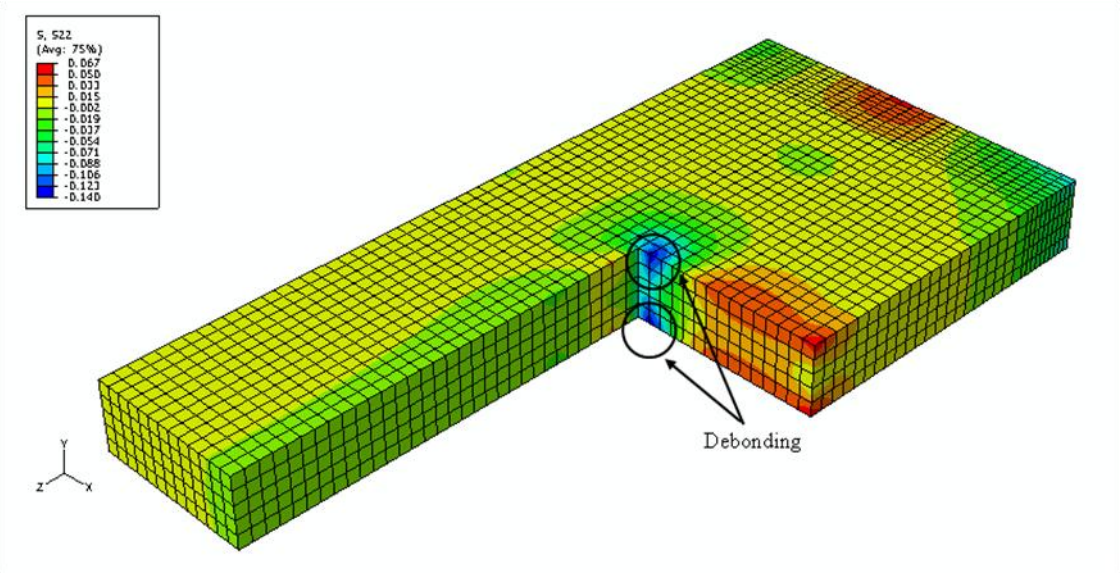

(a) Distribution of the normal stress (S22) of the PUR inner core

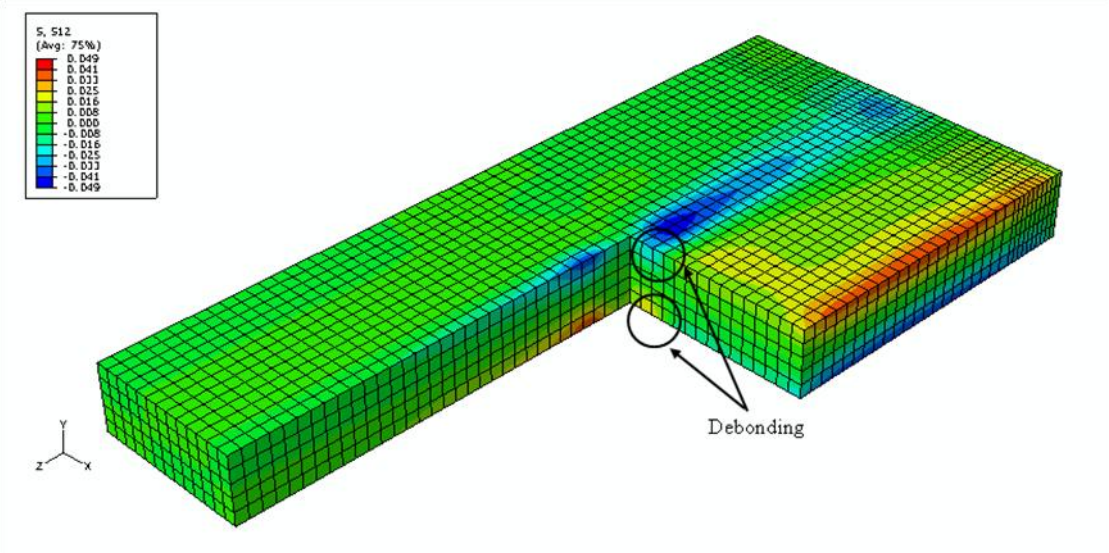

(b) Distribution of the shear stress (S12) of the PUR inner core

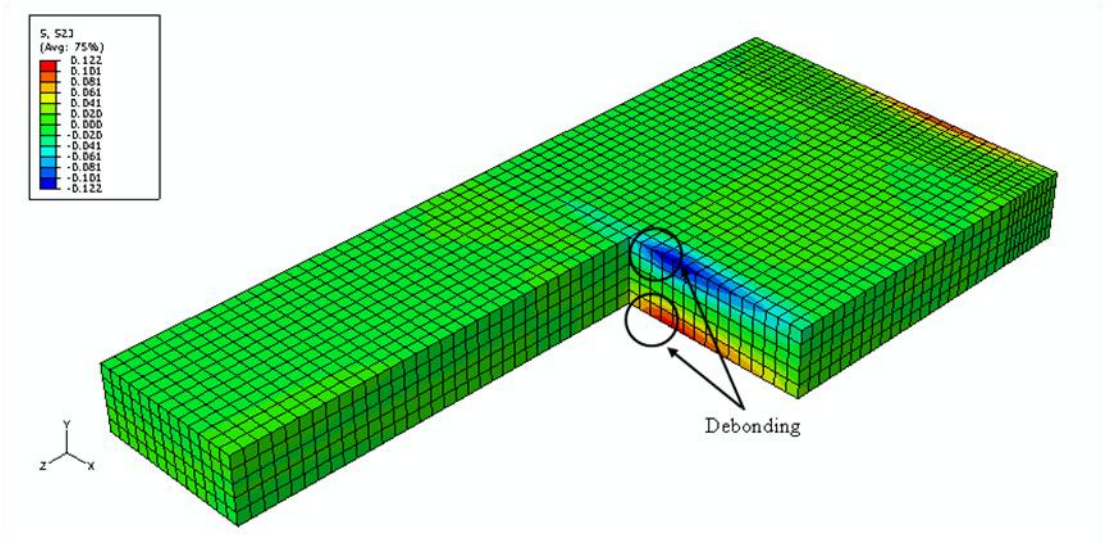

(c) Distribution of the shear stress (S23) of the PUR inner core

Figure 4.72: Distribution of the stresses of the PUR inner core

Further investigations to determine the buckling failure was carried out, the buckling failure load is 115.4 kN. Table 4.30 tabulated the initial failure loads found from the numerical investigations.

Specimen	Load (kN)	Failure
SMCO	115.4	Buckling
	147.1	Debonding
	220.1	Face crushing

Table 4.30: Numerical analysis on SMCO when subjected to axial load

Figure 4.73 shows the load and the displacement curves comparison between the FEM and the mean test results up to the initial failure load i.e. buckling failure load. The displacement has been found small and less concern in engineering practice.

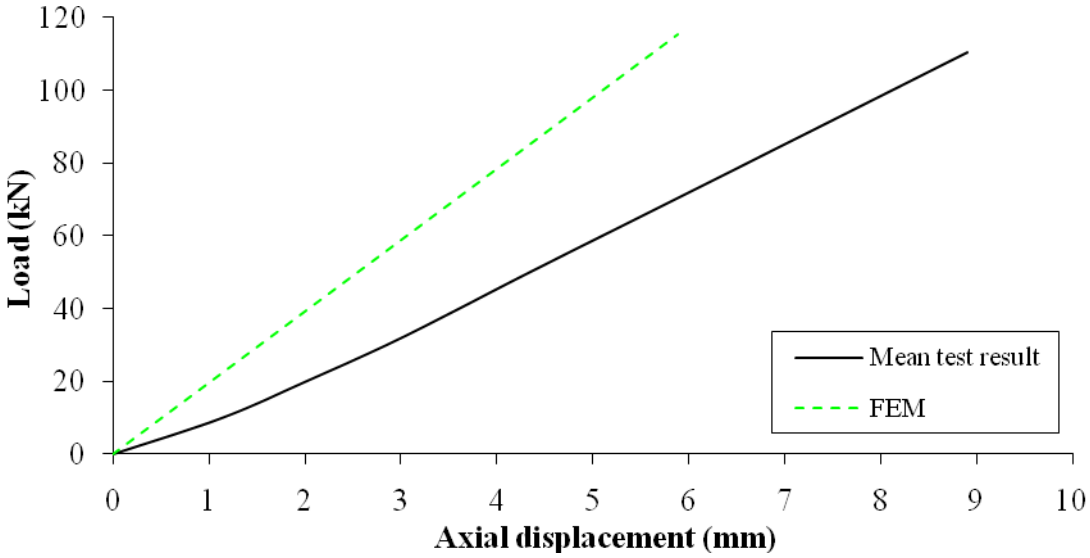

Figure 4.73: Displacement comparison between the FEM and the mean test results

Typical SIPs with openings (STPO) and SIPs with dimensional timber spline connections with openings (SDCO) have not been investigated by the physical test. This section presents the numerical investigations on both STPO and SDCO. The concept to model the STPO and SDCO panels is similar to the SMCO panel. Table 4.31 summarises the initial failure loads due to buckling failure mode as these initial failure loads are the lowest loads in the numerical investigations.

Specimen	Initial failure (kN)	Failure mode
STPO	110.8	Buckling
SMCO	115.4	
SDCO	118.9	

Table 4.31: Summary of FEM investigations for all panels with openings

4.5.7 Investigation summary for panels with different joints and openings

Table 4.32 summarises the test results of the panels when subjected to uniform axial compression. It should be noted that the test results from the SIPs with mini-SIP connection (SMC) and dimensional timber spline connection (SDC) are similar (within 2%) and both failure modes are the same i.e. end bearing. However, their ultimate failure loads are approximately half figures of the analytical and numerical end bearing loads. A possible explanation for this is the due to the dimensional tolerance of facial panels, bearing ends do not provide a flush bearing surface and thus it may be likely only part of facial panels have endured the bearing load. The axial displacement has been found to be small and less concern in engineering practice.

Specimen	Mean ultimate load		Mean axial displacement at failure (mm)	Failure mode
	(kN)	(kN/m)		
SMC	209.0	174.2	9.68	End bearing
SDC	205.0	170.9	10.39	End bearing
SMCO	110.5	92.1	8.90	Face crushing

Table 4.32: Uniform axial compression test result summary

Numerical study reveals the buckling failure mode is governed the loading capacity. It should be noted that the type of longitudinal joint makes an impact on the buckling failure load. Table 4.33 tabulated the initial failure loads found from the numerical investigations.

Specimen	Initial failure		Failure mode
	(kN)	(kN/m)	
STP	210.5	175.4	Buckling
SMC	237.1	197.6	
SDC	307.3	256.1	
STPO	110.8	92.3	
SMCO	115.4	96.2	
SDCO	118.9	99.1	

Table 4.33: Summary of FEM investigations for all panels

4.6 Load case No.3 – Racking loading

As mentioned in the literature review, there is little discussion on SIPs with different joints when subjected to racking loads. Racking load tests were therefore undertaken on SIPs with mini-SIP connections (SMC) and with openings (SMCO) in accordance with BS EN 594 (BSI, 1996). As previously described, the panels with dimensional timber spline connections (SDC) were not tested as it was expected that the failure mode and the ultimate load would be similar to SMC and SMCO. In addition, numerical investigation has not been undertaken since another bonding failure criterion between the OSB faces and the C16 header/footer through nail is required.

Four SIP specimens which are two SMCs and two SMCOs were subjected to racking loading until failure. Each test panel was attached to the test rig by using M8 bolts at 150 mm and 750 mm from the edge of the panel in accordance with BS EN 594. Another end of the panel was supported by two bearing pads at 150 mm from both ends of the panel. The pads (made of PTFE material) are 120 x 120 mm square frictionless and free to move in all horizontal directions as shown in Figure 4.74. The load was then applied at the top of the panel by using a hydraulic hand pump through the load-cell in order to record the applied load magnitudes.

Figure 4.75 illustrates the racking test arrangement. The LVDT positions and the sign convention of displacement are shown in Figure 4.76.

- LVDT No.1 was positioned at the mid-point of the header of the panel for measuring the racking displacement.

- LVDT No.2 was positioned at the mid-point of the footer of the panel for measuring the horizontal displacement.

- LVDT No.3 was positioned at the aluminium bracket, which is attached at mid-point of the footer of the panel for measuring the vertical displacement.

Figure 4.74: 120 x 120 mm square bearing pads

Figure 4.75: Racking test arrangement

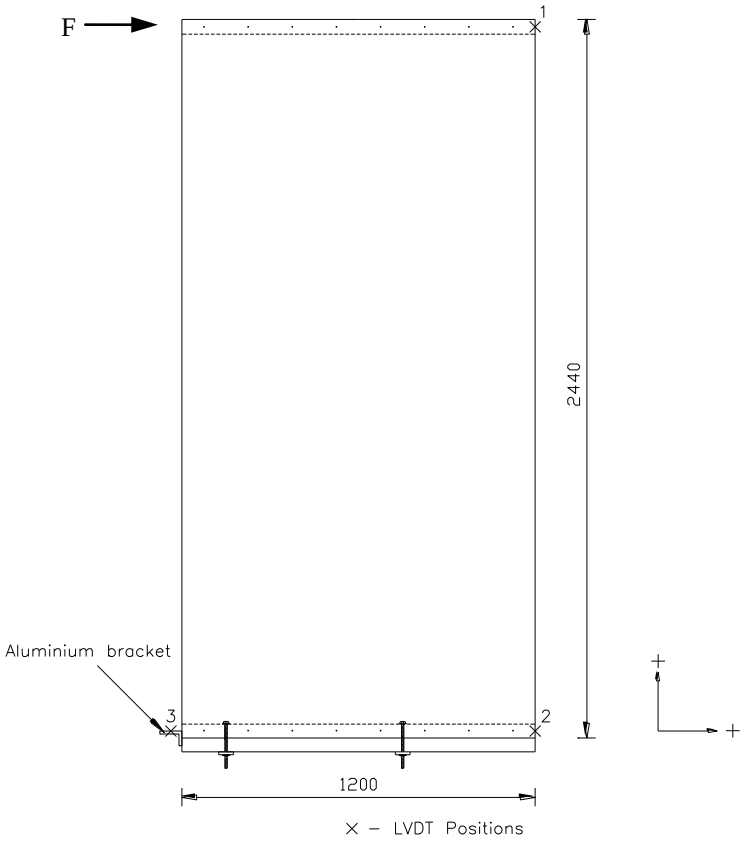

Figure 4.76: LVDT arrangement and sign convention of displacement

4.6.1 Experimental investigation

Figure 4.77 shows the applied loads against the racking displacements of two panels with mini-SIP connections (SMC-1 and 2) and two panels with openings (SMCO-1 and 2).

The mean ultimate loads for the SMC and SMCO panels at failure are 4.16 kN and 4.20 kN, respectively. The failure mode for both SMC specimens is the OSB faces disjointed from the footer indicating a nail connection failure as shown in Figure 4.78 (a) and (b). The failure mode of SMCO-1 is the fracture of the footer plate as shown in Figure 4.78(c). It may explain that this footer plate has less strength to resist the intrusion of the first holding down bolt than the other

panels. However, the failure mode of SMCO-2 is OSB faces were disjointed from the footer as same as previously and shown in Figure 4.78(d).

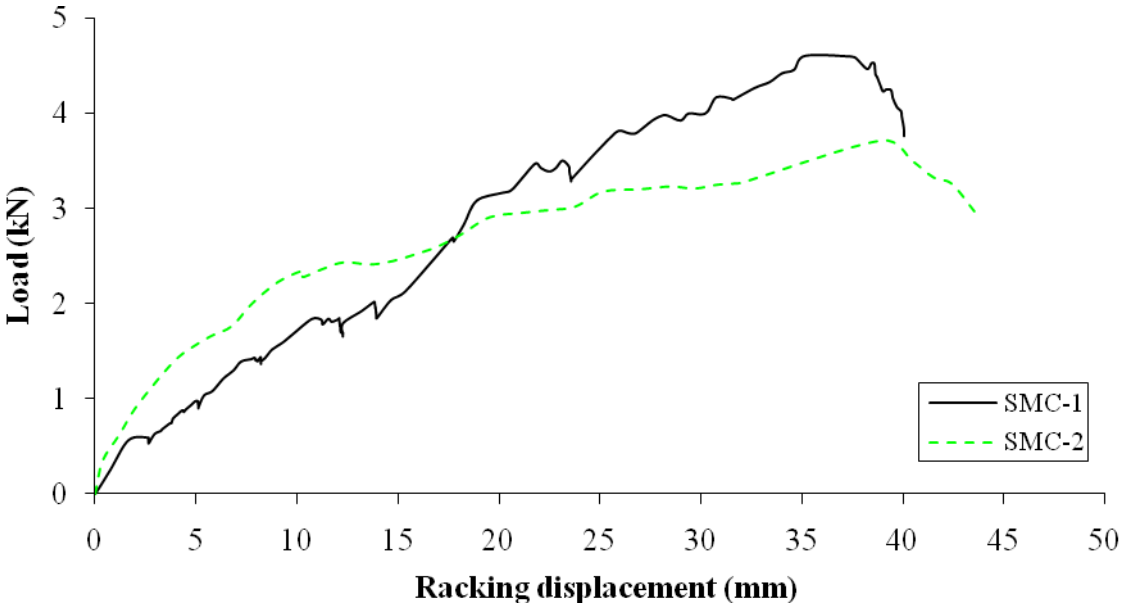

(a) SMC

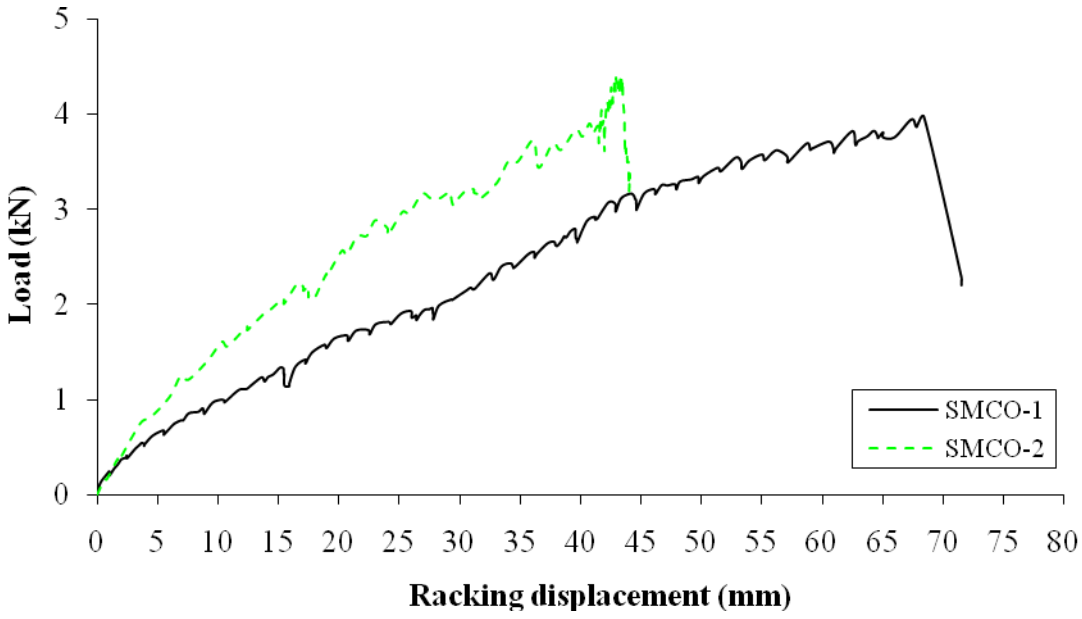

(b) SMCO

Figure 4.77: Load versus racking displacement (LVDT No.1)

(a) SMC-1

(b) SMC-2

(c) SMCO-1

(d) SMCO-2

Figure 4.78: Racking failure modes

Figure 4.79 plots the applied loads against the horizontal displacements at the footer of the panels (LVDT No.2). In comparison to the racking displacement at the top of the panel, the movement at the bottom is minimal.

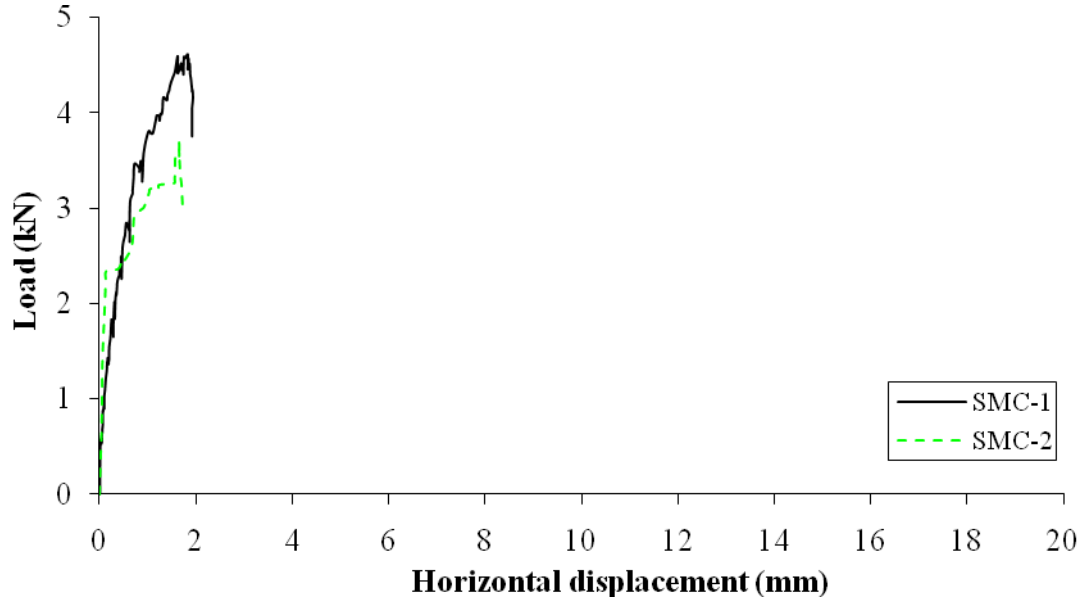

(a) SMC

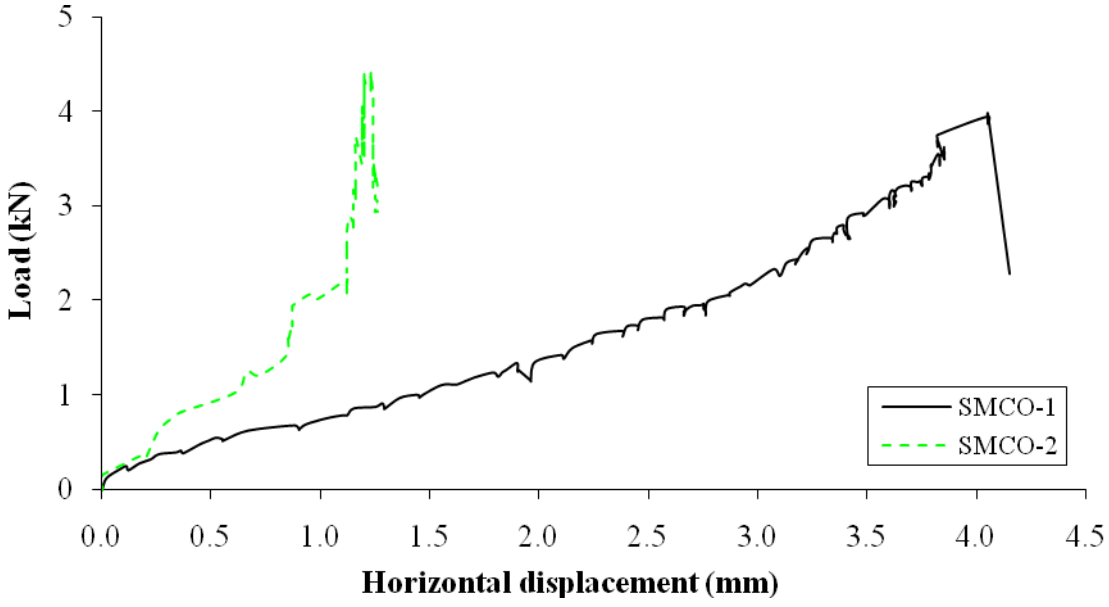

(b) SMCO

Figure 4.79: Load versus horizontal displacement (LVDT No.2)

The vertical displacements of the panels (LVDT No.3) are illustrated in Figure 4.80. The mean displacements found from the test panels are up to a third of the racking displacements at the top of the panels. Nevertheless, it should be noted that the movements measured from LVDT

Nos 2 and 3 were mainly from the rotation movements of the footers that were caused by the applied moments rather than the translational movements caused by the applied shear forces.

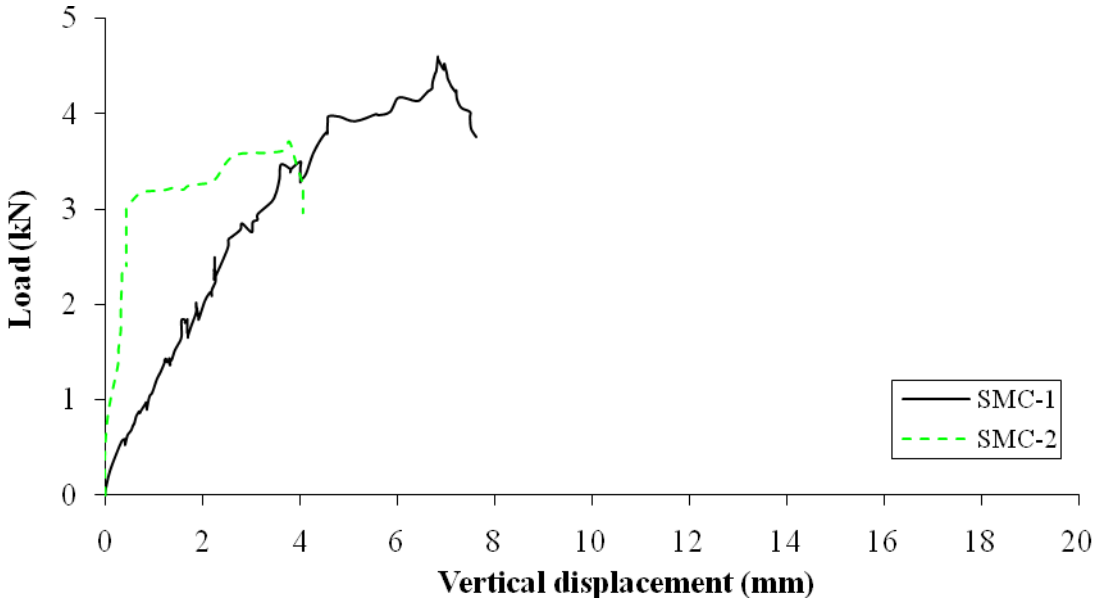

(a) SMC

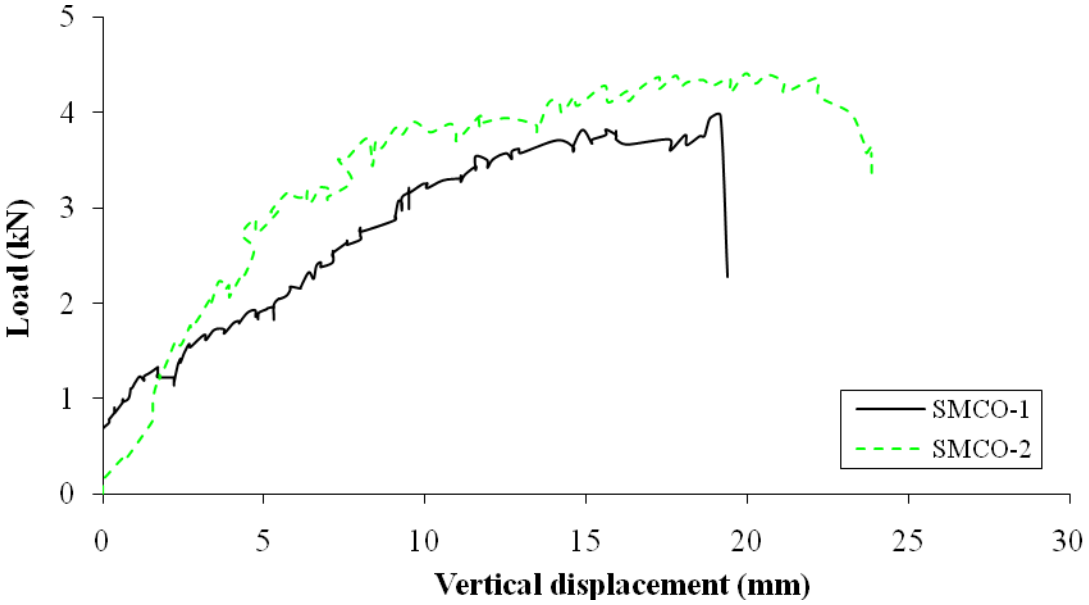

(b) SMCO

Figure 4.80: Load versus vertical displacement (LVDT No. 3)

Table 4.34 summarises the test results of the panels when subjected to the racking loadings. The key findings from the racking loading test are as follows:

- The test results show the panels were not subjected to any damages. Most panels fail by the OSB faces disjoint from the footer, with the exception of SMCO-1 that failed due to fracture of the footer.

- The mean loading capacities from both panel groups are similar which depend upon the strength of the ring shank nail and spacing.

- The horizontal displacements at the footer are negligible in comparison with the racking displacements at the header. The main displacement is due to the rotation rather than the translational movement.

Specimen	**SMC**	**SMCO**
Width (mm)	1,196	1,195
Length (mm)	2,440	2,440
Depth (mm)	125	125
Mean ultimate load (kN)	4.16	4.20
Mean racking displacement at failure (mm)	37.04	55.84
Mean horizontal displacement at failure (mm)	1.65	2.64
Mean vertical displacement at failure (mm)	5.31	19.56
Failure mode	Disjointing	Fracture and Disjointing

Table 4.34: Racking result summary

4.6.2 Racking analytical investigation

The performance of SIP specimen is compared to the stud wall designed to EC5. The characteristic test racking resistance in accordance with BS 5268 Cl. 6.1 (BSI, 1996) is determined and present in Table 4.35. The racking calculation is presented in the Appendix A.

As shown in Table 4.35, SIP specimen without opening are better performance than stud wall designed to EC5 by 15%, whereas outperform by 53% of the panel with opening.

Specimen	**Mean load at failure, F_{max} (kN)**	**Test racking strength load, F_{ult} (kN)**	**Characteristic test racking resistance (kN/m)**	**Stud wall designed to EC5 (kN/m)**
SIPs with mini-SIP connections (SMC)	4.16	3.62	1.48	1.29
SIPs with mini-SIP connections and opening (SMCO)	4.20	3.65	1.50	0.98

Table 4.35: Comparison between the test result and EC5 method

4.7 Summary

Various experimental, analytical and numerical investigations on structural performance of SIPs subjected to single loadings were carried out. The findings can be summarised as follows.

- The failure of SIPs under transverse load is usually governed by the stiffness for normal span length.
- The ranking (high to low) of the panel stiffness found from both experimental and numerical investigations is SDC, SMC and STP, respectively.
- The horizontal displacement is negligible with less concern in engineering practice in comparison with the vertical displacement when SIPs are subjected to transverse load.
- Allen's and TR 019 analytical methods have been found to be favourable to analyse the central displacements for STP and SDC, respectively when subjected to transverse load.

- Under these SIP connection configurations and openings, it has been found that the structural behaviour of SIPs is independent to the different joint designs when subjected to transverse load. This is because the critical section is away from the panel joint line.

- The experimental ultimate failure loads are approximately half the value of the analytical and numerical end bearing loads. A possible explanation for this is the due to the dimensional tolerance of facial panels, bearing ends do not provide a flush bearing surface and thus it may be likely that only part of facial panels have endured the bearing load. To ensure that the maximise end bearing load can be obtained, a flush bearing surface is required.

- A numerical model has been established and validated by the experimental results. The numerical model can well predict the onset of failure load and the failure mode by using the maximum stress criterion for OSB and the linear stress failure criterion for debonding of the PUR.

CHAPTER FIVE

SIPS UNDER COMBINED LOADINGS

5.1 Introduction

This Chapter presents the structural behaviour of SIPs under combined loadings as wall condition. The interactive failure load curves for SIPs under combined axial and transverse loadings, with different joint constructions and with or without openings, are determined and presented.

5.2 Load case No. 4 - Combined axial and transverse loadings

In this test, the structural performance of SIPs subjected to uniform axial compression (8 kN/m) and transverse loadings was examined. For the size of the panel specimen that is normally designed for buildings, an axial load of 8 kN/m is a typical representation of the loading level that they should sustain.

Four SIP specimens, i.e. two SMCs and two SMCOs, were subjected to combined axial and transverse loadings until the ultimate failure. The test setup was similar to the first test series that were described in section 4.4. A 1.2 m steel parallel flange channel section was used to apply a uniform axial compression as shown in Figure 5.1. The axial load (8 kN/m) was applied along the header by using a hydraulic hand pump through the load-cell and then the steel channel. The transverse load was later applied until the failure occured. Three LVDTs were positioned at the following locations as shown in Figure 5.2.

- LVDT No.1 was positioned at the central of the panel for measuring the vertical displacement.

- LVDT No.2 was positioned at the mid-length and approximately 10 mm from the edge of the panel for measuring the vertical displacement.

- LVDT No.3 was positioned at the aluminium bracket, which attached at the header of the panel for measuring the axial displacement.

For the test panels with the openings, the LVDT No.1 was repositioned to be at the mid-length and approximately at 10 mm from the edge of the opening as previously described in section 4.4.

Figure 5.1: Experimental apparatus layout

5.2.1 Experimental investigation

Two SIPs with mini-SIP connections (SMC-1 and 2) and two specimens with openings (SMCO-1 and 2) were subjected to the combined axial and transverse loadings. Figure 5.3 shows the applied loads against central vertical displacements of the two panels with mini-sip connections and other two panels with openings.

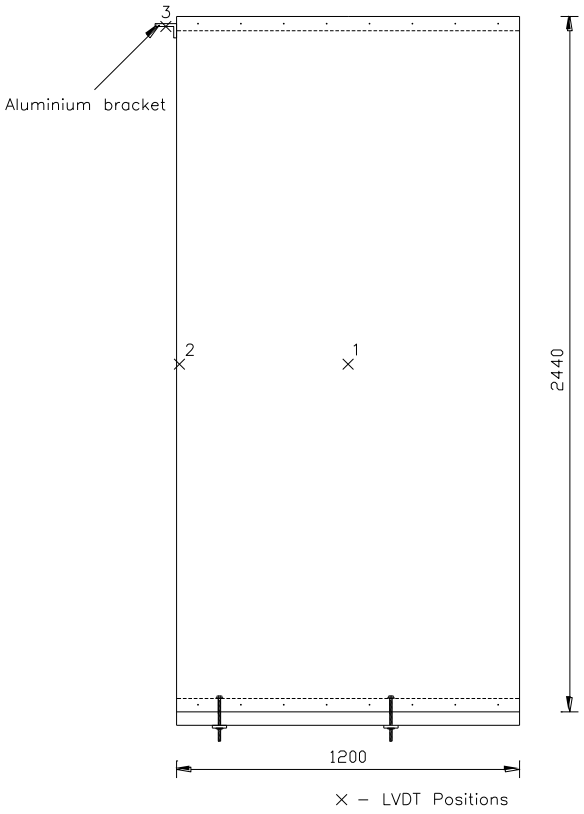

Figure 5.2: LVDT arrangement

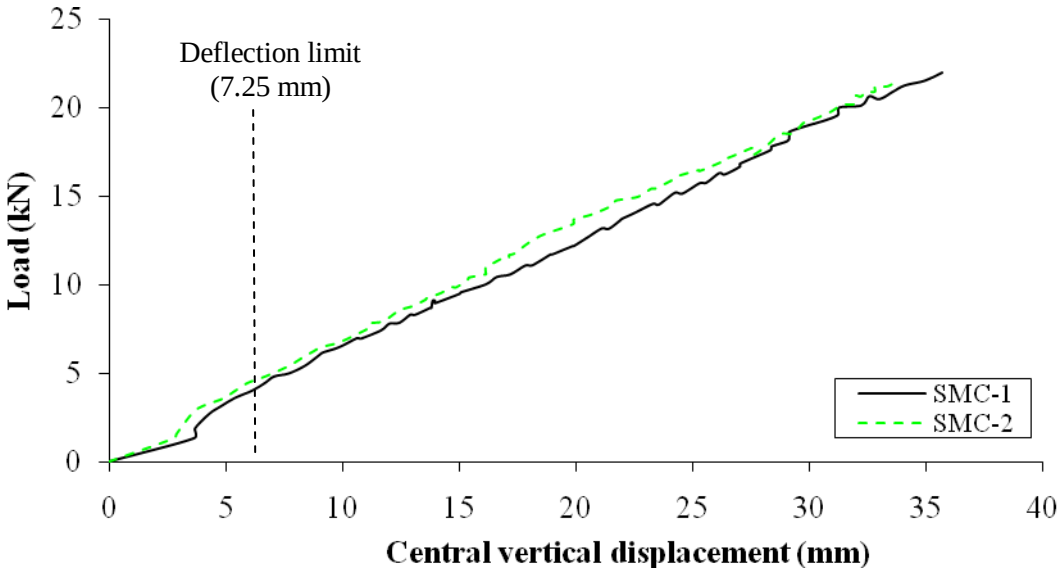

(a) SMC

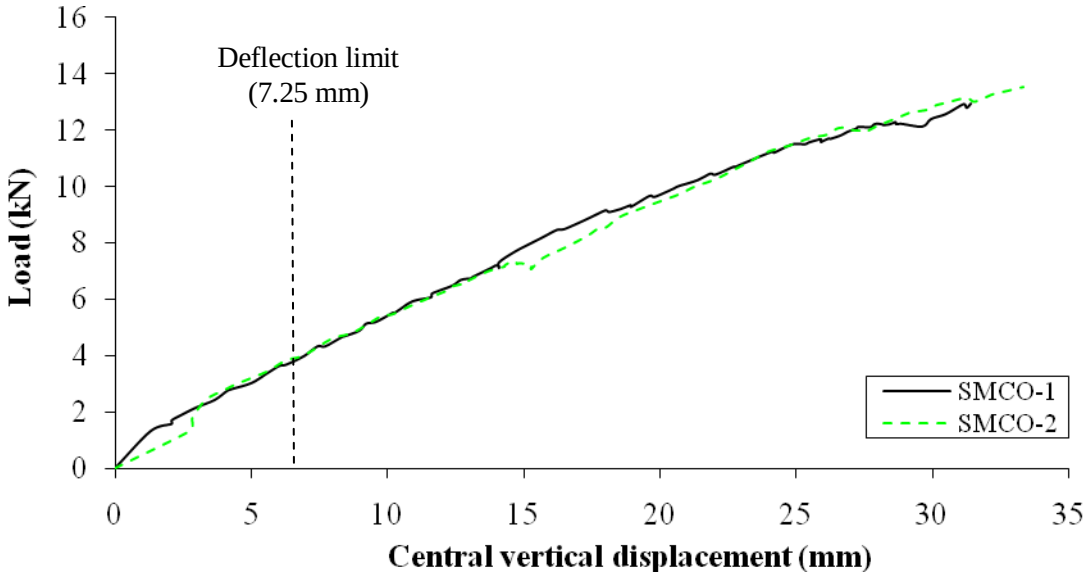

(b) SMCO

Figure 5.3: Load versus central vertical displacement (LVDT No.1)

The mean loading capacities at failure are 21.78 kN (for SMC) and 13.25 kN (for SMCO), this is about 1.7% and 6.6% less than the mean of the panels subjected to transverse load only (22.16 kN and 14.18 kN). The serviceability load again becomes the limiting factor of the loading capacity. The failure modes are as same as previously found from the individual transverse load applied only as shown in Figure 5.4.

Figure 5.5 plots the applied loads against vertical displacements at 10 mm from the edge of the panels.

(a) SMC-1

(b) SMC-2

(c) SMCO-1

(d) SMCO-2

Figure 5.4: Failure mode

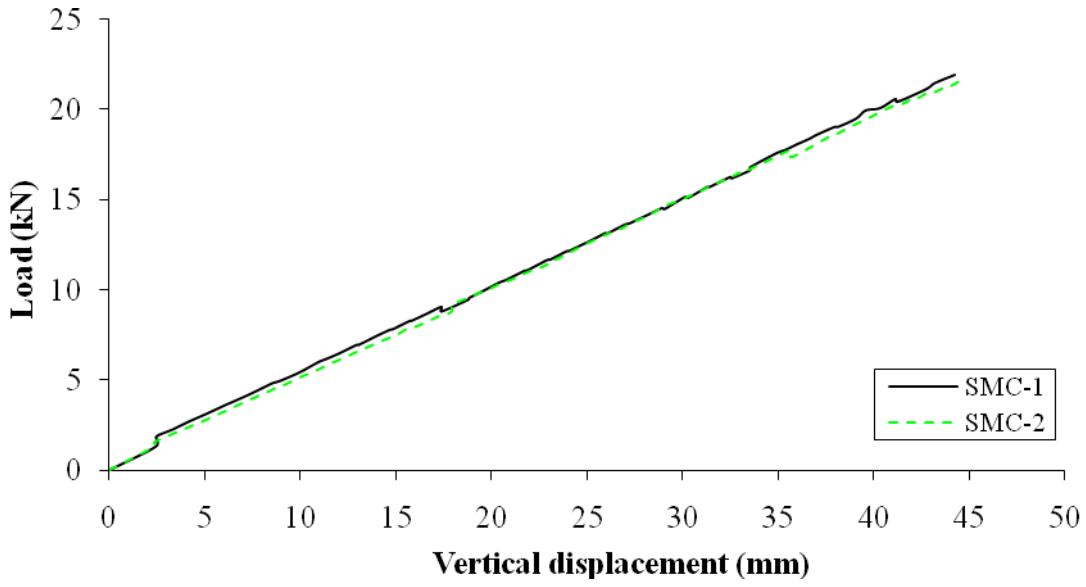

(a) SMC

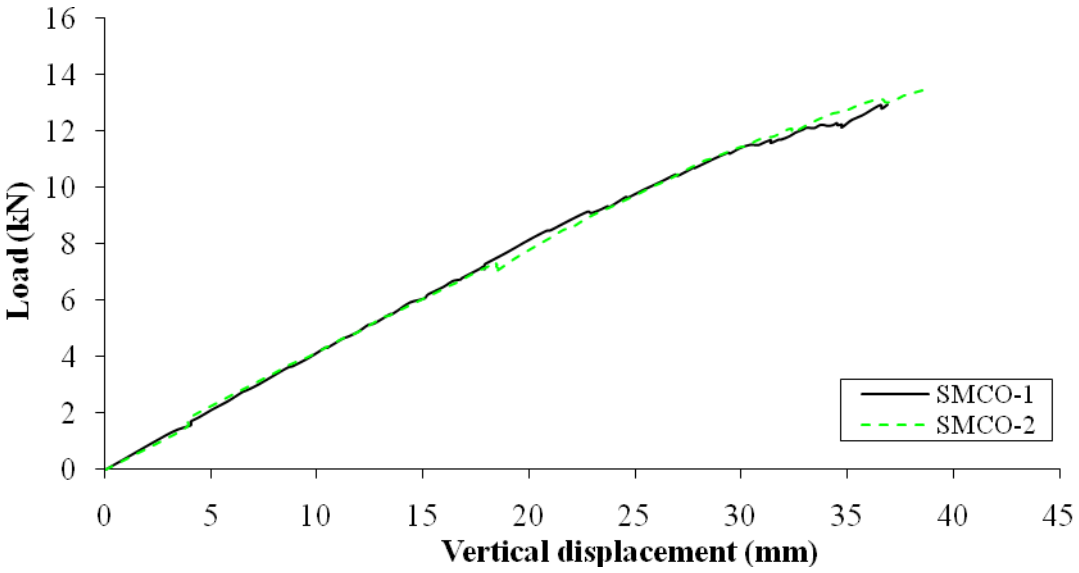

(b) SMCO

Figure 5.5: Load versus vertical displacement (LVDT No.2)

The axial displacements of the panels (LVDT No.3) are small as illustrated in Figure 5. 6. All experimental details and findings are tabulated in Table 5.1.

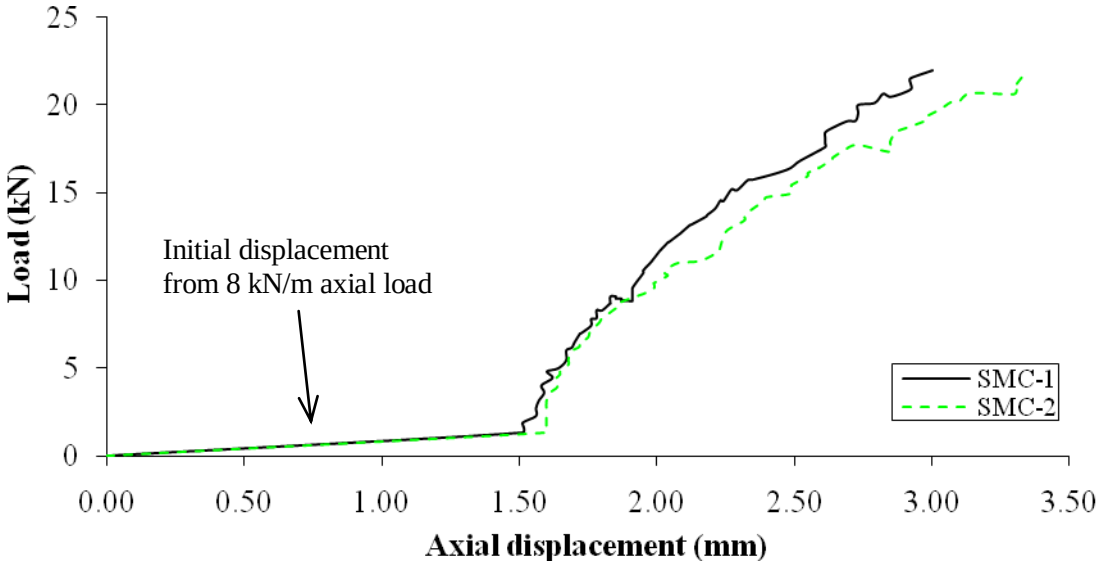

(a) SMC

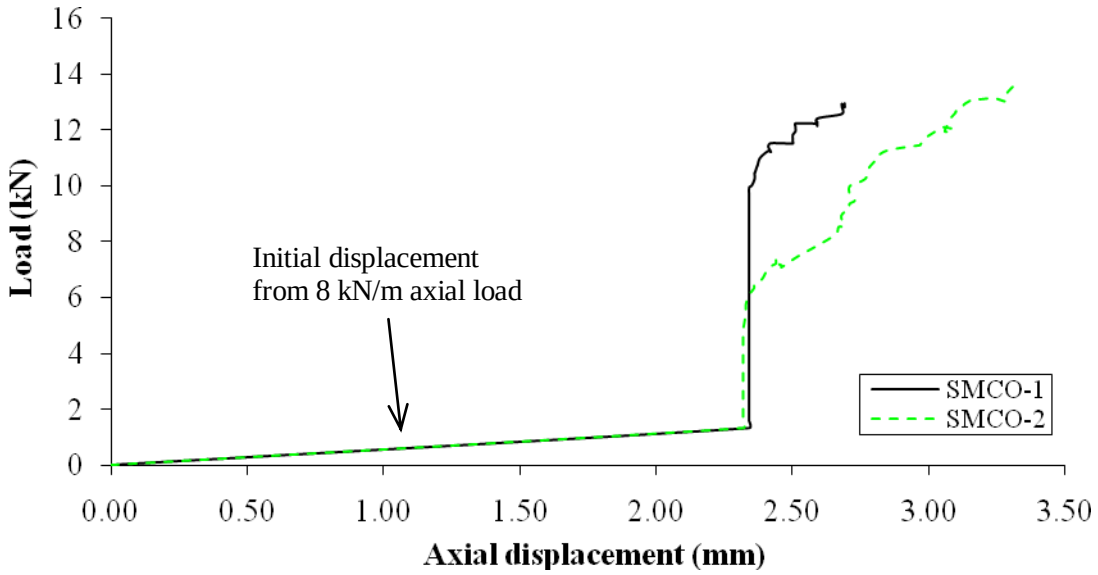

(b) SMCO

Figure 5.6: Load versus axial displacement (LVDT No. 3)

Specimen	SMC-1	SMC-2	Mean
Width (mm)	1,195	1,196	**1,195**
Length (mm)	2,445	2,445	**2,445**
Depth (mm)	125	125	**125**
Ultimate load (kN)	21.94	21.63	**21.78**
Load at deflection limit ℓ/333 (kN)	4.91	5.19	**5.05**
Serviceability load / Ultimate load (%)	22.4	24.0	**23.2**
Maximum central displacement (mm)	35.71	33.81	**34.76**
Maximum edge displacement (mm)	44.25	44.58	**44.42**
Maximum axial displacement (mm)	3.00	3.33	**3.17**
Failure mode	Debonding	Debonding	

(a) SMC

Specimen	SMCO-1	SMCO-2	Mean
Width (mm)	1,193	1,193	**1,193**
Length (mm)	2,445	2,445	**2,445**
Depth (mm)	125	125	**125**
Ultimate load (kN)	12.95	13.55	**13.25**
Load at deflection limit ℓ/333 (kN)	4.13	4.23	**4.18**
Serviceability load / Ultimate load (%)	31.89	31.22	**31.55**
Maximum central displacement (mm)	31.38	33.33	**32.36**
Maximum edge displacement (mm)	36.90	38.96	**37.93**
Maximum axial displacement (mm)	2.69	3.31	**3.00**
Failure mode	Flexure-Shear	Flexure-Shear	

(b) SMCO

Table 5.1: Experimental result summary

5.2.2 Numerical investigation

The SMC and SMCO numerical models are as same as the previous ones as detailed in section 4.4.5. The axial load was applied prior to apply the transverse load. The applied loads of 8 kN/m axial and then 25 kN transverse were applied to the SMC model. This load is again higher than the mean experimental failure loads. Tables 5.2 and 5.3 show the maximum stresses obtained from the finite element analysis for the OSB and the PUR, respectively. The stress distributions and the maximum stresses have been found at the same locations as the case of the transverse load only, the contour plots are therefore not presented. The bending failure does not occur as shown in Table 5.2, whereas the inner core fails due to the debonding as shown in Table 5.3. The initial failure load has been found to be 19.20 kN.

Load (kN)	Failure	S_{11} (N/mm^2)	S_{33} (N/mm^2)	S_{11} / f_{11}	S_{33} / f_{33}	Remark
8 kN/m + 25 kN	Bending	14.48	4.37	0.88	0.53	Pass

Table 5.2: SMC - numerical analysis on the OSB outer faces

Load (kN)	Failure	S_{22} (N/mm^2)	S_{12} (N/mm^2)	S_{23} (N/mm^2)	$S_{22}/f_{11} + S_{12}/f_{12} + S_{23}/f_{23}$	Remark
8 kN/m + 25 kN	Debonding	0.156	0.023	0.032	1.30	Fail
8 kN/m + 19.2 kN		0.120	0.018	0.024	0.99	Pass

Table 5.3: SMC - numerical analysis on the PUR

For SMCO model, the applied loads of 8 kN/m axial and then 15 kN transverse were initially applied to the FEM model. Tables 5.4 and 5.5 show the maximum stresses obtained from the finite element analysis for the OSB and the PUR, respectively. The stress distributions and the maximum stresses have also been found at the same locations of transverse only, the contour plots are therefore not shown. The OSB faces fail due to bending, whereas the inner core fails due to debonding. The lowest initial failure load has been found to be 8.20 kN.

Load (kN)	Failure	S_{11} (N/mm^2)	S_{33} (N/mm^2)	S_{11}/f_{11}	S_{33}/f_{33}	Remark
8 kN/m + 15 kN	Bending	27.66	9.03	1.69	1.10	Fail
8 kN/m + 8.20 kN		16.39	5.34	0.99	0.65	Pass

Table 5.4: SMCO - numerical analysis on the OSB outer faces

Load (kN)	Failure	S_{22} (N/mm^2)	S_{12} (N/mm^2)	S_{23} (N/mm^2)	$S_{22}/f_{11} + S_{12}/f_{12} + S_{23}/f_{23}$	Remark
8 kN/m + 15 kN	Debonding	0.192	0.028	0.028	1.50	Fail
8 kN/m + 9.59 kN		0.125	0.018	0.021	0.99	Pass

Table 5.5: SMCO - numerical analysis on the PUR

Figure 5.7 presents the load and the deflection curves at the central span comparison between the FEM and the mean test results up to the initial failure. The agreement of the central displacements is good. The axial displacements are small and hence less concern in engineering practice, the comparison between the test results and numerical investigations are not presented.

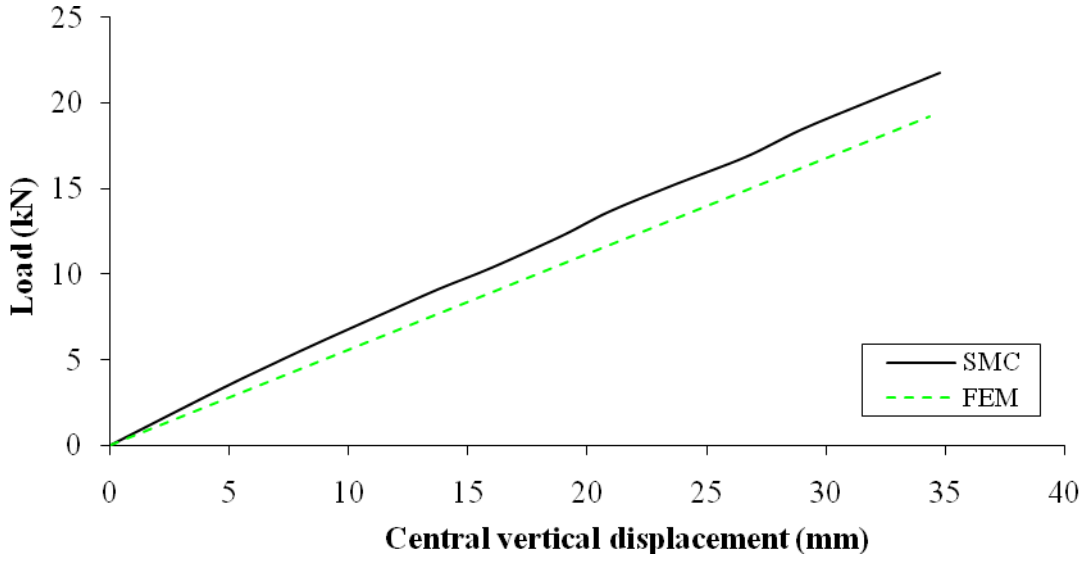

(a) SMC

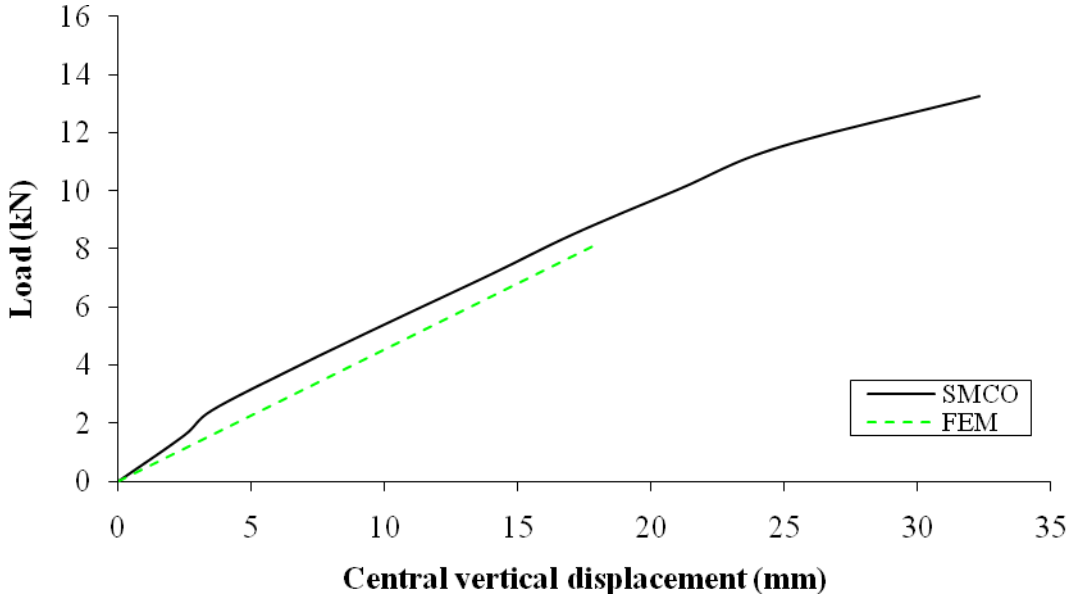

(b) SMCO

Figure 5.7: Central displacement comparison between the FEM and the mean test results

Typical SIPs (STP), SIPs with dimensional timber spline connections (SDC), typical SIPs with openings (STPO) and SIPs with dimensional timber spline connections and openings (SDCO) have not been physically tested as previously described. This section presents the numerical investigations which are summarised in Tables 5.6 and 5.7. A reduction of the initial failure has been found when the axial load is applied to the panel.

Specimen	STP	SDC
FEM initial failure load with 8 kN/m axial load (kN)	17.85	22.94
FEM initial failure load without axial load (kN)	18.70	23.40
Difference (%)	4.55	1.97
Maximum central displacement (mm)	32.76	28.10
Failure mode	Debonding	Debonding

Table 5.6: Summary of numerical results for STP and SDC panels

Specimen	STPO	SDCO
FEM initial failure load with 8 kN/m axial load (kN)	8.17	8.27
FEM initial failure load without axial load (kN)	9.40	9.60
Difference (%)	12	15
Maximum central displacement (mm)	18.51	18.11
Failure mode	Flexure	Flexure

Table 5.7: Summary of numerical results for STPO and SDCO panels

5.2.3 Discussion of results for panels with different joints and openings

Figure 5.8 presents the FEM central displacement results of STP, SMC and SDC. These results are consistent with the expectation in which the SDC shows the best stiffness than the other two panels.

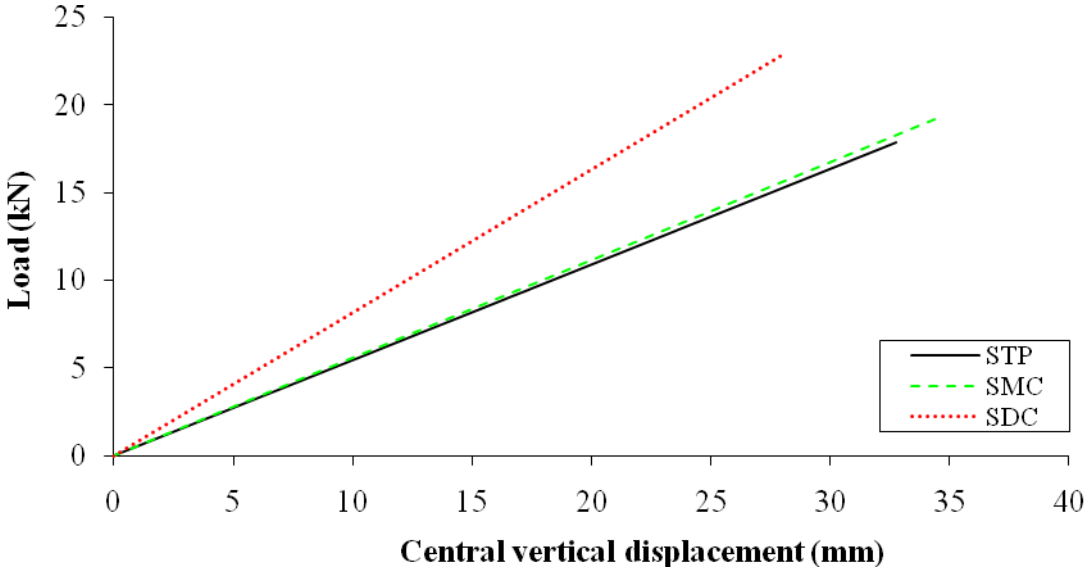

Figure 5.8: Numerical result comparison of SIPs with different connections

For SIPs with different joints and openings under these SIP detail configurations, it has been found that the structural behaviour under the different joint design is not influenced as shown in Figure 5.9 from the FEM investigation. This may be due to the central displacement investigations are at the openings with stiffening by C16 timber blocks. The different in longitudinal joint does therefore not contribute a major impact on the structural behaviour.

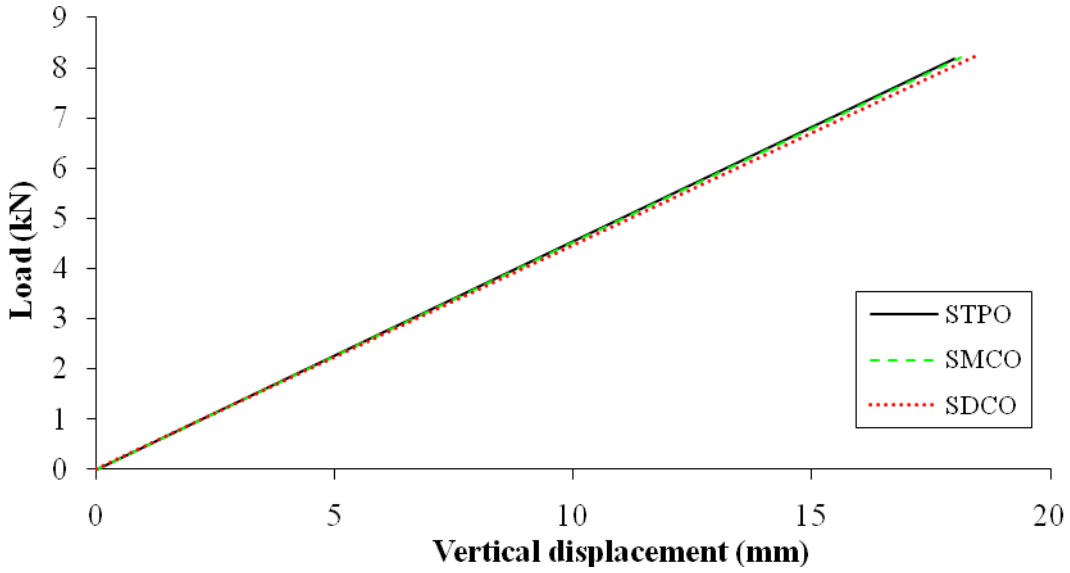

Figure 5.9: Numerical result comparison of SIPs with different connections and openings

Table 5.8 summarises the test results and the numerical investigations of the STP, SMC and SDC panels when subjected to combined axial and transverse loadings. The summary of the STPO, SMCO and SDCO panels are tabulated in Table 5.9.

Specimen	STP	SMC	SDC
Ultimate Limit Load, ULL (kN)	-	21.78	-
Load at deflection limit ℓ/333 (kN)	-	5.05	-
Serviceability load / Ultimate load (%)	-	23.2	-
FEM initial failure (kN)	17.85	19.20	22.94
Maximum central displacement (mm)	-	34.76	-
Maximum edge displacement (mm)	-	44.42	-
Maximum axial displacement (mm)	-	3.17	-
Experimental failure mode	-	Debonding	-
FEM initial failure mode	Debonding		

Table 5.8: STP, SMC and SDC experimental and numerical finding summary

Specimen	STPO	SMCO	SDCO
Ultimate Limit Load, ULL (kN)	-	13.25	-
Load at deflection limit ℓ/333 (kN)	-	4.18	-
Serviceability load / Ultimate load (%)	-	31.55	-
FEM initial failure (kN)	8.17	8.20	8.27
Maximum central displacement (mm)	-	62	-
Maximum edge displacement (mm)	-	32.36	-
Maximum axial displacement (mm)	-	37.93	-
Experimental failure mode	-	3.00	-
FEM initial failure mode	-	Flexure-Shear	-
Ultimate Limit Load, ULL (kN)	Flexure		

Table 5.9: STPO, SMCO and SDCO experimental and numerical finding summary

5.3 Load case No. 5 - Combined racking and transverse loadings

In this test, panels were subjected to combined racking (1 kN) and transverse loadings in order to quantify the structural performance. Although the SIPs can sustain the mean racking load of 4.20 kN found in the racking test, 1 kN racking load (according to the panel size) was chosen to

apply to the test panels as this represents a typical design racking load that the panel requires to sustain in its service life.

One SMC and two SMCOs were subjected to combined racking and transverse loadings until failure. The test setup was similar to the racking loading which previously described in section 4.6. However, another end of the panel was supported by a 30 mm diameter steel roller instead of the two 120 mm square pads. The racking load (1 kN) was applied at the top of the panel by using a hydraulic hand pump through the load-cell. The transverse load was later applied until failure. Figure 5.10 shows the experimental apparatus layout for the combined racking and transverse loading test. The LVDT arrangement is listed below and presented in Figure 5.11.

- LVDT No.1 was positioned at the central of the panel for measuring the vertical displacement.

- LVDT No.2 was positioned at the mid-length and approximately at 10mm from the edge of the panel for measuring the vertical displacement.

- LVDT No.3 was positioned at the header of the panel for measuring the racking displacement.

Likewise, for the test panels with openings, the LVDT No.1 was repositioned to be at the mid-length and approximately at 10 mm from the edge of the opening.

Figure 5.10: Experimental apparatus layout for combined racking and transverse loading test

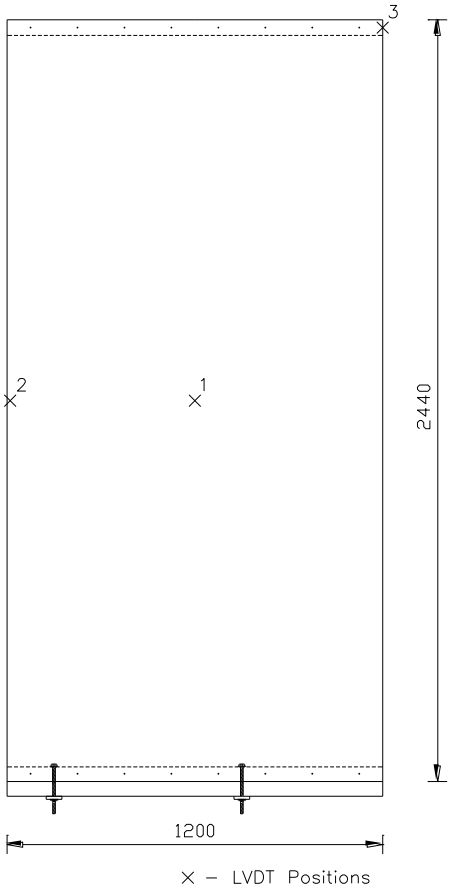

Figure 5.11: LVDT arrangement

5.3.1 Experimental investigation

SMC and SMCO were subjected to combined racking (1 kN) and transverse loadings. Figure 5.12 shows the applied loads against the central vertical displacements. The ultimate loads are 22.05 kN (for SMC) and 13.91 kN (for SMCO), which are 0.5 % and 1.9% slightly lower than the mean ultimate loads of the panels when subjected to individual transverse loading. The failure modes are as same as the individual transverse loading only as shown in Figure 5.13.

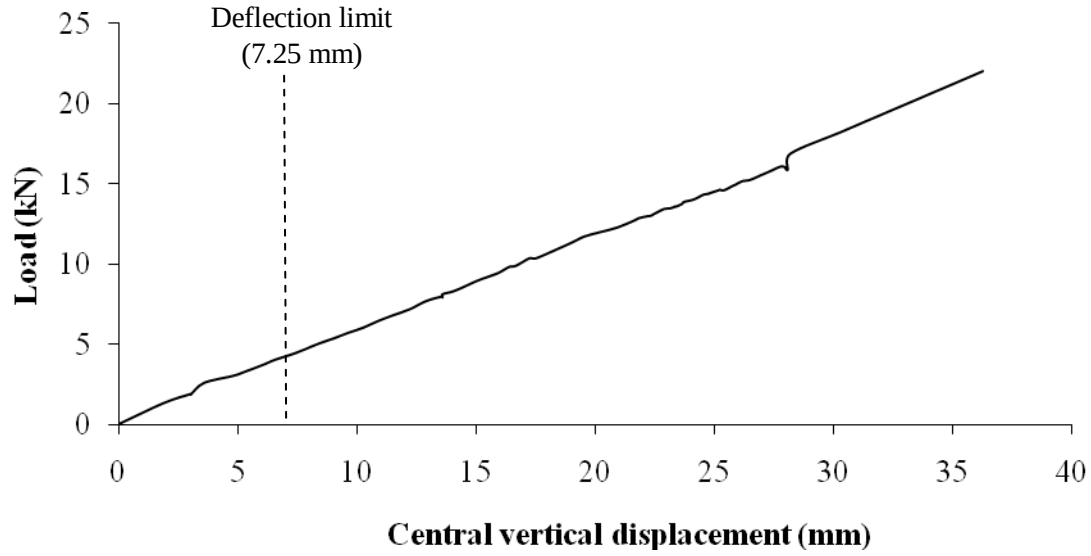

(a) SMC

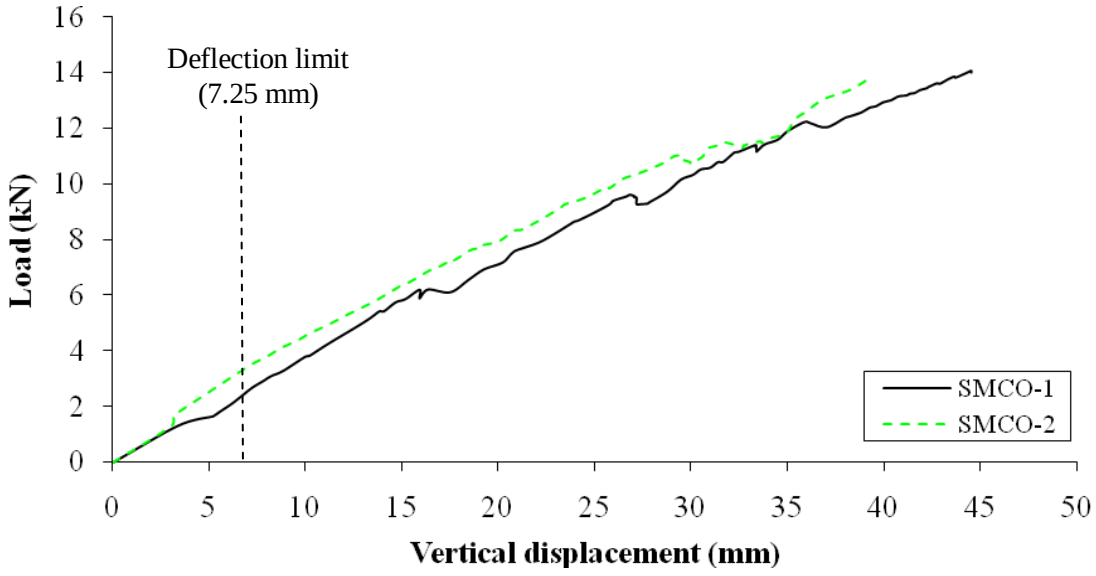

(b) SMCO

Figure 5.12: Load versus vertical displacement (LVDT No.1)

(a) SMC

(b) SMCO-1

(b) SMCO-2

Figure 5.13: Failure modes

Figure 5.14 plots the applied loads against the vertical displacements at 10 mm from the edge of the panel.

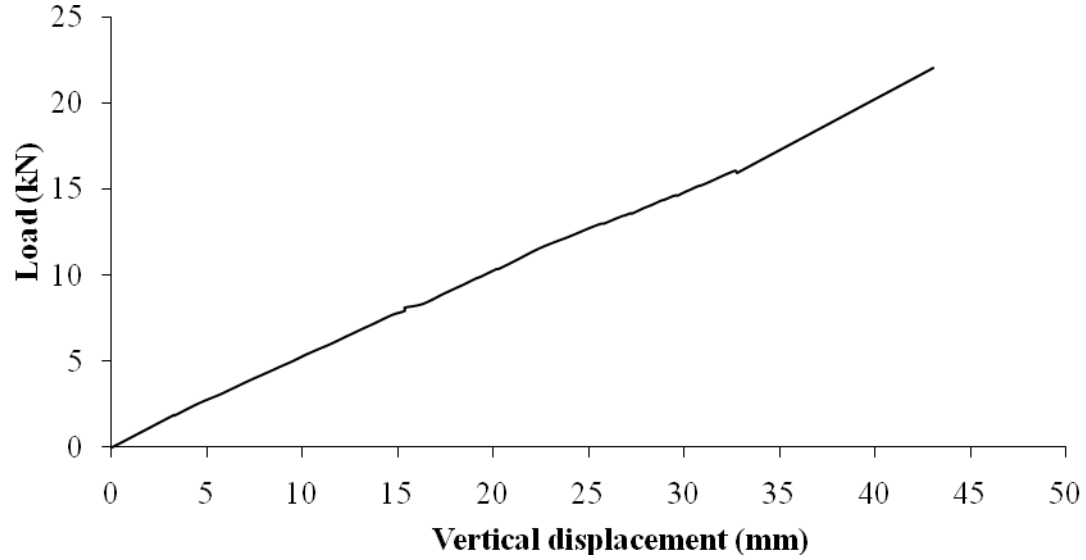

(a) SMC

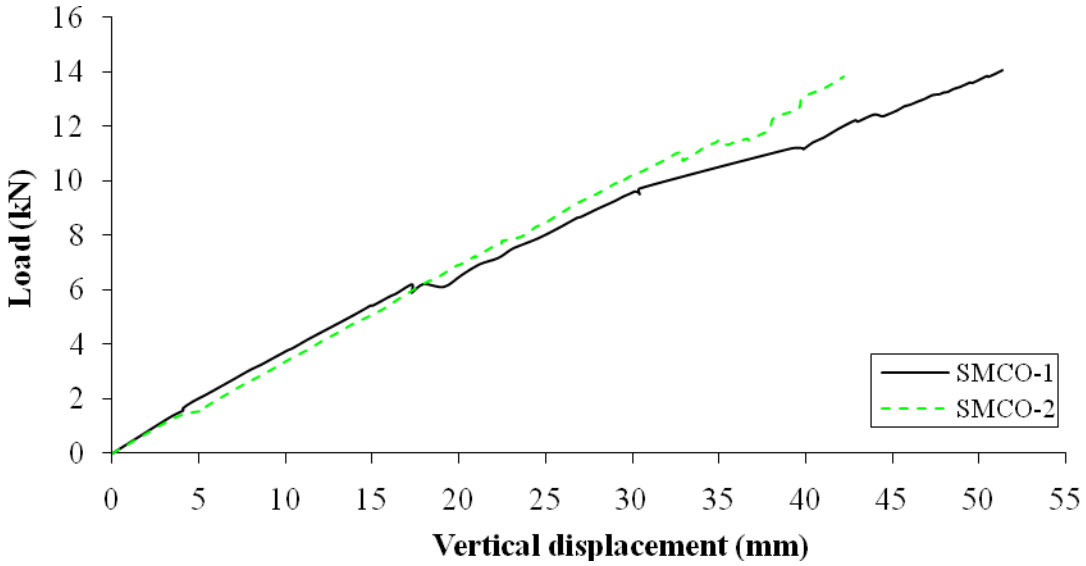

(b) SMCO

Figure 5.14: Load versus vertical displacement (LVDT No.2)

The racking movements at the top of the panels (LVDT No.3) are small (within 2 mm) as illustrated in Figure 5.15.

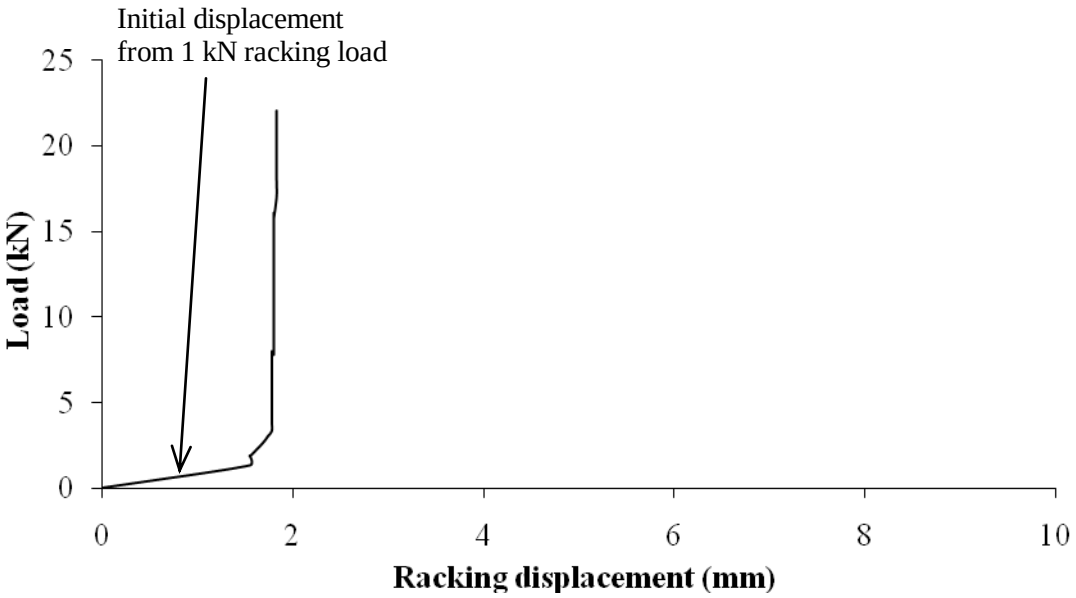

(a) SMC

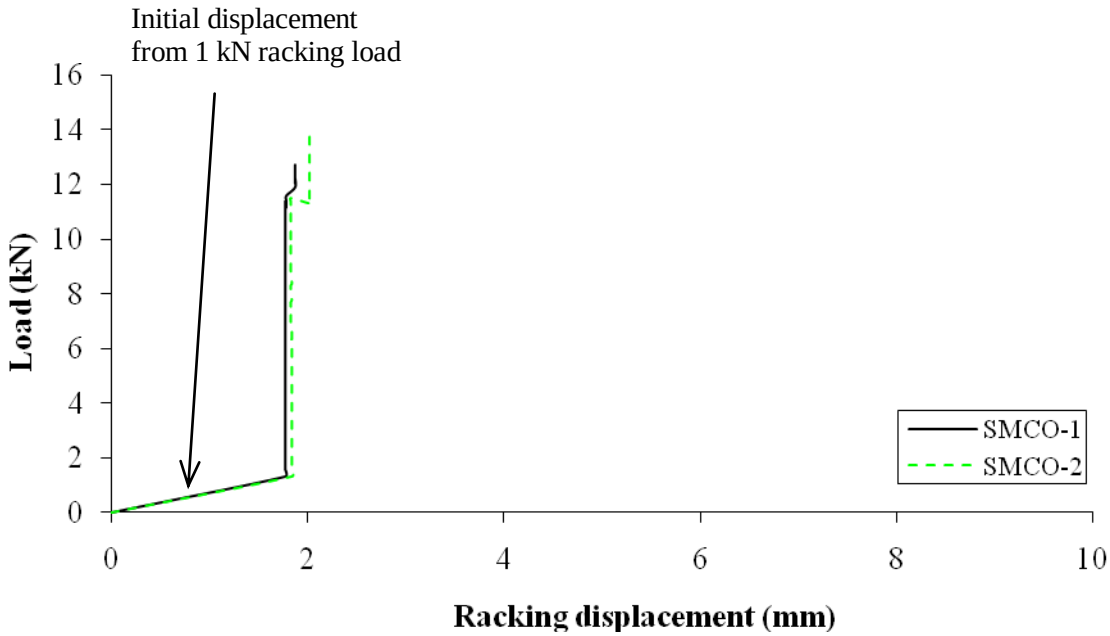

Figure 5.15: Load versus racking displacement (LVDT No. 3)

Table 5.10 summarises the test results of the panels with openings when subjected to the combined racking and transverse loadings. The SMC ultimate load is 22.05 kN, this is slightly (0.5%) less than the mean panels when subjected to transverse loading only (22.16 kN). Whilst, the SMCO ultimate load is 13.91 kN, which is 1.9% lower than the transverse loading only

(14.18 kN). Accordingly, it can be concluded that the 1 kN racking is negligible contributed impact on the structural performance of the panels.

Specimen	SMC	SMCO
Ultimate Limit Load, ULL (kN)	22.05	13.91
Load at deflection limit ℓ/333 (kN)	4.36	3.11
Serviceability load / Ultimate load (%)	19.8	22.4
Maximum central displacement (mm)	36.24	41.90
Maximum edge displacement (mm)	43.02	46.75
Maximum racking displacement (mm)	1.83	1.95
Experimental failure mode	Debonding	Flexure-Shear

Table 5.10: Experimental finding summary

5.4 Load case No. 6 - Combined axial and racking loadings

Previous studies by Kermani and Haristans and (2006) and Bregulla (2003) have revealed an increase in the applied vertical load results in a higher racking resistance. This is due to the vertical load is restraining the panel causing the reduction of the uplift in front of the panel. In this test, the structural performance of SIPs when subjected to uniformly axial compression (8 kN/m) and racking loadings was examined. This axial compression is a normal intended load that the panel requires to sustain in its service life as previously mentioned. The support conditions are as same as the racking test only (section 4.6). Figure 5.16 shows the experimental apparatus layout for combined axial and racking loading test.

Figure 5.16: Experimental apparatus layout for combined axial and racking loading test

One SMC and two SMCO were subjected to combined axial and racking loadings until failure. The test setup was similar to the racking test which previously described in the section 4.6. A 1.2 m steel parallel flange channel section was used to apply a uniformly axial compression. The axial load (8 kN/m) was applied along the header by using a hydraulic hand pump through the load-cell and the steel channel. The racking load was then applied until failure. Three LVDTs were used and positioned as same as in the racking test (section 4.6) to measure the displacements.

5.4.1 Experimental investigation

Figure 5.17 shows the applied load against the racking displacement (LVDT No.1) of the panel with mini-SIP connection (SMC) and with opening (SMCO).

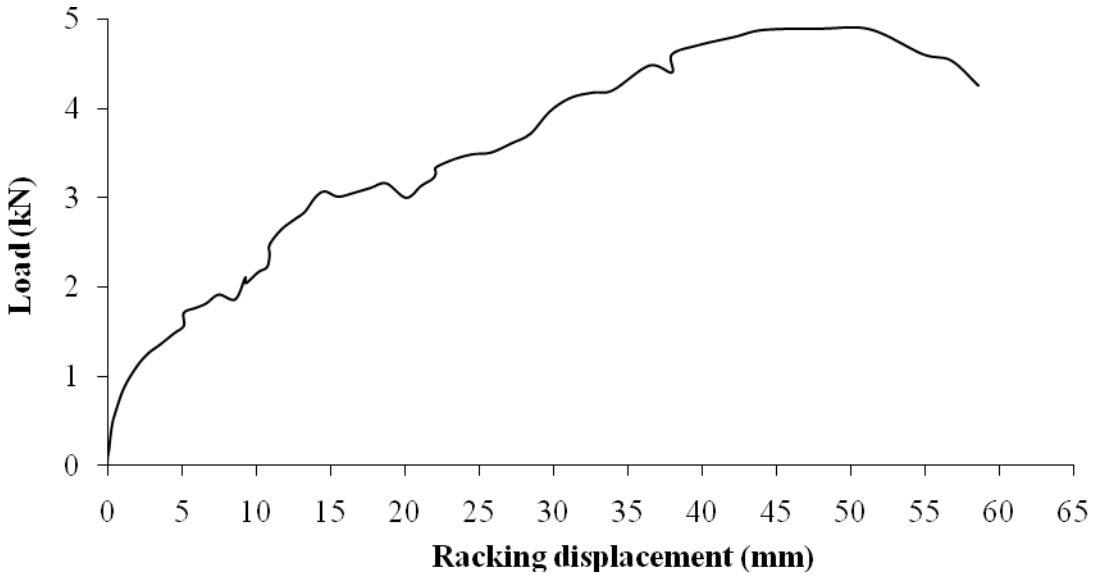

(a) SMC

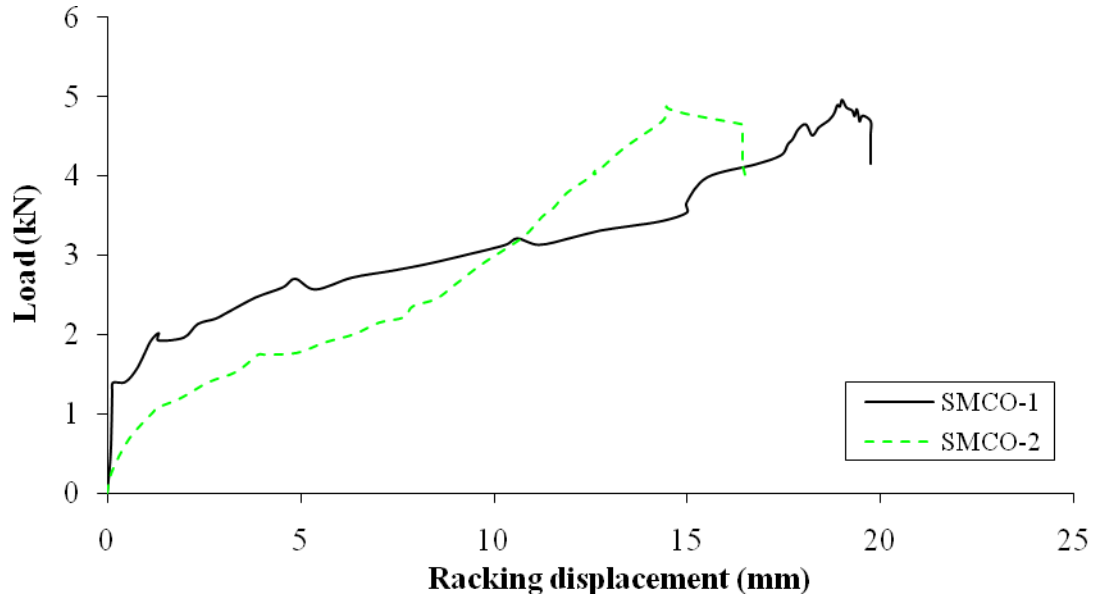

(b) SMCO

Figure 5.17: Load versus racking displacement

The ultimate loads at failure are 4.90 kN and 4.92 kN for SMC and SMCO, respectively. These ultimate loads are 17% higher than the panels without axial loadings (4.20 kN). This is due to the vertical load is restraining the panel causing the reduction of the uplift in front of the panel.

The failure mode for both specimen types are as same as all previous findings which is the OSB faces were disjointed from the footers as shown in Figure 5.18.

(a) SMC

(b) SMCO-1

(c) SMCO-2

Figure 5.18: Disjointed failure

Figure 5.19 plots the applied load against the horizontal displacement at the footer of the panel (LVDT No.2). In comparison to the racking movement at the top of the panel, the movement at the bottom is minimal (1.17 mm maximum at failure).

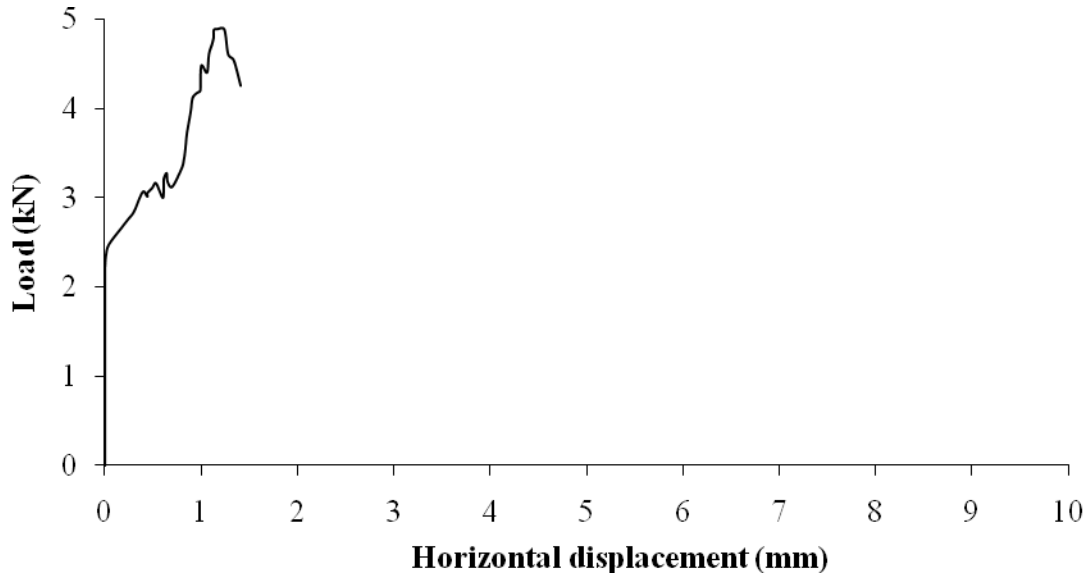

(a) SMC

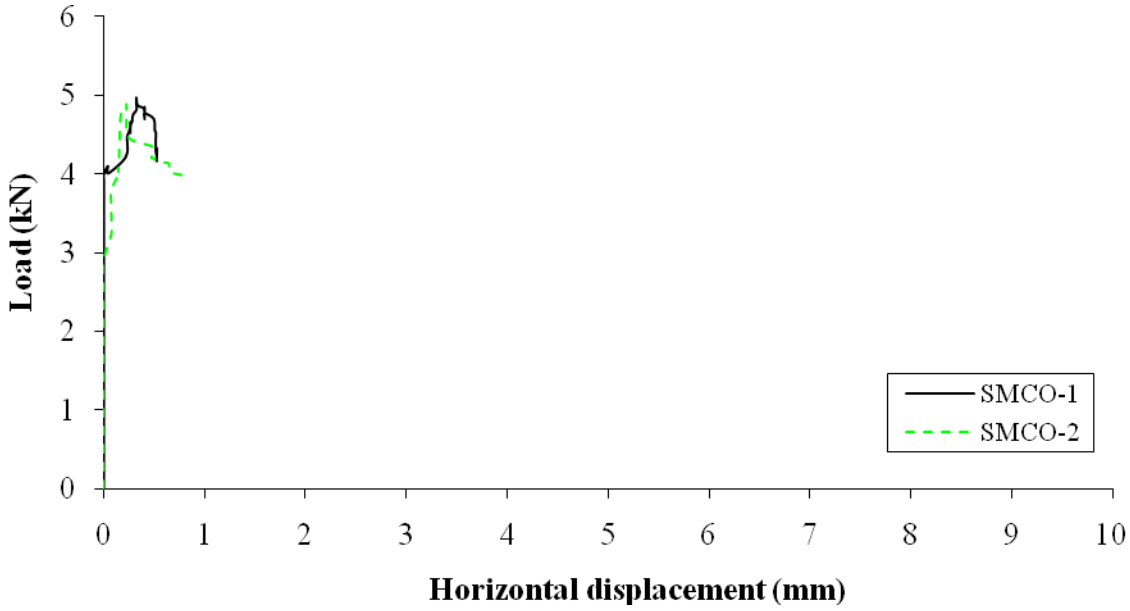

(b) SMCO

Figure 5.19: Load versus horizontal displacement (LVDT No.2)

The vertical displacement of the panel (LVDT No.3) is illustrated in Figure 5.20. The displacement at failure is negligible in comparison to the horizontal displacement at failure at

the top of the panel. Experimental results for both types of panels are tabulated in Tables 5.11 and 5.12.

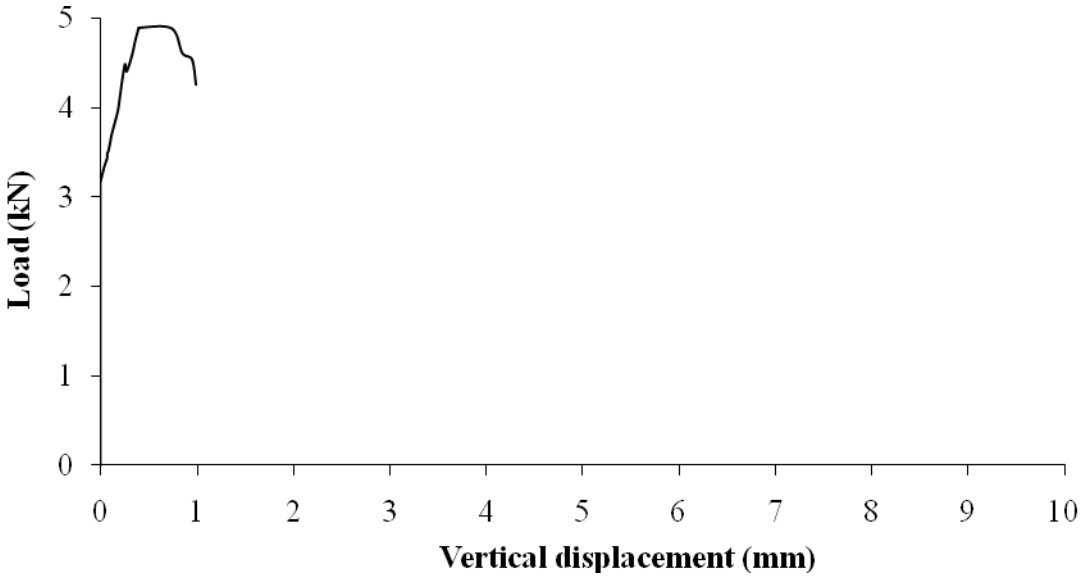

(a) SMC

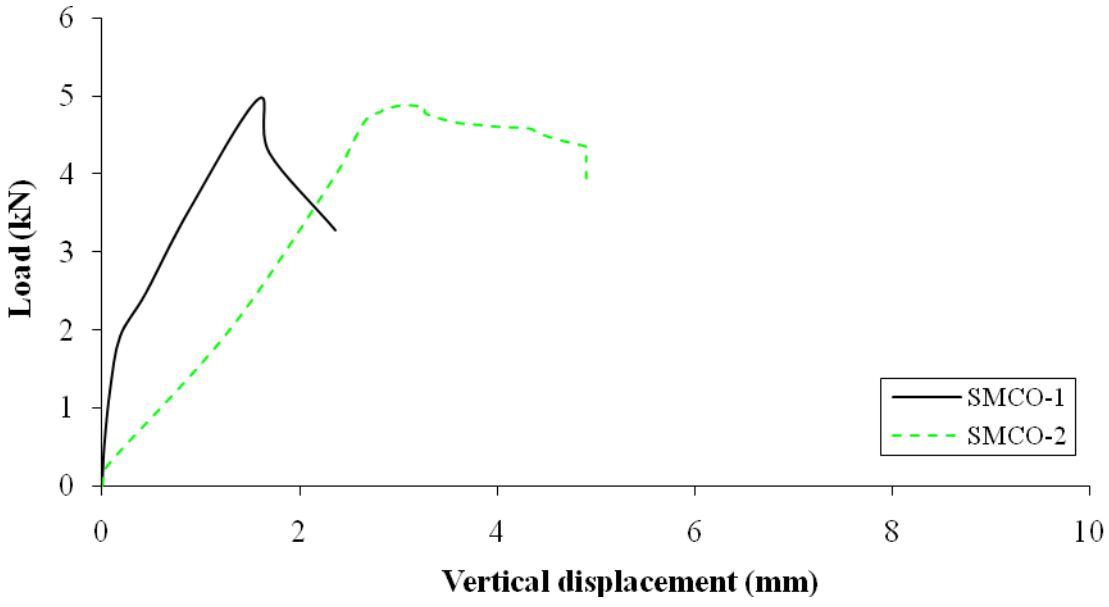

(b) SMCO

Figure 5.20: Load versus vertical displacement (LVDT No. 3)

Specimen	SMC
Width (mm)	1,195
Length (mm)	2,445
Depth (mm)	125
Ultimate load (kN)	4.90
Racking displacement at failure (mm)	47.97
Horizontal displacement at failure (mm)	1.17
Vertical displacement at failure (mm)	0.39
Failure mode	Disjointing

Table 5.11: SMC result summary

Specimen	SMCO-1	SMCO-2	Mean
Width (mm)	1,196	1,194	**1,195**
Length (mm)	2,440	2,441	**2,440**
Depth (mm)	125	125	**125**
Ultimate load (kN)	4.97	4.88	**4.92**
Racking displacement at failure (mm)	18.98	14.45	**16.72**
Horizontal displacement at failure (mm)	0.32	0.23	**0.28**
Vertical displacement at failure (mm)	1.58	3.06	**2.32**
Failure mode	Disjointing	Disjointing	

Table 5.12: SMCO result summary

5.4.2 Racking analytical investigation

The performance of SIP specimen is again compared to the stud wall designed to EC5 (BSI, 2004). The characteristic test racking resistance in accordance with BS 5268 Cl. 6.1 (BSI, 1996) is determined and summarised in Table 5.13. As shown in Table 5.13, a good agreement between SIP specimen with opening (SMCO) and EC5 design has been found, whereas the stud wall designed to EC5 for SMC is 34% higher than the SIP test result. The EC5 design seems to provide an unconservative racking load capacity with the uniformly axial compression, the k_q load factor has been increased by 81% from 8 kN/m axial compression in this study.

Nevertheless, both methods show the applying of the uniformly axial load can increase the racking resistance of the panel.

Specimen	Mean load at failure, F_{max} (kN)	Test racking strength load, F_{ult} (kN)	Characteristic test racking resistance (kN/m)	Stud wall designed to EC5 (kN/m)
SIPs with mini-SIP connections (SMC)	4.90	4.26	1.75	2.34
SIPs with mini-SIP connections and opening (SMCO)	4.92	4.28	1.75	1.77

Table 5.13: Comparison between the test result and EC5 method

5.5 Load cases No. 7 & 8 - Combined axial, racking and transverse loadings

In reality, it is envisaged that SIPs are required to sustain combined axial, racking and transverse loadings at the same time. The structural performances of SIPs when subjected to combined axial, racking and transverse loadings were examined in this section.

Due to the fact that most test results obtained so far were consistency, it was purposed to carry out test on one specimen from Groups No. 2 and 5 only. Two SIP specimens, one SMC (SMC-8A-1R-T) and one SMCO (SMCO-8A-1R-T), were subjected to combined 8 kN axial, 1 kN racking and transverse loadings until failure. The applied loads in both axial and racking loads were later doubled and the test results were examined. One SMC (SMC-16A-2R-T) and one SMCO (SMCO-16A-2R-T) were subjected to combined 16 kN axial, 2 kN racking and transverse loadings until failure.

The test setup for all combination test employed all apparatuses which were previously detailed in the preceding sections. The axial load (8 kN/m or 16 kN/m) was first applied, following by the racking load of 1 or 2 kN. The transverse load was then applied until failure. Figure 5.21

shows the experimental apparatus layout for combined axial, racking and transverse loading test. The LVDT arrangement is shown in Figure 5.22.

- LVDT No.1 was positioned at the central of the panel for measuring the vertical displacement.

- LVDT No.2 was positioned at the mid-length and at approximately 10 mm from the edge of the panel for measuring the vertical displacement.

- LVDT No.3 was positioned at the header of the panel for measuring the horizontal displacement.

- LVDT No.4 was positioned at the aluminium bracket, which attached at the header of the panel for measuring the axial displacement.

For the test panels with openings, the LVDT No.1 was also repositioned to be at the mid-length and approximately at 10 mm from the edge of the opening as previously mentioned.

Figure 5.21: Experimental apparatus layout for combined axial, racking and transverse loading test

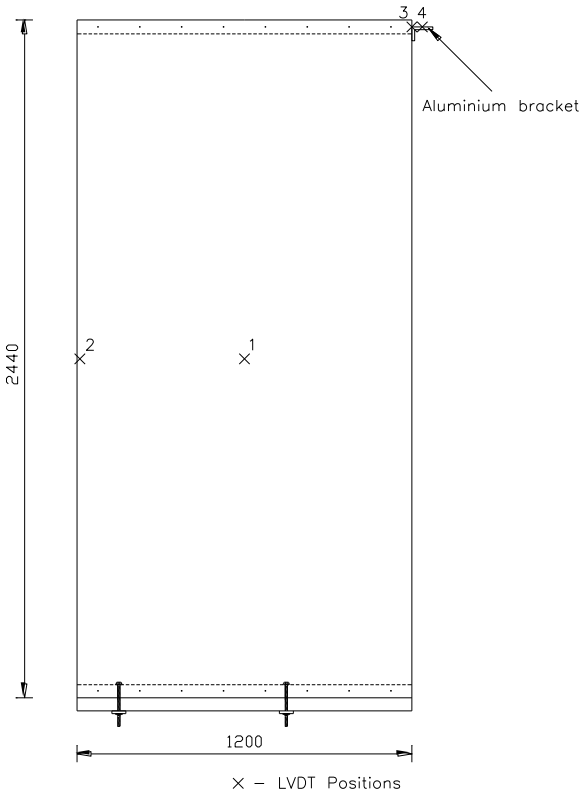

Figure 5.22: LVDT arrangement

5.5.1 Experimental investigation

Two SMC and two SMCO panels were subjected to combined axial, racking and transverse loadings. Figures 5.23 to 5.26 show the loads against displacements at various locations of SIPs with mini-SIP connections and with openings.

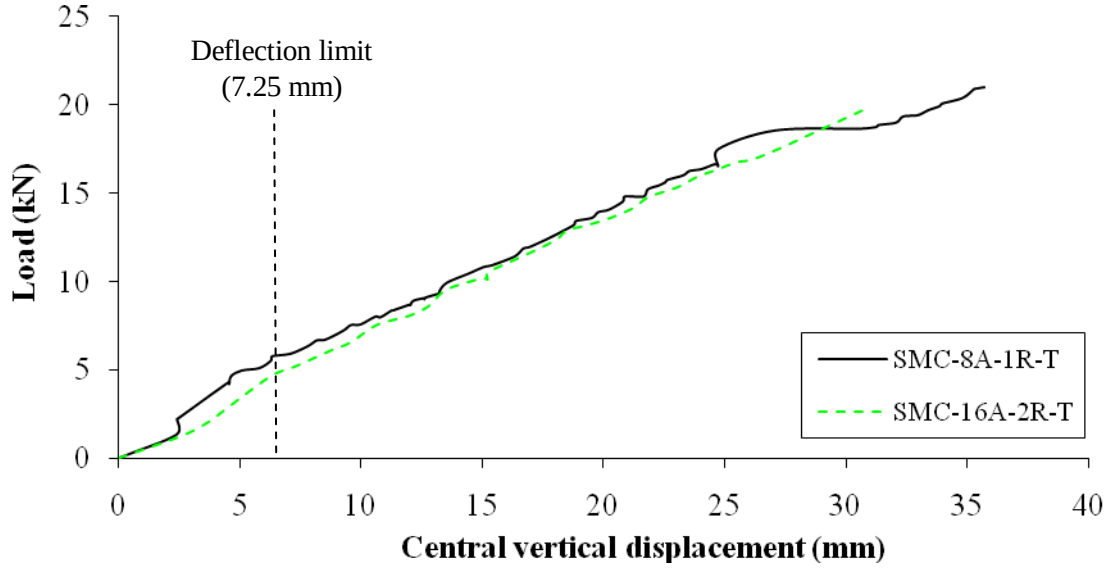

(a) SMC

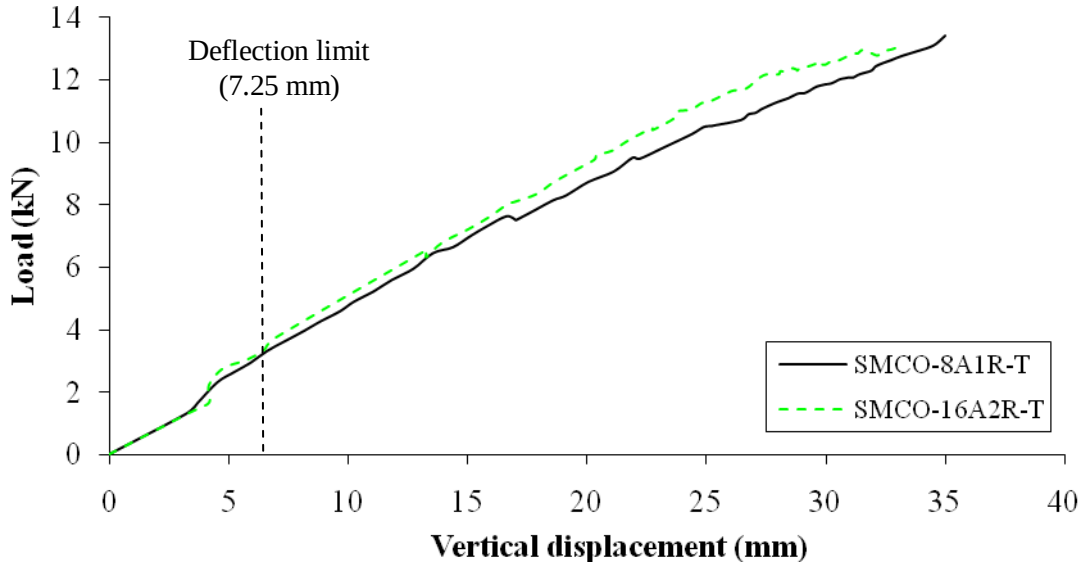

(b) SMCO

Figure 5.23: Load versus central vertical displacement (LVDT No.1)

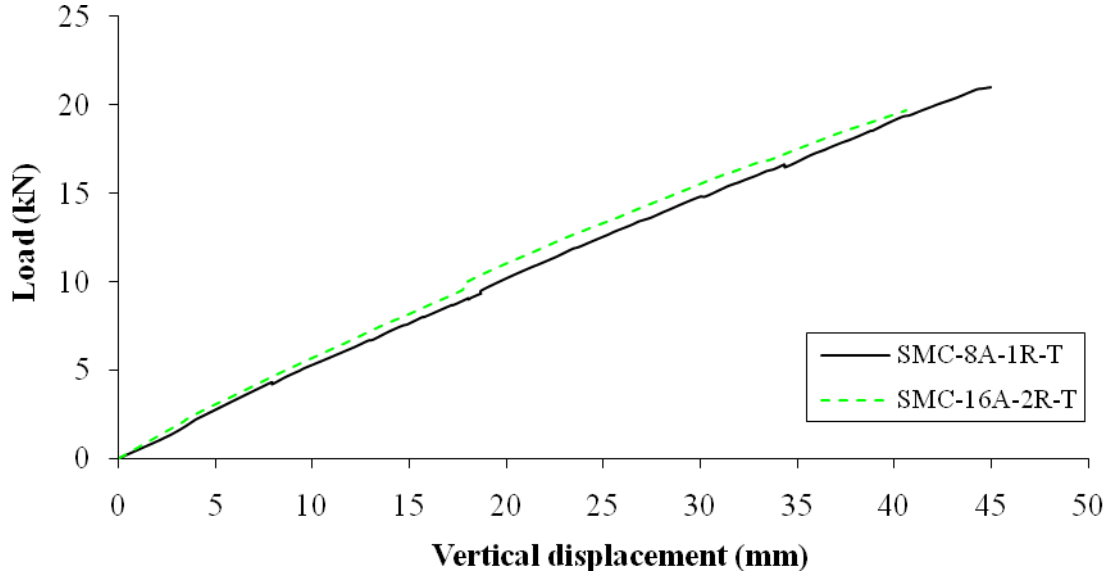

(a) SMC

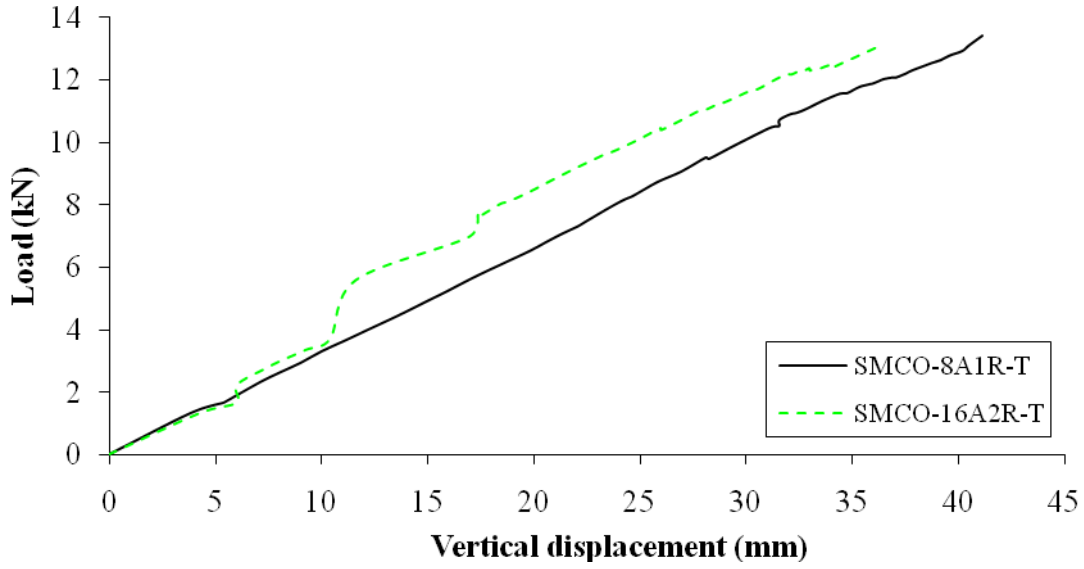

(b) SMCO

Figure 5.24: Load versus vertical displacement (LVDT No.2)

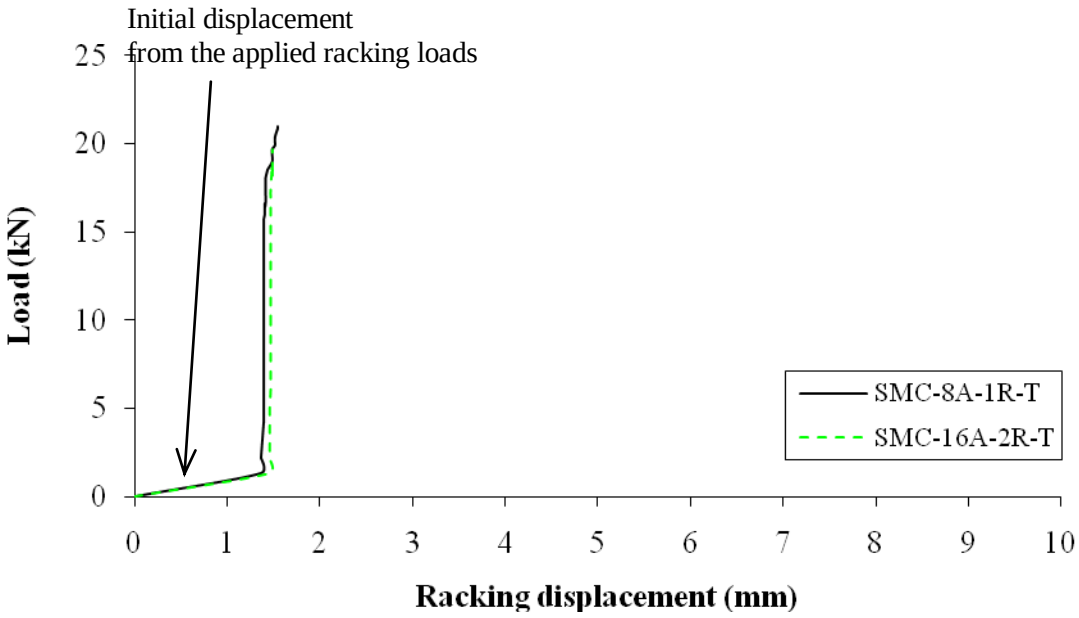

(a) SMC

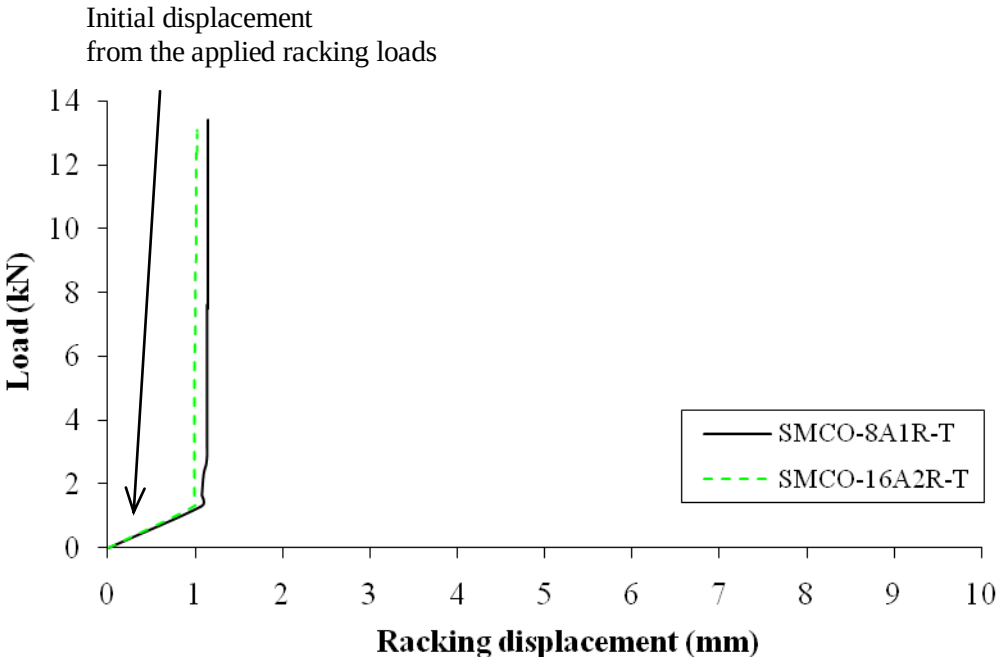

(b) SMCO

Figure 5.25: Load versus racking displacement (LVDT No.3)

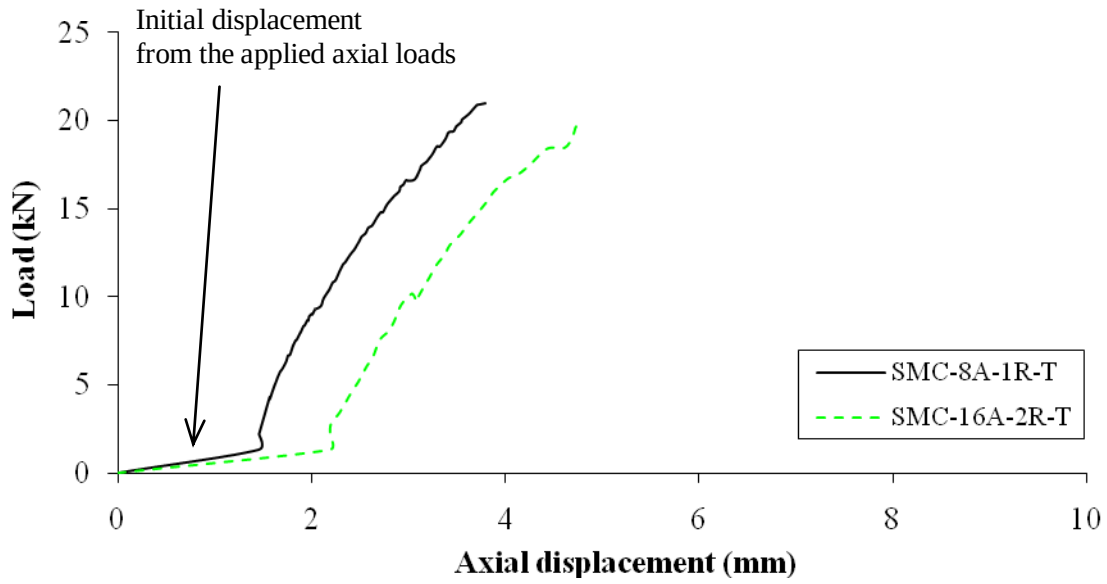

(a) SMC

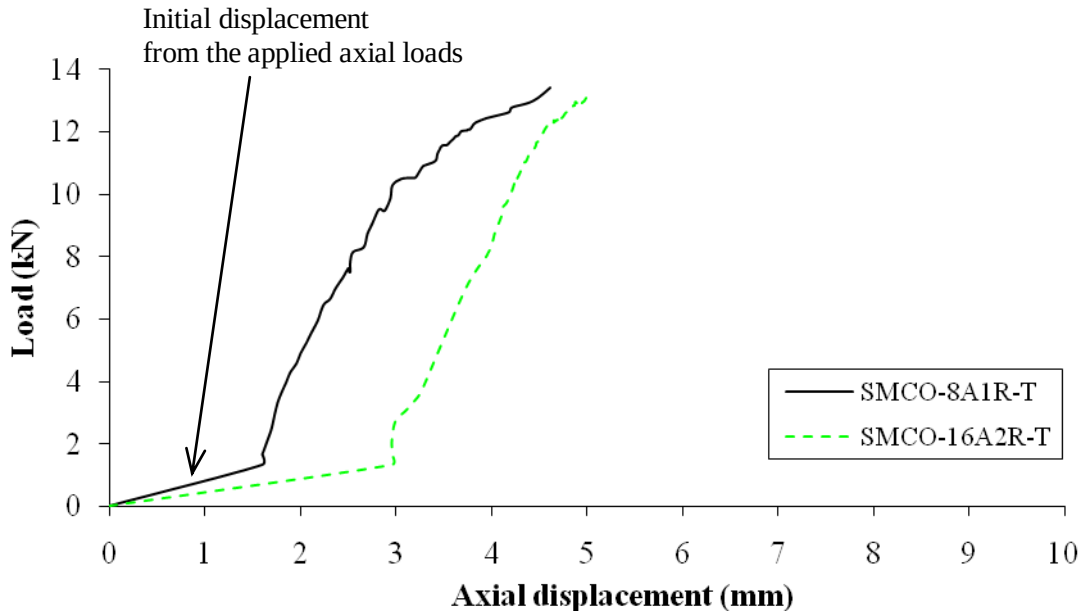

(b) SMCO

Figure 5.26: Load versus axial axis displacement (LVDT No.4)

The failure modes were found to be the same as the individual transverse only i.e. debonding (for SMC) and flexure-shear (for SMCO) as shown in Figure 5.27. Tables 5.14 and 5.15 summarise the experimental results, the reduction of the ultimate load when subjected to combined axial, racking and transverse loadings have been found.

(a) SMC-8A-1R-T

(b) SMC-16A-2R-T

(a) SMCO-8A-1R-T

(b) SMCO-16A-2R-T

Figure 5.27: Failure modes

Specimen	SMC-8A-1R-T	SMC-16A-2R-T
Width (mm)	1,193	1,193
Length (mm)	2,442	2,442
Depth (mm)	125	125
Ultimate load (kN)	20.99	19.70
Reduction of the ultimate load (%) in comparison to the applied transverse load only (22.16 kN)	5.3%	11.1%
Load at deflection limit ℓ/333 (kN)	6.01	5.17
Serviceability load / Ultimate load (%)	28.6	26.2
Maximum central displacement (mm)	35.70	30.70
Maximum edge displacement (mm)	44.95	40.58
Maximum racking displacement (mm)	1.54	1.49
Maximum axial displacement (mm)	3.80	4.73
Failure mode	Debonding	Debonding

Table 5.14: SMC result summary

Specimen	SMCO-8A-1R-T	SMCO-16A-2R-T
Width (mm)	1,195	1,196
Length (mm)	2,444	2,444
Depth (mm)	125	125
Ultimate load (kN)	13.41	13.10
Reduction of the ultimate load (%) in comparison to the applied transverse load only (14.18 kN)	5.4	7.6
Load at deflection limit ℓ/333 (kN)	3.58	3.87
Serviceability load / Ultimate load (%)	26.7	29.5
Maximum central displacement (mm)	34.98	33.14
Maximum edge displacement (mm)	41.14	36.26
Maximum racking displacement (mm)	1.15	1.02
Maximum axial displacement (mm)	4.61	4.99
Failure mode	Flexure-Shear	Flexure-Shear

Table 5.15: SMCO result summary

The experimental result comparison of SMCs and SMCOs with different load cases is tabulated in Tables 5.16 and 5.17. The experimental results are summarised as follows:

- The experimental findings reveal the decrease of panel transverse loading capacity when subjected to the axial load.

- The 1 kN racking is negligible contributed impact on the structural performance of the panels when subjected to combined racking and transverse loadings.

- The failure modes of the panel specimens when subjected to transverse loading are due to debonding (for the test panels without openings) and flexure-shear (for the test panels with openings).

- The ranging (high to low) of the panel stiffness found from the physical experiments is SDC, SMC and STP, respectively.

- The serviceability load becomes the limiting factor of the loading capacity.

Specimen	SMC-T	SMC-1R-T	SMC-8A-T	SMC-8A-1R-T	SMC-16A-2R-T
Ultimate Limit Load, ULL (kN)	22.16	22.05	21.78	20.99	19.70
Index	1.000	0.995	0.983	0.947	0.889
Load at deflection limit ℓ/333 (kN)	4.03	4.36	5.05	6.01	5.17
Serviceability load / Ultimate load (%)	18.2	19.8	23.2	28.6	26.2
Maximum central displacement (mm)	38.05	36.24	34.76	35.70	30.70
Experimental failure mode	Debonding				

Table 5.16: SMC result summary

Specimen	SMCO-T	SMCO-1R-T	SMCO-8A-T	SMCO-8A-1R-T	SMCO-16A-2R-T
Ultimate Limit Load, ULL (kN)	14.18	13.91	13.25	13.41	13.10
Index	1.000	0.981	0.934	0.946	0.924
Load at deflection limit ℓ/333 (kN)	4.03	3.11	4.18	3.58	3.87
Serviceability load / Ultimate load (%)	28.4	22.4	31.6	26.7	29.5
Maximum central displacement (mm)	30.19	41.90	32.36	34.98	33.14
Experimental failure mode	Flexure-Shear				

Table 5.17: SMCO result summary

5.5.2 Numerical investigation on SIPs with combined axial and transverse loadings

Further numerical investigations have been carried out on SIPs with combined axial and transverse loadings. As previously mentioned in section 4.6, the FEM investigation has not included the racking load in this current research since another bonding criterion between the OSB faces and the C16 header/footer through nail is required. Figure 5.28 shows the FEM

results (up to the initial failure load) on SIPs with different joint designs when subjected to the combined axial and transverse loadings.

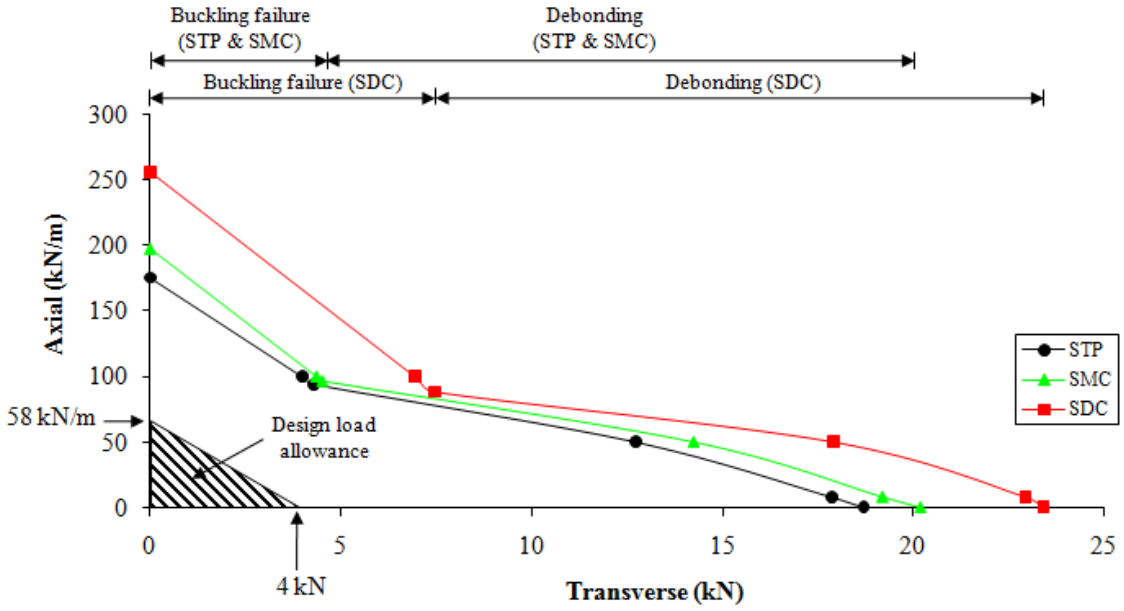

Figure 5.28: Combined axial-transverse capacity of SIPs with different joints

As shown in Figure 5.28, the SDC panel reveals again the highest structural capacity in comparison to STP and SMC. With a relatively high axial load (e.g. greater than 88 kN/m for SDC), the panel tends to fail due to buckling. This failure mode will be shifted to debonding failure when transverse load is increased to a certain level (e.g. 4.3 kN for STP). It is noted that under the pure axial load, the specimen will fail due to buckling.

AC04 (ICC-ES, 2008) provides guidelines for evaluation of sandwich panels. This document suggests the method to determine the allowable load by applying a minimum factor of safety of three to the average ultimate load obtained from the experiment. According to AC04, the design axial load allowance for SIPs is 58 kN/m, whereas the serviceability deflection limit for transverse load is 4 kN. The design load allowance is shown as a triangular area in Figure 5.28. The most interesting finding is that SIPs have a high degree of capacity reserve.

Similarly, Figure 5.29 shows the FEM results (up to the initial failure load) on SIPs with different joint designs and openings when subjected to the combined axial and transverse loadings. The axial-transverse load capacity of SIPs with openings is almost a linear relationship as illustrated in Figure 5.29. As previously presented and concluded, under this SIP detail configurations with the opening, the structural behaviour under the different joint designs is not influenced. The design load allowance is shown as a triangular area in Figure 5.29. Another important finding is that SIPs with openings have a high degree of capacity reserve.

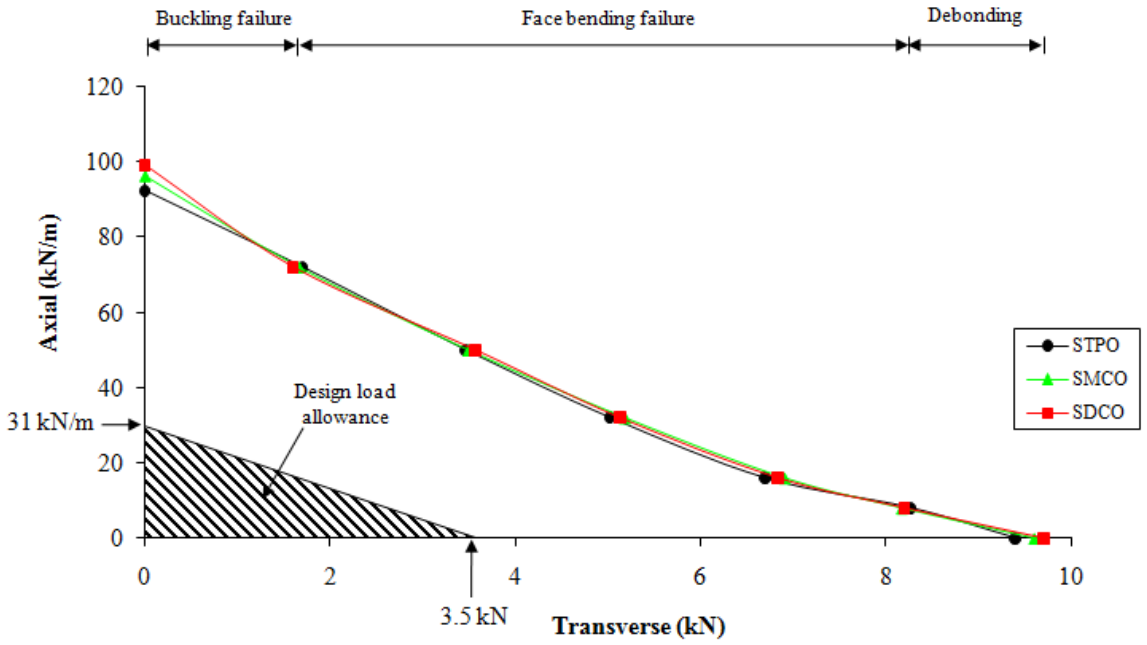

Figure 5.29: Combined axial-transverse capacity of SIPs with openings

5.6 Summary

Structural performance of SIPs subjected to combined loadings were carried out. The findings can be summarised as follows.

- The axial compression load does contribute to the increase of the racking load. This is because the vertical load is restraining the panel causing the reduction of the uplift in front of the panel.

- An interactive failure load curve between axial and transverse loadings has been developed by carrying out a parametric analysis. A linear interaction model appears to be a good representation of such a failure load curve for SIPs with openings. The most interesting finding is that SIPs have a high degree of capacity reserve since the design load allowance is well below the onset of failure load.

CHAPTER SIX

SIPS UNDER LONG-TERM LOADINGS

6.1 Introduction

This chapter presents experimental investigations of SIP constituents (OSB and PUR) and SIPs as beams and panels under long-term loads. Numerical investigations to determine the power-law creep parameters of OSB and PUR are detailed and later employed in the prediction of SIP creep behaviour. The investigations to determine appropriate creep models for predicting the creep behaviours without employing numerical investigation are also presented. Since the numerical investigations provide a good agreement with the creep test results, the numerical models are later studied on SIPs with different joint designs subjected to the applied load for 60 years.

6.2 Experimental study of OSB subjected to long-term loading

Oriented Strand Board (OSB), an engineered panel, has experienced creep at ambient temperature and moisture content. OSB creep behaviour depends on, for instance, stress level, relative humidity, temperature and resin content. Pu et al. (1994) investigated and found that the relative humidity influences the OSB creep behaviour, in which the higher relative humidity, the higher relative creep deformation. This section presents the experimental investigation of the OSB creep behaviour with 10%, 20% and 30% of the ultimate load stress level. The power-law creep parameters will be determined and used to predict the creep behaviour of SIPs in the subsequent sections.

6.2.1 Experimental investigation of long-term performance of OSB

Three OSB specimens (OSB-LT-1, 2 and 3) were approximately 200 mm wide, 800 mm long and 11 mm thick and were cut from a standard 1200 x 2400 mm size. They were subjected to the sustained three-point bending loads for three months under ambient temperature and moisture content in order to investigate their creep behaviours at different levels of applied loads. By initial calculation, it was expected that this size of the OSB specimen would fail due to three-point bending at 0.45 kN by using 20 N/mm^2 as bending failure stress in accordance with BS EN 300 (BSI, 2006). The applied loads at 10%, 20% and 30% of the ultimate load levels were applied to each specimen by steel weights sitting on a 100 mm wide and 200 mm long steel plate at the mid-span. Each OSB specimen was then supported on two movable steel rollers in which one side was welded to the steel plate and another side was free to move horizontally (simply supported condition). The mid-span displacements were recorded by dial gauges (with accuracy of 0.01 mm) at the following times after loading: 0.1, 0.2, 0.5, 1, 2, 5 hours and then every 24 hour in the first week and then every 72 hour interval throughout the test duration. In addition to the recorded displacements, the temperature and humidity level were also recorded. The temperature and humidity were in the range of 23°C ± 3°C and 40 ± 10%, respectively. Figure 6.1 illustrates the long-term three-point bending test apparatus.

Figure 6.1: Long-term OSB experimental apparatus

Figure 6.2 shows the creep deflections of all OSB specimens. The fluctuation in the creep curves may be due to the variations of the temperature and the humidity. However, the effects of temperature and humidity are expected to be negligible impact on the creep behaviours since their variations in the laboratory were small in comparison to the temperature and humidity conditions outside the laboratory which SIPs required to be encountered.

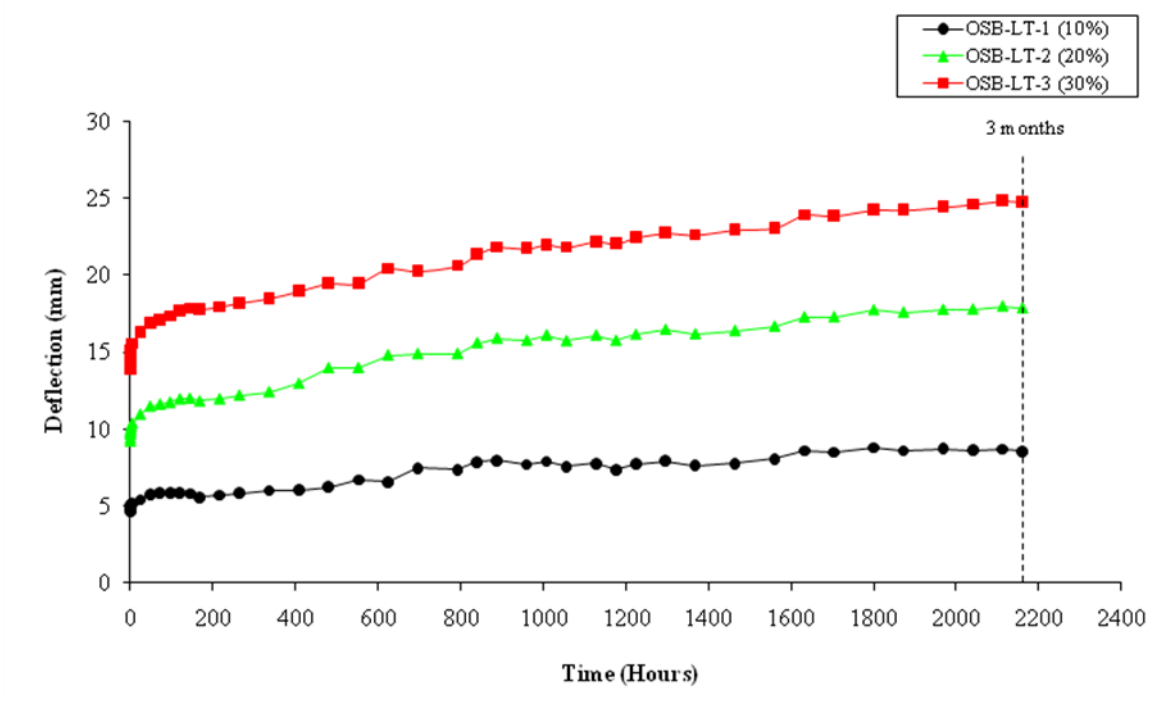

Figure 6.2: Three month creep test results

Table 6.1 summarises the instantaneous and three month deflections of tested specimens loaded at 10%, 20% and 30% of the estimated ultimate load levels, respectively. The relative deflection which is defined as the ratio of long-term to instantaneous deflections is also presented. As expected, the higher the applied stress level, the higher the relative deflection.

Specimen	**Instantaneous deflection**	**Three month deflection**	**Relative deflection[1]**
	(mm)	**(mm)**	
OSB-LT-1 (10%)	4.66	8.56	1.84
OSB-LT-2 (20%)	9.21	17.86	1.94
OSB-LT-3 (30%)	13.90	27.88	2.01

Note 1: Relative deflection equals to the three month deflection divided by the initial deflection

Table 6.1: The applied loads and the instantaneous deflection of each OSB specimen

6.2.2 Numerical investigation of long-term performance of OSBs

The numerical investigation was analysed using the ABAQUS v.6.9-1 finite element programme. The OSB specimen was modelled as a two-dimensional model. A steel support plate was modelled and connected to the OSB bottom face by the contact interaction with the coefficient of friction equal to 0.2.

As the geometry of the specimen is symmetric in the longitudinal direction, only half of the whole specimen was modelled. Thus the symmetric boundary condition about the mid-span section (XSYMM) was applied in the vertical face at the mid-length. This modelling technique can further save the computational efforts. A restraint in the vertical direction ($U_y = 0$) was applied at the centre of the bottom face of the steel support plate. Figure 6.3 depicts the finite element mesh for the OSB model.

The structured meshing technique for this model is an eight-node biquadratic plane strain element with reduced integration (CPE8R). This technique can give the best results together with minimise the computational efforts. OSB faces were then divided into two divisions with a 10 mm element size.

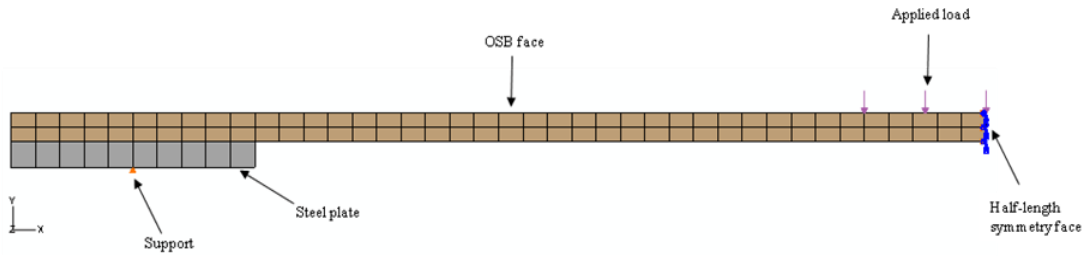

Figure 6.3: OSB finite element model

ABAQUS provides a power-law creep model via the *PLASTIC-CREEP option (ABAQUS, 2010) to deal with creep behaviour. This creep model was employed in this study and three parameters were required, including power law multiplier (A), equivalent deviatoric stress order (n) and time order (m). A curve fitting analysis to the OSB creep tests was used to determine these parameters.

BS EN 14509 (BSI, 2006) recommends undertaking a creep test on a sandwich specimen for up to 1,000 hours in order to obtain the creep parameters as mentioned in section 2.5. The 1,000 hour creep parameters can be adequately used to predict the creep deflections in the longer term. Following this suggestion, the three month creep predictions obtained from the 1,000 hour creep parameters will be compared with the three month creep test results for verification purpose in this study.

Table 6.2 shows the 1,000 hour ABAQUS power-law creep parameters for each applied load which has been found from the curve fitting analysis of the test results. Power law multiplier

(A) value has been found to be the only factor dependant on the load level, whereas the values of equivalent stress order (n) and time order (m) are constant at 2 and -0.5 for all applied loads.

Specimen	Power Law Multiplier (A)	Equivalent Stress Order (n)	Time Order (m)
OSB-LT-1 (10%)	4.90×10^{-6}	2	-0.5
OSB-LT-2 (20%)	2.60×10^{-6}		
OSB-LT-3 (30%)	1.45×10^{-6}		

Table 6.2: 1,000 hour ABAQUS power-law creep parameters

Figure 6.4 shows the comparison of the creep deflection up to 1000 hours from both tests and numerical models by using the parameters listed in Table 6.2. A close agreement between these two sets of data has been revealed.

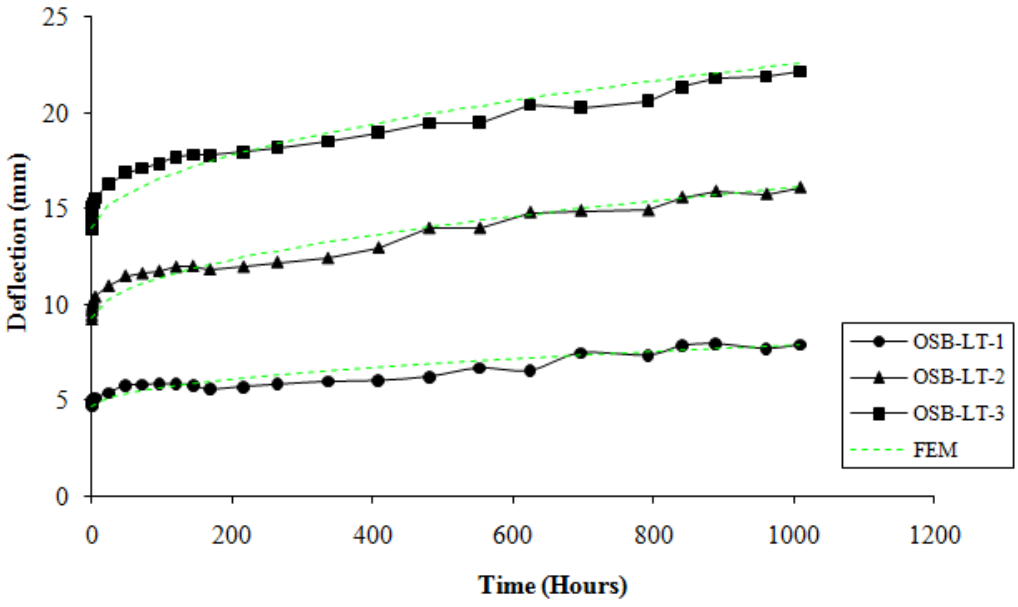

Figure 6.4: 1,000 hour experimental and FEM predicted creep deflections of OSBs

By using the 1,000 hour creep parameters, the modelling was extended to a three month length of time. Figure 6.5 show the comparison between the three month creep test results and the FEM predictions.

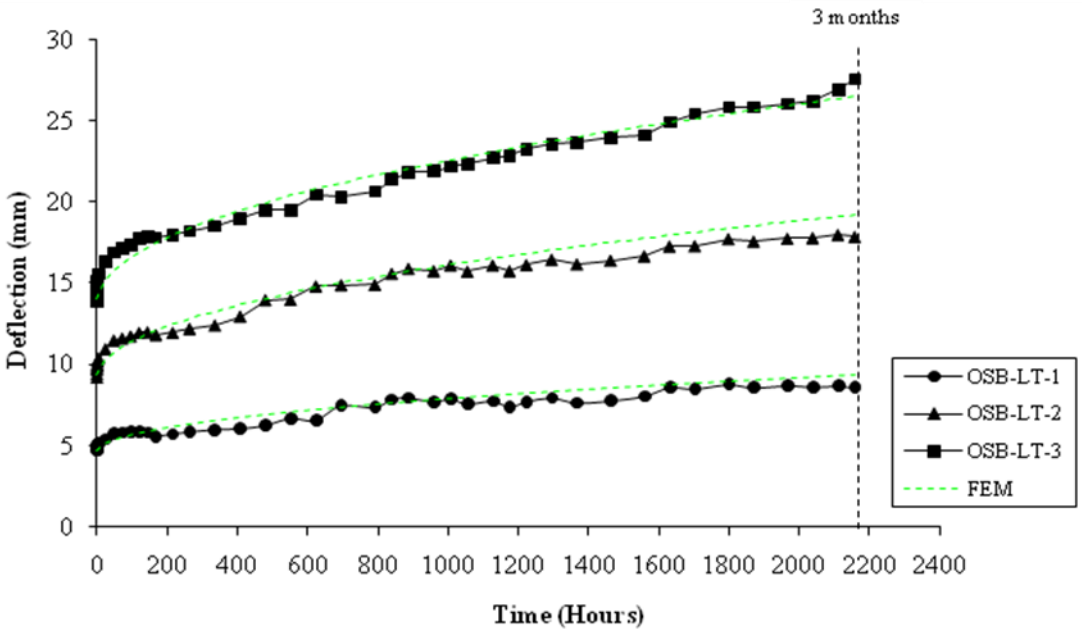

Figure 6.5: Three month experimental and FEM predicted creep deflections of OSBs

Table 6.3 summarises the creep deflection at the mid-span point from test results and the FEM creep predictions. It is noted that the predictions agree well with the three month creep test results. This comparison result indicates that the parameters from 1,000 hour creep tests are adequate to be used to predict the three month creep test results in the numerical. These parameters will be used to predict the SIP beam and panel predictions in the following sections.

Specimen	Three month deflection		Difference
	Test	Prediction	
	(mm)	(mm)	(%)
OSB-LT-1 (10%)	8.56	9.33	9.02
OSB-LT-2 (20%)	17.86	19.20	7.51
OSB-LT-3 (30%)	27.55	26.48	-3.88

Table 6.3: Comparison between the three month creep test results and FEM predictions

6.3 Long-term double shear experimental study of SIPs

Experimental investigation of long-term double shear of SIPs is presented in this section. The 1,000 hour ABAQUS power-law creep parameters were determined and compared with the three month test results for verification. These parameters will be later employed to predict SIP creep behaviours in the subsequent sections.

6.3.1 Experimental investigation of long-term double shear of SIPs

Three sets of SIP specimens (SIPs-LT-DS1, 2 and 3), notionally 100 mm wide, 200 mm long and 125 mm thick, were subjected to the long-term double shear test for three months. SIP specimens were subjected to the applied loads by applying weights at 10% for SIPs-LT-DS1, 20% for SIPs-LT-DS2, and 30% for SIPs-LT-DS3 of the mean ultimate load. The mean ultimate load (4.58 kN) was found from the short-term loading test reported in section 3.6.

The lever and weight-loading apparatus (Figure 6.6) was used for carrying out this long-term experiment. The lever and weight-loading system reduces the number of weights (by approximately 75%) that require applying to the specimens. Three dial gauges were used to monitor the creep displacements at the centre of loading plate at the following times after loading: 0.1, 0.2, 0.5, 1, 2, 5 hours and then every 24 hour in the first week and then every 72 hour interval throughout the test duration. The temperature and humidity were in the range of 23°C ± 3°C and 40 ± 10%, respectively.

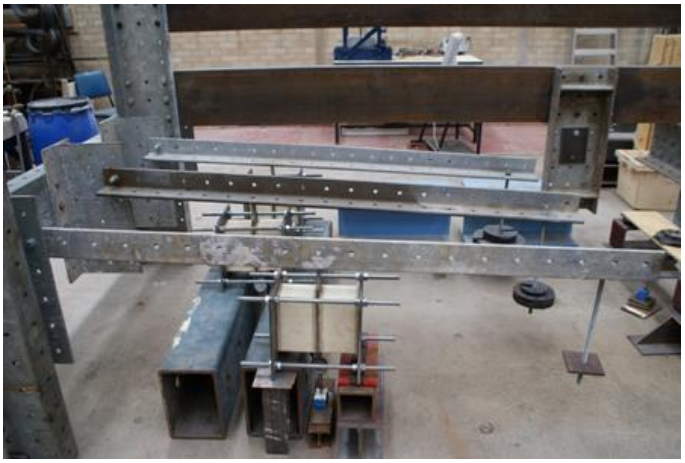

(a)

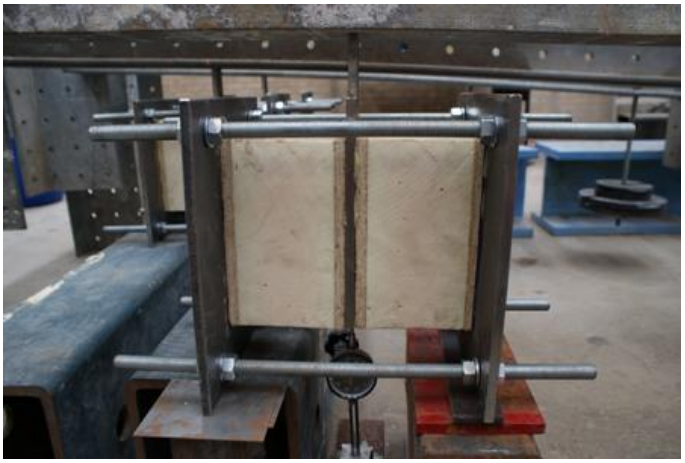

(b)

Figure 6.6: Long-term double shear SIP experimental apparatus

Figure 6.7 shows the creep movements of all specimens. The fluctuation in the creep curves may be again due to the variations of temperature and the humidity. However, the effects of temperature and humidity are again expected to be negligible since their variations are small.

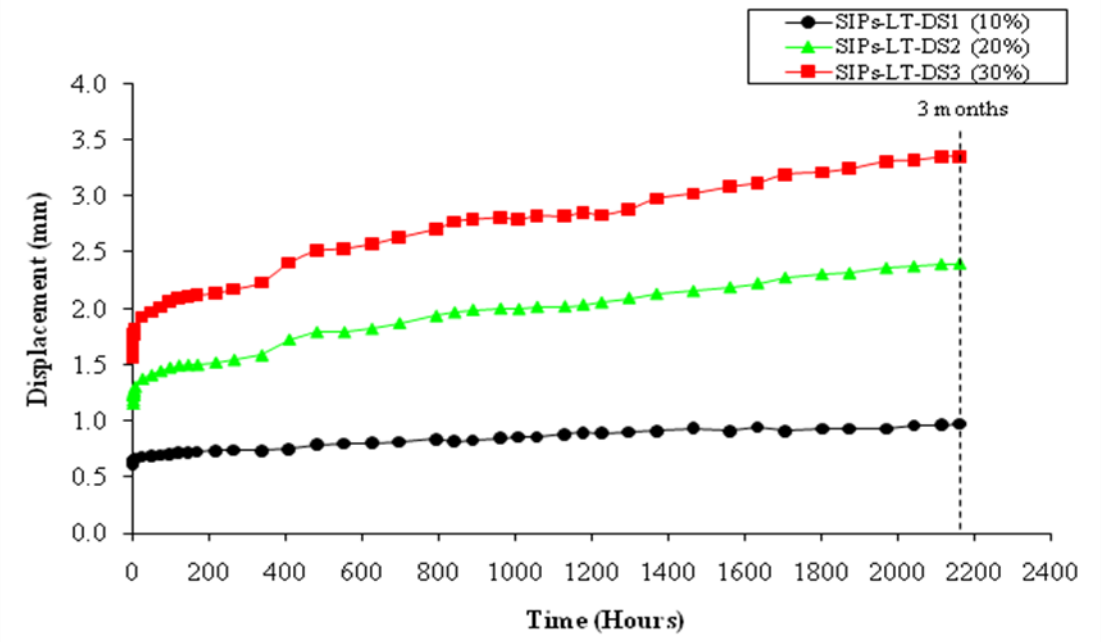

Figure 6.7: Three month creep test results

Table 6.4 summarises the creep test results under 10%, 20% and 30% of the ultimate load, respectively. It is noted that the higher the load applied, the higher the relative deflection as can be seen in Table 6.4.

Specimen	Instantaneous deflection (mm)	Three month deflection (mm)	Relative deflection[1]
SIPs-LT-DS1 (10%)	0.61	0.97	1.59
SIPs-LT-DS2 (20%)	1.15	2.40	2.09
SIPs-LT-DS3 (30%)	1.56	3.35	2.15

Note 1: Relative deflection equals to the three month deflection divided by the instantaneous deflection

Table 6.4: The applied loads and the instantaneous deflection of each SIP specimens

6.3.2 Numerical investigation of long-term SIPs

Since the double shear test was carried out on two symmetric SIP specimens, only one SIP specimen was therefore modelled as a two-dimensional model. The assumption of perfect bond was used at all bonding interfaces. Figure 6.8 depicts finite element mesh for the SIP model.

The structured mesh technique for this model is again an eight-node biquadratic plane strain element with reduced integration (CPE8R). OSB faces were also divided into two divisions with a 10 mm element size in the other direction. Other materials, i.e. PUR and steel plate, were discretised into 10 x 10 mm elements.

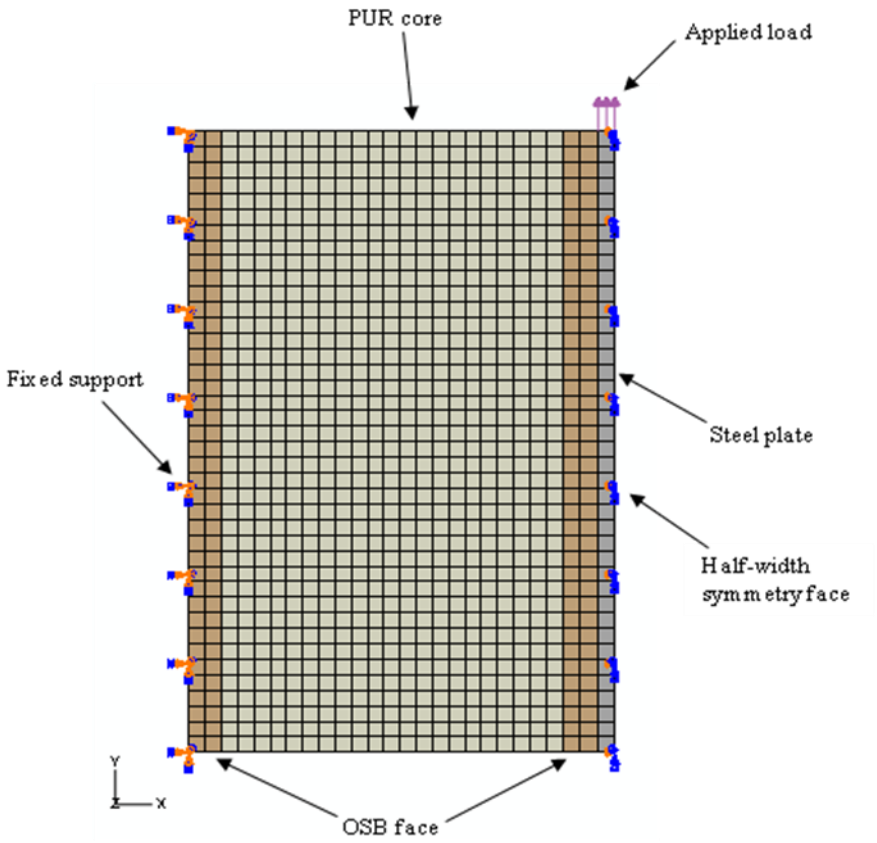

Figure 6.8: SIP double shear finite element model

The 1,000 hour ABAQUS power-law creep parameters for each applied load were again determined by the curve fitting analysis. Power Law Multiplier value has also been found to be the main factor in the creep behaviour, whereas the values of equivalent stress order and time order are again constant at 2 and -0.5 for all applied loads.

Specimen	Power Law Multiplier (A)	Equivalent Stress Order (n)	Time Order (m)
SIPs-LT-DS1 (10%)	0.047	2	-0.5
SIPs-LT-DS2 (20%)	0.037		
SIPs-LT-DS3 (30%)	0.021		

Table 6.5: 1,000 hour ABAQUS power-law creep parameters

By using the above parameters, the creep predictions for the 1,000 hour from the numerical model by using the power-law creep model agree well with the test results as shown in Figure 6.9.

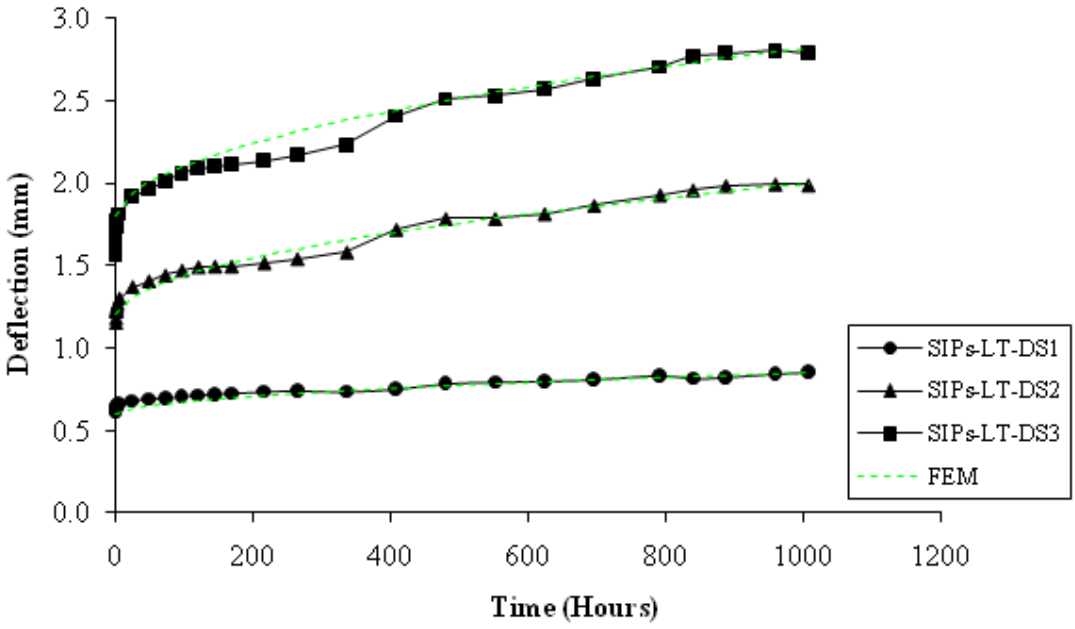

Figure 6.9: 1,000 hour experimental and FEM predicted creep deflections of SIPs

By using the 1,000 hour creep parameters, Figure 6.10 shows the comparison between the three month creep test results and the FEM predictions.

Table 6.6 summarises the creep displacement test results with the FEM creep predictions. It is noted that the predictions agree well with the three month creep test results. These reveal that the 1,000 hour creep parameters are adequate to be used to predict the three month creep test

results. These PUR creep parameters will be used to predict the SIP beam and panel predictions in the following sections.

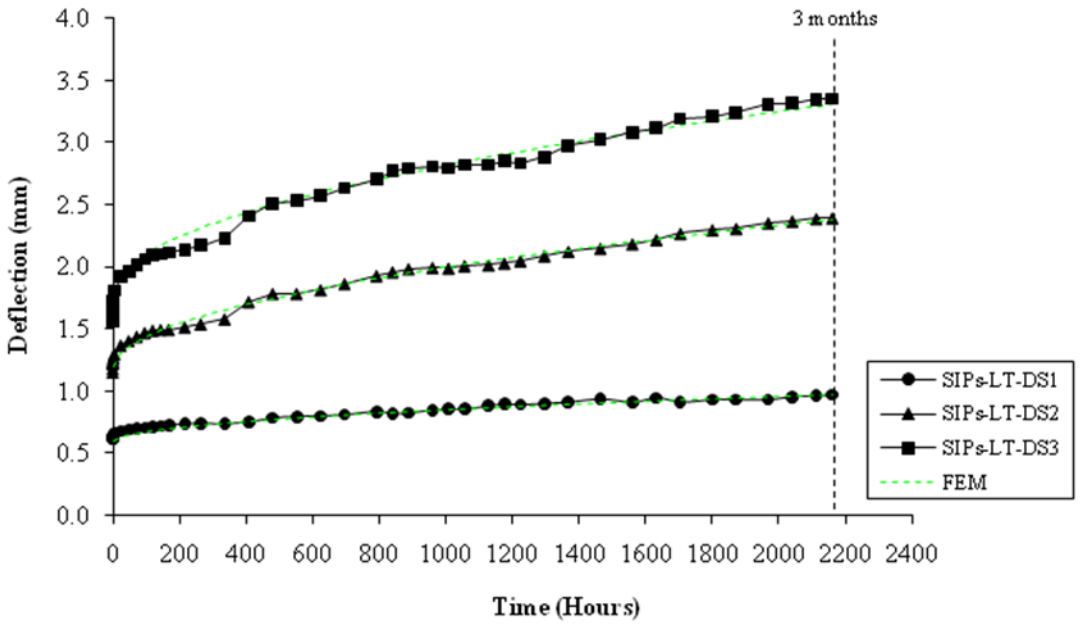

Figure 6.10: Three month experimental and FEM predicted displacements of SIPs

Specimen	Three month deflection		Difference
	Test	Prediction	
	(mm)	(mm)	(%)
SIPs-LT-DS1 (10%)	0.97	0.98	0.55
SIPs-LT-DS2 (20%)	2.40	2.38	-0.77
SIPs-LT-DS3 (30%)	3.35	3.31	-1.34

Table 6.6: Comparison between the three month creep test results and FEM predictions

6.4 Long-term experimental investigation on SIP beams

SIP beams were subjected to sustained three-point bending loads for three months. The aims of this study were as follows:

- To investigate the creep behaviour of SIP beams under different levels of applied loads.

- To investigate the capability of the numerical parameters obtained from OSB and PUR.
- To determine which creep model can be used to predict the flexural mid-span creep deflections.

6.4.1 Experimental investigation of SIP beams under long-term loading

Six SIP beams (SIP-BLT-1 to 6) were subjected to the three-point bending creep tests for three months under ambient temperature and moisture content. Each SIP beam has the same details (200 mm wide, 800 mm long and 125 mm thick) as previously described in the short-term test in section 3.6.

SIP beams were subjected to three-point bending loads applied by weights at 10% for SIP-BLT-1 and 2, 20% for SIP-BLT-3 and 4, and 30% for SIP-BLT-5 and 6 of the mean ultimate load for three months. The mean ultimate load (8.78 kN) was found from the short-term loading test which reported in section 3.6. Two applied loads (20% and 30%) in this long-term test were higher than the mean serviceability load, which is only 10.4% of the mean ultimate load. Therefore, the result of this test can also be used to investigate the behaviour of SIP beams when subjected to the load that is higher than the serviceability design load. However, it should be noted that this investigation was for research purpose only, the design load is less than the serviceability load in engineering practice.

To prevent the SIP specimen slipping from the support steel plates in the longer period, the "Evo Stik Multi Purpose Impact Instant Contact Adhesive" was used to bond them together. All SIP beams were supported and loaded with a 100 mm load spreading plate. These were in the same condition as described in the short-term loading test. The lever and weight-loading

apparatus (Figure 6.11) was used for carrying out this long-term experiment. Four sets of the apparatus were assembled in order to apply 20% and 30% of the ultimate load to four SIP beams (SIP-BLT-3 to 6). For the beam test at the 10% ultimate load level, the applied loads were by weights directly (approximately 90 kg) as these weights were available in the laboratory. A dial gauge was used to monitor the creep deflection at the central span. The creep deflections were then recorded at the same intervals of OSB and double shear tests throughout the test duration. The temperature and humidity were in the range of 20°C ± 4°C and 35 ± 7%, respectively.

Figure 6.11: Long-term experimental apparatus

Due to the fact that the test results for two identical specimens at each loading level were close in the three month duration, it was decided to continue the creep test for one of them beyond three months and unload the other to study the recovery behaviour. Both deflections were again recorded at the regular intervals.

It was found that the creep deflection was still ongoing after five months. Furthermore, the creep recovery was also ongoing after two months. The experimental investigation was therefore stopped since both of them had increased and decreased at a constant or small rate.

Figure 6.12 shows the creep deflections of all specimens. The mean creep deflections of two identical test specimens are illustrated in Figure 6.13.

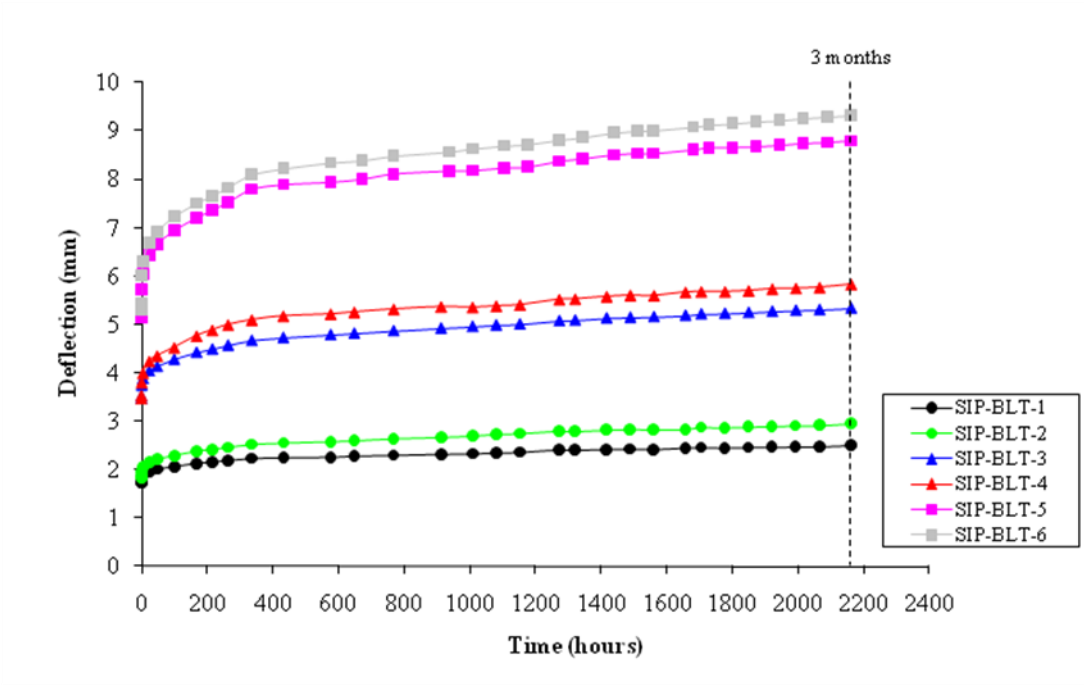

Figure 6.12: Three month creep test results

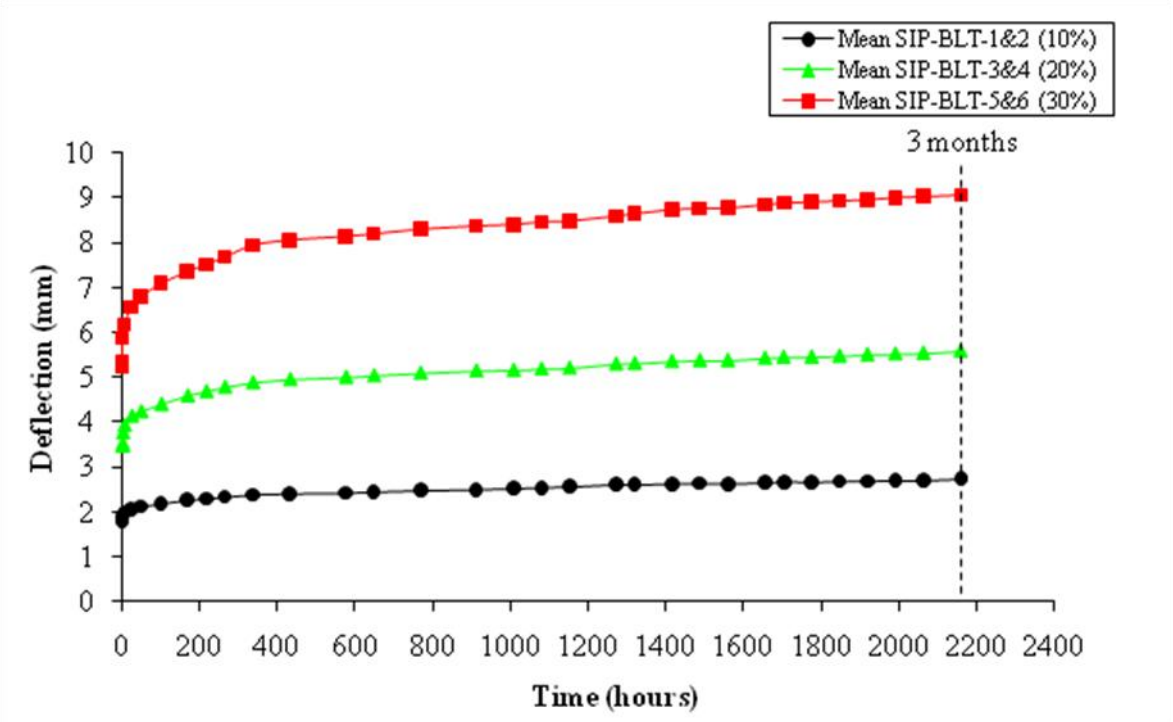

Figure 6.13: Mean creep deflections of two duplicated test specimens

Table 6.7 summarises the mean creep test results under 10%, 20% and 30% of ultimate load, respectively. As expected, the relative deflection is influenced by the applied stress level as can be seen in Table 6.7.

Specimen	Mean instantaneous deflection (mm)	Mean three month deflection (mm)	Relative deflection[1]
SIP-LT-1&2 (10%)	1.78	2.73	1.53
SIP-LT-3&4 (20%)	3.47	5.57	1.61
SIP-LT-5&6 (30%)	5.22	9.06	1.74

Note 1: Relative deflection equals to the three month deflection divided by the instantaneous deflection

Table 6.7: The applied loads and the instantaneous deflection of each SIP specimen

6.4.2 Numerical investigation of long-term SIP beams

The SIP beam numerical model is as same as previously detailed in the short-term investigation section 3.6. The OSB and PUR ABAQUS power-law creep parameters (Table 6.8), which have been found in the previous sections, are employed and the creep predictions are compared to the experimental results for validation.

Specimen	Power Law Multiplier (A)	Equivalent Stress Order (n)	Time Order (m)
OSB-LT-1 (10%)	4.90×10^{-6}	2	-0.5
OSB-LT-2 (20%)	2.60×10^{-6}		
OSB-LT-3 (30%)	1.35×10^{-6}		
SIPs-LT-DS1 (10%)	0.047		
SIPs-LT-DS2 (20%)	0.037		
SIPs-LT-DS3 (30%)	0.021		

Table 6.8: 1,000 hour ABAQUS power-law creep parameters

Figure 6.14 shows the comparison between the three month creep test results and the FEM predictions. It is noted that the predictions are in good agreement with the three month creep test results as summarised in Table 6.9.

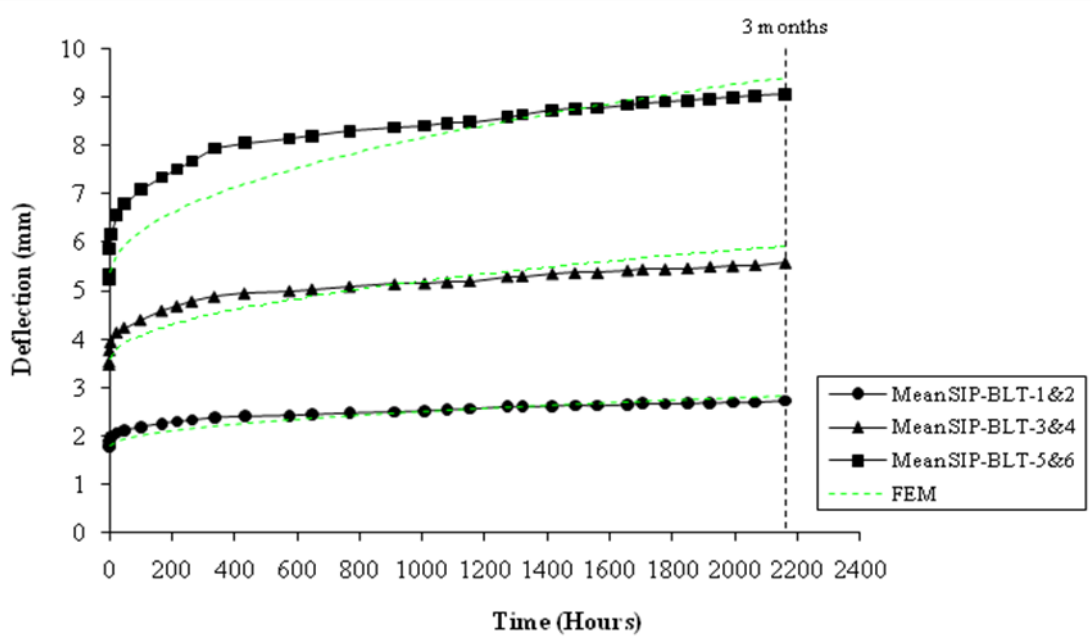

Figure 6.14: Three month comparison of SIP beams

Specimen	Three month deflection		Difference
	Test	Prediction	
	(mm)	(mm)	(%)
Mean SIP-BLT-1&2 (10%)	2.73	2.82	3.51
Mean SIP-BLT-3&4 (20%)	5.57	5.92	6.23
Mean SIP-BLT-5&6 (30%)	9.06	9.41	3.88

Table 6.9: Comparison between the three month creep test results and FEM predictions

Since the predictions provide a good agreement with the three month creep test results, five month creep test results are then compared to the FEM predictions as shown in Figure 6.15.

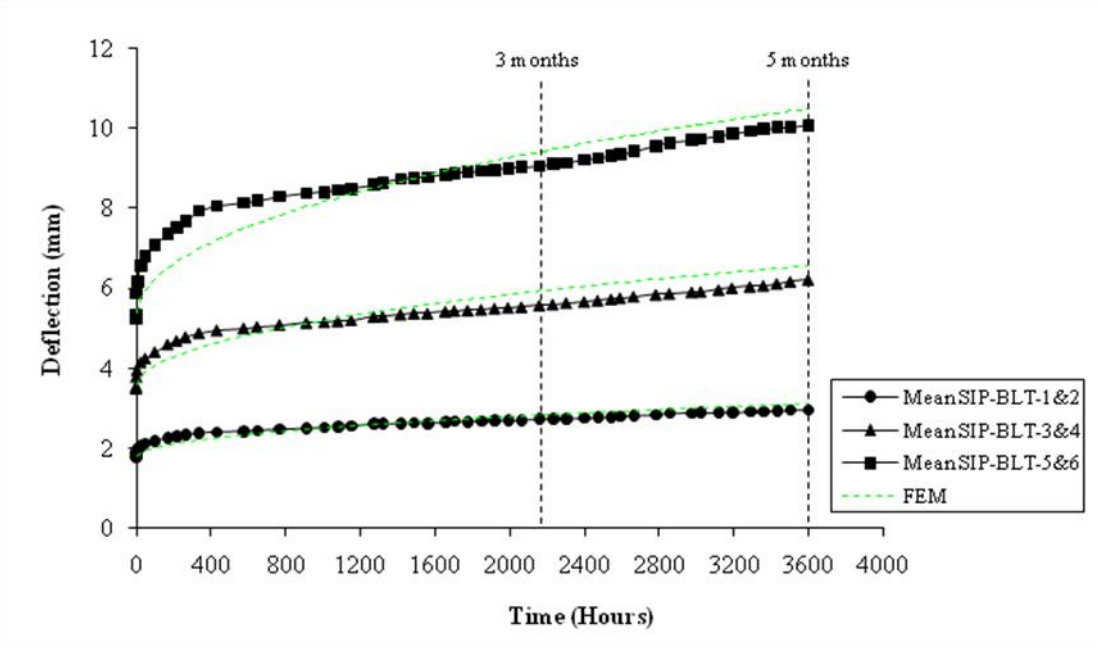

Figure 6.15: Five month comparison of SIP beams

Table 6.10 summarises the five month creep displacement test results with the FEM creep predictions. The predictions are still in good agreement with the five month creep test results.

Specimen	Five month deflection		Difference
	Test	Prediction	
	(mm)	(mm)	(%)
SIP-BLT-1 (10%)	2.96	3.11	5.10
SIP-BLT-3 (20%)	6.23	6.56	5.45
SIP-BLT-5 (30%)	10.08	10.50	4.18

Table 6.10: Comparison between the five month creep test results and FEM predictions

6.4.3 Creep prediction methods for SIP beams

In this section, four creep prediction methods are examined in order to identify the most suitable creep model to describe the flexure mid-span creep deflection of SIP beams without employing numerical investigations. These creep methods have been described in section 2.5.

6.4.3.1 Taylor's models

The creep deflection equations for four creep compliance models are given by Taylor as previously summarised in Table 2.12 and presented again in Table 6.11.

Model	Equation
Power	$\Delta_p(t) = \Delta_0 + A_1 t^{A_2}$
Three element	$\Delta_3(t) = \Delta_0 + A_1[1-\exp(-A_2 t)]$
Four element	$\Delta_4(t) = \Delta_0 + A_1[1-\exp(-A_2 t)] + A_3 t$
Five element	$\Delta_5(t) = \Delta_0 + A_1[1-\exp(-A_2 t)] + A_3 t^{A_4}$
where $\Delta_i(t)$ is total time dependent deflection (minutes); Δ_0 is initial deflection (mm); and A_i is creep parameters associated with creep deflection equations.	

Table 6.11: Creep deflection models proposed by Taylor et al. (1997)

Table 6.12 shows the 1,000 hour creep parameters for each compliance model which found from the regression analysis by using the curve fitting software package i.e. DataFit version 9.0.59 developed by Oakdale Engineering Ltd (Oakdale, 2011). The agreement of the creep predictions from the power and five creep compliance models with the 1,000 hour creep test results is extremely good as shown in Figures 6.16 - 6.18.

Specimen	Model	A_1	A_2	A_3	A_4	R^2
SIP-BLT-1&2 (10%)	Power	0.042	0.261	N/A	N/A	0.997
	Three element	0.640	0.002	N/A	N/A	0.904
	Four element	0.323	0.019	$7.81\text{x}10^{-6}$	N/A	0.911
	Five element	-0.048	2.254	0.063	0.300	0.998
SIP-BLT-3&4 (20%)	Power	0.107	0.254	N/A	N/A	0.997
	Three element	1.508	$2\text{x}10^{-4}$	N/A	N/A	0.902
	Four element	0.892	0.003	$1.62\text{x}10^{-5}$	N/A	0.947
	Five element	-0.093	2.256	0.148	0.228	0.995
SIP-BLT-5&6 (30%)	Power	0.237	0.240	N/A	N/A	0.995
	Three element	2.787	$2.67\text{x}10^{-4}$	N/A	N/A	0.882
	Four element	1.730	0.003	$2.97\text{x}10^{-5}$	N/A	0.948
	Five element	-0.220	2.262	0.346	0.210	0.996

Table 6.12: 1,000 hour creep parameters from regression analysis

The three and four element creep compliance models show less conformity with the test results. The predictions from the three element creep compliance model underestimate the initial creep deflection, whereas the four element model provides an over-estimate.

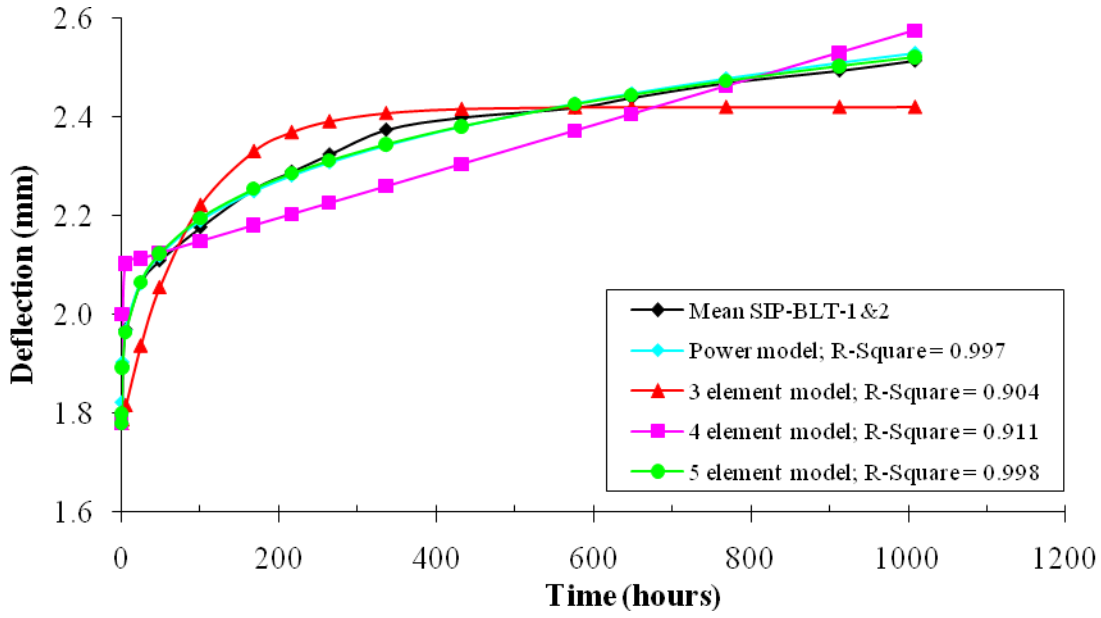

Figure 6.16: 1,000 hour mean experimental and predicted creep deflections of SIP-BLT-1&2

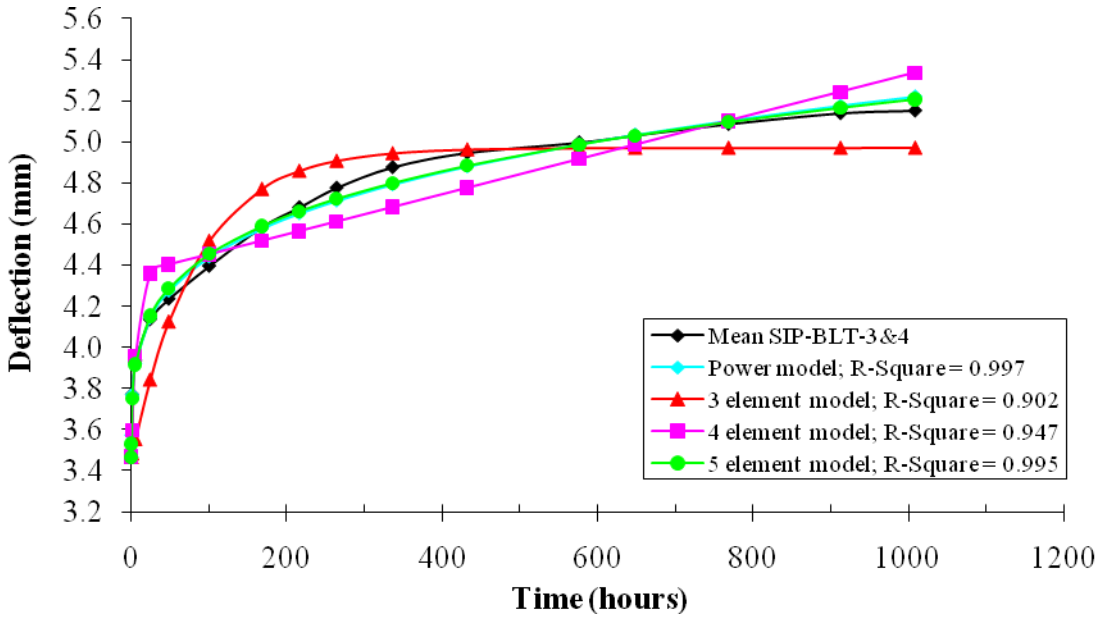

Figure 6.17: 1,000 hour mean experimental and predicted creep deflections of SIP-BLT-3&4

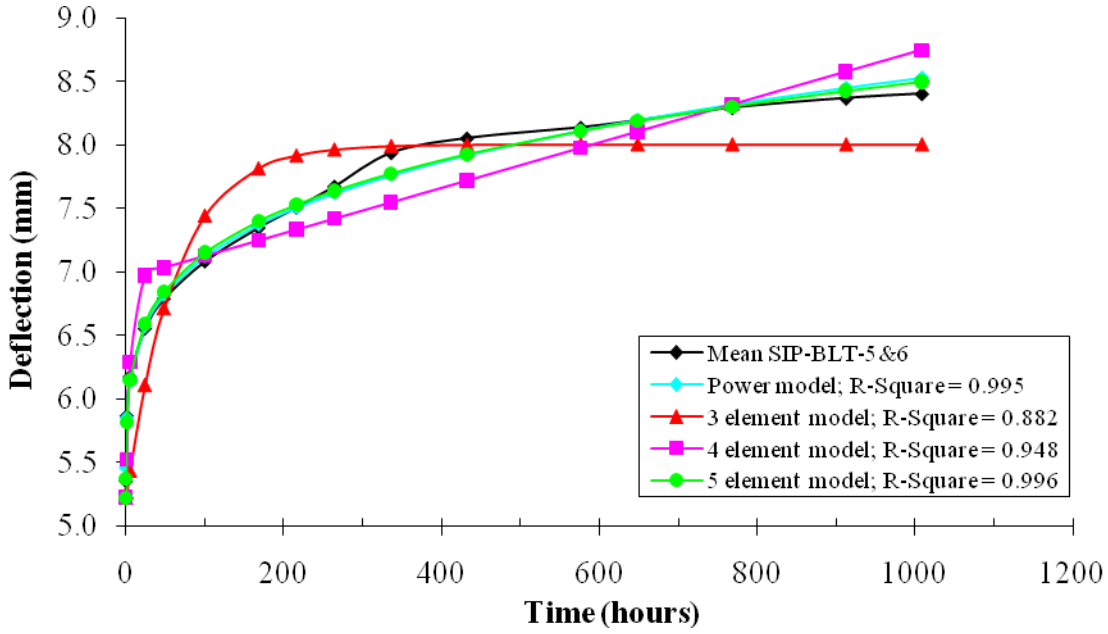

Figure 6.18: 1,000 hour mean experimental and predicted creep deflections of SIP-BLT-5&6

By using the 1,000 hour creep parameters, Figures 6.19 - 6.21 show the comparison between the mean three month creep test results and all four creep compliance model predictions.

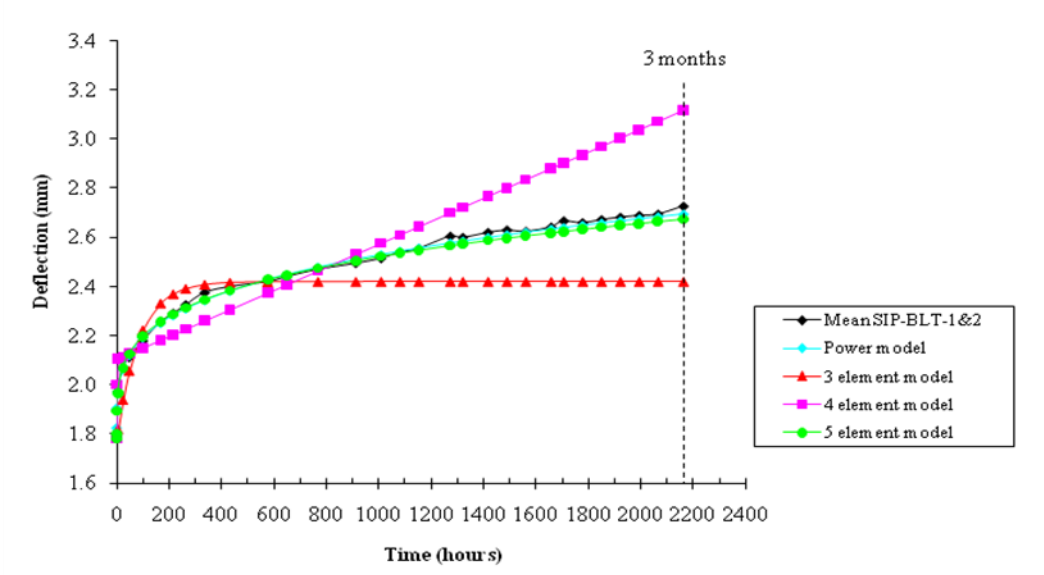

Figure 6.19: Three month experimental and predicted creep deflections of SIP-BLT-1&2

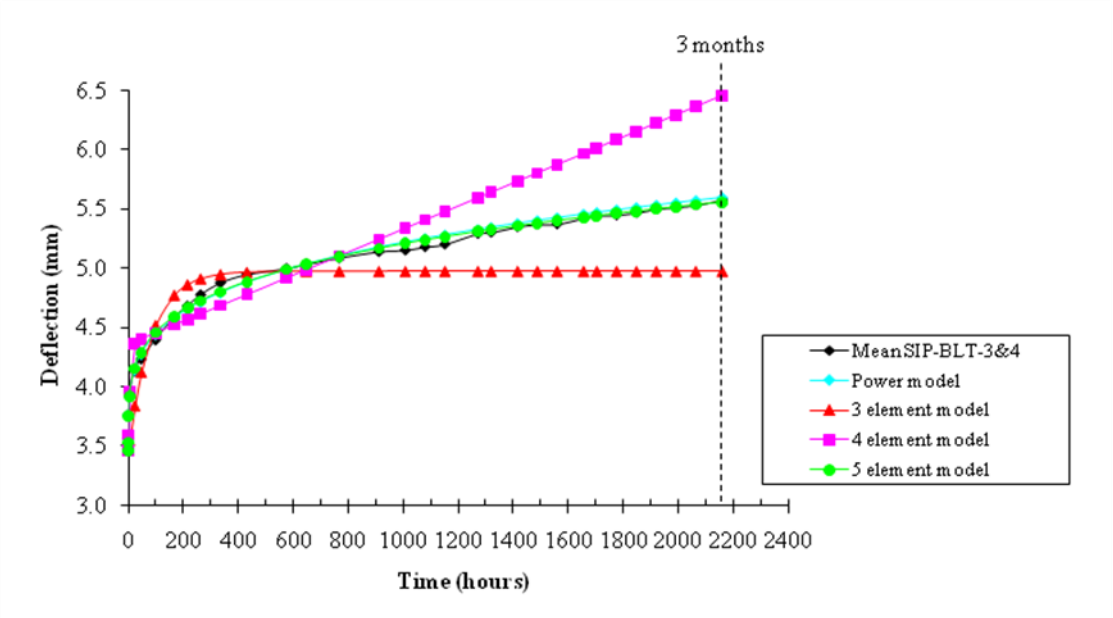

Figure 6.20: Three month experimental and predicted creep deflections of SIP-BLT-3&4

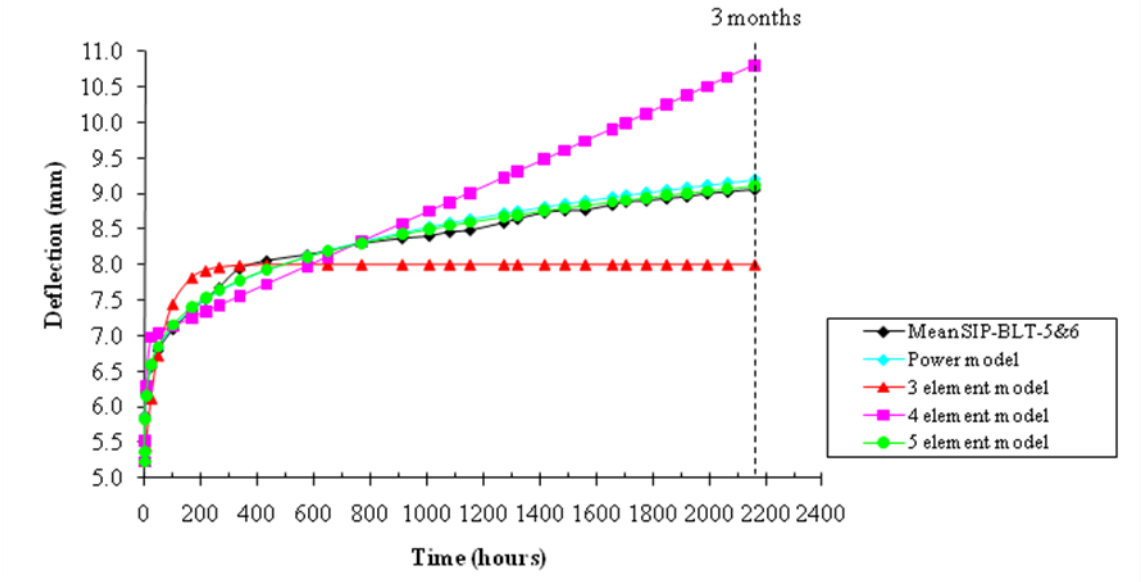

Figure 6.21: Three month experimental and predicted creep deflections of SIP-BLT-5&6

Table 6.13 summarises the creep test result at the mid-span with various creep compliance models. It is noted that the power and five element creep compliance model predictions agree very well with the three month creep test results.

Specimen	Model	Difference (%) to the three month test result
Mean SIP-BLT-1&2 (10%)	Power	-1.20%
	Three element	-11.26%
	Four element	14.22%
	Five element	-1.99%
Mean SIP-BLT-3&4 (20%)	Power	0.40%
	Three element	-10.81%
	Four element	15.74%
	Five element	-0.34%
Mean SIP-BLT-5&6 (30%)	Power	1.55%
	Three element	-11.60%
	Four element	19.30%
	Five element	0.54%

Table 6.13: the creep deflection at mid-span test results with various creep models

By considering the simplicity principle and using the minimal number of creep parameters, the power creep compliance model is the most appropriate method to predict the creep deflection at the mid-span. As previously described, SIP-BLT-1, 3 and 5 were investigated further for two months. Figure 6.22 show the comparison between the five month creep test results with the predictions from the power creep compliance model only. The agreement is good with an underestimate of the test results by 5.34% as summarised in Table 6.14.

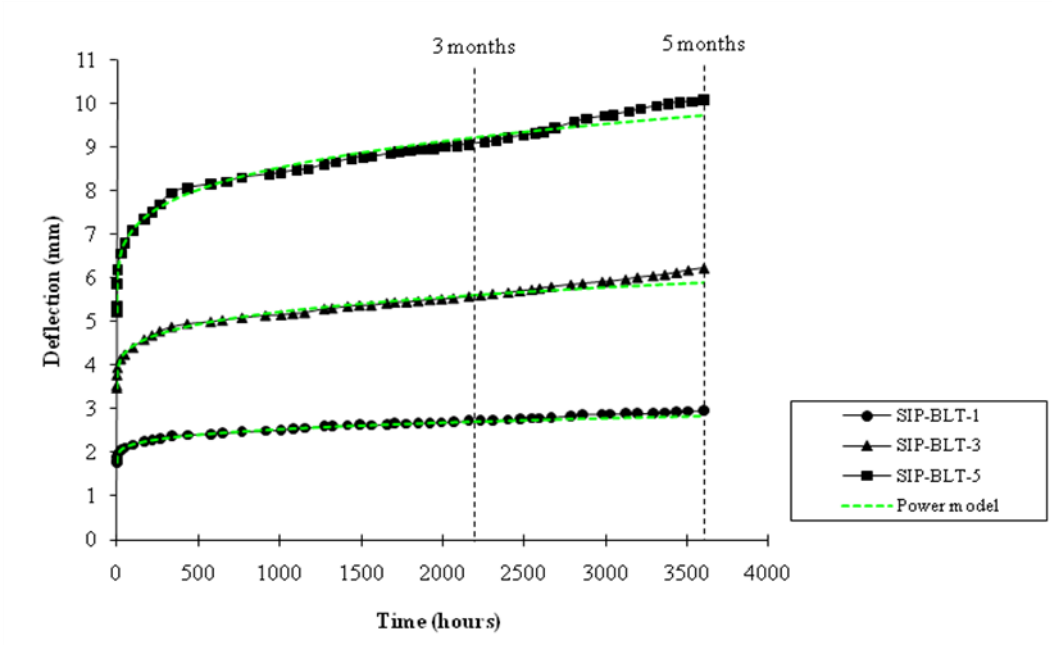

Figure 6.22: Five month experimental and predicted creep deflections of SIP beams

Specimen	Five month deflection		Difference
	Test	Prediction	
	(mm)	(mm)	(%)
SIP-BLT-1 (10%)	2.96	2.83	-4.47
SIP-BLT-3 (20%)	6.23	5.89	-5.34
SIP-BLT-5 (30%)	10.08	9.72	-3.59

Table 6.14: Five month creep test results and predictions from the power model

6.4.3.2 BS EN 1606 (BSI, 1996)

The 1,000 hour material constants were determined using the BS EN 1606 method and are summarised in Table 6.15. By using the 1,000 hour material constants, the creep deflections at time *t* (X_t) can be determined using the equation (6.1). Figure 6.23 depicts the 1,000 hour creep test results and the predictions. The agreement is favourably good with the least R^2 equal to 0.990.

$$X_t = X_0 + mt^b \tag{6.1}$$

where X_t is creep deflection at time t (mm).

X_0 is initial deflection (mm).

m and *b* are material constants.

Specimen	1,000 hour material constants		R^2
	m	b	
SIP-BLT-1&2 (10%)	0.1024	0.2869	0.993
SIP-BLT-3&4 (20%)	0.2527	0.2773	0.990
SIP-BLT-5&6 (30%)	0.5296	0.2606	0.991

Table 6.15: 1,000 hour material constants from BS EN 1606 method

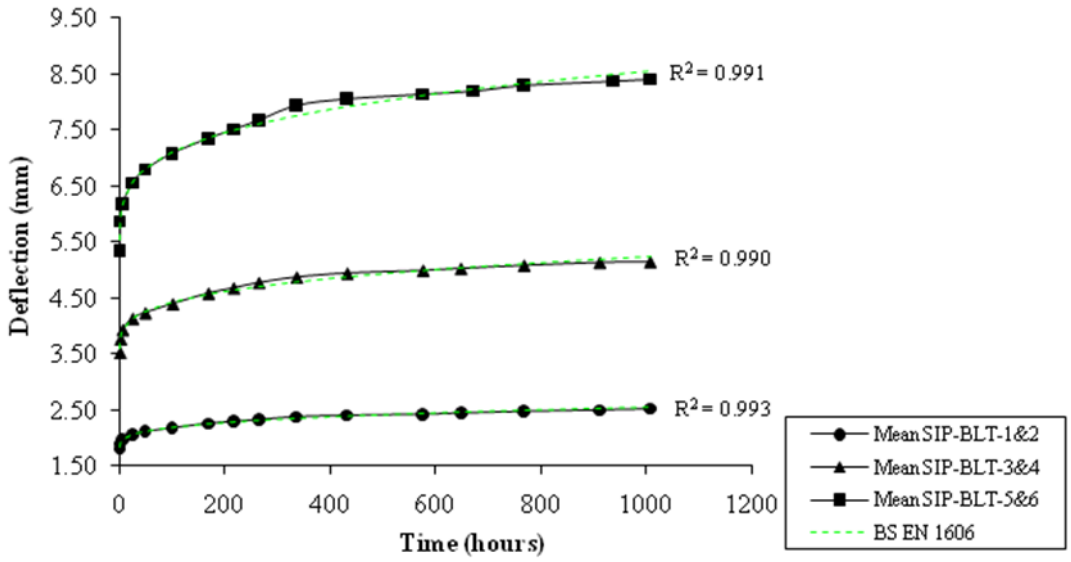

Figure 6.23: Mean 1,000 hour experimental and predicted creep deflections of SIP beams

Figure 6.24 shows the comparison between the mean creep test results and the creep predictions using the material constants from the 1,000 hour creep test. It should be noted that the three month predictions from using the 1,000 hour material constants agree very well with the three month creep test results with 2.21% overestimate as shown in Table 6.16.

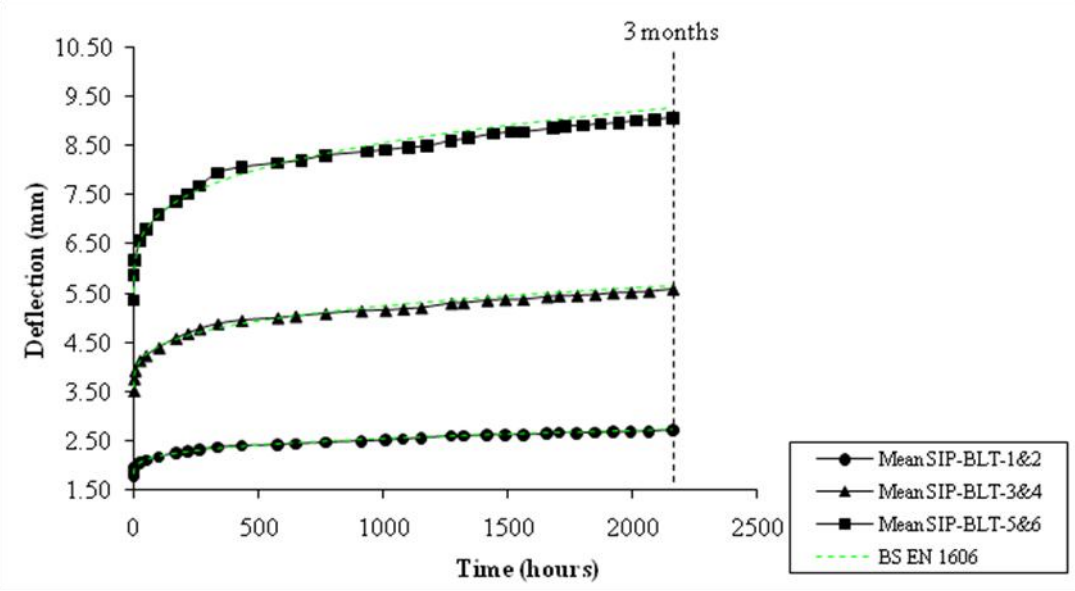

Figure 6.24: Three month mean experimental and predicted creep deflections of SIP beams

Specimen	Three month deflection		Difference
	Test	Prediction	
	(mm)	(mm)	(%)
Mean SIP-BLT-1&2 (10%)	2.73	2.73	0.00
Mean SIP-BLT-3&4 (20%)	5.57	5.65	1.44
Mean SIP-BLT-5&6 (30%)	9.06	9.26	2.21

Table 6.16: Comparison between the three month test results and BS EN 1606 predictions

The 1,000 hour material constants used for the predictions are also acceptable to predict the five month creep test results as shown in Figure 6.25.

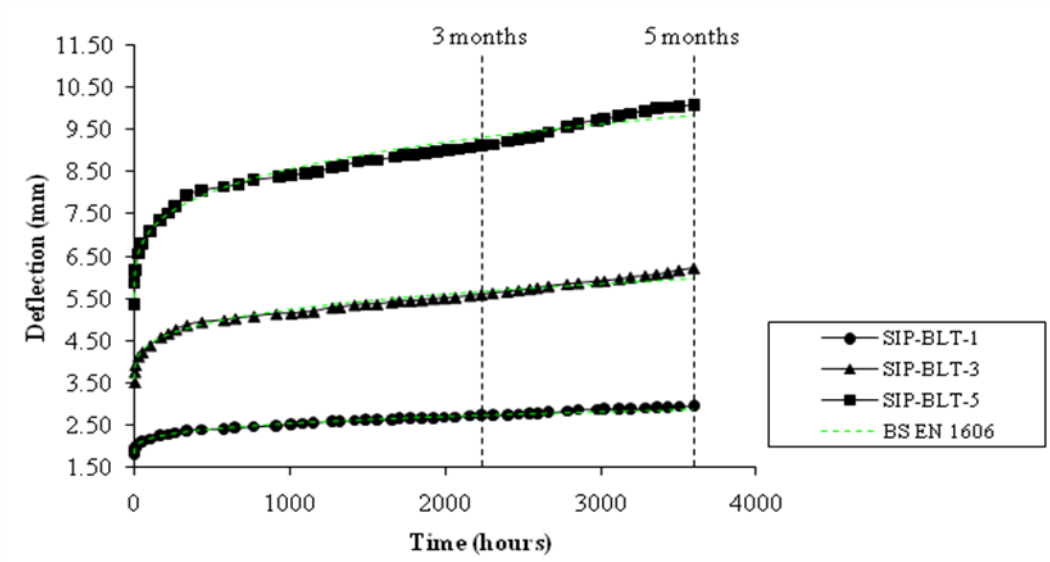

Figure 6.25: Five month experimental and predicted creep deflections of SIP beams

Specimen	Five month deflection		Difference
	Test	Prediction	
	(mm)	(mm)	(%)
SIP-BLT-1 (10%)	2.96	2.87	-3.04
SIP-BLT-3 (20%)	6.22	5.97	-4.02
SIP-BLT-5 (30%)	10.08	9.82	-2.58

Table 6.17: Comparison between the five month test results and BS EN 1606 predictions

Table 6.18 illustrates the comparison between the creep predictions obtained from the BS EN 1606 and the power creep compliance model. The agreement between the creep predictions and the test results obtained from the power model and BS EN 1606 is good.

Model	Three months	Five months
	Utmost Difference (%)	Utmost Difference (%)
BS EN 1606	2.21	-4.02
Power	1.55	-5.34

Table 6.18: Comparison between BS EN 1606 and power model

6.4.3.3 BS EN 14509 (BSI, 2006)

BS EN 14509 - Cl. A.6.5 presents a procedure to obtain the creep coefficients that are required in the design of sandwich panels. The deflection due to bending is a time independent parameter as assumed by BS EN 14509. This is due to that metal faces experience less creep deflection in comparison to the inner foam core at ambient temperature. Therefore, it is acceptable to assume no creep defection due to the metal face bending.

In the test, all SIP beams were supported and loaded with a 100 mm load spreading plate. By assuming that the supported reactions and applied loads as point loads, the bending deflections at the mid-span were overestimated by using the classical sandwich panel theory for point loads (Allen, 1969). The analytical method to determine the deflection with the 100 mm load spreading is unavailable. To tackle this problem, the deflection due to bending was then determined by using a numerical method.

The OSB faces were modelled as a line beam element whereas the steel supported and loaded places were modelled as two-dimensional and deformable body with planar features by using ABAQUS as shown in Figure 6.26. The contact elements with a friction coefficient of 0.2 were

used to connect the beam and the steel supported plates. The second moment of area (I) calculated from the two OSB faces by using the parallel axis theorem was applied to the line beam element. By running this simulation, the real bending deflection (first component of the total deflection) can be obtained by establishing the relationship between the concentrated loading patterns and the patched one. It has been found that the bending deflections are 0.076, 0.152 and 0.228 mm for the 10%, 20% and 30% of the mean ultimate load. Table 6.19 shows the creep coefficients at 200 and 1,000 hours found from the test results.

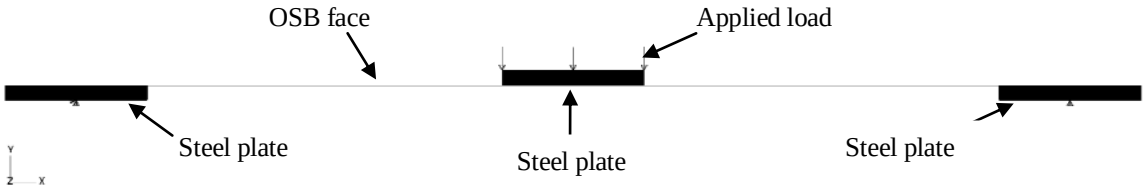

Figure 6.26: OSB face FEM model

Specimen	Creep coefficients	
	φ_{200}	$\varphi_{1,000}$
SIP-BLT-1&2 (10%)	0.2994	0.4314
SIP-BLT-3&4 (20%)	0.3668	0.5087
SIP-BLT-5&6 (30%)	0.4588	0.6382

Table 6.19: Creep coefficient from BS EN 14509 method

Figure 6.27 depicts the creep test results and the design creep deflections. The design creep deflections have been found to be significantly higher than the three month creep test results; these indicate that the design values are acceptable but overly conservative.

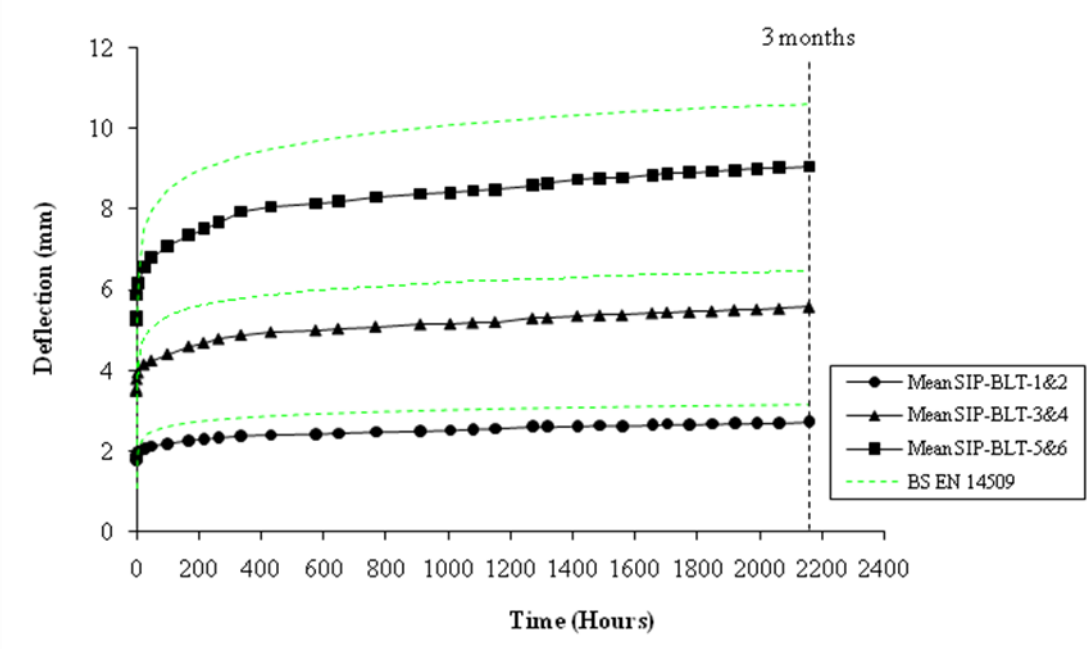

Figure 6.27: Three month experimental and predicted creep deflections of SIP beams

As previously described, BS EN 14509 (BSI, 2006) provides the conservative φ_t values for the design of sandwich panels for polyurethane core when subjected to permanent (100,000 hours) and quasi-permanent (2,000 hours) loads. The experimental φ_t values were calculated at 2,000 and 100,000 hours from the test results using equation 2.20 (presented in section 2.5) with t_1 = 200 hours and t_2 = 1,000 hours, and equation 2.7 to determine φ_{exp1} (t_1 = 200 hours) and φ_{exp2} (t_2 = 1,000 hours). Table 6.20 shows the comparison between the conservative and the experimental φ_t values. It should be noted that the experimental values are lower than the conservative values. Hence, the creep deflections using the conservative φ_t values will be greatly overestimated from the actual creep deflections at 2,000 and 100,000 hours.

Time (hours)	**BS EN 14509 φ_t values**	**Experimental φ_t values**		
		SIP-BLT-1&2	**SIP-BLT-3&4**	**SIP-LT-5&6**
2,000	2.4	0.58	0.68	0.85
100,000	7.0	0.81	0.91	1.15

Table 6.20: Comparison between the conservative and experimental φ_t values

6.4.3.4 *Just's model*

Davies (1987) reported Just's investigation (Just, 1983) on the long-term creep tests of sandwich beams. Just provides the conservative creep coefficient ($\phi_t = 0.12t^{0.36}$) as presented in section 2.5. Figure 6.28 shows the three month experimental and the predicted creep deflections by using Just's creep coefficient. The predictions considerably overestimate and are overly conservative in comparison with the creep test results.

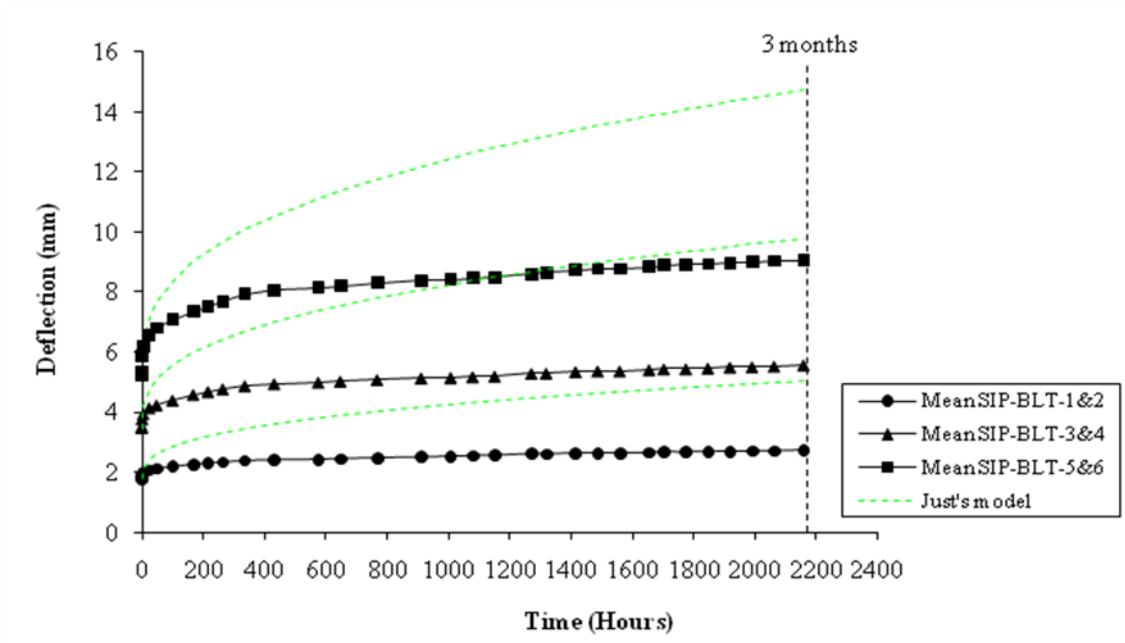

Figure 6.28: Three month experimental and predicted deflections of SIP beams

6.4.3.5 *Huang and Gibson's model*

Huang and Gibson (1990) stated the deflection due to the bending component remained constant. Accordingly, the bending deflections are 0.076, 0.152 and 0.228 mm respectively for the 10%, 20% and 30% of the mean ultimate load as found in the previous section.

By using creep parameters provided by Huang and Gibson (1989) presented in section 2.5, Figure 6.29 presents the creep predictions and the creep experimental results. It should be noted

that deflections predicted by their model overestimate the creep test results. This implies that it is unacceptable to use their creep parameters to predict the creep test results. However, their creep parameters provided a good agreement in their tests. As a result, this reveals that the creep parameters depends on, for instance, type of material and applied load.

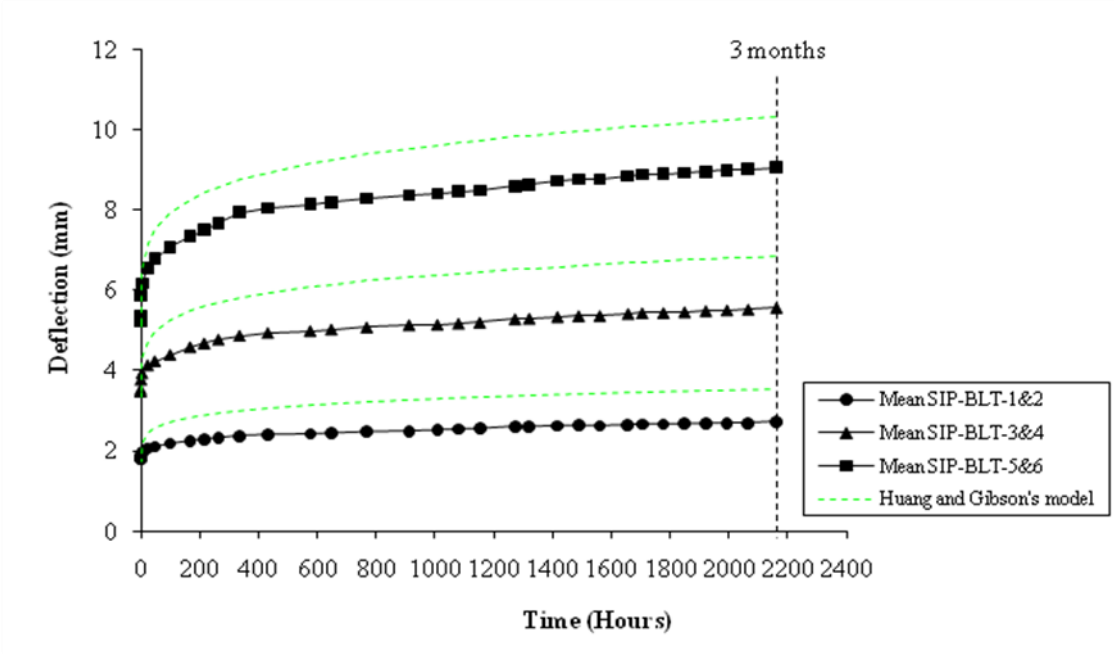

Figure 6.29: Three month mean experimental and predicted creep deflections of SIP beams

6.4.4 Unloaded experimental investigation of SIP beams

As stated in the preceding section, SIP-BLT-2, 4 and 6 were unloaded and the recoveries were then recorded at the following times: 0.1, 0.2, 0.5, 1, 2, 5 hours and then every 24 hour in the first week and then every 72 hour interval for two months as shown in Figure 6.30. The remaining deflections for all SIP beams are plotted against time and presented in Figure 6.31. The initial recoveries were found equal to the initial creep deflections and at least 86.60% of the total deflections can be recovered as can be seen in Table 6.21. These recoveries support Just's

statement (Just, 1983) that at least 50% can be recovered. It should be noted that approximate 70% is recovered after a day unloading.

Figure 6.30: Unloaded experiment

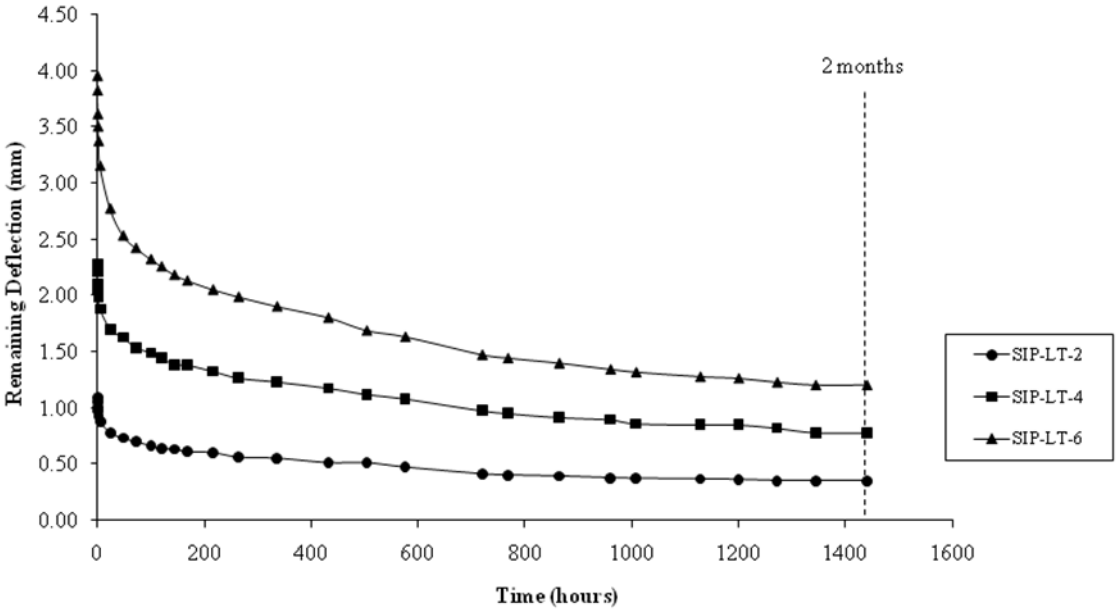

Figure 6.31: Unloaded test results for all SIP beams

Specimen	Recovery (%)					
	0 hour	**1 hour**	**1 day**	**1 week**	**1 month**	**2 months**
SIP-BLT-2 (10%)	63.18%	67.23%	73.65%	79.39%	86.15%	88.18%
SIP-BLT-4 (20%)	60.82%	64.78%	70.79%	76.29%	83.33%	86.60%
SIP-BLT-6 (30%)	57.62%	62.45%	70.28%	77.15%	84.23%	87.12%

Table 6.21: Recovery of each SIP specimen

6.4.5 Unloaded prediction methods for SIP beams

In review literature, there is limited information of SIP behaviours after unloading. Two appropriate creep prediction models (Taylor and BS EN 1606) are modified in order to describe the mid-span deflections after unloading. As the testing results have been recorded for two months, it has been decided to determine the one month recovery parameters that will be later used to predict the two month recovery results for verification. In addition, the recovery results will also compared with the predictions by using Huang and Gibson (1989)'s recovery parameters to verify whether their parameters are capable to be used to predict the SIP recovery.

6.4.5.1 Modified Taylor's models

Taylor's models have been modified and given in Table 6.22. The one month recovery parameters for each compliance model, which are found from DataFit curve fitting software package, are summarised in Table 6.23. The agreement of the remaining predictions from the power and five recovery compliance models with the one month test results is extremely good with the least R^2 equal to 0.991 and 0.999, respectively as shown in Figures 6.32 to 6.34. The three and four element recovery compliance models again show less conformity with the test results.

Model	**Equation**
Power	$\Delta_p(t) = \Delta_0 - A_1 t^{A_2}$
Three element	$\Delta_3(t) = \Delta_0 - A_1[1 - \exp(-A_2 t)]$
Four element	$\Delta_4(t) = \Delta_0 - A_1[1 - \exp(-A_2 t)] - A_3 t$
Five element	$\Delta_5(t) = \Delta_0 - A_1[1 - \exp(-A_2 t)] - A_3 t^{A_4}$
where $\Delta_i(t)$ is total time dependent recovery deflection (minutes); Δ_0 is initial recovery deflection (mm); and A_i is recovery parameters associated with recovery deflection equations.	

Table 6.22: Modified Taylor's models for recovery deflection

Specimen	Model	A_1	A_2	A_3	A_4	R^2
SIP-BLT-2 (10%)	Power	0.062	0.224	N/A	N/A	0.993
	Three element	0.502	$6.95x10^{-4}$	N/A	N/A	0.879
	Four element	0.367	$4.92x10^{-3}$	$1.09x10^{-5}$	N/A	0.974
	Five element	-0.151	2.563	0.160	0.152	0.999
SIP-BLT-4 (20%)	Power	0.114	0.230	N/A	N/A	0.997
	Three element	0.977	$7.13x10^{-4}$	N/A	N/A	0.865
	Four element	0.680	$5.60x10^{-3}$	$2.37x10^{-5}$	N/A	0.974
	Five element	-0.163	2.261	0.211	0.181	0.999
SIP-BLT-6 (30%)	Power	0.251	0.216	N/A	N/A	0.991
	Three element	1.888	$7.31x10^{-4}$	N/A	N/A	0.897
	Four element	1.408	$4.41x10^{-3}$	$3.93x10^{-5}$	N/A	0.977
	Five element	-0.896	2.094	0.846	0.128	0.999

Table 6.23: One month recovery parameters

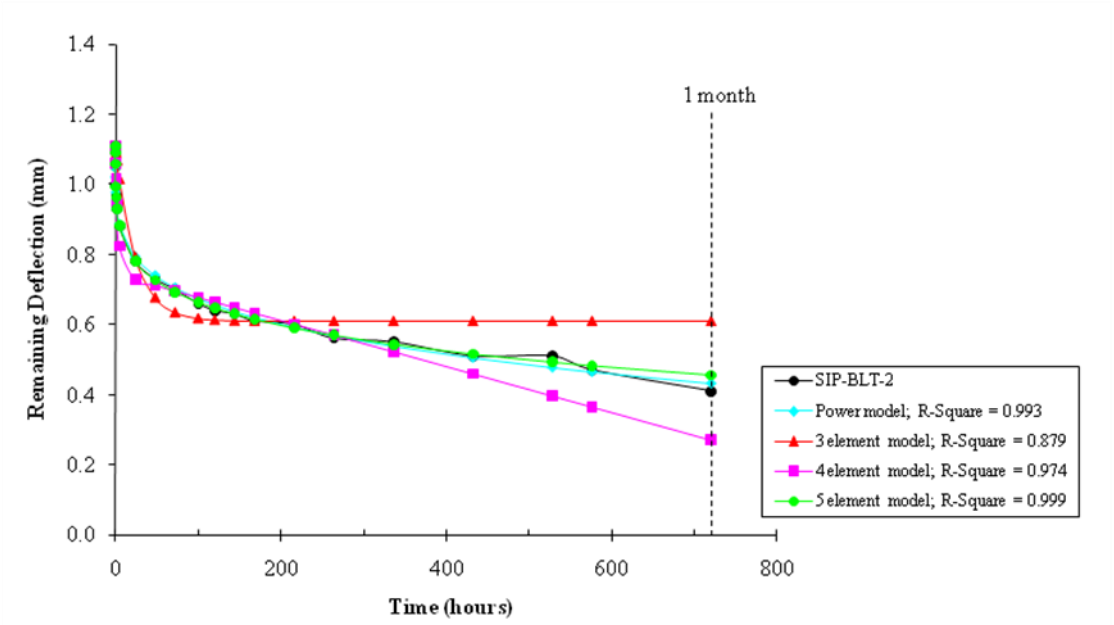

Figure 6.32: Unloaded one month test and predicted remaining deflections of SIP-BLT-2

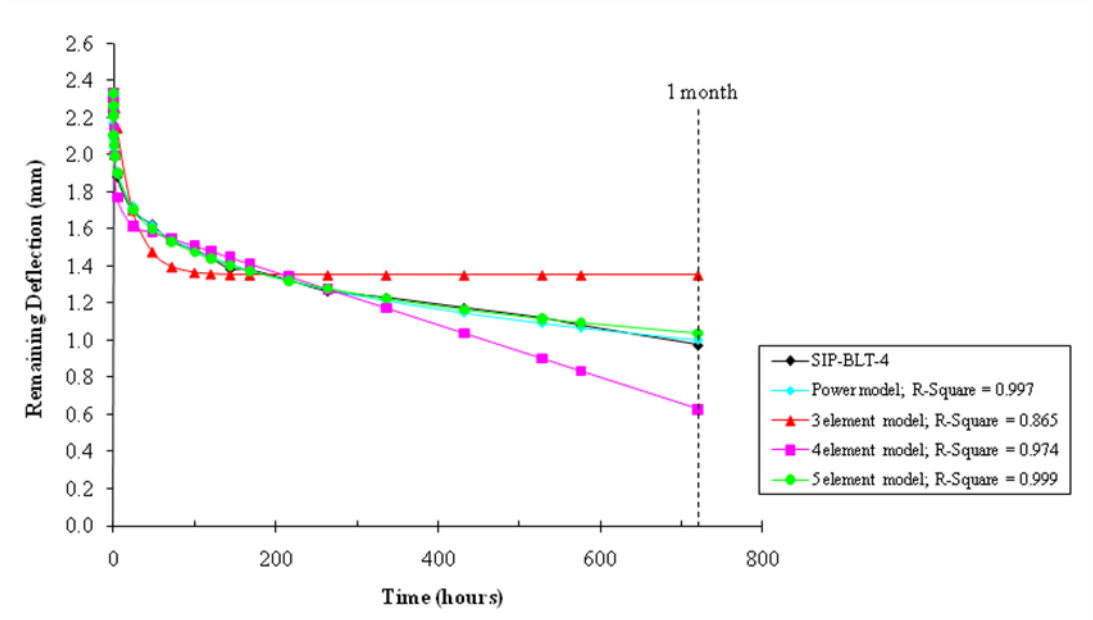

Figure 6.33: Unloaded one month test and predicted remaining deflections of SIP-BLT-4

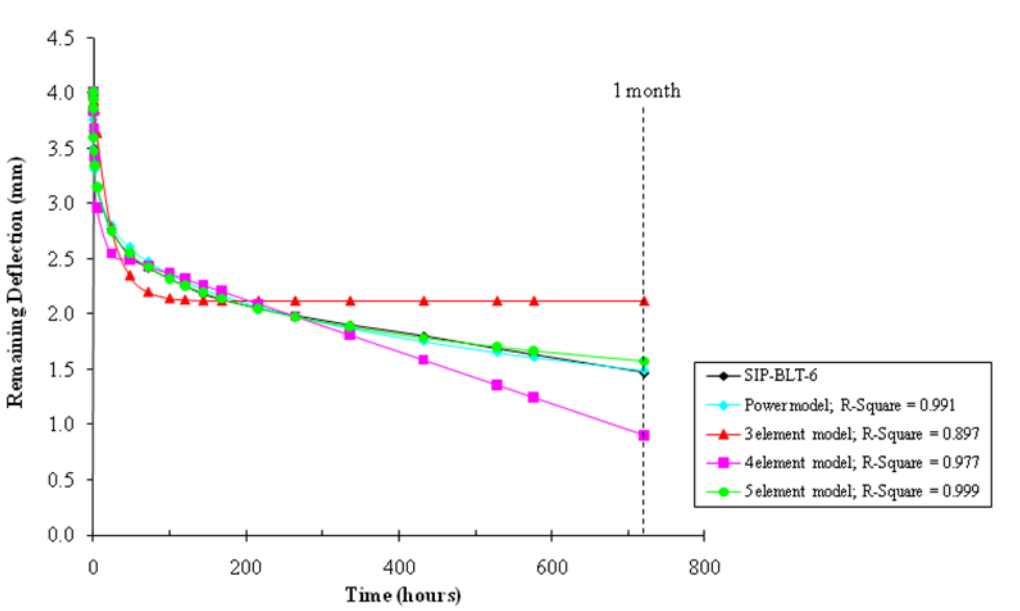

Figure 6.34: Unloaded one month test and predicted remaining deflections of SIP-BLT-6

By using the one month recovery parameters, Figures 6.35 - 6.37 show the comparison between the two month recovery test results and all four recovery compliance model predictions. Table 6.24 provides the comparison between the test results with all recovery models. Although the five element recovery model shows a slightly better agreement with the test results in

comparison with the power model, the power model is favourable account view of the degree of simplicity and number of recovery parameters.

Specimen	Model	Difference (%) to the two month test result
SIP-BLT-2 (10%)	Power	9.66%
	Three element	-73.84%
	Four element	157.81%
	Five element	-4.62%
SIP-BLT-4 (20%)	Power	-0.22%
	Three element	-74.54%
	Four element	150.82%
	Five element	-8.66%
SIP-BLT-6 (30%)	Power	10.07%
	Three element	-76.80%
	Four element	166.06%
	Five element	-5.24%

Table 6.24: Remaining deflection at mid-span test results with various models

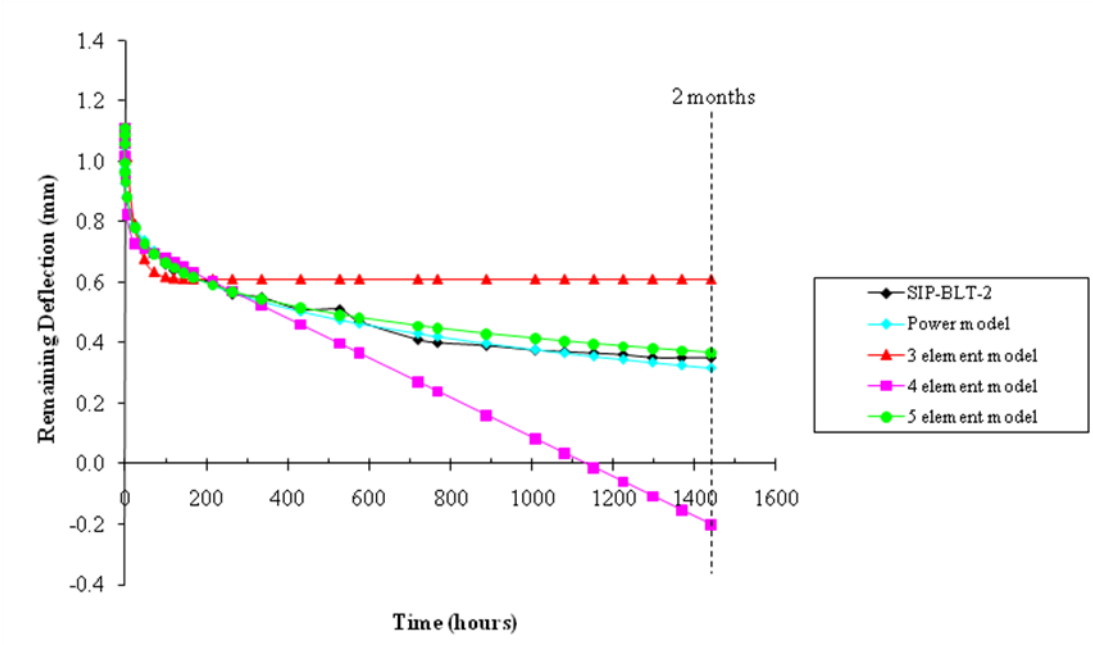

Figure 6.35: Unloaded two month test and predicted remaining deflections of SIP-BLT-2

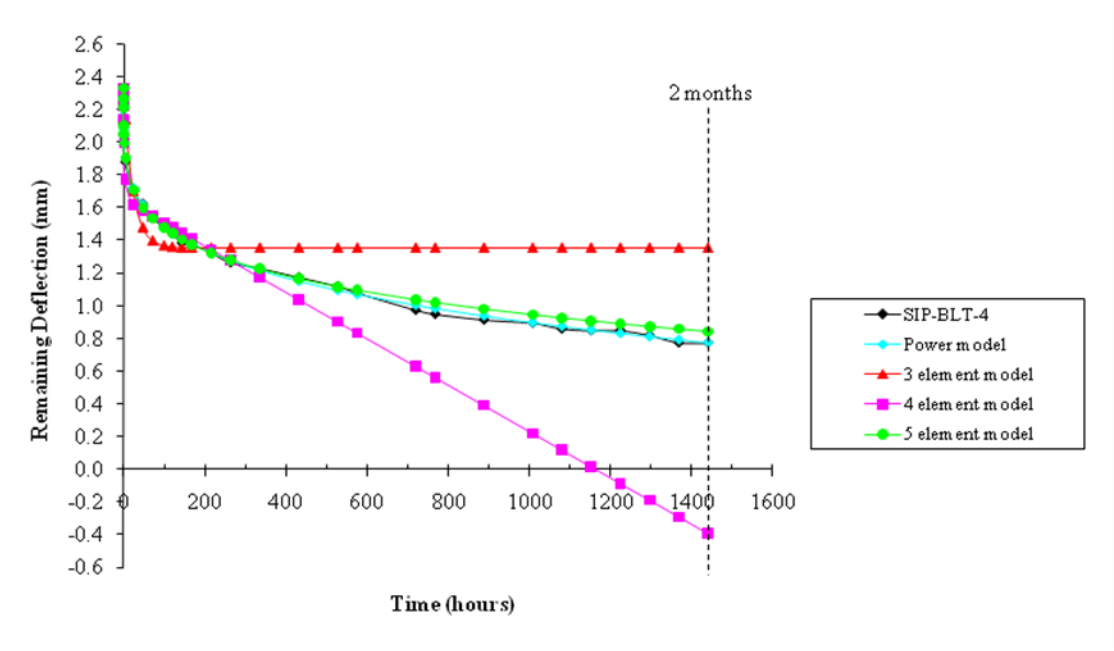

Figure 6.36: Unloaded two month test and predicted remaining deflections of SIP-BLT-4

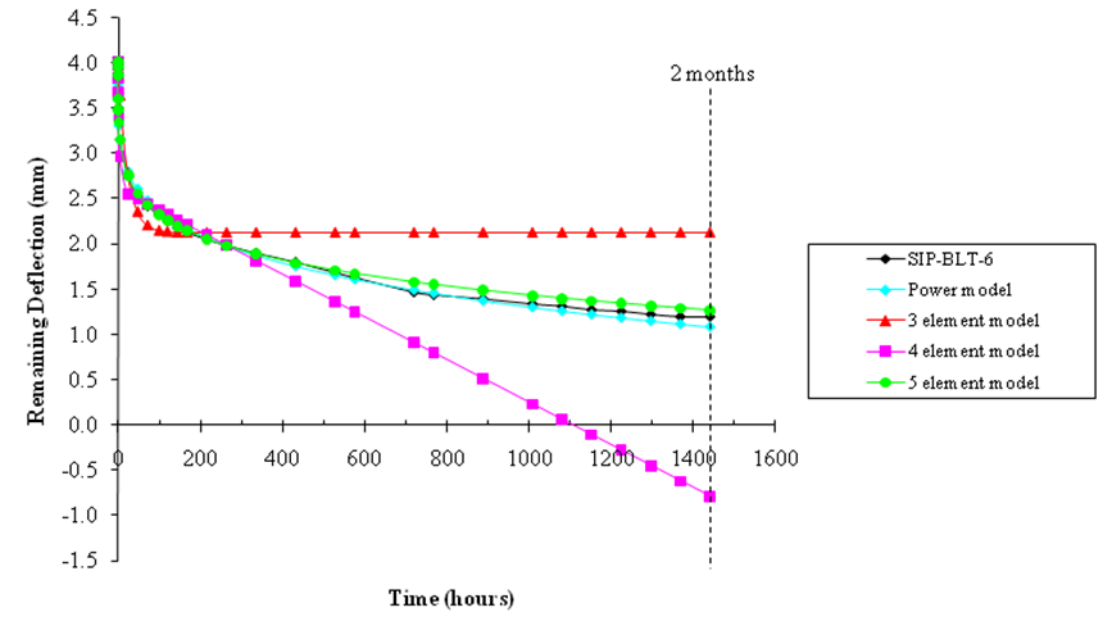

Figure 6.37: Unloaded two month test and predicted remaining deflections of SIP-BLT-6

6.4.5.2 Modified BS EN 1606 (BSI, 1996)

BS EN 1606 method has also been modified, equation 6.2 shows the recovery deflections at time time t (X_t).

$$X_t = X_0 - mt^b \tag{6.2}$$

where X_t is recovery deflection at time t (mm).

X_0 is initial recovery deflection (mm).

m and b are material constants.

The one month material constants are provided in Table 6.25. Figure 6.38 depicts the one month test results and the predictions. The agreement is favourably good with the least R^2 equals to 0.969.

Specimen	One month material constants		R^2
	m	b	
SIP-BLT-2 (10%)	0.1116	0.2823	0.987
SIP-BLT-4 (20%)	0.2076	0.2875	0.985
SIP-BLT-6 (30%)	0.4066	0.2905	0.969

Table 6.25: One month material constants

Figure 6.39 shows the comparison between the test results and the predictions using the material constants from the one month test results. It should be noted that the two month predictions from using the one month material constants has less conformity as shown in Figure 6.39.

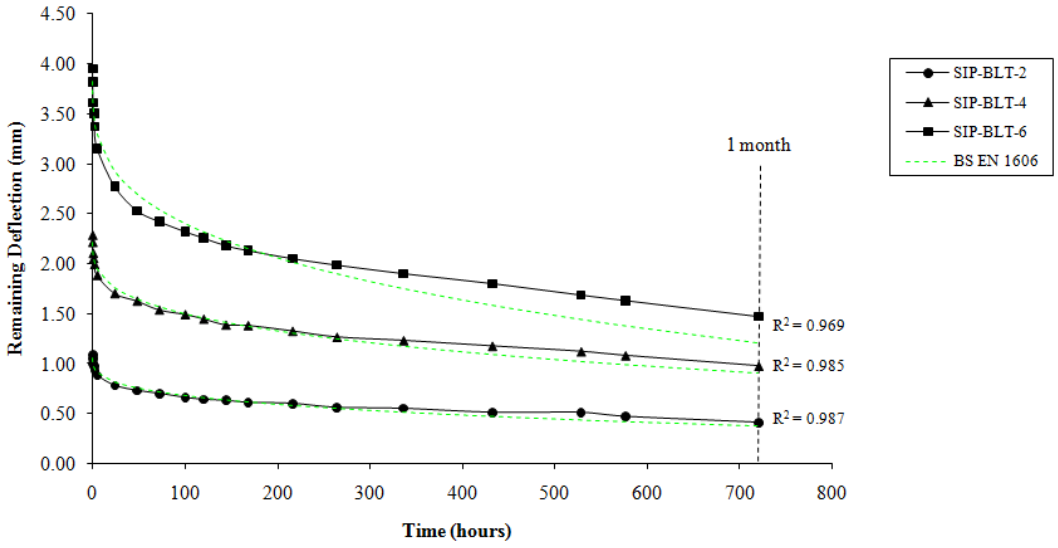

Figure 6.38: Unloaded one month test and predicted remaining deflections of SIP beams

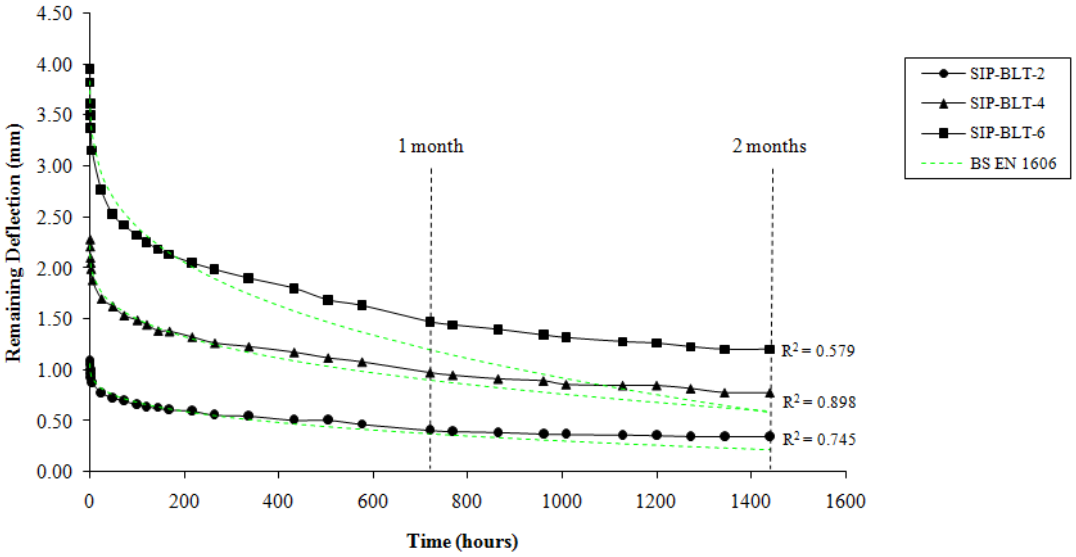

Figure 6.39: Unloaded two month test and predicted remaining deflections of SIP beams

6.4.5.3 Huang and Gibson's model

Figure 6.40 shows the remaining predictions and the experimental results by using the unloading creep parameters provided by Huang and Gibson (1989). It should be noted that the predictions by using Huang and Gibson's model overestimate the test results. This implies that it is unacceptable to use their unloading creep parameters to predict the test results.

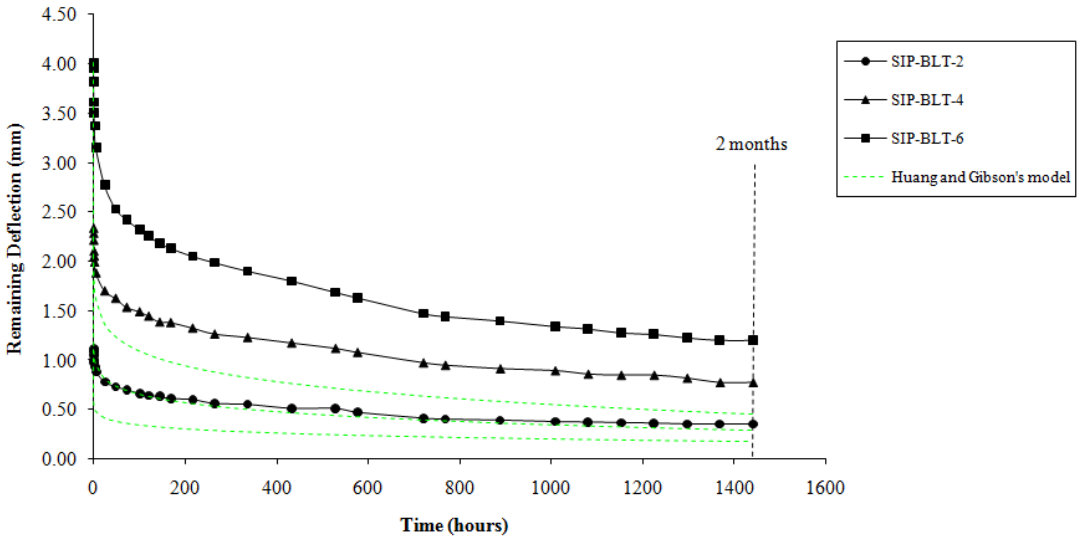

Figure 6.40: Unloaded two month test and predicted remaining deflections of SIP beams

6.4.6 Discussion of SIP beam creep and recovery

The power-law creep parameters obtained from the 1,000 hour creep OSB bending and double shear SIP numerical investigations and later used in the SIP beam predictions provide a good agreement with the three and five month creep test results.

The 1,000 hour creep parameters of the power creep compliance model and BS EN 1606 are adequately to describe the creep test results. Moreover, they can also be used to predict the creep behaviour in longer durations. Both methods are recommended to determine the creep parameters for prototype panels in order to predict the creep deflections for others in longer durations without undertaking numerical investigations on SIP constituents.

Three SIP beams were unloaded for two months, the initial recoveries were found equal to the initial creep deflections and at least 86.60% of the total deflections can be recovered. The modified power model does predict the remaining deflections after unloading very well. The one month recovery parameters can be used to predict and agree well with the two month remaining test results.

6.5 Long-term experimental investigation on SIPs with different joint designs

Although a number of investigations on long-term performance of SIPs are available, there is limited knowledge of long-term performances of SIPs with different joint designs. This section presents the three month experimental investigation on SIPs with different joint designs. The aims of this study were as follows:

- To investigate the creep behaviour of SIPs with different joint designs.
- To investigate the capability of the numerical parameters obtained from OSB and PUR.

- To determine which creep model can be used to predict the flexural mid-span creep deflections.

- To determine the ultimate loads of SIPs after subjected to the three month creep loads.

6.5.1 Experimental investigation of SIPs with different joint designs

All three panels (STP, SMC and SDC), as previously described in section 4.2, were subjected to the four-point bending creep tests for three months under ambient temperature and moisture content. The magnitudes of the applied loads (shown in Table 6.26) are the serviceability loads (at the deflection limits in accordance with BS 5268-2 (BSI, 2002), i.e. ℓ/333) which were found from the short-term test and retained as a constant through the entire testing period. The loads were applied to the panels through loading jacks supported by fixed steel box beams to the strong floor via steel rods. The magnitudes of the applied loads were monitored through the load cells. Figure 6.41 shows the layout of experimental apparatus for this test.

Specimen	**Applied Load (SLS)**	**Weight of supporting elements**	**Total load**	**Applied Load / Short-term Load Capacity**	**Instantaneous deflection**
	(kN)	**(kN)**	**(kN)**	**(%)**	**(mm)**
STP	2.90	0.25	3.15	15.8	4.13
SMC	3.10	0.33	3.43	17.3	3.90
SDC	8.00	0.29	8.29	20.6	4.02

Table 6.26: The applied loads and the instantaneous deflection of each SIP specimen

Figure 6.41: Experimental apparatus

The creep deflections of each SIP specimen together with temperature and humidity were then recorded at the following time intervals after loading: 0.1h, 0.2h, 0.5h, 1h, 2h, 4h, 8h, 24h and then every 24h. At each time of monitoring, the load was increased to its initial level and the set of deflection reading was then recorded. The temperature and humidity were in the range of 20°C ± 5°C and 40 ± 10%, respectively.

Figure 6.42 shows the creep movement of all specimens. The fluctuation in the creep curves may be again due to the variations of temperature and the humidity. However, the effects of temperature and humidity are again expected to be negligible. The creep test results of all SIP specimens are summarised in Table 6.27. The initial creep deflections of all panels are in the range of 3.90 - 4.13 mm and SDC has been found to have the lowest creep deflection at the same time.

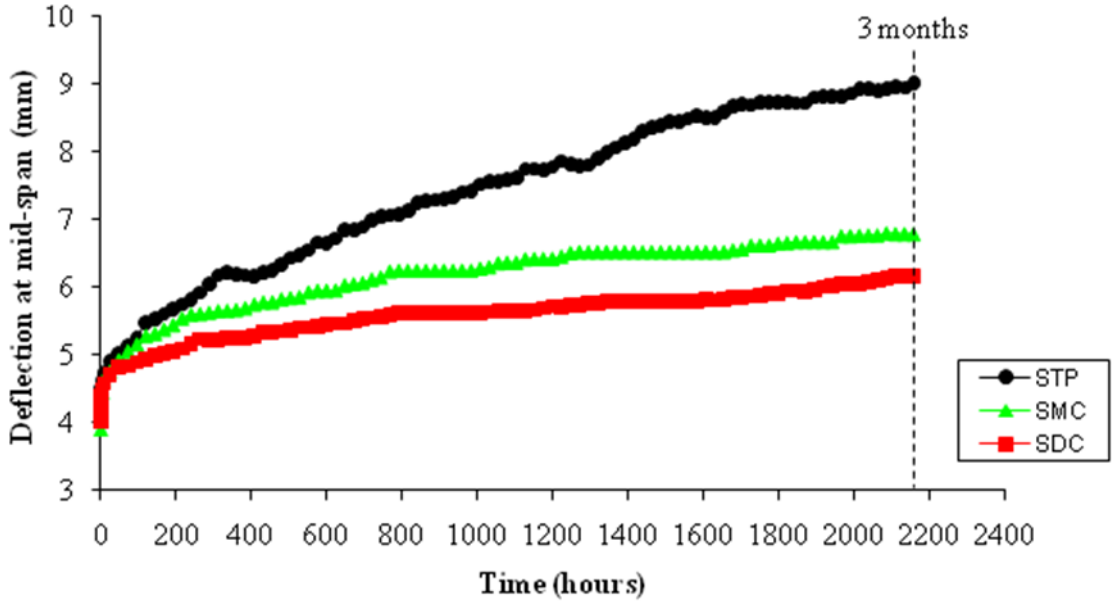

Figure 6.42: Three month creep displacements at the mid-span (Dial Gauge No.1)

Specimen	Instantaneous deflection (mm)	Three month deflection (mm)	Relative deflection[1]
STP	4.13	9.02	2.18
SMC	3.90	6.78	1.74
SDC	4.02	6.17	1.53

Note 1: Relative deflection equals to the three month deflection divided by the instantaneous deflection

Table 6.27: Creep test results of all SIP specimens

Other creep displacements at other locations i.e. at the edge and the end of the panel are shown in Figures 6.43 - 6.45. The creep deflections at the edge are in similar range to the mid-span. In addition, the creep displacements at the end of the panel (Dial Gauge Nos. 3 and 4) are small in comparison with the mid-span creep displacement. Consequently, no further investigations have been carried out.

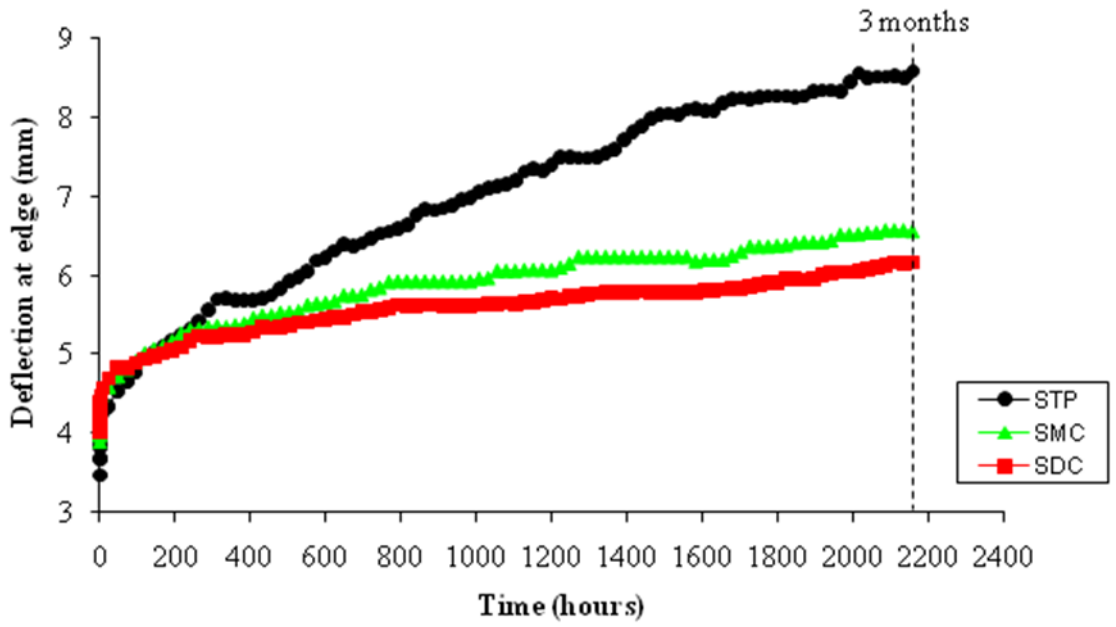

Figure 6.43: Three month vertical creep displacements at the edge (Dial Gauge No.2)

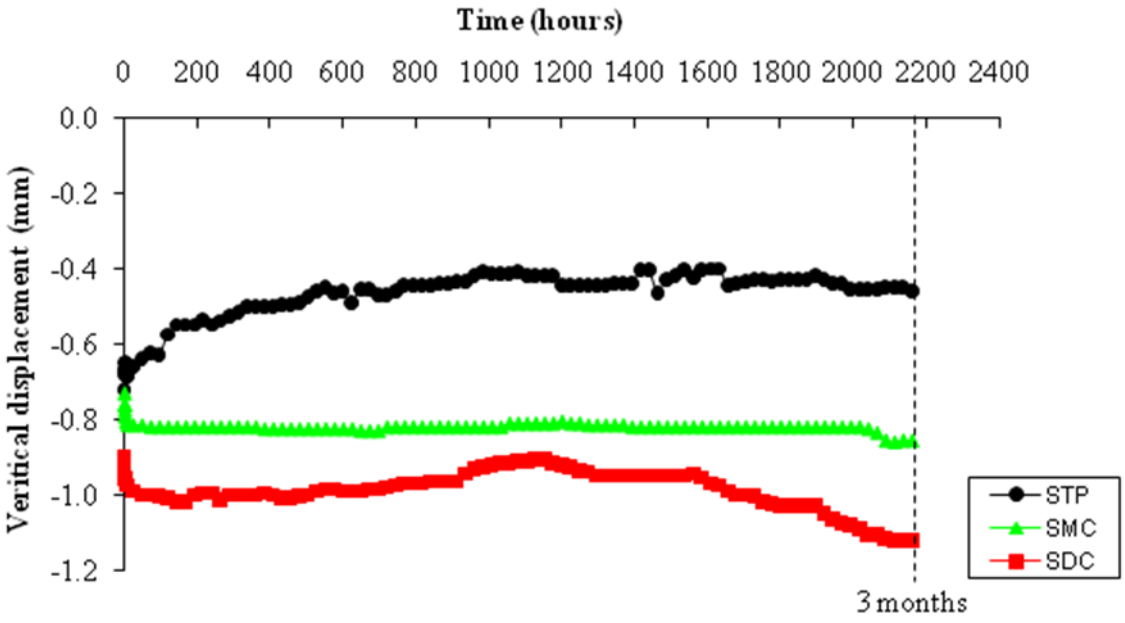

Figure 6.44: Three month vertical creep displacements (Dial Gauge No.3)

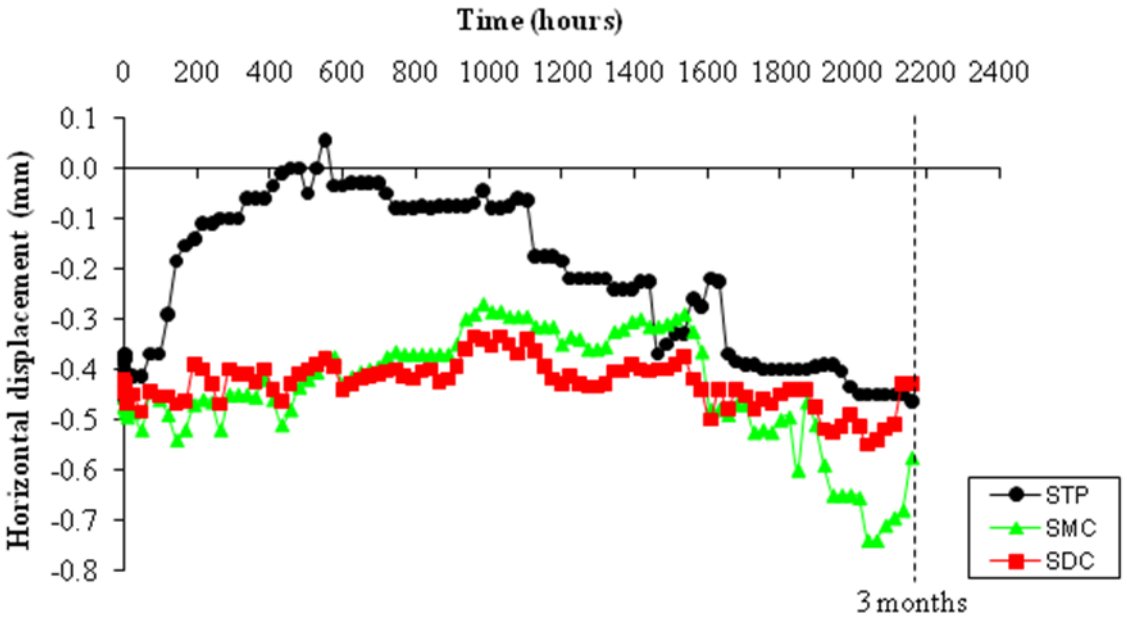

Figure 6.45: Three month horizontal creep displacements (Dial Gauge No.4)

6.5.2 Numerical investigation of long-term SIPs with different joint designs

STP, SMC and SDC numerical models are as same as previously detailed in the short-term investigation section 4.2. The OSB and PUR ABAQUS power-law creep parameters (Table 6.8 in section 6.4), are again employed and the creep predictions are compared to the experimental results for validation. It should be noted that the creep parameters of the header, the footer and the dimensional timber spline connection (all C16 timbers) had not been investigated and did not input in the numerical investigation. It is also expected that the creep parameter and the creep displacement of the C16 timber are smaller than the OSB and PUR.

Figures 6.46 - 6.48 show the comparison between the three month creep test results and the FEM predictions from the 1,000 hour creep parameters.

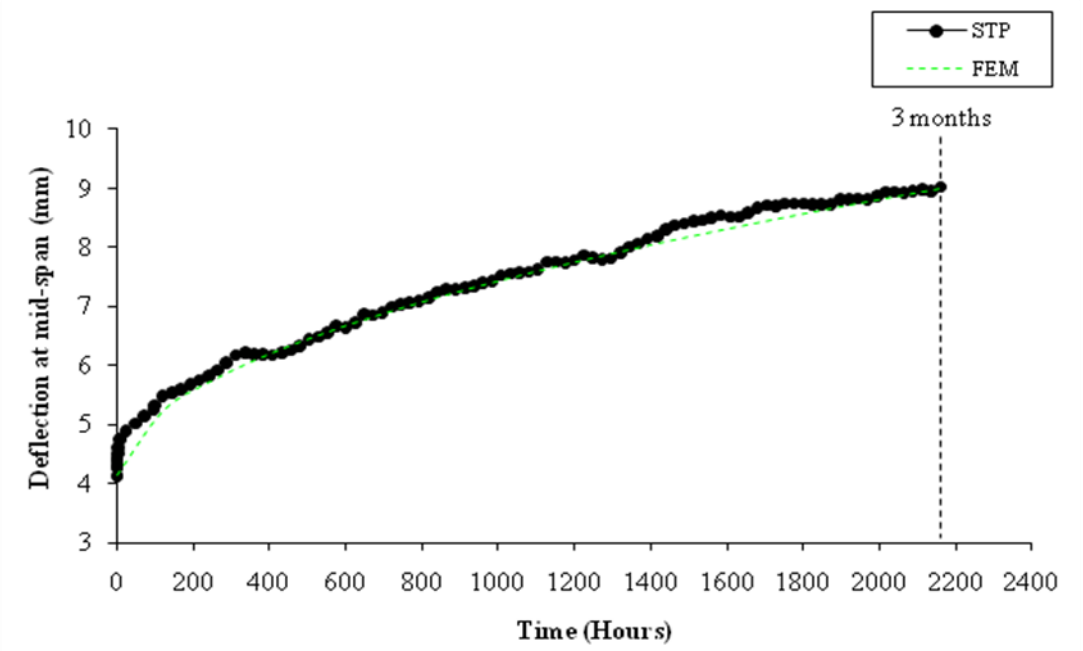

Figure 6.46: Three month comparison of STP

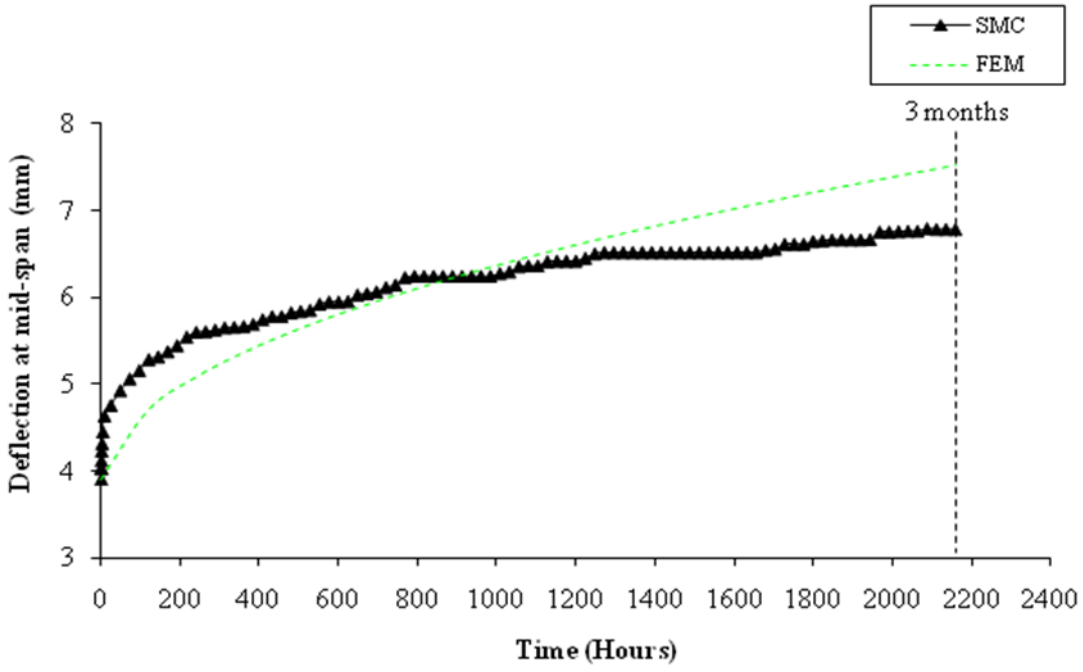

Figure 6.47: Three month comparison of SMC

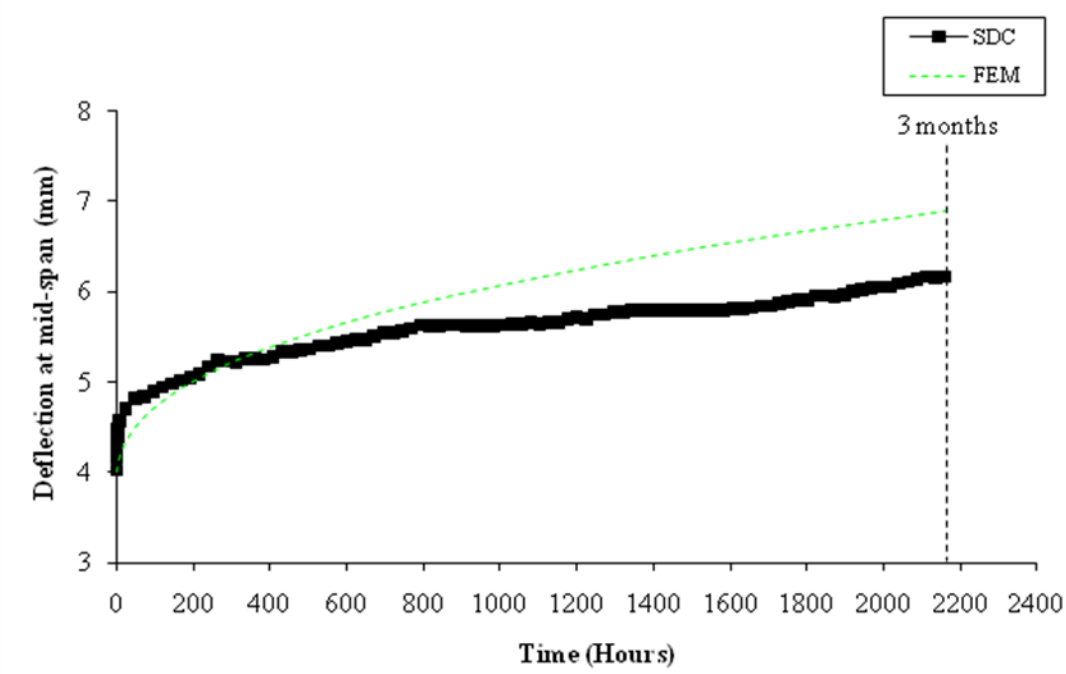

Figure 6.48: Three month comparison of SDC

Table 6.28 summarises the creep displacement test results with the FEM creep predictions. It is noted that the prediction of the STP is in extremely good agreement with the three month creep test results. SMC and SDC panels show less conformity but the predictions are acceptable that just overpredict by 11.73%.

Specimen	**Three month deflection**		**Difference**
	Test	**Prediction**	
	(mm)	**(mm)**	**(%)**
STP	9.02	8.99	-0.33%
SMC	6.78	7.52	9.80%
SDC	6.17	6.89	11.73%

Table 6.28: Comparison between the three month creep test results and FEM predictions

6.5.3 Creep prediction methods for SIPs with different joint designs

In this section, two creep prediction methods, which are found favourable in the previous section, are employed to verify their capabilities.

6.5.3.1 Taylor's models

Taylor's power and five element creep compliance models have been evaluated and found suitable to provide a good agreement with the SIP beams as previously presented in section 6.4. Table 6.29 shows the 1,000 hour creep parameters for the power and five element compliance models which found from the regression analysis. The agreement of the creep predictions with the 1,000 hour creep test results is extremely good with the least R^2 equal to 0.990 and 0.996, respectively.

Specimen	Model	A_1	A_2	A_3	A_4	R^2
STP	Power	0.031	0.422	N/A	N/A	0.990
	Five element	0.361	0.028	0.0062	0.560	0.996
SMC	Power	0.101	0.280	N/A	N/A	0.996
	Five element	0.268	0.0061	0.0582	0.328	0.997
SDC	Power	0.102	0.252	N/A	N/A	0.995
	Five element	0.198	0.031	0.0448	0.316	0.996

Table 6.29: 1,000 hour creep parameters from regression analysis

By using the 1,000 hour creep parameters, Figures 6.49 - 6.51 show the comparison between the three month creep test results and the two creep compliance model predictions.

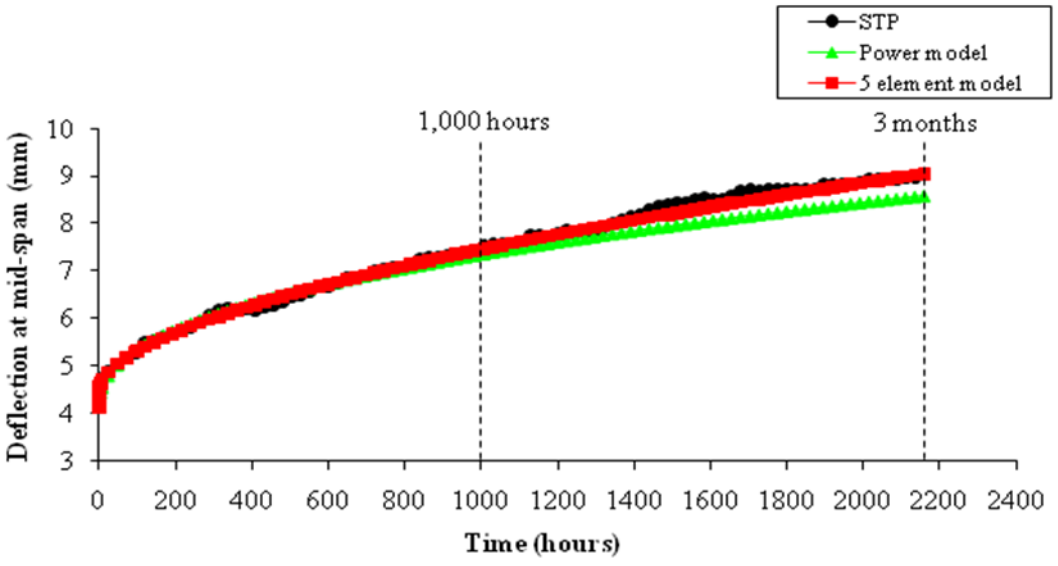

Figure 6.49: Three month experimental and predicted creep deflections of STP

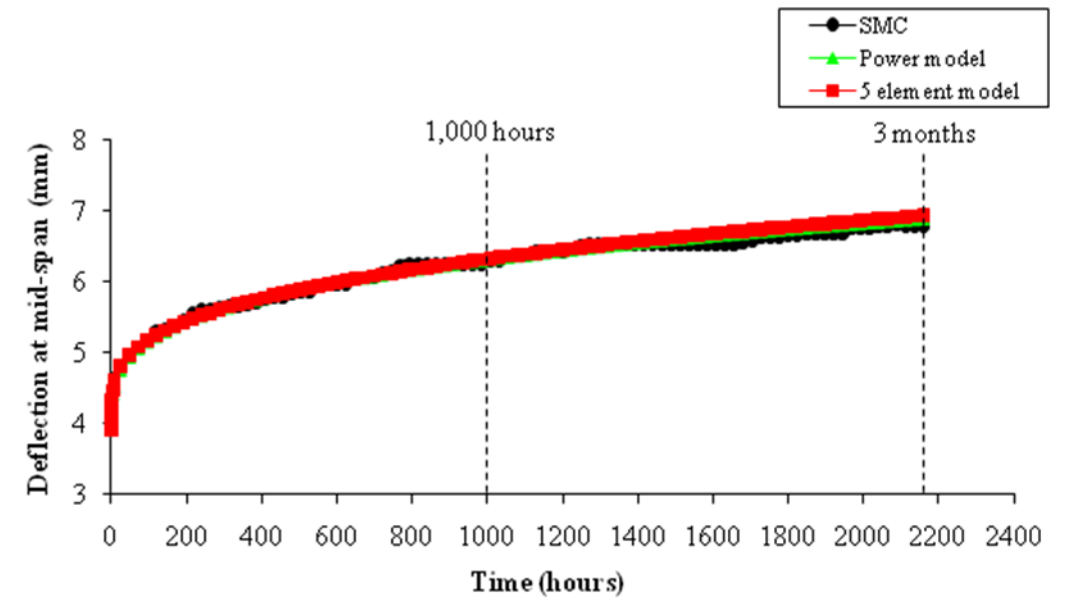

Figure 6.50: Three month experimental and predicted creep deflections of SMC

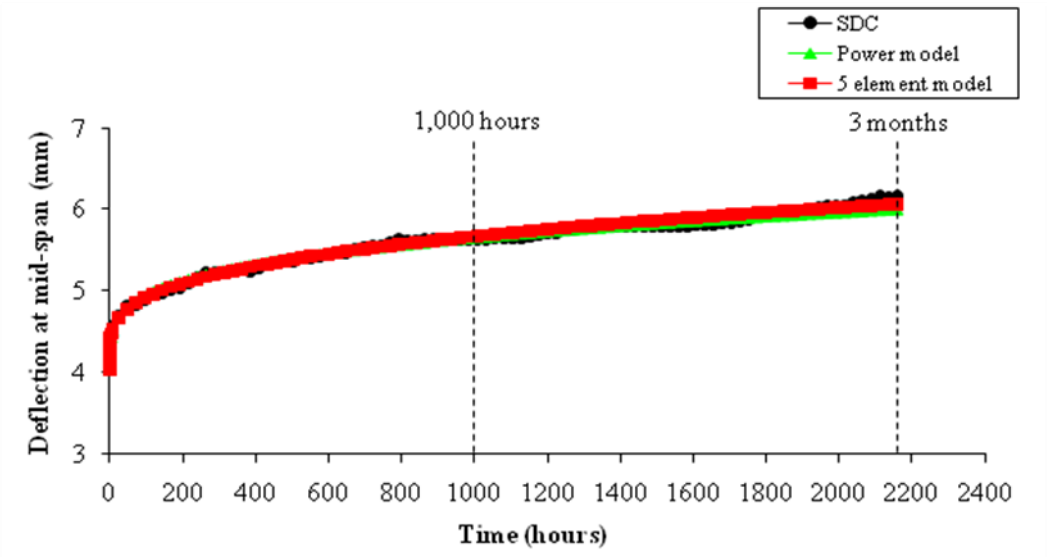

Figure 6.51: Three month experimental and predicted creep deflections of SDC

Table 6.30 summarises the creep deflections at the mid-span test results with the two creep compliance models. It is noted that the power and five element creep compliance model predictions agree very well with the three month creep test results with the least R^2 of 0.959.

Specimen	Model	Difference (%) to the three month test results
STP	Power	-4.88%
	Five element	0.27%
SMC	Power	1.54%
	Five element	-2.11%
SDC	Power	-2.75%
	Five element	-1.63%

Table 6.30: Creep deflection at the mid-span test results with the two creep models

Although five element model has been again found slightly better agreement than the power model, the power model is preferred as its simplicity principle and employing only two creep parameters.

6.5.3.2 BS EN 1606 (BSI, 1996)

The 1,000 hour material constants were determined using BS EN 1606 method and the predicted creep deflections are compared to the creep test results. The agreement is good which is summarised in Table 6.31.

Specimen	1,000 hour material constants		R^2
	m	b	
STP	0.3437	0.2801	0.973
SMC	0.2898	0.3111	0.990
SDC	0.2542	0.2823	0.995

Table 6.31: 1,000 hour material constants from BS EN 1606 method

By using the 1,000 hour creep parameters, Figure 6.52 shows the comparison between the three month creep test results.

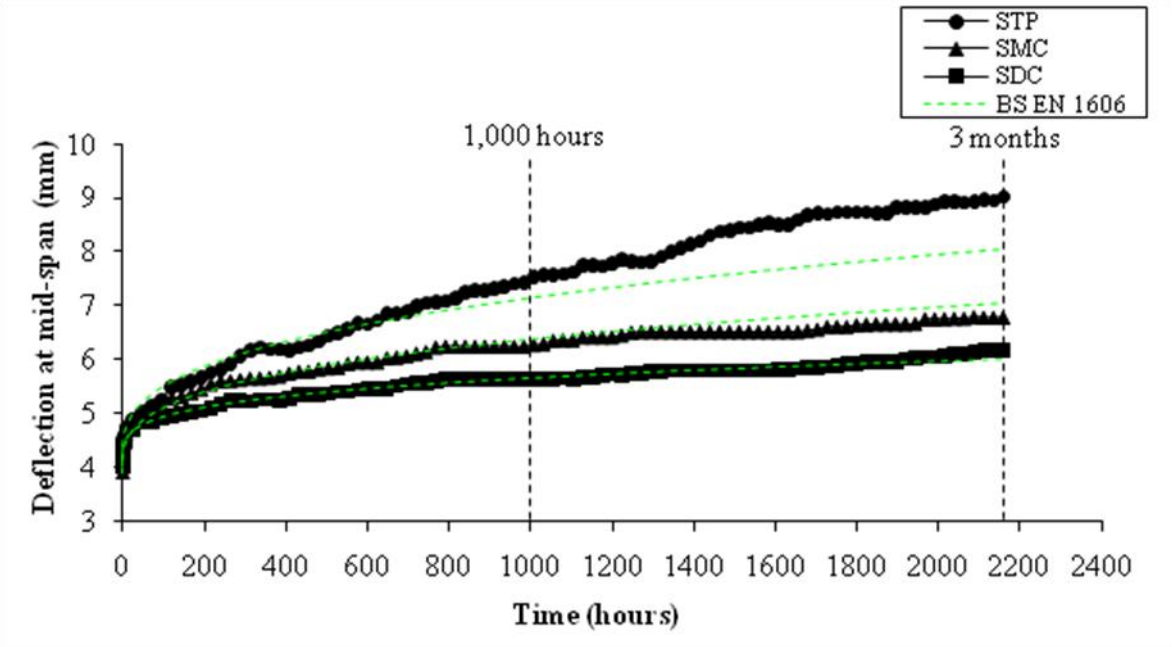

Figure 6.52: Three month experimental and predicted creep deflections

It should be noted that the three month predictions from using the 1,000 hour material constants agree well with the three month creep test results as summarised in Table 6.32. Nevertheless, this BS EN 1606 method provides the lesser agreement in comparison to the power model as previously analysed in section 6.5.3.2.

Specimen	Difference (%) to the three month test results
STP	-10.75%
SMC	4.10%
SDC	-2.55%

Table 6.32: Creep deflection at the mid-span test results with the two creep models

6.5.4 Ultimate load after the creep experiment

At the end of the three month creep test, the applied loads were increased until failure. The ultimate loads were then recorded and compared with the short-term test ultimate loads as summarised in Table 6.33. The failure loads are within 3-7% of their short-term values, and hence there is no significant strength reduction as a result of the long-term loading.

Specimen	Mean short-term ultimate load	Ultimate load at 3 months	Difference	Failure mode
	(kN)	(kN)	(%)	
STP	19.32	18.50	-4.24	Debonding
SMC	19.82	20.50	3.43	
SDC	40.32	43.0	6.64	

Table 6.33: Ultimate loads at 3 months

All SIP specimens failed due to the inner core de-bonding from the top outer face and the timber section as shown in Figure 6.53. The failure mode of STP and SMC specimens is as same as their short-term loading tests. However, the failure mode of SDC is due to the debonding which in different to the short-term test (flexure-shear failure mode). The different in the failure mode is possible as found in the numerical investigation that the debonding failure mode is one of the initial failure modes.

(a) STP

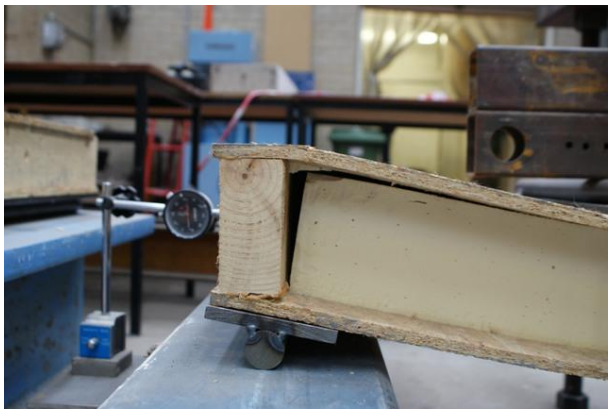

(b) SMC

(c) SDC

Figure 6.53: Debonding failure

6.5.5 60 year SIP performances with different joint designs

SIP manufacturers claim that SIPs will be fit for their intended use for 60 years when they are installed and maintained to the standard as detailed in third-party approval body certificates. Further numerical investigations have been carried out on SIPs with different joint designs subjected to uniformed distributed loads for 60 years.

Nine numerical models with a standard size panel of 1200 mm width and three different lengths without joint (STP) and two different joint designs (SMC and SDC) are presented in Table 6.34. They were all subjected to the uniform distributed loads on simply supported condition to its

own self-weight and 2 kN/m^2 imposed live load for Category A3 (bedrooms in hotels and motels, hospital wards and toilet areas) in accordance with National Annex to BS EN 1995 Part 1 (BSI, 2002). This investigation is purely on the panels with different joint designed; the header and footer were not therefore considered. The principle to model numerical specimens together with their material properties are as same as detailed in previous sections.

Specimen	Width (mm)	Length (mm)	Joint Details
STP-1200x2400	1200	2400	-
STP-1200x3600		3600	
STP-1200x4800		4800	
SMC-1200x2400		2400	100 mm Mini-SIP joint
SMC-1200x3600		3600	
SMC-1200x4800		4800	
SDC-1200x2400		2400	47 mm C16 joint
SDC-1200x3600		3600	
SDC-1200x4800		4800	

Table 6.34: Panel specimen details

Figures 6.54 - 6.56 and Table 6.35 present the FEM predictions for 60 year duration. As expected, SDC specimens reveal the better long-term performance with the lowest deflection at mid-span. The long-term deflections of STP and SMC have been found in similar range. The long-term deflection also depends upon the span length, in which higher the span length, higher the deflection.

Although the maximum relative deflection at 60 year duration is 15.06 time of the instantaneous deflection (shown in Table 6.35), this theoretical large value does not expect to be reached. This is due to the fact that the panel will be unloaded at some stages during its service life and some deflections will be recovered.

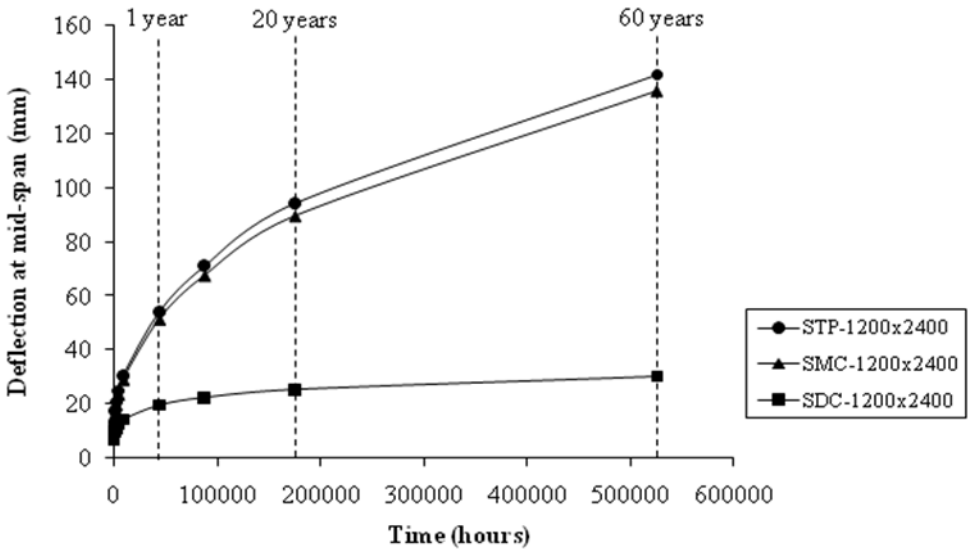

Figure 6.54: Predicted deflections for 2400 mm SIPs with different joint designs

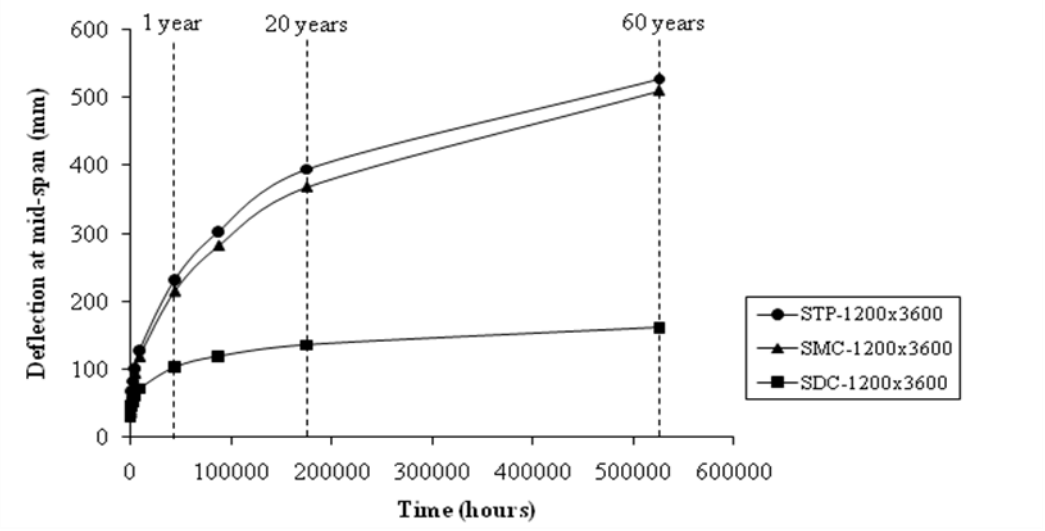

Figure 6.55: Predicted deflections for 3600 mm SIPs with different joint designs

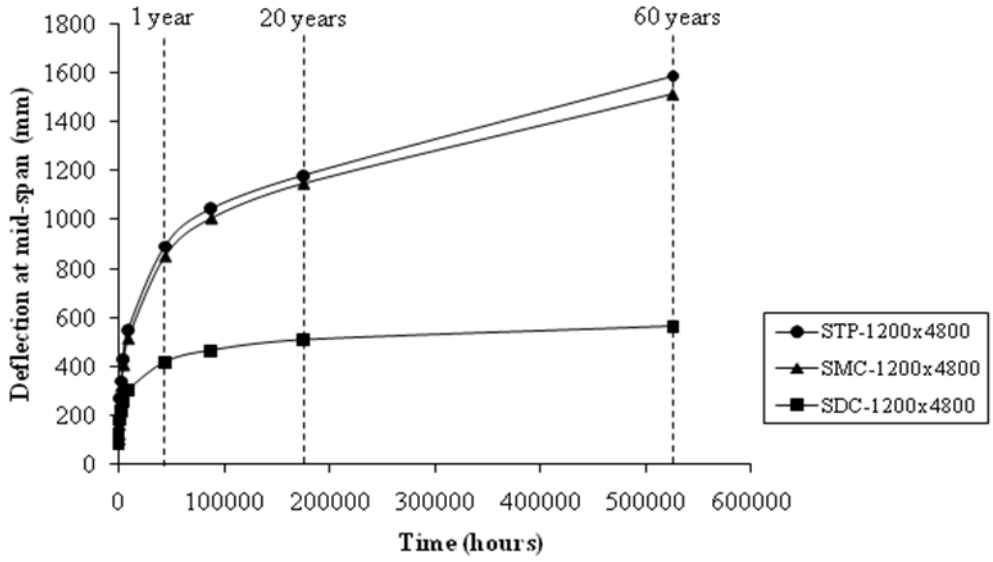

Figure 6.56: Predicted deflections for 4800 mm SIPs with different joint designs

6.5.6 Discussion of SIPs with different joint designs

Four-point bending creep tests were conducted to investigate the creep behaviour of typical panel (STP), mini-sip connection panel (SMC) and dimensional timber connection panel (SDC). The initial creep deflections of all panels are in the range of 3.90 – 4.13 mm and SDC has been found to have the lowest creep deflection at the same time.

The ABAQUS power-law creep parameters (Table 6.8 in section 6.4), are employed and the creep prediction for STP is in extremely good agreement with the three month creep test results. SMC and SDC panels show less conformity but the predictions are acceptable that just overpredicted by 11.73%.

Without employing numerical investigations, power model and BS EN 1606 methods provide good agreement between the creep test results and the predictions. It has been found that 1,000 hour parameters are adequate to provide good agreement to SIP physical test and can be used to predict the creep behaviour in a longer duration.

Specimen		Duration					
		Initial	**1,000 hours**	**1 year**	**10 years**	**20 years**	**60 years**
STP-1200x2400	Deflection (mm)	10.89	17.58	30.64	71.01	94.19	141.64
	Relative Deflection	1.00	1.61	2.81	6.52	8.65	13.00
STP-1200x3600	Deflection (mm)	38.01	67.93	127.29	302.50	393.67	526.44
	Relative Deflection	1.00	1.79	3.35	7.96	10.36	13.85
STP-1200x4800	Deflection (mm)	105.28	269.64	547.52	1043.83	1180.45	1585.68
	Relative Deflection	1.00	2.56	5.20	9.91	11.21	15.06
SMC-1200x2400	Deflection (mm)	10.51	16.77	29.05	67.34	89.37	135.52
	Relative Deflection	1.00	1.60	2.76	6.41	8.50	12.89
SMC-1200x3600	Deflection (mm)	36.31	63.80	118.47	281.54	367.82	509.28
	Relative Deflection	1.00	1.76	3.26	7.75	10.13	14.03
SMC-1200x4800	Deflection (mm)	101.26	251.87	511.57	1003.21	1145.13	1509.84
	Relative Deflection	1.00	2.49	5.05	9.91	11.31	14.91
SDC-1200x2400	Deflection (mm)	7.12	9.98	14.25	22.41	25.38	30.16
	Relative Deflection	1.00	1.40	2.00	3.15	3.57	4.24
SDC-1200x3600	Deflection (mm)	29.25	45.84	71.14	118.93	135.70	161.25
	Relative Deflection	1.00	1.57	2.43	4.07	4.64	5.51
SDC-1200x4800	Deflection (mm)	86.47	180.76	301.68	464.44	506.96	562.11
	Relative Deflection	1.00	2.09	3.49	5.37	5.86	6.50

Table 6.35: Creep deflections of different numerical models

At the end of the creep test, the applied loads were increased until the panels failed. The failure loads were within 3-7% of their short-term values, and hence there was no significant strength reduction as a result of the long-term loading.

Further numerical investigations were carried out on SIPs with different joint designs subjected to uniformed distributed loads for 60 years. SDC specimens again reveal the better long-term

performance with the lowest deflection at mid-span. The long-term deflections of STP and SMC have been found in similar range. In addition, the deflection also depends upon the span length in which higher the span length, higher the deflection.

6.6 Summary

This chapter presented experimental investigations of SIP constituents (OSB and PUR) and SIPs as beams and panels under long-term loads. The investigation began with OSB and PUR to determine the power-law creep parameters and found these parameters provided the creep predictions which agreed well with the SIP beams and panels.

Without employing numerical investigations, power model and BS EN 1606 methods provide good agreement between the creep test results and predictions. It has been found that 1,000 hour parameters are adequate to provide good agreement to SIP physical test.

As expected, SDC specimens reveal the better long-term performance with the lowest deflection at mid-span. The displacements at panel edges are small and can be negligible in engineering practice. At the end of the creep test, the applied loads were increased until the panels failed, there was no significant strength reduction as a result of the long-term loading.

Further numerical investigations were carried out on SIPs with different joint designs subjected to uniformed distributed loads for 60 years. The maximum relative deflection at 60 year duration is 15.06 time of the instantaneous deflection (from STP investigation), this theoretical large value does not expect to be reached. This is due to the fact that the panel will be unloaded at some stages during its service life and some deflections will be recovered.

CHAPTER SEVEN

CONCLUSIONS AND RECOMMENDATIONS

In this chapter, the main contributions achieved and conclusions drawn from the experimental and numerical findings of this doctoral investigation are presented. The implications for design practice and recommendations for future work are also outlined.

7.1 Contribution to knowledge

Various experimental and numerical investigations on structural performance of SIPs were carried out. The contributions of this doctoral study can be summarised as follows:

- A new set of test data pool of the structural performance of SIPs under both short and long-term loadings were established; details on test set-up, testing methods and instrumentations were well documented.

- The typical failure of SIPs under transverse load is usually governed by the stiffness for normal span length.

- The ranking (high to low) of the panel stiffness found from both experimental and numerical investigations is panel with dimensional timber connection (SDC), panel with mini-sip connection (SMC) and typical panel (STP), respectively.

- A numerical model has been established and validated by the experimental results. The numerical model can accurately predict the onset of failure load and the failure mode by using the maximum stress criterion for OSB and the linear interactive failure criterion for debonding of the PUR.

- An interactive failure load curve between axial and transverse loadings has been developed by carrying out a parametric analysis. A linear interaction model appears to be a good representation of such a failure load curve for SIPs with openings. The most interesting finding is that SIPs have a high degree of capacity reserve since the design load allowance is well below the onset of failure load.

- Four-point bending creep tests were conducted to investigate the creep behaviour of a typical panel (STP), mini-sip connection panel (SMC) and dimensional timber connection panel (SDC). The initial creep deflections of all panels are in the range of 3.90 - 4.13 mm and SDC has been found to have the lowest creep deflection at the same duration. At the end of the three month creep test, the applied loads were increased until failure. The failure loads have been found within 3-7% of their short-term values, and hence there is no significant strength reduction as a result of the long-term loading.

- Without employing numerical investigations, power model and BS EN 1606 methods provide good agreement between the creep test results and the predictions. It has been found that 1,000 hour parameters are adequate to provide good agreement to the SIP physical test and can be used to predict the creep behaviour in a longer duration.

- Numerical investigations were carried out on SIPs with different joint designs subjected to uniformed distributed loads for 60 years. The SDC panel again reveals the better long-term performance with the lowest deflection at mid-span. The long-term deflections of STP and SMC panels have been found in similar range. In addition, the deflection also depends upon the span length where higher the span length, higher the deflection. The maximum relative deflection at 60 year duration is 15.06 times that of the instantaneous deflection (from STP investigation), this theoretical large value is not

expected to be reached. This is due to the fact that the panel will be unloaded at some stages during its service life and some deflections will be recovered.

7.2 Implications for design practice

This doctoral research has made a number of findings which can be used to inform the design practice for SIPs, i.e.:

- Allen's analytical method (Allen, 1969) has been found to be favourable in designing SIPs without any joints (STP) that are subjected to a transverse load; whilst TR 019 analytical method (EOTA, 2005) is more suitable for SIPs with dimensional timber joints (SDC).

- When SIPs are subjected to transverse loads, it has been found that the deflection is more sensitive to the shear modulus (G) of the inner core than the material properties of the OSB outer faces and the modulus of elasticity (E) of the inner core. The shear modulus obtained from the bending test can be used to provide a better prediction on the deflection of SIPs as is compared to the same value obtained from the single and double shear tests. Therefore, it is recommended to follow the procedures provided by BS EN 14509 (BSI, 2006) to carry out the bending test and obtain the shear modulus.

- The horizontal displacement is negligible with less concern in engineering practice in comparison with the vertical displacement when SIPs are subjected to transverse load. This displacement can be ignored in the SIP design.

- To enable the SIPs to gain the optimum axial capacity, appropriate assembling provisions should be made or a tight dimensional tolerance control should be exercised

to encourage both facial panels to endure the bearing load. To that end, a flush bearing surface should be provided prior to installing the panel. One of the viable options is to use the proprietary gap filling adhesive to even out the surface before the installation of panels.

- It is suitable to design SIPs subjected to combined axial and racking loadings by employing EC5 design code (BSI, 2004). SIPs have been found to better perform in the combined axial and racking loadings than the stud wall.

- There is currently no analytical method to design SIPs subjected to combined axial, racking and transverse loadings simultaneously. Finite element analysis should be carried out to assist the design. Likewise, panels with openings should also be designed by using the finite element analysis due to the lack of analytical analysis available.

- To determine the long-term behaviour of SIPs, the power model (Taylor et al., 1997) and BS EN 1606 (BSI, 1996) methods are suitable to predict the creep deflection of longer duration from a short length of observation, e.g. 1000 hours.

7.3 Recommendations for future work

This doctoral research highlights a number of issues which require further investigations. These recommendations are as follows:

- Although the research findings of SIPs in terms of structural performance can be applicable to other SIP constituent materials, it is recommended to examine other type of SIPs to establish the applicability of the conclusions obtained from this research program.

- Different temperatures between internal and external environments can induce stresses and deflections. Davies (1987) emphasises these temperature stresses and deflections are sufficiently large and cannot be ignored in the design consideration. Limited publication is currently available in this field.

- SIP system has been reported to perform well in various natural disasters, which are the earthquakes in Kobe Japan and North Ridge, hurricane Andrew, a Colorado tornado, a Portland gas explosion and an Omaha fire (all in the USA). However, their dynamic response behaviour research is limited.

- This research only focuses on a rectangular opening with rectangular in the middle with a 600 x 1200 mm^2 opening area (25% of the panel area). However, the opening such as window or door can be placed in any other locations of the panel. Moreover, different numbers, sizes and shapes can also be cut on the panel. More research is required to further quantify the effects of different opening combinations.

- Long-term SIP performance should be further researched on other SIP constituent materials with different span lengths and also different environmental impacts such as moisture attack and UV exposure.

- It should be noted that the FEM investigation in this research mainly focuses on the structural response of SIPs up to the onset of failure. The modelling of the damage evolution has not been included due to time constraints. However, the initial failure mode, which is obtained from this numerical investigation, can be adequately used to predict the ultimate failure mode of SIP as a beam or a panel. Further research should

incorporate the damage evolution in the numerical investigation in order to investigate the structural performance after the initial failure load.

- The performance and design of SIP structures is also worth studying as part of a system where the effect of roof-wall and floor-wall connections can be investigated.

REFERENCES

ABAQUS (2010) **ABAQUS Version 6.9 Documentation.** http://bbdoc.bham.ac.uk:2080/v6.9 [Accessed May 12th 2010]

Allen, H. G. (1969) **Analysis and Design of Structural Sandwich Panels.** Oxford, Pergamon Press.

Alwin, H. Z. (2002), **Development of a method to analyze structural insulated panels under transverse loading**. Master Thesis, Washington State University.

American Plywood Association or The Engineered Wood Association (APA) (1993) **Design and Fabrication of Plywood Sandwich Panels.** Supplement No. 4. Tacoma, WA.

American Plywood Association or The Engineered Wood Association (APA) (2006) **APA Report T2006P-33: Standardization Testing of Structural Insulated Panels (SIPs) - for The Structural Insulated Panel Association**. Gig Harbor, Washington.

American Plywood Association or The Engineered Wood Association (APA) (2007) **APA Report No. T2007P-40: Standardization Testing of Structural Insulated Panels (SIPs) - BASF Polyurethane**. Tacoma,Washington.

American Plywood Association or The Engineered Wood Association (APA) (2008) **APA Report T2008P-77: Standardization Testing of Structural Insulated Panels (SIPs) - Extruded Polystyrene (XPS) for The Structural Insulated Panel Association**. Gig Harbor, Washington.

American Plywood Association or The Engineered Wood Association (APA) and Structural Insulated Panel Association (SIPA) (2007) **Structural Insulated Panels – Product Guide.**

American Plywood Association or The Engineered Wood Association (APA) (2008) **ANSI/APA PRS-610.1 Standard for Performance-Rated Structural Insulated Panels in Wall Applications.** Draft 4 December 2008.

Apetre, N. A., Sankar, B. V. and Ambur, D. R. (2008) **Analytical Modeling of Sandwich Beams with Functionally Graded Core**. Journal of Sandwich Structures and Materials, Volume 10, January 2008 pp. 53-74.

ASTM (American Society of Testing and Material) (2005), ASTM E72-05. **Standard Test Methods of Conducting Strength Tests of Panels for Building Construction**. West Conshohocken, PA.

ASTM (American Society of Testing and Material) (2010), ASTM D2559-10a. **Standard Specification for Adhesives for Bonded Structural Wood Products for Use Under Exterior Exposure Conditions**. West Conshohocken, PA.

BBA (British Board of Agrément) (2004) BBA No. 04/4099, **SIPs Eco Panels - Structural Insulated Panels Scotland**.

BBA (British Board of Agrément) (2006) BBA No. 06/4312, S**IP Building System - SIP loadbearing wall and roof panels - SIP Building Systems Ltd**.

BBA (British Board of Agrément) (2006) BBA No. 06/4374, **Hemsec SIPs panels - SIP loadbearing wall and roof panels - Hemsec Sips Ltd**.

BBA (British Board of Agrément) (2007) www.bbacerts.co.uk [Accessed December 12th 2007]

BBA (British Board of Agrément) (2009) BBA No. 09/S043, **i-S Manufacturing Ltd**.

Berner, K. and Pfaff, U. (2005) **Openings in sandwich panels**. Institute for Sandwich technology, Mainz.

Bregulla, J. (2003) **Investigation into the fire and racking performance of structuralsandwich panel walls - a methodology to assess loadbearing sandwich panel walls in fire**. PhD thesis, University of Surrey.

Bregulla, J. and Enjily, V. (2004) **An introduction to building with Structural Insulated Panels (SIPs).** IP 13/04, Building Research Establishment.

British Standards Institution (BSI) (1987), BS 476-21. **Fire tests on building materials and structures - Methods for determination of the fire resistance of loadbearing elements of construction**. London.

British Standards Institution (BSI) (1997), BS EN 594. **Timber Structures - Test methods - Racking strength and stiffness of timber frame wall panels**. London.

British Standards Institution (BSI) (1997), BS EN 1606. **Thermal insulating products for building applications - Determination of compressive creep.** London.

British Standards Institution (BSI) (1997), BS EN 12090. **Thermal insulating products for building applications - Determination of shear behaviour.** London.

British Standards Institution (BSI) (2001), BS EN 12369-1. **Wood-based panels - Characteristic values for structural design. Part 1: OSB, particleboards and fibreboards**. London.

British Standards Institution (BSI) (2002), BS 5268-2. **Structural use of timber - Part 2: Code of practice for permissible stress design, materials and workmanship.** London.

British Standards Institution (BSI) (2002), BS EN 1991-1-1. **Eurocode 1: Actions on structures - General actions - Densities, self-weight, imposed loads for buildings**. London.

British Standards Institution (BSI) (2003), BS EN 1991-1-1. **Eurocode 1: Actions on structures - General actions - Densities, self-weight, imposed loads for buildings**. London.

British Standards Institution (BSI) (2004), BS EN 789. **Timber structures - Test methods - Determination of mechanical properties of wood based panels**. London.

British Standards Institution (BSI) (2004), BS EN 1995-1-1. **Eurocode 5: Design of timber structures - Part 1-1: General – Common rules and rules for buildings**. London.

British Standards Institution (BSI) (2005), BS EN 1993-1-1. **Eurocode 3: Design of steel structures - Design of steel structures - General rules and rules for buildings**. London.

British Standards Institution (BSI) (2006), BS EN 300. **Oriented strand boards (OSB). Definitions, classification and specifications.** London.

British Standards Institution (BSI) (2006), BS EN 14509. **Self-supporting double skin metal faced insulating panels – Factory made products – Specifications.** London.

ISO (International Organization for Standardization) (2011), ISO 22452. **Timber structures - Structural insulated panel walls - Test methods.**

Burton, W. S. and Noor, A. K. (1995) **Assessment of computational models for sandwich panels and shells.** Computer methods in applied mechanics and engineering, 124 (1995), pp. 125-151.

Caprino, G. and Langelan, A. (2000) **Study of a Three-Point Bending Specimen for Shear Characterization of Sandwich Cores**, Journal of Composite Materials, Vol. 34, No. 9, 2000, pp. 791-814.

Carradine, D. M., Woeste, F. E. and Dolan, J. D. (2004) **Utilising diaphragm action for wind load design of timber frame and structural insulated panel buildings.** Forest Products Journal, Vol.54 No.5, pp. 73-80.

Case J., Chilver, A. H. And Ross, C. T. F. (1999) **Strength of Materials and Structures**. 4th Edition, Butterworth-Heinemann, Oxford.

Cobb, F. (2009) **Structural Engineer's Pocket Book.** 2nd Edition, Elsevier Ltd.

Communities and Local Government (2008) **BD 2503 Innovative Construction Products and Techniques** www.communities.gov.uk [Accessed January 12th 2011]

Dai, J. and Hahn, H.T. (2003), **Flexural behavior of sandwich beams fabricated by vacuum assisted resin transfer molding**. Composite Structures, Volume 61, Issue 3, August 2003, pp. 247-253.

Davies, J. M. (1987) **Design Criteria for Structural Sandwich Panels.** The Structural Engineer, 65A(12), pp. 435-441.

Davies, J.M. (1993) **Sandwich Panels**. Thin-Walled Structures, Vol. 16, pp. 179-198.

Davies, J. M. (2001) **Lightweight Sandwich Construction**, Blackwell Science, Oxford.

DCLG (Department for Communities and Local Government) (2010) **The performance in fire of structural insulated panels - BD2710**. December 2010, DCLG Publications.

Del Coz Diaz, J. J., García Nietob, P. J., Alvarez Rabanala, P. J. and Betegon Biempicaa, C. (2008) **Finite element analysis of thin-walled composite two-span wood-based loadbearing stressed skin roof panels and experimental validation**. Thin-Walled Structures, Volume 46, Issue 3, March 2008, pp. 276-289.

Diab (2010), Sandwich Concept. Diab Sandwich Handbook,

www.diabgroup.com/europe/literature/e_pdf_files/man_pdf/sandwich_hb.pdf

[Accessed October 10th 2010]

Dinwoodie, J. M. And Enjily, V. (2003) **Wood-based panels: Oriented Strand Board (OSB)**, Digest 477 Part 1, Building Research Establishment.

ErgoHome Ltd (2010) www.ergohome.co.uk [Accessed December 10th 2010]

Esvelt, J. J. (1999) **Behavior of Structural Insulated Panels under Transverse Loading**, Master Thesis, Washington State University.

ECCS (European Convention for Constructional Steelwork) (2001) **European Recommendations for Sandwich Panels: Part I: Design**, ECCS Publication No. 115.

EOTA (European Organization for Technical Approvals) (2005) **TR 019 Calculation models for prefabricated wood-based loadbearing stressed skin panels for use in roofs**. Bruxelles.

Findley, W. N., Lai, J. S. and Onaran, K. (1976) **Creep and Relaxation of nonlinear viscoelastic materials**. Dove Publications, Inc., New York, pp.3-4.

Forestry (2010) www.forestry.gov.uk [Accessed December 10th 2010]

Foster, D. C. (2008) **Development of a Micromechanics Based Failure Criteria for Transversely Loaded Composite Materials**. PhD Thesis, University of Dayton.

Frostig, Y. (2003) **Classical and high-order computational models in the analysis of modernsandwich panels**. Composites Part B: Engineering, Volume 34, Issue 1, January 2003, pp. 83-100.

Gibson, L. J. and Ashby, M. F. (1999), **Cellular Solids : Structure and Properties,** 2nd Edition Cambridge University Press, Cambridge, UK.

Hairstans, R. and Kermani, A. (2007) **Briefing: Structural insulated panels in modern construction**. Proceedings of the ICE - Construction Materials, Volume 160, Issue 3, 1st August 2007, pp. 91 –94.

Hemsec SIPs Ltd (2007) **Structural Insulated Panel Technology – The modern method of Construction with Added Benefits**.

Huang, J. S. and Gibson, L. J. (1990) **Creep of sandwich beams with polymer foam cores.** Journal of Materials in Civil Engineering, ASCE, Vol. 2 No.3, pp. 171-182.

Huang, J. S. and Gibson, L. J. (1991) **Creep of Polymer Foams.** Journal of Materials Science, 26, pp. 637-647.

HUD (U.S. Department of Housing and Urban Development) (2007), **Prescriptive Method for Structural Insulated Panels (SIPs) Used in Wall Systems in Residential Construction**. March 2007.

ICC-ES (ICC Evaluation Service, Inc.) (2008) **Acceptance Criteria for Sandwich Panel Adhesives AC05.**

ICC-ES (ICC Evaluation Service, Inc.) (2009) **Acceptance Criteria for Sandwich Panel AC04.**

Illston, J. M. and Domone, P. L. J. (2010), **Construction Materials: Their Nature and Behaviour**. 4th Edition, Spon Press, London.

Innovaré System Ltd (2010) **Guide to i-SIP construction**.

International Barrier Technology (2008) **Fire-Resistance Treatment of Structural Insulated Panels (SIPs) for Commercial Roofing Systems**. www.intlbarrier.com [Accessed December 10th 2010]

Just, M. (1983) **Ergebnisse Experimenteller Untersuchungen Zum Langzeitverhalten Von Pur-Hartschaumstoff-Stutzkernbauteilen Und Schlussfolgerungen Fur Die Anwendung (the Results of an Experimental Investigation of the Long-Term Behavior of Building Elements Utilizing a Rigid Plastic Foam Core and Conclusions Regarding Their Use).** IfL-Mitt., 22 (Heft 3), pp. 95-104.

Kawasaki, T. and Kawai, S. (2006) **Thermal insulation properties of wood-based sandwich panel for use as structural insulated walls and floors.** The Japan Wood Research Society. Vol. 52, Issue N1, pp. 75-83.

Kenyangi, O. B. (2010) **A study of the use of Structural Insulated Panels (SIPs) in the UK construction industry**. MEng Dissertation, School of Civil Engineering, University of Birmingham.

Kermani, A. (2006) **Performance of structural insulated panels.** Proceedings of the Institution of Civil Engineers, Structures & Buildings 159, Issue SB1, pp. 13-19.

Kermani, A. and Hairstans, R. (2006) **Racking Performance of Structural Insulated Panels.** Journal of Structural Engineering, ASCE. Vol. 132, No. 11, pp. 1806-1812.

Kim J. and Swanson S.R. (2001) **Design of sandwich structures for concentrated loading**. Composite Structures, Volume 52, Number 3, May 2001, pp. 365-373.

Kim, N.H. and Sankar, B.V. (2009) **Introduction to finite element analysis and design**. New York, John Wiley & Sons, Inc.

Kingspan TEK (2007) **Kingspan TEK Building System Brochure**. 5th edition, June 2007.

Kingspan TEK (2007) www.kingspantek.co.uk [Accessed December 10th 2007]

Koschade R. (2002) **Sandwich Panel Construction**, Ernst & Sohn, Berlin.

Lim, T. S., Lee, C. S. and Lee, D. G. (2004) **Failure Modes of Foam Core Sandwich Beams under Static and Impact Loads**. Journal of Composite Materials, Vol. 38, No. 18, pp. 1640-1662.

Lyons, A. (2010) **Materials for Architects and Builders**. 4th Edition, Butterworth-Heinemann, Oxford.

McCormack T. M., Miller R., Kesler O. And Gibson L. J. (2001) **Failure of sandwich beams with metallic foam cores**. International Journal of Solids and Structures, Volume 38, Issues 28-29, July 2001, pp. 4901-4920.

McIntosh, J. (2008) **Learning from Hurricane Katrina: The Case for Structural Insulated Panel Systems**. 4th International i-Rec Conference 2008, Building resilience: achieving effective post-disaster reconstruction, Christchurch, New Zealand. 30 April - 2 May 2008.

Milner, M. (2003) **A briefing guide to the use of structural insulate panel (SIP)**. TRADA Technology Publication, U.K.

Morley, M. (2000) **Building with Structural Insulated Panels (SIPs).** The Taunton Press.

Mullens, M. A. and Arif, M. (2006) **Structural Insulated Panels: Impact on the Residential Construction Process.** Journal of Construction Engineering and Management, July 2006 Vol. 132, No. 7.

Noakes, K. (2008) **Successful composite techniques : a practical introduction to the use of modern composite materials**. 4th edition, Ramsbury, Crowood.

Oakdale Engineer (2011) www.oakdaleengr.com [Accessed January 15th 2011]

PATH (The Partnership for Advancing Technology in Housing) (2007) **Structural Insulated Panels**. www.pathnet.org [Accessed December 7th 2007]

Plantema, F. J. (1966) **Sandwich construction.** New York, Wiley.

Pokharel, N. (2003) **Behaviour and Design of Sandwich Panels Subject to Local Buckling and Flexural Wrinkling Effects**. PhD Thesis, Queensland University of Technology.

Pu, J.H., Tang, R.C. and Hse, Chung-Yun (1994) **Creep behavior of sweetgum OSB: effect of load level and relative humidity**. Forest Products Journal, Vol. 44, pp. 45-50

Pugh, G. (2006) **Building with Structural Insulated Panels.** JLC, August 2006.

Rizov, V., Shipsha, A. and Zenkart, D. (2005) **Indentation study of foam core sandwich composite panels**. Computational Materials Science, Volume 69, Issue 1, June 2005, pp. 95-102.

Rungthonkit, P. and Yang, J (2009). **Behaviour of Structural Insulated Panels (SIPs) under both short-term and long-term loadings**. 11th International Conference on Non-conventional Materials and Technologies Materials for Sustainable and Affordable Construction, University of Bath, Bath, UK, 6th - 9th Sep 2009.

Said, M. N. A. (2006) **Task 2: Literature Review: Building Envelope, Heating, and Ventilating Practices and Technologies for Extreme Climates.** Institute for Research in Construction National Research Council Canada Ottawa, Ontario, Canada.

SIP Build Ltd (2007) **SIP Build Limited Brochure.**

SIP Build Ltd (2007) www.sipbuildltd.co.uk/download3.html [Accessed December 10th 2007]

SIP Building Systems Ltd (2010) **Design Guide – Part 1: Structural Design**.

SIP Industries Ltd (2010) www.sipsindustries.com [Accessed November 10th 2010]

SIPA (Structural Insulated Panel Association) (2008) **Department of Energy laboratory shows new way to win the energy wars at home**. Form No. L-206 May 2008.

Sun, C. T. And Tao, J. (1998) **Prediction of failure envelopes and stress/strain behaviour of composite laminates**. Composites Science and Technology, Volume 58, Issue 7, July 1998, pp. 1125-1136.

Sun, Y. (2007) **Structural Aspects of Sandwich Panels With and Without Openings.** Master of Philosophy Thesis, Department of Architecture and Civil Engineering, University of Bath.

Sunley, J. and Bedding, B. (1985) **Timber in construction**. Batsford: TRADA.

Swanson, S. R. (2001) **Anticlastic effects and the transition from narrow to wide behavior in orthotropic beams**. Composite Structures, Volume 53, Issue 4, September 2001, pp. 449-455.

Structural Insulated Panels Association (SIPA) (2010) www.sips.org [Accessed December 10th 2010]

Taylor, S. B., Manbeck, H. B. and Janowiak, J. J. (1997) **Modeling Structural Insulated Panel (SIP) Flexural Creep Deflection.** Journal of Structural Engineering, ASCE. Vol. 123, No. 12, pp. 1658-1665.

Thomas, D., Mantell, S. C., Davidson, J. H., Goldberg, L. F. and Carmody, J. (2005) **Analysis of Sandwich Panels for an Energy Efficient and Self-Supporting Residential Roof.** Proceedings of 2005 International Solar Energy Conference (ISEC2005), 6-12 August 2005, Orlando, Florida.

Tracy, J. M. (2000) **SIPs overcoming the elements.** Forest Products Journal. Madison March 2000. Vol. 50 Issue 3.

TRADA Technology Ltd (2007) **Timber frame construction : Sole plates**. TRADA Technology, August 2007.

Triantafillou T. C. and Gibson L. J. (1987) **Failure mode maps for foam core sandwich beams**. Materials Science and Engineering, Volume 95, November 1987, pp. 37-53.

UKSIPS (UK SIPS ASSOCIATION) (2010) www.uksips.org.uk [Accessed December 10th 2010]

Unidek Ltd (2010) **Unidek: SIPS Sense Brochure**.

Vaidya, A., Uddin, N. and Vaidya, U. (2010) Structural Characterization of Composite Structural Insulated Panels for Exterior Wall Applications, ASCE Journal of Composites for Construction Volume 14, No.4, August 2010, pp. 464-469.

Vinson, J. R. (1999) **The behavior of sandwich structures of isotropic and composite materials.** Lancaster, Technomic.

Yeh, B., Williamson, T. And Keith, E. (2008) **Development of Structural Insulated Panel Standards**. Proceedings of the 2008 Structures Congress.

Zarghooni, M. and Sennah, K. (2010) **Development of creep model for structural insulated timber-foam panels for roof construction under sustained loading**. Proceedings, Annual Conference - Canadian Society for Civil Engineering 2010 (CSCE 2010), 9 - 12 June 2010 Volume 2, pp. 961-970.

Zenkert, D. (1995) **An introduction to sandwich construction.** London, Chameleon Press Ltd.

Zenkert, D. (1997) **The Handbook of Sandwich Construction**, EMAS, Cradley Heath, UK.

Zhou, D.W., Louca, L.A. and Saunders, M. (2008) **Numerical simulation of sandwich T-joints under dynamic loading**. Composites Part B: Engineering, Volume 39, Issue 6, September 2008, pp. 973-985.

Zhu, E.C., Guan, Z. W., Rodd, P. D. and Pope, J. D. (2005) **A constitutive model for OSB and its application in finite element analysis**. European Journal of Wood and Wood Products Volume 63, Number 2, pp. 87-93.

APPENDICES

Appendix A - Analytical method calculations

Appendix B - Published paper

Appendix A

Analytical method calculations

	Project		Job ref
UNIVERSITY OF BIRMINGHAM	Allen's method - SIP calculation		PhD Research
	Part of structure		Calc sheet no
	Typical SIPs		1/1
	Drawing ref	Calc by	Date
	-	Prathan Rungthonkit	6/12/2010

Ref.	Calculations	Output

Allen's method - Typical SIPs (STP)

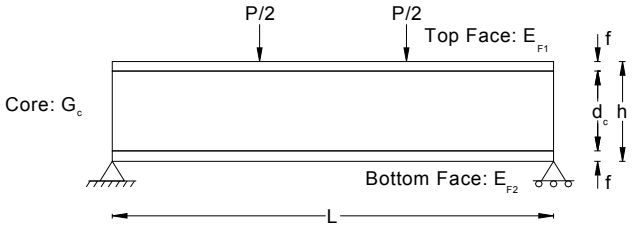

Input parameters:

Applied Load, P	19.32	kN
The span of the panel, L	1100	mm
The width of the panel, B	500	mm
The outer face thickness, f	11	mm
The inner core thickness, d_c	103	mm
Modulus of the top face, E_{F1}	3844	N/mm^2
Modulus of the bottom face,E_{F2}	3844	N/mm^2
Core shear modulus, G_c	2.3	N/mm^2
Modulus of the bottom face, E_c	6.442	N/mm^2

Output:

The sum of flexural rigidity, D	1.38E+11	Nmm^2
Bending deflection at midspan, Δw_B	3.30	mm
Shear deflection at midspan, Δw_s	24.41	mm
Total deflection, Δw	27.72	mm
Tensile and Compressive stress in the outer face	5.62	N/mm^2
Shear stress in the inner core	0.188	N/mm^2

	Project			Job ref
UNIVERSITY OF BIRMINGHAM	TR019 - Wood-Based Section with C16			PhD Research
	Part of structure			Calc sheet no
	SDC			1/2
	Drawing ref	Calc by	Date	
	-	Prathan Rungthonkit	6/12/2010	

ref.	Calculations			Output
	TR019 - Wood-Based Section with C16 - SDC			
	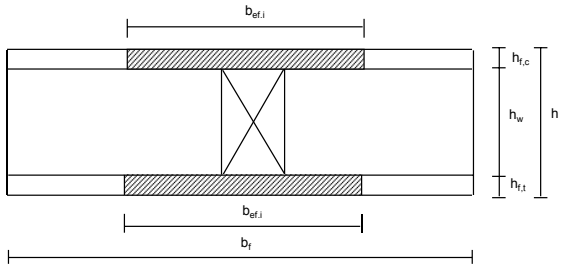			
TR 019 - C.3.1.1.2	Applied Load	40.32	kN	
	The span of the beam, l	1100	mm	
	The web spacing, b_f	600	mm	
	The rib width, b_w	47	mm	
	$E_{t(c),//,0,mean,i}$	3844	N/mm^2	
	$E_{t(c),//,90,mean,i}$	3615	N/mm^2	
	$G_{//,mean,i}$	1080	N/mm^2	
	m_i	0.24		
	a_i	1.434		
	c_i	0.940		
	$l_{1,i}$	1.578		
	$l_{2,i}$	0.615		
	$a_{1,i}$	1.352		
	$a_{2,i}$	0.527		
	Effective flange width of the wood-base skins, $b_{ef,i}$	406.1591	mm	
	Clear distance between webs, b_f	1200	mm	
	Web:			
	Width of the web, b_w	47	mm	
	Clear height between the flanges, h_w	103	mm	
	Area of the web, A_w	4841	mm	
	Flanges:			
	Top flange thickness, ht_f	11	mm	
	Bottom flange thickness, hb_f	11	mm	
	Panel depth, h	125	mm	
	2. Material strength properties			
BS EN 338:2003	C16:			
Table 1	Mean modulus of elasticity, $E_{C16.mean}$	8000	N/mm^2	
	Mean shear modulus, $G_{C16.mean}$	500	N/mm^2	
BS EN 12369-1:2001	OSB:			
Table 2	Mean modulus of elasticity, $E_{OSB.mean}$	3844	N/mm^2	

	Project			Job ref
UNIVERSITY OF BIRMINGHAM	TR019 - Wood-Based Section with C16			PhD Research
	Part of structure			Calc sheet no
	SDC			2/2
	Drawing ref	Calc by	Date	
	-	Prathan Rungthonkit	6/12/2010	

ref.	Calculations			Output
	Effective flange width in compression, $b_{ef.c}$	406.1591	mm	
	Effective flange width in compression, $b_{ef.t}$	406.1591	mm	
	3. Transformed section properties			
	Transformed web thickness into OSB, $b_{w.tfd}$	97.81	mm	
	Area of flange in compression, $A_{ef.f.c}$	4468	mm^2	
	Area of flange in tension, $A_{ef.f.t}$	4468	mm^2	
	Area of web, $A_{ef.w}$	10075	mm^2	
	Transformed area, A_{ef}	19010	mm^2	
	First moment of area of the section abot the top face, A_{1st}	1188151	mm^3	
	Neutral axis depth from the top face, y_t	63	mm	
	Second moment of area of the web about the NA, $I_{ef.w}$	8907071	mm^4	
	Second moment of area of the top flange about the NA, $I_{ef.f.t.f}$	14516093	mm^4	
	Second moment of area of the bottom flange about the NA, $I_{ef.f.b.f}$	14560770	mm^4	
	Instantaneous second moment of area the transformed section, I_{ef}	37983933	mm^4	
	5. Deflection of the panel			
	Bending deflection at midspan	6.52	mm	
	Shear deflection at midspan	3.05	mm	
	Total deflection	9.58	mm	

	Project			Job ref
UNIVERSITY OF BIRMINGHAM	EC5 Racking Resistance			PhD Research
	Part of structure			Calc sheet no
	Stud wall			1/2
	Drawing ref	Calc by	Date	
	-	Prathan Rungthonkit	15/8/2010	

ref.	Calculations				Output
	EC5 stud wall racking resistance				
	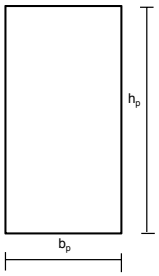				
EC5	1. Geometric properties:				
	Width of each stud, b	47	mm		
	Depth of each stud, h	103	mm		
	Wall height, h_p	2440	mm		
	Lateral spacing of each stud, S_{stud}	600	mm		
	Wall panel width, b	1200	mm		
	Wall panel ratio, r	2.03			< 4 => OK
	Wall length, b_p	1200	mm		
	Thickness of OSB, t_{OSB}	11	mm		
	Fastener diameter, d_n	2.8	mm		
	Fastener spacing, s	150	mm		
	2. Timber and nail properties:				
BS EN 338 (2003)	Characterisic of C16, r_k	310	kg/m^3		
Table 1	Design strength of fixing, $F_{f,Rd}$	638	N		
	3. Modification factors:				
Cl.9.2.4.3.2 (4)	Basic fastener spacing, s_o	0	mm		
eq 9.27	k_d	0.49			< 1 => OK
eq 9.28	k_q	1.00			
eq 9.29	k_s	0.49			
eq 9.30	k_n	1.5		(For both sides)	
	5. Racking resistance:				
	Racking resistance of wall, $F_{v,Rd}$	3.16	kN	1.29 kN/m	

Appendix B

Behaviour of Structural Insulated Panels (SIPs) under both short-term and long-term loadings

Proceedings of the 11th International Conference on
Non-conventional Materials and Technologies (NOCMAT 2009)
6-9 September 2009, Bath, UK

BEHAVIOUR OF STRUCTURAL INSULATED PANELS (SIPS) UNDER BOTH SHORT-TERM AND LONG-TERM LOADINGS

Prathan Rungthonkit[1] and Jian Yang[2]

School of Civil Engineering, University of Birmingham

Abstract: Structural Insulated Panels (SIPs), as a load-bearing construction material, have recently attracted continuingly growing interest. They are structurally sufficient, energy efficient, easy to use in construction and more sustainable. SIPs are a composite sandwich panel system, typically made of two oriented strand board (OSB) panels and one insulation core material such as expanded polystyrene (EPS) or polyurethane (PUR). They have high strength-to-weight ratio and can resist axial, transverse and racking loads. Therefore, they can be used as structural materials for roof, wall and floor panels. An entire building structure can be made of SIPs without including many conventional construction materials such as steel or masonry. Due to the limited application and research on SIPs, the knowledge of this material is still lacking. This is exacerbated by the fact that the structural performance of SIPs has been reported varies from manufacturer to manufacturer as they use different SIP construction and connection details. In applying SIPs as structural materials, apart from addressing conventional structural issues, there is another major concern related to their long-term performance, mainly caused by creep. Both facial and core materials experience high creep behaviour, and it has been found that the creep of SIPs is predominantly caused by the core material. This paper will report studies conducted at University of Birmingham on structural behaviours of SIPs under both short-term and long-term loadings.

Keywords: *Structural insulated panels; SIPs; Panel-to-panel connections; Structural behaviour; Creep*

1. Introduction

Structural Insulated Panels (SIPs) are high performance load-supporting panels, which are considered to be the next generation of timber construction in the UK. A typical make-up of SIPs comprises insulation core materials adhesively bonded to outer skins such as oriented strand board (OSB). As a novel structural material, they offer key advantages including satisfactory structural strength, super thermal performance, high strength-to-weight ratio and low environmental impact. The knowledge of SIPs as a load-supporting construction material is still very limited. This is exacerbated by the fact that the structural performance of SIPs has been reported to vary from manufacturer to manufacturer as they use different SIP construction and connection details.

SIP connections encompass panel-to-panel joints and connections between different structure members, such as wall-to-floor connections. There are a number of different panel-to-panel joint designs from various manufacturers. However, no universal standards or codes of practice are currently available for designing and detailing SIP connections.

[1] Researcher, pxr735@bham.ac.uk
[2] Lecturer, j.yang.3@bham.ac.uk

Most existing designs recommended by manufacturers need to be tested and approved by independent approval bodies.

Literature survey reveals three typical panel-to-panel joints, including OSB thin spline, foam block spline (or referred to as mini-SIP spline) and dimensional lumber spline. Figures 1 illustrates the typical panel-to-panel joints.

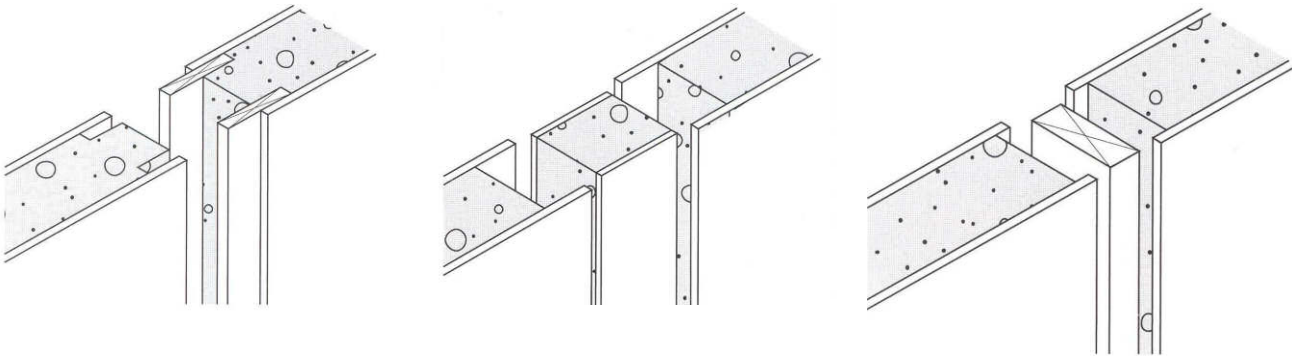

(a) OSB thin spline (b) Mini-SIP spline (c) Dimensional lumber spline

Figure 1: Typical panel-to-panel joints (Morley, 2000)

This paper will report studies conducted at University of Birmingham on structural behaviour of SIPs under both short-term and long-term loadings. The main objective of this study is to investigate structural behaviour (e.g. stiffness, loading capacity and creep) of SIPs with various panel-to-panel joints. A series of purposely selected SIP samples have been subjected to both short-term and long-term transverse loading test. Testing results have provided the first-hand data, which are not readily available in open literature. In this study, special focus has been placed on the effect of panel-to-panel joint on structural behaviour of SIPs under both short-term and long-term loading conditions. Displacements at various locations have been recorded throughout the entire loading regime. Failure loads and the corresponding failure modes have been identified. The obtained testing results can be used to validate the subsequent numerical modelling results.

2. Short-term experimental investigation on SIPs with various panel-to-panel joints

Short-term four-point bending tests of a series of SIP samples were undertaken at University of Birmingham. In this test program, joints with mini-SIP connections and dimensional lumber spline connections have been studied. The first type of joint in Figure 1 with OSB thin spline was not included due to the difficulty of fabrication in engineering practice. Since neither British nor European standards has specified standard testing method for SIPs, the four-point bending test for double skin metal faced insulating panels specified in BS EN 14509 was found suitable and hence employed. Figure 2 illustrates the four-point bending test details.

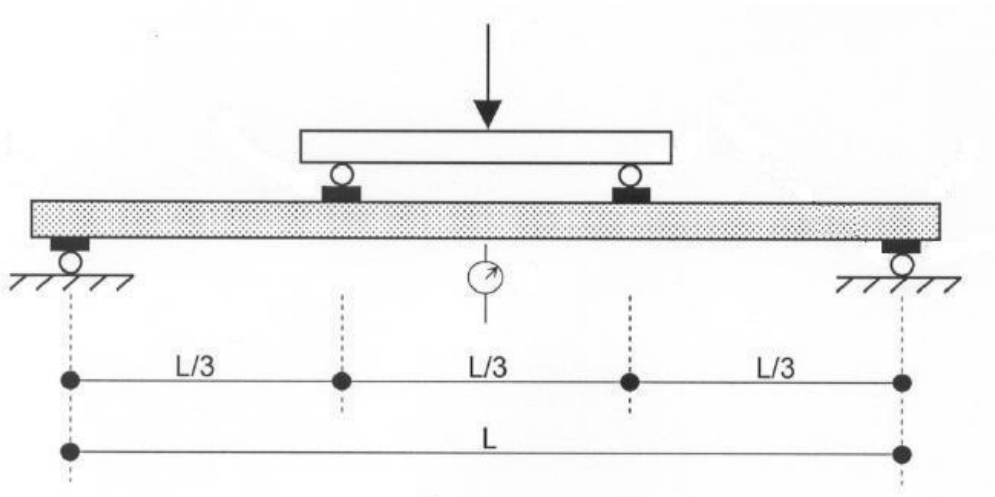

Figure 2: Four-point bending test (BS EN 14509, 2006)

2.1 SIP testing samples

Six SIP samples of three groups, i.e. two typical panels without any connections (TP1-1 and 2), two panels with the mini-SIP spline connection (TP2-1 and 2) and two panels with the dimensional lumber spline connection (TP3-1 and 2), were subjected to the four-point bending test until failure. The expected failure modes in this test include the inner core shear, debonding and outer face fracture/crushing. All test samples have half of the standard product size, i.e. 600 mm x 1200 mm. The principle of selecting sample size is that by testing most economic panel size, tests should be able to supply adequate results to fulfil the designated purpose. For instance, conclusions on the impact of joints drawn through these half-size samples can be rationally extended to full-size panels. It is obvious that results obtained from these tests may adequately serve as the benchmark example of the subsequent numerical modelling.

All panel samples were manufactured by SIP Build Ltd. The technique used to bond the inner core and outer faces is by injecting the PUR foam into the spacing between the two OSB skins and then curing to produce a strong bond.

TP1 has a 600 mm width and 1200 mm length with 11 mm thick OSB/3 facings and a 103 mm thick polyurethane inner core (overall thickness of 125 mm). Both short edges of the panel are inserted with C16 50x103 mm timber sections fastened by 2.8 mm diameter and 63 mm long nails with 150mm spacing, and also glued to the OSB faces and PUR core. Both long edges of the specimens are not inserted with any timber sections and are left with 50x103 mm rebates. Figure 3 shows the sample details of the first group of panel.

TP2 panel consists of two small panels, each being 300 mm wide by 1200 mm long with 11 mm thick OSB/3 facings and a 103 mm thick polyurethane inner core (overall thickness of 125 mm). The two small panels are joined along the centre-line by a mini-SIP spline fastened by 2.8 mm diameter and 63 mm long nails with 150mm spacing. Like TP1, both short edges are inserted with 50x103 mm timber sections. Both long sides of the sample are left with 50x103 mm rebates as previously described. Figure 4 shows the specimen details of the second group of panel.

Like TP2, TP3 consists of two identical small panels but is jointed by C16 dimensional lumber spline fastened by 2.8 mm diameter 63 mm long nails with 150mm spacing. The edge configurations are the same as TP1 and TP2. Figure 5 shows the specimen details of the third group of panel.

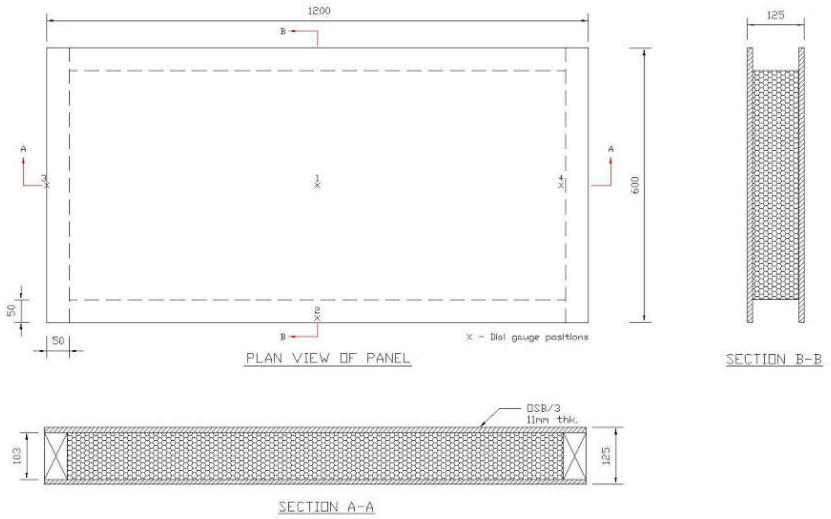

Figure 3: TP1 sample details

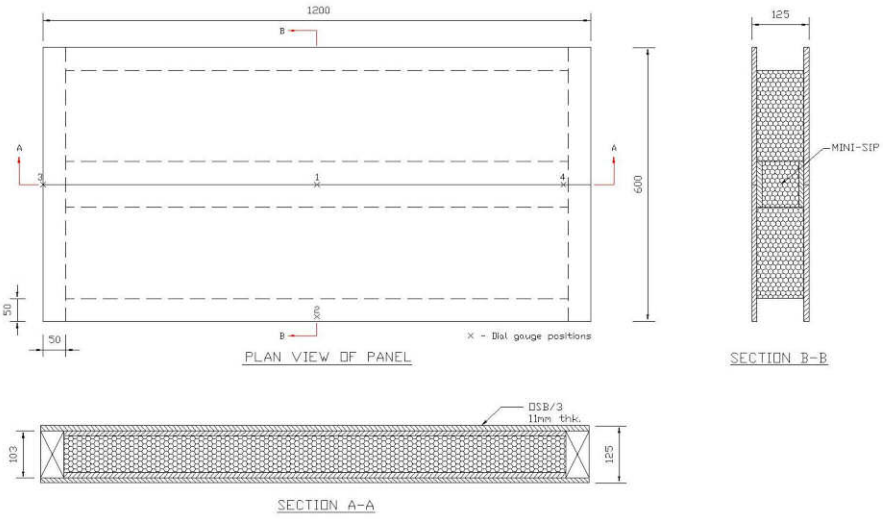

Figure 4: TP2 sample details

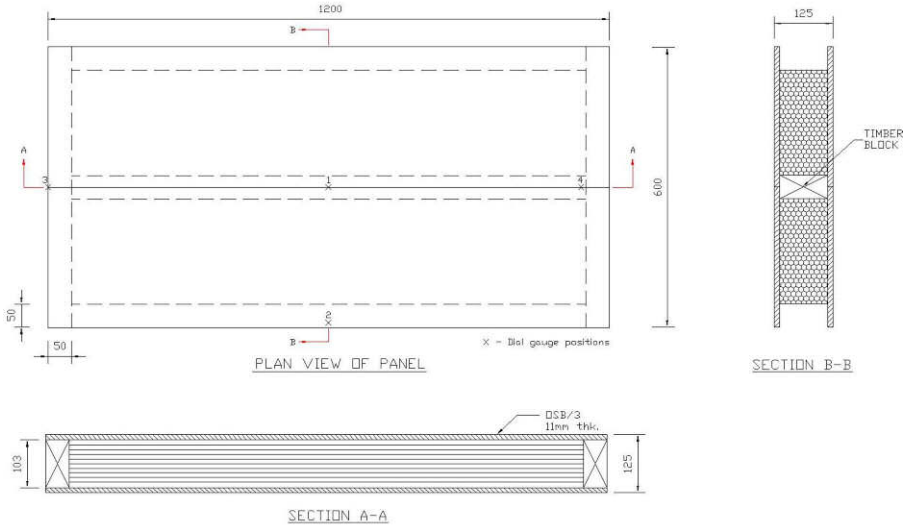

Figure 5: TP3 sample details

2.2 Experimental apparatus

Test panels were supported on two movable steel rollers which are placed on two steel I-beams. Between the roller and the panel, a 100 mm wide steel plate was placed to spread the reaction (see Fig. 6). Two line loads, which are 366 mm apart, were symmetrically applied through load spreading steel plates of size 600x100x10 mm and a steel roller of 30 mm diameter. The loads were then applied at suitable increments and the centre displacements were recorded until failure by using Mand Testing Machine. Figure 6 shows the layout of experimental apparatus for this test.

Figure 6: Experimental apparatus

2.3 Short-term test results

Table 1 shows the summary of the testing. It should be noted that the deflection of the panel becomes the governing factor of the loading capacity.

Table 1: Experimental findings summary

Specimen	***Load at Failure (kN)***	***Displacement at Failure (mm)***	***Load at deflection limit L/333 (kN)***	***Serviceability Load / Load at Failure (%)***	***Failure Mode***	***Increase of design loading capacity (%)***
TP1-1	19.32	34.84	2.87	15	Shear	0
TP1-2	19.32	42.90			De-Bonding	
TP2-1	20.32	42.35	3.06	15	De-Bonding	7
TP2-2	19.32	39.65			De-Bonding	
TP3-1	44.32	23.05	7.98	20	Flexural-Shear	178
TP3-2	36.32	21.54			Flexural-Shear	

Figure 7 shows the applied loads against vertical centre displacements of all three groups of panel.

As can be seen from Table 1 and Figure 7, TP3 panels (jointed by dimensional lumber spline connections) are the stiffest, which offers highest load capacity; whereas TP2

panels (jointed by mini-SIP connections) exhibit almost identical stiffness and failure loads to TP1. The loading capacity of TP3 governed by the deflection limit is 178% higher those of TP1 and TP2.

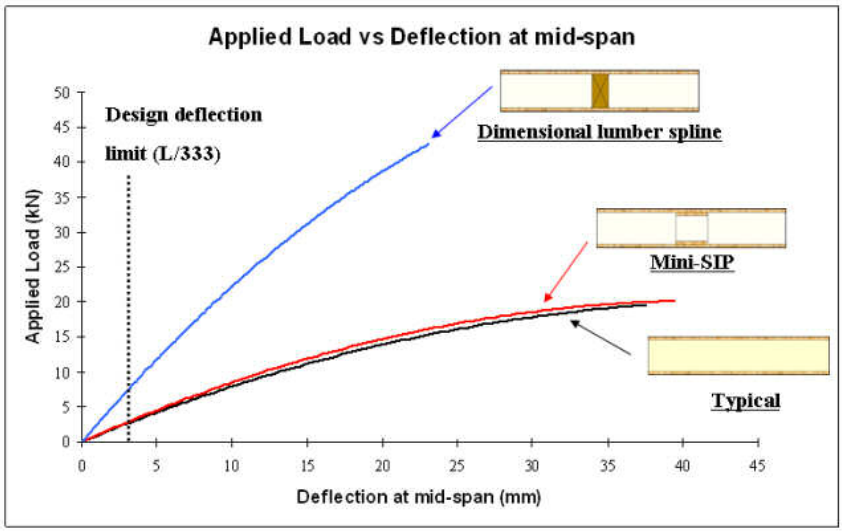

Figure 7: Load vs centre vertical displacement

This observation reveals that the mini-SIP joint has negligible impact on structural behaviours of SIPs whereas the lumber spline joint has significant impact. To increase the structural efficiency, the lumber spline joint is preferred. The quantitative increase of loading capacity, which may be affected by the dimension, the space of the lumber and the connection between the lumber and SIPs, e.g. the size and space of nails, is to be investigated.

3. Long-term experimental investigations on SIPs with various panel-to-panel joints

3.1 SIP samples and experimental apparatus

All three panels (TP1, TP2 and TP3), as previously described in Section 2.1, were subjected to the four-point bending creep test for three months under ambient temperature and moisture content. The magnitudes of the applied loads (shown in Table 2) are the serviceability loads (at the deflection limits in accordance with BS 5268-2, 2002, i.e. L/333) which were found from the short-term test and retained as a constant through the entire testing duration. The loads were applied to the panels through loading jacks supported by fixed steel box beams. Steel box beams were hold down onto the strong floor via threaded steel rods. The magnitudes of the applied loads were monitored by load cells. Figure 8 shows the layout of experimental apparatus for this test.

The creep deflections of each SIP samples together with temperature and relative humidity were then recorded at the following time points after initial loading: 0.1h, 0.2h, 0.5h, 1h, 2h, 4h, 8h, 24h and then every 24h. At each time of monitoring, the load was increased to its initial level and the set of deflection reading was also recorded.

3.2 Long-term experimental test results

The initial creep deflection of all panels is in the range of 3.9 - 4.1 mm, TP3 is found to have the lowest creep deflections at the same time. Figure 9 shows the comparison of the creep test results among all test panels.

Table 2: The applied loads and the initial deflection of each SIP specimen

Specimen	*Applied Load (SLS)*	*Weight of supporting elements*	*Total load*	*Applied Load / Short-term Load Capacity*	*Initial Deflection*
	(kN)	**(kN)**	**(kN)**	**(%)**	**mm**
TP1	2.9	0.25	3.15	15.8	4.1
TP2	3.1	0.33	3.43	17.3	3.9
TP3	8.0	0.29	8.29	20.6	4.0

Figure 8: Experimental apparatus

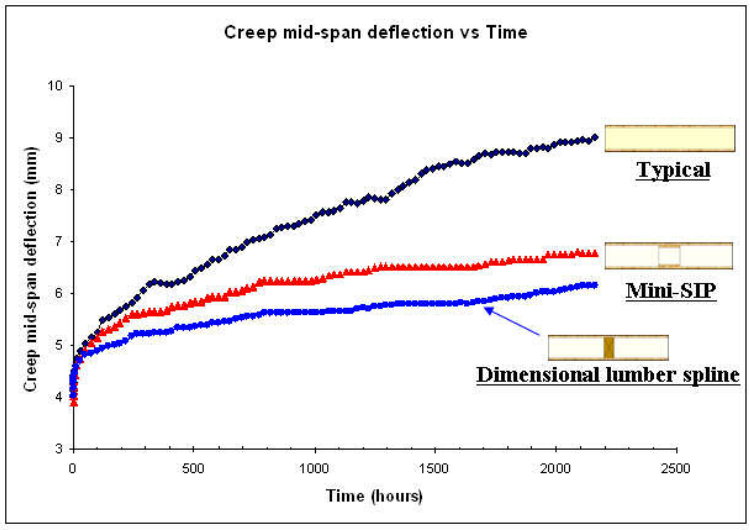

Figure 9: Three month creep test results

Test results show that the five element creep compliance model, provided by Taylor (1997) in Equation 1, is adequate to describe the three month creep test result. Moreover, creep parameters can be used to predict the creep behaviour at longer durations. Figure 10 illustrates five element creep compliance model prediction with three month creep test results.

$$\Delta(t) = \Delta_0 + A_1[1 - \exp(-A_2 t)] + A_3 t^{A_4} \quad (1)$$

where $\Delta(t)$ is total time dependent deflection (mm);
Δ_0 is initial deflection (mm);
A_i is creep parameters associated with creep deflection equations; and
t is duration (hour)

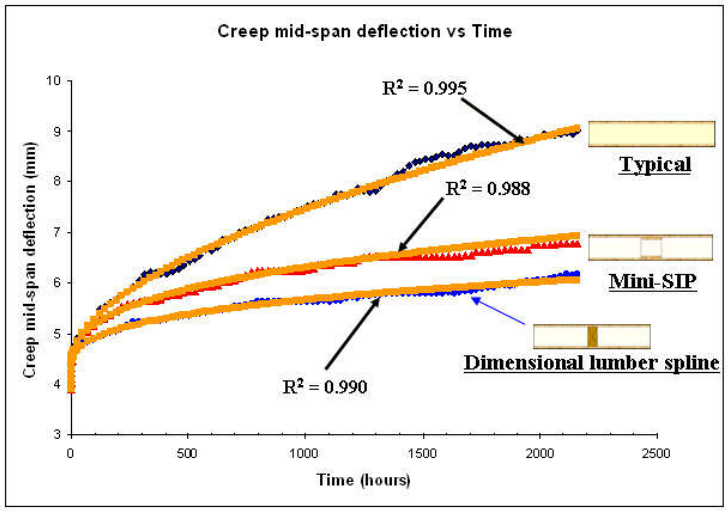

Figure 10: Five element creep compliance model prediction

4 Conclusions

The popularity of SIPs is increasing because of their favourable features. The short-term transverse loading test was carried out and test results show that the panels with dimensional lumber spline connections are the stiffest and therefore provide highest design loading capacity. Loading capacities of panels with mini-sip connections are found to be similar to the typical panels without any connections. Consequently, this indicates that the loading capacity is not subjected to any deduction when the mini-SIP connection is used. It has been also found that the serviceability ultimate limit load usually governs the design.

The long-term transverse creep test was also carried out and it has been found that the panel with dimensional lumber spline connection has the lowest creep deflections within the same duration. Furthermore, the five element creep compliance model has been found to be able to adequately describe creep test results and can be used to predict the creep behaviour in longer durations.

5 References

BRITISH STANDARD: BS 5268-2, 2002. Structural use of timber - Code of practice for permissible stress design, materials and workmanship.

BRITISH STANDARD: BS EN 14509, 2006. Self-supporting double skin metal faced insulating panels – Factory made products – Specifications.

MORLEY, M., 2000. Building with Structural Insulated Panels (SIPs). *The Taunton Press*. pp. 82.

TAYLOR, S. B., MANBECK, H. B. AND JANOWIAK, J. J., 1997. Modeling Structural Insulated Panel (SIP) Flexural Creep Deflection. *Journal of Structural Engineering*, ASCE. Vol. 123, No. 12, pp. 1658-1665.